Imperial College
London

Bioorthogonal Chemistry for Pretargeted PET Imaging

A thesis submitted in fulfilment of the requirements for the degree of
Doctor of Philosophy at Imperial College London

Helen Louise Evans

Department of Surgery and Cancer

Declaration

I hereby declare that the work described in this thesis is based upon my own independent research and when others have contributed this is clearly acknowledged.

Finally, my warmest thanks go to my support system, my friends and family who made all of this possible. To my housemate Ruth, for always being there for me, and for providing me with endless cakes and M&S treats, these were always appreciated. To all of my other friends who have been there since the beginning, and through all of my undergraduate days, I've been so lucky to have you all. To Lucy, for being a fantastic sister and friend, and for joining me on some amazing adventures! Thanks also to my Grandparents, who have always believed in me, I hope you will be able to understand some of my thesis when I show it to you! Last, but certainly not least, I want to thank my parents for their unconditional love and support, and for letting me be the independent person that I have become. I owe so much to each of you, and I would not have achieved all of this without you by my side.

Abstract

Positron Emission Tomography (PET) is emerging as a powerful method for imaging cancer through the design and development of new radiotracers. Antibodies have promising properties as ligands for targeting cancer, as they have the advantage of displaying high affinity for their respective receptors. However, the use of antibodies as radiotracers is limited to the use of long-lived isotopes, as these large biomolecules additionally display slow blood circulation and clearance. The use of short-lived isotopes such as ^{18}F or ^{68}Ga, in combination with antibodies, would provide the ideal balance between targetability and clearance. This may be achieved by use of a two-step pretargeting strategy, whereby a reactive tag is conjugated to the antibody and allowed to localise in the tissue to be imaged, before systemic administration of a chemical reporter (e.g. a labelled reactive partner) which allows the 'pretargeted' tissue to be imaged.

The Strain-Promoted Azide/Alkyne Cycloaddition (SPAAC) reaction between cyclooctynes and azides was evaluated as an appropriate bioorthogonal reaction for application to a pretargeting strategy using short-lived isotopes. The synthesis of a library of cyclooctyne precursors was carried out, which were evaluated in terms of their reactivity with azides, and their suitability for *in vivo* applications. An ^{18}F-labelled version of the SPAAC reaction was developed, demonstrating the ability of the reaction to be carried out under different conditions. This model reaction was translated to *in vivo* pretargeting using a cyclooctyne modified Herceptin monoclonal antibody and an ^{18}F-labelled azide. These initial experiments indicated that the SPAAC reaction may not be fast enough to occur at the low concentrations which are found *in vivo*. The reaction was thoroughly examined in terms of kinetics at different concentrations, and a high concentration-dependence upon rate of reaction was confirmed. This was supported by a ^{68}Ga-labelled SPAAC reaction, which was carried out using reportedly more reactive cyclooctynes than those used in the initial experiments. In general, the reaction showed a greater preference to be carried out in organic solvents such

as acetonitrile, and under closer to physiological conditions the reactions were less likely to proceed.

The Inverse-electron-Demand Diels-Alder (IeDDA) reaction between tetrazines and strained alkenes was evaluated as an alternative bioorthogonal reaction for demonstrating *in vivo* pretargeting. A series of ^{68}Ga-labelled IeDDA reactions between a ^{68}Ga-labelled tetrazine and a series of norbornene analogues demonstrated the superior reaction kinetics and biocompatibility of the IeDDA reaction. The initial translation of the IeDDA reaction to a proof-of-concept for pretargeting using cyclic RGD pentapeptides was initially unsuccessful, attributed to the surprisingly poor reactivity of norbornene-modified cyclic RGD pentapeptides towards a ^{68}Ga-labelled tetrazine. The reaction between a ^{68}Ga-labelled tetrazine and a Cetuximab antibody, which had been modified with the more reactive *trans*-cyclooctene (TCO) moiety, was successfully demonstrated. The hypothesised pretargeting strategy using this model reaction was achieved on high EGFR expressing cells, validating the IeDDA reaction in this context. These results suggested tantalising opportunities for application of the IeDDA reaction to *in vivo* pretargeting for PET imaging using short-lived isotopes such as ^{18}F and [68]Ga.

Glossary of Terms

Ac	Acetate anion
ADME	Absorption, Distribution, Metabolism and Excretion
BARAC	Biarylazacyclooctyne
BCN	Bicyclo[6.1.0]nonyne
Boc	Di-*tert*-butyl dicarbonate
BPDS	*n*-(*m*-trifluoromethylphenyl)phenoxazine-4,6-dicarboxylic acid
n-BuLi	*n*-Butyllithium
CCD	Charge-Coupled Device
Cps	Counts per second
CT	X-ray computed tomography
CuAAC	Copper-catalysed Azide/Alkyne Cycloaddition
Cyclen	1,4,7,10-tetraazacyclododecane
C225	Cetuximab monoclonal antibody
DBU	1,8-Diazabicyclo[5.4.0]undec-7-ene
DDQ	2,3-Dichloro-5,6-dicyano-1,4-benzoquinone
DMP	1,1,1-Triacetoxy-1,1-dihydro-1,2-benziodoxol-3(1H)-one
DFO	Desferrioxamine-B
DIBAC	Aza-dibenzocyclooctyne
DIBAL-H	Diisobutylaluminum hydride
DIBO	Dibenzocyclooctynol
DIBOD	*sym*-Dibenzo-1,5-cyclooctadinene-3,7-diyne
DIFO	Difluorinated cyclooctyne
DIMAC	Aza-dimethoxycyclooctyne
DIPEA	*N*,*N*-Diisopropylethylamine
DMA	*N*,*N*-Dimethylacetamide
DMAP	4-Dimethylaminopyridine
DMF	*N*,*N*-Dimethylformamide
DMSO	Dimethylsulfoxide
DOTA	1,4,7,10-Tetraazacyclododecane-1,4,7,10-tetraacetic acid
DOTA-Az	2,2′,2″-(11-Azido-3,6,9-trioxaundecan-1-amino)-2-oxoethyl)-1,4,7,10-tetraazacyclododecane-1,4,7-triyl)triacetic acid
DOTA-GA-NH$_2$	2,2',2''-(10-(1-Carboxy-4-((2-(2,5-dioxo-2,5-dihydro-1H-pyrrol-1-yl)ethyl)amino)-4-oxobutyl)-1,4,7,10-tetraazacyclododecane-1,4,7-triyl)triacetic acid

DOTA-GA-Tz	2,2',2''-(10-(1-Carboxy-4-((4-(6-methyl-1,2,4,5-tetrazin-3-yl)benzyl)amino)-4-oxobutyl)-1,4,7,10-tetraazacyclododecane-1,4,7-triyl)triacetic acid
DOTA-Tz	2,2′,2″-(10-(2-((4-(6-Methyl-1,2,4,5-tetrazin-3-yl)benzyl)amino)-2-oxoethyl)-1,4,7,10-tetraazacyclododecane-1,4,7-triyl)triacetic acid
Dppf	1,1'-Bis(diphenylphosphino)ferrocene
DTPA	Diethylene triamine pentaacetic acid
2D	2-Dimensional space
3D	3-Dimensional space
EDTA	Ethylenediaminetetraacetic acid
EGFR	Epidermal Growth Factor Receptor
EMA	European Medicines Agency
EWG	Electron-withdrawing group
E&Z	Eckert & Ziegler
FBA	4-Fluorobenzaldehyde
FBS	Fetal bovine serum
FEA	2-Fluoroethylazide
FET	Fluoroethyltyrosine
FDA	Food Drug Administration
FDG	2-Fluoro-2-deoxy-D-glucose
FII	Flourescence Intensity Imaging
FLT	Flourothymidine
FT	Fourier Transform
GFP	Green fluorescent protein
HBTU	O-(Benzotriazol-1-yl)-N,N,N',N'-tetramethyluronium hexafluorophosphate
HER	Human Epidermal growth factor Receptor
HOMO	Highest occupied molecular orbital
HPLC	High performance liquid chromatography
HRMS	High Resolution Mass Spectrometry
IBX	O-Iodobenzoic acid
ID	Infected Dose
IeDDA	Inverse-electron-Demand Diels-Alder
IgG	Immunoglobulin G
IHC	Immunohistochemistry
KHMDS	Potassium bis(trimethylsilyl)amide
LDA	Lithium diisopropylamine
LiHMDS	Lithium bis(trimethylsilyl)amide

LOR	Line of Response
Log*P*	Log (partition coefficient)
LUMO	Lowest unoccupied molecular orbital
mAb	Monoclonal antibody
m-CPBA	*meta*-Chloroperoxybenzoic acid
MOFO	Mono-fluorinated cyclooctyne
MRI	Magnetic Resonance Imaging
MSA	Murine Serum Albumin
NaHMDS	Sodium bis(trimethylsilyl)amide
NB	Norbornene
NCA	No-carrier-added
NCE	New Chemical Entities
n.d.c	Non-decay-corrected
NHS	*N*-Hydroxysuccinimide
NIR	Near Infrared
NIS	*N*-Iodosuccinimide
NMR	Nuclear Magnetic Resonance spectroscopy
NOTA	2,2',2''-(1,4,7-Triazacyclononane-1,4,7-triyl)triacetic acid
NOTP	1,4,7-Triazacyclononane-1,4,7-tris(methylenephosphonate)
NOTPME	1,4,7-Triazacyclononane-1,4,7-tris(methylenephosphonate monoethylester)
OCT	Cyclooct-1-yn-3-glycolic acid (and derivatives)
ORTEP	Oak Ridge Thermal-Ellipsoid Plot
PBS	Phosphate Buffered Saline
PCC	Pyridinium chlorochromate
PEG	Polyethelene glycol
PTC	Phase-transfer Catalyst
PET	Positron Emission Tomography
*p*NP	*para*-Nitro phenyl
PyBOP	Benzotriazol-1-yl-oxytripyrrolidinophosphonium hexafluorophosphate
pyr	Pyridine
RCM	Ring-Closing Metathesis
RCY	Radiochemical yield
RF	Radio-frequency
R*f*	Retardation factor
RIT	Radioimmunotherapy

RT	Room temperature
Ruppert's reagent	Trifluoromethyltrimethylsilane
Selectfluor™	Chloromethyl-4-fluoro-1,4-diazoniabicyclo[2.2.2]octane bis(tetrafluoroborate)
S_NAr	Nucleophilic Aromatic Substitution
S_N2	Bi-molecular Nucleophilic Substitution
SPAAC	Strain-Promoted Azide-Alkyne Cycloaddition
SPDC	Strain-Promoted 'Double-Click'
SPECT	Single-Photon Emission Computed Tomography
TACN	1,4,7-Triazacyclononane
TBAF	Tetra-*n*-butylammonium fluoride
TBS	*tert*-Butyl dimethylsilyl group
TCO	(*E*) or *trans*-cyclooctene
TESCl	Triethyl silyl chloride
TFA	Trifluoroacetic acid
THF	Tetrahydofuran
TLC	Thin Layer Chromatography
TMDIBO	3-Hydroxy-2',3',2",3"-tetramethoxy-7,8-didehydro-1,2:5,6-dibenzocyclocta-1,5,7-triene
TMSCl	Trimethyl silyl chloride
TMSI	Trimethyl silyl iodide
TOCA	[Tyr³]Octreotate
Togni™ reagent	3,3-Dimethyl-1-(trifluoromethyl)-1,2-benziodoxole (and derivatives)
Traut's reagent	2-Imino thiolane
UV	Ultra-violet
VEGF	Vascular Endothelial Growth Factor

Contents

Chapter 1 – Introduction

1.1   Cancer and Detection

Cancer may be defined in broad terms as being a set of diseases in which there is an uncontrolled multiplication and spread within the body of abnormal forms of the body's own cells.[1] There are numerous causes of cancer, and these remain only partially understood, due to the complexity and invasive nature of the diseases. Understanding cancer is essential to the development of new therapies, and one important way in which this can be explored is through the use of molecular imaging.

1.1.1 The Hallmarks of Cancer

There are relatively few exploitable chemical differences between cancerous and normal cells, and hence it remains highly challenging to target. In 2000, however, six main characteristic hallmarks were defined as being the integral components of most forms of cancer. These hallmarks include sustaining proliferative signalling (uncontrolled cell division), resisting cell death, inducing angiogenesis, enabling replicative immortality, activating invasiveness and metastases, and evading growth suppressors.[2] Although these hallmarks are still considered to be the main characteristics of most cancer types, these are now described in more detail due to the increased understanding of oncology (Figure 1).[2, 3]
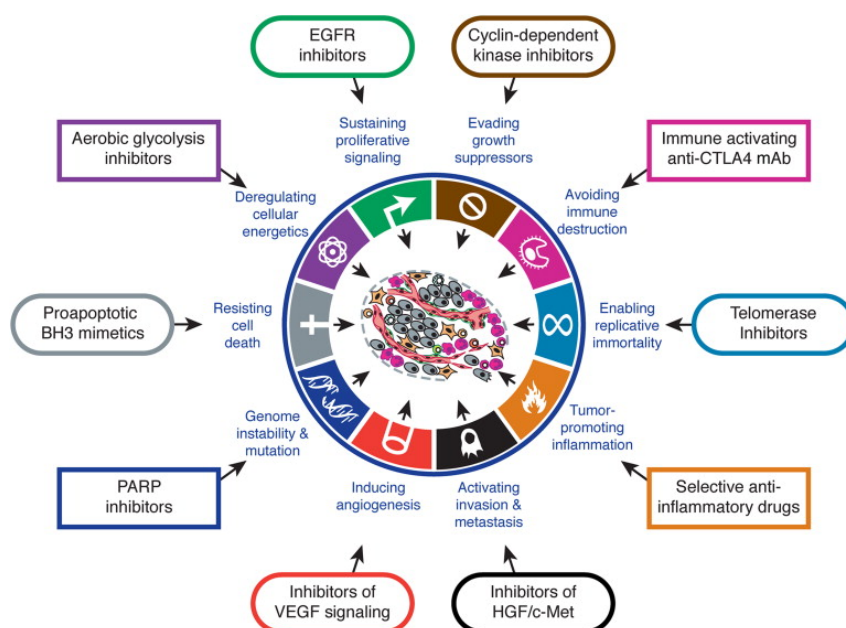
Figure 1. The characteristic hallmarks of cancer, taken from Cell, 2011[3]

The change in our understanding of the cancer phenotypes are partly a result of the improved therapies that have been developed, as well as monitoring the mechanisms by which these therapies are controlling the diseases. The basis of cancer lies at the fundamental difference between the cells which contain one or more of these defined hallmarks and healthy cells.

For example, cell proliferation and cell death are both essential during an organism's development, and these two features are tightly controlled by the cell cycle. Each phase of the cell cycle is responsible for dictating and controlling a particular cellular event, and these are strongly monitored by specific molecular checkpoints.[4] These checkpoints determine whether progression from one phase of the cell cycle to another is allowed, and small irregularities are corrected quickly by repair mechanisms, whereas larger defects may instead be committed to programmed cell death or apoptosis (Figure 2).
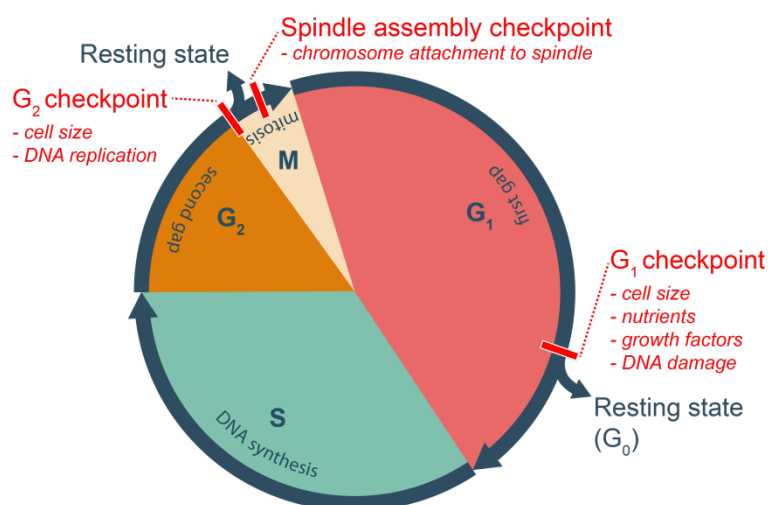
Figure 2. A general overview of the cell cycle, showing the key checkpoints which determine the progression from one stage to another[4]

Deregulated cell proliferation and apoptosis lie at the foundation of all tumour development and are obvious targets for anticancer therapeutics for this reason. However, cancer is much more complex than at first glance; proliferative signals are coupled to a variety of growth-inhibitory processes such as apoptosis, differentiation and senescence, making the development of cancer therapeutics a highly complex process.

Coupled to this is the fact that design and development of cancer therapeutics is a lengthy and costly process, and the drug candidates often have adverse effects, with low response rates relative to drugs in other therapeutic areas.[5] For these reasons, rationalising and shortening drug discovery and development is critical to improving cancer drug discovery, by characterising compounds in the early phases of the discovery and development, and within clinical use. In addition, the key to successful cancer therapeutics lies in early diagnosis and monitoring the response to therapy, and one way in which this may be achieved this is through the discovery, development and validation of oncology biomarkers, including molecular imaging biomarkers.[6]

1.1.2 Molecular Imaging Biomarkers for Cancer Detection

Biomarkers are used to measure and evaluate normal biological processes, pathological processes, or pharmacological responses to therapeutic intervention.[7, 8] Molecular imaging biomarkers may improve the precision, and decrease the invasiveness of cancer diagnosis, and may allow non-invasively imaging of whole tumour masses. New imaging biomarkers that fulfil these criteria allow for the non-invasive imaging of cancer before, during and after therapy, and could increase our understanding of cancer biology, as well as providing earlier diagnosis, and act as a useful method to monitor the responses to therapy.[1]

Molecular imaging requires the use of multimodality techniques, involving the collaboration between chemists, biologists, physicists and clinicians, and is developing both in terms of the range of modalities available, and in the diversity of the molecular probes used. Several stages are required for the development of new molecular imaging probes, starting from the identification of molecular targets and the development of chemistry, through to cell and small animal imaging, and finally computer modelling and clinical imaging (Figure 3).
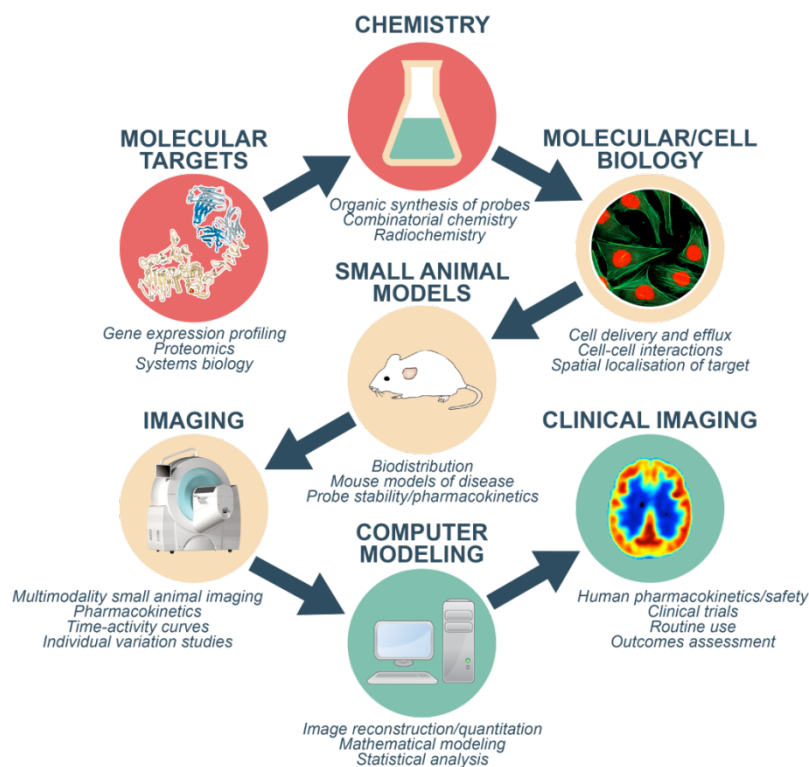
Figure 3. An overview of the process of molecular imaging; from deciding the molecular target to imaging in a clinical setting *via in vitro* models and small animal studies.[9]

Molecular imaging allows for the characterisation and quantification of biological processes at the cellular and molecular level in intact living subjects, and new methods now have enough spatial and temporal resolution for studying biological processes *in vivo*. Small animal imaging may be used to determine the biodistribution of a molecular probe before use in humans, and may be used to mechanistically understand biological responses to treatment. Repetitive, non-invasive, uniform and relatively automated studies of the same living subjects may be carried out, using biological imaging assays at different time points, which is statistically more powerful and more cost-effective than using single experiments with numerous subjects.[10]

Imaging modalities include optical imaging (bioluminescence and fluorescence), ultrasound, magnetic resonance imaging (MRI), X-ray computed tomography (CT), and the nuclear imaging methods; positron emission tomography (PET) and single photon emission computed tomography (SPECT).[6, 11] Each of these modalities has its own strengths and

weaknesses, varying in terms of sensitivity, spatial resolution, temporal resolution, cost, and depth of tissue penetration for carrying out small animal imaging (Table 1).

Imaging method	Imaging time	Spatial resolution[a]	Main purpose	Advantages	Disadvantages
Optical: Bioluminescence and fluorescence	Sec–min	Organ: 50 μm Whole body: 1–5 mm	Monitoring tumour response to treatment in deep-seated/ orthotopic sites and metastatic spread; imaging gene expression and protein– protein interactions	Relatively non-invasive (requires restraint), high sensitivity (amol–nmol); many fluorescent and near-infrared probes available; amenable to use of gene reporters; relatively cheap	In most cases, these methods require genetic modification of tumour cells for detection; quantitation relies on 2D images in current imaging systems; nude or shaved animals are required
Three-dimensional high-frequency ultrasonography	Sec–min	100 μm in-plane resolution	Relative measure of tissue blood flow; three-dimensional measurement of tumour size	Relatively non-invasive (requires restraint), high sensitivity (single particle); absolute measurements are possible with suitable contrast agents, e.g.. microbubbles	Specialized application
Magnetic resonance imaging (MRI), spectroscopy (MRS) or spectroscopy imaging (MRSI)	Min–hours	100 μm in-plane resolution (7 T); much higher for spectroscopy without imaging	Pharmacodynamics, pathophysiology, pharmacokinetics, anatomy	Some techniques use endogenous contrast; good spatial resolution (imaging)	Poor sensitivity (mmol), so that exogenous contrast agents and drugs need to be given at high concentration
Standard or contrast-enhanced computed tomography (CT)	Sec–min	100 μm	Pharmacodynamics, anatomy	Very good spatial resolution combined with relatively good sensitivity	High radiation dose (for standard CT, 2 cGy for most currently available systems), limited number of contrast agents, which may be nephrotoxic
Single photon emission computed tomography (SPECT)	Min	1–2 mm	Pharmacodynamics, pathophysiology, pharmacokinetics	High sensitivity (pmol) Radiochemistry can be performed in nuclear medicine department	Limited radiochemicals available compared with PET, less quantitative
Positron emission tomography (PET)	Min	1–2 mm	Pharmacodynamics, pathophysiology, pharmacokinetics	High sensitivity (pmol) allowing true tracer kinetics; unlimited range of radiochemicals making it very flexible; fully quantitative	Poor spatial resolution; full quantitation requires cannulation (for kinetic studies); requires specialized radiochemistry in most situations

[a]Optimum spatial resolution is usually achieved at the expense of ability to obtain fast kinetics.

Table 1. Examples of imaging modalities and their advantages and disadvantages for carrying out small animal imaging, adapted from *Workman, 2010*.[10]

Optical Imaging

Optical molecular imaging techniques image photons using charge-coupled device (CCD) cameras.[6] This allows for the imaging of light in both the ultraviolet (UV) and near infrared (NIR) regions. Most *in vivo* optical imaging is obtained using fluorescence, whereby light is emitted from an electronically excited molecule when the energy of the molecule drops from its lowest singlet state to its ground state. Optical imaging is widely available due to the low cost of the technique, and the most utilised modalities are bioluminescence and fluorescence imaging (FLI). Bioluminescence is limited due to the requirement of the production of cross-species of proteins, making the method irrelevant in clinical applications. However, FLI has seen the development of numerous molecular probes, and is a highly

21

sensitive technique. The wide range of fluorophores that are available, as well as the use of non-ionising radiation, make this an attractive method for molecular imaging. However, the method is limited due to the poor methods of quantification that exist, as well as the depth of tissue penetration in a clinical setting, which is much lower than for the other imaging modalities. For this reason, in the clinic, FLI imaging probes are most useful for studying superficial tissues; for example breast cancers and lymph nodes, or when coupled with invasive techniques (e.g. using an endoscope or open surgery).

Ultrasound

Ultrasound is a fairly robust and inexpensive method for imaging soft tissue, and uses high-frequency sound waves, which are reflected or refracted back to the transducer, allowing for reconstruction of the tissue under study. An image known as a sonogram is produced, and is used particularly for measuring the progression of pregnancy.[12] In oncology, this technique is useful for imaging tumours by contrast to other tissue, and distinguishing these areas from fluid-filled compartments such as cysts. Ultrasound is useful for diagnostic purposes, and for measuring changes in tumour size, particularly when aided by 3D techniques and through the use of contrast agents.[13] It is possible to distinguish between benign and malignant tumours when microbubble contrast agents are employed.

The main advantages for use as a molecular imaging modality include the low risks associated with the technique (as unlike CT it does not use ionising radiation), and the small size of the equipment, making the method widely available at relatively low cost. However, the technique is limited to studying areas that are not overlaid by bone, and the waves are reflected more strongly at air-tissue interfaces.[14] This modality also has the disadvantage of being operator dependent, making reproducibility of the procedure for a wide range of applications challenging.

Magnetic Resonance Imaging (MRI)

MRI is one of the most highly utilised methods for imaging cancer, and, unlike the nuclear imaging methods (PET and SPECT) and CT, this method does not rely on the use of ionising radiation.[15] Instead, nuclear magnetic resonance (NMR) is used to visualise nuclei inside the body. A strong magnetic field is used to align the protons inside the subject, which is then exposed to a varying electromagnetic field (pulse).[6] This electromagnetic field has the correct resonance frequency to alter the spin of the nuclei within the magnetic field, and when this radiofrequency pulse is turned off, the protons re-align to the bulk magnetic field. This is known as the relaxation, and the radiofrequency produced from this event is recorded by the receiver coils in the MRI scanner. Additional magnetic fields may be used in order to obtain useful 3D information, and a Fourier Transform (FT) is used in order to mathematically determine the distribution of protons within the subject. Protons in different tissue-types display differing relaxation rates, and hence this can be used to generate, or construct images, based upon variables such as the T_1 and T_2 relaxation times, spin density, flow and spectral shifts. Contrast between different tissue may be visualised using this method, and for this reason it is particularly useful for imaging tissues that contain many hydrogen nuclei and low density contrast, such as the brain, and most types of tumours.

The main advantages of MRI over other molecular imaging modalities are the high contrast to other tissue, and high spatial resolution that may be obtained, providing superior anatomical information when compared to optical and nuclear imaging. A significant advantage of MRI over modalities such as CT is the use of non-ionising radio frequency (RF), which has a lower overall risk to patients than the use of ionising radiation.[16] However, there are some limitations associated with the sensitivity of the technique. In order to achieve imaging of disease biomarkers using MRI, targeted MRI contrast agents are required, such as gadolinium-based chelates, which improve the visibility of internal body structures by altering the relaxation times of atoms within the treated tissue.[17] The sensitivity may be enhanced by increasing the molecular field strength, or by use of hyperpolarisation.

A significant disadvantage is that the technique is relatively expensive, having a similar overall cost to nuclear imaging modalities.[6]

X-Ray Computed Tomography (CT)

CT is a medical imaging technique that produces tomotographic images through the use of computer-processed X-rays. Since its introduction in the 1970s, it remains the most widely used method of transaxial imaging, and is used for both diagnosis and staging of most soft-tissue and bone cancers, as well as to assess response to treatment. This is largely due to the fact that this method provides excellent tissue contrast, allowing for the disease to be visualised in 3 dimensions (3D), by use of a series of 2D X-ray images around a single axis of rotation. CT allows for a quantitative assessment of the change in tumour volume in response to treatment, and the functional properties of tumours may be assessed with the aid of contrast agents.[18]

This method is useful for determining the boundaries of the tumour, and therefore the extent to which invasiveness into other tissue has occurred, due to the detailed anatomical image that may be obtained. Another advantage is the wide availability of the technique, coupled with the low cost as compared to other imaging modalities, as well as the speed of the scan acquisition. For assessing cancer, CT is most commonly used to evaluate the primary tumour size, as well as determining the levels of metastasis, but it may be used in combination with other imaging modalities in order to obtain further molecular information.The main limitation of this method for imaging cancer is the use of ionising radiation, which has many health implications for the patient.[19] The use of this modality for some particular applications is currently being eclipsed by other imaging modalities such as MRI.

Single Photon Emission Computed Tomography (SPECT)

Nuclear imaging may be defined as being the temporal and spatial detection of ionising radiation from injected radionuclides.[6] SPECT and PET are two key molecular imaging

modalities that are able to functionally map the distribution in the body of a radiotracer. Both of these techniques are 3D, and are 'powered' by use of nuclear imaging. These imaging modalities are, in a simiar manner to CT, limited in terms of radiation exposure.

SPECT relies on the delivery of a gamma-emitting radioisotope, which is usually administered through the blood stream. In most circumstances, the radioisotope is attached to a ligand which is of interest due to its chemical binding, forming a radioligand which may be delivered selectively to the part of the body under study. The concentration of the radioligand may subsequently be detected by a gamma camera, creating a series of 2D images, which when combined and reconstructed allows a 3D dataset to be produced. Due to the functional images that may be obtained, SPECT is often coupled with CT in order to obtain more detailed anatomical information (Figure 4).
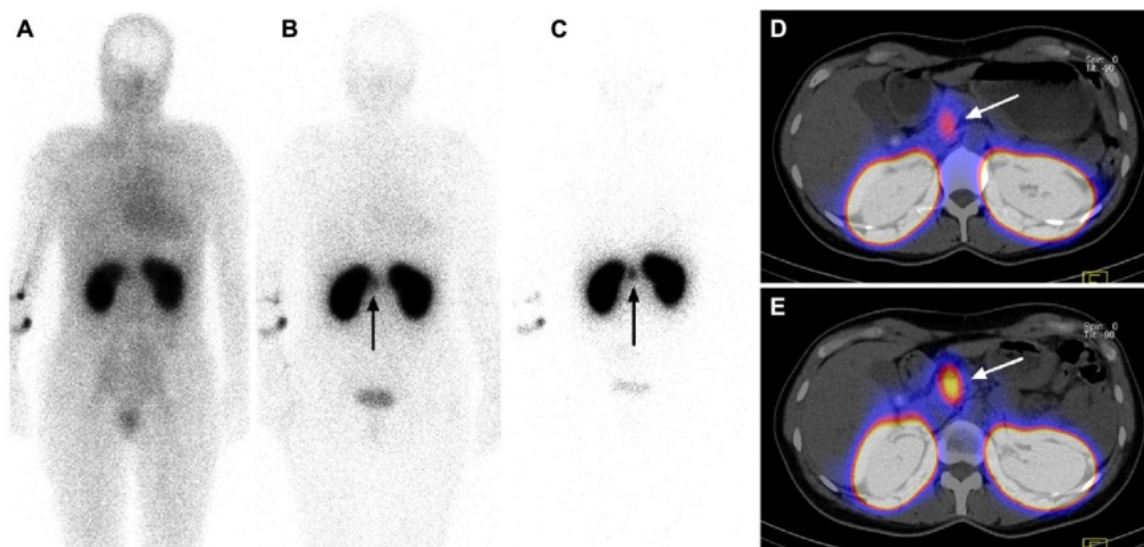
Figure 4. ^{111}In-DOTA-exendin-4 whole-body planar images (A–C) and ^{111}In-DOTA-exendin-4 SPECT/CT images (D, E) from the same patient. ^{111}In-DOTA-exendin-4 uptake visible in the head of the pancreas (arrow) on whole-body (B) and SPECT/CT (D) scans. Reproduced from Christ, 2009[20, 21]

SPECT is a relatively low-cost nuclear imaging technique, using longer-lived and more easily obtained radioisotopes than PET. However, the resolution of a SPECT image is limited due to the use of measurement of directly emitted gamma rays. PET, however, detects emissions in coincidence, providing more information on the exact radiation event, and is subsequently 2 to 3 times more sensitive than SPECT.

1.2   Positron Emission Tomography (PET)

PET is a powerful molecular and functional imaging modality, which can be used to non-invasively measure *in vivo* biodistribution of molecular probes which are labelled with a positron-emitting nuclide, and allows for biological processes in intact living systems to be imaged.[22-24] PET involves the administration of a positron-emitting isotope, which is bound to a targeting ligand, and may either be a substrate for a normal physiological pathway, or is designed to have specific binding interactions with a particular biological target.[25] These radiolabelled probes are administered intravenously in trace amounts, so as to not interfere with normal physiological processes, and for this reason are known as radiotracers. PET can be used to observe complex biological processes such as metabolism and receptor/enzyme interactions, and can also be used to image tissue function at the molecular level.[26] Unlike with CT and MRI, PET is a functional imaging modality, and a detailed anatomical image is not produced.

A PET scan can, however, enable early detection of a potential disease through an observation of chemical changes which may already have occurred.[27] This is an advantage over other imaging techniques such as MRI and CT, which rely upon observation of structural changes, and do not provide any information on metabolic or molecular events.[15] For these reasons, PET has now become an invaluable technique in drug discovery and development due to the ability to facilitate the early detection of disease.[28] PET requires the use of multidisciplinary resources, and on the expertise in a number of scientific areas including synthetic organic chemistry, radiochemistry, pharmacology, cell biology, physics, image analysis and oncology.

1.2.1 Principles of PET Imaging

Probes designed for use in a PET study are labelled with a positron-emitting nuclide, such as ^{18}F, ^{11}C or ^{68}Ga. These radionuclides achieve stability either by electron capture; whereby a nearby orbital electron is captured by the nuclei, or by emission of a positron, which has equal mass but opposite charge to an electron (β^+).[24, 29, 30] Each radionuclide has a

26

characteristic kinetic energy profile, and the positron emitted during this process loses its relative kinetic energy whilst travelling through the host system, *via* electrostatic interactions with neighbouring electrons and protons. These particles of antimatter travel very short distances (~2 mm) within a living organism, dependent upon the particular energy of the positron and hence the radioisotope used, eventually slowing and colliding with an electron from surrounding tissue, forming an ultra-short-lived entity called a positronium (Figure 5).[31]
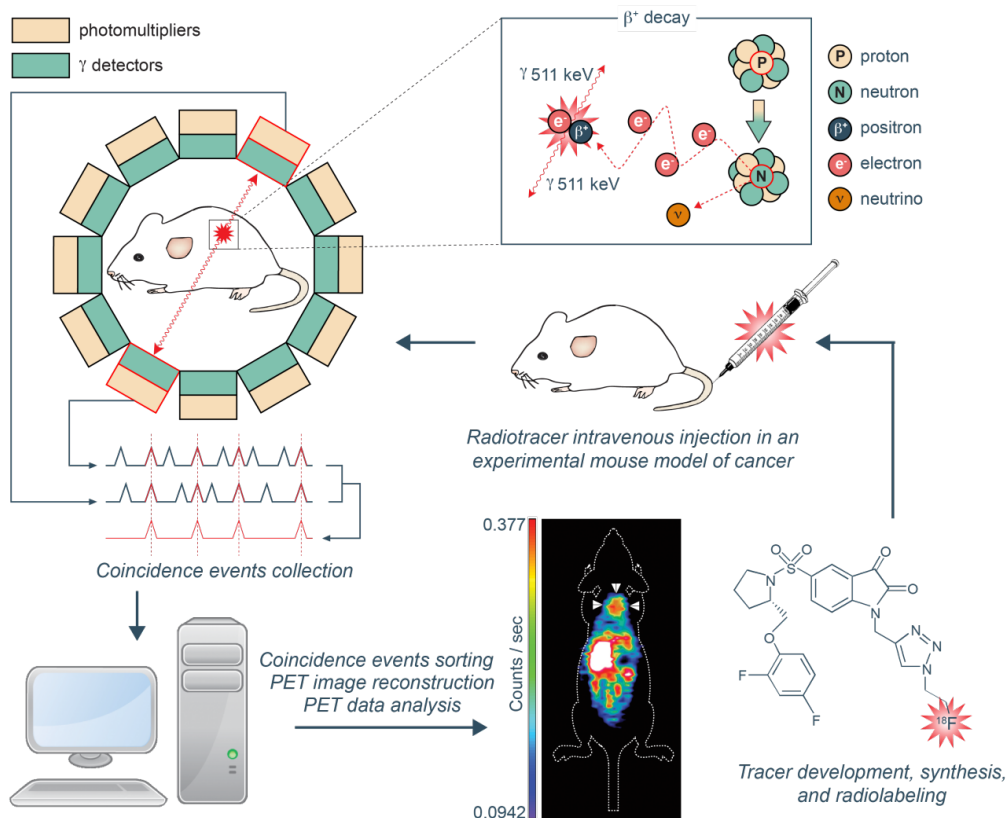
Figure 5. The principal of PET imaging, showing the decay of a positron-emitting isotope, and subsequent collision of the positron with an electron, forming two high-energy γ rays. Adapted from Nguyen, 2010[1]

Two high-energy γ-rays (511 keV) are formed as a result of the positronium annihilation, at approximately 180° angles from each other, which travel at the speed of light (30 cm ns^{-1}) through the host system.[32] A radiation detector can be used to detect both of the γ-rays from an external source, generating detailed information on the origin of the annihilation event.

By use of an array of detectors circulating the object under study, the annihilation information can be used to produce a time resolved image of the distribution of radioactivity within the human body, with very little perturbation of the biological system.[33] PET scanners consist of

a series of pairs of opposing radiation detectors, arranged geometrically to approximately a circle in 2D, and a cylinder in 3D. A line of response (LOR) is defined by a combination of the detection of the coincident event (photons detected in opposite directions) within a finite time span (nanosec). These events are reconstructed into images of representative slices of the subject, using mathematical tomographic image algorithms.[34]

The instruments used for PET are frequently being developed and improved, and their enhancements have been a cornerstone in the development of PET and its introduction into the clinic. These have developed from being solely confined to whole-body scanners, to organ-dedicated instruments such as positron emission mammography, as well as dedicated brain and prostate scanners, and systems designed specifically to image small animals.

1.2.2 Clinical Applications of PET Imaging

Labelling a molecule which targets a specific biological process or marker allows for the spatial distribution of a labelled molecule to be imaged dynamically *in vivo*. PET imaging has already had a large number of applications in disease; the most predominant of these being the non-invasive imaging of cancer.[35] The method not only allows us to visualise the disease, but can also be used to plan suitable therapies and monitor the effectiveness of these treatments.[36, 37] Existing radioligands have been used, for example, to study blood flow, metabolism, cell surface receptor expression, angiogenesis, gene expression, proliferation and apoptosis (Table 2).[25]

Radiotracer	Molecular Target
[^{18}F]FDG	Glucose metabolism
3-[^{18}F]Fluoro-3-deoxythymidine	Tumor proliferation
[^{11}C]Choline/[^{18}F]fluorocholine	Choline metabolism
[^{18}F]Fluoro-L-DOPA	Neuroendocrine tumors
[^{18}F]Fluoroethyltyrosine	Amino acid transport
[^{18}F]AH111585 ([^{18}F]fluciclatide)	Angiogenesis
[^{18}F]FACBC	Amino acid transport
[^{18}F]FMISO	Hypoxia
[^{18}F]HX4	Hypoxia
[^{18}F]EF5	Hypoxia
[^{64}Cu]ATSM	Hypoxia
[^{68}Ga]DOTATATE	Neuroendocrine tumors
[^{18}F]FES	Estrogen receptor
[^{18}F]RGD-K5	Angiogenesis
[^{68}Ga]BNOTA-PRGD2	Angiogenesis
[^{18}F]Paclitaxel	Multi-drug resistance
[^{89}Zr]Bevacizumab	VEGF
[^{18}F]VM4-037	Carbonic anhydrase IX
[^{89}Zr]Cetuximab	EGFR
[^{18}F]FFNP	Progesterone receptor
[^{64}Cu]DOTA-U3-1287	HER3
[^{18}F]BAY94-9392	Amino acid transport
[^{124}I]NM404	Brain glioma
[^{124}I]cG250	Carbonic anhydrase IX
[^{18}F]ML-10	Apoptosis
[^{11}C]Lapatinib	Her2
[^{18}F]Annexin V	Apoptosis
[^{18}F]FAC	Tumor proliferation
[^{11}C]Verapamil	P-gp expression

Table 2. Radiotracers that are currently reported in clinical studies or are listed as in the clinical trial on the clinicaltrials.org website[25]

Although PET has obvious uses in the imaging of cancer, it is a potential 'multipurpose' imaging tool, and has numerous applications in other biomedical, clinical and research areas. PET has also been used to gain a greater understanding of complex receptor systems and their relevance to a particular disease. In particular, imaging agents have been designed to bind to various receptors in the human brain, and can allow for detailed analysis of the role of these receptors in brain diseases such as Parkinson's and Alzheimer's diseases.[29, 38] As well as having the ability to diagnose some neurologic and psychiatric disorders, the technique may also be used for the non-invasive quantification of cerebral blood flow and metabolism, as well as other disease types.

1.2.3 Advantages and Limitations of PET as an Imaging Technique

PET imaging displays a number of advantages as an imaging modality; in particular, it has higher sensitivity (up to 10^{-12}mol l^{-1}) than all of the other techniques, meaning that tracers with very low (i.e. nano or pico molar) concentrations can be detected, therefore lowering the requirement to inject harmful levels of ionising radiation. The method also allows for the distribution of radiotracer to be measured quantitatively; accurately measuring the amount of tracer transported to, and deposited in, the tissue under study, and it is largely independent of the thickness of the object and depth of the source within the subject.

A significant disadvantage of PET as a molecular imaging modality is the low spatial resolution of the images that may be obtained as compared to other imaging techniques, owing to the fact that PET is essentially a functional imaging modality. Hybrid PET/CT systems are now most commonly used, as these allow for the functional information obtained by a PET image to be combined with the morphologic data obtained from a diagnostic CT scan.[36] Merging of two techniques allows for an overall more confident and accurate diagnosis, and has led to an increase in the success of patient diagnosis, disease staging, and therapy monitoring (Figure 6).
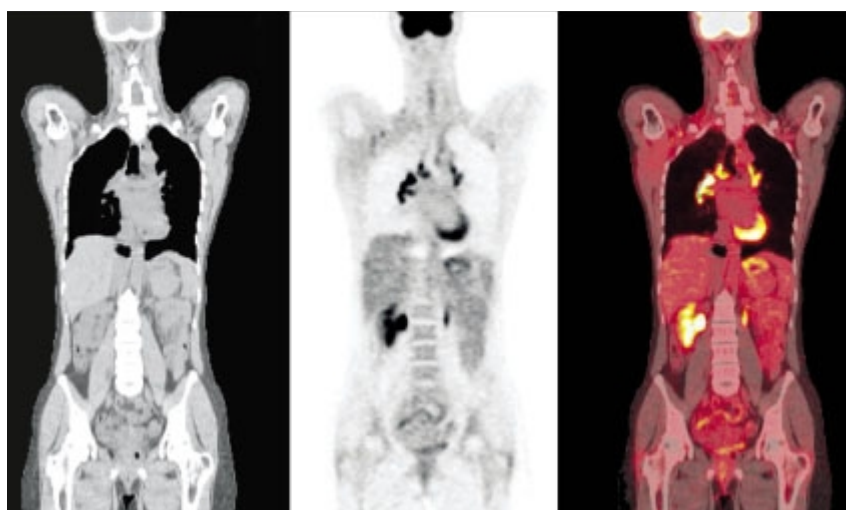
Figure 6. From left to right: A whole body CT scan, a PET scan, and A PET/CT scan[39]

The use of a combined technique also increases patient comfort, and importantly, has a higher clinical throughput and success rate than when the two modalities are used separately. The main limitation of combining these two techniques is the fact that the use of ionising radiation in CT outweighs some of the main advantages of PET, and subsequently the overall risk to patients is higher.

The future of PET may in fact lie in alternative hybrid systems such as PET/MRI, which again allows for the combination of metabolic and anatomical information.[40] This certainly has advantages of improving the success of disease detection, as well as involving lower exposure to ionising radiation; these advances suggest that the diagnostic research area will, in the future, be dominated by hybrid molecular approaches.

1.3   Designing and Synthesising Radiotracers for PET Imaging

When designing a new radiotracer for PET imaging applications, a number of factors must be taken into consideration. This is due to the use of short-lived, positron emitting isotopes, which have unique properties to enable their function for imaging applications. As discussed, the development of molecular imaging probes involves collaboration between scientists of a number of different disciplines, and this begins with the identification of the molecular target, which is followed by the development of the chemistry (Figure 7).[41]
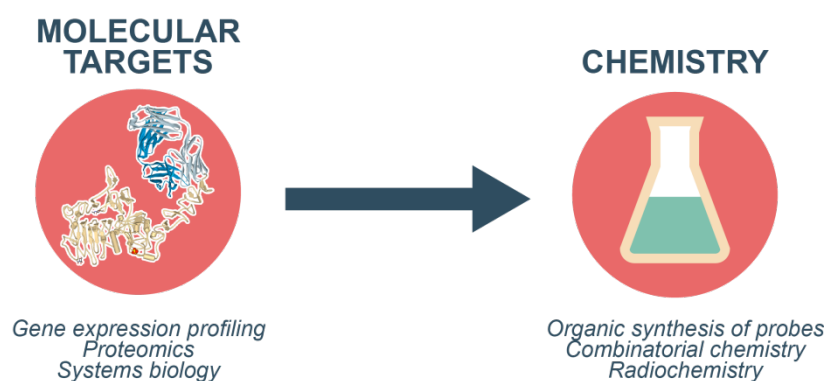
Figure 7. Development of a radiotracer for PET, including target selection, choice of a suitable biomarker, and radiochemistry development

1.3.1 Molecular Target Selection

A radiotracer is most often designed with a particular biological target in mind; for oncology applications this is usually a receptor that is up-regulated in particular tumour types, and may be related directly to one of the hallmarks of cancer (e.g. proliferation, apoptosis etc.). Once the target has been chosen, the biomarker may be designed based upon either an existing ligand for this receptor (for example an existing cancer therapy), or by structure-based design. Many types of compound may be considered as potential radioligands, varying from small molecules to macromolecules, such as peptides and antibodies.[25]

Often, a library of radioligands is synthesised with the target in mind, and this may consist of a series of structural analogues of a parent compound, which has a known affinity for the molecular target. The chosen radioligand should ideally have sub-nanomolar or nanomolar affinity for the target, so that only trace amounts are required. In addition to these factors, the structure of the ligand or biomarker should not be significantly altered by the introduction of the radionuclide, so as not to alter the overall binding affinity of the labelled compound relative to its unlabelled parent compound.

Isotopes of carbon (^{11}C $t_{1/2}$ = 20.3 min), nitrogen (^{13}N, $t_{1/2}$ = 9.97 min), oxygen (^{15}O; $t_{1/2}$ = 2.03 min), and fluorine (^{18}F; $t_{1/2}$ = 109.8 min) are particularly useful as they correspond to some of the most common naturally-occurring elements in living systems. This means that the introduction of the radionuclide may be possible *via* direct isotopic substitution; for example, the radioligand may have the same fundamental structure as the biologically active molecule (e.g. ^{12}C may be replaced directly by ^{11}C). This means that radiolabelled versions of molecules of biological interest can often be synthesised without significantly altering the biological function of a molecule; and in fact, the labelled version may sometimes be modified to be more biologically active than the native form.

1.3.2 Suitable Radionuclides

One of the most challenging aspects of probe development for PET imaging is the short half-lives of the isotopes involved; the fast decay rate means that the tracer must be synthesised rapidly, as imaging must take place within one or two half-lives after completion of radiosynthesis in order to attain useable levels of signal-to-noise. This often suggests that there is a requirement for isotopes to be produced within an on-site cyclotron facility, significantly increasing the cost of this method. However, ^{18}F ($t_{1/2}$ = 109 min) has a longer half-life than other isotopes used, and may be outsourced from non-site-based facilities, making this a more popular isotope when costs are an issue. A preferred metal-chelating isotope may also be considered in this case; ^{68}Ga ($t_{1/2}$ = 68 min) may be produced by a relatively low-cost ^{68}Ge generator (see sections 1.5 and 1.6).

As well as the synthetic considerations that must be taken into account, when deciding upon the radionuclide used for the specific tracer, the half-life of the isotope must be tailored towards the application and pharmacokinetic properties of the radiotracer. Different radionuclides for PET have varying properties in terms of radioactive half-life, decay pattern and positron energy (Table 3).[42]

Radionuclide	Half-life	% β^+ decay	Mean positron energy (MeV)	Mean range in water (mm)	Specific activity (GBq/µmol)
Carbon-11	20 min	100.0	0.39	1.10	341140
Fluorine-18	109 min	97.0	0.25	0.60	102342
Copper-64	12.7 h	17.0	0.28	0.64	63270
Gallium-68	68 min	89.0	0.83	2.90	9065
Yttrium-86	14.7 h	34.0	0.55	1.80	N/A
Zirconium-89	78.4 h	22.7	0.40	1.20	7881
Iodine-124	4.2 days	11.0 (23 % total) 12.0	0.69 0.97	2.30 3.50	1147

Table 3. Physical data for common PET radionuclides used in oncology applications. The quoted specific activity is the maximum achievable (or theoretical) value for the given isotope[42]

These properties have a significant effect on the image that may be obtained, as the radioisotope chosen will alter the image resolution due to the differing decay properties. The isotopes displaying the highest positron energy (for example gallium-68 and Iodine-124) will

produce the lowest resolution images, and will subsequently require the highest level of expertise to reconstruct.

^{11}C is an ideal nuclide for labelling molecules of biological interest, due to the ideal positron energy and range in physiological (aqueous) tissue. However, the half-life of the isotope is too short for use in tracers that require significant distribution and commercialisation, and is therefore most applicable for labelling small molecule tracers. ^{18}F displays a good balance between positron energy and physical half-life, and has a number of other properties that make it attractive for the synthesis of tracers (see section 1.5). Metallic nuclides such as ^{64}Cu and ^{86}Y are appropriate for developing tracers based on peptides and proteins, as these ligands take a longer time to accumulate sufficiently at the target. ^{124}I is good for labelling peptides and larger proteins such as antibodies, due to its long half-life, but this is balanced by a relatively low achievable specific activity compared with other positron-emitting nuclides.

1.3.3 Synthetic Considerations

Once the radionuclide has been chosen, the synthetic strategy by which to incorporate the isotope into the tracer must be developed. The radioisotope chosen is produced by charged particle nuclear reactions, usually from a cyclotron. A cyclotron is an instrument which contains a gas or liquid target, which is bombarded by either protons or deuterons, and once obtained, the isotope is usually formulated for use in the synthesis of the radiotracer.[25]

In order for a radiotracer to be developed, the following characteristics of the synthetic strategy must be achievable:

- Sufficient radiochemical yields

- An adequate radiochemical purity (95 % or higher for human clinical scans)

- High enough specific radioactivity for imaging by administration of trace amounts

- Formulation of the radiotracer into a form which is approved by the European Medicines Agency (EMA) or the Food and Drug Administration (FDA)

Fast and robust strategies are preferred when working with short-lived isotopes, and generally, the total time from the start of the radiosynthesis to the time when the tracer is ready for injection should be no longer than 2 times the half-life of the isotope chosen. For obvious reasons, the synthesis should be as high yielding as possible, and the isotope is ideally introduced at the last stage of the synthesis in order to reduce the amount of time pre-injection that the radionuclide is allowed to decay. Long synthetic strategies may hinder the use of a radiopharmaceutical in a clinical setting, and so careful consideration must be taken to insure that the synthetic time and complexity is kept to a minimum.[43] Often, a multi-step synthetic pathway is chosen, where a prosthetic group containing the radionuclide is synthesised first, and is subsequently introduced onto the compound of interest (see section 1.5).[25] The method of purification of a radiotracer is also of high importance, and isolation is often achieved using High-Performance Liquid Chromatography (HPLC), which would eliminate any unreacted precursors and by-products obtained from the reaction.

Due to the use of high levels of radioactivity during radiosynthesis, adequate shielding is required for the radiochemist and the exposure to radiation must be kept as low as possible by taking all necessary safety precautions. For this reason, as well as keeping the synthesis time low and reproducibility high, automated synthesis platforms are often developed for well-established radiosynthetic procedures; and these are particularly useful when synthesising radiotracers for routine clinical use.

1.3.4 Specific Activity

One of the most important considerations when designing and developing the synthesis of a new radioligand is the specific activity; which is the amount of radioactivity per mole of the 'cold' or non-radiolabelled compound. This value is usually stated in units of GBq or µCi µmol^{-1}, which gives a quantitative value for the ratio of radionuclide to non-labelled material. Each radionuclide has a maximum theoretical specific activity, which is inversely proportional to the physical half-life and mass number of the isotope (*cf.* Table 3).[41]

This maximum theoretical value is almost impossible to achieve, and so the precise specific activity of the particular radiolgiand must be calculated. A high specific activity is often necessary in order to achieve maximum accumulation of the radioligand over the non-labelled compound, especially when the ligand binds irreversibly to the receptor (Figure 8).
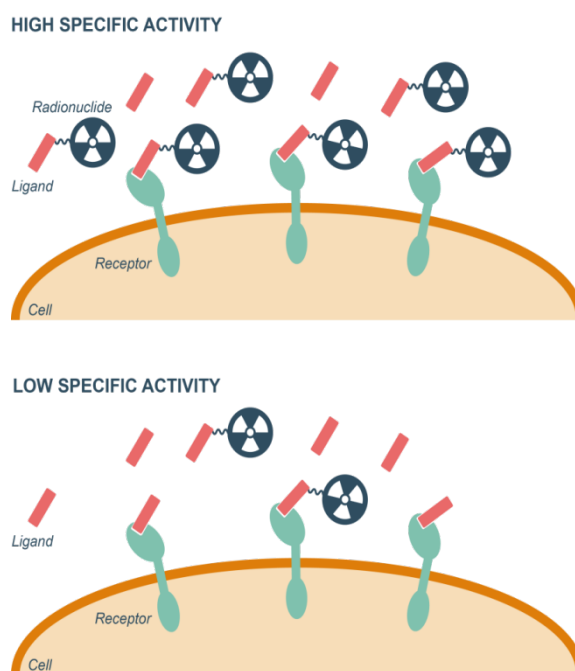
Figure 8. A schematic representation of the difference between a high specific activity (top) low specific activity (bottom) radioligand *in vivo*, using a ligand that binds irreversibly to the receptor

This in turn may alter the required dose of the tracer, and therefore the amount of radiation exposure to the subject. The required specific activity will, however, be dependent on the relative affinity of the radiopharmaceutical for the receptor, balanced by the number of receptors available for binding.

1.3.5 Pharmacokinetics

Even when a radioligand has been designed for a specific biological target, the *in vivo* stability and metabolic fate may be difficult to predict. Due to the fact that only trace amounts are injected, there is not so much interest in the pharmacodynamic fate of the radioligand; it is more important to determine how the distribution of the tracer will alter the outcome of the PET measurement. There are numerous ways to predict the pharmacokinetics profile of a molecule; including measuring its Log$P$, which has a significant effect of the binding of the

ligand to the receptor target, and on the adsorption, distribution, metabolism and excretion (ADME) of the tracer (see chapter 3 for more details). Additionally, the metabolic fate of the tracer may have an effect on the outcome of the PET experiment; one specific example is *in vivo* defluorination, which is a common occurrence with ^{18}F-labelled radiotracers. For example, the defluorination of [18F]arenes and [18F]fluoromethyl groups attached to heteroatoms, leads to the production of 'free' ^{18}F-flouride, which accumulates in bone tissue, and therefore affects any PET measurements in these areas.[44]

1.4   Radiolabelling with [18]F

1.4.1 Properties of ^{18}F as a Radionuclide for PET

Fluorine is the most electronegative element in the periodic table (4 on the Pauling scale), and the element forms extremely strong bonds with carbon (105.4 kcal mol^{-1}).[45] This combination of factors makes fluorine an attractive choice for introduction into biologically active compounds for the development of pharmaceuticals and radioligands.[46] The C-F bond is consequently found in approximately one-fifth of pharmaceuticals and generally displays good metabolic stability; probably a result of the electrostatic attraction between the polarised C and F atoms. In addition to this, fluorine acts as a bioisostere of the hydrogen atom, possessing the smallest atomic radius of the Period 2 elements due to its high nuclear charge (Table 4).[47]

Van der Waals radii (Å)	H (1.2)	C (1.70)	N (1.55)	O (1.52)	F (1.47)
	Si (2.1)	P (1.8)	S (1.8)	Cl (1.74)	
Bond lengths (Å)	C–H (1.09)	C–C (1.54)	C–N (1.47)	C–O (1.43)	C–F (1.35)
	C–Si (1.85)	C–P(1.84)	C–S (1.82)	C–Cl (1.77)	

Table 4. The van der Waals radii and average C–X bond lengths of some common elements, *adapted from O'Hagan 2008*[46]

The C-H bond is often replaced directly by a C-F bond with minimal perturbation of the molecule on steric grounds. However, on electronic grounds, this substitution has a much more significant effect, often altering the pharmacokinetic properties of the molecule.

^{18}F has a number of important characteristics that make it an attractive radionuclide for PET imaging applications. Most importantly, it displays relatively low positron energy (maximum 0.635 MeV), which means it has a relatively short range in tissue, allowing for the production of high resolution images. ^{18}F has a half-life of 109.7 min (97% β+ decay), which is significantly longer than other positron-emitting nuclides such as ^{11}C (20.4 min), ^{13}N (9.9 min) or ^{15}O (2.1 min), increasing the synthetic feasibility of introduction of the isotope. This also allows for potential transportation of the isotope or synthesised tracer from a production site (or site containing a cyclotron) to an off-site facility. However, the costs associated with this are still high for the user, and additional transportation may have certain time-associated problems, especially when carrying out radiosynthesis that has a clinical end-point.

As discussed, the specific activity of a radioligand is very important in order to obtain maximum uptake of the labelled over the non-radioactive or 'cold' compound. When obtained as nucleophilic [^{18}F]fluoride, ^{18}F can display a higher specific activity (maximum = 6.3 x 10^{10} GBq mol^{-1}), compared to other isotopes such as ^{64}Cu, making tracers labelled by ^{18}F potentially more efficient than those incorporating other radionuclides. ^{18}F may also be produced in large quantities by a cyclotron (>10 Ci) and the labelling techniques often allow for PET tracers to be produced in high radiochemical yields. Importantly, due to the relatively low positron energy of this isotope, as well as the high specific activity of these tracers, the radiation dosimetry received by a patient is usually acceptable in order for multiple studies to be carried out.

1.4.2 Obtaining [^{18}F]Fluoride for Probe Synthesis

[^{18}F]Fluoride may be used as a nucleophile for the direct incorporation onto aliphatic and aromatic carbons, provided that a precursor is available for carrying out traditional S$_N$2 and S$_N$Ar reactions. There are numerous methods which have been adopted for the preparation of nucleophilic ^{18}F, and in all cases there is of course a charged counter-ion.[48] The most effective method for the initial production of aqueous [^{18}F]fluoride is by use of a cyclotron, which produces ^{18}O-enriched water (Figure 9).

Figure 9. Example of a PET cyclotron used to produce ^{18}F

The very high yielding nuclear reaction ^{18}O(p,n) forms the [^{18}F]fluoride ion as a solution in the irradiated target water, producing no-carrier-added (NCA) [^{18}F]fluoride.[23] This is a useful attribute of radiotracers, as it improves the specific activity of the final tracer by removal of the non-radioactive species.

Usually, nucleophilic fluoride is used directly for synthesis, as it is the most straight-forward to obtain, and allows access to the most synthetic possibilities, but it is possible to obtain electrophilic fluorine-18 (^{18}F$^+$) (see section 1.6.3). The nucleophilic species may be obtained by a variety of different methods, which should be achievable in time-periods within the half-life of the isotope.[23] The first step always involves the removal of the bulk [^{18}O]water, followed by solubilisation in a suitable organic solvent. The [^{18}O]water is recovered by use of an ion exchange resin, adsorbing the [^{18}F]fluoride ion which can then be eluted into a small volume of aqueous weak base such as potassium carbonate.

The next stage of recovering [18F]fluoride involves the removal of water, which may be achieved by azeotropic evaporation with acetonitrile. The [18F]fluoride ion is solubilised into an organic solvent such as acetonitrile during this process, which can be achieved using a kryptand such as aminopolyether 2.2.2 (K2.2.2) (Figure 10).
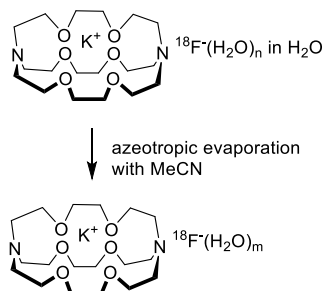
Figure 10. The [18F]fluoride ion – K2.2.2-K+ complex[23]

The kryptand is responsible for capturing the positive counter-ion, separating it from the nucleophilic [18F]- and enhancing its reactivity. A truly 'naked' fluoride ion is thought not to be obtained during this process, as some degree of hydration will still remain when any residual water is present, and so careful consideration must be taken when carrying out a reaction that does not tolerate water.

Purification of [18F]fluoride is often carried out before it can be applied to a chemical reaction, as a number of contaminants may result from the cyclotron sources and may become more concentrated after evaporation of the irradiated water.[23] These impurities may cause problems with probe synthesis if not properly removed. For example, the ion may be converted into [18F]fluorotrimethylsilane, which can be distilled and then converted back to purified [18F]fluoride, which may be particularly useful when carrying out more challenging reactions for probe synthesis.

1.4.3 Electrophilic Fluorinations for the Introduction of ^{18}F

Elemental fluorine, F_2, is one of the most reactive known substances, due to the weak bond formed between two atoms of fluorine, and the contrastingly strong bonds that are formed with other elements, such as carbon, hydrogen and silicon. Electrophilic fluorinations may be

carried out using elemental fluorine, and for radiosynthesis, a number of electrophilic fluorinating reagents now exist.[47] For example, ^{18}F-F$_2$ is a widely-applicable electrophilic fluorinating reagent, in which fluorine is transiently highly polarised with a partial positive charge (Figure 11).
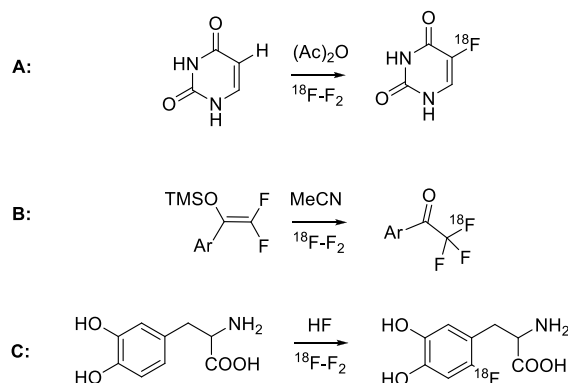
Figure 11 Examples of electrophilic fluorinations using ^{18}F-F$_2$, *adapted from Alauddin 2012[47]*

Using these methods, electron-rich arenes and aliphatic compounds act as nucleophiles and become fluorinated. Electrophilic fluorinations are fairly fast and efficient, making these reactions feasible for obtaining ^{18}F-labelled tracers. However, the products obtained from this type of reaction are often formed with low specific activity due to the necessity that ^{18}F$_2$ is contaminated with non-radioactive F$_2$, and hence is carrier-added.[47]

1.4.4 Nucleophilic [^{18}F]Fluoride for Radiolabelling

A number of methods now exist for carrying out nucleophilic [^{18}F]fluorinations. Aryl C-^{18}F bonds generally have a greater *in vivo* stability than alkyl C-^{18}F bonds, but the chemistry involved in the synthesis of aromatic C-^{18}F bonds is significantly more challenging. Large biomolecules and electron-rich arenes are not readily labelled directly using NCA nucleophilic fluorination due to the low reactivity and high proton affinity of [^{18}F]fluoride. The traditional methods to introduce fluorine atoms onto an aromatic ring usually require harsh conditions such as those involved in direct fluorination, the Balz-Scheimann reaction between anilines and HBF$_4$/NaNO$_2$, nucleophilic substitutions of bromo- or chloro- arenes with KF, and reaction of aryl iodides with CuF$_2$.[49]

Improved methods for introducing ^{18}F onto aromatic rings include the reactions of [^{18}F]fluoride with diaryliodonium salts, triarylsulfonium salts, or diaryl sulfoxides.[50] These methods, have improved the ability to incorporate [^{18}F]fluoride onto electron-rich arenes, and the nuclide may be introduced onto the *meta-* as well as *ortho-* and *para-* positions relative to existing substituents (Figure 12).

$$Ar\bar{}\text{—}I^{+}\text{—}Ar' \xrightarrow{\ ^{18}F^{-}\ } Ar\text{-}^{18}F \quad \text{and/or} \quad Ar'\text{-}^{18}F$$

$$\underset{R^{-}}{|}$$

R = OTs, OTf, halogen *etc.*
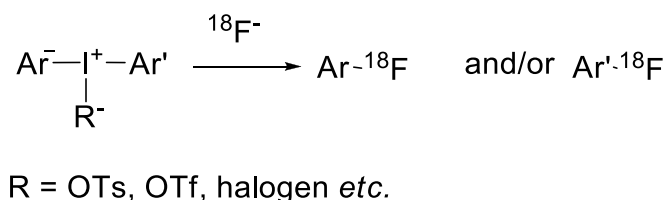
Figure 12. The use of diaryliodonium salts for nucleophilic ^{18}F-fluorination, *adapted from Chun and Pike 2013*[50]

This method is still utilised mainly for the synthesis of small molecule, or low molecular weight radiotracers (< 500 Da), and so alternative methods are still required for the introduction of ^{18}F into more complex, higher molecular weight structures. This may require the use of prosthetic groups, which are readily prepared reactive species' containing ^{18}F, and can be used to introduce the radioisotope into the target compound.[49] A number of methods may be used for the synthesis of such prosthetic groups, which can be used to label both small molecules and macromolecules, and may be either aliphatic or aromatic.[51, 52] Examples of these groups, also known as labelling synthons, include ^{18}F-labelled haloketones, esters, benzyl halides, and benzaldehydes. These have been used for labelling PET radiotracers of more complex molecules, such as amino acid receptor ligands, peptides and proteins.[50]

Peptides are particularly useful targets for cancer detection, as highly specific tissue uptake may be achieved. A radiolabelled small molecule prosthetic group, once synthesised, may be attached to the peptide without significant alteration of its biological function, which is usually achieved using simple reactions with fast reaction kinetics.[53] Chemoselective reactions which proceed under mild conditions have been increasingly utilised for introduction of suitable NCA ^{18}F-labelled prosthetic groups.

One type of reaction in particular has been used for the synthesis of [18F]fluoropeptides, known as 'click' chemistry.[54] The term 'click' chemistry usually refers to the highly regioselective copper(I) catalysed reaction between azides and terminal acetylenes to form 1,4-disubstituted 1,2,3-triazoles, also known as the copper-catalysed azide/alkyne cycloaddition (CuAAC) reaction.[55] Reactions between azides and alkynes originally involved the use of elevated temperatures to increase the rate of this reaction and typically resulted in an ~1:1 mixture of the 1,4- and the 1,5-disubstituted triazoles.[56] The formation of catalytic copper(I) *in situ* from copper(II) salts using sodium L-ascorbate allows for the regiospecific preparation of a large spectrum of 1,4-triazole products in high yield (Figure 13).[57-59]

a) RN_3 + ≡—R^1 $\xrightarrow{\triangle}$ (triazole products)

b) RN_3 + ≡—R^1 $\xrightarrow[\substack{H_2O/^tBuOH\ (1:1) \\ r.t.\ 12\text{-}24\ h}]{\substack{1mol\%\ CuSO_4 \\ 0.1\ eq.\ sodium\ ascorbate}}$ (triazole product)
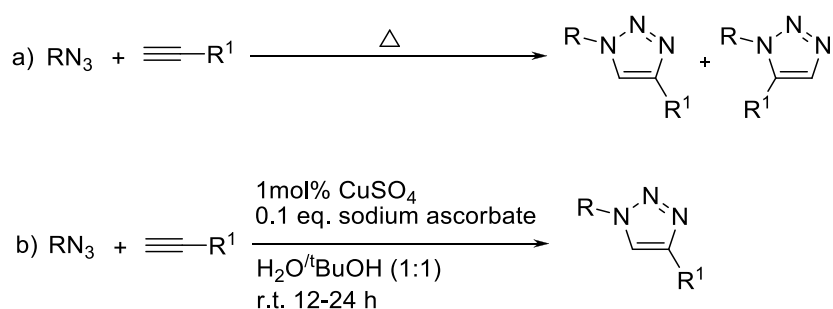
Figure 13. a) Huisgens 1,3-dipolar cycloaddition between azides and alkynes, b) The modified version using copper(I) catalysis, known as the CuAAC reaction

The product triazoles have desirable physiological properties, being topologically and electronically similar to naturally occurring secondary amide functional groups.[29] The former are more stable to hydrolysis and contain very rigid linking units, placing the carbon atoms within the triazole ring at distances of 5.0 Å to one another, compared to 3.8 Å in the C-α amide bond. Unlike benzene derivatives and related aromatic heterocycles, the triazole group is very difficult to oxidise or reduce, and has a large dipole moment of 5 debye, which allows it to form stable hydrogen bonds.[60]

For example, the synthesis of peptidic radioligands using the CuAAC reaction was demonstrated using a series of [Tyr]^{3}octreotate (TOCA) analogues, which are used to target somatostatin receptors, and have been labelled in one step from readily-synthesised [18F]2-fluoroethyl azide ([18F]FEA) (Figure 14).[54, 61, 62]
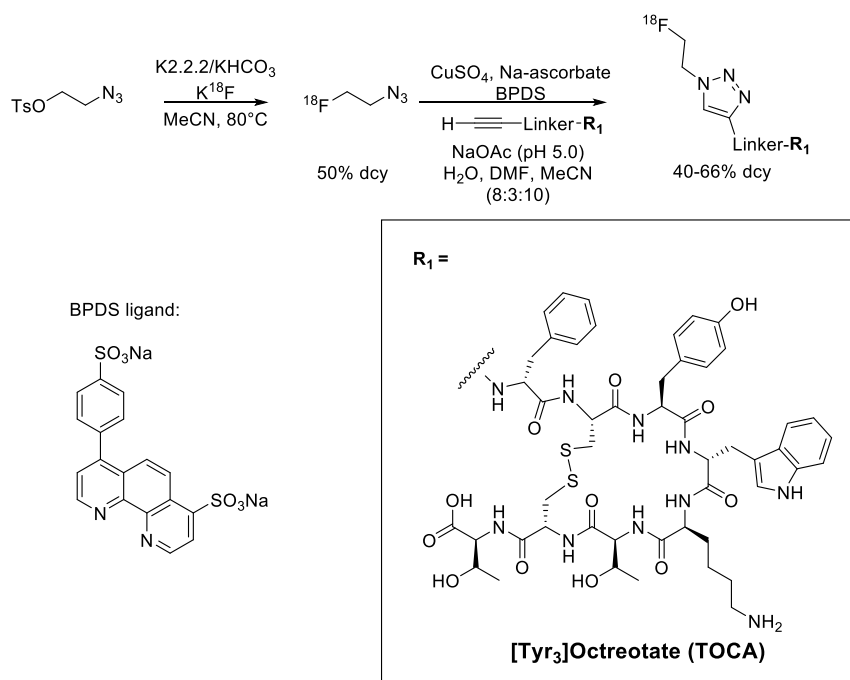
Figure 14. Aboagye's use of 'click' chemistry for radiolabelling TOCA peptides using [^{18}F]FEA as a prosthetic group[61]

By incorporating an alkyne moiety onto the peptide, radiolabelling was achieved by reaction with the ^{18}F-labelled azide using a copper(I) catalyst. This method allowed for the synthesis of a library of ^{18}F-labelled octreotate analogues in good radiochemical yields. The stability of the triazole group had little impact on the biological efficacy of the peptides, as compared to analogues that had been labelled by alternative methods.[61]

Click chemistry has been highly utilised for radiolabelling peptides using prosthetic groups, due to the accessibility of ^{18}F-labelled azides, as well as the high radiochemical yields that may be obtained; a combination of properties that is ideal when working with short-lived isotopes.[53, 63, 64] This method is useful for labelling small molecules and peptides using isotopes such as ^{18}F, but is less efficient for labelling larger biomolecules such as antibodies due to the requirement for the use of higher concentrations, and hence toxic dose levels, of copper(I) catalyst. A number of alternative methods for ^{18}F-labelling are being developed, relying on either the synthesis of prosthetic groups as mentioned, or by direct labelling methods, and these often rely upon the use of metal catalysts.

1.4.5 Existing [18]F Radiotracers in Oncology

The most significant example of the use of ^{18}F in oncology is [^{18}F]2-fluoro-2-deoxy-D-glucose (FDG), which was originally designed to study glucose metabolism.[23] [^{18}F]FDG was developed in 1977 by Ido and coworkers, and it was considered to be the first major breakthrough in terms of radiopharmaceutical development.[65] The discovery that an increase in glucose uptake in tumour cells as compared to normal cells meant that [^{18}F]FDG became a very useful radiotracer for imaging cancer. Phosphorylated [^{18}F]FDG accumulates in cells where glycolysis and glucose transport is enhanced, making the radiotracer more highly concentrated in these areas.[66], [67] The synthesis of [^{18}F]FDG was improved in 1986, which led to the increased use of this tracer for clinical applications (Figure 15).

[18]FDG
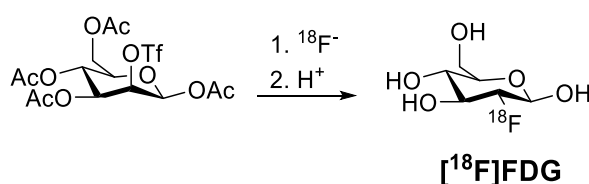
Figure 15. Stocklin's formation of 2-[^{18}F] fluoro-2-deoxy-D-glucose ([^{18}F]FDG) from 2-deoxyglucose.[68]

The compound is most commonly synthesised *via* a straight-forward nucleophilic substitution of a triflate by cyclotron-produced [^{18}F]fluoride, and may now be produced on automated synthesis platforms, allowing for large-scale synthesis of the tracer. The tracer may, however, be synthesised *via* both nucleophilic and electrophilic fluorination methods.[47] The development of [^{18}F]FDG led to a gradual increase in developing the technology associated with PET, especially towards a clinical end-point. However, although this major breakthrough in PET radiopharmaceuticals dates back to the 1980s, this is still the most significant advancement in PET radiotracers to date, and [^{18}F]FDG remains the most important compound for carrying out PET measurements for oncology.

There are now, however, a number of ^{18}F-labelled radiopharmaceuticals that have been developed for PET imaging in oncology, and which are in clinical use (Figure 16).
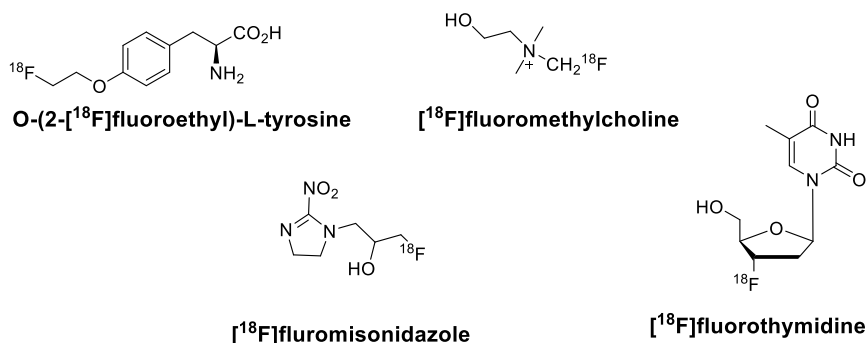
Figure 16. Some of the key clinically used [^{18}F]-labelled tracers for oncology

Cancer cells also demonstrate an increase in uptake of particular amino acids such as [^{18}F]fluoroethyltyrosine ([^{18}F]FET), which has particular use in imaging brain tumours.[69] Other examples of ^{18}F-labelled tracers include analogues of choline (for example [^{18}F]fluoromethylcholine) which are involved in the synthetic pathway for forming cell membranes, and are particularly useful for prostate cancer detection.[70] [^{18}F]Fluorothymidine ([^{18}F]FLT) is another important tracer, which is used to determine response to therapy, and is designed to target the up-regulated cell proliferation observed in cancerous cells.[71] Resistance to radiotherapy is another key area which may be evaluated using PET, an example being the imaging of hypoxia in tumours. For example [^{18}F]fluromisonidazole was designed as a biomarker for hypoxia in order to identify when radiotherapy treatments are likely to be most effective.[72] [41]

Increasing interest has been placed recently upon designing alternative compounds for better tumour characterisation, which have higher tumour specificity and should aid better patient management through improved diagnosis of disease and in evaluating response to treatment. A greater range of more accurate probes would also be of benefit in clinical trials to evaluate the efficacy of New Chemical Entities (NCEs).[12]

1.5   Radiolabelling with Gallium-68

^{68}Ga, although having a shorter half-life (67.71 min) than ^{18}F, and emitting a higher energy positron ($E^{+}_{\beta max}$ = 1899 keV), (decaying to 89% *via* positron emission, and to 11% by electron capture) has some attractive properties for the synthesis of radiolabelled probes for

PET imaging.[73] This is largely due to the relatively low production costs of the isotope, which relies on a generator containing the parent radionuclide ^{68}Ge, as well as the relatively simple and short radiolabelling methods that are used for metal isotopes, utilising chelating ligands attached to a targeting molecule. The half-life of ^{68}Ga, although lower than that of ^{18}F, is also compatible with the pharmacokinetics of most radionuclides of relatively low molecular weight, such as antibody fragments, peptides, aptamers and oligonucleotides.

1.5.1 ^{68}Ga Generation

^{68}Ga is produced by electron capture from its parent nuclide ^{68}Ge ($t_{1/2}$ = 270.95 days), and must be separated from ^{68}Ge into its ionic form in order to be useful for chelation chemistry. This separation is achieved by use of a chromatographic methods; the ^{68}Ge is adsorbed onto the stationary phase, which is usually alumina, TiO_2, or SnO_2, whereas the mobile phase is a solvent which is able to elute the ^{68}Ga (usually 1 M or 0.1 M HCl).

The production of ^{68}Ga is achieved using relatively low-cost generators, which allow for clinical studies to be carried out without requiring the use of an on-site cyclotron, and may provide the radionuclide for synthesis of radioactive probes at any time, and on demand. Automated synthesis platforms now exist, for example Eckert & Ziegler (E&Z) Modular Lab system,[74] that allow for both the generation and synthesis of ^{68}Ga labelled compounds to be controlled by a computer platform (Figure 17).
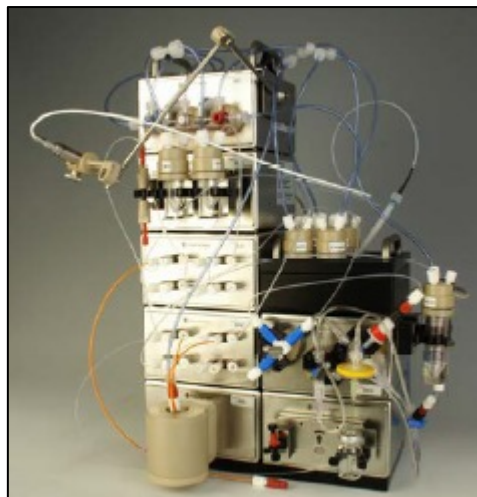
Figure 17. A Modular Lab system (by E&Z) for the elution, purification and synthesis of ^{68}Ga radiotracers[74]

These automated platforms are very robust, and when properly utilised may allow for ^{68}Ga radiotracer production, from elution to purification of the product, without the need for carrying out hands-on radiochemistry. This is particularly advantageous from a safety perspective, as it significantly lowers the dose of radiation to the radiochemist, as well as lowering the overall time of the synthesis.

1.5.2 Use of ^{68}Ga for Radiolabelling

Methods for the incorporation of metal isotopes for radiolabelling are often more efficient than those for non-metal isotopes, and usually involve the use of suitable chelating ligands. In addition to this, solid-phase purification methods may often be used, minimising the problems associated with isotope decay during synthesis.[75]

Ga(III) is the only stable and relevant oxidation state of gallium in aqueous solution, and the free hydrated Ga^{3+} ion is only stable under acidic conditions. If the concentration of the Ga^{3+} exceeds nanomolar level within pH ranges 3-7, then it can become the insoluble $Ga(OH)_3$ form; however, at physiological pH, the much more soluble $[Ga(OH)_4]$ form dominates.[76, 77] Ga^{3+} may be incorporated into a radiotracer *via* use of a suitable chelating ligand, and a number of these ligands now exist, several of which have become popular, and form the basis of robust methods for introduction of this radionuclide into the target compound.

1.5.3 ^{68}Ga Coordination Chemistry

Ga^{3+} has similar coordination chemistry to Fe^{3+}; both species have a similar ionic radius and have a dominant coordination number of six (Ga^{3+} can also, however, display a coordination number of four or five). Ga^{3+} is a hard Lewis acid, and consequently it will form thermodynamically stable complexes with ligands that exhibit hard Lewis base properties. The types of ligand fulfilling these criteria typically contain a combination of oxygen and nitrogen donor atoms. Examples of the kind of functional groups that may be appropriate for coordination to Ga^{3+} include carboxylates, phosphonates, hydroxamates, and amines, as well as softer functional groups such as phenolates and thiols.

1.5.4 Development of Chelators for ^{68}Ga Labelling

Suitable chelators for Ga^{3+} must be stable to hydrolysis, and must also be kinetically inert within the period of clinical use, in order to avoid any ligand exchange with the protein transferrin. This protein is found in blood serum and any ion exchange with this protein would lead to liver and lung accumulation of the metal.

The majority of chelators for incorporation of $^{68}Ga^{3+}$ are hexadentate, due to the preferred coordination number of six of the Ga^{3+} ion.[78] Usually, the chelate also contains a functional group which allows it to be incorporated into the targeting moiety (e.g. peptide), and in this situation is referred to as a bifunctional chelator. As discussed, the chelate formed must be kinetically stable within the pH range 4-8, and in the presence of other metal cations such as Ca^{2+}, Zn^{2+} and Mg^{2+}. The method for introduction of the radiometal (i.e. ^{68}Ga) must additionally be rapid and high yielding, due to the relatively short half-life of the isotope. Other considerations when choosing an appropriate chelating group include the compatibility with peptide synthesis (e.g. ability to incorporate protecting groups) and solvent solubility, and each of these will be specific to the particular situation and the chemistry required in order to introduce the chelating group.[79]

An octreotate analogue of desferrioxamine-B (DFO) was one of the first molecules to be labelled with ^{68}Ga, and this was achieved in high radiochemical yield (Figure 18).
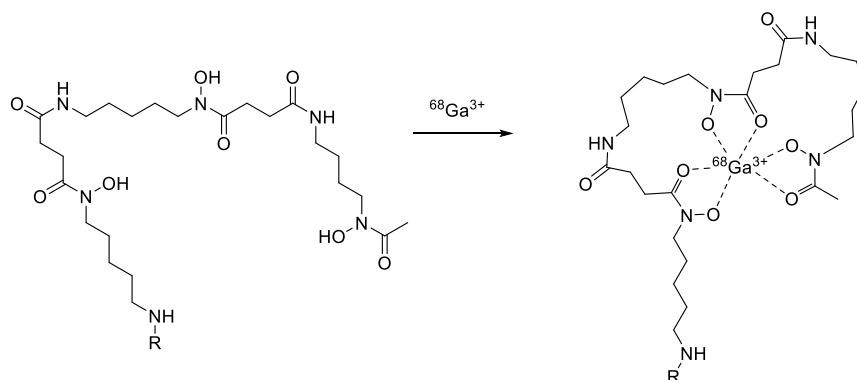
Figure 18. Van Dongen's use of Desferrioxamine-B (DFO) as a ^{68}Ga chelator[80]

The three hydroxamate groups in DFO are available for rapid and high affinity metal coordination to Ga^{3+} ions, and the molecule serves as a bifunctional chelator through its available amine group. However, the main limitation of this first-generation chelator is the fact that high concentrations (>5 µM) are required in order to achieve acceptable radiochemical yields. It was found, through use of assays into the stability of a series of mercapto amino ligands, that sufficiently stable complexes may be formed with tetra- and pentadentade ligands, but hexadentate ligands demonstrate far superior properties in terms of bifunctional chelation through covalent linkage to biomolecules.[79]

The tetraaza tetraacetic acid chelator DOTA is one of the most common chelators for radiometals possessing the +3 oxidation state, including many examples of ^{68}Ga incorporation (Figure 19).[81-84]

DOTA

TACN-TN $R = CH_2CH_2SH$
NOTA $R = CH_2COOH$
NOTP $R = CH_2PO_4H_2$
NOTPME $R = CH_2PO_2H(OC_2H_5)$
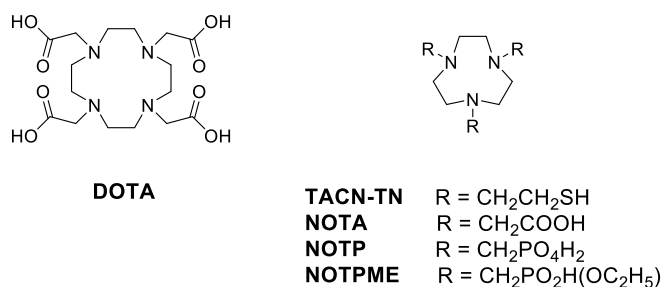
Figure 19. Structures of DOTA and NOTA chelates for ^{68}Ga-labelling

Ga(DOTA)[-] has now been extensively studied as a potential prosthetic group for radiolabelling targeting groups, and demonstrates sufficient stability for use in a clinical setting.[85] It is possible to introduce DOTA to peptides efficiently using the tri-*tert*-butyl protected synthon DOTA(*t*-Bu)$_3$, which has one available acid functional group for reaction with an N-terminus. Deprotection under acidic conditions will afford the DOTA-functionalised peptide, which will now be available for chelation to the [68]Ga^{3+} ion.[86]

Crystal structures of the model peptide Ga^{3+}-DOTA-D-PheNH$_2$ have indicated that the chelated DOTA adopts a *cis*-pseudooctahedral geometry, whereby the macrocycle is in a folded conformation. The two transannular nitrogens and two of the oxygens from the carboxylate groups occupy the equatorial plane, whereas the axial positions are formed by the remaining two cyclen nitrogens (Figure 20).[79]
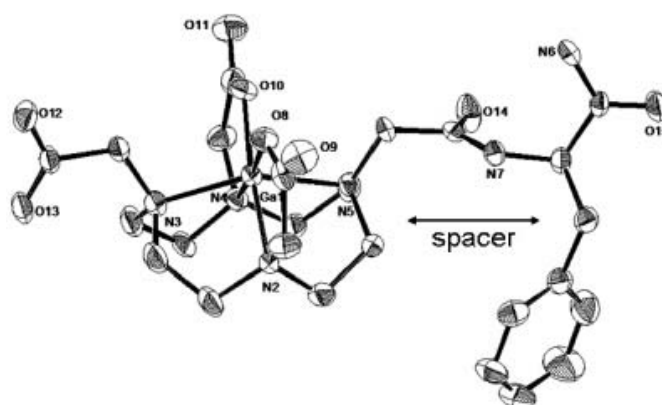
Figure 20. Molecular structure (ORTEP plot) of 6-coordinate [GaIII-DOTA-D-PheNH2] as suggested by the single crystal X-ray structure, adapted from Hennig *2009*.[87]

More recently, it was found that triaza triacetic acid chelators (e.g. NOTA) have a greater thermodynamic stability constant with [68]Ga^{3+} (logK = 30.98)[88] than the tetraaza tetraacetic

acid chelators (e.g. DOTA) (logK = 21.33)[89], due to the fact that this ligand has a smaller cavity in which the Ga^{3+} ion can sit. These macrocycles demonstrate high conformational and size selectivity towards Ga^{3+} ions, and for this reason they can encapsulate the metal ions with high efficiency. Examples of some of the most common hexadentate triaza chelators for ^{68}Ga include TACN-TM, a ligand with three mercaptoethanol arms[90]; NOTA, a tricarboxylic acid ligand[89, 91, 92]; as well as phosphonate-bearing ligands such as NOTP and NOTPME.[93, 94] Due to the particularly high affinity of this family of chelators towards $^{68}Ga^{3+}$, radiolabelling is usually achieved at lower temperatures than with DOTA compounds, and a smaller amount of precursor is required, resulting in a higher specific activity (*cf.* Figure 19).[95]

1.5.5 Existing ^{68}Ga Radioligands in Oncology

A number of radioligands using gallium-68 as the isotope now exist, and some are now routinely used in a clinical setting. [^{68}Ga-DOTA, Tyr^3] octreotide ([^{68}Ga]DOTA-TOC) is probably the most important of these (Figure 21).[79, 96]
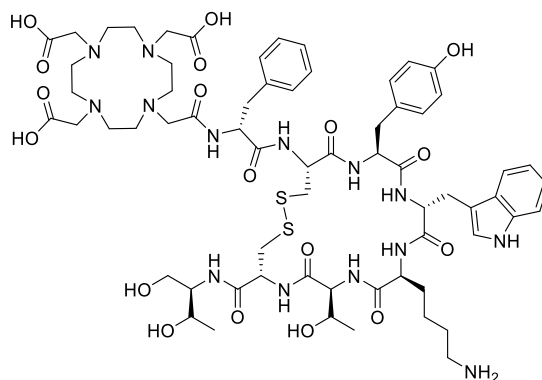
Figure 21. Structure of DOTA-TOC

[^{68}Ga]DOTA-TOC was developed in order to target somatostatin receptor subtype-2, and this compound was found to exhibit promising *in vitro* and *in vivo* properties. It has been tested in a clinical setting, where it exhibits higher tumour specificity than the analogous [^{111}In]DTPA-octreotide (Figure 22).[96]

In-111 Octreotide   Ga-68 DOTATOC
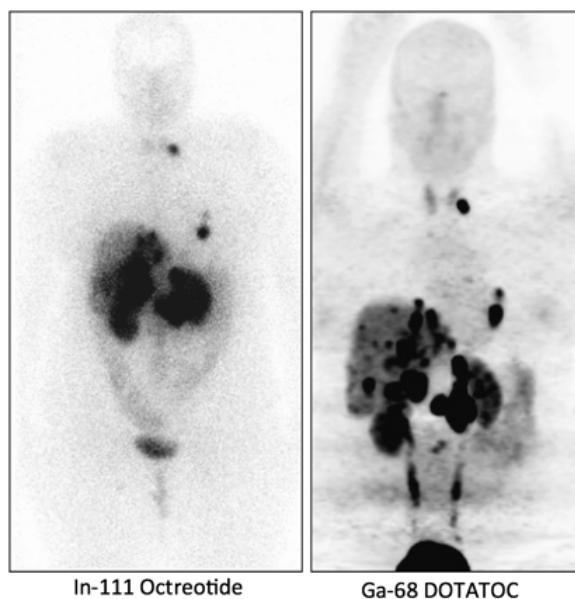
Figure 22. Comparative images of the same tumour patient obtained using [^{111}In]DTPA-octreotide and [^{68}Ga]DOTA-TOC, respectively. Taken of the same patient, with a metastatic gastrinoma, *adapted from Graham and Menda 2011[97]*

Other similar structures were developed as tracers for different subtypes of somatostatin receptors: [^{68}Ga-DOTA, 1-Nal[3]] octreotide (DOTA-NOC), [^{68}Ga-DOTA, Tyr[3]Thr[8]] octreotide (DOTA-TATE) and [^{68}Ga-DOTA-2-Nal, Tyr[3], ThrNH82] octreotide (DOTA-lanreotide). Other gallium-68 labelled radiopharmaceuticals also exist, including [^{68}Ga]-DOTA-bombesin, which binds to three bombesin receptor subtypes, and has been studied for imaging gastrointestinal, colon and prostate tumours.

1.5.6 Limitations and Advantages

^{68}Ga emits a higher energy positron (1.899 keV), than ^{18}F, and subsequently this leads to a lower image resolution. As discussed, however, gallium-68 is produced by a relatively low-cost generator, making the isotope more accessible to the user than other isotopes. In addition to this, the use of chelators such as DOTA and NOTA are highly robust, and result in very reproducible and high radiochemical conversions. The combination of these factors often results in short synthetic strategies, which may now be fully automated, and produce the ^{68}Ga radioligand in high radiochemical yields, and with reasonable to good specific activity.

1.6   Pretargeting as a Molecular Imaging Tool

Pretargeting is a two-step targeting approach, by which the delivery of a radionuclide is separated from that of a functional biomolecule. This may involve the biomolecule being modified with a group which has high affinity for the radiolabelled compound, or more specifically, it may contain a moiety which is highly reactive under physiological conditions towards a functional group on the radiolabelled partner.[98]

Pretargeting is particularly advantageous when monoclonal antibodies are used as the tumour-targeting species. These have a high specificity for tumours, and may be considered very useful PET imaging agents for this reason. However, they also have the disadvantage of displaying slow tumour accumulation and retention, as well as long blood clearance time, especially when compared to small targeting molecules. Pretargeting may therefore be used as a tool to allow the non-radiolabelled antibody to achieve maximum tumour uptake and sufficient blood clearance, before administration of a radiolabelled probe, which has affinity for the targeted antibody. The small and fast clearing molecule, will bind rapidly to the accumulated antibody, while any unbound radiolabel will be quickly cleared from the subject (Figure 23).
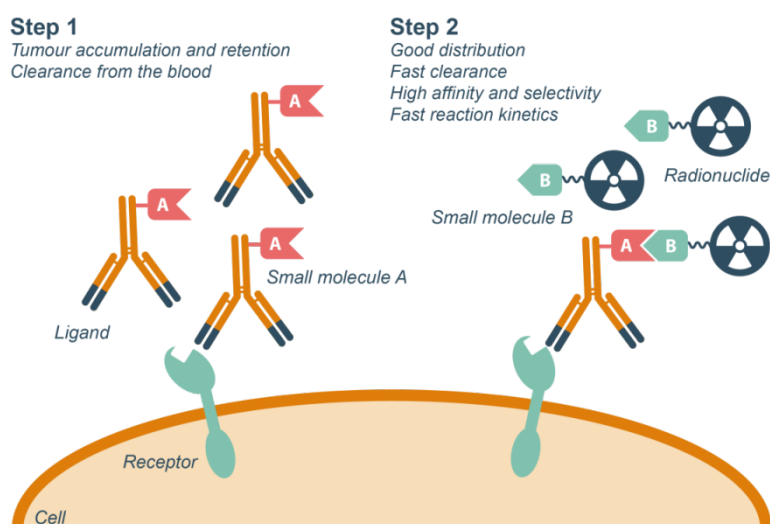
Figure 23. A schematic representation of the principle of pretargeting using monoclonal antibodies for molecular imaging

This method leads to a desirable combination between the high tumour affinities of monoclonal antibodies, with the fast distributing and clearing properties of small molecule probes. More specifically, this method has the advantage of demonstrating greater tumour-to-background activity than with direct targeting approaches.

1.6.1 Existing Methods for Pretargeting

Pretargeting was first demonstrated in 1985 by Frincke and co-workers, during research into the development of radiochemistry chelates. This concept was based upon the principle that chelated radiometals clear much more quickly from the body than radiolabelled antibodies, as well as the fact that the radiolabelling methods for small molecule chelates are more efficient than those for large molecules such as antibodies.[99] This consequently led to the development of a new construct, which involved the design of a monoclonal antibody which could bind independently to both the tumour and to the radiolabelled chelate EDTA. Pre-injection of a non-radiolabelled antibody, followed by subsequent administration of the radiolabelled chelate, resulted in specific binding of the radiolabelled small molecule to the pre-localised antibody.

A number of pretargeting approaches have now been demonstrated, and the application of this method to PET imaging has had a significant contribution to this field. In addition, the technique has been found to be a particularly useful strategy in the area of radioimmunotherapy (RIT) for the delivery of bifunctional monoclonal antibodies (Figure 24).
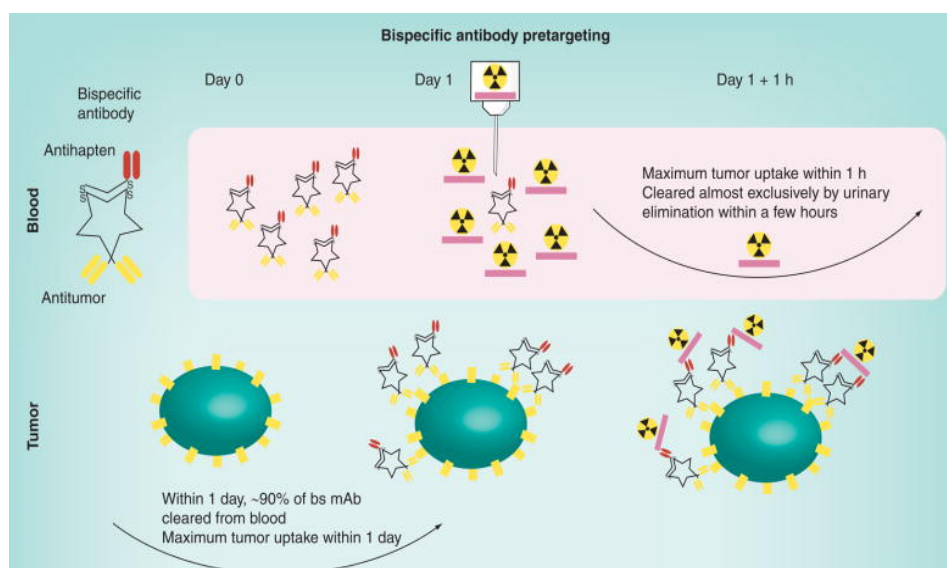
Figure 24. A general schematic of prertargeting for radioimmunotherapy (RIT), adapted from *Sharkey and Goldenberg, 2011*[98]

Pretargeting for RIT has several distinct advantages; it has the potential to increase the achievable dose to tumours, improve tumour tissue: normal tissue dose ratios, and subsequently improve the overall therapeutic index of pretargeted monoclonal antibodies over direct targeting methods.[100]

Two strategies in particular have received a large amount of attention; the first of these involves the use of bispecific antibodies which are capable of binding both a radiolabelled hapten and an antigen, and the second are modified antibodies that contain both oligomeric nucleic acids (acting as targeting vectors) and radioligands. There are, however, significant problems associated with the current methods of pretargeting; the synthesis of bispecific antibodies is often not simply achieved using direct modification of the parent antibody, and is a highly complex and expensive procedure involving molecular engineering (Figure 25).[101]
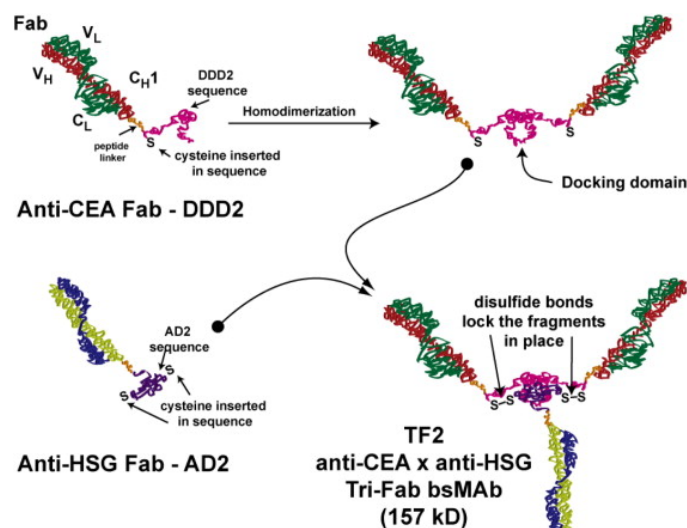
Figure 25. Assembly of bispecific antibodies using 'Dock-and-Lock' modules, demonstrating the complexity and high costs associated with this approach, adapted from *Goldenberg, 2010*[101]

There are also a number of concerns around the use of these olignomeric nucleic acid systems which involves the use of non-natural nucleic acids. They constitute expensive processes, and additionally, these complexes potentially do not demonstrate sufficient *in vivo* stability for use in a wide range of pretargeting applications.

Another specific example is a strategy that is based upon the high binding affinity ($K_D = 10^{15}$ M) of the avidin-biotin complex, which is the strongest known non-covalent interaction (Figure 26).[102]
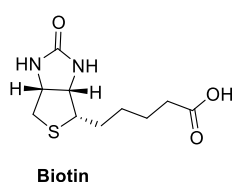
Biotin

Figure 26. Structure of biotin, which binds to the protein avidin with a high binding affinity.

The bond formed is extremely stable to changes in pH, temperature, organic solvents and other denaturing agents, and avidin may bind up to four biotin molecules, making this interaction attractive for pretargeting applications. In one approach, streptavidin (which has a similar structure to avidin) may be first ligated to an antibody, which is intravenously injected. After a time-point of several days, a radiolabelled biotin is injected, which rapidly binds to the streptavidin localised at the tumour. A clearing agent may be used to remove any of the

excess streptavin-antibody conjugate from the blood, prior to injection of the radiolabelled probe. The opposite method may alternatively be used, by which biotin is attached to the targeting molecule (antibody), and streptavidin is used as the labelled tag.[102] The former approach has been applied in a clinical setting using a three-step method involving the sequential introduction of a streptavidin-antibody followed by ^{90}Yttrium-DOTA-biotin. This approach allowed doses of the radiolabelled partner to be five times higher than when the antibody was directly labelled, due to a significantly lower radioactive concentration in the blood, and this significantly increased survival time of the patients (33.5 months *vs.* 8 months for the control group).[100, 103, 104] The main disadvantage of this approach, however, is that any biotin-rich tissue (biotin is a biological molecule) will cause unwanted background and specificity issues, by binding competitively with the streptavidin complex.[102]

A more general problem with using pretargeting is associated with the potential internalisation of antibodies, which will result in difficulties in accessing the modified antibody by the radiolabelled small molecule. For these reasons, methods are being developed in order to overcome these problems, and to allow for a pretargeting system to be established that is more versatile for a wider range of imaging applications, including using short-lived isotopes for PET imaging.

1.7   Development of Bioorthogonal Chemistry

The term 'click' chemistry was defined by Sharpless *et al.* as being a set of reactions that are able to proceed under mild conditions and can be applied to the efficient synthesis of a broad variety of compounds.[105],[29] These reactions are characterised by fast kinetics and high selectivity for covalent linking of molecular compounds and are particularly useful for the production of non-natural heteroatom linkages.[106] 'Click' reactions are modular and wide in scope, give consistently high yields, and form products which are stable under physiological conditions.[105]

Bioorthogonal chemical reactions are closely associated with the characteristics of 'click' chemistry, and are defined as being a set of reactions which may occur under physiological conditions, without interfering with any of the native biological processes to which they may be exposed (Figure 27).[57, 107, 108]
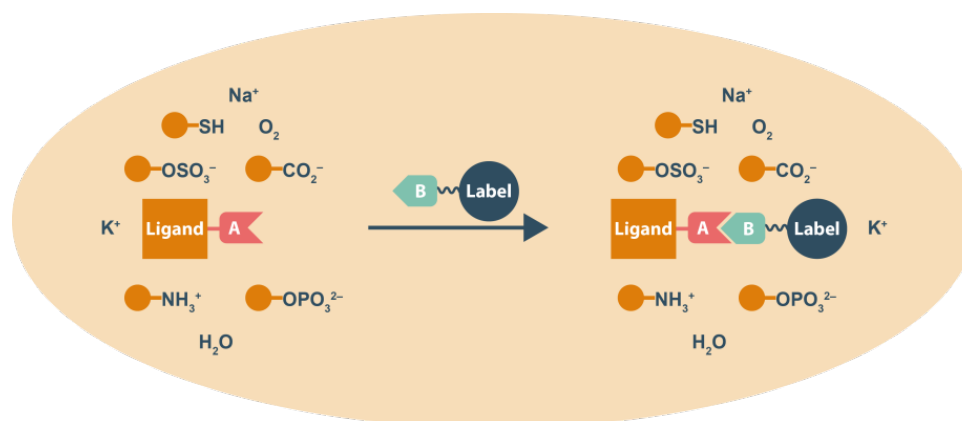
Figure 27. Cartoon of a bioorthogonal chemical reaction[106]

These reactions are also considered to be fast, occurring at low reactant concentrations, without the need for metal catalysts. For these reasons, bioorthogonal chemistry has received increasing interest as a tool for chemical reporter strategies, including pretargeting, and it may be envisioned that the two reactive partners may be separately incorporated into the targeting biomolecule and the radiolabelled probe, respectively, allowing for this fast and highly stable reaction to occur *in vivo*.[106] An advantage over the previously discussed methods for pretargeting is the fact that these reactions form strong covalent bonds, and therefore the introduction of the radiolabelled partner is irreversible.

A number of bioorthogonal chemical reactions now exist, and handles which have been shown to be applicable to modifications within biological settings include aldehydes, azides, nitrones, nitrile oxides, diazo compounds, tetrazines, tetrazoles, quadrocyclanes, alkenes, and iodobenzenes.[109] The two most utilised functional handles for carrying out bioorthogonal ligations are carbonyl groups (which were the first non-natural functional groups to be incorporated for protein modifications) and organic azides (the most commonly used reagents for the modification of biological systems). Some of the most important

bioorthogonal reactions are summarised in the following table. Only the bioorthogonal reactions not requiring metal catalysis or some other form of activation (such as UV-light) are included (Table 5).[109]

Entry	Functional handle	Reaction partner	Product
1			
2			
3			
4			
5			
6[a]			
7[a]			
8[a]			
9[a]			
10[a]			

60

Entry	Functional handle	Reaction partner	Product
11[a]			
12[a]			
13[a]			
14[a]			
15[a]			
16[a]			
17[a]			
18[a]			
19[a]			

[a]More than one regioisomer is obtained, but only one is shown in the table

Table 5. Summary of the reaction partners for bioorthogonal conjugation, which have been used in the modification of biomolecules

Aldehydes and ketones form stable covalent bonds with alkoxyamines in the form of oxime ethers, and this reaction has been applied to chemical reporter strategies, including the labelling of living cells, virus particles, and cell surfaces.[110, 111] Organic azides are particularly inert, making them very popular functional handles, and their small size means

that they only minimally perturb the substrate to which they are introduced.[112] Azides are reactive towards a number of different functional groups (Entries 4-6, Table 5) and the most significant bioorthogonal reactions involving this functional handle are the Staudinger-Bertozzi Ligation and the Strain-promoted Azide/Alkyne cycloaddition (SPAAC).[113, 114] In addition to these two functional handles is the tetrazine (Entries 13-18,Table 5) which is reactive towards a number of unsaturated compounds with a high level of biocompatibility, and with improved reaction rates over the ligations involving azides.[115, 116] These three functional handles, coupled with their appropriate reaction partners, have particularly gained interest for chemical reporter strategies, and will later be discussed in more detail as potential tools for pretargeted PET imaging.

1.7.1 The Staudinger-Bertozzi Ligation

The first bioorthogonal reaction to be reported for use in living systems was the 'traced' Staudinger ligation, a modification of the Staudinger reaction involving an azide and an ester-derived phosphine to form an amide bond [Figure 28, pathway (b)].[107, 108, 117]
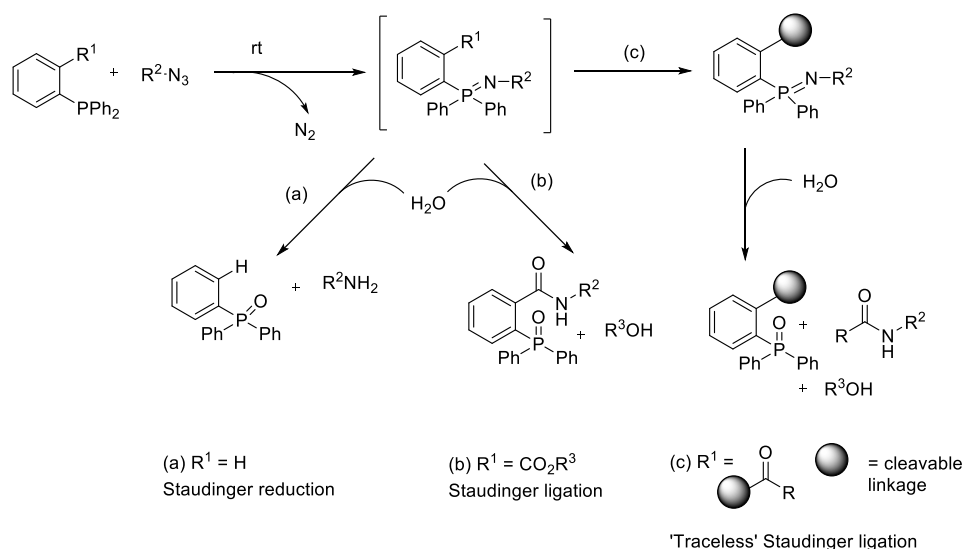
Figure 28. The Staudinger reaction and the Staudinger ligation ('traced' and 'traceless').

This reaction exploits the selective acylation of the α-nitrogen on the intermediate, the product of which is capable of undergoing an intramolecular reaction with a methoxycarbonyl group at the R^1 position, forming an amide-linked phosphine oxide upon hydrolysis.[57] This

pathway was designed to overcome the problems associated with the instability of the azaphosphorane intermediate in water, by trapping this with an ester.

A 'traceless' Staudinger ligation was later developed to minimise interference from the phosphine oxide by incorporating a cleavable linkage between the aryl group and the newly formed amide (R^1).[107] Upon nucleophilic attack from the nitrogen, the phosphine-containing aryl group is liberated, forming an amide as a separate molecule from the phosphine oxide [Figure 28, pathway (c)]. The traceless reaction is highly chemoselective and proceeds at pH 7 with no observable azidephosphorane hydrolysis in aqueous solution. [118], [108] Adding to the reaction's high level of utility is the small size of the azide and the structural resemblance between the product and biological compounds, such as proteins and lipids.[58] The phosphine and the azide are both stable in a biological environment, and they react selectively, with the intramolecular reaction occurring fast enough for it to be carried out in aqueous medium on the surface of cells.[108]

The Staudinger ligation has been utilised in a number of biological applications for these reasons, and importantly shows very low levels of toxicity in mammalian cells.[119] The reaction can be used to covalently attach probes to azide-bearing biomolecules but is not able to detect species in low abundance or processes which are occurring within the body on a fast time-scale; problems which can both be attributed to non-optimised reaction kinetics (second order rate constant with benzyl azide = 2.5 x 10^{-3} $M^{-1}s^{-1}$).[57], [120] For this reason, the Staudinger ligation has not been demonstrated as a potential tool for carrying out *in vivo* pretargeted imaging, and a reaction which with more desirable reaction kinetics at low reaction concentrations is required for this purpose.

1.7.2 The Strain-Promoted Azide/Alkyne Cycloaddion (SPAAC)

The CuAAC reaction, as previously described, allows for high-sensitivity detection of azides, suggesting its potential usefulness *in vivo* for use in a chemical reporter strategy. However, the reaction is only useful in this regard when toxicity is irrelevant; for example in probing

enzyme activity in cell lysates or in visualising biomolecules in stationary cells.[58],[121] Copper is an essential trace element but is toxic at dose levels above about 5 mgL^{-1}, causing nausea, cramps, emesis and diarrhoea in some cases.[122] [123] [124] As well as the apparent toxicological effects associated with copper accumulation in the body, the difficulty in delivery of copper to the tumour hinders the usefulness of this reaction for *in vivo* pretargeting. The copper-free 'click' reaction however makes use of a strained ring system to promote the well-established [3+2] cycloaddition, with little or no observed cytotoxicity.[125] A combination of the biocompatibility observed with the Staudinger ligation and the fast reaction kinetics of 'click' chemistry were demonstrated by Bertozzi's strain-promoted, copper-free azide-alkyne [3+2] cycloaddition (SPAAC) (Figure 29).[58]
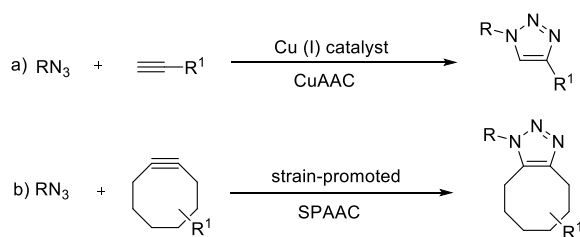
Figure 29. a) Cu(I)-catalysed Huisgen 'click' chemistry. b) Strain-promoted [3+2] cycloaddition between azides and cyclooctynes[126]

The cyclooctyne is the smallest ring size that can accommodate the alkyne functional group and still be isolated as a stable molecule. The strained system has been found to improve the rate of the copper-free reaction by lowering the activation energy, which was achieved by distorting the bond angles of the sp-hybridised carbons by about 17° from the idealised 180° angles of a C-C triple bond, forming comparable angles to those involved in the transition state of the cycloaddition (~160°). Much of the ring strain which is contained in the cyclooctyne skeleton (~18 kcal mol^{-1}) is released upon [3+2] cycloaddition with the azide, making this a favourable process.[127] The relationship between strain energy and reactivity is therefore related to the degree of strain in the alkyne as well as the amount of relief of ring or twist strain upon conversion to the corresponding alkene.

Increased reactivity of the cyclooctyne may be achieved by certain structural modifications. For example, the introduction of electron-withdrawing groups onto one side of the alkyne moiety withdraws electron density away from the triple bond, making reaction with the azide more favourable (Figure 30).[55]

OCT1
$k = 0.0024$ $M^{-1}s^{-1}$
3 Steps
75% yield

MOFO
$k = 0.0043$ $M^{-1}s^{-1}$
6 Steps
11% yield

DIFO2
$k = 0.042$ $M^{-1}s^{-1}$
6 Steps
36% yield

TMDIBO
$k = 0.094$ $M^{-1}s^{-1}$
8 Steps
57% yield

BARAC
$k = 0.96$ $M^{-1}s^{-1}$
8 Steps
18% yield

BCN
$k = 0.14$ $M^{-1}s^{-1}$
4 Steps
46% yield
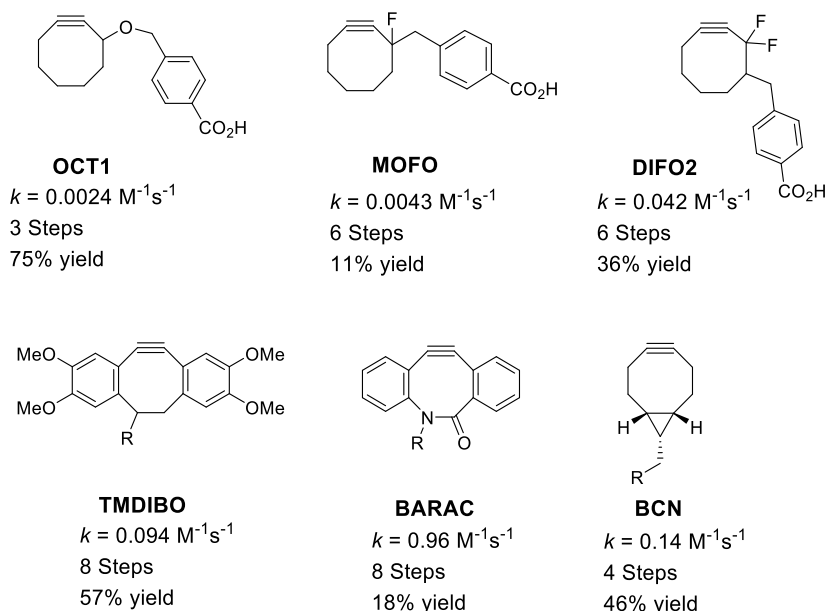
Figure 30. A series of modified cyclooctynes, with the number of synthetic steps, overall chemical yield and 2nd order rate constants for reaction with simple azides[128]

This was demonstrated by Bertozzi and coworkers by introduction of fluorine; the monofluorinated analogue **MOFO** (k = 4.3 x 10^{-3} $M^{-1}s^{-1}$) showed improved kinetics in the strain-promoted cycloaddition with benzyl azide as compared to the equivalent non-fluorinated analogue **OCT1** (k = 2.4 x 10^{-3} $M^{-1}s^{-1}$), and the addition of a second fluorine atom (**DIFO2**) increased the rate by approximately 60 times more (k = 4.2 x 10^{-2} $M^{-1}s^{-1}$) than with **MOFO** (see section 2.2).[106] The rate of reaction with azides can similarly be modulated by inducing greater ring strain in the core cyclooctyne, which could be achieved by conjugation of the alkyne with aromatic groups, such as those in dibenzocyclooctynol (DIBO) reagents such as **TMDIBO** (9.4 x 10^{-2} $M^{-1}s^{-1}$) (see section 2.3).[127] It was found by Bertozzi *et al.*, that addition of a further sp^2-like centre to the already highly strained system in the DIBO template could lead to greater enhancement of 1,3-dipolar cycloaddition reaction kinetics, for example by incorporation of an amide group within the cyclooctyne ring in

biarylazacyclooctynes such as **BARAC** (0.96 $M^{-1}s^{-1}$).[129, 130] More recently, bicyclo[6.1.0]nonyns (**BCN**) have been developed, which introduce increased ring strain over earlier analogues, and can be synthesised in 61% overall yield (in the case of the *endo*-isomer). The increased strain over first-generation reagents such as **OCT1** and **DIFO2** gave rise to improved second-order rate constants for cycloaddition reactions with azides, which were comparable to those demonstrated by **TMDIBO** (k = 0.14 $M^{-1}s^{-1}$).[131]

Although a number of cyclooctynes have now been developed, and their reaction kinetics with azides demonstrated as being superior to the first-generation reagents, the chemical synthesis of cyclooctynes remains one of the most challenging aspects of the SPAAC reaction, and some of the later generation cyclooctynes may take up to 8 steps to synthesise (see chapter 2). In general, more steps are required in order to prepare the cyclooctynes with the highest rate constants, and the time required to access most is still greater than that for the corresponding Staudinger ligation substrates. However, optimisation of the synthetic procedures is possible, and groups are working on ways to improve the synthetic accessibility of these compounds.[128]

The application of the SPAAC reaction towards pretargeting was first successfully validated by Bertozzi and co-workers, who established that this reaction could occur on the surface of living cells.[58] In this first breakthrough in pretargeting using bioorthogonal chemistry, **DIFO** was modified with fluorescent tags, which were subsequently reacted with azide modified glycans on Jurkat cells. This early demonstration of the SPAAC reaction *in vitro* has since been demonstrated in different settings; for example, the reaction was achieved on zebrafish embryos, where the pretargeted area was successfully visualised after incubation with the fluorescently-labelled cyclooctyne (Figure 31).[132-134]
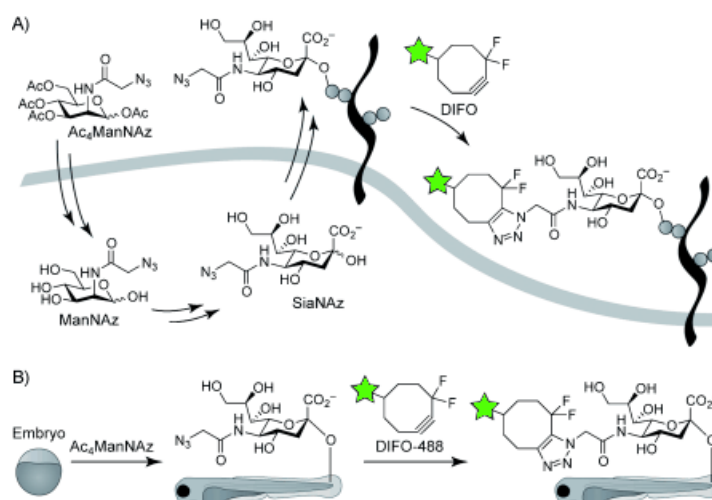
Figure 31. Bertozzi's demonstration of pretargeting using fluorescence on living cells[132]

Although this was a major advancement in the field of pretargeting, the method was only demonstrated using fluorescence, which is not useful for a clinical application as it involves imaging of the subject *ex vivo* (and therefore is an invasive technique). Another major drawback of this reaction as a potential pretargeting tool is the apparent binding of cyclooctynes to albumin in red blood cells and plasma proteins, as well as their generally poor pharmacokinetic profile (see chapter 2). This is due to the generally lipophilic nature of the cyclooctyne structure, which renders the compounds poorly soluble in aqueous media, and ultimately leads to poor *in vivo* biodistribution due to a large amount of uptake in all tissue types.

Perhaps the most significant flaw to this method, however, is the less than ideal reaction kinetics that may be obtained, which, although substantially improved over the Staudinger ligation, are still inferior to the CuAAC reaction (k = 1-10 $M^{-1}s^{-1}$).[135] This combination of factors means that this reaction has yet to be demonstrated as a tool for pretargeted imaging using short-lived isotopes *in vivo*. The reaction is arguably too slow to be carried out in this setting, as discussed in Chapter 3.

1.7.3 An Inverse Electron Demand Diels-Alder (IeDDA) Reaction

A more recent advancement in the field of bioorthogonal chemistry is the use of the Inverse-electron-Demand Diels-Alder (IeDDA) reaction between tetrazines and strained alkenes,

which was initially recognised as being bioorthogonal by Fox and co-workers in 2008.[116] This reaction was first demonstrated as early as 1959, where the reaction between a fluorinated tetrazine and polystyrene was observed to occur rapidly at room temperature (Figure 32).[136]
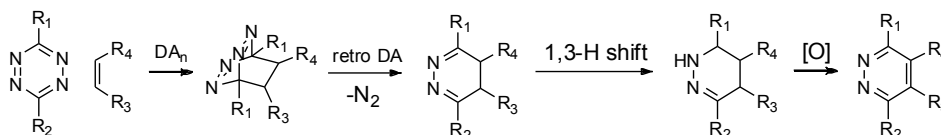
Figure 32. The IeDDA reaction between a tetrazine and an alkene

In a similar manner to the reaction of cyclooctynes with azides, norbornenes and (*E*)-(or *trans-)*cyclooctenes (TCOs) were shown to be the most reactive partners in this cycloaddition, due to the large amount of relief of ring strain upon reaction with the tetrazine (second-order rate constants of up to $k = 6000$ $M^{-1}s^{-1}$).[116, 137] The reaction was shown to occur rapidly in aqueous media, suggesting a high level of biocompatibility. Moreover, this reaction demonstrated some significant improvements over the SPAAC reaction in relation to its use for pretargeting (see chapter 5).[115, 138-143] The reaction kinetics are up to 5 orders of magnitude higher than those demonstrated by the SPAAC reaction, and up to 7 orders of magnitude higher than the Staudinger Ligation, making this ligation far more comparable to the rates displayed by biochemical processes.

In addition to the greatly enhanced reaction kinetics over earlier reported bioorthogonal reactions, as well as the improved pharmacokinetic profile, is the reduced number of steps required in order to synthesise the reaction partners, as compared to the cyclooctyne substrates (See Chapter 4).[144, 145] The reaction was initially demonstrated in a pretargeting setting using fluorescence on living cells, whereby the tetrazine partner was ligated to a fluorophore, and was subsequently reacted with an antibody modified with a norbornene moiety (Figure 33).[115]
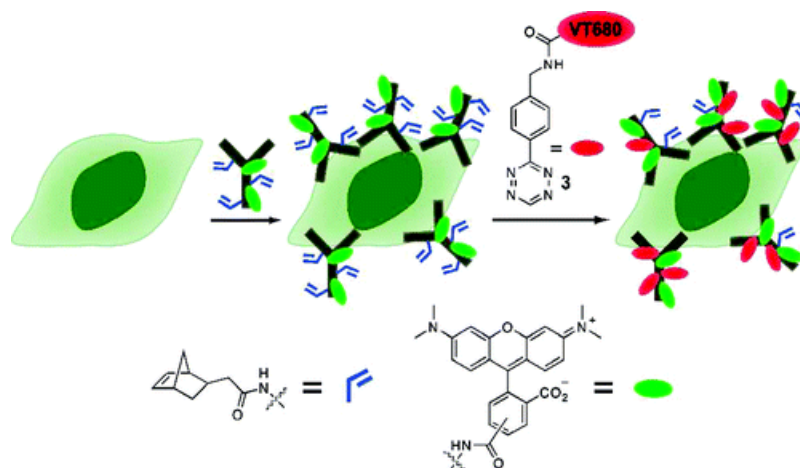
Figure 33. Hilderbrand's use of the IeDDA reaction for fluorescence imaging on live cells[115]

The kinetics of the reaction may be improved using the more reactive TCO reaction partner, which has been ligated to the anti-EGFR (a receptor over-expressed in cancer cells) monoclonal antibody Cetuximab.[140] The results of these *in vitro* experiments showed that the tetrazine is highly selective for cells expressing the ligated antibodies, suggesting that the reaction is occurring on the surface of the cells.

For these reasons, this reaction is currently receiving significant attention in the field of pretargeting for PET, and it is thought that it may display kinetics which are sufficient in order for the reaction to occur using short-lived isotopes in the time-scale of a PET experiment (see Chapter 5).[138, 143, 146, 147]

1.8   Aims and Hypothesis

For the reasons discussed, bioorthogonal chemistry has become a very useful method for developing radiolabelling methods towards the synthesis of tracers for PET imaging. The aim of this project was to validate bioorthogonal chemistry as a potential tool for pretargeting, and ultimately for PET imaging.

The two main reactions that were considered as prospectively demonstrating the ideal properties required for this application were the strain-promoted azide-alkyne cycloaddition (SPAAC) between cyclooctynes and azides, and the Inverse-electron-Demand Diels-Alder (IeDDA) reaction between tetrazines and strained alkenes.

This would first involve the design and synthesise a library of cyclooctynes, as well as radiolabelled azides (using both ^{18}F and ^{68}Ga), as precursors for application to the SPAAC reaction. The relative reactivity of the cyclooctynes with different azides will be demonstrated, highlighting the relevance of the use of different solvents and temperatures in applying this reaction to a pretargeting strategy (Figure 34).
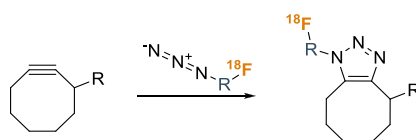
Figure 34. A general scheme for labelling cyclooctynes with ^{18}F-labelled azide prosthetic groups

Once a full range of these precursors have been developed and optimised through kinetic studies of the SPAAC reaction, the cyclooctynes may be ligated to a chosen biomolecule and reacted with radiolabelled azides, with the intention that this reaction could ultimately be utilised for pretargeted *in vivo* imaging.

A similar strategy could be applied to the IeDDA reaction between tetrazines and strained alkenes. This would first involve synthesis of tetrazine precursors, which would be evaluated in terms of their reactivity towards dienophiles such as norbornene and TCO. A radiolabelled version of this reaction could be developed, in a similar manner to that described for the SPAAC reaction, for example using a ^{68}Ga-labelled tetrazine and a series of strained alkenes (Figure 35).

C = chelate (e.g. DOTA)
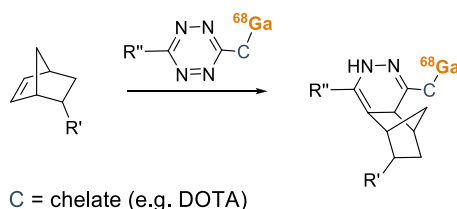
Figure 35. A general scheme for radiolabelling norbornenes with ^{68}Ga-labelled tetrazine prosthetic groups

This reaction may be applied to a pretargeting strategy in a similar manner, for example by ligating norbornene to a chosen biomolecule and reacting with the radiolabelled tetrazine prosthetic group. The reaction will be optimised in a vial and *in vitro*, before being applied to

an *in vivo* pretargeting strategy for PET imaging, by which the modified biomolecule will be administered prior to introduction of the radiolabelled prosthetic group.

It is hypothesised that one, or both of these reactions, will display the desired balance between reaction kinetics and stability, under the conditions and low concentrations that are observed *in vivo*, for a pretargeting strategy for PET imaging to be successfully demonstrated.

Chapter 2 – Synthesis and Development of Cyclooctynes for the SPAAC Reaction

2.1   First generation cyclooctynes (OCTs)

2.1.1 Introduction to OCT Cyclooctynes

As discussed, the SPAAC reaction is one of the key bioorthogonal reactions that may be considered for pretargeting applications. The basic cyclooctyne structure was initially modified by Bertozzi and co-workers by the addition of carboxylic acids, which can be regarded as simple and easily functionalised side chains. These first-generation reagents were known as **OCT1** and **OCT2** (Figure 36).[109, 126, 148]
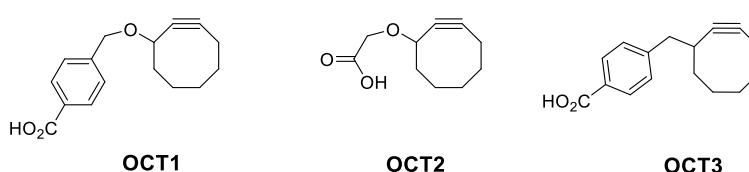
Figure 36. Bertozzi's first-generation cyclooctyne (OCT) reagents[126]

These compounds were found to have suitable properties for application to copper-free click ligation chemistry, such as good solubility in a number of solvents, and were found to exhibit promising reaction kinetics in their cycloaddition reactions with benzyl azide ($k = 2.4 \times 10^{-3}$ $M^{-1}s^{-1}$ for **OCT1** and $k = 1.3 \times 10^{-3}$ $M^{-1}s^{-1}$ for **OCT2**), which are comparable to those demonstrated by the Staudinger ligation ($k = 2.4 \times 10^{-3}$ M^{-1} s^{-1}).[57] These reagents have been used for a number of applications, including for the functionalisation of quantum dots.[149]

The main drawbacks of compounds **OCT1** and **OCT2** include their relatively short shelf-lives, showing decomposition when stored at -20°C for long periods. This led to the development of a more stable analogue of these compounds, **OCT3**, in which the ether linkage is replaced by an alkyl chain (Figure 1).[113, 148] However, this increase in stability was counter-balanced by a lower reactivity ($k = 1.2 \times 10^{-3}$ $M^{-1}s^{-1}$) towards cycloaddition with benzyl azide (see chapter 3).

2.1.2 Synthesis of OCT2

The most simple cyclooctyne structure (**OCT2**) was chosen to be synthesised, as this was considered to be a useful first-generation compound to use as a reference for comparison with future cyclooctynes. The best described strategy in the literature towards the synthesis of this type of compound was carried out in three steps from cycloheptene **1**.[113, 149, 150] The carboxylic acid group was expected to allow for the introduction of further functionality and would provide a useful point of attachment for chemical probes (Figure 37).
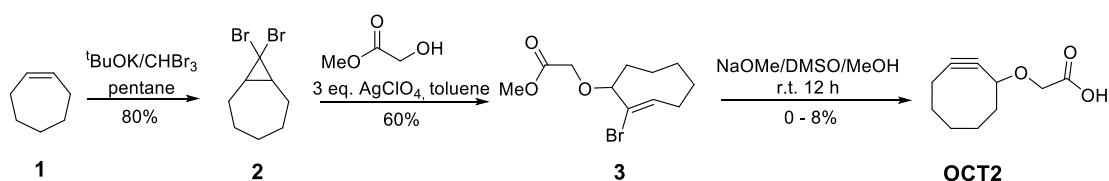
Figure 37. The total synthesis of **OCT2** from cycloheptene **1**[113]

The first step towards the synthesis of **OCT2** involved treatment of cycloheptene **1** initially with potassium *tert*-butoxide and subsequently with bromoform to afford 8,8-dibromobicyclo[5.0.1]octane **2**. This reaction was complete after stirring at room temperature over night and was purified using column chromatography yielding cyclopropane **2** as a colourless oil in 80% yield. Initial conditions using cycloheptene and potassium *tert*-butoxide in *tert*-butanol rather than pentane provided lower yields of approximately 50%, and so the aforementioned conditions were chosen as the standard procedure.

The next step was to perform a 'ring-expansion' using methyl glycolate and silver perchlorate to form methyl 2-bromocycloct-1-en-3-glycolate **3**. This reaction proceeded within 1.5 h at room temperature in reasonable yields of 60%. However, the silver precipitate had to be removed and the purification carried out immediately upon completion of the work-up, as the product was unstable to the silver salts formed.

The final step was the elimination of the bromine to give the alkyne and ester deprotection to give the carboxylic acid to form the final cyclooctyne **OCT2**. Initial attempts towards the synthesis of this compound relied upon the use of sodium methoxide as base, but

elimination of bromine did not occur under these conditions, and the major isolated compound was the hydrolysed starting material. Attempts were made to improve the conditions of this reaction by ensuring that the solvents were completely dry, and also by synthesising the sodium methoxide *in situ* through the use of sodium metal and methanol. Low yields of the final compound were observed using this method (approximately 8%), and so attempts were made to improve the synthesis using alternative bases (Table 6).

Entry	Base	Yield (%)
1	NaOMe (solid form)	0
2	NaOMe (formed in situ from Na and MeOH)	8
3	DBU	0
4	Kt-BuO	0

Table 6. Attempted elimination of bromine to form cyclooctyne **OCT2**.

DBU and potassium *tert*-butoxide were both investigated as potential bases in order to eliminate bromine, but were found to be unsuccessful, and so only the strategy involving the *in situ* formation of sodium methoxide allowed for the product to be isolated upon scale-up, be it in low overall yield.

An analogue of **OCT2** was synthesised in order to test the versatility of the 'click' reaction with cyclooctynes containing different side-chains (see chapter 3).[151] 4-Methoxy benzylamine **4** was reacted with the first-generation cyclooctyne **OCT2** at room temperature using HBTU as a coupling agent, to form **OCT4** in 60% yield after column chromatography (Figure 38).
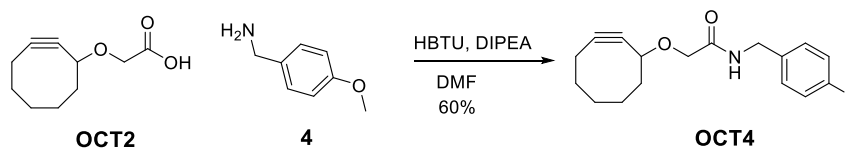
Figure 38. Synthesis of **OCT4** *via* an amide coupling using HBTU

2.1.3 Conclusions

The difficulties involved with the final step of the synthesis of **OCT2** limits the attractiveness of this particular compound towards the hypothesised pretargeting application. It was therefore concluded that a cyclooctyne with more advanced structural modifications, displaying more desirable physicochemical properties, would be more useful for this purpose. However, significant material was obtained for carrying out example SPAAC reactions with OCT reagents, as demonstrated in Chapter 3.

Although the first-generation **OCT** reagents developed by Bertozzi and co-workers demonstrated comparable reaction kinetics to the Staudinger ligation, one of the main limitations of these compounds is that they have less than desirable physicochemical properties.[113, 114] Although these properties could be partially improved by attaching different side-chains onto the molecule, such as with the **OCT4**, the core cyclooctyne is still highly lipophilic. This may lead to problems such as plasma-protein binding and poor *in vivo* biodistribution, which would limit their application to pretargeting, a problem which has been observed when applying these systems *in vivo*.[114, 128] It was additionally considered that the OCT compounds probably did not show rapid enough reaction kinetics for the SPAAC reaction to be demonstrated *in vivo*, as discussed in Chapter 3, as the reaction needs to occur at very low concentrations under biological conditions.[151] For these reasons, alternative cyclooctynes were explored as potential compounds for use in the proposed pretargeting strategy.

2.2 Halogenated Cyclooctynes

2.2.1 Introduction to MOFO and DIFO Analogues

Bertozzi found that the lower reactivity observed upon introduction of the alkyl moiety in the **OCT3** reagent, as compared to the less stable **OCT1** reagent, could be overcome by introduction of a fluorine substituent.[55, 113] The mono-fluorinated cyclooctyne **MOFO** (k = 4.3 x 10^{-3} $M^{-1}s^{-1}$) showed enhanced reaction kinetics in the strain-promoted cycloaddition over the equivalent non-fluorinated analogue (**OCT1**) due to the addition of one fluorine atom on the carbon adjacent to the alkyne moiety (Figure 39).[113]


MOFO   **DIFO1**
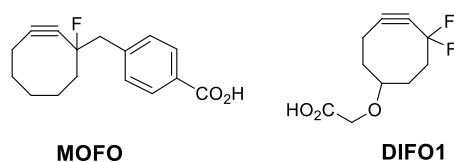
Figure 39. The structures of the mono- and di- fluorinated cyclooctynes **MOFO** and **DIFO1**[57]

The incorporation of a suitable electron-withdrawing group (EWG) within the cyclooctyne skeleton lowers the activation energy of the SPAAC reaction through electronic effects. One way of understanding this effect is by use of the molecular orbital theory (Figure 5).[55] During a reaction, the HOMO of one species and the LUMO of another interact to form a bonding orbital (and an antibody orbital) in the newly formed species. The LUMO and HOMO are the two orbitals which lie closest in energy between the two reacting species, which allows them to interact most strongly. By addition of an EWG on one side of the alkyne, the empty orbital (LUMO) of the alkyne bond becomes lower in energy, making this reaction more favourable.[55]

It was observed that the addition of a second fluorine atom, to form a di-fluorinated cyclooctyne such as **DIFO1** (Figure 39) increased the rate by approximately 60 times (k = 7.6 x 10^{-2} $M^{-1}s^{-1}$) relative to **MOFO**.[55, 58, 113, 148] This can be explained by the shorter C-F bond lengths that are observed with di-fluorinated $(C^*H)_2$-C-F_2 (1.348 Å) as compared to mono-fluorinated groups C_2CH-F (1.399 Å).[106] Enhancing the polarity of both C-F bonds has a

greater effect on the kinetics than would be expected for two isolated C-F groups, such as with the equivalent 3,8-difluorocyclooctyne skeleton.[152] As a consequence of these electron-withdrawing effects, the energy barrier for the [3+2] cycloaddition of methyl azide to **DIFO1** is computed to be 2.1 kcal mol^{-1} lower than its parent non-fluorinated cyclooctyne.

DIFO1 was found to exhibit particularly promising reactivity and properties, reacting with azides on intact proteins at a comparable rate to that observed with copper-catalysed 'click' chemistry.[148] The *syn* regioisomer, whereby the R_1 group is adjacent to the CF_2 group, is favoured over the opposite *anti* orientation ($\Delta\Delta E \approx 1.2$ kcal mol^{-1}) due to an enhanced alignment of atoms in the transition state (Figure 40).[137, 153]
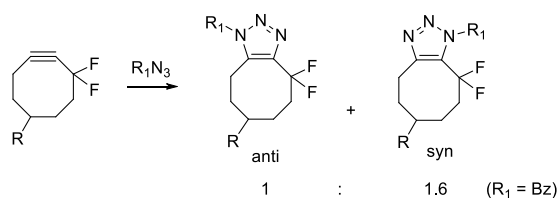
Figure 40. Bertozzi's reaction of DIFO reagents with functionalised azides[55]

The use of the difluoromethylene moiety in **DIFO1** is significant as it not only acts as a good EWG through inductive effects, but it is also particularly inert. Unlike other potential substituents that might have been incorporated, such as carbonyl groups, the difluoro functionality does not create a Michael acceptor capable of alkylating biological nucleophiles.[148] **DIFO1** is stable in water, suggesting that this compound will be similarly stable in a biological environment, lowering the likelihood of cross-reactions with biomolecules. It should be noted that the rate of reaction of **DIFO1** with azides was between 17-63 times greater than any of the reactions previously reported with either the Staudinger ligation or other strain-promoted cycloadditions, displaying encouraging biocompatibility.[148] In the literature, DIFO reagents were successfully applied to *in vitro* studies, such as the imaging of glycans in developing zebrafish.[154] **DIFO1** was also compared to other cyclooctyne reagents for staining Jurkat cells, where a biotinylated version of the cyclooctyne was shown to have excellent intrinsic reactivity with cells bearing SiaNAz

(azides), with the reaction occurring up to 20-fold faster than with previously identified cyclooctynes such as **OCT1** and **MOFO**.[155]

DIFO1 was originally synthesised by Bertozzi *et al*. in 12 steps and in an overall yield of only ~1% (Figure 41).[106, 148]
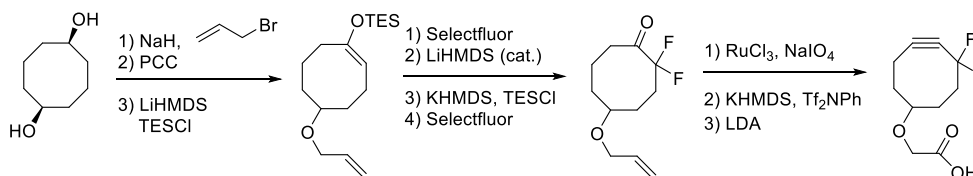

Figure 41. Bertozzi's initial synthesis of **DIFO1**[148]

This synthesis involves an often problematic elimination step to install the alkyne functional group, which is an issue observed with the formation of the cyclooctyne structure in general. This limitation led to the development of a second generation of DIFO related compounds, whereby a more practical synthetic route was adopted.[55] The Bertozzi group aimed to reduce the synthetic complexity involved with the difluorinated core by replacing the ether linker on the C-4 substituent with a more simple alkyl linker. It was hoped that by doing so, the SPAAC reaction could be utilised in a more diverse range of applications.

The literature synthesis of a second-generation compound **DIFO2** was completed in 6 steps from 1,3-cyclooctanedione **5**, which itself is synthesised in ~67% overall yield, as described in section 2.2.2 (Figure 42).[55, 156]

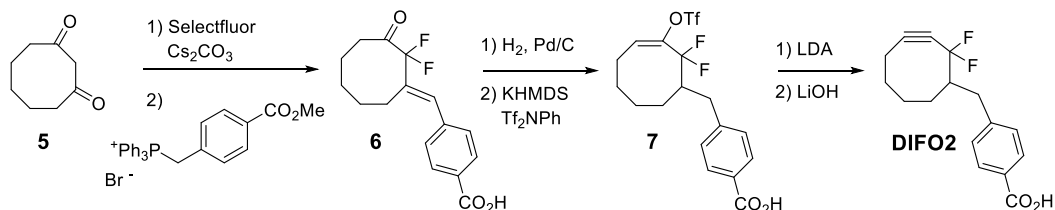

Figure 42. The improved synthesis of **DIFO2** which was completed in 36% yield from 1,3-cyclooctanedione **5**[55]

Difluroination of 1,3-carbonyls had been previously carried out using Selectfluor™, and the studies have shown that elevated temperatures and pressures, or the formation of enamine intermediates were required in order for the reactions to proceed successfully.[157] However,

Bertozzi *et al.* found that 2,2-difluoro-1,3-cyclooctanedione could be produced in 73% yield *via* simple treatment of diketone **5** with Selectfluor™ and Cs_2CO_3, which aids the deprotontaion of the α-carbon.[55] The next step of the synthesis involved a Wittig reaction using a phosphonium salt in order to produce the carbon-carbon linker.[156] The alkene was then reduced, which was followed by triflation of the enol form of ketone **6**, which could subsequently be converted to the alkyne **7** by use of a strong base. **DIFO2** was finally formed in an overall yield of 36% from the synthesised diketone **5** (in 21% overall yield and 10 steps from the diester).

DIFO2 and **DIFO3** (a derivative not containing the phenyl ring), were termed 2nd generation DIFO compounds, and shown to display comparable reaction kinetics to **DIFO1** (k = 4.2 x 10^{-2} $M^{-1}s^{-1}$ for **DIFO2** and k = 5.2 x 10^{-2} $M^{-1}s^{-1}$ for **DIFO3**) in their 1,3-diploar cycloadditions with benzyl azide.[55, 158] The lack of the phenyl ring in **DIFO3** also improved the physicochemical properties, showing lower background labelling in the staining of Jurkat cells, which was attributed to the lower lipophilicity of this compound.[55, 109, 132, 134, 148, 159]

2.2.2 Hypothesis for a 'Trifluoromethylated' Cyclooctyne

Due to the promising reaction kinetics demonstrated by Bertozzi's DIFO analogues, as well as the relatively short total synthesis, it was postulated that these compounds could be a useful class of compound for application to pretargeting.[55] Based upon the improved synthetic route towards DIFO compounds (Figure 8), we hypothesised that it might be possible to introduce other electronegative atoms or groups may be introduced into the same position as the fluorine atoms, due to the acidity of the methylene proton positioned between the two ketone functional groups in 1,3-cyclooctanone **5**. It could be envisaged that a trifluoromethyl group would be similarly electronegative to the difluorine moiety, whilst also introducing a significant amount of steric bulk onto the position. It has been demonstrated that the CF_3 group is significantly larger (2.70 Å) than the CH_3 group (2.29 Å), but not as sterically demanding as a *tert*-butyl substituent (2.83 Å). A single fluorine atom, on the other

hand, has a van der Waals radius that is only marginally larger than that of a hydrogen atom, and subsequently does not have a significant steric effect (Figure 43).
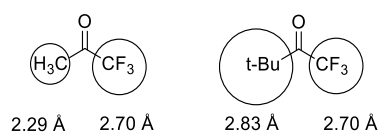
Figure 43. The difference in reported van der Waals radii of methyl, trifluoromethyl and *tert*-butyl substituents adjacent to a ketone moiety

It was anticipated that introduction of the CF_3 group would lead to an increase in the formation of one regioisomer over the other upon reaction with the azide in the SPAAC reaction (*i.e.* make the reaction more stereoselective), by making one end of the alkyne bond less accessible. Two trifluoromethyl groups could potentially be introduced onto this position simultaneously, to increase the electronegativity and the steric bulk even further (Figure 44).
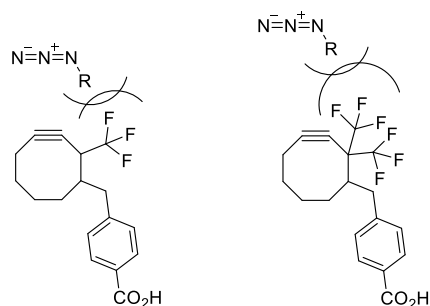
Figure 44. Hypothetical effect of addition of a) one and b) two trifluoromethyl groups, respectively onto the carbon α- to the alkyne on the SPAAC reaction with a substituted azide

The difluorine moiety in the DIFO class of cyclooctynes is introduced to 1,2-cyclooctadione using Selecfluor™, and it was imagined that an electrophilic trifluoromethylating reagent such as the a Togni™ reagent, could be used to introduce one or two trifluoromethyl groups into the same position.[55] The subsequent steps towards the synthesis of the cyclooctyne would then be identical to the conditions employed for the synthesis of **DIFO2** (Figure 45).
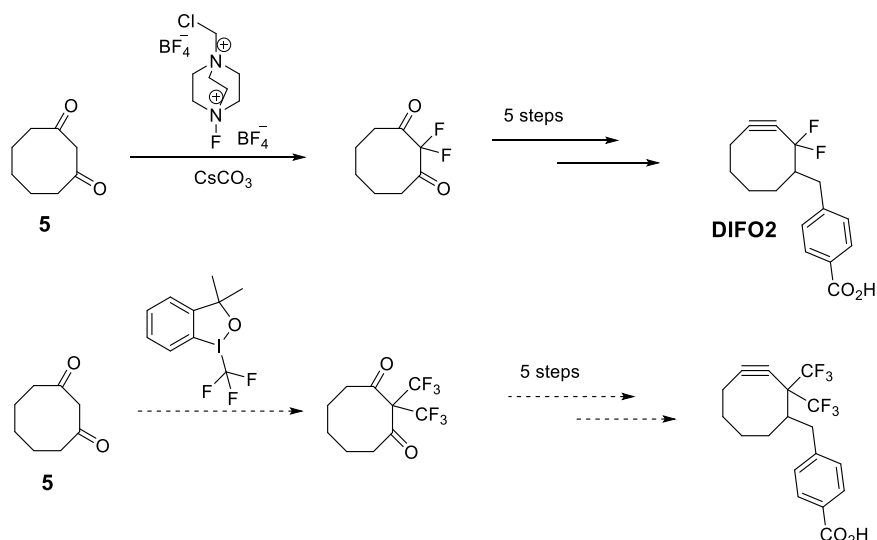
Figure 45. Proposed trifluromethylation of diketone **5** using an electophilic trifluromethylating (Togni[TM]) reagent, as a parallel to the difluorination using Selectflour[TM] towards the synthesis of **DIFO2**[55]

Several literature procedures have been described towards the synthesis of 1,3-cyclooctadione **5**, which would be the precursor for carrying out the synthesis of halogenated analogues.[156, 160] However, two main routes are employed; both of which start from commercially available diethyl pimelate **8** (Figure 46).
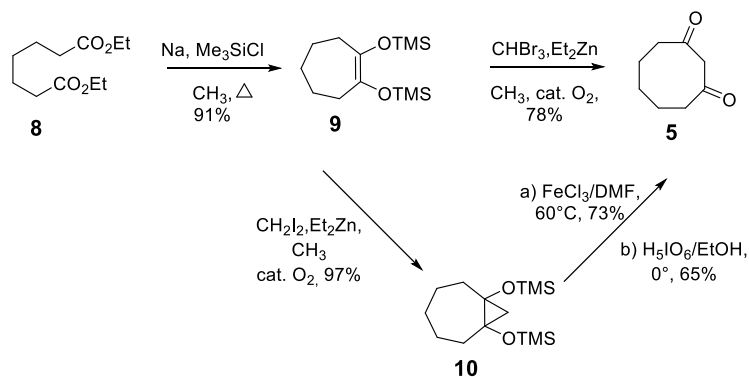
Figure 46. Literature procedures for the synthesis of 1,3-cylooctadione **5**[156]

The first method utilises the cyclooproponation of silylated alkene **9** *via* treatment with diiodomethane and diethylzinc to form a strained bicyclo[5.0.1]octane **10**. Two methods are then reported for the catalytic oxidation of the cyclopropane **10**.[156, 160] The first uses FeCl₃, forming the dione **5** in 73% yield, but a sub-optimal work-up procedure is reported, which renders this route less favourable. An alternative oxidation is carried out using periodic acid, in which diketone **5** may apparently be formed cleanly in 65% yield from the cyclopropane.

The second method instead forms the bromocarbene *in situ* using bromoform and diethylzinc directly from alkene **9**, which is then treated with molecular oxygen to form the ring expansion product **5** in 78% yield.

After optimisation of the synthetic route to compound **5**, the most succesful method was acheived in three steps from diethyl pimelate **8**, and in a good overall yield of 54%. This strategy followed the literature procedure *via* the cyclopropane **10** fairly closely, demonstrating camparable (and in some cases improved) yields.[156] The first step to form alkene **9** was fairly straight-forward, but relied on the use of elemental sodium, which is difficult to handle. This step formed the trimethylsilyl protected alkene **9** in excellent yield (84%), and was shown to be reproducible when carried out on different scales of up to 5 g of diethyl pimelate **8**. Diiodomethane and diethyl zinc were found to be the most effective for the formation of cyclopropane **10**, which could be synthesised in 81% yield. The final step of the synthesis was similarly high yielding, and treatment of cyclopropane **10** with periodic acid afforded the 1,3-substituted diketone **5** in 80% yield following column chromatography (Figure 47).
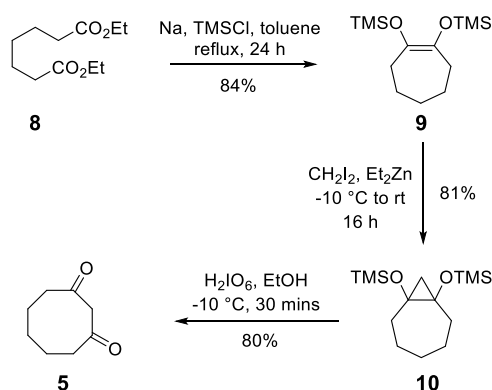

Figure 47. The optimised route for synthesis of 1,3-cyclooctadione **5**

The diketone **5** obtained from this synthesis was used to reproduce the synthesis of **DIFO2** (*cf.* Figure 45), and was also used to carry out attempted trifluoromethylations, towards the synthesis of a triflouromethylated cyclooctyne analogue.[55, 113]

The development of fluoro-alkylated compounds has received significant attention in the context of medicinal chemistry due to the interesting properties that these functional groups can display, for example by enhancing the lipophilicity of a molecule or by modifying its metabolic behaviour.[161, 162] The use of reagents such as SF_4, SbF_3, BrF_3, and HF as reagents for the conversion of CH_3 to CF_3 groups, usually require harsh conditions, which may have detrimental effects towards other functional groups within the target molecule.[162] A number of less harsh strategies now exist for the introduction of the CF_3 group, with the most widely-explored methods being based upon the use of nucleophilic trifluoromethylating reagents such as (trifluoromethyl)trimethylsilane (Me_3SiCF_3), or Ruppert's reagent.[163] Although nucleophilic reagents remain the most popular choice for carrying out these transformations, methods relying on the use of radical and electrophilic trifluoromethylations also exist, and allow for the CF_3 group to be introduced into a wider range of compounds.[164, 165]

In 2006, Togni *et al*. developed a family of formally electrophilic CF_3 transfer reagents, based upon hypervalent iodine, with the two most significant and widely-used compounds being the acid-derived reagent **11** and the alcohol-derived reagent **12** (Figure 48).[162]

11   **12**
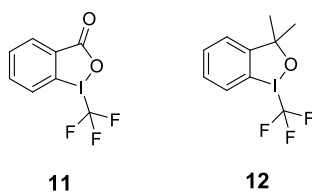
Figure 48. The two most commonly utilised Togni[TM] reagents based upon trifluoromethylated hypervalent iodine

These reagents have now been successfully applied to the trifluoromethylation of both soft nucleophiles (such as phosphorous-, sulfur-, and carbon-centred nucleophiles, thiols, α-nitroesters, β-ketoesters, phosphorothiolates and aromatics), and more recently hard O-centred nucleophiles (such as alcohols, sulfonic acids and hydrogen phosphates).[166]

The initial work carried out by Togni and co-workers demonstrated that the alcohol-derived reagent **12** could be applied to the trifluoromethylation of β-ketoester **13** using polar, aprotic

and nucleophilic solvents, under phase-transfer catalyst (PTC) conditions and in the presence of a mild base.[162] Both reagents **11** and **12** have been used for carrying out similar transformations with α-nitroesters, with the alcohol-derived reagent **12** being the most widely used reagent for the trifluoromethylation of this type of compound. The same reagent could be used to successfully introduce the CF_3 group into Evans-type chiral enolates, as well as more recently being applied to α-trifluoromethylation of aldehydes when combined with organocatalysts.[166] The acid-derived reagent **11**, however, has primarily been used for the introduction of CF_3 onto soft nucleophilic centres, and it is generally acknowledged that the 'alcohol' reagent **12** is preferred for carrying out triflouromethylations of carbonyl compounds (Figure 49).[167]
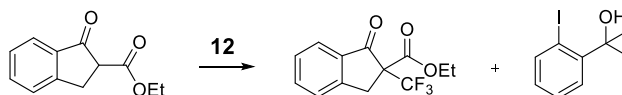

Figure 49. Togni's transformation of β-keto esters to their trifluoromethylated products using reagent **12**[168]

Based on the findings reported by Togni *et al*., as well as more recent developments into this type of transformation, we hypothesised that we could apply the Togni™ reagent **12** to our diketone precursor and achieve a trifluoromethylation at the targeted α-carbon centre in compound **5**. However, it should be noted that these reagents have yet to be demonstrated for the introduction of CF_3 onto ketone substrates.

The trifluoromethylation step was carried out as a test reaction on a small amount of diketone **5** (10 mg).[169] The initial conditions investigated were standard conditions for the electrophilic triflouromethylation using reagent **12**, with potassium carbonate as base and under PTC conditions. The stoichiometry of the reaction was controlled using 1.1 equivalents **12** so that only one trifluoromethylation would occur. However, under these conditions, the only isolated compound was the diketone starting material **5**, suggesting that these conditions are not optimal for carrying out trifluoromethylation of the diketone (Figure 50).
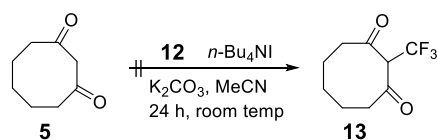
Figure 50. Attempted triflouoromethylation of diketone **5** using Togni[TM] reagent **12**

Raising the temperature of the reaction may additionally lead to competing nucleophilic attack on the ketone. It was therefore hypothesised that an alternative base could be employed for this reaction, which would allow for the formation of the anion on the α-carbon, rendering this position more reactive towards the electrophilic trifluoromethylating reagent. By using a stronger base, such as *n*-BuLi, it could be anticipated that the deprotonation could be rendered irreversible, making the introduction of the trifluromethyl group highly selective at this position. Diketone **5** was first treated with *n*-BuLi at -78°C, and was then allowed to stir for 30 min in order to fully deprotonate the α-position. After warming to room temperature, the mixture was treated with reagent **12**, and the reaction progress was monitored by TLC. However, after several attempts at this reaction, the product **13** still remained to be isolated. It is possible that in the presence of strong bases such as *n*-BuLi, defluorination may occur, as trifluoromethyl groups tend to be unstable, especially when the α-carbon is not fully substituted (Figure 51).
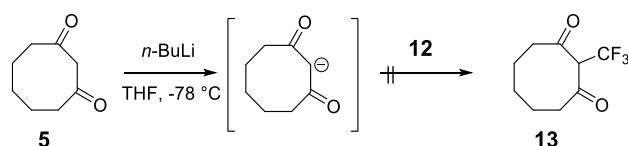
Figure 51. Attempted triflouoromethylation of diketone **5** using **12** *via* the anion intermediate using *n*-BuLi

It was concluded that this is a very challenging transformation to achieve, and this is supported by the fact that, as far as we are aware, no electrophilic α-trifluoromethylations of ketones have been reported in the literature. Coupled to this is the apparent instability of the trifluoromethane group towards strongly basic conditions; LDA is required in order to eliminate the triflate in the final step of the cyclooctyne synthesis (*cf.* Figure 42), potentially resulting in defluorinations during the final step of the synthesis. It was considered that it would potentially require a large amount of optimisation to attain the product, and we

therefore postulated that it would be easier to introduce an alternative moiety, which would display similar properties to the trifluoromethane group, without having the associated synthetic complexity.

2.2.3 Hypothesis for an Iodinated Cyclooctyne

Iodine has a larger van der Waals radius (between 2.03 and 2.15 Å) than fluorine (between 1.35 and 1.47 Å), but it still has a relatively high electronegativity on the Pauling scale (2.66 *vs.* 3.98 for fluorine).[170] However, an iodine is often more straight-forward to introduce than a CF_3 group, and subsequently it could be envisaged diketone **5** could be α,α-diiodinated, and subsequently used to synthesise diiodinated analogue **16**, in a similar manner to the proposed route to the di-trifluoromethylated compound (Figure 52).[55]
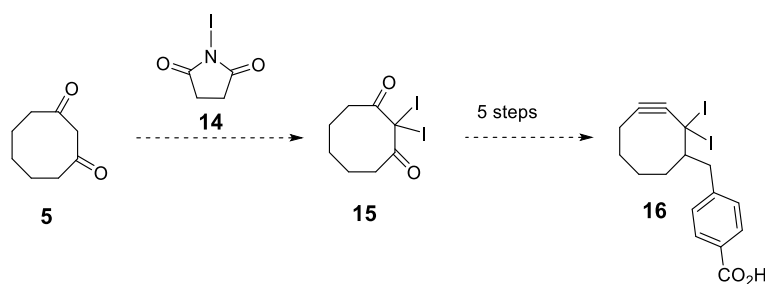
Figure 52. Proposed approach to diiodinated cyclooctyne **16**

The α-idoination of ketones has been reported several times in the literature, and the most promising conditions could be evaluated in the context of synthesising compound **16**.[171-173] It is possible that Iodine in this position would be unstable to the strongly basic conditions required to carry out the subsequent synthetic steps to cyclooctyne **16**, and consequently it was important to test this before applying this chemistry to the synthesised diketone **5**.

Therefore, the same synthetic procedure was initially tested by carrying out a similar synthesis using α-iodo cyclooctanone **17** (Figure 53).[55]
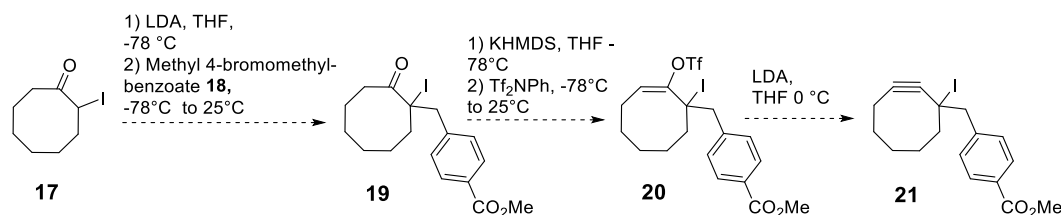
Figure 53. Proposed synthetic route to a mono-iodinated cyclooctyne **21**

If the synthesis were to be successful, this compound could potentially be used to synthesise a mono-iodinated cyclooctyne **21**, following a similar procedure to the synthesis of **MOFO**, and would additionally enable us to compare the effects of addition of one or two iodines onto this position.[113] The α-proton must be blocked in this case, as with compound **19** by addition of an alkyl group, in order to afford the subsequent triflate **20** by deprotonation from only one side of the ketone.

The conditions for the synthesis of α-iodo cyclooctanone **17** were first tested and optimised, as this would enable us to test the feasibility of introducing iodine α- to the ketone in only a few steps. Introduction of iodine was carried out according to literature procedures (Table 7).[172-174]

Entry	Starting material	Conditions	Diiodination feasible?	Time (hours)	Yield (%)
1	22	NIS/IBX, DMSO	N	2	70
2	23	NIS, DMSO, rt	Optimisation required	2	10
				4	15
				16	25
3	23	1. NaI, H_2O, 0ºC 2. H_2SO_4/H_2O_2, 40ºC	Y	3	90

Table 7. Methods employed for the synthesis of α–iodocyclooctanone **17**[172-174]

N-Iodosuccinimide (NIS) **14** is commonly used for carrying out α-iodinations, and has been used to synthesise cyclic α-iodo ketones from the respective cyclic alkene, including for the

synthesis of α-iodocyclooctanone **17**.[173] This method is advantageous as it uses cyclooctene **22** (which is cheaper than cyclooctanone **23**) but requires the use of *o*-iodoxybenzoic acid (IBX) (Figure 54).
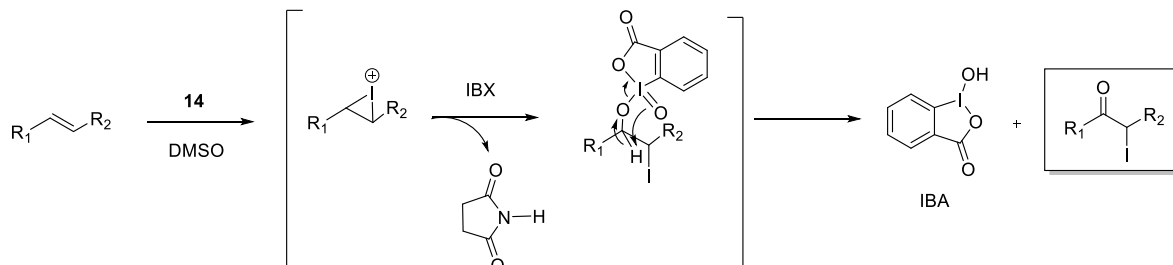
Figure 54. Nidhi's proposed mechanism of the formation of α-iodo ketones from alkenes using NIS/IBX in DMSO[173]

This reaction allowed for the formation of **17** in good yield (70%), and it could be achieved in 2 h at room temperature in DMSO (Table 7, Entry 1). However, although this proved very efficient for the formation of **17**, the proposed mechanism of the reaction prohibits the formation of the α,α-diiodinated product.

NIS has similarly been used to introduce Iodine α- to ketones in DMSO at room temperature, in high selectivity and without the need for catalysis.[172] This method has been used for the successful α-iodination of cyclic ketones such as cyclohexanone and 1,3-cyclohexadione, and for this reason was anticipated to be a useful method for the synthesis of α-iodoketone **17**. Cyclooctanone **23** was consequently treated with 1.05 equivalents of NIS in DMSO, and the reaction was monitored by TLC. Using this method, a significant amount of the ketone starting material remained, even when the reaction time was increased, although it was possible to isolate the product using distillation (Table 7, Entry 2). It may also be difficult to achieve bis-iodination using this method, as relatively mild reaction conditions are used; harsher conditions are usually necessary in order to achieve the α,α-diiodination.

An alternative method for the iodination was explored, which would allow for the compound to be synthesised in greater yield.[174] This method reportedly allows for almost quantitative formation of α-iodinated ketone **17**, and the mechanism of the reaction should permit for introduction of two iodines onto the α-carbon (Figure 55).
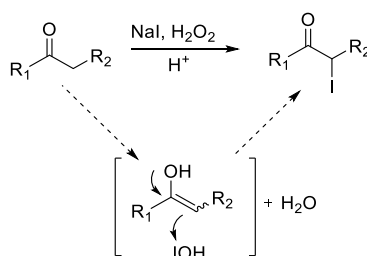
Figure 55. Proposed mechanism for the α- iodination of ketones using the NaI/H_2O_2/H^+ system[174]

Both alcohols and ketones may be treated with sodium iodide in water, in the presence of an acid to form the α-iodinated ketone. Cyclic ketones were shown to be the most reactive substrates for these transformations, and sulfuric acid was found to be the most effective acid to aid the reaction, and the conditions were successfully applied to the synthesis of α-iodocyclooctanone **17** from cyclooctanone **23**, forming the product in ~90% yield under the literature conditions (Table 7, Entry 3).[174] The formation of the enol is the driving force for this reaction, and so it may be hypothesised that two iodinations may be achieved by forming a second enol, using two equivalents of sodium iodide.

The iodinated product **17** was subsequently treated to the alkylating conditions employed by Bertozzi *et al* (*cf.* Figure 53).[55, 113] This first involved treating the ketone with LDA at -78°C, followed by dropwise addition of the alkylating agent in THF upon warming to room temperature. Complete consumption of the starting material had occurred after stirring for 1 h at room temperature, however after work-up and purification, it was determined by NMR that the Iodine had been eliminated forming ketone **24**. It is possible that the elimination was occurred *via* halophilic attack of the LDA on the iodine to generate the lithium enolate **25** in a Reformatsky-type process (Figure 56).
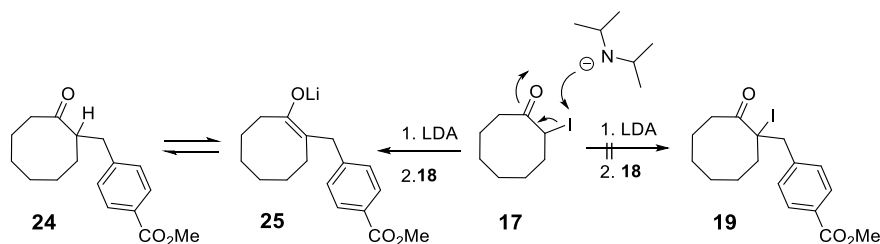
Figure 56. Attempted alkylation of α-iodocyclooctanone **19**, forming only the de-iodinated product, and plausible mechanism for the elimination of iodine

Due to the poor stability of Iodine under highly basic conditions, it was concluded that the iodinated cyclooctyne **19** would be very difficult to synthesise, as the formation of the cyclooctyne requires the use of a strong base. Therefore, attempts were not made to synthesise **19**, as it could be anticipated that diiodinated compound **15** would be equally unstable. The product obtained from this reaction was instead used to synthesise the first-generation methyl ester of cyclooctyne **OCT3** (Figure 57).[113]
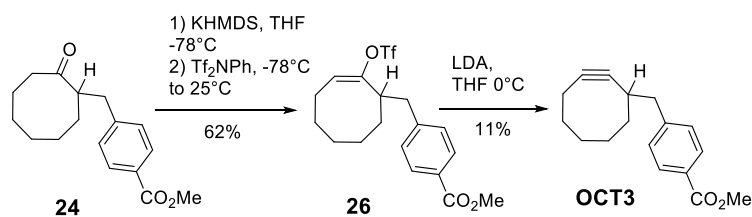
Figure 57. The synthesis of **OCT3** from ketone **24**

This compound was used to evaluate the SPAAC reaction in terms of the kinetics of first-generation cyclooctynes as compared to later-generation compounds (see chapter 3).

2.2.3 Conclusions

It was found that introduction of a trifluoromethyl group, and similarly an iodine atom, into the α-position to the cyclooctyne, was difficult to achieve. It could be hypothesised that an alternative bulky substituent, such as a *tert*-butyl group, may be introduced more easily. However, the lack of electronegativity which would be attained as compared to the halogenated substituents, would most probably result in a reduction in the rate of reaction of the derived cyclooctyne with azides. It was considered that a balance of reactivity and steric bulk must be achieved, whilst maintaining a low level of synthetic complexity. Future work

would therefore be to design a cyclooctyne which combines these factors, for example by incorporation of steric bulk onto one side of the alkyne, and electronegative moieties on the other (Figure 58).[175]
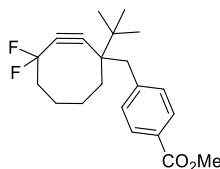
Figure 58. Proposed cyclooctyne containing steric bulk (*tert*-butyl group) and electron-withdrawing groups (diflourine)

Such a molecule should enable favourable reaction kinetics to be maintained, whilst introducing improved regioselectivity, in terms of 1,3-dipolar cycloadditions, over existing cyclooctynes.

2.3   Dibenzocyclooctynol (DIBO) Cyclooctynes

2.3.1 Introduction to DIBO Reagents

Boons and co-workers aimed to enhance the rate of the reaction of cyclooctynes in click-type reactions by increasing the amount of ring strain and conjugation in the cyclooctyne partner, using dibenzocyclooctynol reagents **DIBO1** and **DIBO2** (Figure 59).[127]
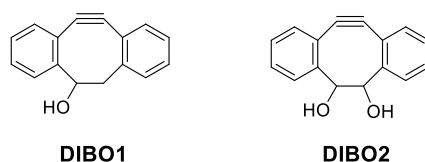
Figure 59. Boons' dibenzocyclootynol reagents **DIBO1** and **DIBO2**[106]

Boons anticipated that these reagents might react quickly enough with azides to be applicable to a wider range of applications than previous designs.[127] These compounds may be functionalised *via* the hydroxyl group; which is a useful handle for radiolabelling applications or for attaching the cyclooctyne to biologically active compounds.

The incorporation of two aromatic rings in these compounds proved to increase the reactivity of the cyclooctyne, as they impose increased strain on the alkyne, and also result in a

reduction in the energy of the alkyne LUMO as the electron density is distributed more evenly across the conjugated system.[127, 176] The aromatic rings also improved the biological stability of this compound over the earlier generation cyclooctynes, as these rings appear to help to block the attack of nucleophiles onto the alkyne.[106] **DIBO1** importantly showed comparable reaction kinetics (k = 5.7 x 10^{-2} M^{-1}s^{-1}) to second-generation cyclooctynes such as the difluorinated compound **DIFO1** (k = 7.6 x 10^{-2} M^{-1}s^{-1}) when reacted with benzyl azide, thus displaying a reasonable balance between stability and reactivity.[57, 127] The synthesis of **DIBO1** was described by Boons *et al.* in 5 steps from phenylacetaldehyde, in an overall yield of 10% (Figure 60).[127, 177]
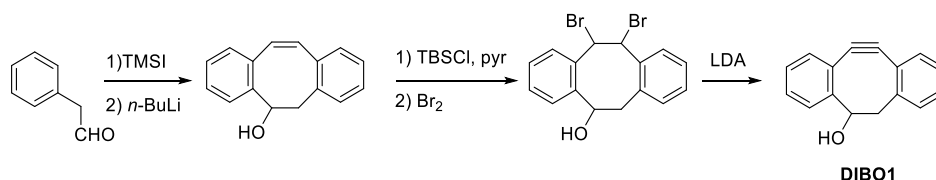
Figure 60. Boons' synthesis of **DIBO1** from phenylacetaldehyde in overall yield of 10%[127]

A modified variant of this compound was later developed by Leeper and co-workers.[178, 179] 3-Hydroxy-2',3',2",3"-tetramethoxy-7,8-didehydro-1,2:5,6-dibenzocyclocta-1,5,7-triene (**TMDIBO)** is a compound which shows structural resemblance to the DIBO reagents; but displays enhanced stability due to the introduction of four methoxy groups onto the aromatic rings (Figure 61).
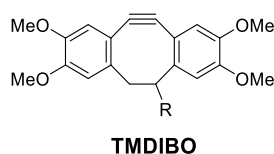
TMDIBO

Figure 61. Leeper's **TMDIBO** cyclooctyne[178]

As well as improving the stability of the cyclooctyne, the methoxy groups also stabilise the intermediates *en route* to this type of compound, making the synthesis of **TMDIBO** more straight-forward than that of **DIBO1**.[127] The rate constant of the reaction with benzyl azide,

as measured in methanol (k = 9.4 ± 0.4 x 10^{-2} $M^{-1}s^{-1}$), was also found to be even greater than that of **DIBO1**, demonstrating an attractive balance between reactivity and stability.[180]

2.3.2 Synthesis of TMDIBO1

The *p*NP carbonate analogue, **TMDIBO1** showed promising reactivity in the SPAAC reaction (see chapter 3), as well as apparently displaying a promising level of biocompatibility, and for this reason was chosen as a suitable cyclooctyne to synthesise.[151] The synthesis of **TMDIBO1** was achieved as described by Leeper *et al.* who described the synthesis in 8 steps, in an analogous manner to the synthesis of **DIBO1** (Figure 62).[178]
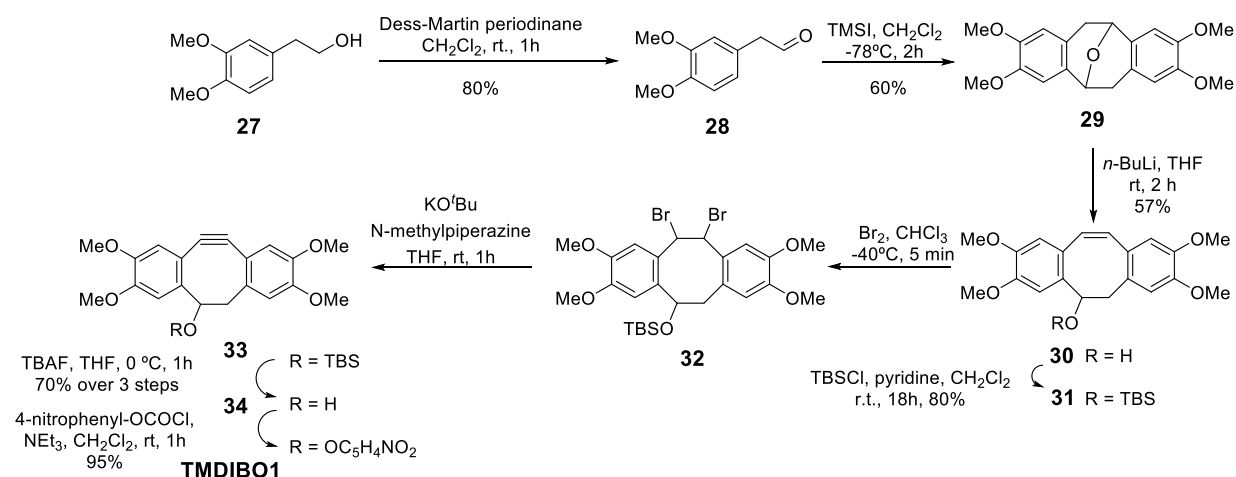
Figure 62. The synthesis of TMDIBO-*p*NP carbonate **TMDIBO1** from 2-(3,4-dimethoxyphenyl)ethanol **27**[178]

The first step towards the total synthesis of **TMDIBO1** involved the oxidation of 2-(3,4-dimethoxyphenyl)ethanol **27** to aldehyde **28** using the Dess-Martin periodinane (DMP). This reaction proceeds at ambient temperature in 1 h, to yield pure aldehyde **28** after column chromatography. This reaction was successfully carried out on various scales from 1g to 8g and, forming **28** in excellent yield (80-90%) in each case.

Subsequent addition of TMSI to a solution of aldehyde **28** in methylene dichloride at -78°C, followed by warming to room temperature for 2 h afforded the dimerised ether **29** after quenching with sodium thiosulfate. This could be recrystallised from methanol to produce pure product **29** in a yield of 45%. This dimerization step is far more efficient than is reported

for the equivalent compound without the methoxy groups, which is evidence of the enhanced stability of this class of compound.[127] Ether **29** was consequently treated with *n*-BuLi to promote ring-opening to give alcohol **30**. This reaction was complete after 2 h at room temperature and gave alcohol **30** in 57% yield after column chromatography. The next step was protection of **30** to give the silyl ether **31**, which went to completion at room temperature in 16 h.

The alkene in derivative **31** was di-brominated using elemental bromine, which could be achieved in 5 min; a significant improvement over the formation of brominated compound **26**, which takes 7 days, allowing for isolation of the product in only 50% yield. The brominated product **31** was reported to be labile, and so the subsequent dehydrobromination reaction was carried out in one-pot without any workup or isolation. The dehydrobromination to afford the cyclooctyne **33** was achieved in 70% yield over 3 steps, by treating **32** with 1-methylpiperazine and KO^{t}Bu for 1 h at room temperature, as reported. The silyl ether was deprotected using TBAF, which could be achieved in 1 h at 0°C, to form the alcohol derivative **34** and the side-chain was functionalised by generation of the 4-nitro-phenyl carbonate to give **TMDIBO1** as the final product after recrystallisation.

2.3.3 Conclusions

TMDIBO1 has been synthesised with only a small decrease in the overall yield as compared to the literature procedure.[178] The stability that may be achieved by introduction of the methoxy groups makes the synthesis of this compound more efficient and more reproducible than for **DIBO1**, and with no observed sacrifice of its reaction kinetics with azides. The carbonate side-chain also allows for simple structural modifications to be made to this compound, and **TMDIBO** may be introduced to a biomolecule or radiolabel by direct substitution with a primary amine to form the respective carbamate. For these reasons, **TMDIBO1** was chosen as the first cyclooctyne to be used for demonstrating the utility of the SPAAC reaction towards the pretargeting application (see chapter 4).[151]

2.4   A Strain Promoted 'Double-Click' (SPDC) Reagent

2.4.1 Introduction to the 'SPDC' Reaction

Hosoya and co-workers aimed to improve the incorporation of cyclooctynes into a biological setting through the use of a new mechanistic concept, referred to as the strain-promoted double-click reaction (SPDC), by which two alkyne groups are available for reaction with azides, such as with *sym*-dibenzo-1,5-cyclooctadiene-3,7-diyne (**DIBOD**) (Figure 63).[181]
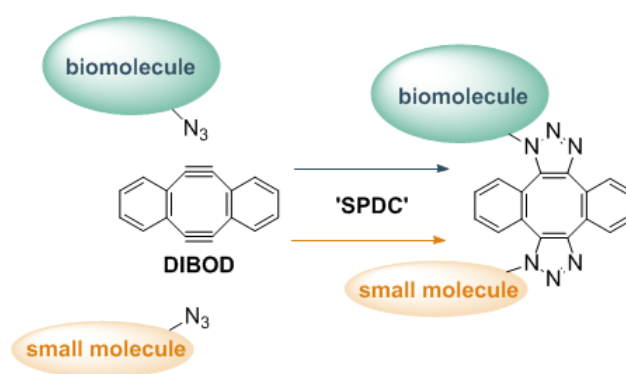
Figure 63. Hosoya's strain-promoted double-click (SPDC) reaction using **DIBOD**[181]

For example, it was shown that it was possible to form a mono-cycloadduct containing a small molecule prior to incorporation into the biomolecule, potentially opening up the possibility of introducing a large range of functionality using a relatively simple synthetic strategy. In particular, the second alkyne group could then be available for reaction with the azide-containing biomolecule by the SPAAC reaction.

The capabilities of the SPDC reaction have been demonstrated by Hosoya *et al.* in living cells.[181] **DIBOD** was reacted with excess amounts of simple azides, in which the *trans*-isomer **36** was generally shown to dominate over the *cis*-isomer **37**, the geometries of which were determined by single crystal X-ray crystallography. The mono-cycloadduct **35** was found to be more reactive than the starting alkyne, possibly due to the amount of steric repulsion between the triazole substituent and the *ortho*-proton on the benzene ring, producing a distorted and more reactive alkyne bond.[181] The reaction was similarly demonstrated using an equimolar amount of two different azides, showing the hetero-

cycloadducts as the major products and producing two sets of homo-cycloadducts (Figure 64).
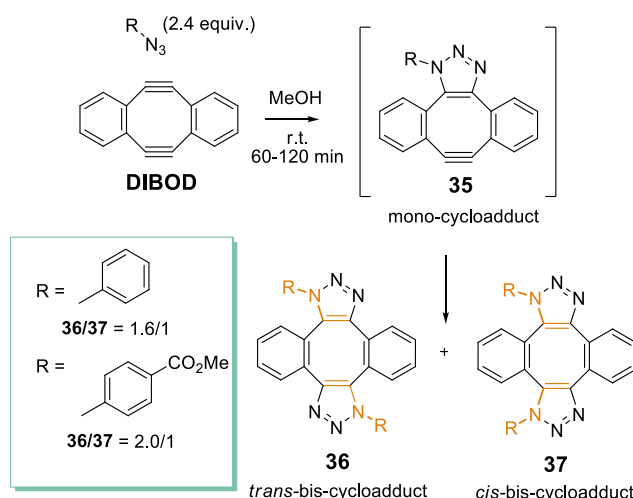
Figure 64. Hosoya's reaction of the SPDC reagent **DIBOD** with an azide, showing the formation of mono-cycloadduct a as a more reactive intermediate[181]

The reaction of the dialkyne **DIBOD** was found to have reaction kinetics comparable to that of the second-generation reagent **DIFO1**, when reacted with benzyl azide under similar conditions (k~ 62.9 x 10^{-3} M^{-1}s^{-1}).[55, 181]

2.4.2 Synthesis of the 'SPDC' Reagent DIBOD

The SPDC compound **DIBOD** was identified as being particularly interesting from a pretargeting perspective as there is potential for two 'click' reactions to be carried out *in vivo*, or for functionality to be introduced by one 'click' reaction and for the other alkyne to be available for reaction with an azide. The synthesis of **DIBOD** was therefore carried out in four steps from commercially available α-bromotolunitrile **38**, as described by Otera *et al.* (Figure 65).[182]
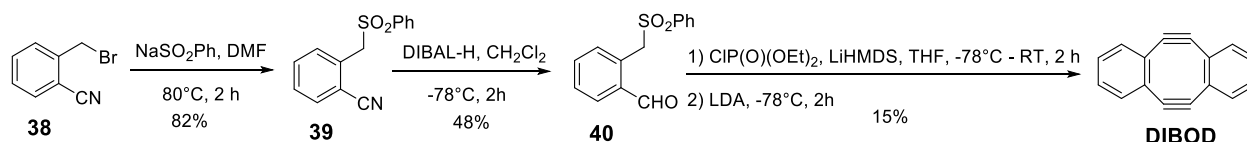
Figure 65. Otera's synthesis of the SPDC reagent **DIBOD** from α-bromotolunitrile **38**[182]

The first step of the synthesis involved sulfonylation of α-bromotolunitrile **38**, which is commercially available, but also easily synthesised from *ortho*-tolunitrile. The reaction uses benzenesulfinic acid sodium salt in DMF to form *ortho*-(phenylsulfonylmethyl)benzonitrile **39**, which was formed in 81% yield after purification by recrystallisation. The second step was reduction to aldehyde **40** using DIBAL-H, which was complete after 2 h at -78°C, giving a yield of 50%.

The final step of the synthesis was a Wittig-Horner reaction using $POCl(OEt)_2$ to form a bicyclic ether, which upon treatment with strong base was reduced to **DIBOD** in just 15% yield when carried out on a 500 mg scale. The Wittig-Horner reaction is a modification of the standard Wittig reaction, forming alkenes from phosphonates (Figure 66).[183]
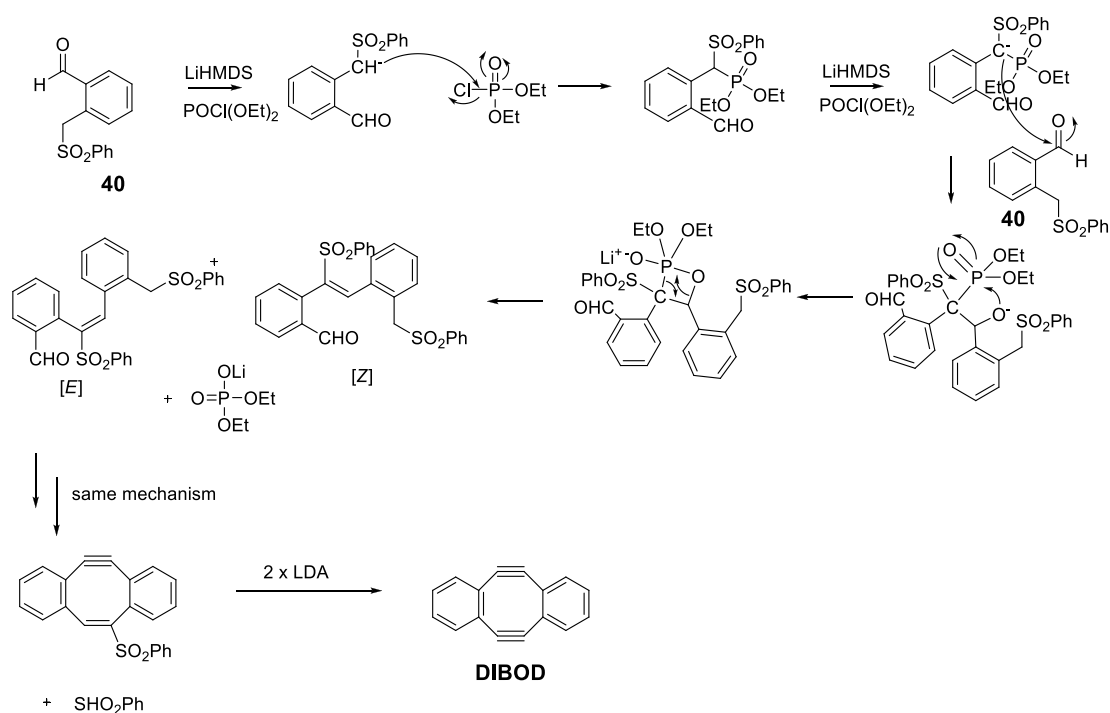
Figure 66. The Wittig-Horner reaction as applied to the formation of the 'SPDC' reagent **DIBOD**

In this case, aldehyde **40** is dimerised using two molecules of $POCl(OEt)_2$. A carbon-phosphorous bond is first formed with the methyl carbon adjacent to the phenyl sulfonyl group, and the subsequently formed ylid reacts with the aldehyde carbon, forming a carbon-carbon bond. $PO(OEt)_2(OLi)$ is eliminated as a by-product *via* a 4-membered transition state, driven by the formation of a strong P=O bond. The *E*-isomer subsequently undergoes a

second intermolecular Wittig-Horner reaction to form the di-cyclooctene ring. In the final step, the phenyl sulfonyl groups are eliminated by use of a strong base in order to afford the dialkyne. The final elimination step towards the synthesis of this cyclooctyne was found to be low yielding, as is observed with a number of the other cyclooctynes, exemplifying the difficulty involved in introducing such a large amount of strain into a medium-sized ring.

Although there were difficulties involved in the final step, and only a small amount of this compound was isolated, attempts to improve the yield of this compound using this strategy were not carried out, and it was instead envisioned that dialkyne, or 'SPDC' reagents such as these could be synthesised *via* an alternative route.

2.4.3 A 'Dual' Sonogashira Reaction for the Synthesis of 'SPDC' Reagents

One of the main challenges in synthesising cyclooctynes is often the final elimination step, resulting in low yields, and often requiring harsh conditions. This is due to the large amount of strain that is contained in the newly formed cycloalkyne as compared to the preceding cycloalkene, meaning that the formation of the cyclooctyne core is disfavoured. This is demonstrated through their spontaneous reaction towards azides; it is this ring strain which drives the SPAAC reaction to go to completion and form the more stable triazole product.

It can therefore be imagined that a method to form the cyclooctyne which does not involve this final and problematic elimination step may be preferred, and may result in a more efficient overall synthesis. One particularly useful method for forming carbon-carbon bonds is through the use of metal catalysis.[184] The use of metal catalysis is particularly advantageous, as this often enables carbon-carbon bonds to form which are otherwise difficult to achieve. For this reason, it was postulated that metal catalysed reactions may be a useful and robust method for forming the cyclooctyne core, and if successful, could be applied to the synthesis of a number of structural analogues with only minor modifications to the synthetic route.

The Sonogashira reaction is one of such metal catalysed reactions, which is used to form carbon-carbon bonds between terminal alkynes and either vinyl or aryl halides. The reaction

usually uses a combination of a palladium catalyst and a copper catalyst, and the couplings can usually be achieved using mild conditions, and are often carried out at ambient temperature (Figure 67).[185]
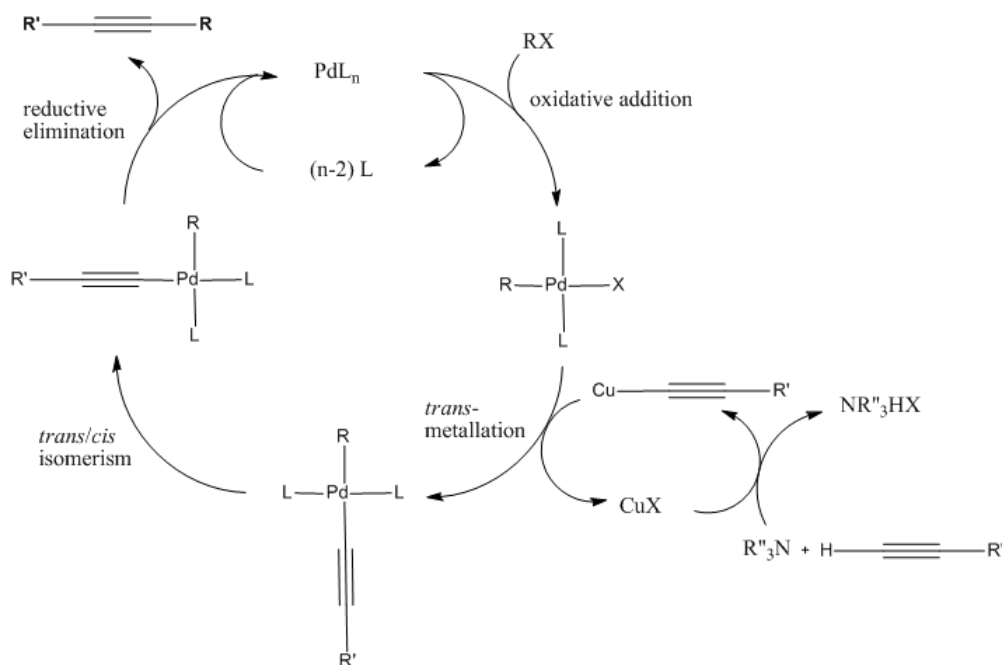
Figure 67. Sonogashira reaction catalytic cycle, involving both palladium and copper[185]

The first key step of the Sonogashira reaction involves insertion of palladium into the halogen-containing species, and parallel insertion of copper into the species containing the triple bond. *Trans*-metallation followed by *trans*/*cis* isomerism and reductive elimination results in the formation of the desired alkyne, as well as catalytic formation of the original palladium species.

As mentioned, **DIBOD,** or 'SPDC' reagent may be considered useful in a pretargeting setting. For this reason, a one-step synthetic procedure to synthesise this type of compound could be a valuable contribution to the field, and could allow for the synthesis of more suitably functionalised analogues *via* a robust and straight-forward route. In a *retro*-synthetic manner, it can be imagined that **DIBOD** could be prepared *via* two identical Sonogashira coupling reactions, whereby two alkynes react with two halogens through metal catalysis in order to construct the dialkyne core (Figure 68).

Figure 68. Reterosynthesis of the dialkyne **DIBOD** *via* two different 'dual' Sonogashira reactions (routes a and b)

This transformation would either be achieved by having both halogens on one aromatic ring (**41**), and having both of the acetylene functional groups on the other (**42**) (Route A, Figure 68); or, it could be envisioned that two equivalents of an α–halogen substituted phenyl acetylene **43** may be reacted together in a similar manner (Route B, Figure 68).

It was first necessary to synthesise the acetylene precursors that would be required for carrying out the Sonogashira coupling reactions. Two silyl protected acetylene analogues **44** and **45** were synthesised from commercially available 1,2-diiodobenzne **41**, using a Sonogashira coupling with varying equivalents of trimethylsilyl acetylene (Figure 69).[186, 187]
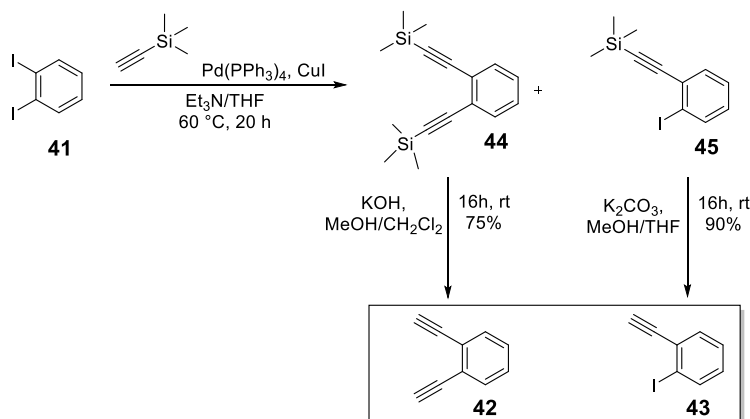
Figure 69. Synthesis of the acetylene precursors **42** and **43** for application to Sonogashira reactions

Dependent upon the number of equivalents of trimethylsilyl acetylene used, and upon the reaction time, the reaction could be adapted to favour either the single Sonogashira product or the double-Sonogashira product, which could be easily separated using column chromatography. The silyl protected compounds **44** and **45** were then deprotected to the free alkynes **42** and **43**, respectively, under basic conditions, and up to 90% yields were

observed for this step, ensuring that care was taken during isolation, due to the volatile nature of these two compounds. The two products were subjected to different Sonogashira reaction conditions, towards the synthesis of the SPDC reagent **DIBOD**. The first attempts towards the 'dual' Sonogashira coupling step were carried out using 2 equivalents of iodo acetylene **43** under standard Sonogashira coupling conditions (Figure 70).
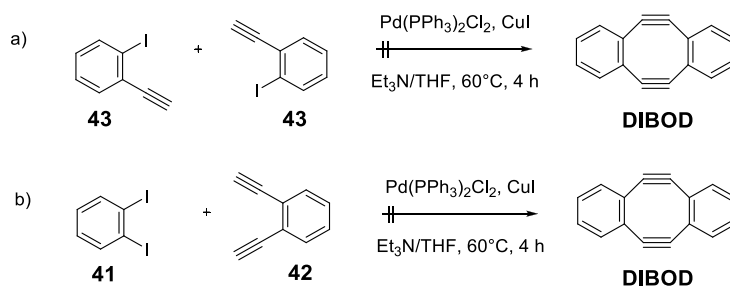
Figure 70. First attempts towards a 'dual' Sonogashira reaction towards the synthesis of **DIBOD** on using palladium and copper catalysts

Complete consumption of the starting material **43** was observed, however **DIBOD** was not formed under these conditions. It was hypothesised that this could be attributed to Glaser couplings due to the presence of Cu(I) salts in the reaction mixture, leading to catalysis of linear diyne products, and this idea was supported by the presence of numerous fluorescent spots on the TLC plate. These products were not easily separable by column chromatography, and therefore full characterisation of these compounds was not carried out. The copper-catalysed reaction was also attempted using the alternative precursors **41** and **42**, as formation of the diyne may be more likely to occur with 2-iodo acetylene **43** than a combination of **41** and **42**; the former may easily react with itself linearly, whereas the second Sonogashira reaction (an intramolecular ring closure) is less favourable. However, the alternative reagents **41** and **42** also showed similar results, showing a large number of inseparable by-products but no desired product. This suggests that formation of the linear diyne by-products is a result of the presence of the copper salts, and is independent of the reactants used. One possible method to overcome the observed formation of the linear products was to use the silyl-protected alkyne precursors, and to generate the 'free' alkyne *in situ*.[188] The reaction was carried out in two steps; first adding the palladium catalyst, and

subsequently adding the copper after 20 min, in order to try and avoid the formation of the Cu(I) salts (Figure 71).
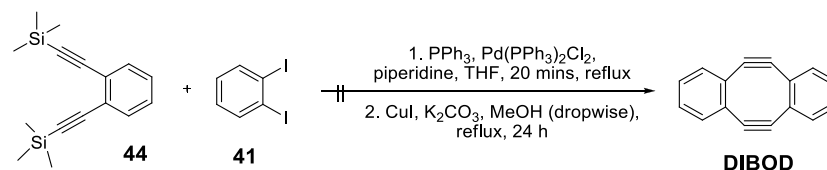
Figure 71. Attempted Sonogashira reaction using protected dialkyne **44** towards the synthesis of the SPDC reagent **DIBOD**

This was initially attempted under reflux, whereby methanol was added dropwise to the mixture in order to generate the 'free' alkyne slowly. This resulted in deprotection of the starting materials, but no formation of the desired product was observed, with trace amounts of the diyne by-products. The reaction was subsequently attempted at lower temperatures (40°C), but this resulted in poor deprotection of the starting material, and no Sonogashira products.

It was therefore envisaged that using a copper-free method for the Sonogashira coupling step might result in fewer side reactions, and would not require deprotection *in situ*. A number of copper-free 'Sonogashira'-type conditions have now been described in the literature in order to try and circumvent the problems associated with formation of the undesired diyne products.[189, 190] The one which was chosen to be applied to this synthesis relied on gold(I) iodide as catalyst and dppf as a ligand (Figure 72).[190]
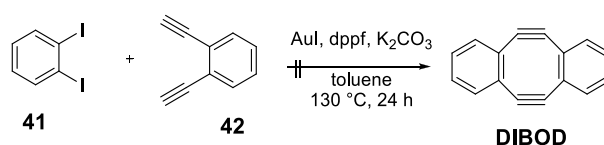
Figure 72. Attempted Sonogashira reaction using gold catalysis, towards the formation of the SPDC reagent **DIBOD**[190]

These conditions were initially tested with precursors **41** and **42**, and the mixture was stirred at 130°C for 24 h. After filtration of the reaction mixture, only 1,2-diiodobenzene **41** was isolated, and no other compounds were visible by TLC. It was found that diacetylene **42** is volatile (bp = 80°C) and therefore the reaction was repeated in a sealed pressure tube in order to avoid any loss of the starting material from the reaction mixture. The reaction was also carried out at higher dilution, in the hope that this would aid the second intramolecular

Sonogashira reaction over the competing linear reactions. TLC analysis after the reaction was carried out under these conditions indicated that no reaction had occurred.

Due to the difficulties in obtaining **DIBOD** using this method, it was deduced that the gold-catalysed reaction conditions would be tested on some standard reagents, which had been reported as being able to form the Sonogashira products under these conditions.[190] The chosen reaction conditions were subsequently applied to different starting materials, in order to validate the reaction conditions for carrying out a 'simple' Sonogashira coupling (Figure 73).[190]
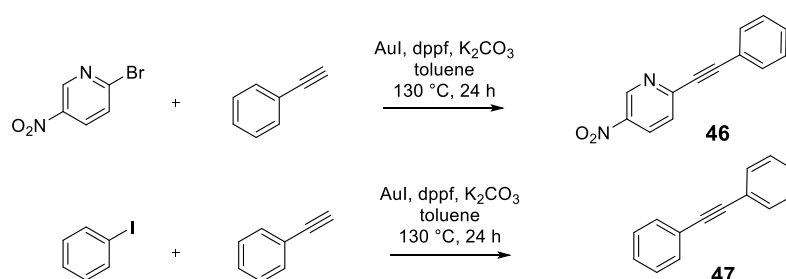
Figure 73. Validation of the Sonogashira reaction conditions using gold catalysis

These reactions were both complete after 24 h under reflux, and the crude products **46** and **47** were isolated and characterised. This result suggests that the conditions are suitable for carrying out simple Sonogashira couplings, and that it is the nature of the product that is preventing from the reaction from occurring in the case of the transformation shown in Figure 72.

Therefore, future work could include activating the aromatic rings to make them more reactive towards the Sonogashira coupling reaction. Additionally, different catalyst loadings and concentrations could be investigated, which might result in preferential formation of the desired product over the 'linear' Sonogashira products. Alternative catalysts may also be considered, which also do not involve the use of copper as a co-catalyst, and could result in a higher probability of the second intramolecular Sonogashira reaction occurring towards the formation of the SPDC reagent **DIBOD**.

2.4.3 Conclusions

It is possible that through further optimisation, this type of double Sonogashira coupling reaction could allow for preparation of a number of symmetrical cyclooctynes such as **DIBOD**. However, due to the low observed reactivity in the SPAAC reaction, it may also be necessary to increase the hydrophilicity of this type of compound, for example through the addition of methoxy groups onto the aromatic ring, in order to make them more suitable for a pretargeting application (see Chapter 3).[106, 151]

2.5   Overall Conclusions

In general, the synthesis of cyclooctynes is challenging, requiring multiple steps, and often in low overall yield. The most reactive cyclooctynes are often the most difficult to synthesise, which may be attributed to the introduction of further strain into the 8-memebered ring.[125] Subsequently, the final step of the synthesis, which involves introducing this strain, is usually the most demanding.[106, 109] For this reason, we sought to find an alternative method for the synthesis of such cyclooctynes, for example using Sonogashira-type reactions, which could potentially allow access to a range of functionalised cyclooctyne structures in only a few steps. It may be possible to optimise these conditions towards the synthesis of analogues of the SPDC reagent, and potentially alternative metal-catalysed reactions (for example Heck and ring-closing metathesis (RCM)) could be considered towards similar structures.

Sufficient material was obtained of each of the literature cyclooctynes to take forward into the hypothesised SPAAC reaction, and the application of these compounds is discussed in detail in chapter 3. The recent development of more water-soluble cyclooctynes, which may be synthesised in a few steps, has additionally led to the commercial availability of such compounds, and these may be considered as alternatives for application to *in vivo* applications such as pretargeting (see chapter 3).[176]

Chapter 3 - Evaluating the SPAAC Reaction

for Pretargeting

3.1 Radiolabelled SPAAC Reaction between Cyclooctynes and [^{18}F]FEA

3.1.1 Hypothesis for an ^{18}F-labelled SPAAC Reaction

In order to validate the SPAAC reaction between cyclooctynes and azides in the context of pretargeting, a radiolabelled version was developed. The radiolabelled partner (or chemical reporter) in this reaction was chosen to be the azide, as cyclooctynes have been reported to demonstrate poor physicochemical properties, including high lipophilicity and potential binding to murine serum albumin (MSA).[114, 155]

The purpose of the planned study was to determine which cyclooctynes are most reactive towards our radiolabelled azide, and ultimately which would be most suitable for application to a pretargeting strategy for PET, which would involve attaching the cyclooctyne to a suitable targeting biomolecule. Six literature cyclooctynes were chosen for carrying out the radiolabelled SPAAC reaction, and these were chosen based upon the different levels of reactivity that were displayed by these compounds previously in the SPAAC reaction with azides (Figure 74).
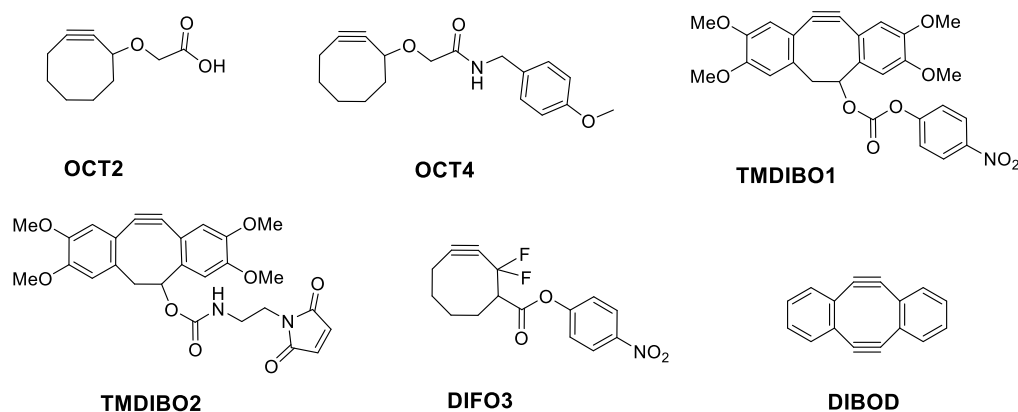
Figure 74. The six cyclooctynes used in the radiolabelling study

The first two cyclooctynes are derivatives of the first-generation OCT reagents; **OCT2** contains a carboxylic acid side-chain, whereas **OCT4** has been modified with an amide functional group (see section 2.1).[113, 126] These compounds are expected to demonstrate the lowest overall reactivity in the SPAAC reaction with azides, as discussed in chapters 1 and 2.[113]

The second class of reagents are analogues of the TMDIBO structure developed by Leeper *et al.*, containing a *p*NP carbonate side-chain (**TMDIBO1**), and a maleimide (**TMDIBO2**), respectively.[191] These compounds show improved reactivity over the first-generation cyclooctynes due to the introduction of further strain (a result of the addition of two aryl rings onto the ring), and improved water solubility over dibenzocylooctynes (**DIBO**) due to the addition of four methoxy groups onto the aromatic rings (see section 2.3).[127]

DIFO3 is a derivative of the difluorinated cyclooctyne, which was originally developed by Bertozzi, and was synthesised *via* a modified procedure as reported by Leeper *et al.*, incorporating a *p*NP carbonate side-chain.[55, 178] These cyclooctynes are expected to show improved reactivity over OCT reagents with azides, as the fluorine atoms adjacent to the alkyne moiety act as electron-withdrawing groups, enhancing the reactivity of the triple bond towards cycloaddition reactions (see section 2.2).

The final compound used in this study was the SPDC reagent **DIBOD**, which was developed by Hosoya and co-workers. This compound is reported to be able to react with two azide molecules (see section 2.4).[181]

3.1.2 Evaluation of the ^{18}F-labelled SPAAC Reaction

[^{18}F]2-fluoroethyl azide (**[^{18}F]FEA**) may be synthesised *via* a well-established procedure, and is commonly used for radiolabelling prosthetic groups using the CuAAC reaction.[54, 61, 62] **[^{18}F]FEA** was synthesised from tosylethyl azide **48** using the method of Glaser *et al* (Figure 75).[62]
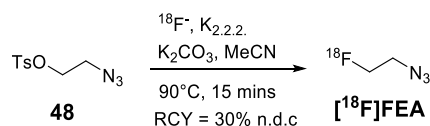

Figure 75. Synthesis of **[^{18}F]FEA**

Tosylate **48** was reacted with a mixture of [^{18}F]fluoride and K[2.2.2] in MeCN under basic conditions, forming the desired labelled **[^{18}F]FEA** in 30% radiochemical yield (RCY), non-

decay-corrected (n.d.c), after distillation.[62]

Each cyclooctyne was subsequently reacted with the radiolabelled azide at 40°C and at 90°C, primarily using MeCN as solvent. The reactions were carried out in a sealed reaction vial (initially for 15 min), and the experiments were repeated at least three times in order to ensure that the results were reproducible.[151] In certain cases, the reactions were carried out for 1 h in order to determine how the reaction proceeds within the time-frame of a PET scan (which is limited by the half-life of ^{18}F), and additionally in water in order to replicate close to physiological conditions.

The relative reactivity of the different cyclooctynes (Entries 1-6) with **[^{18}F]FEA** clearly varied when using different solvents and temperatures. These reactions were monitored by HPLC, and the conversions (%) were determined by the relative proportion of the **[^{18}F]FEA** reference radio-HPLC trace against the ^{18}F-labelled triazole product HPLC traces, which are quoted as the summation of the two regioisomers formed (Table 8).

[18F]49-54

mixture of regioisomers in ratio ~2:1

Cyclooctyne[a]	Entry	Temperature (ºC)	Time (mins)	Solvent	RCY (%)[b]
OCT2	1	40	15	MeCN	4.4
	2	40	15	H_2O	0.3
	3	90	15	MeCN	24.9
OCT4	4	90	15	MeCN	60.4
TMDIBO1	5	40	15	MeCN	7.1
	6	40	15	H_2O	33.3
	7	40	60	H_2O	36.2
	8	90	15	MeCN	31.5
TMDIBO2	9	40	15	MeCN	3.2
	10	90	15	MeCN	9.6
DIFO3	11	40	15	MeCN	62.1
	12	40	15	H_2O	26.1
	13	40	60	H_2O	17.8
	14	90	15	MeCN	97.1
DIBOD	15	40	15	MeCN	0.0
	16	90	15	MeCN	0.8

[a] Each reaction carried out using 50 µL of **[18F]FEA** (typical activity of ~ 5 MBq); *n* = 3 in all cases.

[b]Radiochemical yield as determined *via* radio-HPLC showing conversion of **[18F]FEA** into the summation of the regioisomers.

Table 8. The results of radiolabelling cyclooctynes with **[18F]FEA** under different reaction conditions

As anticipated, **OCT2** showed relatively low reactivity, giving conversions of only 4.4% after 15 min in MeCN at 40°C (Entry 1, Table 8). Significantly higher reactivity was observed at 90°C, producing conversions of 24.9% conversion after 15 min in the same solvent (Entry 3, Table 8). Its lack of reactivity at 40°C (0.3% conversion after 15 min) in water (Entry 2, Table 8) may be attributed to the lipophilic structure of the first-generation cyclooctynes, which had not been developed in terms of their physicochemical properties (see chapter 2). The relatively low overall observed reactivity towards the azide is not entirely surprising, as **OCT2**

has reportedly lower reaction kinetics in the SPAAC reaction than the cyclooctynes developed later (k = 1.3×10^{-3} $M^{-1}s^{-1}$).[57, 113]

OCT4 showed improved reactivity over **OCT2**, and introducing an amide side-chain increased its reactivity at 90°C in MeCN (Entry 4, Table 8) by more than two-fold (60% *vs.* 25% conversion after 15 min), suggesting that addition of a side-chain may enhance its reactivity towards azides. This result is promising, as it demonstrates the feasibility of introducing a different functional group onto the cyclooctyne structure without interfering with the reactivity of the compound, and it can be imagined that a biologically active molecule may be introduced in a similar manner. It could be anticipated that the introduction of an antibody could, in addition, significantly improve the solubility of these first-generation cyclooctynes in water, and therefore will not prohibit these as potential compounds for use *in vivo*.

TMDIBO1, showed lower reactivity than **DIFO3** in MeCN at 40°C, giving conversions of only 7% after 15 min (Entry 5,Table 8), and at 90°C the conversion to the triazole products was only improved to 31.5% (Entry 8, Table 8). In contrast, this compound showed slightly enhanced reactivity in water, giving conversions of 33% after 15 min (Entry 6, Table 8) *vs.* 26% conversion for **DIFO3** (Entry 12, Table 8) under the same conditions. The reactivity was not compromised at a longer time-point of 1 h, showing conversions of 36% (Entry 7, Table 8).

Pleasingly, it was observed that **TMDIBO1** was particularly stable in aqueous media, and no decomposition products were observed over 1 h when the reaction was carried out in water at 37°C. These results suggest that **TMDIBO1** may be a potential compound for application to the pretargeting strategy, showing more promising reactivity and stability in solvents and temperatures that are closer to physiological conditions.[178] It should still be noted, however, that the highest radiochemical yield observed using this compound was 36%, and these yields may not be achievable at very low reaction concentrations such as those found *in vivo*.

Replacement of the *p*NP-carbonate in **TMDIBO1** with a maleimide substituent, to form **TMDIBO2** compromised some of its reactivity in MeCN (Entries 9 and 10,Table 8) at both 40°C (3% *vs.* 7% conversion after 15 min) and at 90°C (10% *vs.* 35.5% conversion after 15 min), which could be a result of an increase in flexibility of the side-chain as compared to the carbonate linker, potentially causing an increase in the steric bulk onto one side of the molecule. The maleimide functional group is a useful handle by which to incorporate the cyclooctyne onto a biomolecule through a thiol moiety (see section 3.2.1), and it is hoped that this compound will maintain its reactivity with azides even when substituted with a much larger group.

**DIFO3** showed the highest overall levels of reactivity in the SPAAC reaction with **[^{18}F]FEA**, especially when the reactions were carried out in MeCN. At the higher temperature of 90°C, almost quantitative conversions were observed within 15 min (Entry 14, Table 8). At 40°C not much of the reactivity was compromised, showing conversions of 62% within 15 min (Entry 11, Table 8) (Figure 76).
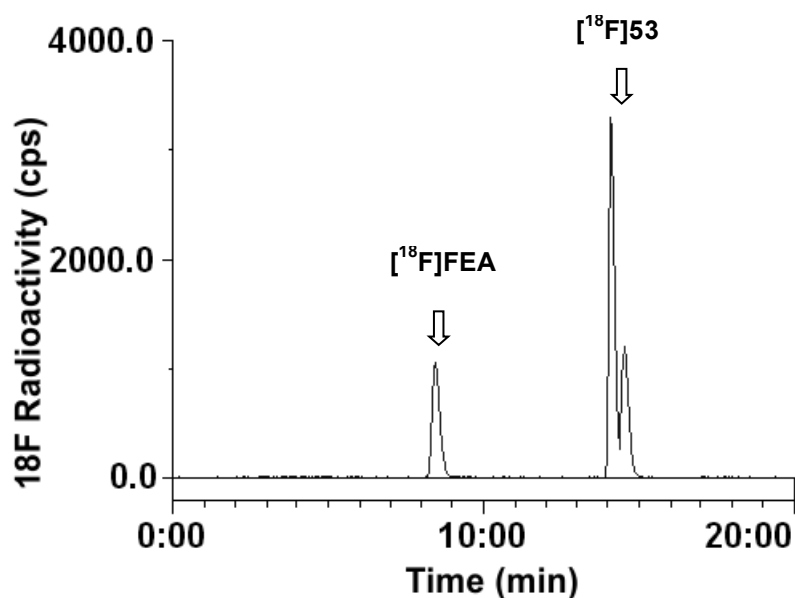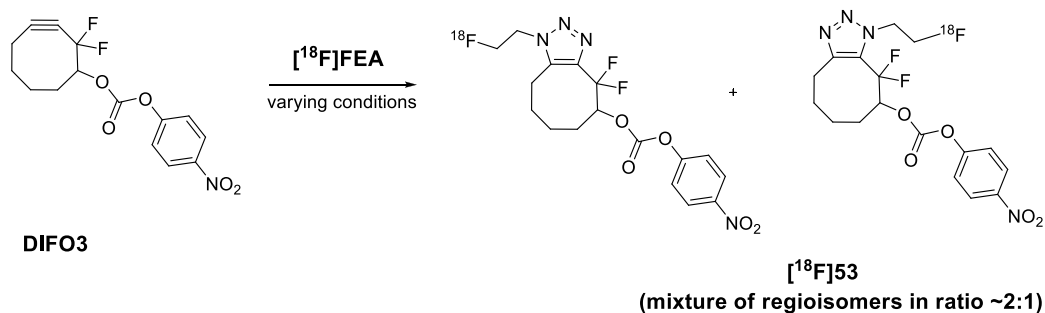
Figure 76. Reaction of **DIFO3** with **[¹⁸F]FEA** to form the triazole regioisomers and example radio-HPLC trace at 40°C in MeCN after 15 min

Conversely, when the reaction with **DIFO3** was carried out in water, a greater than two-fold drop in reactivity was observed, giving conversions to the triazole regioisomers of only 26% (Entry 12, Table 8), owing in part to the formation of many decomposition products. Bertozzi and co-workers previously observed similar results when the cycloaddition reactions of fluorinated cyclooctynes (**MOFO**) were carried out in aqueous media (Figure 77).[113]
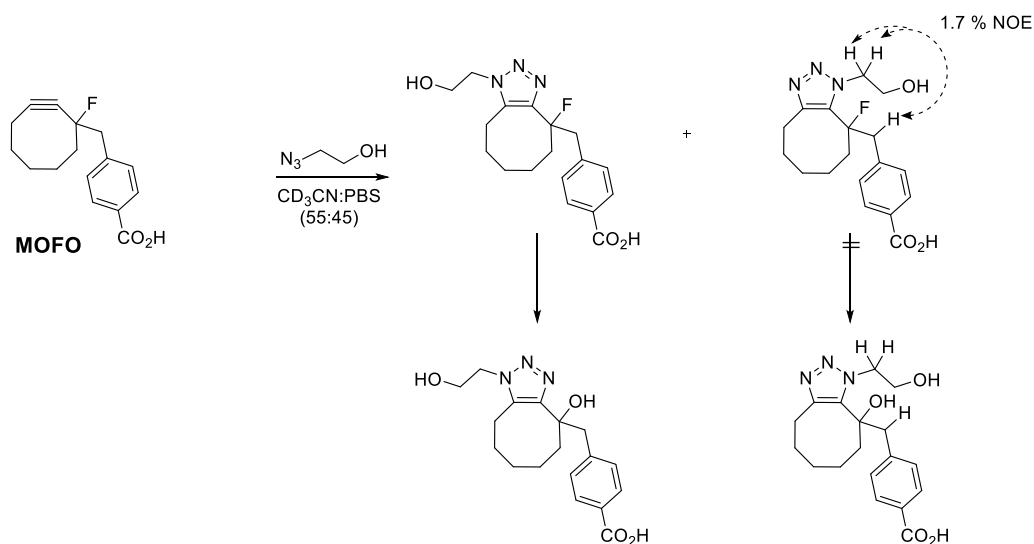
Figure 77. The deflourination reaction observed by Bertozzi *et al*. of the mono-fluorinated cyclooctyne **MOFO**[113]

Bertozzi *et al*. attributed this observation to the displacement of fluorine by a hydroxyl group in the least sterically hindered of the two triazole regioisomers, which was confirmed by characterisation of the products formed by mass spectrometry.[113] It was subsequently concluded that with the fluorinated cyclooctynes, the reaction was non-ideal in aqueous media at longer-time points such as those used in PET experiments, as this led to the formation of a greater number of decomposition products.[114]

Surprisingly, the SPDC reagent **DIBOD** did not show any of the previously observed reactivity in the SPAAC reaction when carried out in MeCN at 40°C after 15 min, showing no observed conversion to the triazole products (Entry 15, Table 8).[181] This lack of reactivity may be a result of poor solubility of the cyclooctyne in the solvents used, or compound decomposition over the time frame of the experiment, as this cyclooctyne has lower reported stability than the other cyclooctynes.

3.1.3 Synthesis of the 'Cold' Reference Compounds

The synthesis of 2-fluoroethyl azide (**FEA**) was carried out in order to make the reference triazole compounds with each of the cyclooctynes (Entries 1-6, Table 8) used in the radiolabelling study (Figure 78).[62, 192]
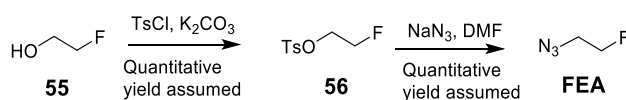
Figure 78. Synthesis of **FEA** from 2-flouroethanol **55**

This first involved tosylation of 2-fluoroethanol **55**, which proceeded at ambient temperature in 12 h. The next step was to form **FEA** from the tosylate **56** using sodium azide. This reaction was monitored by TLC and was complete after 24 h at ambient temperature. After this time, the white precipitate formed was filtered off and the crude filtrate was used for the copper-free 'click' reactions with each of the cyclooctynes, as it has been reported that isolation of **FEA** may result in an explosion.[62] All of the cyclooctynes used in the radiolabelling study were reacted with **FEA** in CDCl₃, by heating to 40°C for 2 h (Figure 79).
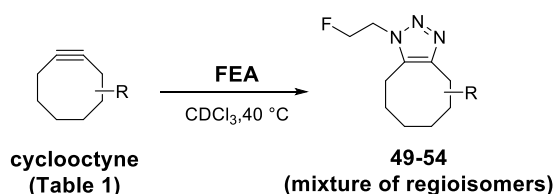
Figure 79. Reaction of the cyclooctynes (Table 8)

The resulting reaction mixtures were concentrated *in vacuo* in order to remove any excess **FEA**, as this compound is volatile, and the crude compounds were re-dissolved in CDCl₃ for NMR analysis. Initial confirmation that the reactions had occurred was obtained by examination of the ^{19}F NMR spectra of these crude mixtures, which indicated the presence of the triazole fluorine substituents at δ_F ~-225 ppm. The ratio of regioisomers could additionally be determined as the two regioisomeric triazole fluorine peaks are clearly separated by their relative chemical shifts (δ_F). Further proof that the triazoles had been formed was obtained by ^{1}H NMR, HRMS and HPLC analysis and by ^{13}C NMR analysis when possible (see experimental section for further details and for example spectra).

Each of the 'cold' reference compounds was used to confirm the identity of the products formed in the radiolabelled SPAAC reaction with **[^{18}F]FEA**, by comparing the retention times of the HPLC UV trace with the radio-HPLC trace of the ^{18}F-labelled compounds (see experimental section).

3.1.4 Conclusions

In conclusion, the radiolabelled SPAAC reaction between **[^{18}F]FEA** and the six cyclooctynes used in this study gave a good overview of the ability of these reactions to be carried out under different conditions of solvent, temperature and duration.[151] The early-generation cyclooctynes (Entries 1-4, Table 8) as expected, showed relatively low conversion to the triazole regioisomers, as compared to the more developed cyclooctyne structures, **DIFO3** and **TMDIBO** (Entries 5-14, Table 8).

The optimum conditions for carrying out the SPAAC reaction were in MeCN, and required elevated temperatures in order for the reaction to proceed efficiently. Using media that replicates *in vivo* conditions, such as using water and longer reaction times, resulted in lower conversions, or decomposition in the case of the fluorinated cyclooctyne **DIFO3**. However, in some cases this may be considered to be a result of the poor water solubility of these compounds, and should not hinder their application to pretargeting, as attaching to a large biomolecule such as an antibody would be expected to greatly enhance the solubility of the cyclooctynes. The **TMDIBO1** construct was to be taken forward to *in vivo* studies, as this derivative displayed the most optimal combination of stability and reactivity in the reaction with **[^{18}F]FEA** in water at 40°C, over a time-point of 1 h. In addition, a cell viability assay was carried out in HCT116 human colon cancer cells, and no toxicity of **TMDIBO1** was observed at concentrations up to 100 mM (see experimental section for further details).

3.2   Evaluation of [^{18}F]FEA as a Chemical Reporter

3.2.1 Introduction to [^{18}F]FEA as a Potential Chemical Reporter

Based on the results obtained from the ^{18}F-labelling, it was hypothesised that the most promising cyclooctyne could be ligated to a chosen biomolecule, and applied to a pretargeting strategy using **[^{18}F]FEA** as the radiolabelled 'tag'. Due to the reasonable reactivity demonstrated by the most reactive cyclooctynes (in particular **TMDIBO1**), we decided to apply the SPAAC reaction in our pretargeting strategy *in vivo* (Figure 80).
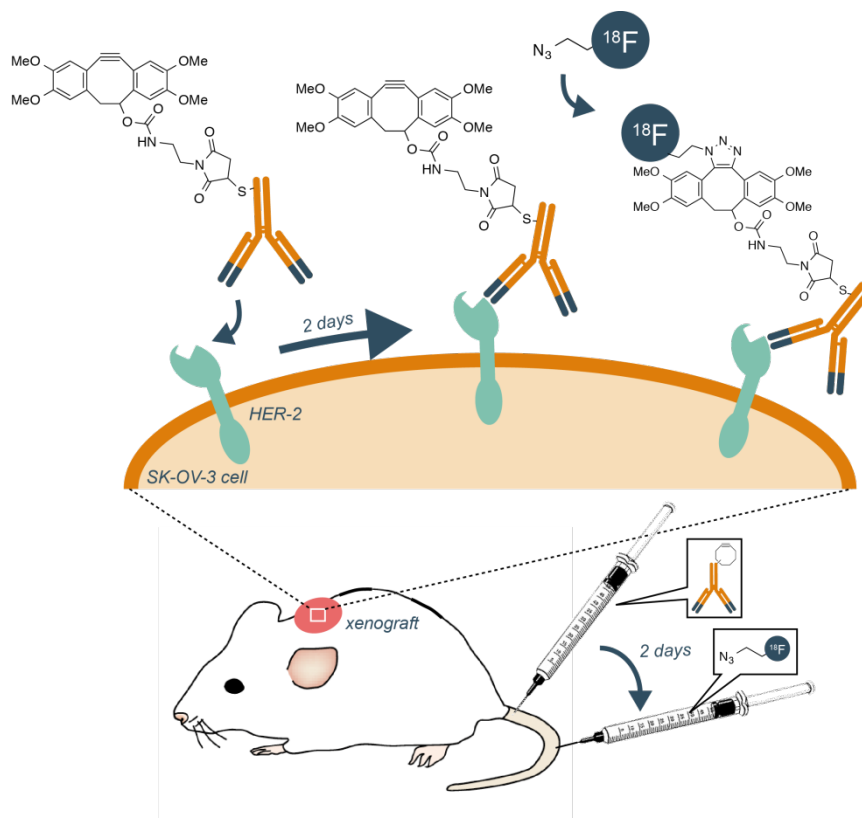
Figure 80. The SPAAC reaction as applied to the proposed pre-targeting strategy

Prior to attempting the *in vivo* SPAAC reaction, it was necessary to validate **[^{18}F]FEA** as a potential radiolabelled pull-down reagent or 'tag', by predicting and evaluating the behaviour of the compound *in vivo*.

3.2.2 Measuring the Log*P* of [^{18}F]FEA

For a pretargeting application, it is important that **[^{18}F]FEA** reaches the site at which the biologically active molecule containing the cyclooctyne is localised. This is essential for the reaction to occur *in vivo*, and for the targeted tissue to be imaged successfully in contrast to the background tissue. One method which will aid prediction of the fate of the azide *in vivo* is by measuring its Log*P*.

The value of Log*P* is an important consideration when designing a radiotracer, as the relative hydrophilic *vs.* hydrophobic properties have a large influence on the tracer's, absorption, distribution, metabolism and excretion (ADME).[193] For example, highly hydrophilic compounds are more prone to plasma protein binding and will not cross the cell

membrane, but very hydrophobic compounds often suffer from poor absorption. It is consequently important that a correct balance is achieved and that Log*P* is considered when designing a radiotracer.

Log*P* can be measured experimentally by observing the relative distribution of the compound in a mixture of *n*-octanol and water.[194] Hydrophilic molecules will prefer the aqueous phase, whereas more hydrophobic molecules will dissolve more readily in the organic layer. The partition coefficient (*P*) is a measure of the concentration of the tracer that is dissolved in the *n*-octanol layer relative to the aqueous layer, and therefore a very hydrophobic compound will have a high partition coefficient, and consequently the Log*P* scale is a measure of the hydrophobicity of a tracer. The Log*P* value of **[¹⁸F]FEA** was measured using this method, and the average value was found to be -0.44 (Table 9).

[Octanol]	[Aqueous]	Partition coefficient (*P*)	Log*P*
236.4	679.3	0.35	-0.46
279.4	739.1	0.38	-0.42
267.3	721.0	0.37	-0.43
198.8	587.7	0.34	-0.47
266.0	665.6	0.40	-0.40
		Average Log*P*=	**-0.44**

Table 9. Calculating the log*P* of **[¹⁸F]FEA**

This value suggests that **[¹⁸F]FEA** is relatively hydrophilic, but tracers such as [¹⁸F]FDG also have similar measured Log*P*s (Log*P* = -0.67).[195] This implies that although the azide has a slightly lower than ideal Log*P*, it does not inhibit the use of **[¹⁸F]FEA** as a radiotracer. It should be noted, however, that the azide was shown to be relatively volatile, and evaporation may have affected the outcome of the Log*P* determination.

3.2.3 *In vivo* Biodistribution of [¹⁸F]FEA

We planned to evaluate the behaviour of the azide *in vivo* prior to attempting pretargeting.[151] Therefore, we injected **[¹⁸F]FEA** into normal Balb/c mice (*n* = 3), enabling the biodistribution of the compound to be observed and to test for any associated toxicity. This would enable us

to determine the level of background radiation due to the distribution of the azide alone, which could be expected when applying the SPAAC reaction *in vivo*. This study generally showed that the radiotracer distributed evenly throughout the tissues, but that a small accumulation occured in the liver and bone joints (Figure 81).
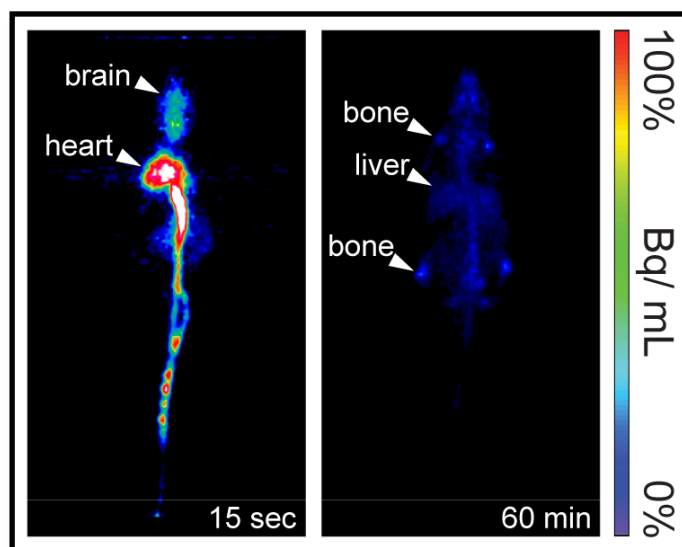
Figure 81. *In vivo* Biodistribution of [18F]FEA* Representative small animal PET images of a Balb/c nude mouse at: t = 15 sec and t = 60 min after intravenous injection in the tail of 3.7 MBq of **[18F]FEA**. *In vivo work was carried out by Dr Quang-De Nguyen.

The image suggests a small amount of elimination to the [18F]fluoride anion, due to accumulation in the bone, however this is only observed in small amounts relative to the initial injection. A decrease in the overall amount of radiotracer in the animal was observed over the 60 min time-course of the experiment, possibly attributable to the volatile nature of this compound, but perhaps also caused by bodily excretion. The azide was found to be stable in PBS (pH = 7.4), MeCN and DMSO for up to 6 h at room temperature, and displayed relatively rapid clearance from the body over the 60 min time frame, suggesting that this could initially be a useful azide for the proposed pretargeting strategy. The volatility of this compound, as well as the undesirable Log*P*, may however cause some problems for the long-term use of this azide as the radiolabelled reaction partner.

3.2.3 Conclusions

[^{18}F]FEA demonstrated reasonable *in vivo* biodistribution, showing clearance of the compound from the body within 1 h. The good stability of this compound in different media also makes it attractive as a chemical reporter, as does its demonstrated reactivity with the cyclooctynes used in the radiolabelling study. However, the small size of this compound renders it volatile, making it difficult to handle, and the Log*P* may need to be improved if it were to be used for a wider range of applications. The ease of synthesis of this compound, which could be achieved by an automated process, meant that this azide was used for initial *in vivo* validation of this reaction, and optimisation of the compound would be postponed until required for future studies.

3.3   Attempted *In vivo* SPAAC Reaction Using Her-TMDIBO and [^{18}F]FEA

It was anticipated that the **TMDIBO** structure would be the most suitable cyclooctyne for ligation to a monoclonal antibody, as it demonstrated the most promising combination of stability and reactivity in the SPAAC reactions with **[^{18}F]FEA** (Entries 5-10, Table 8).[113, 126]

Cyclooctynes **OCT2** and **TMDIBO** were therefore conjugated to the Trastuzumab (Herceptin) monoclonal antibody, which would be used to target high HER2 receptor expressing tumours. After 2 days, the cyclooctyne-ligated antibodies were considered to have had enough time to localise at the targeted tissue, and **[^{18}F]FEA** was then to be injected, allowing for the SPAAC reaction to occur at the HER2 target (*cf.* Figure 80). The distribution of ^{18}F within the whole body would then be monitored over a time point of 60 min, with the intention that the SPAAC reaction would occur specifically in the tumour, allowing for effective visualisation using PET imaging, with minimal background signal.

3.3.1 Introduction to Herceptin as an Antibody for the HER2 Receptor

Herceptin is a monoclonal antibody (mAb) which is used to treat particular forms of breast cancer, and does so by interfering with the HER2/*neu* receptor.[196, 197] The Human Epidermal Growth Factor Receptors (HER1, HER2, HER3 and HER4) are responsible for regulating

cell growth and survival, adhesion, migration and differentiation, as well as other cellular responses. Amplification of the HER2 gene is observed in 20-30% of early stage breast cancers, leading to an over-expression of the receptors in the cell membrane and uncontrolled proliferation of the cells. Herceptin contains two antigen-specific sites that bind to the extracellular domain of the HER2 receptor.

As discussed (see chapter 1 – Introduction), antibodies have desirable characteristics for targeting tumours, including a high specificity and affinity for the targeted receptor. Herceptin is one of such monoclonal antibodies, and could therefore be used to target cells over-expressing the HER2 receptor.[196] The long circulation time of the antibody, combined with slow clearance means that it would be difficult to use such an antibody for direct labelling using short-lived isotopes (such as ^{18}F or ^{68}Ga), for use as a radiotracer, and traditionally this may only be achieved using long-lived isotopes (for example ^{111}I).[198] The pretargeting strategy may be used to overcome some of these limitations by separating the delivery of the antibody with that of the radionuclide. Additionally, Herceptin was considered as a suitable antibody for pretargeting as it is not rapidly internalised into the cell, which is a common problem when separating the delivery of the antibody with that of the chemical reporter.

### 3.3.2 Synthesis of Herceptin-Ligated Cyclooctynes

In order to conjugate the two cyclooctynes **OCT2** and **TMDIBO1** to Herceptin (which has a molecular weight of approximately 145 kDa) it was necessary to introduce a suitable linker to each of the compounds that would allow a point of attachment to the protein. The maleimide group was chosen as a suitable linker group as this can specifically react with free thiol groups in the antibody to form a stable carbon-sulfur bond. **OCT2** and **TMDIBO1** were both reacted with *N*-(2-aminoethyl) maleimide **57** under amide coupling conditions to form the maleimide-substituted amides **OCT5** and **TMDIBO2** respectively. (Figure 82).[199]
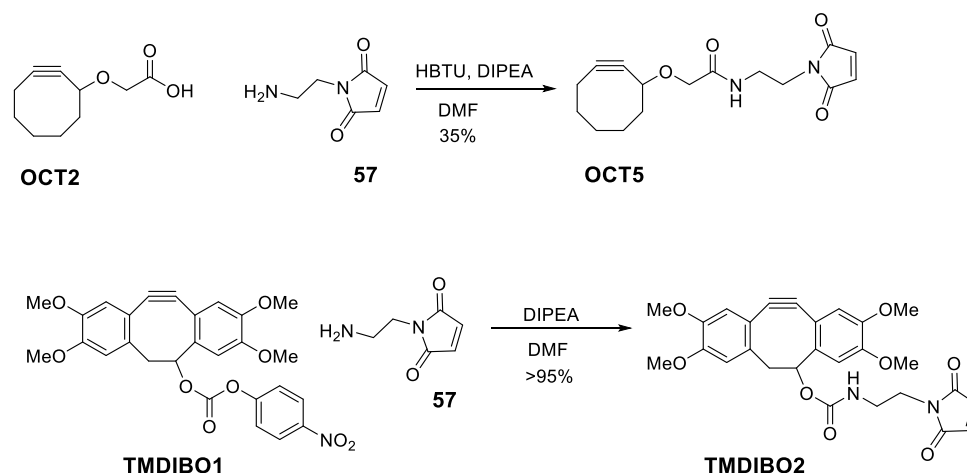
**Figure 82.** Coupling of **OCT2** and **TMDIBO1** to introduce a maleimide linker

HBTU was used as the coupling agent for the synthesis of **OCT5**, in order to introduce an active ester (Scheme 28), however the *p*NP-carbonate group on **TMDIBO1** allowed for the reaction to occur without the aid of a coupling agent.[178]

Herceptin, as well as a control antibody, Immunoglobin (IgG$_1$), (which possesses a similar size to Herceptin, but lacks specificity to the Her2 target), were both modified so that they would be reactive towards the maleimide moiety (Figure 83).
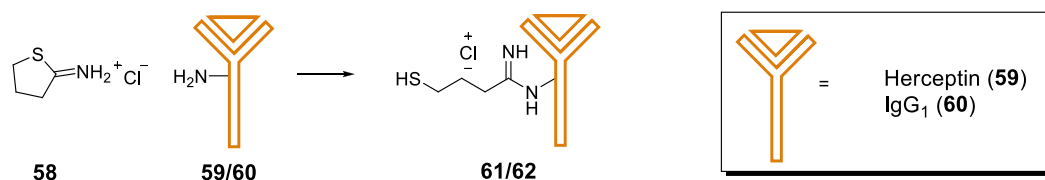
Figure 83. Example of the use of 'Traut's' reagent to introduce thiol groups to free lysine residues onto the Herceptin and IgG$_1$

Traut's reagent (2-imino thiolane) **58** was used to introduce 'free' thiol groups to the antibodies, *via* the available lysine residues.[200] Traut's reagent is highly electrophilic at the tertiary carbon centre, allowing for nucleophilic substitution of the amine and subsequent ring-opening of 2-imino thiolane to form the available thiol group.[201] Use of this reagent also introduces a short linker for attachment to the small molecule, increasing the availability of the thiol towards reaction with the maleimide.

The maleimide-substituted cyclooctynes **OCT5** and **TMDIBO2** were subsequently conjugated to the respective antibodies using the newly formed thiol groups as points of attachment (Figure 84).
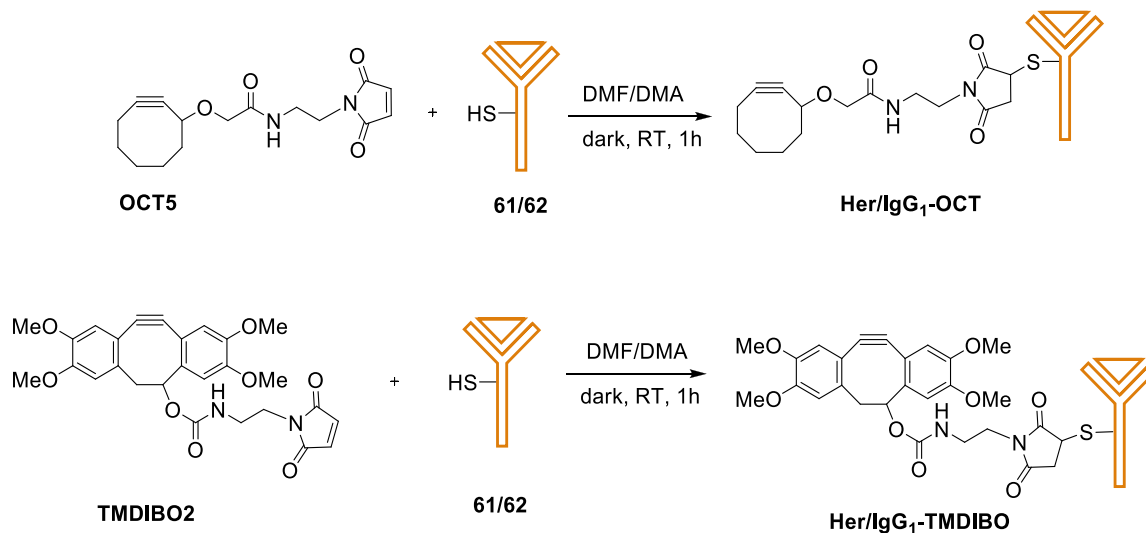
Figure 84. Reaction of thiol-functionalised Herceptin with maleimide-containing **OCT5** and **TMDIBO2**

The conjugated products were purified by passing through a NAP^{TM}-5 column, and were eluted using a sodium acetate buffer. The characterisation of products **Her/IgG$_1$-OCT** and **Her/IgG$_1$-TMDIBO** was carried out by mass spectrometry in order to confirm the number of cyclooctynes conjugated to the antibody. These results indicated that a mixture of 1, 2 and 3 small molecules were attached to each of the antibodies, with 2 being the major isoform. This could be seen by the average difference in mass between the antibody alone and the cyclooctyne conjugated antibody (see experimental section for further details).

The ligated antibodies were tested for their immunoreactivity by western-blot, which showed that the ligated (Herceptin) antibodies were still active towards the HER2 receptor (Figure 85).

SK-OV-3 (1%FBS)
Her, Her-TMDIBO, IgG1-TMDIBO = 40µg.mL^{-1}
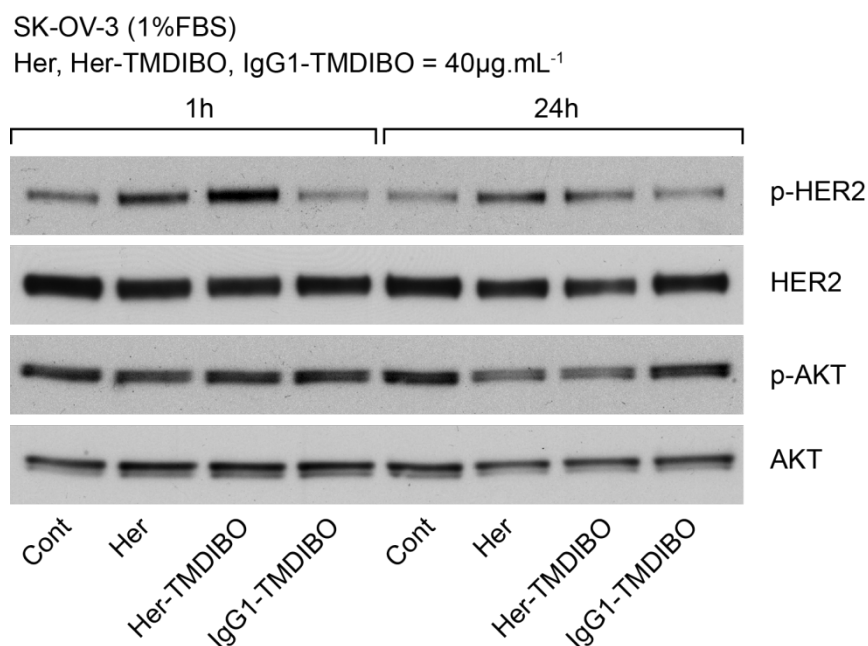
Figure 85. Immunoreactivity assessment of Her-TMDIBO* Human ovarian carcinoma SK-OV-3 cells were incubated in the absence or presence of 40µg/mL Herceptin, Her-TMDIBO or IgG$_1$-TMDIBO for the indicated time. Whole cell lysates were prepared and 30µg processed for immunoblot analysis using primary antibodies against phosphorylated-HER2 (p-HER2), total HER2 (HER2), phosphorylated-AKT (p-AKT), and total AKT (AKT).*Immunoreactivity assessment by western blot was carried out by Dr Quang-De Nguyen.

This data showed that the modified Herceptin and IgG$_1$ antibodies maintained the same levels of affinity for the HER2 receptor as the unmodified antibodies, and a similar level of expression was observed after both the 1 and 24 h time-points. Phosphorylation of HER2 was only observed with the Herceptin antibodies, as expected, and the IgG$_1$ antibody did not activate the receptor. This confirmed the use of each of the antibodies for use in the hypothesised pretargeting model, with the modified IgG$_1$ being used as a negative control.

3.3.4 Attempted Pretargeting Using the SPAAC Reaction

Once the biodistribution of [^{18}F]FEA had been evaluated, and the chemical reporter was confirmed as having a reasonable *in vivo* profile in terms of distribution and clearance, the SPAAC reaction was evaluated in a tumour-bearing mouse model. The mice were treated with SKOV-3 human ovarian adenocarcima (HER2 over-expressing) cells, forming tumours suitable for imaging 14-days post-implantation.

Three main steps were carried out with the tumour-bearing mice, which would validate the pretargeting strategy *in vivo*:

a) Pre-treatment with cyclooctyne-ligated Herceptin (or corresponding negative controls), 48 h before imaging, 100µg in 100µL *i.v.* per mouse.

b) CT/ 60 min dynamic PET imaging, bolus *i.v.* injection of ~3.7MBq (~100µL) **[^{18}F]FEA** per mouse.

c) Post-imaging biodistribution and IHC tumour HER2/*neu* assessment

The main observations from this experiment were that there was a slight increase in uptake in the tumour tissue that was pretargeted with the **Her-TMDIBO** antibody, as compared to the tissue that was treated with the non-ligated cyclooctyne (**TMDIBO1**), or with the vehicle (PBS) (Figure 86).
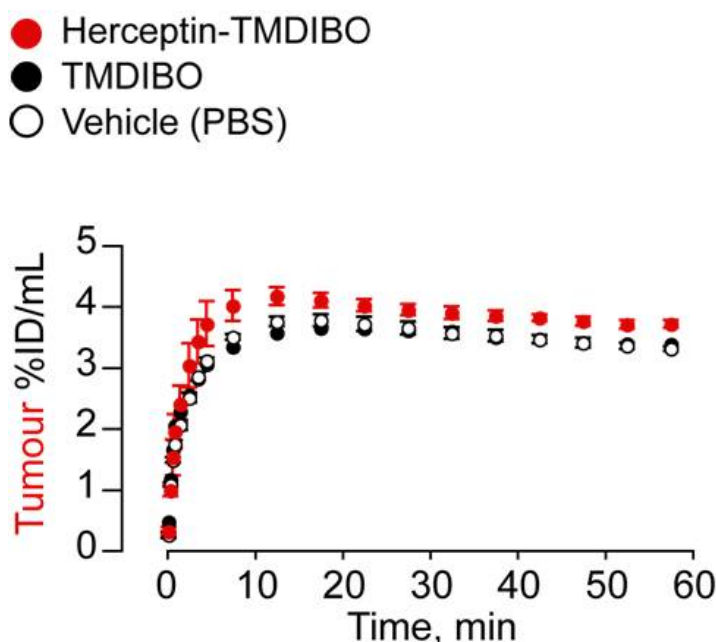
Figure 86. A significant difference in ^{18}F uptake was not observed between control and pretargeted HER2 over-expressing tumours* SKOV-3 human ovarian adenocarcima tumour bearing mice were injected intraveneously with the vehicle (PBS), or with 100µg **TMDIBO1** or **Herceptin-TMDIBO** 48 h prior to bolus *i.v.* injection of ~3.7MBq (~100µL) **[^{18}F]FEA** per mouse. The line graphs show the mean relative uptake (%ID per mL) of ^{18}F in each treatment group. *In vivo work was carried out by Dr Quang-De Nguyen.

Although a difference between the treated and non-treated tissue was observed, this variance was not significant, suggesting that this observation was not solely to the SPAAC reaction occurring in the tumour. This was supported by the fact that a similar pattern was also observed in other tissues, as evidenced from the biodistribution studies (Figure 87).
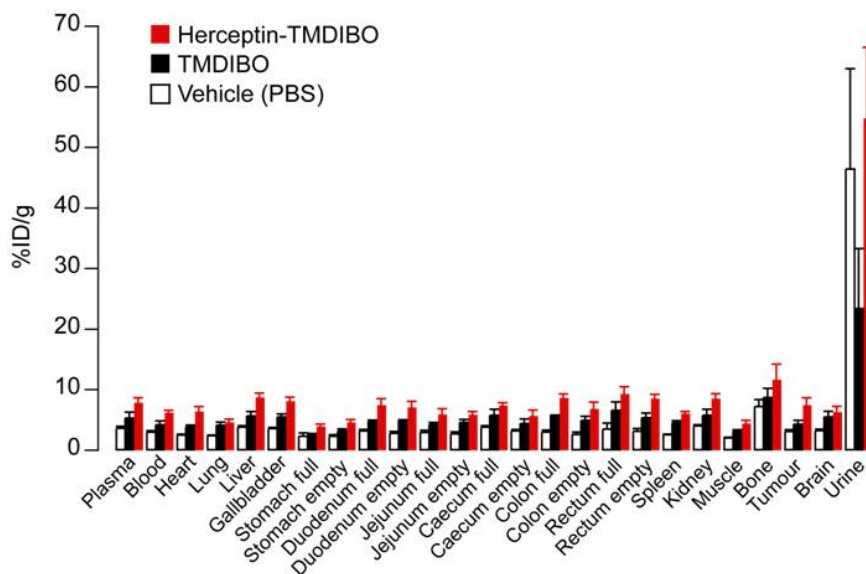
Figure 87. Biodistribution experiment* The uptake of ^{18}F in selected organs of SKOV-3 human ovarian adenocarcima tumour-bearing mice was measured 1 h after intraveneous injection of a) vehicle (PBS) + ~3.7MBq (~100µL) **[18F]FEA** (white bars); b) 100µg **TMDIBO1** + ~3.7MBq (~100µL) **[18F]FEA** (black bars); c) 100µg **Herceptin-TMDIBO** + ~3.7MBq (~100µL) **[18F]FEA** (red bars). The bar graphs show the mean relative uptake of [8]F after 1 h in each treatment group. *In vivo work was carried out by Dr Quang-De Nguyen.

The biodistribution data indicated a similar increase in uptake in the pretargeted mouse across all of the tissue types, with a significant accumulation in the bone joints. This showed us that the uptake of ^{18}F in the tumour was not enhanced over the uptake in other tissue, suggesting that unfortunately the SPAAC reaction was not occurring *in vivo* as anticipated, or is at least was not specific for the targeted tissue.

3.3.5 Conclusions

It was concluded that further optimisation of the reaction was required in order to determine whether the SPAAC reaction is achievable *in vivo*. This could require the use of a different cyclooctyne, which would demonstrates a better balance between reactivity in the SPAAC reaction with *in vivo* stability. In addition to the reactivity considerations, it was hypothesised that an alternative azide may be required, which also displays better *in vivo* biodistribution; for example using a less volatile compound, which has an improved Log*P*.

3.4   Kinetic Evaluation of the SPAAC Reaction

The results obtained up to this point seem to suggest that the SPAAC reaction is not fast enough to occur *in vivo*. However, in order to corroborate this reaction, it was determined

that it should be evaluated in terms of the kinetics, and more specifically, that the effect of concentration on the rate of reaction should be considered. Such a study would allow us to determine how effective a given SPAAC reaction would be at concentrations relevant to an *in vivo* experiment. An alternative cyclooctyne was considered at this stage, with the hope that this compound could be applied to a similar pretargeting application for future studies.

3.4.1 Introduction to Aza-Dibenzocyclooctyne (DIBAC) Reagents

The aza-dibenzocyclooctyne (**DIBAC**) was developed by Van Delft and co-workers,[129] with the intention to combine the favourable reaction kinetics in the cycloaddition reaction displayed by dibenzocyclooctyne (**DIBO**) reagents, developed by Boons *et al.*[127], and the improved hydrophilicity of the aza-dimethoxycyclooctyne (**DIMAC**) derivatives synthesised by Bertozzi and co-workers (Figure 88).[202]

Figure 88. The structures of **DIMAC**, **DIBO** and **DIBAC**

The nitrogen moiety on **DIBAC** potentially allows for simple structural modifications to be made, providing a useful point of attachment for side-chains, and therefore might be anticipated to be easily functionalised for attachment to a biomolecule. These compound could additionally be synthesised in 70% overall yield in only five steps, making them desirable cyclooctynes for numerous applications, and for this reason a range of these reagents are now commercially available.

These cyclooctynes have been reported to have superior reaction kinetics (k = 0.31 M^{-1}s^{-1}) in the SPAAC reaction with benzyl azide in CD$_3$OD, as compared to **DIBO** (k = 0.17 M^{-1}s^{-1}) and **DIFO** (k = 0.076 M^{-1}s^{-1}) and reacts approximately 100-fold faster than the hydrophilic **DIMAC** system (k = 3×10^{-3}M^{-1}s^{-1}).[55, 127, 129] This may be explained by the increased strain accruing from the introduction of two aryl rings adjacent to the alkyne and increased

hydrophilicity over the earlier **DIBO** analogues as the result of incorporation of a nitrogen atom into the cyclooctyne ring.[109, 129] Due to the availability of the **DIBAC** reagents, and the fact that these compounds have improved reactivity in the SPAAC reaction, it was determined that these reagents might be more suitable than the earlier cyclooctynes application to pretargeting. In order to validate these compounds thoroughly in this context, the kinetics of these compounds were more extensively evaluated.

3.4.2 Determining the Rate of Reaction of OCT3 and DIBAC Cyclooctynes

The direct comparison between a carboxylic acid-derived **DIBAC** analogue (**DIBAC1**) and **OCT3** (a first generation cyclooctyne), was initially carried out, by measuring the reaction rates of both of these compounds towards benzyl azide. The kinetics of the reaction between **OCT3** and benzyl azide **63** has been measured previously by Bertozzi and co-workers using ^{1}H NMR analysis.[113] This work was repeated in order to validate the method and ensure for the reproducibility of the results. **OCT3**, which was synthesised as described in Chapter 2, was reacted using this method; a 1:1 molar ratio of starting materials was employed with a concentration of 40 mM (Figure 89).
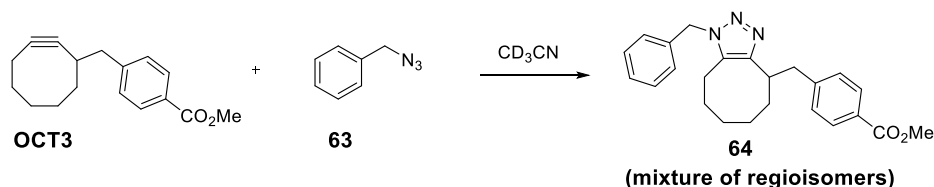
Figure 89. The reaction of **OCT3** with benzyl azide **63**

An NMR tube was treated with a solution containing **OCT3**, to which another solution containing an equimolar amount azide **63** was added. The progress of the reaction was monitored using ^{1}H NMR, at a number of time-points up to 16 h. The first time-point measured was 15 min, followed by 30 min and 1 h, after which measurement was taken every hour up to 8 h after mixing. After 16 h a final ^{1}H NMR was taken, and the relative concentration of azide **63** as compared to the initial concentration was measured at each time-point (Figure 90).
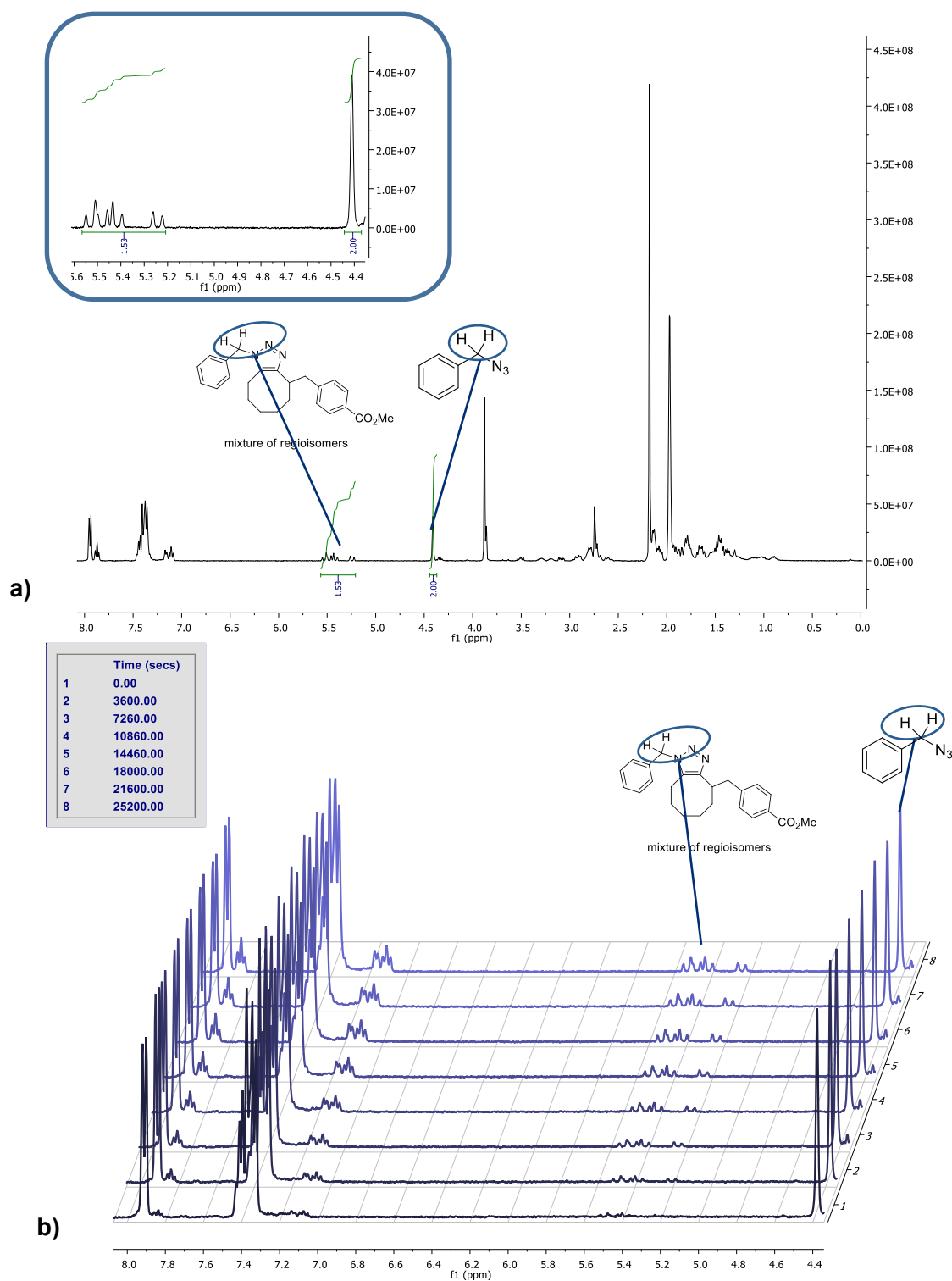
Figure 90. a) Example ^{1}H NMR spectrum of the reaction mixture at 16 h, showing the relative proportion of the starting material protons as compared to the triazole product protons b) A stacked plot of the ^{1}H NMR at different time-points showing the progress of the reaction over time

The concentration of benzyl azide **63** remaining in the mixture was calculated based upon the relative integration of the benzylic protons at δ_H ~4.4 ppm in the starting material, as compared to those at δ_H ~ 5.2-5.6 ppm observed in the regioisomeric triazole products **64**.

The calculation was also confirmed using the integration of other reference peaks, such as the change in integration of the aromatic protons, which also gave similar results. The rate of reaction was calculated using the slope of the line of the graph of 1/[benzyl azide] *vs*. time (Figure 91).
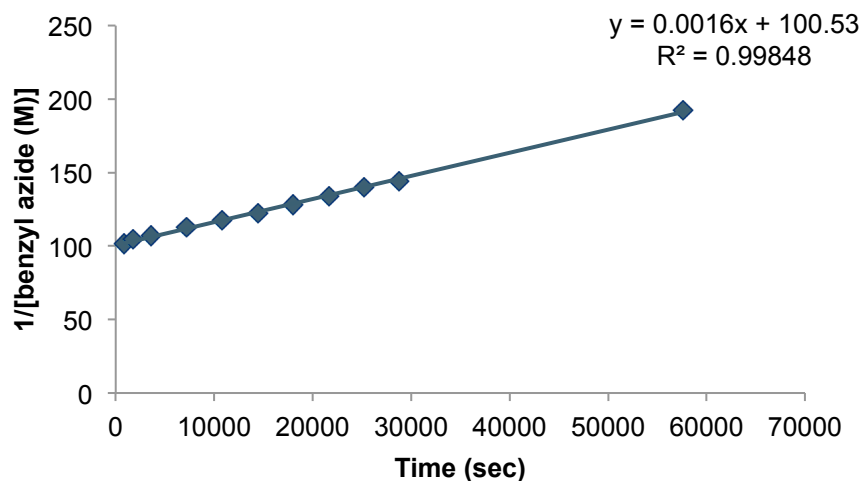
Figure 91. A graph showing time *vs*. 1/[benzyl azide], which was used to calculate the rate constant for the reaction with **OCT3**
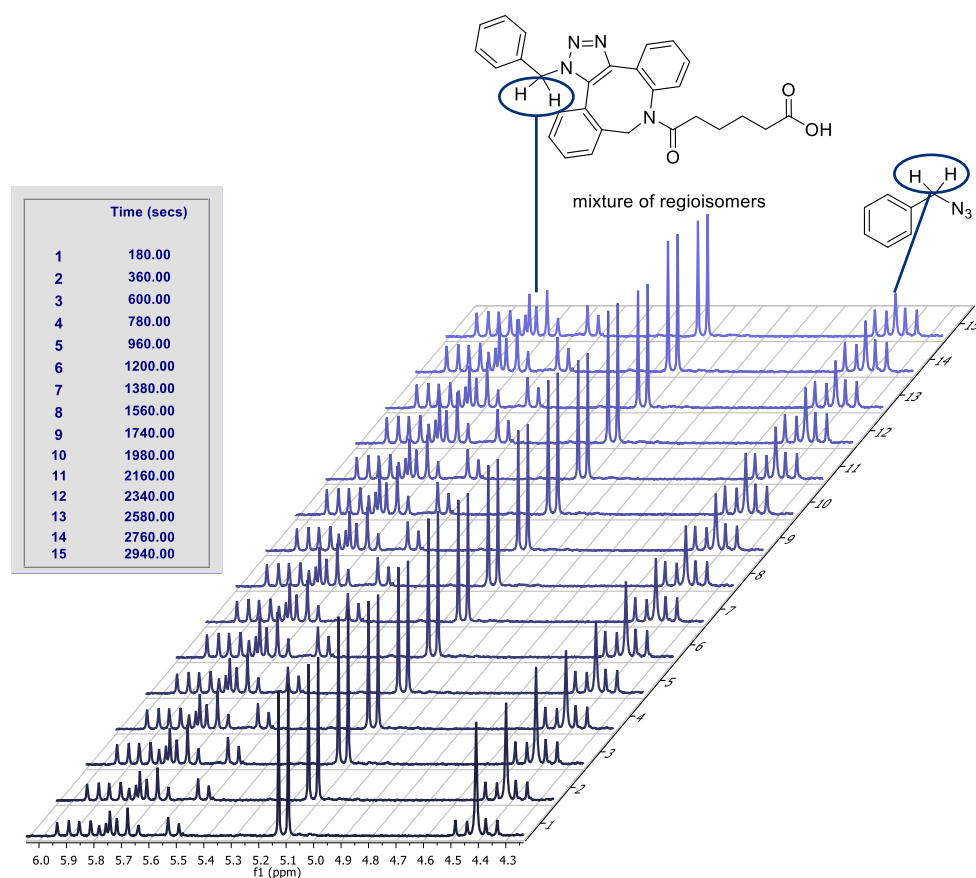
These data were collected three times in order to confirm the reproducibility of the results, and the graph was plotted based upon the average of the three experiments. The average rate of reaction was found to be k = 1.6 x 10^{-3} M^{-1}s^{-1}, which is comparable to Bertozzi's value of k = 1.3 x 10^{-3} M^{-1}s^{-1} for the carboxylic acid analogue of this ester.[113] The same experiment was subsequently carried out using **DIBAC1**, in order to compare a first-generation cyclooctyne to the commercially-available, and reportedly more reactive cyclooctyne **DIBAC1** (Figure 92).[129]
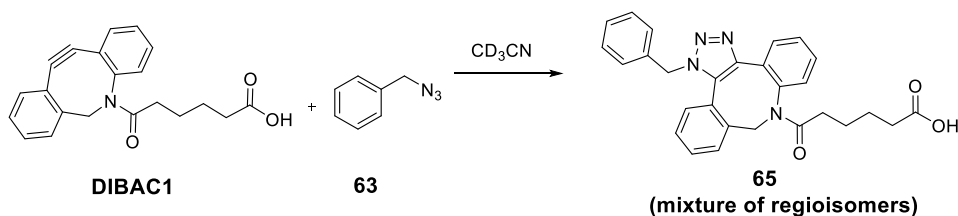
Figure 92. The reaction of **DIBAC1** with benzyl azide **63** in CD$_3$CN, which was monitored by ^{1}H NMR

The reaction was carried out using identical conditions to those used for the reaction of **OCT3** with azide **63**, and it was found that most of the starting material had reacted to form

the triazole regioisomers **65** within 30 min. Therefore, in order to calculate the rate of reaction more accurately, the reaction was carried out again, this time monitoring the mixture at shorter time-points (every 3 min), up to 49 min. The reaction was carried out in triplicate, as with the previous experiment, and the conversion to the triazole products was similarly calculated based upon the relative integration of the benzylic protons (δ_H ~ 4.4 ppm) in the azide starting material **63**, as compared to the benzylic protons (δ_H ~ 5.5 - 6.0 ppm) of the regioisomeric triazole products **65** (Figure 93).

	Time (secs)
1	180.00
2	360.00
3	600.00
4	780.00
5	960.00
6	1200.00
7	1380.00
8	1560.00
9	1740.00
10	1980.00
11	2160.00
12	2340.00
13	2580.00
14	2760.00
15	2940.00

Figure 93. A stacked plot of the ^{1}H NMR at different time-points showing the progress of the reaction over time

The rate of reaction was subsequently calculated, as with the previous experiment, by plotting a graph of 1/[benzyl azide] against time (Figure 94).
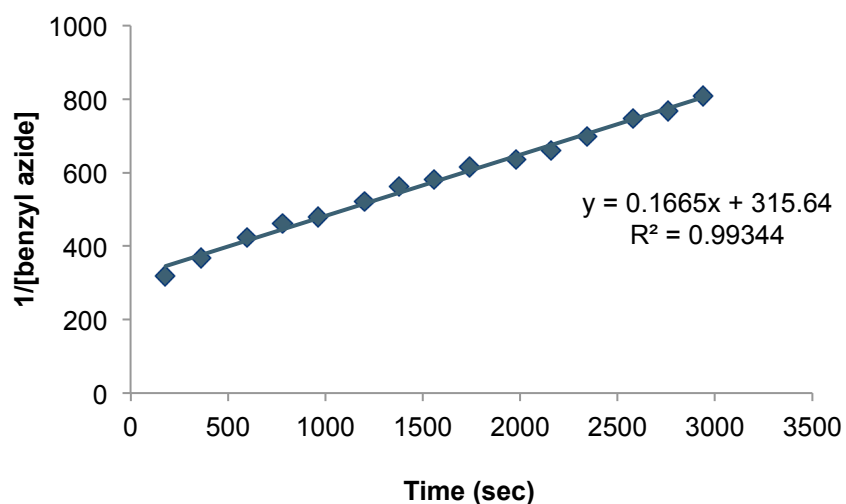
Figure 94. A graph showing time *vs*. 1/[benzyl azide], which was used to calculate the rate constant for the reaction with **DIBAC1**

Pleasingly, the rate of reaction was calculated to be 0.17 $M^{-1}s^{-1}$; approximately 100-fold faster than **OCT3**. This value is comparable to, but lower than the reported value of 0.31 $M^{-1}s^{-1}$, and the discrepancies may be attributed to the difference in method for calculating the rate constant, which were determined by Van Delft *et al.* using the following equation:[129]

$$kt = \frac{1}{[B]_0 - [A]_0} \times \ln \frac{[A]_0([B]_0 - [P])}{([A]_0 - [P])[B]_0}$$

These initial studies into the kinetics of the SPAAC reaction demonstrate the significant difference between the first-generation cyclooctynes as compared to the more recent congeners, and that judicious modification of the cyclooctyne structure can have a significant positive impact on their rate of reaction with azides.

These results, however, gave us no indication of how the reaction rates depend upon the concentration of the reactants, and consequently whether the reaction will be compatible with the very low concentrations required in order for the reaction to occur *in vivo*. Since we wanted to monitor how the reaction performs at much lower concentrations, we envisaged that these reactions would need to be evaluated by a more sensitive detection method.

3.4.3 Evaluating the Effect of Concentration upon Rate of Reaction

Due to the relatively impressive reaction kinetics that were demonstrated by **DIBAC1** in the SPAAC reaction with benzyl azide, it was decided that the rate of reaction should be more carefully evaluated in terms of concentration of the cyclooctyne. A maleimide derivative (**DIBAC2**) of this compound was chosen for carrying out these studies, as it would be necessary to use such a functional group for attachment to a chosen biomolecule.[129]

A sugar-derived azide **66** was reacted with **DIBAC2** under various conditions, observing the effects of modifying the concentration of the cyclooctyne on the rate of reaction within 15 min at 40°C (Figure 95)
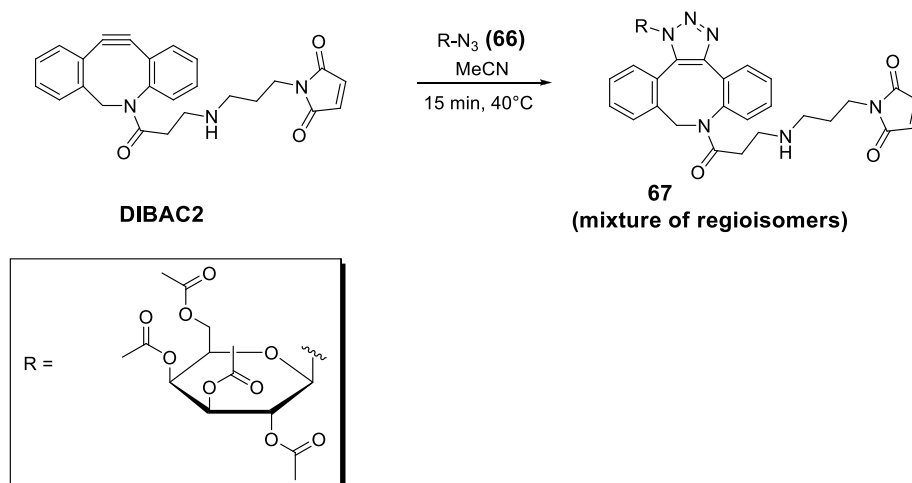
Figure 95. The reaction of **DIBAC2** with a sugar azide **66** in MeCN, which was monitored by HPLC

Azide **66** was chosen as it contains a suitable amount of functionality, without containing a UV chromophore, and would therefore not itself be detected at 254 nm by the UV detector of the HPLC instrument. It was planned that the reaction would be monitored at one time-point only, and under the optimum conditions for this type of reaction (i.e. using MeCN as solvent and at 40°C). ^{1}H NMR analysis of the reaction would not be possible at very low reagent concentrations, and for this reason HPLC analysis was chosen in order to observe the progress of the reaction. The triazole product **67** could be detected by HPLC, and was significantly separated from the **DIBAC2** starting material in terms of retention time.

The reaction was initially carried out at 90°C, and the two regioisomers of the triazole products were observed on the UV trace of the analytical HPLC. The reaction was subsequently carried out at 40°C, at four different concentrations of cyclooctyne, and each reaction was repeated four times (Figure 96).
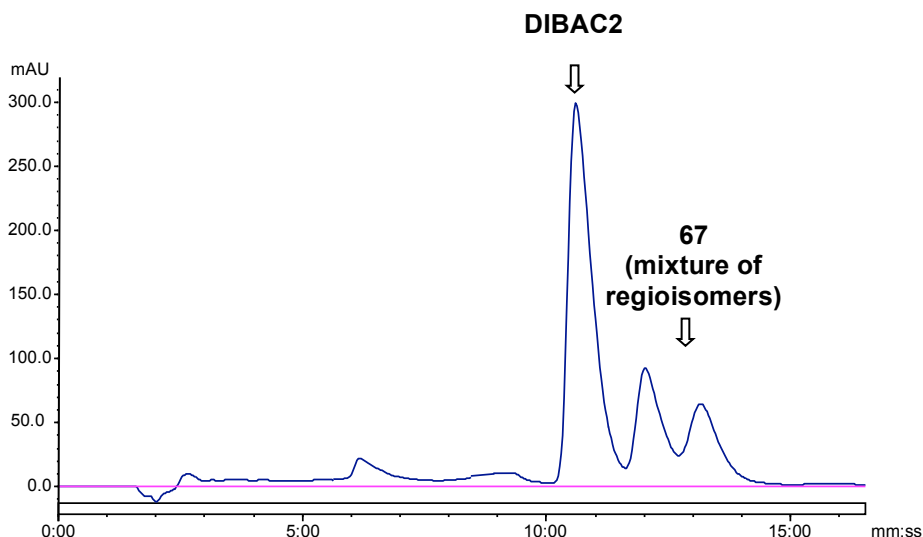
Figure 96. An example HPLC trace at 254 nm of the reaction mixture after heating to 40°C for 15 min

Some decomposition products were observed in the HPLC trace of the reaction mixture when carried out at 90°C, presumably attributable to the high temperatures used. The reaction proceeded smoothly at 40°C however, forming a lower number of decomposition products. The number of equivalents of azide **66** added in each case was kept constant, and the same stock solution of **DIBAC2** was used in order to ensure reproducibility. A linear dependence on the concentration of **DIBAC2** and the area under the curve (AUC) on the UV trace (at 254 nm) was demonstrated by injecting known concentrations of the stock solution, in order to obtain a calibration curve.

The conversion to the triazole products **67** was plotted as a function of initial **DIBAC2** concentration, which allowed us to estimate that a concentration of 8.7 M of **DIBAC2** would be required in order to achieve 100% conversion to the triazole products **67** within 15 min at 40°C (Figure 97).
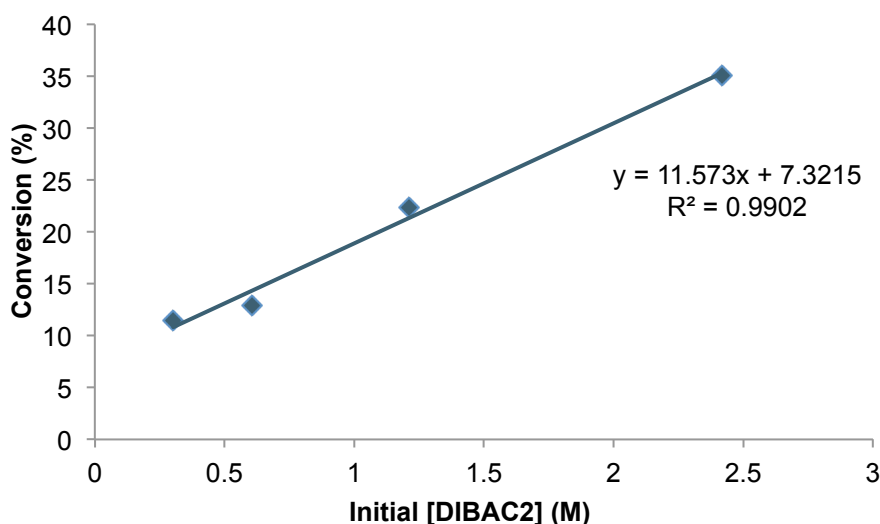
Figure 97. A graph showing initial [**DIBAC2**] *vs.* conversion (%) to the triazole products **67**

The maximum conversion to the triazole products **67** within 15 min was observed at the highest concentration of **DIBAC2** (2.4 M), with only 35% of the cyclooctyne reacting to form the triazoles **67**. A fairly linear decrease in the reactivity was observed when decreasing the concentration of **DIBAC2** sequentially by 2-fold for each data point, and only 11.5% of the cyclooctyne was reacting by the time the initial concentration was reduced to 0.3 M.

3.4.4 Conclusions

The concentrations required in order for the reaction to proceed efficiently are not achievable *in vivo*, and therefore it is unlikely that sufficient reaction will occur within the time-frame of a PET experiment for the targeted tissue to show significantly higher uptake than background tissue. It should additionally be noted that these studies were carried out in MeCN, as **DIBAC2** was insoluble in water in the absence of other solvents. However, it could be expected that incorporating a more water-soluble side-chain (such as a biomolecule) could improve the compatibility of the SPAAC reactions with aqueous media.

3.5 ^{68}Ga-labelled SPAAC Reactions

3.5.1 Hypothesis for a ^{68}Ga-Labelled SPAAC Reaction

In order to test the reactivity of **DIBAC** cyclooctynes further in the context of PET imaging applications, we hypothesised that a ^{68}Ga-labelled (DOTA) azide could be synthesised,

which could be tested for its reactivity with these cyclooctynes, in a similar manner to the study carried out with **[^{18}F]FEA**. The high volatility of **[^{18}F]FEA**, coupled with its reasonable, but not optimal measured Log$P$, encouraged us to find a more suitable prosthetic group for the radiolabelling of small molecules and peptides using the SPAAC reaction (see section 3.2). The radiochemical yields that may be achieved using ^{68}Ga chelates such as DOTA are usually very reproducible, are frequently superior to those that may be obtained using ^{18}F-labelling chemistry.[73, 84] In addition, ^{68}Ga is generally produced by a generator containing ^{68}Ge (see Introduction), and for this reason is a less expensive option than having an on-site cyclotron facility.

For these reasons, we designed a DOTA-containing azide (**DOTA-Az**), which would be readily radiolabelled using standard ^{68}Ga chelation chemistry (Figure 98).
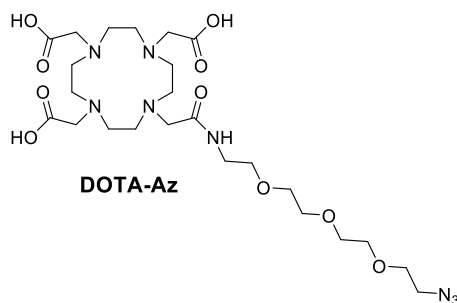
Figure 98. Structure of DOTA-PEG3-azide (**DOTA-Az**)

A PEG3 linker was inserted in between the DOTA chelate and the azide moiety, which it was anticipated would make the azide more accessible to the SPAAC reaction with cyclooctynes, whilst also making the compound more hydrophilic.

3.5.2 Synthesis of DOTA-Az

Two different methods were explored towards the synthesis of the azide **DOTA-Az**; the first

involved the synthesis of the tri-*tert*-butyl protected DOTA, which would have one available

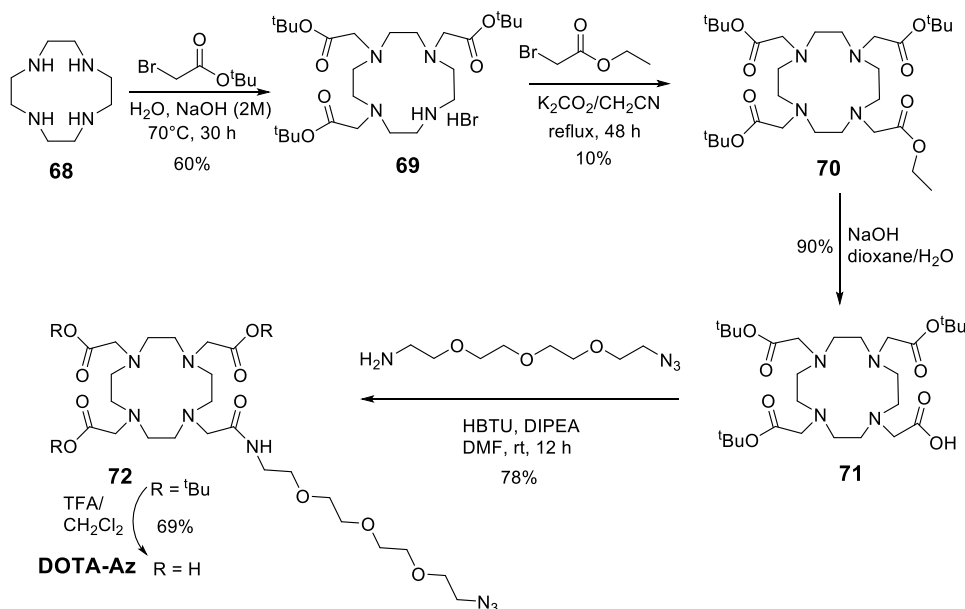acid group for amide coupling with the azide-containing amine (Figure 99).[203]

Figure 99. The total synthesis of **DOTA-Az** from cyclen **68**

The synthesis of the *tri*-protected DOTA is a literature procedure, and may be achieved in

three steps from commercially-available 1,4,7,10-tetraazacyclododecane (cyclen) **68**.[204, 205]

The first step of the synthesis involved treating cyclen **68** with three equivalents of *tert*-butyl

bromo acetate; this reaction proceeded in 30 h at 70°C, forming the product **69** in a yield of

60% after recrystallisation. The product **69** was subsequently treated with benzyl

bromoacetate, in order to introduce an ester onto the remaining position of the cyclen

structure. This step could be carried out in good conversion, but the purification often

resulted in the loss of material, and so the product **70** was isolated in yields of just 10% after

column chromatography. Some of the reported methods for the deprotection of the ethyl

ester to form the free acid **71** required the use of hydrogenation,[204] but this could be avoided

by using an alternative method utilising 0.1 M NaOH in dioxane.[205] This reaction proceeded

in 36 h, and the product **71** could be isolated in 90% yield following work-up.

The synthesised DOTA derivative **71** is protected on three of the carboxylic acid groups using *tert*-butyl groups, leaving one available acid for reaction with amine. HBTU was used as coupling agent to achieve the amide coupling to form protected form of the azide **72** in 78% yield. This compound was finally deprotected under acidic conditions to form azide **DOTA-Az** in 68% yield, which has available carboxylic acid groups for chelation to ^{68}Ga.

Due to the difficulty involved in the second step of the synthesis to form ester **70**, and the low overall yields that were obtained, an alternative method was employed when repeating the synthesis of azide **DOTA-Az** (Figure 100).
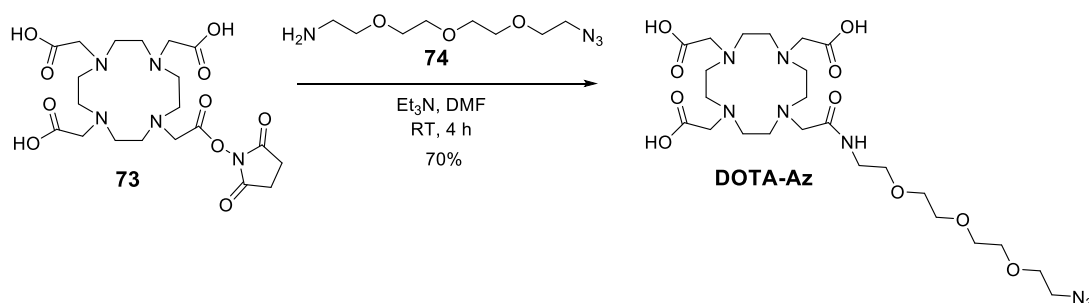
**Figure 100.** An alternative method for the synthesis of **DOTA-Az** from DOTA-NHS ester **73**

The second method towards the synthesis relied on the use of commercially-available DOTA-*N*-succinimide ester (DOTA-NHS) **73**, which may be directly reacted with the amine **74** to form azide **DOTA-Az** in one step under mildly basic conditions.[206] This reaction proceeded in good yields, forming the product in up to 70% yield after purification by preparative HPLC.

The purity of azide **DOTA-Az** was confirmed using ^{1}H NMR, HPLC and HRMS (see experimental section). Once synthesised, **DOTA-Az** could be used for radiolabelling with ^{68}Ga, and subsequently applied to a ^{68}Ga-labelled SPAAC reaction.

3.5.3 Radiosynthesis of [^{68}Ga]DOTA-Az

Once synthesised, the conditions for the radiolabelling of azide **DOTA-Az** with ^{68}GaCl$_3$ were tested and optimised. ^{68}GaCl$_3$ was eluted in 2 mL of a 0.1 M HCl solution, and this eluent could be buffered to a higher pH before reaction with the DOTA chelate. **DOTA-Az** was

dissolved in DMSO to a concentration of 1 mg mL^{-1}, and then added to the solution containing the buffered ^{68}GaCl$_3$. Two different NaOAc buffers were tested for this particular chelation; one at pH 5 and the other at pH 4. The resulting reaction mixture was heated to 90°C for 10 min, and the progress of the reaction was determined using radio-HPLC (Figure 101).
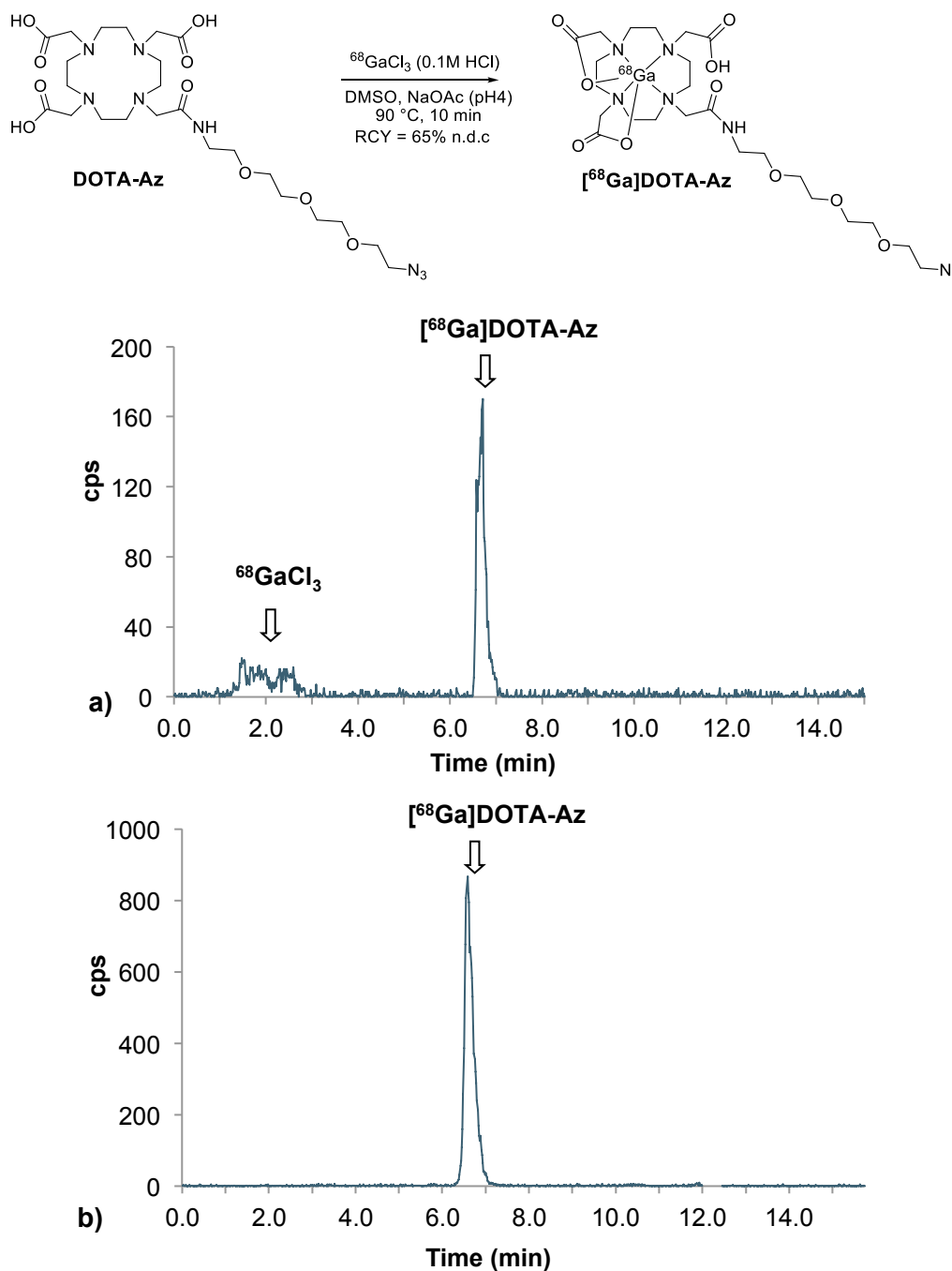
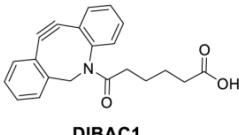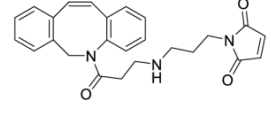**Figure 101.** Radiosynthesis of **[^{68}Ga]DOTA-Az** and radio-HPLC trace of a) **[^{68}Ga]DOTA-Az** prior to purification, b) **^{68}Ga]DOTA-Az** after purification

Although both of these buffers allowed for the formation of the labelled azide **[^{68}Ga]DOTA-Az** in >80% conversion from ^{68}GaCl$_3$, the pH 4 buffer provided the optimum pH for this reaction, allowing for radiochemical conversions of up to 95%. The radiosynthesis of ^{68}Ga-labelled azide **[^{68}Ga]DOTA-Az**, once optimised, are a significant improvement over the previously synthesised ^{18}F-labelled azide **[^{18}F]FEA**. **[^{68}Ga]DOTA-Az** could be successfully purified using a SepPak light C$_{18}$ cartridge, which allows for the larger compound to be retained on the cartridge when washing with water, whilst the smaller molecules, such as ^{68}GaCl$_3$ are eluted. The purified ^{68}Ga-labelled azide **[^{68}Ga]DOTA-Az** was then eluted from the cartridge using an organic solvent such as EtOH (typically 500 µL). The purity of the eluted **[^{68}Ga]DOTA-Az** fraction was determined using radio-HPLC, which showed that the ^{68}GaCl$_3$ had been successfully removed from the mixture. **[^{68}Ga]DOTA-Az** could be radiolabelled in isolated yields of up to 65% (n.d.c) after purification, starting with approximately 1 mCi of activity, and in >95% radiochemical purity (at least 5 repeats of the radiosynthesis were carried out).

3.5.4 Radiolabelled SPAAC Reactions with [^{68}Ga]DOTA-Az

The radiolabelled azide **[^{68}Ga]DOTA-Az** was subsequently used for a series of SPAAC reactions with two analogues of commercially-available aza-dibenzocyclooctyne (**DIBAC**).[127, 129, 202] The two cyclooctynes used in this study were **DIBAC1** and **DIBAC2** (containing a carboxylic acid or maleimide functional group, respectively) as the rates of reaction of these compounds had previously been evaluated. The progress of the reaction in each case was monitored by radio-HPLC, which was used to calculate the conversion from the azide **[^{68}Ga]DOTA-Az** to the regioisomeric triazole products **[^{68}Ga]75** and **[^{68}Ga]76.** In general, the results were improved over those demonstrated by the ^{18}F-labelled reaction, which may be attributed to the improved reactivity of the DIBAC cyclooctynes over the reagents explored earlier (Table 10).

Cyclooctyne[a]	Entry	Temperature (ºC)	Time (mins)	Solvent	RCY (%)[b]
DIBAC1	1	37	15	MeCN[c]	94.2
	2	90	10	MeCN[c]	100.0
	3	37	10	H_2O[d]	15.2
	4	90	10	H_2O[d]	97.3
DIBAC2	5	37	15	MeCN	51.4
	6	50	15	MeCN	79.2
	7	90	10	MeCN	99.4
	8	N/A	N/A	H_2O[d]	insoluble

[a] Each reaction carried out using 100 µL of [**68Ga]DOTA-Az** (typical activity of ~ 5 MBq); *n* = 3 in all cases. [b] Radiochemical yield as determined *via* radio-HPLC showing conversion of [**68Ga]DOTA-Az** into the summation of the regioisomers. [c] 1% DMSO was added to the reaction mixture [d] 10% DMSO was added to the reaction mixture

Table 10. Radiolabelled SPAAC reactions between DIBAC cyclooctynes and [**68Ga]DOTA-Az** under different conditions.

The carboxylic acid analogue **DIBAC1** formed the triazole isomers in radiochemical conversions of approximately 95% from the radiolabelled azide [**68Ga]DOTA-Az** at 37°C in MeCN within 15 min (Entry 1, Table 10). A higher temperature of 90°C allowed for complete conversion to the click products within just 10 min (Entry 2, Table 10). Cyclooctyne **DIBAC1** similarly performed well in the SPAAC reaction with the azide [**68Ga]DOTA-Az** in water, but the addition of 10% DMSO was required in order for the compound to dissolve fully. Low conversions of 15% to the triazole products were demonstrated in water at 37°C after 10 min (Entry 3, Table 10) but heating to 90°C allowed for the triazoles to be formed in near to quantitative yields (Entry 4, Table 10) possibly, at least in part, attributable to the increased solubility of the cyclooctyne at higher temperatures.

The maleimide analogue **DIBAC2** demonstrated poor water solubility, even with the addition of 10% DMSO, and so the reactivity of this compound in aqueous media was not successfully demonstrated (Entry 8, Table 10). Conversely, cyclooctyne **DIBAC2**

demonstrated reasonable reactivity with the azide **[^{68}Ga]DOTA-Az** in MeCN giving almost quantitative conversions to the triazole products at higher temperatures of 90°C (Entry 7, Table 10). However, slightly lower conversions of 51.4% and 79.2% were observed at lower temperatures of 37°C and 50°C respectively (Entries 5 and 6, Table 10) (Figure 102).
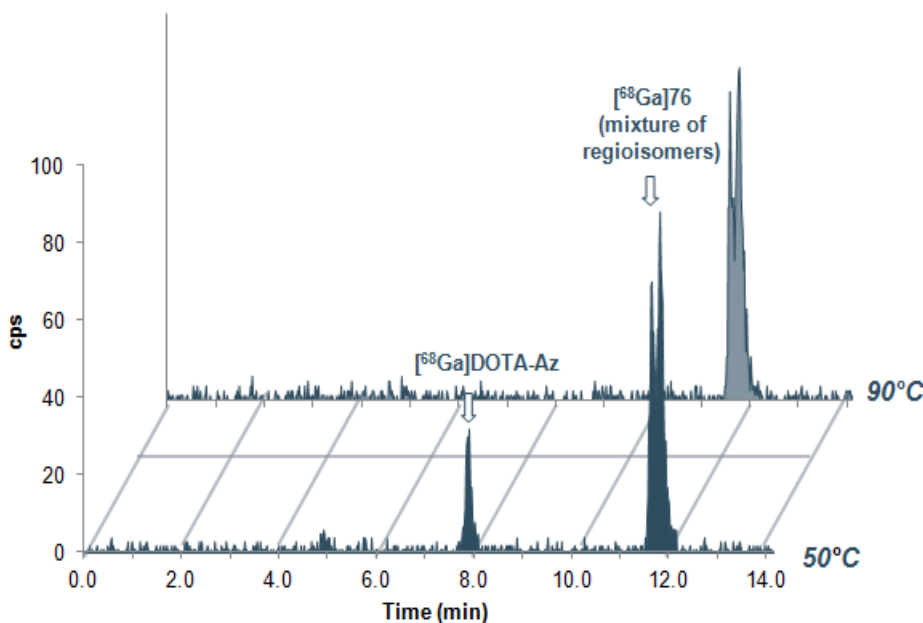
Figure 102. Example radio-HPLC traces of the reaction between [68Ga]DOTA-Az and DIBAC2 at; 50°C in MeCN for 15 min, 90°C in MeCN for 15 min

In order to demonstrate the usefulness of the SPAAC reaction when radiolabelling with metal chelators, we also decided to compare these results to those obtained using the traditional CuAAC radiolabelling method, by reaction of ^{68}Ga-labelled azide **[^{68}Ga]DOTA-Az** with an alkyne under standard CuAAC reaction conditions.[61] Octreotate analogue **77** was chosen for this purpose as this peptide is readily radiolabelled using CuAAC chemistry by reacting with previously synthesised azide **[^{18}F]FEA**. Compound **77** was reacted with **[^{68}Ga]DOTA-Az** under identical reaction conditions to a literature ^{18}F-labeling procedure,[61] but no conversion to the triazole product [^{68}Ga]**78** resulted (Figure 103).
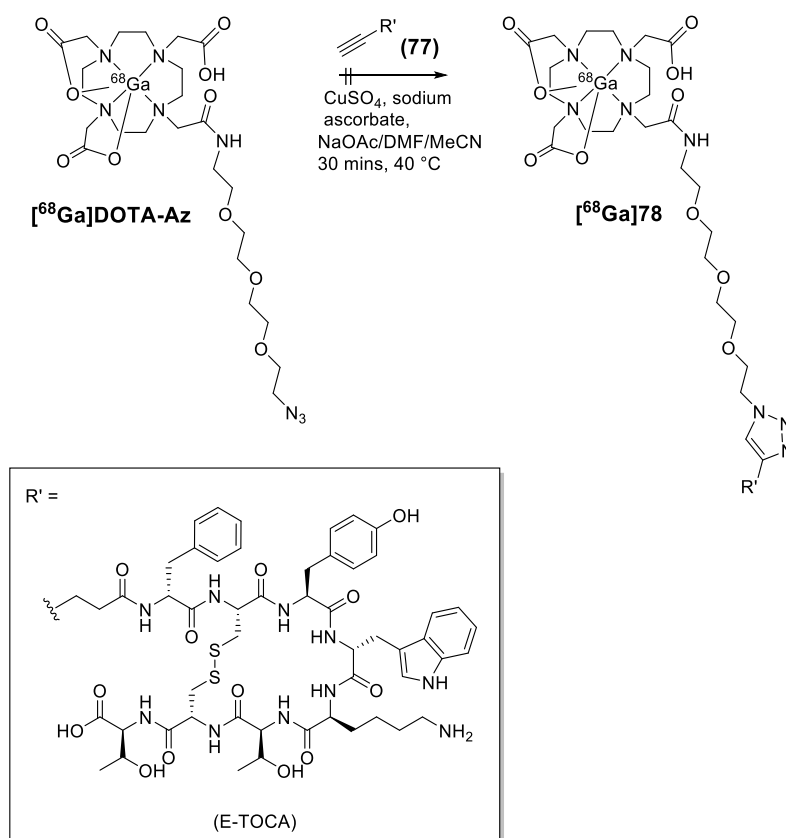
Figure 103. Attempted CuAAC reaction with **[^{68}Ga]DOTA-Az** and octreotate analogue **77**

This lack of reactivity may be attributed to the deactivation of the copper catalyst in the presence of excess DOTA chelate from solid-phase (SP) purification, a problem which is not observed in the copper-free version of the reaction. This highlights the utility of the SPAAC reaction for labelling biomolecules which cannot tolerate copper catalysts.

3.5.5 Conclusions

The radiolabelled azide **[^{68}Ga]DOTA-Az** has been demonstrated as a useful prosthetic group for the radiolabelling of cyclooctyne-containing compounds with ^{68}Ga. The SPAAC reaction may be considered as a useful method for labelling biomolecules with ^{68}Ga, due to the demonstrated difficulties involved in using the CuAAC in this context. These reactions may be particularly useful when aprotic organic solvents can be tolerated (*e.g.* MeCN), and it could be hypothesised that a similar level of reactivity may be achievable *in vivo* if the cyclooctyne were to be attached to a water-soluble biomolecule. However, the reaction may not be fast enough to occur on the time-scales required for a PET experiment (the highest

radiochemical conversions observed in water were ~15%) and this may be hindered even further by the low reactant concentrations that would be found *in vivo*, as was demonstrated in the kinetics studies.

3.6 Overall Conclusions

The SPAAC reaction has been described as being bioorthogonal, due to its ability to occur quickly and without the need for catalysis.[57, 58, 113] Studying this reaction in more detail, however, has enabled us to conclude that the reaction is not optimal within an *in vivo* setting. This was demonstrated initially using an ^{18}F-labelled model reaction between azide **^{18}F[FEA]** and a series of cyclooctynes, both in a vial and *in vivo*, which showed that the reaction required elevated temperatures or organic solvents in order to proceed efficiently. Radiolabelled azide **[^{18}F]FEA** also displayed less than ideal properties as the radiolabelled 'tag' molecule, as it was shown to be volatile, additionally having relatively low Log*P*, suggesting a less than ideal biocompatibility.[151] The potential binding of cyclooctynes to MSA has, in addition, been observed by other groups, significantly lowering the reaction rate of the SPAAC reaction *in vivo*. However, this observation may additionally be attributed to accumulation of azides in background tissue.[114, 155]

The kinetics of the SPAAC reaction could be improved by using the later-generation cyclooctynes based on the DIBAC core, which showed enhanced reactivity towards benzyl azide **63**, and efficient labelling of the alternative azide **[^{68}Ga]DOTA-Az** could be achieved at low temperatures and at short time-points. However, the SPAAC reaction was still significantly more efficient in polar aprotic solvents such as MeCN than in water, and high temperatures were required in order to achieve quantitative conversions. It was concluded from these results that a reaction possessing superior reaction kinetics was required for the desired *in vivo* pretargeting applications.

Chapter 4 - Synthesis and Reactivity of Tetrazines in the IeDDA Reaction
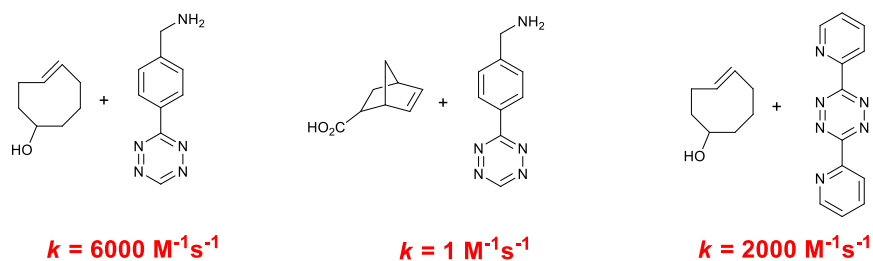
4.1 Synthesis of Tetrazines

4.1.1 Introduction to Tetrazines for IeDDA Reactions with Strained Alkenes

As described previously (see chapter 1 – Introduction), the [4+2] cycloaddition reaction between tetrazines and strained alkenes has increasingly received attention as an alternative bioorthogonal reaction to the SPAAC reaction. This is due to the superior rates of reactions that may be obtained, coupled with the vastly increased compatibility with aqueous and biological media. In addition to this is the fact that, unlike many other Diels-Alder cycloadditions, these reactions are irreversible (due to the elimination of elemental nitrogen); an essential feature to achieve biological labelling (Figure 104).[136, 207, 208]
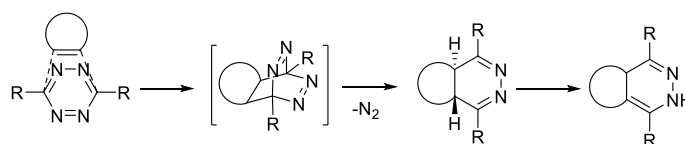
Figure 104. General reaction mechanism for the [4+2] cycloaddition reaction between tetrazines and dienophiles

A number of tetrazine reagents now exist for application to the inverse electron demand Diels-Alder (IeDDA) reactions with alkenes.[209] Modification of the chemical structure can help to 'tune' the reactivity and the stability of tetrazines by several orders of magnitude, and the most appropriate compound for application to pretargeting must be carefully considered, to obtain an ideal balance between ease of synthesis, stability and reactivity in the [4+2] cycloaddition reaction (Figure 105).

k = 6000 M^{-1}s^{-1} k = 1 M^{-1}s^{-1} k = 2000 M^{-1}s^{-1}

Figure 105. The reaction rates of selected tetrazines with norbornene and *trans*-cyclooctene (TCO) dienophiles[128]

## 4.1.2 Synthesis of a 'Symmetrical' Bipyridyl Tetrazine

The first tetrazine to be synthesised was a 'symmetrical' tetrazine **Tz1** with two pyridine groups; one of which contained an amine to facilitate subsequent attachment to a radiolabel or fluorescent probe (Figure 106).[116, 138, 145]

Tz1
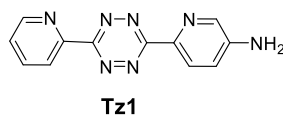
Figure 106. Tetrazine **Tz1** containing two pyridine groups and an amine

Tetrazine **Tz1** reportedly has impressive reaction kinetics in the cycloaddition reaction with strained alkenes, and has been applied to a number of applications including pretargeted *in vivo* chemistry using fluorescence.[138] Other tetrazines containing pyridine groups have also been used for alternative applications with the IeDDA reaction, such as the post-synthetic modifications of DNA, and for the synthesis of a 'Bio Shuttle' that helps to transport cargo into cells. [210, 211]

The synthesis of tetrazine **Tz1** was reported in two steps from nitriles **79** and **80,** and we attempted to replicate this synthesis (Figure 107).[116]
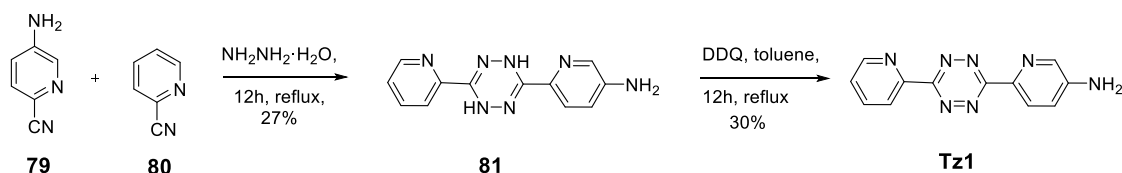

Figure 107. Fox's synthesis of tetrazine **Tz1** from nitriles **79** and **80**[116]

The first step was the reaction of 5-amino-2-cyanopyridine **79** and 2-cyanopyridine **80**, using hydrazine to form the dihydrate **81**. This compound was formed in only ~30 % yield after column chromatography, which was in accordance with literature protocols.[116] The dihydrate **81** was then reacted with DDQ *via* an oxidation to form the dehydrated tetrazine **Tz1**. Obtaining pure desired product was found to be difficult on the first attempts, with a large number of impurities making purification challenging. Column chromatography using silica

gel deactivated with triethylamine allowed for more successful separation of the desired product, forming the product in improved yields of 30%, when compared to previous attempts (~10%).

It was hypothesised that tetrazine **Tz1** could be ligated to a side-chain such as DOTA, which would serve as a chelate for ^{68}Ga labelling, and this approach was explored. This would enable the tetrazine to be radiolabelled using ^{68}Ga, and consequently could allow for a radiolabelled IeDDA reaction to be demonstrated, in parallel to the previously demonstrated ^{68}Ga-labelled SPAAC reaction. This first involved introduction of a suitable linker which would serve as a point of attachment to the DOTA chelate (Figure 108).
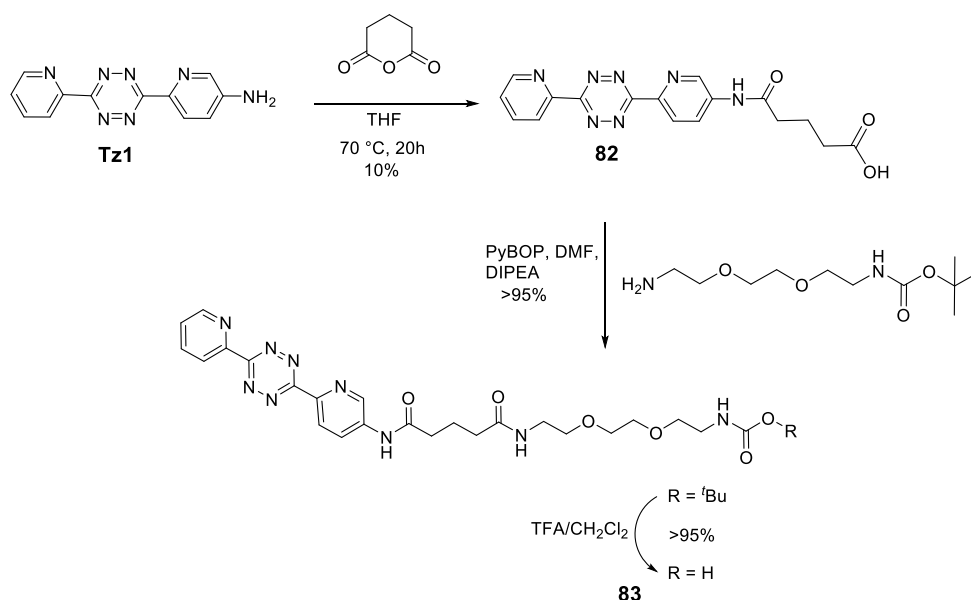
Figure 108. Introduction of a carboxylic acid side-chain, followed by a PEG2 linker onto tetrazine **Tz1**

The first step involved introduction of a carboxylic side chain onto the amine of tetrazine **Tz1**, which would serve as a linker between the tetrazine and PEG2 chain. This reaction was carried out according to a literature procedure, but only 10% yields were observed, compared to the 40% reported yields for the formation of carboxylic acid analogue **82**.[212] Attempts were made to improve the yields of this reaction by addition of a catalytic amount of DMAP, which it was anticipated, should aid the formation of the amide bond by activation of glutaric anhydride. However, the yields for formation of **82** were only marginally improved

to 15% using this method. This could be attributed to the poor availability of the amine group as a nucleophile, due to localisation of the nitrogen lone pair into the aromatic system. The obtained acid **82** was reacted with a Boc-protected PEG2-amine, and almost quantitative yields for the formation of the amide coupling product **83** were observed after column chromatography, using PyBop as the coupling reagent. The BOC-protected amine was consequently deprotected to the free amine **83** using TFA; this reaction was complete within 30 min, as determined by TLC, and the crude material was to be used for coupling to the DOTA chelate.

The free amine **83** was reacted with DOTA-NHS **73**, forming the desired DOTA-tetrazine **84** by addition of mild base (Figure 109).
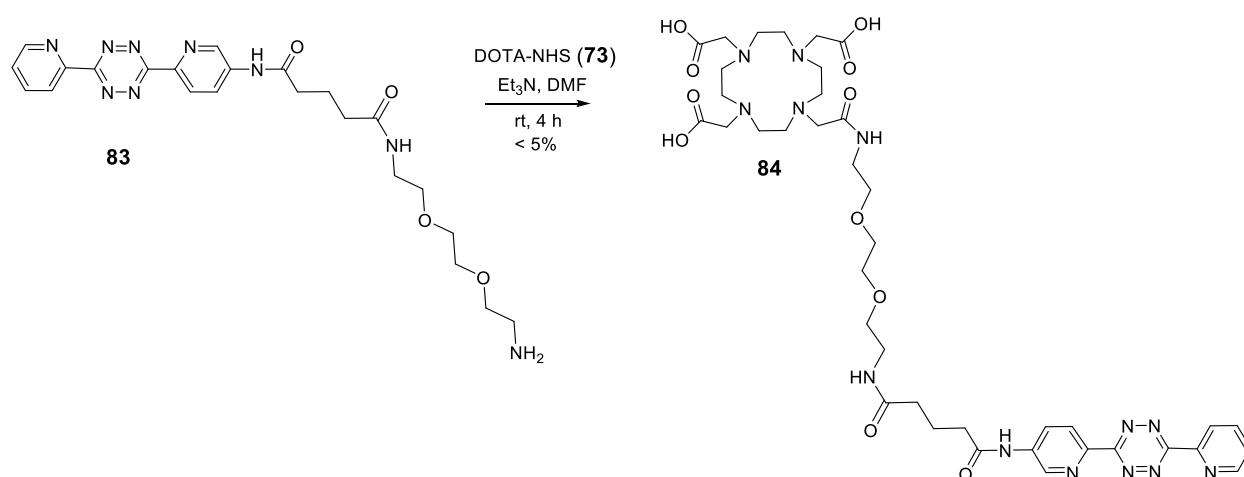
Figure 109. The attempted synthesis of DOTA-tetrazine **84**

The desired product **84** was formed by this method, as was determined by HRMS, but the compound was difficult to purify using preparative HPLC. Only trace amounts of the final compound were isolated, and attempts to repeat the synthesis of this compound resulted in lower overall yields. For this reason, a different method towards the synthesis of a DOTA-containing tetrazine was explored.

In addition to the very low overall yields obtained for this synthesis is that these tetrazines have apparently lower water solubility and stability in aqueous media than other tetrazines.[145] The strategy employed for the synthesis of this tetrazine, using the addition of

hydrazine to aromatic nitriles, as described, is limited to activated nitriles such as **79** and **80**, and this therefore prohibits access to a diverse range of tetrazines using an analogous approach. Alternative methods towards the synthesis of tetrazines, which do not require the use of aromatic nitriles, have been recently reported, allowing for the synthesis of a wider range of both symmetric and unsymmetrical tetrazines.[144, 145]

4.1.3 Synthesis of 'Asymmetric' Benzylamino Tetrazines

The methods which allow for the synthesis of asymmetric tetrazines rely upon the use of Lewis acid catalysis, presumably in order to activate the nitriles towards addition with hydrazine, which allows for even aliphatic nitriles to be used. Tetrazines such as 3-(4-benzylamino)-1,2,4,5-tetrazine **Tz2** were reportedly synthesised in good yield, which have greater water solubility and reactivity in aqueous media relative to the diaromatic compounds, such as tetrazine **Tz1**, owing to their slightly reduced lipophilicity (Figure 110).[115]


Tz2
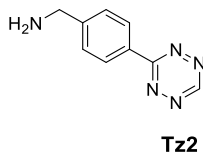
Figure 110. Structure of tetrazine **Tz2** containing only one aromatic ring

Tetrazine **Tz2** was demonstrated by Hilderbrand *et al*. as displaying excellent stability in PBS, with no decomposition products observed at room temperature after several hours.[115] A small amount of decomposition was observed in fetal bovine serum (FBS); however over a time-point of 15 h this resulted in only 15% decomposition. This tetrazine demonstrates good reaction kinetics with strained alkenes (see section 4.2), and for these reasons have been increasingly utilised for numerous applications.

First attempts towards the synthesis of tetrazine **Tz2** relied on repeating the literature procedure reported by Hilderbrand *et al*. whereby 4-(aminomethyl)benzonitrile **85** is reacted with formamidine acetate **86** and anhydrous hydrazine in the presence of elemental

sulfur.[115] The dihydrotetrazine products formed is subsequently oxidised to the tetrazine **Tz2** using sodium nitrite in acetic acid. Hilderbrand *et al.* synthesised **Tz2** in 20% overall yield, in a one-pot procedure, making this method very attractive for the synthesis of these reportedly stable and reactive tetrazines (Figure 111).
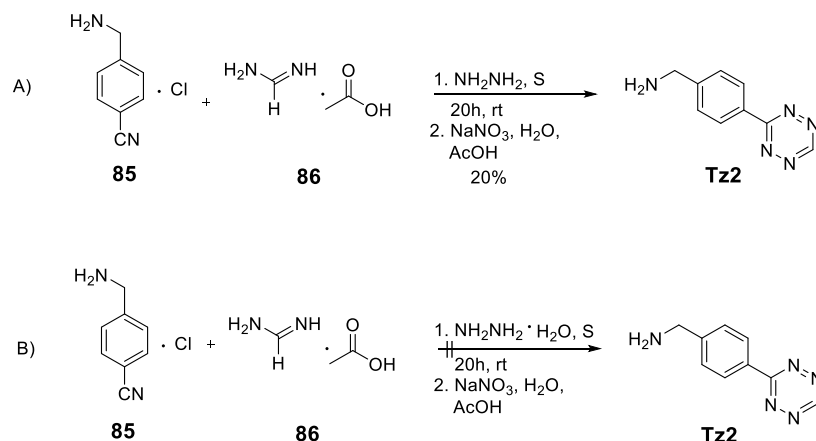
Figure 111. A) The synthesis of **Tz2** as described by Hilderbrand *et al*; B) The modified method using hydrazine hydrate, which resulted in poor conversion to the desired product[115]

As anhydrous hydrazine is not commercially available in the UK, hydrazine hydrate was used as a substitute, using the appropriate number of equivalents. However, this method only formed trace amounts of tetrazine **Tz2**, and attempts to isolate this compound *via* this method were unsuccessful. This was attributed to the use of a lower concentration of hydrazine in the mixture, potentially lowering the rate at which the reaction occurred.

More recently, the Deveraj group developed an alternative method for synthesising this type of tetrazine, utilising zinc and nickel salts as catalysts (Figure 112).[144]
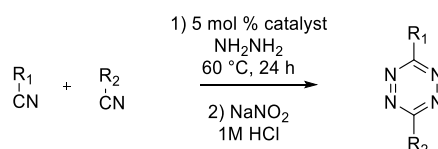
Figure 112. Deveraj's synthesis of 1,2,4,5-tetrazines directly from nitriles catalyzed by Ni(OTf)$_2$ or Zn(OTf)$_2$[144]

19 examples of this type of reaction were demonstrated, allowing for the formation of a mixture of symmetric and asymmetric tetrazines. A range of yields was reported, ranging from 12% to 95%, and the catalyst used was dependent upon the nitrile substrate selected.

It was hypothesised by Devaraj *et al.* that the metal ion acts as a Lewis acid for the formation of the amidrazone intermediate by coordinating to both the nitrile and the hydrazine.[145, 213] Alternatively, the metal may coordinate to the nitrile only, still promoting nucleophilic attack from the hydrazine (Figure 113).[214]
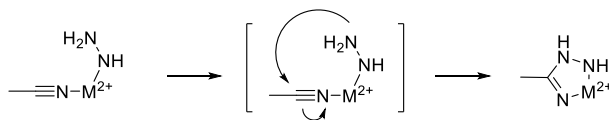
Figure 113. Hilderbrand's proposed reaction mechanism for the activation of nitriles by Lewis acid catalysis[144]

The synthesis of tetrazine **Tz2** was described using this method, and first involved the protection of the amine side-chain with a Boc group, which could prevent hydrolysis to the alcohol; a likely by-product of this reaction (Figure 114).[144]
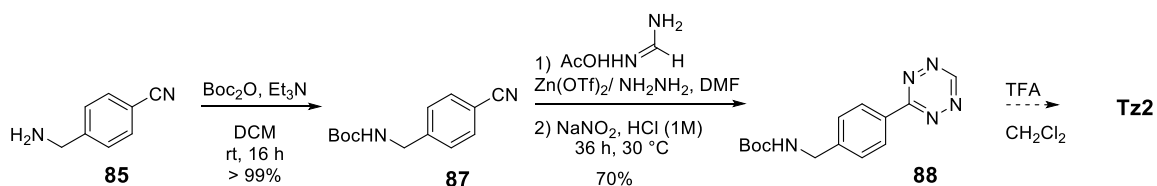
**Figure 114.** Devaraj's synthesis of Boc-protected tetrazine **Tz2**[144]

Due to the reportedly improved yields of tetrazine **Tz2**, attempts were made in order to follow the described literature procedure.[144] The protection of nitrile **85** was achieved in quantitative yields, and could be carried out on a gram-scale, allowing for formation of large quantities of Boc-protected material **87** for further reactions towards tetrazines. The Boc-protected nitrile **88** was then reacted with formamidine acetate and hydrazine, with zinc triflate as the Lewis acid catalyst. DMF was also used as a co-solvent for synthesis of this particular tetrazine, owing to the poor solubility of the starting materials in hydrazine.[144]

First attempts towards the synthesis of tetrazine *via* this method were carried out in hydrazine (1 M) in THF, and using this method the Boc-protected tetrazine **88** was formed in approximately 5% conversion after oxidation using sodium nitrite and HCl (1 M). The product **88** could not be isolated using this method, and the low yields were presumably due to the

lower concentration of hydrazine in the mixture as compared to the anhydrous version used in the literature procedure. Similar results were obtained using hydrazine hydrate, and it was concluded that higher temperatures would be required in order to get the reaction to go to completion using this more dilute solution of hydrazine. However, attempts to carry out this reaction at 60°C resulted in the formation of unknown by-products, with only trace amounts of the desired product being formed.

The same method was consequently applied to a similar tetrazine **Tz3** (1-[4-(6-methyl-1,2,4,5-tetrazin-3-yl)phenyl]methanamine), containing a methyl group at C3 of the tetrazine core. Temperatures of 60°C had been used for the synthesis of this compound following Devaraj's literature procedure (Figure 115).[144]
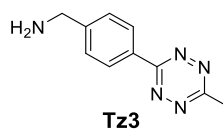
Figure 115. Structure of **Tz3**; the methyl group at C3 is expected to enhance stability

The methyl group is reported by Hilderbrand *et al*. to increase the stability of the tetrazine relative to tetrazine **Tz2**, which could potentially make the compound easier to synthesise, as it is more stable to higher temperatures and harsher reaction conditions (Figure 116).[145]
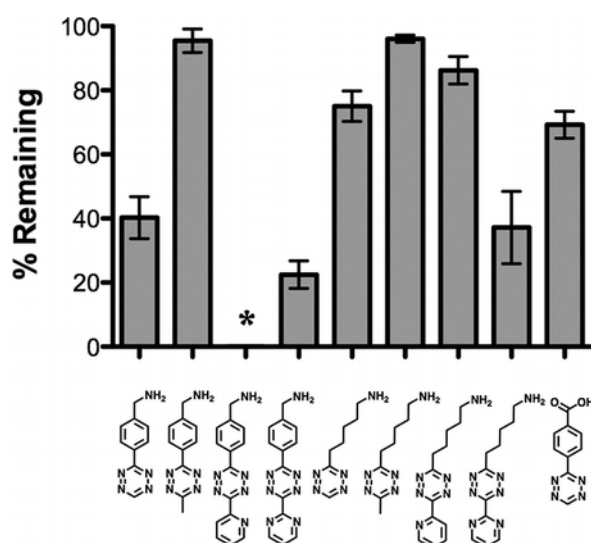
Figure 116. Hilderbrand's demonstration of the stability of a series of tetrazines in FBS at 37°C after 10 h, showing the significance of introducing a methyl group onto C3[145]

This improved stability would also be advantageous when considering using the compound for radiolabelling (temperatures of 90°C are required for ^{68}Ga labelling with DOTA), and later for *in vivo* applications. Tetrazine **Tz3** was synthesised by reacting the Boc-protected nitrile **87** with acetonitrile in hydrazine, this time using nickel triflate as the catalyst, with no problems associated with the solubility of the starting materials (Figure 117).
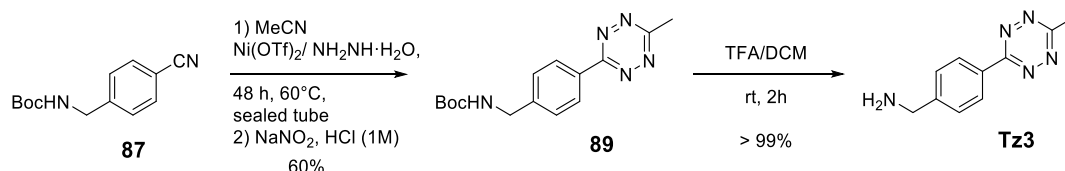

Figure 117. Synthesis of tetrazine **Tz3** from Boc-protected nitrile **87**

The literature procedure again relies on the use of anhydrous hydrazine, and so initial attempts towards the formation of the tetrazine were carried out using a 1 M hydrazine solution in THF. However, no product **89** was observed *via* this method, owing to the use of a low concentration of hydrazine solution. The reaction was consequently carried out using hydrazine hydrate (55-60%), which formed the Boc-protected tetrazine **89** in ~20% yield after oxidation and column chromatography when carried out at 60°C for 24 h. These yields could be improved significantly (up to 60%) by increasing the reaction time to 48 h, and by carrying out the reaction in a sealed tube. The Boc group in derivative **89** could then be removed by simple deprotection in TFA to form tetrazine **Tz3** in quantitative yield. Tetrazine **Tz3** could be obtained in overall yields of up to 59% from nitrile **87** on scales of up to 1g, making this a very attractive method for the synthesis of this compound.

4.2 Evaluating the Reaction Kinetics of the IeDDA Reaction

Due to the strong concentration dependence on rate of reaction demonstrated with the SPAAC reaction (see chapter 3), it was decided that a model IeDDA reaction should be evaluated for its concentration dependence. This would enable us to compare the two reactions directly, and evaluate their relative merits for use *in vivo*.

4.2.1 Introduction to Norbornenes as Dienopohiles in the IeDDA Reaction

Norbornenes have been used extensively as the dienophile in the IeDDA reaction with tetrazines, due to the overall balance between their reactivity towards tetrazines and their general chemical stability. This example of an IeDDA reaction has been applied to a variety of *in vivo* applications for this reason. [115, 145, 211, 215] Additionally, a number of norbornenes containing functional handles are commercially available, allowing for straight-forward modifications of biological molecules to be made.

The norbornene functional group demonstrates good reactivity as a dienophile with tetrazines, and its reaction with tetrazine **Tz2** was evaluated in detail by Hilderbrand *et al* (Figure 118).[115]
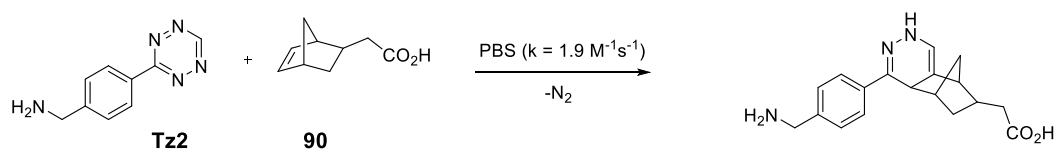

Figure 118. Hilderbrand's demonstration of the reaction between tetrazine **Tz2** and a norbornene dienophile **90**

Tetrazine **Tz2** displayed a second-order rate constant of 1.9 $M^{-1}s^{-1}$ in aqueous buffer with norbornene analogue **90**, which demonstrates the improved water-compatibility of these reactions as compared to the SPAAC reactions (rate constants for the SPAAC reactions were calculated in either acetonitrile or methanol). A rate constant of 1.6 $M^{-1}s^{-1}$ could also be demonstrated in FBS, further demonstrating the bioorthogonality of these reactions.

4.2.2 Evaluating the Rate of the IeDDA Reaction at Varying Concentrations

The incorporation of a methyl group at C3 of the tetrazine core was demonstrated to improve their stability in biological media, with marginal compromise to the reaction kinetics.[145] We therefore planned to evaluate the kinetics of tetrazine **Tz3** in more detail, and in particular to focus on the effect of altering the concentration of the tetrazine on the rate of reaction with norbornene dienophiles. Unlike symmetrical tetrazine **Tz1**, tetrazine **Tz3** was found to be

highly soluble in water; no difficulties were encountered dissolving the compound, even at the highest concentrations used. The rate of reaction of tetrazine **Tz3** with commercially available norbornene analogue **91** was determined at varying concentrations, to evaluate if the reaction was likely to occur at concentrations comparable to those expected *in vivo*. The reaction was carried out in aqueous media at 37°C, to demonstrate most effectively the applicability of this reaction to biological environments (Figure 119).
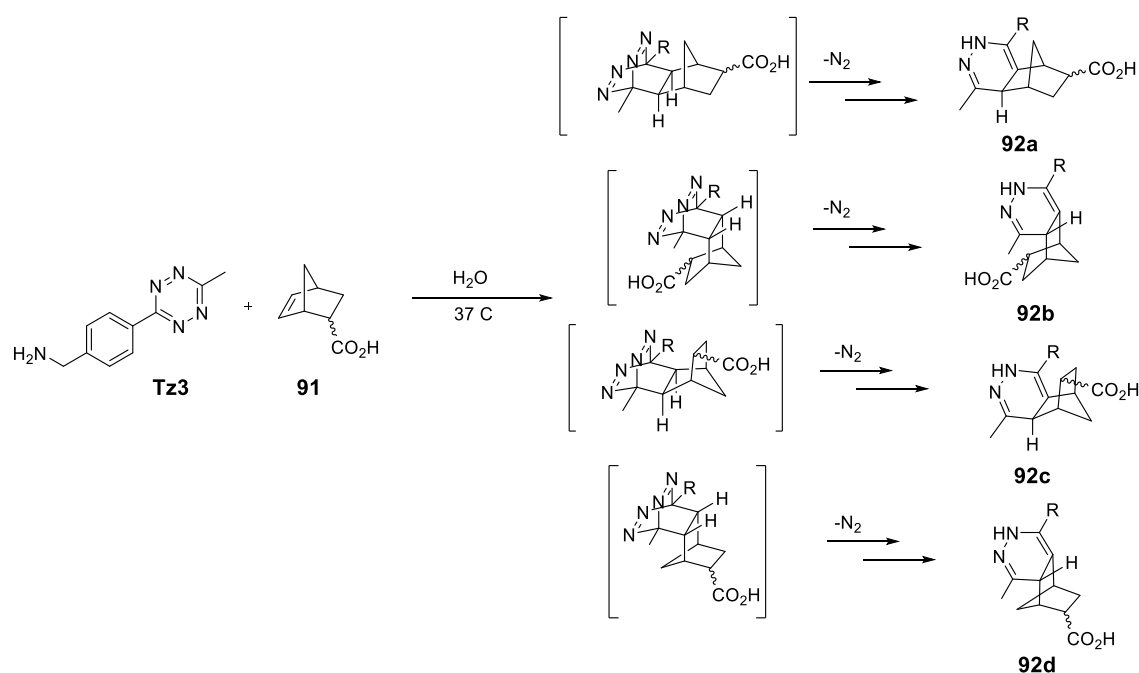
Figure 119. Reaction of tetrazine **Tz3** with norbornene **91**, resulting in four dihydropyridazine product regioisomers

Due to its asymmetric structure, tetrazine **Tz3**, can react with alkenes *via* the IeDDA reaction to give four isomeric dihydropyridazine products (**92a-d**). Moreover, when using an asymmetric alkene such as norbornene **91**, 8 isomeric products can form (the *endo* and *exo* isomers of products **92a-d**). In the event, the reaction between tetrazine **Tz3** and the norbornene **91** produced the four distinguishable dihydropyridazines (**92a-d)**, which could be observed by monitoring the progress of the reaction using the UV detector on a HPLC instrument (Figure 120).
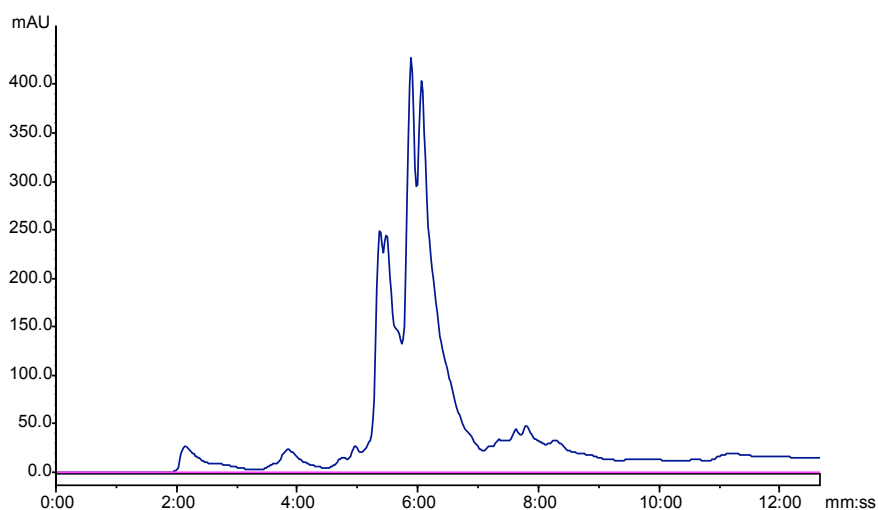
Figure 120. Example HPLC trace of the isomeric dihydropyridazine products **92a-d**

Tetrazine **Tz3** was used as the standard in this reaction, and known concentrations of this compound were first injected into the HPLC instrument to confirm that lowering the concentration of tetrazine **Tz3** decreased the area under the UV peak in a linear fashion, by plotting a calibration curve. This was found to be an accurate way to measure the change in concentration of the tetrazine, and so the AUC could be used to determine the effective change in tetrazine concentration in the reaction mixture.

The progress of the reaction was subsequently monitored at 4 time-points: 5, 10, 30 and 60 min, at each of the concentrations used. Due to the formation of multiple products, the consumption of the tetrazine **Tz3** starting material was calculated. This data was plotted at each of the concentrations used (Figure 121).
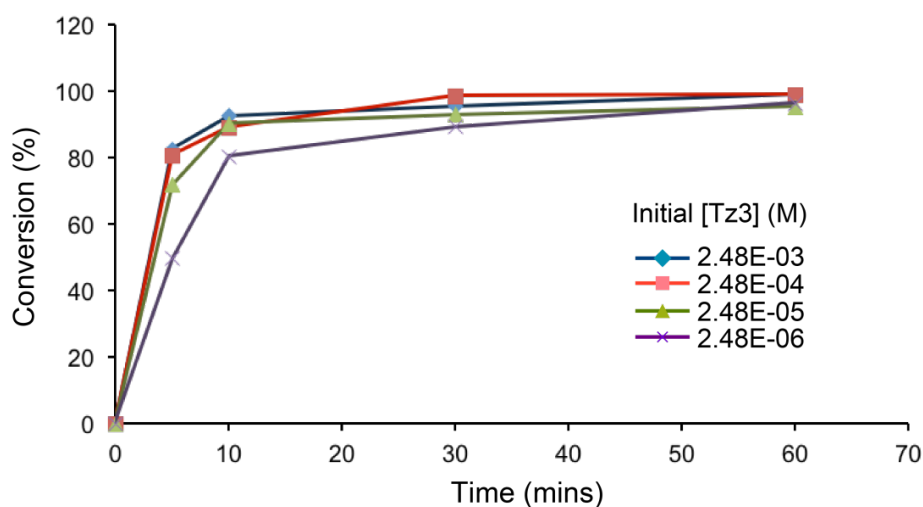

Figure 121. A plot of time (sec) *vs*. conversion (%), showing the effect of altering the initial concentration of **Tz3**

157

It was concluded from these results that the rate of this IeDDA reaction was only weakly dependent on the concentration of the tetrazine **Tz3**, with the lowest measurable concentration (using this HPLC method) of 2.5×10^{-6} M allowing for the formation of the product in almost quantitative yields within 60 min. The most significant difference in conversion was observed within the first 5 min, but after 10 min the products had formed to almost the same extent, independent of the concentration of tetrazine used. Pleasingly, at all of the concentrations used, greater than 95% conversions to the dihydropyridazine products was achieved within 60 min, which suggests that this reaction may be suitable for an *in vivo* application.

The lowest concentration measured for the cycloaddition reaction between tetrazine **Tz3** and norbornene **91** was 10,000 times higher than the lowest concentration measured for the SPAAC reaction between cyclooctyne **DIBAC1** and a simple azide, as described in chapter 3. The highest conversion that was measured for the SPAAC reaction within 15 min to the triazole regioisomers from cyclooctyne **DIBAC1** was 35%, which is almost 3 times lower than that which was achieved using this IeDDA reaction. In addition, the IeDDA reaction was carried out in aqueous media, whereas the SPAAC reaction was measured in MeCN, owing to the poor solubility of the cyclooctyne precursors in water.

4.2.3 Conclusions

In general, the cycloaddition reactions between tetrazines and strained alkenes appear to display great biocompatibility as compared to those between cyclooctynes and azides, combining excellent levels of reactivity at low temperatures and at low concentrations in water. The reaction between tetrazine **Tz3** and norbornene **91**, in particular, appears to be a promising bioorthogonal ligation reaction, demonstrating a favourable balance of reaction rate and stability in water. For this reason, it was hoped that this reaction could be useful for application to a pretargeting. The plan was to first validate this concept using a radiolabelled version of this reaction.

4.3 Radiolabelled IeDDA Reactions Using [^{68}Ga]DOTA-Tz

4.3.1 Hypothesis for a ^{68}Ga - Labelled IeDDA Reaction

Due to the promising results obtained from the concentration dependence studies, it was determined that a radiolabelled version of the cycloaddition reaction between tetrazine **Tz3** and norbornenes, and potentially other dienophiles, could be developed. This would initially involve the synthesis of a DOTA-tetrazine for labelling with ^{68}Ga, which could then be reacted with a series of alkenes in order to demonstrate a radiolabelled IeDDA reaction.

4.3.1 Synthesis of DOTA-Tz

It was planned to construct a simple DOTA-tetrazine in which the tetrazine moiety is ligated *via* a free amine residue to one of the available carboxylic acids on DOTA. Thus, **DOTA-Tz** was synthesised by reacting the amine with a commercially available DOTA-NHS **73** (Figure 122).
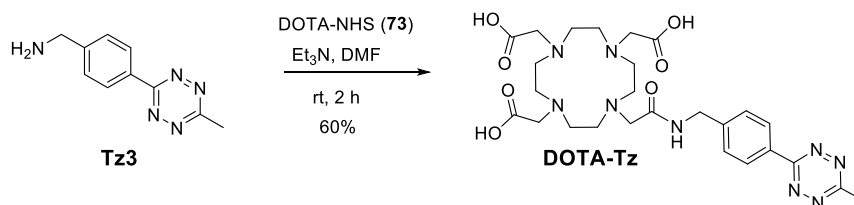
Figure 122. Synthesis of **DOTA-Tz** using tetrazine **Tz3** and DOTA-NHS ester **73**

DOTA-Tz could be isolated in much more acceptable yields (60%) than the previously synthesised DOTA-tetrazine **84** (*cf.* Figure 110), and could be isolated in high purity (>95%) after purification by preparative HPLC. Due to the enhanced total synthesis of **DOTA-Tz** as compared to the previous compound **84**, in addition to the reportedly enhanced stability of this type of compound, we decided that this would be the initial construct to take forward to radiolabelling reactions, and studies would be carried out into the potential use of this compound for pretargeting applications.

4.3.1 Radiosynthesis of [^{68}Ga]DOTA-Tz

Initial radiolabelling with tetrazine **DOTA-Tz** was challenging, resulting in only 40% radiochemical conversions from ^{68}GaCl$_3$. This was attributed to some traces of metal

impurity in the material as the synthesis of the tetrazine was achieved using Nickel salts, which were subsequently removed by carrying out a second purification by preparative HPLC.

A number of different buffers of NaOAc, of varying pH values (ranging from 3.5 - 6.5), were evaluated for carrying out the radiolabelling reaction, and the optimum pH was found to be 6. Using these conditions, tetrazine **DOTA-Tz** was radiolabelled in up to 95% radiochemical conversions within 10 min at 90°C. The radiolabelled product **[68Ga]DOTA-Tz** could be obtained in >95% purity by use of a SepPak light C_{18} cartridge, in a similar manner as with the purification of labelled azide **[68Ga]DOTA-Az** (Figure 123).
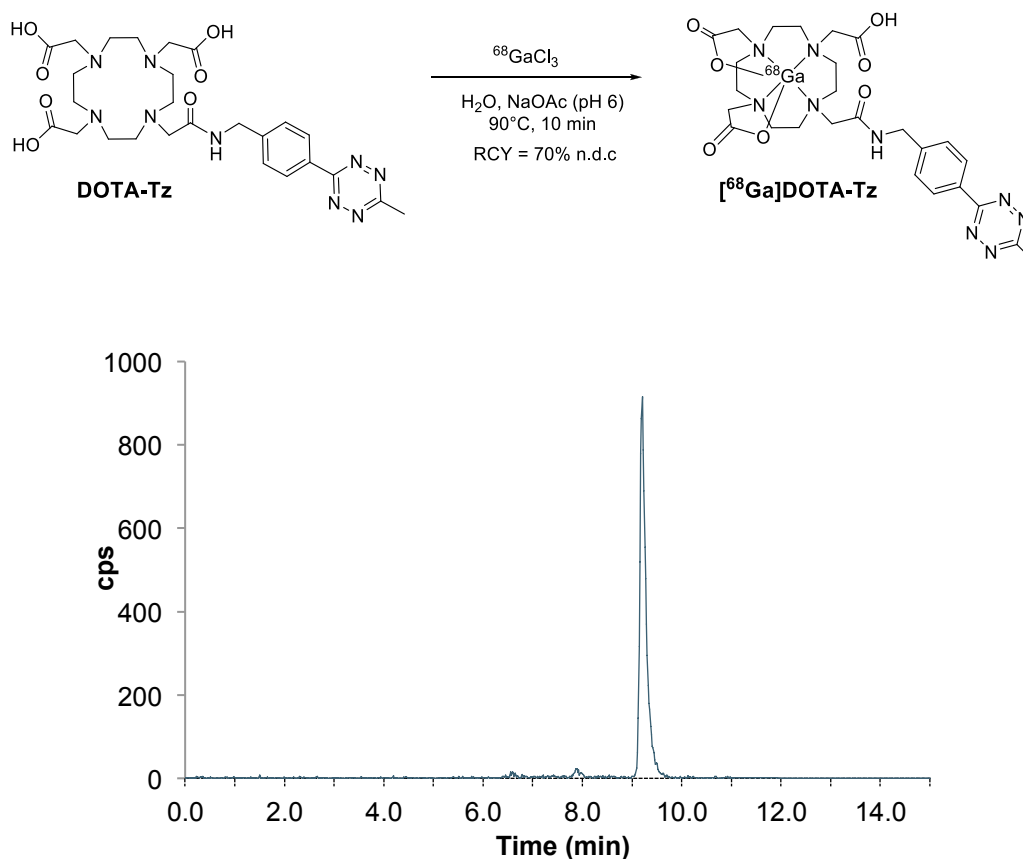
Figure 123. Radiosynthesis of **[68Ga]DOTA-Tz** and example HPLC trace of the purified product

Up to 70% overall radiochemical yields (n.d.c) could be obtained 'end-of-synthesis' for this reaction, and the synthesis was found to be highly reproducible. The product was eluted in 0.5 mL of pure ethanol, and could be divided into 100 µL fractions, with up to 2.5 mCi of activity being obtained in the most concentrated fractions, and these results were consistent

across each experiment ($n > 10$). The initial $^{68}GaCl_3$ used in these experiments had an activity of 6.6 mCi at the start of the synthesis. The aliquots obtained were sufficient for the labelled product to be used for both *in vitro* and *in vivo* studies.

The specific activity of **[^{68}Ga]DOTA-Tz** was calculated for each of the fractions containing the product, in order to determine the relative amount of ^{68}Ga-labelled compound as compared to the 'cold', non-radiolabelled materials. This is an essential factor when considering the use a compound as a potential radiotracer or chemical reporter, for application to *in vivo* pretargeting. This was calculated by injecting known concentrations of cold **DOTA-Tz**, and measuring the AUC at each known concentration. This data was plotted as a calibration of the concentration of **DOTA-Tz** against the AUC in the UV trace (Figure 124).
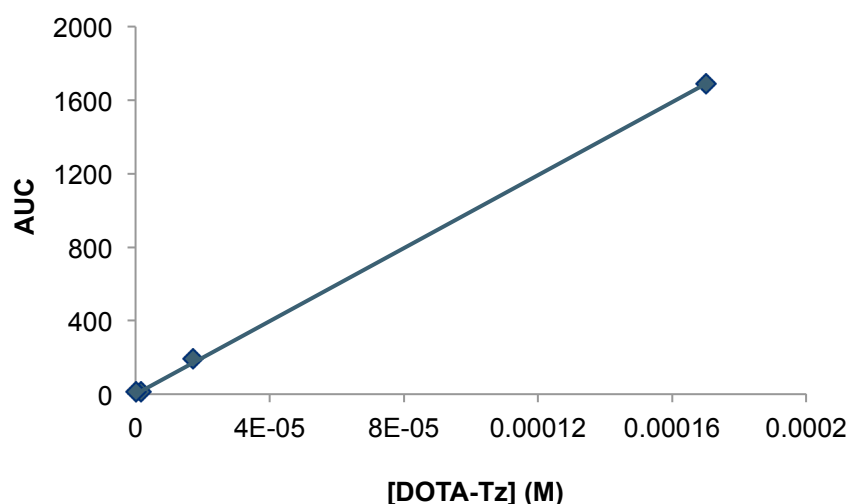
Figure 124. A plot of concentration of **DOTA-Tz** *vs*. AUC in the UV trace, used to calculate the specific activity

This plot could be used to determine the concentration of 'cold' material in any injected sample of the radiolabelled tetrazine **[^{68}Ga]DOTA-Tz**. This was subsequently used to calculate the specific activity of the sample. When starting the synthesis with approximately 1 mCi of $GaCl_3$, this value was found to be 17 Gbµmol^{-1}.

[^{68}Ga]DOTA-Tz was additionally tested for its stability in PBS, in order to ascertain whether it would be suitable for *in vivo* applications (Figure 125).
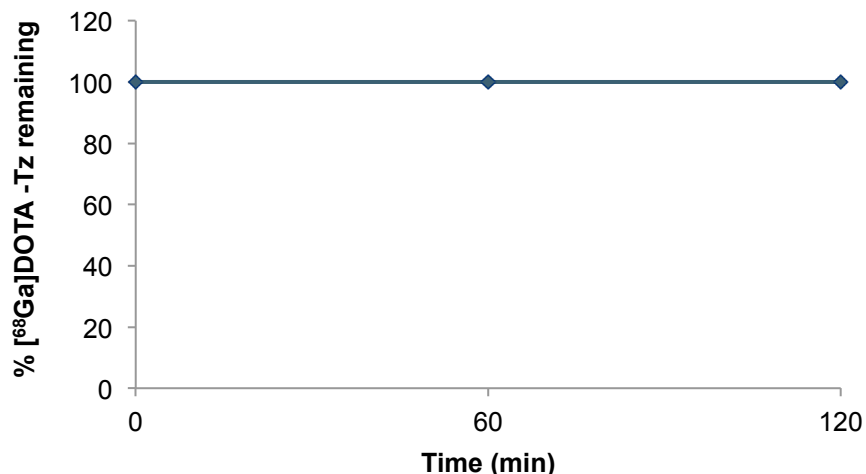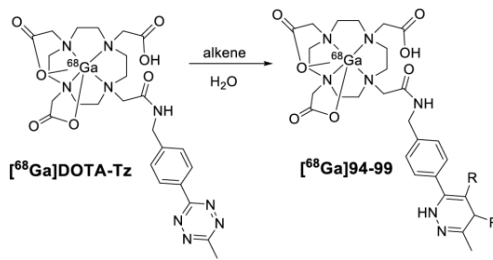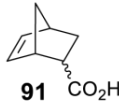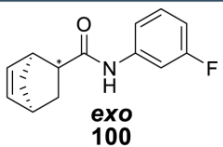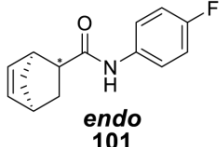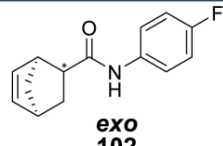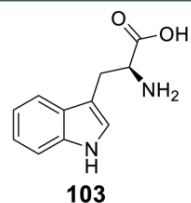
Figure 125. A plot demonstrating the stability of **[⁶⁸Ga]DOTA-Tz** after 1 and 2 h incubation in PBS, as monitored by the permanence of the **[⁶⁸Ga]DOTA-Tz** radio-HPLC trace

Pleasingly, the compound demonstrated good stability after 1 and 2 h incubation in PBS, showing no decomposition products within this time-frame. This is significant when considering this compound as a potential chemical reporter, as the radiolabelled tetrazine must remain stable throughout the pretargeting experiment. Due to these results, it was established that the radiolabelled tetrazine **[⁶⁸Ga]DOTA-Tz** would be a suitable compound for use as a chemical reporter in the hypothesised pretargeting strategy. In order to confirm this, it was necessary to demonstrate the reactivity of this compound towards alkenes, and show that it displays a good level of biocompatibility.

4.3.2 Demonstrating the ⁶⁸Ga - Labelled IeDDA Reaction

The radiolabelled tetrazine **[⁶⁸Ga]DOTA-Tz** was reacted with a series of alkenes in order to demonstrate that the IeDDA reaction, could be carried out using this compound, and in order to find the most appropriate coupling partner for pretargeting (Table 11).

| Alkene[a]	Entry	Temperature (ºC)	Time (mins)	Solvent	RCY (%)[b]
93	1	37	10	H_2O	10.5
	2	90	10	H_2O	27.2
91 CO_2H	3	37	10	H_2O	79.9
	4	37	20	H_2O	93.6
	5	37	10	MeCN	0[c]
exo **100**	6	37	10	H_2O	25.5
	7	37	20	H_2O	39.0
endo **101**	8	37	10	H_2O	49.2
exo **102**	9	37	10	H_2O	20.3
103	10	37	60	H_2O	0

[a] Each reaction was carried out using 100 µL of [68Ga]DOTA-Tz (typical activity of ~ 5 MBq); *n* = 3 in all cases. [b]Radiochemical yield as determined via radio-HPLC showing conversion of [68Ga]DOTA-Tz into the summation of the product isomers. [c]Decomposition of [68Ga]DOTA-Tz was observed

Table 11. Radiolabelled IeDDA reactions between a series of alkenes and [68Ga]DOTA-Tz under different conditions

The reaction was initially carried out using ethyl vinyl ether **93**, in order to demonstrate that the tetrazine is reactive towards alkenes which do not contain any ring strain, but which are electronically activated. Ethyl vinyl ether **93** gave approximately 10% conversion to the corresponding dihydropyridazine product from [68Ga]DOTA-Tz at 37°C in 10 min (Entry 1,

Table 11), and increasing the temperature to 90°C (Entry 2, Table 11) increased this conversion to nearly 30% (Figure 126).
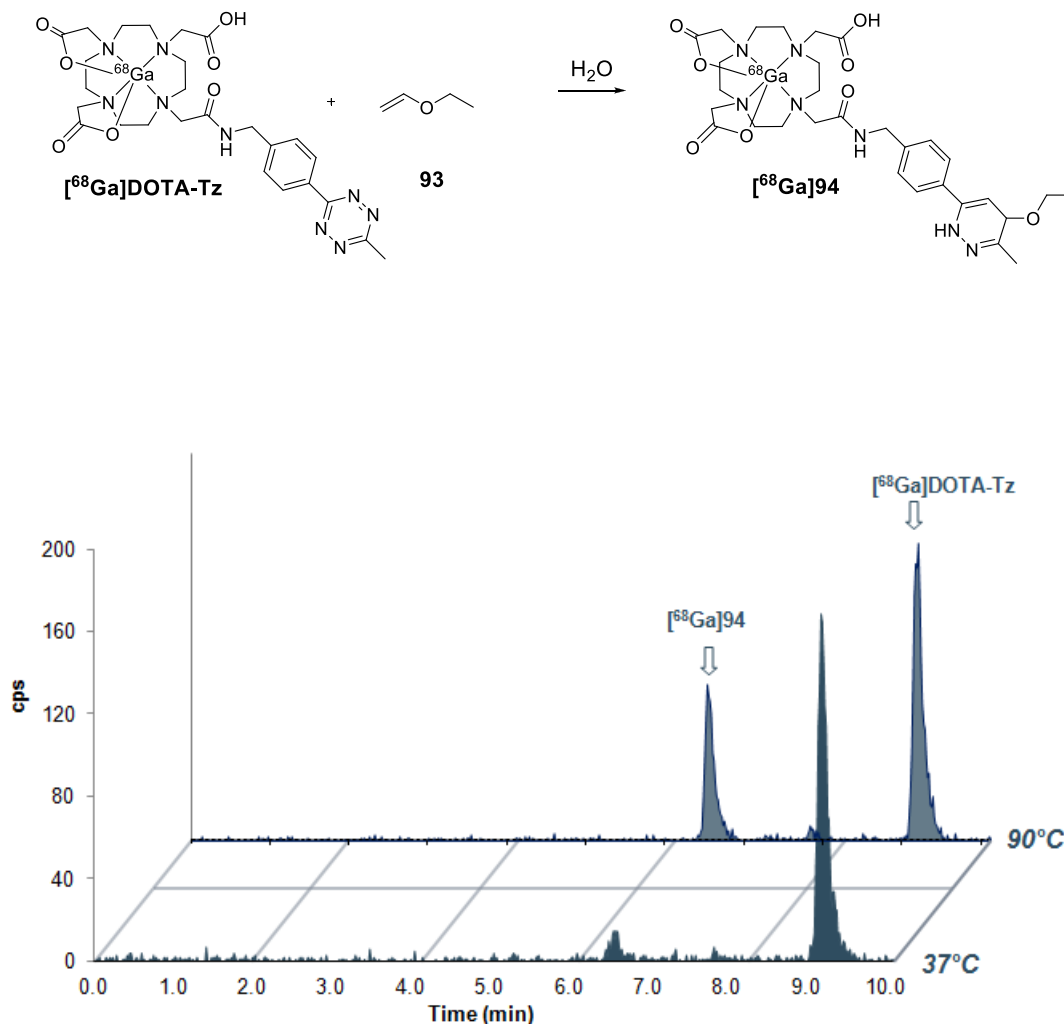
Figure 126. Radio-HPLC traces of a) The reaction mixture between [^{68}Ga]DOTA-Tz and **93** at: 37°C in H_2O after 10 min, 90°C in H_2O after 10 min

Although these results were not very impressive when compared to the strain-promoted reactions, and the reaction lacks the same levels of bioorthogonality, this demonstrates the possible utility of labelled tetrazines such as [^{68}Ga]DOTA-Tz for a wide range of labelling applications. For example, it could be envisaged that these conversions could be greatly enhanced by optimisation of the reaction conditions, through use of different co-solvents and by increasing the reaction temperatures and time.

As mentioned, norbornenes have been shown to react rapidly with tetrazines, due to the large amount of strain contained in the alkene. [115, 215] It was not surprising therefore to find that radiolabelled tetrazine **[^{68}Ga]DOTA-Tz** showed high levels of reactivity with this alkene (Figure 127).
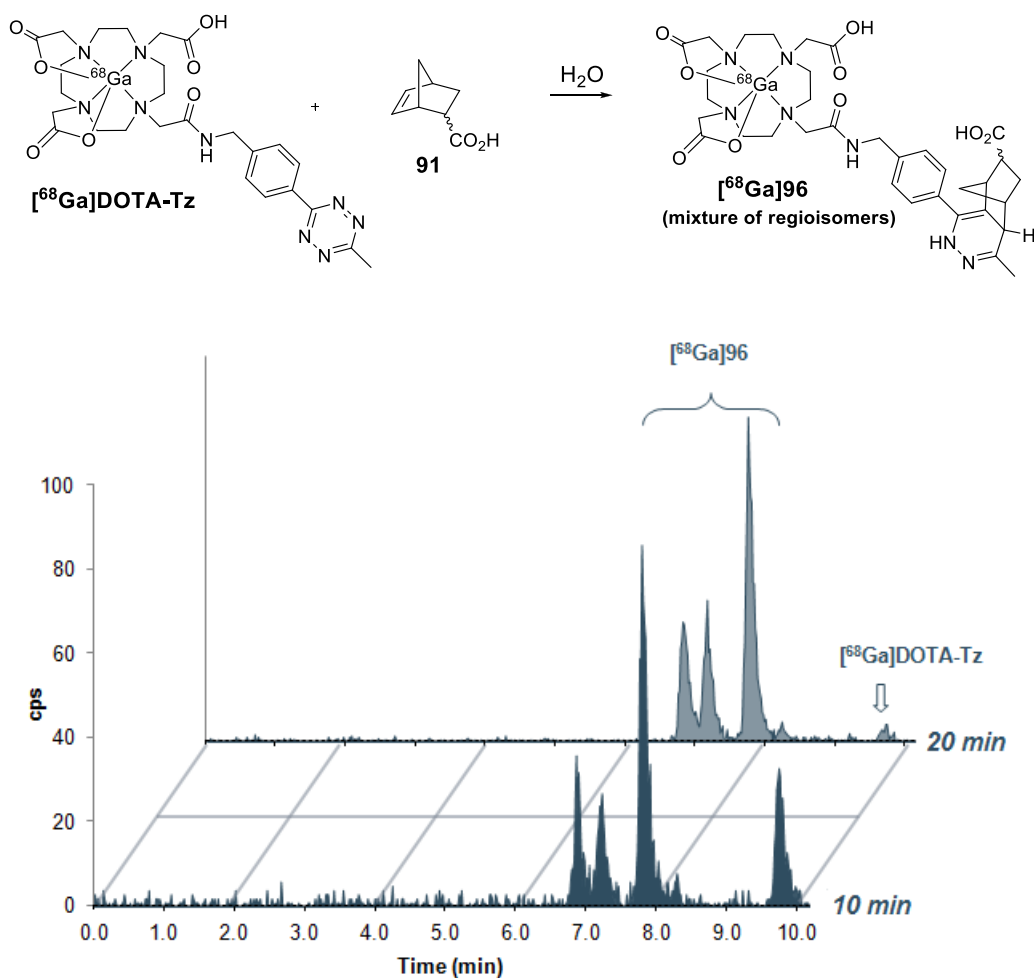

Figure 127. Radio-HPLC traces of a) The reaction mixture between **[^{68}Ga]DOTA-Tz** and **91** at 37°C in H_2O after 10 min; b) The same reaction mixture after 20 min

The conversion to the 4 dihydropyridazine products **[^{68}Ga]96** was measured using the AUC for the starting material **[^{68}Ga]DOTA-Tz** radio-HPLC peak, as compared to the summation of the AUC for the radio-HPLC peaks of the products. When the carboxylic acid functionalised norbornene **91** was reacted with **[^{68}Ga]DOTA-Tz** at 37°C in H_2O for 10 min, almost 80% radiochemical conversion to the dihydropyridazine isomers was observed within just 10 min

(Entry 3, Table 11). Almost quantitative conversion to [⁶⁸Ga]96 was achieved within 20 min under the same conditions (Entry 4, Table 11).

Due to the impressive yields obtained in the reaction of radiolabelled tetrazine **[⁶⁸Ga]DOTA-Tz** with norbornene **91**, a series of modified norbornenes were reacted with **[⁶⁸Ga]DOTA-Tz**, in order to demonstrate that the tetrazine ligation could be carried out using norbornenes containing different side-chains (Entries 6-10, Table 11).

The effect of altering the side chain on norbornene was demonstrated by reacting the radiolabelled tetrazine **[⁶⁸Ga]DOTA-Tz** with a number of fluoroaniline derivatives of norbornene **91** (**100-102**). These compounds were synthesised using the amine coupling reaction between the carboxylic acid **91** and the respective fluoroanilines **104** and **105** (Figure 128).
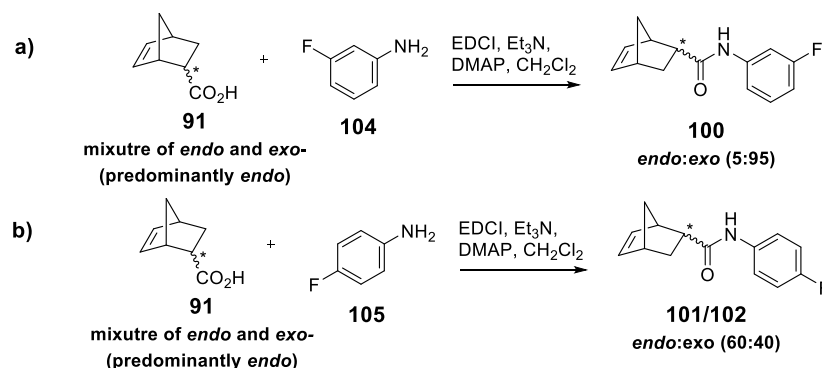

Figure 128. Reaction of norbornene-carboxylic acid **91** with a) 3-fluoroaniline **104** and b) 4-fluoroaniline **105**

The products from these reactions were obtained in good yield (>70%) and were isolated as separate *endo* and *exo* regioisomers after column chromatography and recrystallisation from a mixture of ethyl acetate and hexane.

Introducing the fluoroaniline side-chain appeared to have a pronounced effect on the radiochemical conversion to the dihydropyridazine products within 10 min. This may, at least in part, be attributable to their reduced water solubility as compared to compound **91**. The lower reactivity of radiolabelled tetrazine **[⁶⁸Ga]DOTA-Tz** towards these compounds may also have been due to the introduction of a slightly larger side-chain, as the most significant difference in the rate was observed with the *exo* isomers **100/102**, which formed the

respective dihydropyridazine products in ~20-25% conversions in 10 min at 37°C (Entries 6, 7 and 9, Table 11). The *endo* 4-fluoroaniline analogue **101** showed the most comparable reaction rate to norbornene **91**, forming the products in ~50% conversion (*vs.* 80% for **91**) within 10 min at 37°C (Entry 10, Table 11) which may reflect the better alignment between the tetrazine and the double bond in the transition state for the cycloaddition (Figure 129).
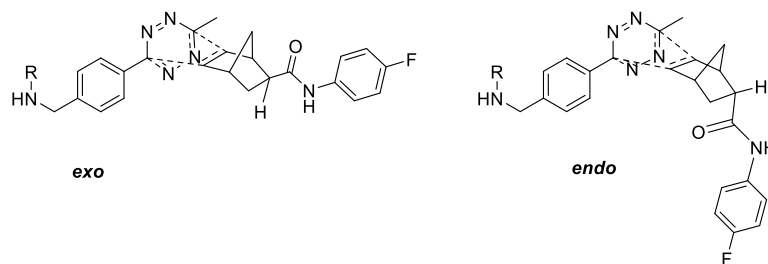
Figure 129. Possible transition states for the favoured (*exo*) orientation between the tetrazine [⁶⁸Ga]DOTA-Tz and norbornenes **101** and **102**

In order to demonstrate the biocompatibility of the IeDDA reaction, we also tested the reactivity of the tetrazine towards L-tryptophan **103**; an "alkene"-containing α-amino acid, which is found in high abundance in the human body. Reaction of **[⁶⁸Ga]DOTA-Tz** with this compound under physiological conditions would hinder the use of this strategy in biological applications, such as pretargeted imaging. However, despite containing an alkene, which displays enamine type reactivity despite also being part of the aromatic indole ring, compound **103** did not show any reactivity towards out tetrazine under these conditions (Entry 11, Table 11), eliminating this as a potential problem, and demonstrating further the reaction's utility in biological applications.

In order to make a direct comparison with the SPAAC reaction, the reaction with the 'simple' norbornene was also carried out in acetonitrile as solvent. However, rather than observing the expected dihydropyridazine products, a different product was formed which had a similar retention time to the radiolabelled tetrazine **[⁶⁸Ga]DOTA-Tz**. It was proposed that this product was formed as a result of a different cycloaddition reaction between the tetrazine

and the nitrile moiety of acetonitrile, presumably by a similar mechanism to that proposed for the reaction of tetrazines with isonitriles.[216]

Each of the alkenes used in the radiolabelling experiment was reacted with 'cold' tetrazine **DOTA-Tz**, and the products were conjugated with ^{69}Ga using Ga(NO$_3$)$_3$, in order to confirm the products formed from the radiolabelling experiment (Figure 130).
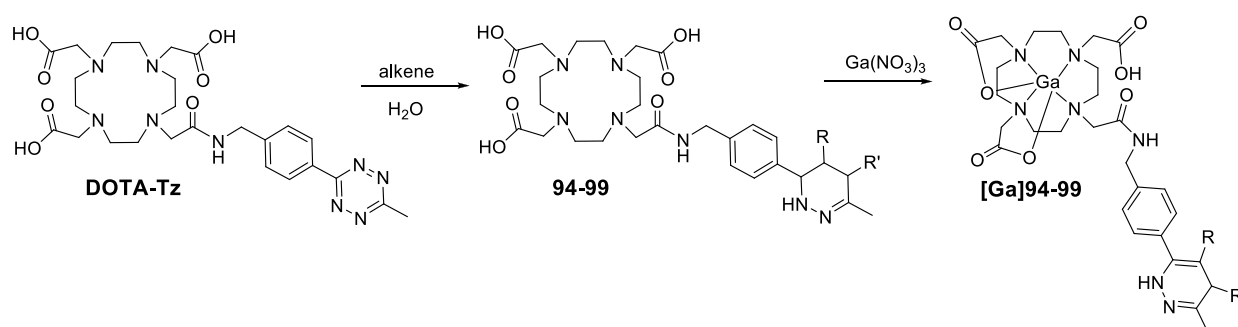

Figure 130. Synthesis of 'cold' labelled dihydropyridazine products

All of the 'cold' labelled compounds were characterised by HRMS and the products **94-99** obtained from these reactions were additionally used as 'cold references' for confirmation of the identity of the radiolabelled products (see experimental section for more details).

4.3.3 Conclusions

The readily synthesised ^{68}Ga-labelled tetrazine **[^{68}Ga]DOTA-Tz** was demonstrated as useful prosthetic group for radiolabelling of an array of small molecules *via* bioorthogonal chemistry. Norbornenes, in particular, appeared to show impressive reaction rates with the radiolabelled tetrazine, and may be considered as a potential chemical handle for the pretargeting approach. These reactions could be applied to the labelling of suitably functionalised biomolecules, and ultimately could be applied to pretargeted imaging. Moreover, it was anticipated that the already impressive rates could be improved, for example by use of a more strained dienophile, which would expand further the potential for these compounds to be used for a wide range of applications.

4.4. Overall Conclusions

The main advantages of the IeDDA cycloaddition over the SPAAC reaction include the improved compatibility with aqueous media, and the ability to achieve reasonable to high radiochemical conversions at low temperatures (37°C), and at low concentrations. In addition to this was the more achievable synthesis of the tetrazine precursors (which may be prepared in just 1 step) as compared to cyclooctynes. Dienophiles such as norbornene are commercially available, containing functional groups which enable simple modifications to be made, such as ligation to biomolecules.

For these reasons, radiolabelled tetrazine **[^{68}Ga]DOTA-Tz** could be used for a number of applications, including labelling biomolecules containing strained alkenes such as norbornenes or TCO.[217] The radiolabelled tetrazine **[^{68}Ga]DOTA-Tz** additionally demonstrated good stability in PBS within 2 h, complying with a high level of biocompatibility. It was therefore imagined that the prosthetic group **[^{68}Ga]DOTA-Tz** may be considered as a potential chemical reporter for the hypothesised pretargeting strategy, and this idea would consequently be explored in more detail.

Chapter 5 – Application of the IeDDA

Reaction To Pretargeting

5.1   RGD Cyclic Pentapeptides for an Attempted *in vitro* IeDDA Reaction

5.1.1 Hypothesis for Pretargeting Using RGD Cyclic Pentapeptides

Due to the large size, and ensuing difficulties involved in the characterisation of antibodies, we hypothesised that it would be worthwhile validating the IeDDA using smaller biomolecules such as peptides. As directly-labelled cyclic RGD peptides are already being evaluated as tracers for PET imaging, it would be possible to compare the developed direct targeting method, in which the radiolabelled RGD peptide is introduced directly onto high $\alpha_v\beta_3$ integrin expressing cells, with the postulated pretargeting strategy.[218-224] Based on the promising reactivity of norbornene in the IeDDA reaction with the radiolabelled tetrazine **[68Ga]DOTA-Tz**, as discussed in Chapter 4, this strategy would involve ligating the norbornene to a cyclic RGD pentapeptide. Accumulation of the modified peptide onto high $\alpha_v\beta_3$ integrin cells would be followed by introduction of the radiolabelled chemical reporter **[68Ga]DOTA-Tz**, with the expectation that the IeDDA reaction would occur on the cell surface (Figure 131).
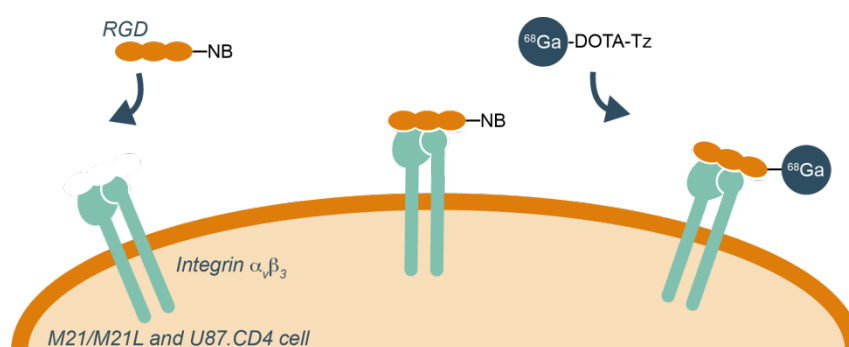
Figure 131. Proposed *in vitro* pretargeting between RGD cyclic pentapeptides (RGD) ligated with a norbornene functional group (NB) and **[68Ga]DOTA-Tz**

It was anticipated that this method would help to provide us with proof-of-principle for pretargeting using the IeDDA reaction using the tetrazine/norbornene reaction partner.

5.1.2 Introduction to RGD Cyclopentapeptides for Targeting $\alpha_v\beta_3$ Integrin

The integrin family are heterodimers of 19 α- and 8 β- subunits non-covalently imbedded into the cell membrane, for which there are 25 known members.[218] The binding of integrins to

their respective ligands plays a critical role in processes such as cell attachment, proliferation, tumour invasion, angiogenesis and metastasis, as well as a number of other significant pathological events. For this reason, integrins have been utilised as targets for cancer therapy and imaging, and $\alpha_v\beta_3$ integrin has been extensively evaluated for its role in tumour growth and angiogenesis.

The $\alpha_v\beta_3$ receptor ligand has demonstrated good affinity for the RGD (Arg-Gly-Asp) tripeptide sequence, as it is the minimum sequence in naturally-occurring ligands that bind the $\alpha_v\beta_3$ receptor, and for this reason peptides containing this sequence have often been used as targets for the receptor over other integrins. Linear RGD peptides, for example GRGDS (Gly-Arg-Gly-Asp-Ser), often have lower affinity ($IC_{50} > 100$ nM) than cyclised RGD peptides, as the fourth amino acid alters the binding specificity and are often susceptible to chemical degradation.[225] Structure-activity-relationship (SAR) studies have shown that incorporating the RGD sequence into a cyclic pentapeptide framework leads to further selectivity and binding affinity for the receptor. The rigidity that is conferred by cyclisation prevents degradation, and for this reason, cyclic peptides are more stable, potent and specific for the $\alpha_v\beta_3$ receptor. Additional amino acids are required to build the ring system, and the RGD sequence can be placed in a conformation that is specific for the integrin. For example, c(RGDfK) is one of such cyclic pentapeptides, whereby an unnatural D-Phe amino acid and a lysine (K) residue has been incorporated (Figure 132).

| The original RGD sequence | Cyclic peptide c(RGDfK) | Modified RGD peptide 'RGD-NB' |
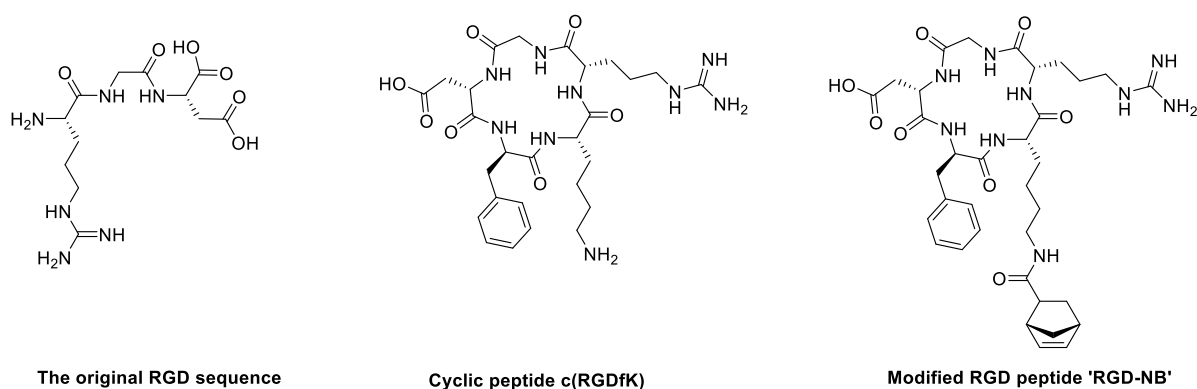
Figure 132. (left) the original straight-chain Arg-Gly-Asp (RGD) tripeptide sequence, (middle) c(RGDfK); an example of a cyclic pentapeptide incorporating a D-Phe amino acid and a lysine residue (right) 'RGD-NB', the hypothesised modified cyclic pentapeptide incorporating a norbornene moiety

172

As a consequence of the high selectivity of RGD cyclic pentapeptides to the $\alpha_v\beta_3$ receptor binding site, these peptides have been evaluated as PET potential tracers for imaging angiogenesis in tumours by direct labelling of the peptides, for example through introduction of a DOTA or NOTA chelate for ^{68}Ga labelling.[218-224]

5.1.3 Synthesis of a Norbornene Modified RGD Cyclopentapeptide

In light of the reactivity of norbornene derivatives in the radiolabelling studies and kinetic experiments described in chapter 4, we envisaged synthesis of a norbornene-functionalised RGD peptide, which would be reactive towards radiolabelled tetrazine **[^{68}Ga]DOTA-Tz**. The norbornene moiety was introduced onto the lysine residue of the peptide, as it has been demonstrated that functionalising this amino acid has little effect on the binding affinity of RGD to the $\alpha_v\beta_3$ receptor.[224] The RGD cyclic pentapeptide was synthesised on a 2-chlorotrityl resin using a solid-support peptide coupling procedure, which has previously been described for the synthesis of this peptide sequence. Introduction of the norbornene group was carried out with the peptide still on the solid support, as three additional amino acid residues were required to complete the peptide sequence after introduction of this group (Figure 133).[43, 224, 225]

Figure 133. Synthesis of the RGD cyclic pentapeptide **RGD-NB** on a 2-chlorotrityl resin.

Once the amino acid sequence was completed, the fully functionalised peptide was cleaved from the resin and the cyclisation reaction was carried out using a mixture of sodium bicarbonate and DPPA in DMF. The remaining protecting groups (*tert*-butyl and Pbf) were subsequently removed using a mixture of TFA, TIS and water to give the final crude peptide **RGD-NB** in an overall yield of 15%. The obtained peptide was purified, first by precipitating

174

in diethyl ether to form a white solid, and then using preparative HPLC to obtain the pure peptide.

An alternative method was additionally used for synthesis of the modified peptide **RGD-NB**, which was achieved in 60% overall yield from commercially available protected cyclic RGD peptide **104** (Figure 134).

Figure 134. An alternative method used for the synthesis of **RGD-NB** from commercially available protected c(RGDfK) **104** using NB-NHS

This method involved coupling a norbornene-NHS ester to the available lysine residue on peptide **104**. The modified peptide **RGD-NB** was deprotected under the same deprotection conditions as before, using a mixture of TFA, TIS, and water, and the resulting material was purified as previously described. All of the obtained peptide products were characterised by HRMS and the purity was confirmed using analytical HPLC (see experimental section for example spectra and HPLC traces).

5.1.4 *In Vitro* Control Experiments by Direct Targeting

Two control experiments were carried out in order to validate the RGD binding affinity using the assay that would be used for the pretargeting strategy. The first of these control experiments was carried out using a DOTA-containing **RGD-dimer**, which is a commercially available peptide and is routinely labelled using ^{68}Ga. This peptide has been demonstrated to show a higher affinity for the $\alpha_v\beta_3$ receptor than the monomeric peptide, and so may be

considered an alternative structure for modification in the future.[220, 226] The second control experiment was carried out using a DOTA-containing **RGD-monomer**, which is structurally more similar to the modified peptide **RGD-NB**, and was synthesised on the 2-chlorotrityl resin as described previously (*cf.* Figure 133). Both of the control RGD peptides were labelled with ^{68}Ga using similar conditions to those described for the radiolabelled DOTA-tetrazine **[68Ga]DOTA-Tz** (Figure 135).[224]
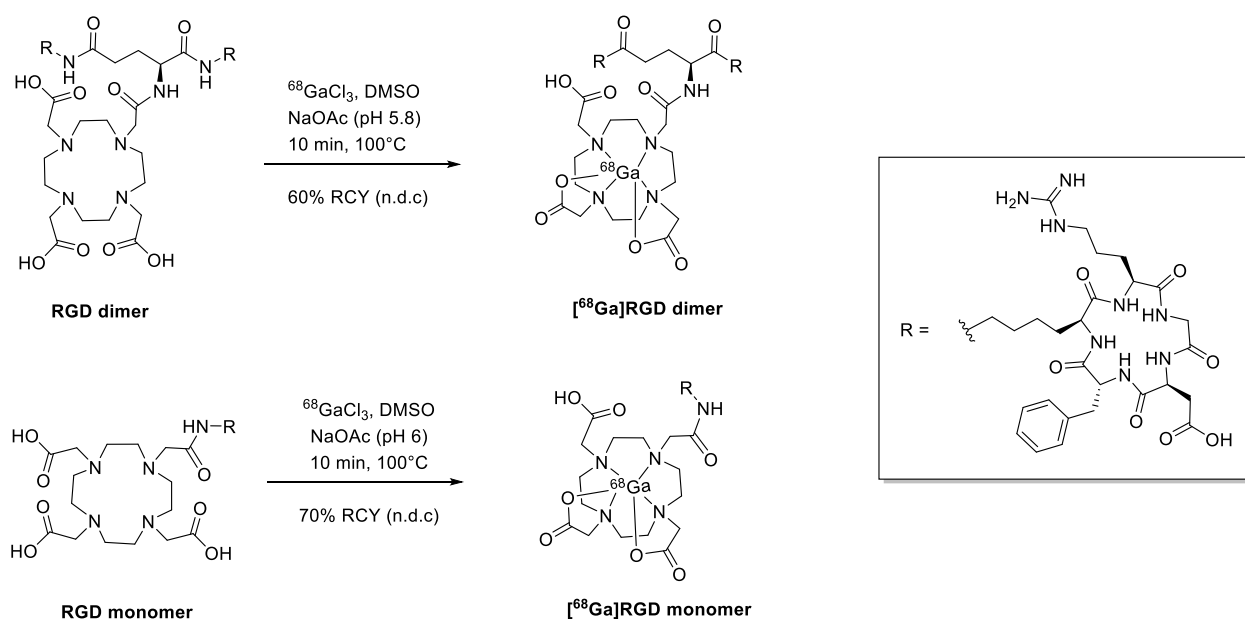
Figure 135. Radiosynthesis of **[68Ga]RGD-dimer** and **[68Ga]RGD-monomer**

The two labelled peptides were obtained in good overall radiochemical yields (60% and 70% n.d.c at the end of synthesis). The slightly lower than expected yields for **[68Ga]RGD-dimer** were a result of the difficulties in eluting the compound from the C_{18} cartridge, which consequently lead to a portion of the activity being retained on the cartridge. In both cases, however, the radiolabelling was achieved in >95% radiochemical conversion from [68]GaCl$_3$, with >95% radiochemical purity (*n* = 3 for both reactions), and sufficient material was obtained for carrying out the proposed biology experiments.

Cell lines, each expressing different levels of $\alpha_v\beta_3$ integrin receptor, were treated directly with the radiolabelled RGD peptides. Each experiment was repeated at least three times in order

to validate the assay for potential use for the pretargeting approach, which was to be demonstrated in ensuing experiments (Figure 136).
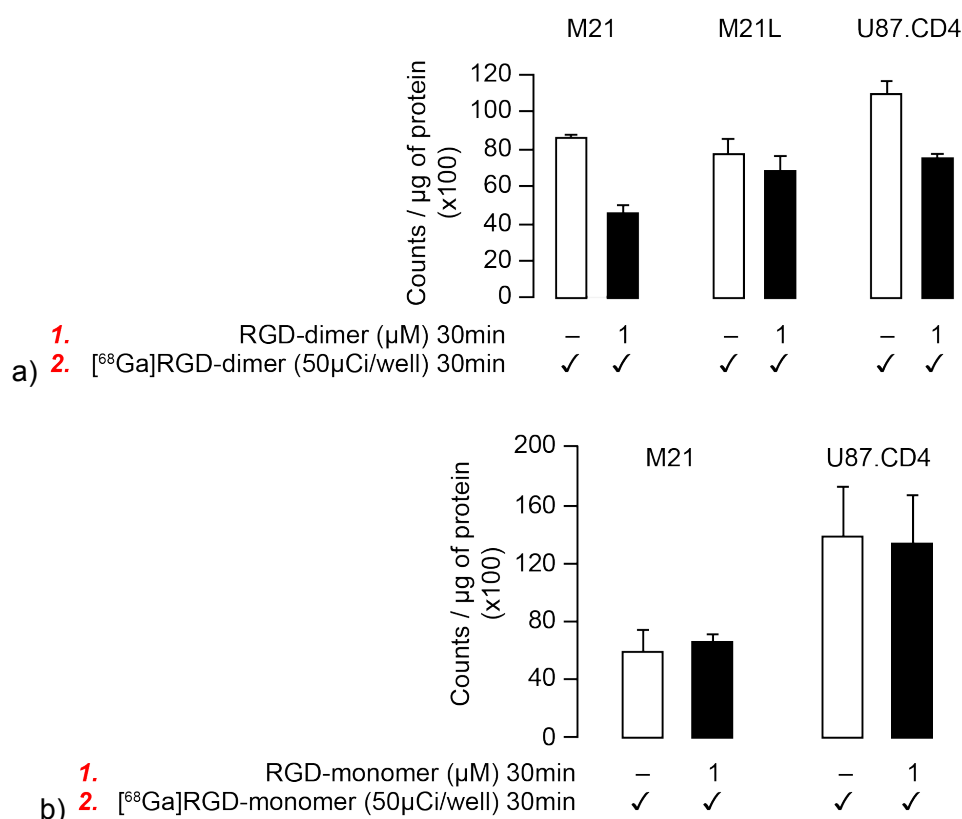
**Figure 136. Control *in vitro* experiments using 'direct' targeting*** Low (M21L) and high (U87.CD4 and M21) $\alpha_v\beta_3$ integrin expressing cell lines were treated with with a) 50 **µCi [68Ga]RGD-dimer** (white bars), or 1 µM **RGD-dimer** for 30 min + 50 µCi **[68Ga]RGD-dimer** (black bars); b) 50 µCi **[68Ga]RGD monomer** (white bars), or 1 µM **RGD-monomer** for 30 min + **[68Ga]RGD monomer** (black bars). The bars represent the mean uptake of 68Ga in each cell line after 30 min incubation. Error bars represent the standard errors of the mean. **In vitro* work was carried out by Dr Quang-De Nguyen.

As anticipated, the radiolabelled dimeric peptide **[68Ga]RGD-dimer** showed the highest levels of affinity towards the high $\alpha_v\beta_3$ integrin expressing cell line (U87.CD4), as evidenced by the highest uptake of radioactivity in these cells.[226] Pre-treating these cells with the 'cold' peptide **RGD-dimer** showed a marked reduction of the uptake in these cells, presumably due to blocking of the $\alpha_v\beta_3$ integrin receptors.

The second control experiment was required as it provided a more accurate demonstration of the binding affinity of a single molecule of RGD, and gave an indication as to the levels of uptake that we might expect to achieve using the pretargeted approach. The smaller peptide **[68Ga]RGD-monomer** expressed similar levels of activity on the high integrin expressing cell line (U87.CD4) as the larger dimeric peptide. However, there was no apparent difference

between the cell lines which were blocked with 'cold' peptide **RGD-monomer** and those which were not pre-treated, suggesting a substantially lower overall affinity for the $\alpha_v\beta_3$ integrin receptor than the dimeric peptide. This was later confirmed by blocking the cells with the 'cold' dimeric peptide **RGD-dimer**, which showed a more significant decrease in the observed activity following treatment with radiolabelled monomeric peptide **[^{68}Ga]RGD-monomer**.

As a consequence of these preliminary studies, it was decided that the dimeric peptide **RGD-dimer** would be used for carrying out the blocking studies for the proposed *in vitro* pretargeting. As this peptide showed the highest overall affinity for the receptor, this would in theory allow for the greatest difference in signal between the pre-treated cells and those which were not blocked by the peptide to be demonstrated.

5.1.4 Attempted *In Vitro* Pretargeting Using Norbornene Modified RGD

The cell lines used for the previous control experiments were used for application to the pretargeting strategy. This first involved incubating the cells with the modified peptide **RGD-NB** for 30 min, followed by treatment with approximately 50 µCi of the radiolabelled tetrazine **[^{68}Ga]DOTA-Tz** per well (Figure 137).

	M21		M21L		U87.CD4	
1. RGD-dimer (µM) 30min	–	1	–	1	–	1
2. RGD-NB (µM) 30min	1	1	1	1	1	1
3. [^{68}Ga]DOTA-Tz (50µCi/well) 30min	✓	✓	✓	✓	✓	✓
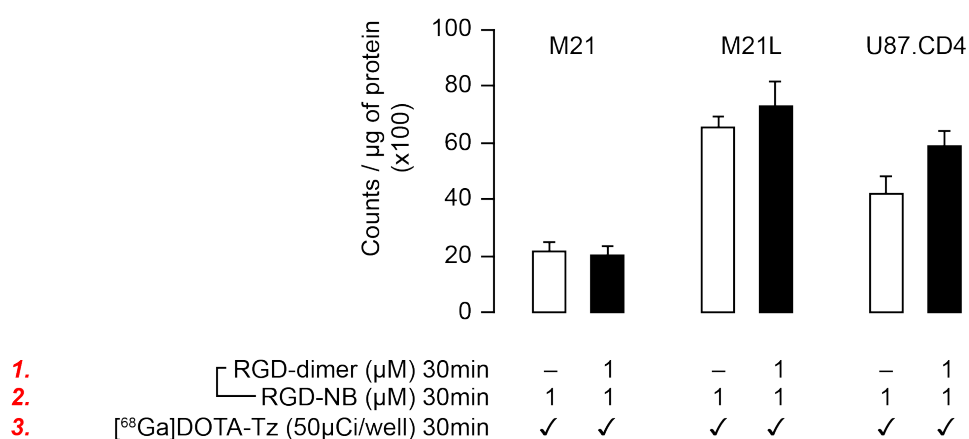
Figure 137. Attempted *in vitro* pretargeting* Low (M21L) and high (U87.CD4 and M21) $\alpha_v\beta_3$ integrin expressing cell lines were treated with a) 1 µM **RGD-NB** for 30 min + 50 µCi of **[^{68}Ga]DOTA-Tz** (white bars); b) (1 µM **RGD-dimer** + 1 µM **RGD-NB**) for 30 min + 50 µCi of **[^{68}Ga]DOTA-Tz** (black bars) . The bars represent the mean uptake of ^{68}Ga in each cell line after 30 min incubation. Error bars represent the standard errors of the mean. *In vitro work was carried out by Dr Quang-De Nguyen.

Unlike with the control experiment with **RGD-dimer**, the pattern of activity in each cell line suggested that non-specific binding was occurring. Specifically, the low uptake pattern in the low expressing cell line (M21L) was not substantially different to the higher expressing cell lines (M21 and U87.CD4) and none of the observed activity could be successfully blocked by the dimeric peptide. This suggested that the observed activity was caused by background from the radiolabelled tetrazine **[^{68}Ga]DOTA-Tz**, rather than been related to the affinity of the monomeric peptide, or by the IeDDA reaction occurring on the surface of the cells. This was additionally confirmed by treating the cells with the tetrazine **[^{68}Ga]DOTA-Tz** only, which displayed similarly high levels of activity.

It was concluded from these experiments that either the IeDDA reaction was not occurring on the cells, or that the monomeric peptide **RGD-monomer** did not have high enough affinity for the $\alpha_v\beta_3$ integrin receptor, suggesting that some further optimisation would be required in order to achieve significant results *in vitro*.

The first strategy explored in order to improve the *in vitro* reaction was to validate the reaction in a vial, using the functionalised peptide, with the intention to improve the reactivity of the two cycloaddition partners. Surprisingly, when the reaction between the modified peptide **RGD-NB** and the radiolabelled tetrazine **[^{68}Ga]DOTA-Tz** was attempted in a vial, no product was formed, as determined by monitoring the reaction on the radio-HPLC trace after 15, 30 or 60 min after incubation in PBS at 37°C. These observations were attributed to the reactive site (i.e. the alkene functional group) perhaps having become too hindered by the large cyclic pentapeptide structure to allow reaction with the tetrazine.

Due to these findings, a PEG3 chain was introduced in order to create more distance between the RGD structure and the reactive norbornene, with the hope that this would enhance the reactivity of the available alkene functional group towards ligation with the tetrazine (Figure 138).
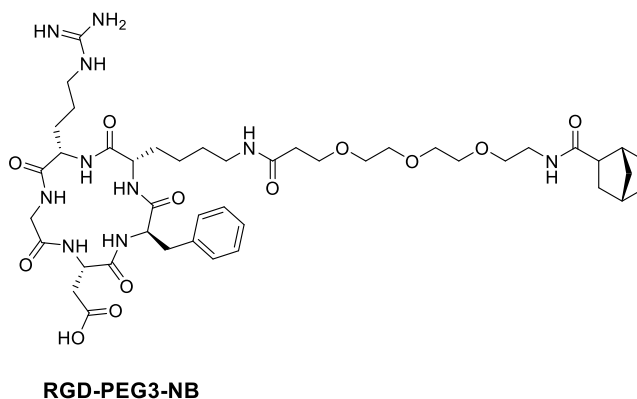
RGD-PEG3-NB

Figure 138. An alternative RGD peptide, **RGD-PEG3-NB**

This compound was synthesised in the same manner as the original modified peptide **RGD-NB** (*cf*. Figure 133). However, even this peptide **RGD-PEG3-NB** did not show any reaction with the radiolabelled tetrazine **[^{68}Ga]DOTA-Tz** under the conditions used. This result suggested that the reason for the lack of reactivity between the tetrazine and the modified peptides could be more complex than at first glance. It was concluded that further optimisation of the reaction partners would be required in order to validate the IeDDA reaction *in vitro*.

5.1.6 Conclusions

None of the norbornene-modified RGD cyclic pentapeptides developed so far had demonstrated the expected reactivity with radiolabelled tetrazine **[^{68}Ga]DOTA-Tz** in a vial or *in vitro*. However, cyclic RGD peptides have previously been used for carrying out 'click'-type reactions with ^{18}F-labelled prosthetic groups, and so these results may be considered unexpected, especially considering the reactivity of norbornenes towards the radiolabelled tetrazine **[^{68}Ga]DOTA-Tz** in previous experiments.[63] It was concluded, therefore, that further modifications needed to be made in order for the IeDDA reaction to be demonstrated for the required pretargeting approach.

5.2   An Alternative DOTA-Tetrazine for [68]Ga Radiolabelling

5.2.1 Synthesis of DOTA-GA-Tz

Due to the observed lack of reactivity of our radiolabelled tetrazine **[68Ga]DOTA-Tz** towards the norbornene-modified RGD peptides, an alternative method towards improving the reactivity was explored. It was hypothesised that the introduction of a linker between the DOTA chelate and the tetrazine moiety might improve the availability of the tetrazine for cycloaddition with alkenes containing bulky side-chains, such as biomolecules. An alternative DOTA-ligated tetrazine **DOTA-GA-Tz** was therefore synthesised from tetrazine **Tz3**. The synthesis of this compound involved introduction of a carboxylic acid side-chain onto tetrazine **Tz3**, initially by reaction of the amine residue with glutaric anhydride. Unlike when the same reaction was carried out with symmetrical tetrazine **Tz1** (*cf.* section 4.1), this reaction proceeded efficiently, affording the acid product **105** in almost quantitative yields after purification by column chromatography (Figure 139).
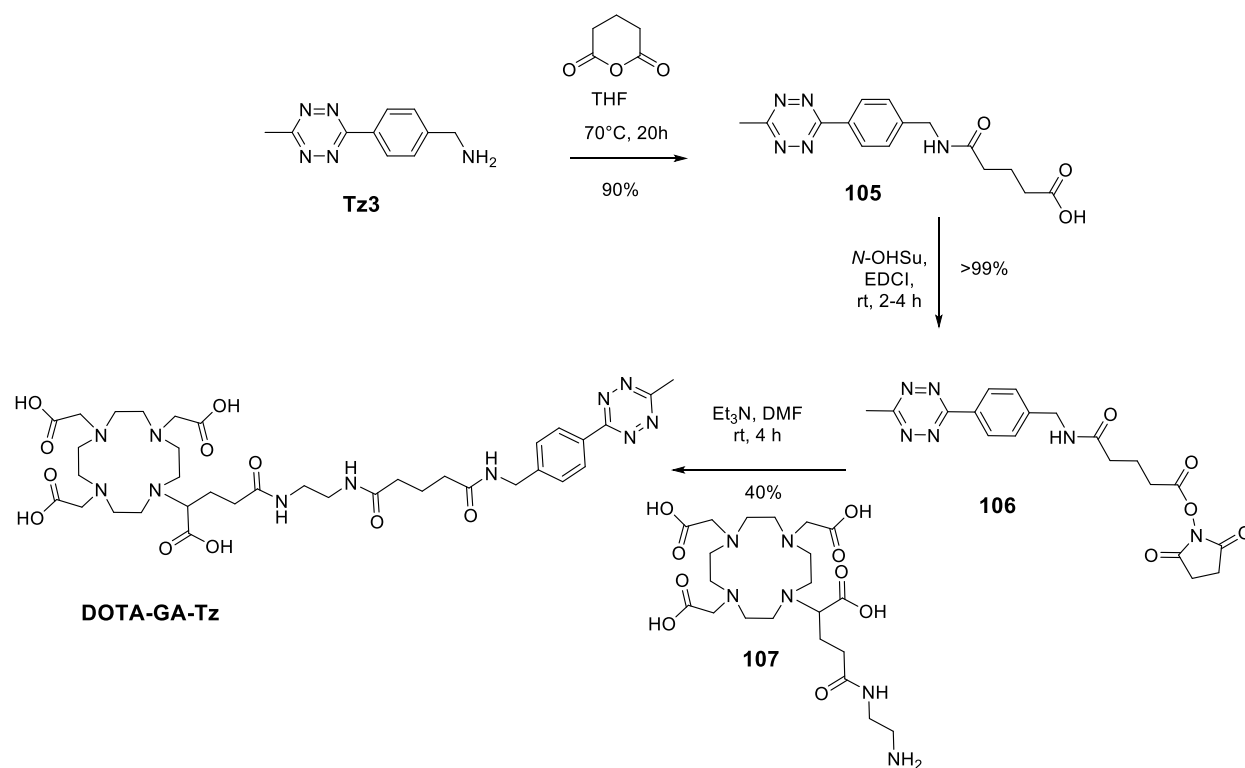
Figure 139. Synthesis of **DOTA-GA-Tz** from **Tz3**

A simple reaction of the carboxylic acid **105** with NHS allowed for the formation of a succinimide ester activated acid derivative **106**, which could subsequently be reacted with the free amine on the DOTA-derivative **107** in the presence of a mild base. The final DOTA analogue **DOTA-GA-Tz** could be purified by preparative HPLC, and was isolated in 40% yield. The lower than expected yield for this final step was a consequence of problems during purification; the multiple protonation states in the product resulted in the product eluting from the HPLC at different retention times. This situation could be moderately improved by dissolving the crude material in acidic media prior to purification.

5.2.2 Radiosynthesis of [^{68}Ga]DOTA-GA-Tz

The structurally modified DOTA chelate containing the tetrazine moiety **DOTA-GA-Tz** was radiolabelled under the same conditions as the original compound **DOTA-Tz**, and up to 95% conversions to the labelled product were observed from ^{68}GaCl$_3$ when the reaction was carried out in pH6 NaOAc buffer. The crude material could be purified by passing through a Sep-Pak light C$_{18}$ cartridge, as was described for the radiosynthesis of previously labelled **[^{68}Ga]DOTA-Tz** (see section 4.3), forming the radiolabelled product in >95 % radiochemical purity (Figure 140).
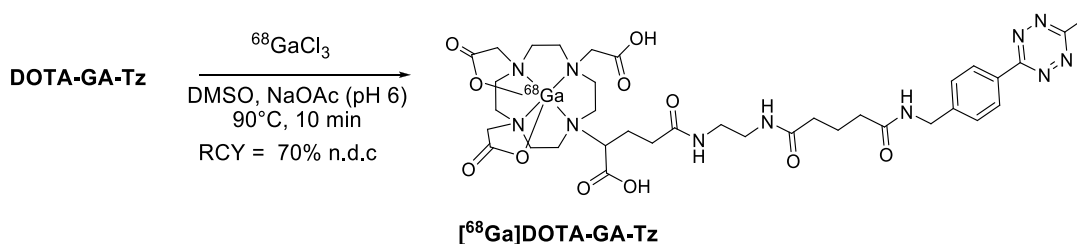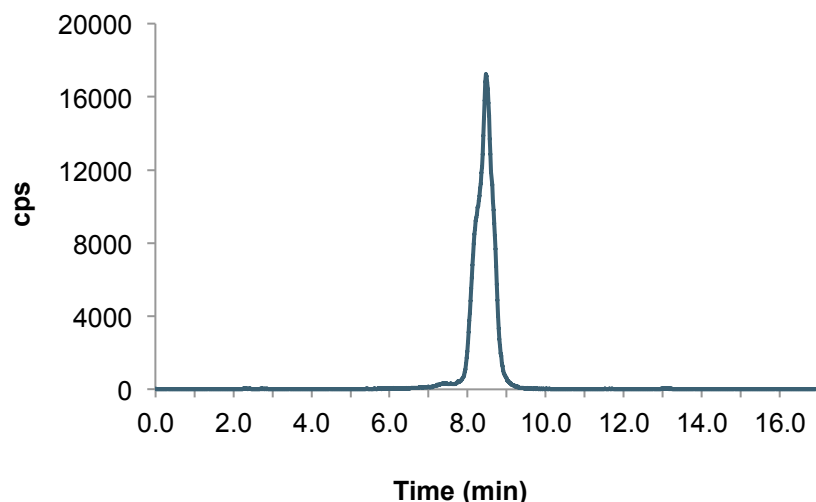
Figure 140. Radiosynthesis of **[^{68}Ga]DOTA-GA-Tz** from **DOTA-GA-Tz**, and radio-HPLC trace of purified **[^{68}Ga]DOTA-GA-Tz**

The ^{68}Ga-labelled product was obtained by treating the conditioned C_{18} cartridge with the crude material, and subsequently washing with 500 μL of water, before eluting the product in five 100 μL fractions of ethanol. When starting the reaction with 6.8 mCi of ^{68}GaCl$_3$, a maximum of 2.5 mCi of the product could be eluted in the most concentrated fraction, with a total of 4.7 mCi of the product being obtained 'end-of-synthesis'; equivalent to a radiochemical yield of 70% (n.d.c).

The specific activity of the obtained fractions of radiolabelled tetrazine **[^{68}Ga]DOTA-GA-Tz** was calculated in a similar manner to the previously purified compound **[^{68}Ga]DOTA-Tz** (*cf.* section 4.3). Known concentrations of 'cold' compound were injected, and the AUC was measured at each of the known concentrations, providing a linear plot, which could be used to calculate the concentration of the non-labelled compound in the sample (Figure 141).
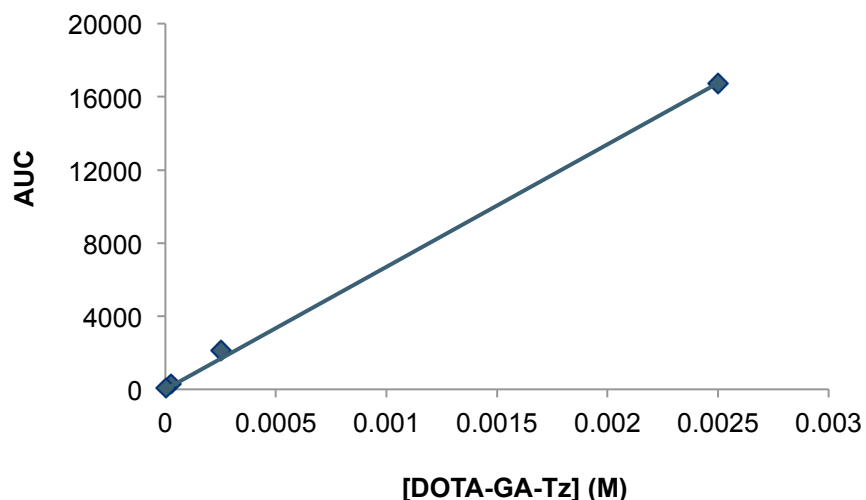
Figure 141. A graph showing [**DOTA-GA-Tz3**] *vs.* the measured AUC from the UV trace, used to measure the specific activity of [**^{68}Ga]DOTA-GA-Tz3**

Initially, the specific activity of the labelled compound was calculated at 162 µCi µmol^{-1}, as determined from the synthesis starting with approximately 900 µCi of ^{68}GaCl$_3$. This specific activity was obtained using 50 µL of a 1 mgmL^{-1} solution of the **DOTA-GA-Tz** (equivalent to 0.06 µmol) at the start of the synthesis. Using 6.5 mCi of ^{68}GaCl$_3$ at the start of the synthesis, the specific activity could be improved to 540 µCi µmol^{-1} (using a new ^{68}Ga generator), using the same amount of precursor **DOTA-GA-Tz**. This could be significantly enhanced by using only 25 µL of the stock solution of **DOTA-GA-Tz** (0.03 µmol). Using these parameters, the purified compound could be obtained with a specific activity of up to1.5 Ci µmol^{-1}, and this value was calculated for each of the radiolabelling experiments that were carried out, and was found to be consistent across each subsequent experiment (*n* > 10).

In order to demonstrate the biocompatibility of this compound further, the stability of this compound was tested, by incubating ~100 µCi of conjugate **[^{68}Ga]DOTA-GA-Tz** in PBS. The radio-HPLC of the solution was taken after 1 and 2 h after incubation at 40°C, and the experiment was repeated at least 3 times in order to ensure reproducibility (Figure 142).
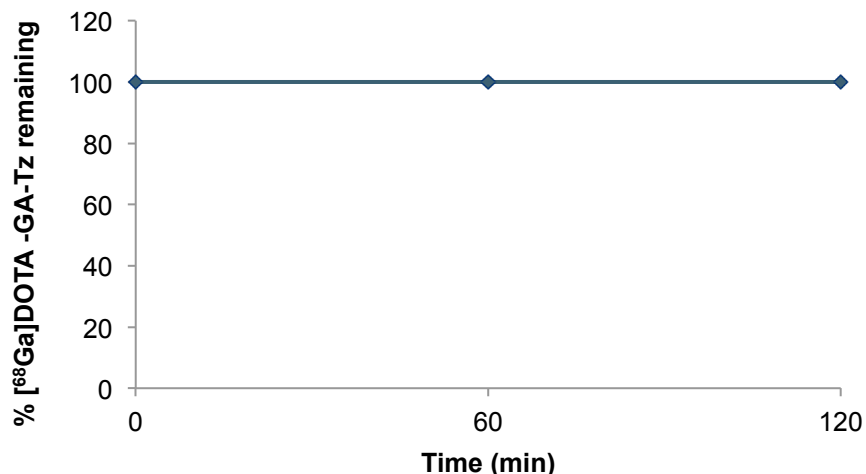
Figure 142. A graph demonstrating the stability of **[^{68}Ga]DOTA-GA-Tz** in PBS buffer after 1 and 2 h

As was observed when carrying out the same experiment with the original radiolabelled tetrazine **[^{68}Ga]DOTA-Tz**, no decomposition of the radiolabelled product was observed at the time-points measured, suggesting that this compound would be similarly stable in a biological environment, and importantly, *in vivo*.

Due to the high purity, and good specific activity of the radiolabelled tetrazine **[^{68}Ga]DOTA-GA-Tz**, we hypothesised that this compound could be used as an alternative to the previously radiolabelled tetrazine **[^{68}Ga]DOTA-Tz** as a chemical reporter in the pretargeting strategy, with the hope that introduction of the linker would make the tetrazine more available for reaction with highly substituted dienophiles, such as the norbornene functionalised RGD peptides.

5.2.3 Testing the IeDDA Reaction with [^{68}Ga]DOTA-GA-Tz

Unfortunately, attempted reaction between the radiolabelled tetrazine **[^{68}Ga]DOTA-GA-Tz** and the modified peptides **RGD-NB** and **RGD-PEG3-NB**, were unsuccessful (Figure 143).
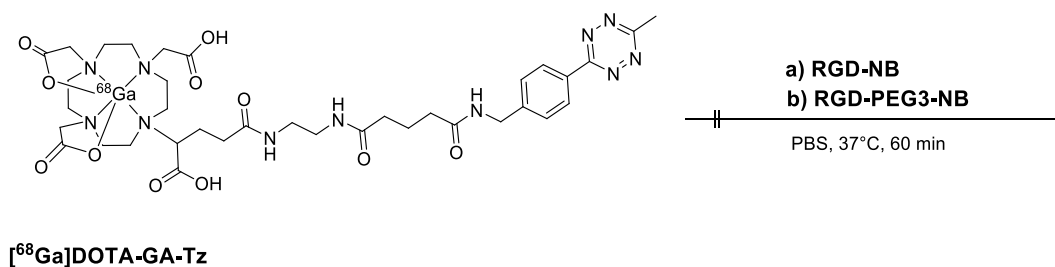
Figure 143. Attempted reaction between **[⁶⁸Ga]DOTA-GA-Tz** and a) **RGD-NB** and b) **RGD-PEG3-NB**

The lack of reactivity of the modified radiolabelled tetrazine **[⁶⁸Ga]DOTA-GA-Tz** towards both of the RGD cyclic pentapeptides, suggests that the cyclic peptide was in some way hindering the reactivity of the dienophile towards reaction with the tetrazine. One possible explanation for this observation is that the chain containing the strained alkene adopted a folded conformation inside the structure of the cyclic RGD, and subsequently blocked the alkene functional group from being available for reaction. Future work could therefore be to synthesise a linear RGD peptide in order to test this hypothesis. It should be noted however, that the linear structure does not have the same binding affinity for the $\alpha_v\beta_3$ integrin receptor as the cyclic peptide, and so it would not enable us to fully demonstrate the proof-of-principle concept for pretargeting by direct comparison to the direct targeting approach.[225] A similar reaction, however, was demonstrated by Conti and co-workers between an ¹⁸F-labelled TCO and a tetrazine-modified cyclic RGD peptide, suggesting the problems in reactivity that we observed may instead have been caused by the lower reaction rate of the norbornene moiety as compared to TCO towards IeDDA reactions with tetrazines.[227]

5.2.4 Conclusions

As a result of these observations, it was concluded that more detailed characterisation of the structure of the RGD peptides would be required in order to fully understand the negative results obtained. As was observed with the radiolabelling studies between the radiolabelled tetrazine **[⁶⁸Ga]DOTA-Tz** and norbornenes (see chapter 4), the addition of even a small a side-chain can have a significant effect on the reactivity of an appended dienophile towards tetrazines. An alternative strategy would be to introduce a greater number of norbornene

functional groups per biomolecule, which would be difficult to achieve using relatively small biomolecules such as the RGD peptides, without significantly altering the binding affinity. An alternative biomolecule would be preferable for validating the pretargeting strategy, which would allow for the addition of multiple dienophiles, and would moreover increase the probability of the reaction occurring. It was additionally considered that a more reactive dienophile would circumvent the problems observed with the reactivity of the modified biomolecules, as the increased rate of the cycloaddition must outweigh any steric problems that may prevent the reaction from occurring.

5.3   *In Vitro* Pretargeting Using TCO Modified Cetuximab

5.3.1 Hypothesis for Pretargeting Using Cetuximab-TCO

Monoclonal antibodies, as discussed previously, are particularly amenable to pretargeting due to the balance between high affinity and specificity for their receptors, coupled with slow physiological half-lives, circulation time and clearance.[139, 143, 228, 229]   Due to the apparently high reactivity of the TCO dienophile towards tetrazines, it was hypothesised that this could be ligated to the Cetuximab (C225) monoclonal antibody for subsequent application to a pretargeting strategy, using radiolabelled tetrazine **[^{68}Ga]DOTA-GA-Tz** as the chemical reporter (Figure 144).
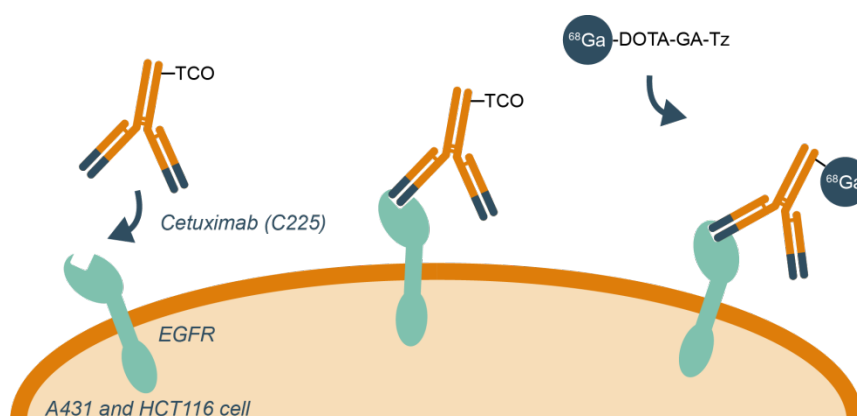
Figure 144. Proposed *in vitro* pretargeting between Cetuximab (C225) ligated with a *TCO* functional group

5.3.2 Introduction to Cetuximab as an Antibody for EGFR

Cetuximab (Erbitux/C225) is a monoclonal antibody that is used for treatment of colorectal cancer and head and neck cancer, by inhibiting the epidermal growth factor receptor (EGFR).[230] Growth factors bind to their respective receptors on the surface of the cell, which causes the receptors to produce a signal, ultimately leading to cell division.[231, 232] Mutated receptors may lead to the production of a signal which causes the cells to divide without the use of a growth factor, and hence cause uncontrolled proliferation, which may ultimately lead to cancer. The inhibition of these receptors, for example using the C225 antibody, subsequently prevents the uncontrolled growth of cells in EGFR mutated cancers.

It was anticipated that this monoclonal antibody could be used for the pretargeting strategy, as it has high affinity for the EGFR receptor, and could be used to target cells over-expressing EGFR, prior to introduction of the radiolabelled chemical reporter. Significantly, C225 would not be readily internalised into the cell, which is an important consideration in order to achieve pretargeting, especially when using a non-cell penetrating chemical reporter.

5.3.3 Introduction to *trans*-Cyclooctenes (TCOs) as Dienophiles

As was observed during the radiolabelling experiments between tetrazine **[⁶⁸Ga]DOTA-Tz** and the series of alkenes that altering the side-chain of the norbornene can have a significant effect on the rate of reaction with the tetrazine (see section 4.3). When large cyclic peptides such as the RGD cyclopentapeptide are used as the side-chain, it may be expected that this effect will be even more significant. We therefore decided to explore the use of a more reactive alkene in place of the norbornene. The hope was that the improved reaction kinetics of the small molecule with tetrazines would out-weigh any steric problems that may be caused by the peptide.

Trans-cyclooctenes (TCOs) have received increasing attention as the dienophile in the IeDDA reaction with tetrazines.[116, 136, 140, 147, 217, 233-240] These highly strained alkenes

demonstrate superior reaction kinetics with tetrazines over norbornenes, due to the increased strain that is imposed on the double bond; Weissleider and co-workers measured second order rate constants of $6000 \pm 200\,M^{-1}\,s^{-1}$ at 37°C for TCO, as compared to previously measured rate constants of $1.6\,M^{-1}\,s^{-1}$ at 20°C for norbornene using the same tetrazine.[115, 140, 207] The mechanism of the reaction is similar to that described for the IeDDA reaction with norbornenes (see chapter 4), and in the presence of protic solvents the intermediate dihydropyridizine rearranges to form isomeric dihydropyridazines products (Figure 145).[116]
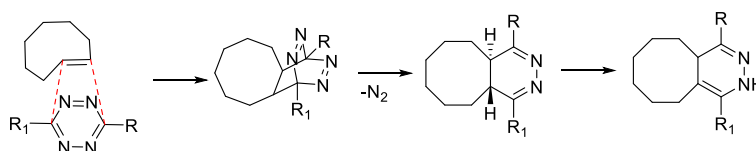
Figure 145. The IeDDA reaction between tetrazines and TCO to form dihydropyridazines, showing the mechanism of the cycloaddition and the intermediate dihydropyridizine formed

However, this increase in reactivity is balanced by a slightly lower *in vivo* stability due to the spontaneous *trans*/*cis* isomerism which may occur over time.[138, 241] The synthesis of *trans* cyclooctenes requires photochemical irradiation of the corresponding *cis* isomers,[217] but fortunately the increasing interest in the IeDDA reaction means that a number of these compounds are now commercially available, containing a range of functional side-chains, suitable for attaching to biomolecules (Figure 146).[138, 141, 242]
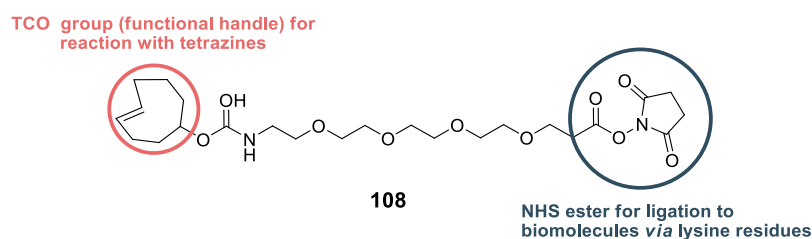
Figure 146. The structure of TCO-PEG4-NHS **108**

Due to the availability of the TCO functional handle, coupled with its promising kinetic profile with tetrazines, the IeDDA reaction between these two reaction partners has become the

most utilised bioorthogonal ligation for use *in vivo*, and has started to be utilised for pretargeted PET imaging applications, as well as for pretargeted RIT.[139, 143, 228, 229]

5.3.3 Synthesis of TCO Modified Cetuximab

A number of procedures have been reported for the ligation of norbornenes and TCOs to antibodies, all of which involve the reaction of the available lysine residues on the antibody with an NHS ester group.[140-143] The use of the NHS ester rather than an alternative activating group towards amide couplings (for example PyBOP or HBTU) is desirable in this case, as only mildly basic conditions are required in order for the reaction to proceed, and NHS is the only major by-product formed (Figure 147).
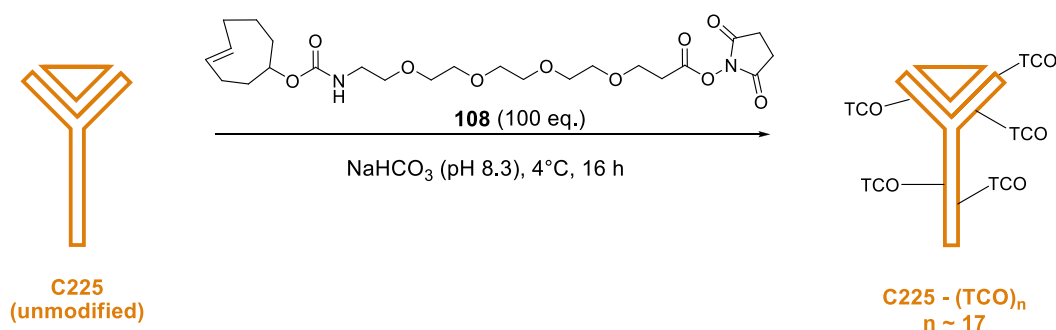
Figure 147. Ligation of Cetuximab (C225) with TCO-PEG4-NHS to form TCO-modified antibody (**C225-TCO**)

Commercially available TCO containing a PEG4 linker **108**, was used so that a linker between the antibody and the TCO functional group would be introduced, in the same manner as with the RGD peptides. This would help to ensure that the strained alkene functional group was still available for reaction with the tetrazine.

A large excess of TCO-PEG4-NHS ester **108** (100 molar equivalents) was used for the ligation reaction, in order to ensure that a sufficient number of TCO molecules would be introduced. The reaction was carried out at 4°C for 16 h, following gentle agitation, after which time the crude mixture (containing both the modified antibody and a significant amount of unreacted TCO small molecule) was purified using centrifugal filtration, using Amicon Ultra® Centrifugal filters. This purification method utilises the difference in size of the antibody and small molecules, by using filters which retain molecules of a certain size (in this

case 30 kDa), letting any molecules of a smaller size pass through. As a result, any antibody molecules (both modified and unmodified) are separated from any small molecules in the mixture.

The amount of time required in order to achieve successful separation was optimised, and the removal of the small molecule was monitored using size-exclusion column (SEC) HPLC, requiring approximately 40 min of spin time in order to obtain pure modified antibody. This method also relies on the separation of molecules by size, but in this case molecules of a larger size are eluted first, with small molecules eluting later. A sample of unmodified antibody (**C225**) was initially injected onto the SEC column, and the retention time of the compound was observed to be ~6 min, which was confirmed by injecting the compound multiple times (n = 3). It was anticipated, based on the theory of SEC, that the unmodified and modified antibodies would have similar, if not identical, retention times, as it is unlikely that either of these can fit into even the largest pores in the column. This was found to be the case, and any unreacted small molecule was observed significantly later in the UV trace (Figure 148).

a)

b)
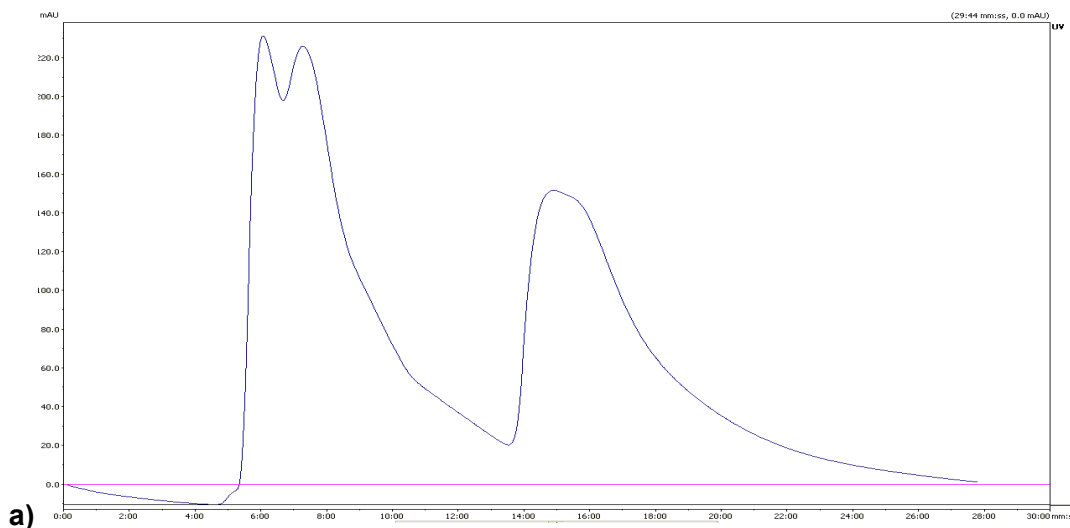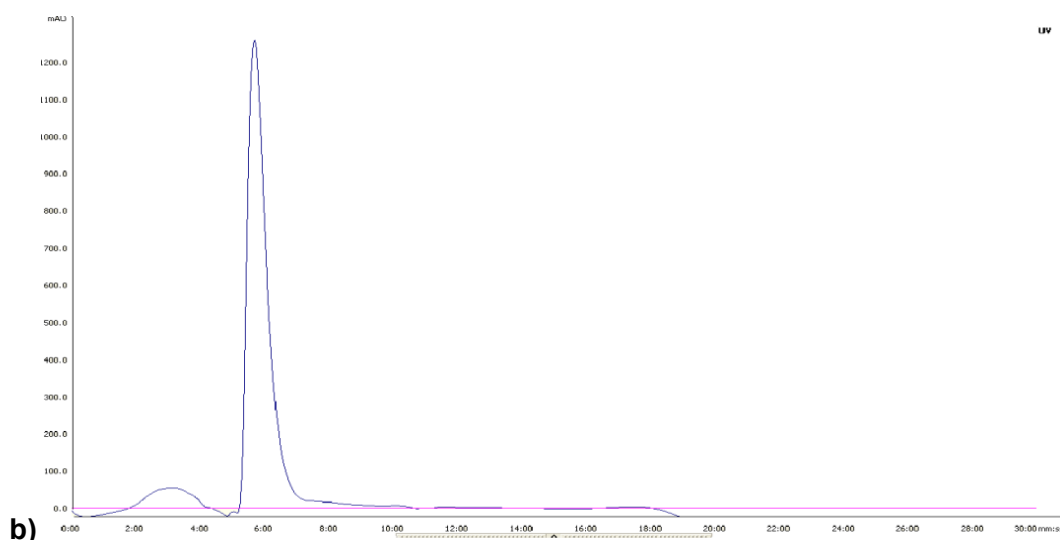
Figure 148. HPLC traces of the modified antibody after a) 20 min of purification b) 40 min of purification (at 215 nm). The UV peak corresponding to the antibody has a retention time of 6 min.

After 40 min of filtration, the small molecule had been removed successfully, as evidenced by the UV trace at both 215 nm and 254 nm. The collected waste from the centrifugal filtration was additionally retained, and a sample was injected into the SEC column, in order to check for any traces of antibody. This showed that none of the modified antibody had passed through the filter, implying that at least 95% of the antibody was in the purified fraction. The purified fractions were made up to an estimated concentration of 5 mgmL^{-1} in PBS (pH 7.4), and the actually concentrations were measured using a bicinchroninic acid (BSA) assay and this confirmed a relatively consistent concentration of approximately 5 mgmL^{-1} across each batch of antibody.

After successful optimisation of the purification method, it was determined that an average of 17 molecules of TCO had been added to each molecule of antibody (using MALDI mass spectrometry), by calculating the difference in mass between the unmodified antibody and the average mass of the modified antibody **C225-TCO** (see experimental section for details and spectra).

The immunoreactivity of the modified antibody **C225-TCO** was confirmed by carrying out a western-blot (Figure 149).
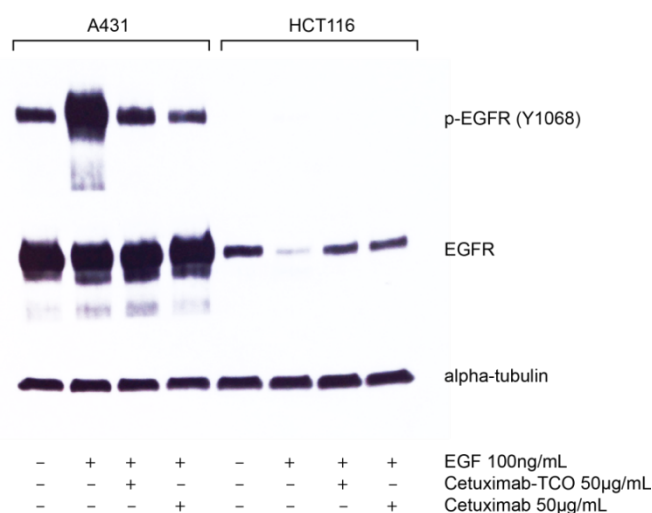
Figure 149. **Immunoreactivity assessment of C225-TCO*** High and low EGFR expressing cell lines (human epidermoid carcinoma A431 cells and human colon carcinoma HCT116 cells, respectively) were incubated in the absence or presence of EGF (100 ng/mL) for 15 min, prior to incubation with C225-TCO (50 µg/mL) or C225 (50 µg/mL) for a 24 h. Whole cell lysates were prepared and 30µg processed for immunoblot analysis using primary antibodies against phosphorylated-EGFR (p-EGFR), total EGFR (EGFR), and alpha-tubulin. *Immunoreactivity assessment was carried out by Dr Quang-De Nguyen.

The western blot generally showed that the modified antibody still maintained its immunoreactivity towards the EGFR receptor. On the high EGFR expressing cell-line (A431), a similar level of expression of phosporolated EGFR was observed for both the unmodified (Cetuximab) and the modified antibody. The same was not observed in the low EGFR expressing cell-line (HCT116), demonstrating selectivity of the antibody for the receptor. The level of immunoreactivity is important, as the antibody must maintain its specificity for EGFR in order to demonstrate the pretargeting strategy *in vitro* and *in vivo*.

5.3.4 *In vitro* IeDDA Reactions Using TCO Modified Cetuximab

In order to demonstrate that the IeDDA reaction could be carried out using the modified antibody **C225-TCO**, it was first necessary to validate the reaction in a vial, by incubating **C225-TCO** with the radiolabelled tetrazine **[⁶⁸Ga]DOTA-GA-Tz** in PBS, and observing the progress of the reaction by SEC HPLC (Figure 150).
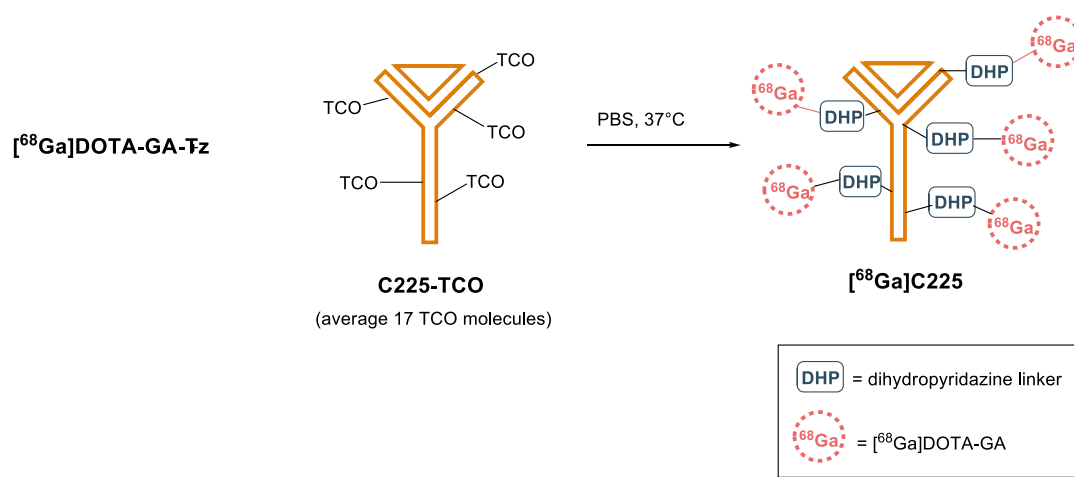
Figure 150. General scheme for the reaction of **[^{68}Ga]DOTA-GA-Tz** with **C225-TCO.** The number of [^{68}Ga]DOTA-GA molecules introduced per antibody is unknown, but is based on an average of 17 TCO molecules in the original antibody

Prior to carrying out the reaction with the modified antibody, a sample of tetrazine **[^{68}Ga]DOTA-GA-Tz** was injected onto the SEC column, in order to determine the retention time of the starting material, and to ensure that sufficient separation from the antibody could be achieved. The peak obtained for the tetrazine was very broad, lying between 10 and 14 min (see experimental section for example spectra), which may be expected considering the principles of size-exclusion chromatography. However, sufficient separation was achieved from the labelled antibody in order for the conversion to the radiolabelled antibody **[^{68}Ga]C225** be quantified, which was expected to have a retention time of 6 min, based upon the UV trace obtained from the cold material (*cf.* Figure 148).

A series of reactions were carried out with the radiolabelled tetrazine **[^{68}Ga]DOTA-GA-Tz**, and each experiment was carried out twice times using the initial batch of antibody. The reaction was carried out using 2 initial volumes of the modified antibody **C225-TCO**, and the progress of the reaction was monitored by injection of a portion of the reaction mixture onto the SEC column and observing the resultant radio-HPLC trace. The conversion to the radiolabelled antibody was measured using the relative AUC of the radio-peak estimated as corresponding to the antibody as compared to the AUC of the radio-peak corresponding to the tetrazine (Figure 151).
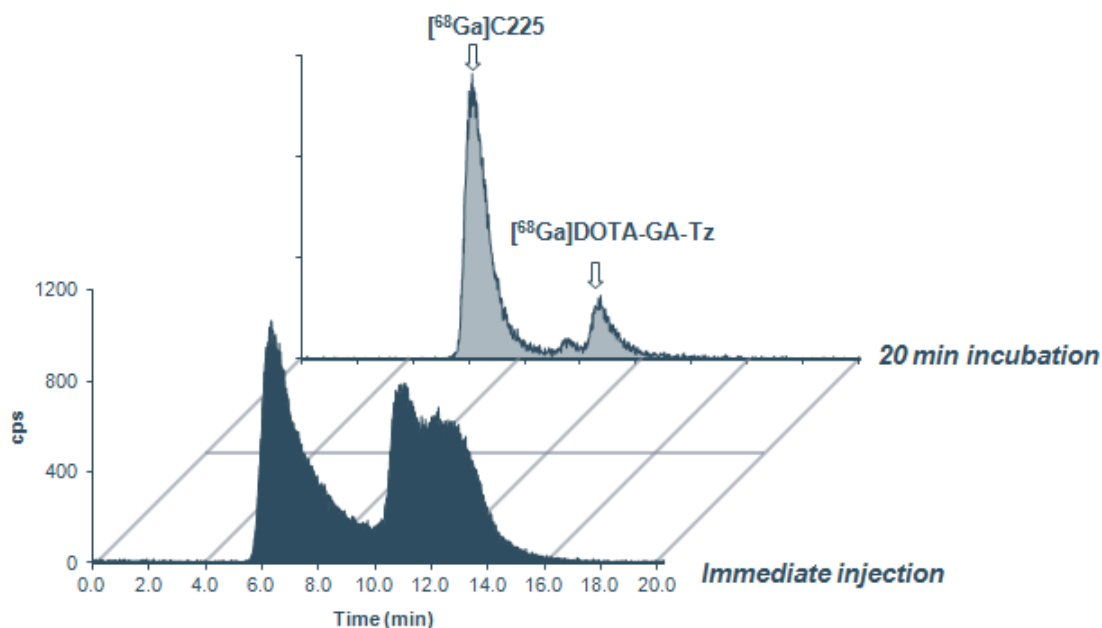
Figure 151. Radio-HPLC traces of The reaction between **C225-TCO** and **[⁶⁸Ga]DOTA-GA-Tz** in PBS after; immediate injection, the same reaction mixture after 20 min incubation at 37°C

Using 10 µL of a 2 mgmL^{-1} solution (2 µg) of this batch of modified antibody **C225-TCO** (diluted to 1 mgmL^{-1} using 10 µL PBS for the reaction), and ~50 µCi of tetrazine **[⁶⁸Ga]DOTA-GA-Tz**, the reaction formed ~10% of the radiolabelled antibody after injection of the reaction mixture as soon as the two components were incubated (Figure 152).
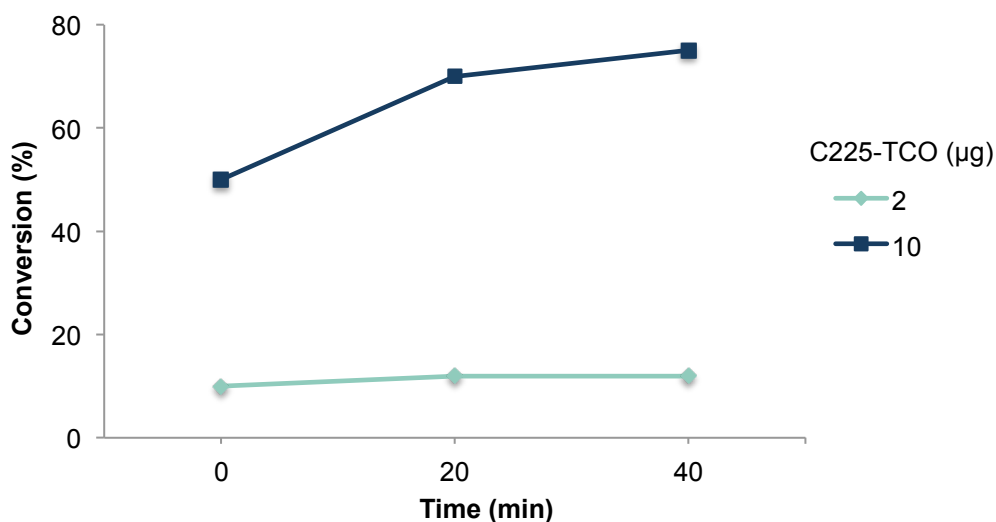
Figure 152. The conversion to the radiolabelled antibody measured as a percentage from the radiolabelled tetrazine radio-HPLC trace, using 2 different volumes (2 and 10 µg) of **C225-TCO**

The reaction did not appear to proceed significantly over a time-point of 40 min, showing only a small increase in the conversion to the product after this time (~12%). A second experiment was carried out using a larger initial volume of **C225-TCO** of 50 µL, equivalent to 10 µg, diluted to the same concentration as with the first experiment. In this case, a significant increase in the formation of the radiolabelled product was observed, and 50% conversion was observed when injected immediately after incubation. This could be increased to 70% after incubating the reaction mixture at 37°C for 20 min, and a maximum conversion of 75% to radiolabelled C225 was observed after 40 min incubation, suggesting that the reaction had reached a plateau. These results suggested that the reaction of modified antibody **C225-TCO** with the radiolabelled tetrazine **[^{68}Ga]DOTA-GA-Tz** was dependent on the concentration of antibody used. This was considered to be significant for carrying out subsequent *in vitro* and *in vivo* experiments, due to the requirement for the amount of the modified antibody used to be controlled. However, in general the results obtained from this experiment were promising, and the ability to radiolabel antibodies *via* a two-step labelling procedure was demonstrated. Sufficient labelling of the modified antibody could be achieved within 40 min, and this result was considered extremely important in the context of pretargeting as the reaction must be achievable within the half-life of ^{68}Ga (68 min) in order to attain sufficient accumulation of ^{68}Ga in the targeted tissue.

Due to the ability to demonstrate reaction between the modified antibody **C225-TCO** and radiolabelled tetrazine **[^{68}Ga]DOTA-GA-Tz** in a vial, the reaction was next carried out *in vitro*. This was demonstrated by using two cell lines (A431 and HCT116) which each expressed different levels (high and low, respectively) of EGFR. The first experiment was carried out using the same batch of modified antibody **C225-TCO** as was used in the initial radiolabelling experiments. The cells were initially incubated either with 100 µgmL^{-1} of unmodified C225 (as a control experiment), or with **C225-TCO** at varying concentrations (5, 10 and 20 µgmL^{-1} respectively). After a 15 min incubation, ~50 µCi of tetrazine **[^{68}Ga]DOTA-**

GA-Tz was introduced to each well, and the cells were incubated for a further 45 min, after which time the uptake of activity in each cell line was measured (Figure 153).

	A431						HCT116					
1. C225 (μg/mL) / 5min	-	-	-	-	100	-	-	-	-	-	100	-
2. C225-TCO (μg/mL) / 15min	-	5	10	20	20	-	-	5	10	20	20	-
3. [⁶⁸Ga]TZ (~50μCi per well) / 45min	✓	✓	✓	✓	✓	-	✓	✓	✓	✓	✓	-
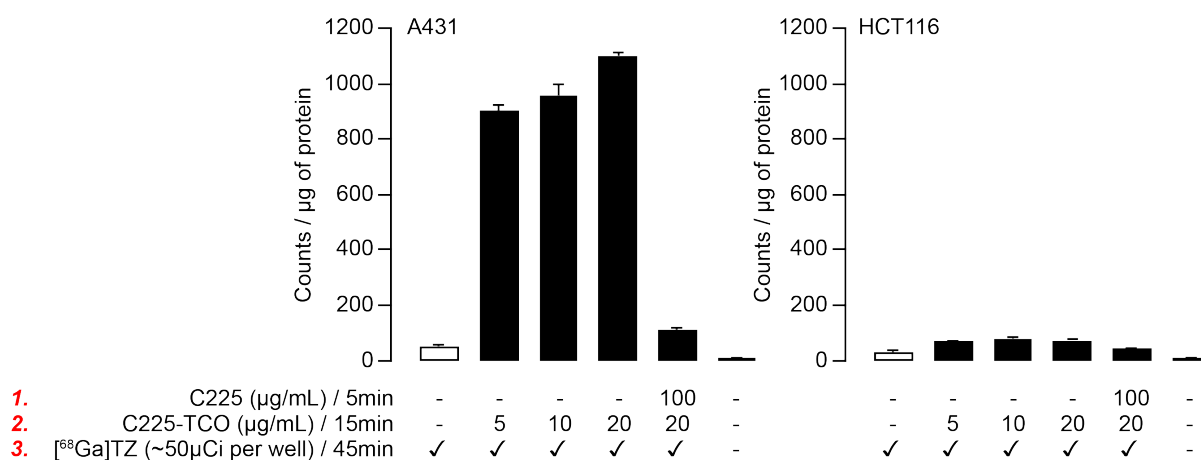
Figure 153. *In vitro* **pretargeting was successfully demonstrated on high EGFR expressing cells*** High (A431) and Low (HCT116) and EGFR expressing cell lines were treated with 50 μCi of **[⁶⁸Ga]DOTA-GA-Tz,** following either: no treatment (white bars), treatment with 5, 10, or 20 μg/mL **C225-TCO** for 15 min, or with 100 μg/mL **C225-TCO** for 5 min **+** 20 μg/mL **C225-TCO** for 15 min (black bars). The bars represent the mean uptake of ⁶⁸Ga in each cell line after 45 min incubation. Error bars represent the standard errors of the mean. *In vitro work was carried out by Dr Quang-De Nguyen.

It was generally observed in the high EGFR expressing cells (A431) that significantly higher uptake was measured in the pretargeted cells *vs.* the cells which had not been treated, as well as those which had been pre-treated with the unmodified antibody, which demonstrated blocking of the receptor. This observation was further validated using the negative cell line (HCT116), which pleasingly did not show the same increase in uptake in the pretargeted cells. It was concluded from these results that the pretargeting strategy could be demonstrated using this approach, and that the IeDDA reaction was occurring on the high EGFR expressing cells.

For future application of this method towards an *in vivo* setting, it was determined that the optimum concentration of the modified antibody **C225-TCO** required in order for the reaction to occur *in vitro* would be calculated. As could be observed from the initial experiment, a slight decrease in uptake was observed when lowering the concentration of **C225-TCO** from 20 μgmL⁻¹ to 10 μgmL⁻¹, and subsequently to 5 μgmL⁻¹, however these differences were not significant. A second experiment was carried out using the same batch of antibody and the concentration of the modified **C225-TCO** antibody used was consequently lowered

successively by 10-fold, so that the cells were incubated with pretargeted concentrations of 0.2, 2 and 20 µgmL^{-1} of **C225-TCO** respectively (Figure 154).

1.	C225 (µg/mL) / 5min	-	-	-	-	100	-
2.	C225-TCO (µg/mL) / 15min	-	0.2	2	20	20	-
3.	[^{68}Ga]Tz (~50µCi per well) / 45min	✓	✓	✓	✓	✓	-
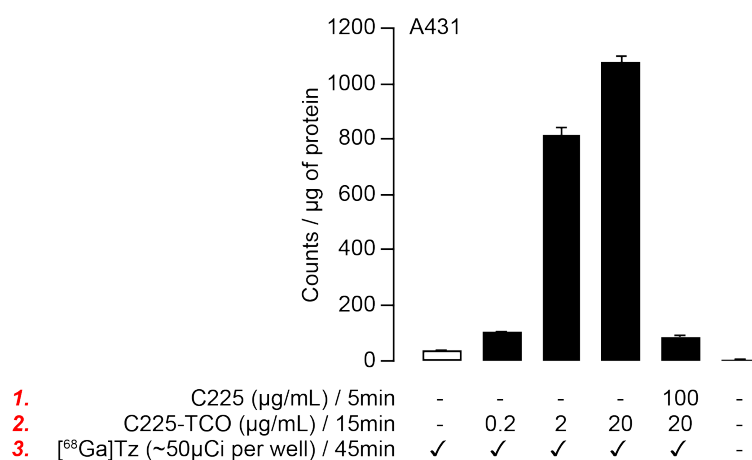
Figure 154. *In vitro* pretargeting on high EGFR expressing cells was dependent upon the concentration of C225-TCO used* High (A431) EGFR expressing cell lines were treated with 50 µCi of **[^{68}Ga]DOTA-GA-Tz,** following either: no treatment (white bars), treatment with 0.2, 2, or 20 µg/mL **C225-TCO** for 15 min, or with 100 µg/mL **C225-TCO** for 5 min **+** 20 µg/mL **C225-TCO** for 15 min (black bars). The bars represent the mean uptake of ^{68}Ga in each cell line after 45 min incubation. Error bars represent the standard errors of the mean. *In vitro work was carried out by Dr Quang-De Nguyen.

This experiment showed us that there was a dependence on concentration of the modified antibody **C225-TCO** used upon the reaction occurring within the time-frame of the experiment (45 min), which was supported by the observations found from the radiolabelling experiments (see section 5.3.3). The optimum concentration of **C225-TCO** for carrying out the *in vitro* experiments was found to lie between 2 and 20 µgmL^{-1}, with only a minimal observed difference in uptake between the two experiments. Decreasing the concentration to 0.2 µgmL^{-1} had a much more pronounced effect, lowering the measured uptake significantly, suggesting that careful consideration must be taken when considering the concentration that would be required for achieving the reaction *in vivo.*

Due to the results obtained to this point, it was determined that a second batch of antibody would be required in order to carry out further *in vitro* and *in vivo* experiments. The second batch was synthesised using the same method as described, other than that the modification was carried out using a stock solution of TCO-PEG4-NHS ester **108**, which had been stored in the freezer for 1 month. Using this batch of modified antibody (Batch 2), as well as with the initial batch (Batch 1), a repeat of the described radiolabelling experiment was carried

out in a vial. A single experiment was carried out using 10 µg of the initial stock solution of each batch of modified antibody, injecting the reaction mixture 0, 15 and 30 min after incubation in PBS (Figure 155).
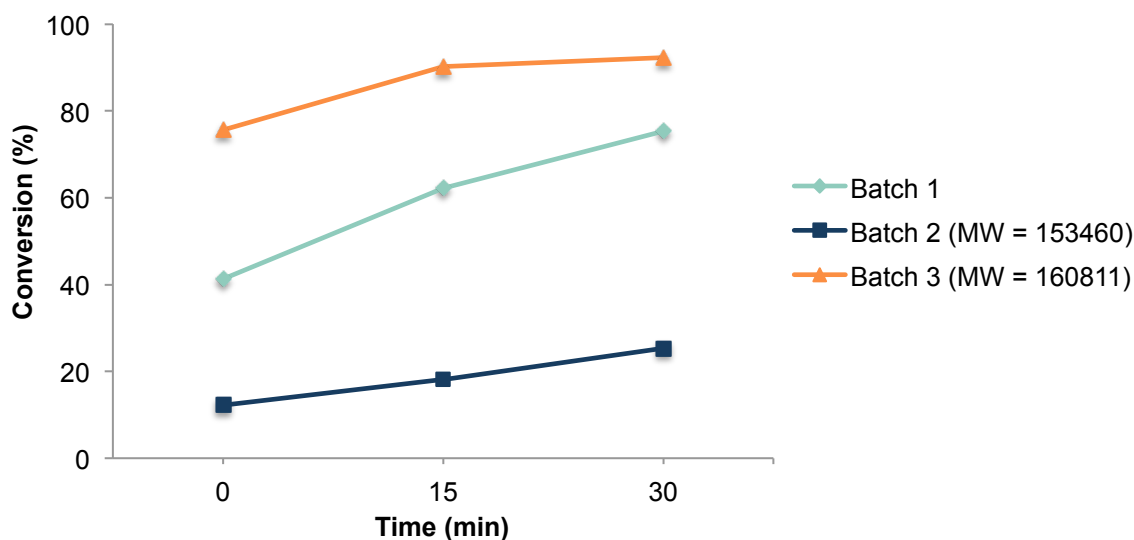
Figure 155. The conversion to the radiolabelled antibody measured as a percentage from the radiolabelled tetrazine radio-HPLC trace, using 3 batches of **C225-TCO**

From this experiment it was observed that a maximum of only 25% conversion to the radiolabelled antibody could be achieved using Batch 2 after 30 min incubation in PBS showing only a minimal increase in labelling following the initial injection (~12% conversion). The rate of reaction appeared to be increasing linearly, but at a considerably slower rate than Batch 1. The first batch however, performed in a similar manner to when the reaction was carried out previously, showing a range of conversions to the radiolabelled product between 40 and 75% within the 30 min time-frame (*cf.* Figure 152). The rate of reaction of Batch 1 appeared to be increasing linearly, and the reaction had yet to reach the plateau that was observed after the 40 min time-point in the previous experiments.

A third batch of the modified antibody **C225-TCO** was synthesised in light of these experiments, whereby the modification reaction was carried out using a fresh batch of the NHS ester **108**. As can be seen from the graph, this batch of antibody gave impressive radiochemical conversions to the labelled antibody within 30 min, with 75% of the activity

being associated with the antibody upon initial injection of the reaction mixture. Almost quantitative conversions to the radiolabelled product were observed after 30 min, with only a minimal increase as compared to the 15 min time-point, which was suggestive of saturation of the reactive TCO functional groups. It was hypothesised that these observations were mostly a result of the introduction of a range of TCO molecules per C225 molecule, and this theory was confirmed by obtaining the MALDI mass spectra for Batches 2 and 3 (a sufficient signal was not obtained from Batch 1) of the modified antibody (Figure 156).

Figure 156. The MALDI mass spectra for a) Unmodified C225 antibody and modified C225-TCO antibodies b) Batch 2 (approximately 1 TCO molecule), c) Batch 3 (approximately 17 TCO molecules)

It was found that the Batch 2 had an average molecular weight of 153460, indicating the addition of an average of only 1 TCO molecule per antibody, by calculating the difference in average mass from the unmodified antibody C225. In contrast, Batch 3 was found to have an average molecular weight of 160811, indicative of 17 additions of TCO onto the antibody. This explained the observed difference in the ability to radiolabel the respective antibodies, and highlighted the importance of using a consistent method for the modification step. It may be imagined that this observation is a result of the use of an older stock solution of TCO-

NHS ester **108**; the instability of the NHS group towards hydrolysis lowered the reactivity of the compound towards free lysine residues on the antibody.

In order to validate these findings further, the *in vitro* experiment was carried out with each of the 3 batches of antibody (Figure 157).

		#1		#2		#3	
1. C225 (µg/mL) / 5min	-	-	-	100	-	100	-	-	-	100
2. C225-TCO (µg/mL) / 15min	-	-	20	20	20	20	-	-	20	20
3. [68Ga]Tz (~50µCi per well) / 45min	-	✓	✓	✓	✓	✓	-	✓	✓	✓
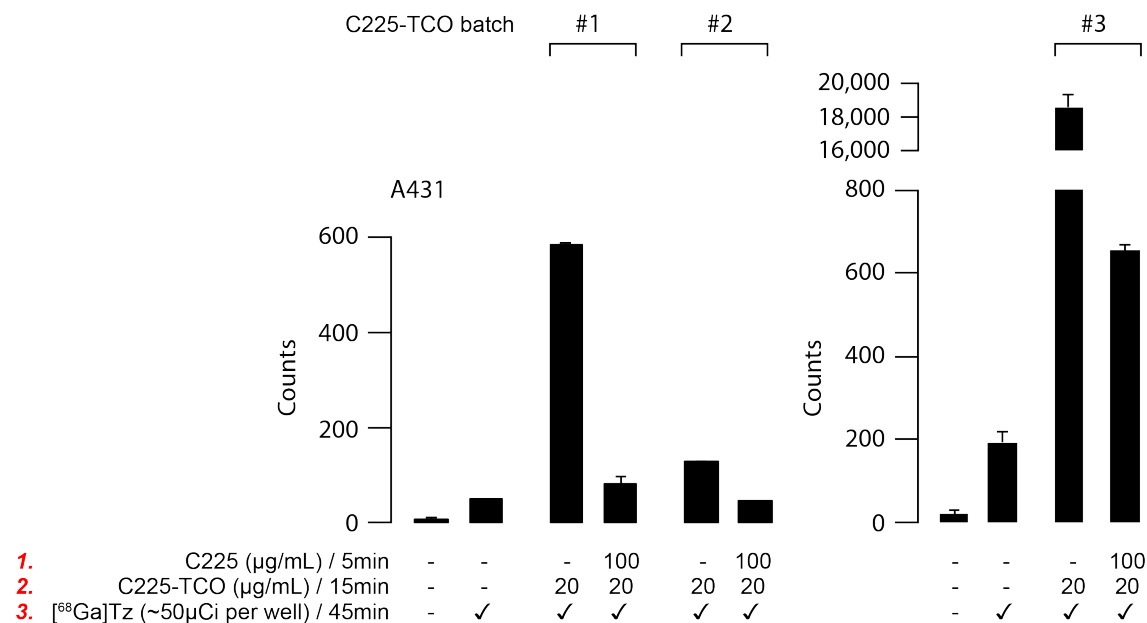
Figure 157. *In vitro* **pretargeting was demonstrated on high EGFR expressing cells using 3 different batches of C225-TCO*** High (A431) EGFR expressing cell lines were treated with 50 µCi of **[68Ga]DOTA-GA-Tz,** following either: no treatment, treatment with 20 µg/mL **C225-TCO** for 15 min, or with 100 µg/mL **C225-TCO** for 5 min + 20 µg/mL **C225-TCO** for 15 min. The bars represent the mean uptake of 68Ga in each cell line after 45 min incubation. Error bars represent the standard errors of the mean. *In vitro work was carried out by Dr Quang-De Nguyen.

When the *in vitro* experiments were repeated with the second batch of **C225-TCO** (Batch 2), it was found that the uptake (in the high EGFR expressing cells), which was observed using the first batch was not achieved, showing an uptake in the pretargeted cells that was not significantly greater than the non targeted or blocked cells. These observations were in accordance with the experiments that were carried out in a vial, and it was seen by the mass spectra that the second batch did not contain enough TCO molecules for successful reaction with the radiolabelled tetrazine under these conditions.

This observation was further supported by repeating the experiment with Batch 3, which showed a greater than 30-fold increase in uptake in the pretargeted cells as compared to Batch 1, and almost 200-fold increase as compared to Batch 2. The observed difference

between batches of the modified antibody **C225-TCO** was found to be more significant *in vitro* than in a vial, possibly due to the more quantitative nature of the results obtained. This highlights the importance of carrying out full characterisation of the antibody post-modification, as small discrepancies in the method for carrying out the ligation reaction can lead to significantly different levels of reactivity.

This was attributed to the significantly increased probability of the IeDDA reaction occurring in the presence of a greater number of TCO groups. It was deduced, therefore, that Batch 3 would be used for each subsequent experiment so as to ensure reliable results, and would be used for carrying out future work into *in vivo* pretargeting with the radiolabelled tetrazine **[^{68}Ga]DOTA-GA-Tz**.

5.3.5 Conclusions

The *in vitro* data obtained for the reaction between the modified antibody **C225-TCO** and the radiolabelled tetrazine **[^{68}Ga]DOTA-GA-Tz** provided some very promising results, suggesting the potential for use of this model reaction for *in vivo* pretargeting. The successful labelling of the C225 antibody was demonstrated, suggesting that a similar method may be used for labelling alternative antibodies for both direct targeting and pretargeting approaches.

Using the first batch of modified antibody **C225-TCO**, the observed increase in uptake in the pretargeted A431 cells *vs.* the non-targeted cells was significant, and implied a selective IeDDA reaction was occurring on the cells. This was supported by the reactivity of the two species in a vial, which enabled for the C225 antibody to be radiolabelled with ^{68}Ga *via* the IeDDA reaction, in 70% radiochemical conversions at 37°C within 20 min. These initial results suggested a potential for the IeDDA reaction for performing *in vivo* pretargeting, and therefore successive batches of the modified antibody were synthesised. However, considerable differences in reactivity were observed between the different batches of modified antibody, with the most significant difference observed in the *in vitro* experiments.

The third batch of the modified antibody **C225-TCO** confirmed that an average of 17 copies of TCO could be added to each antibody molecule, and extremely promising reactivity of this modified antibody towards the radiolabelled tetrazine in a vial and *in vitro* were demonstrated.

The most significant variable to consider when applying the strategy *in vivo* is the amount of the modified antibody **C225-TCO** (and initial injected concentration) used, which must be high enough for the reaction to occur at the low concentrations *in vivo*, but not too high as to exceed the recommended injected dose. Future work will therefore be to adapt these initial positive *in vitro* results, and to translate them into a small animal *in vivo* model.

5.4 Overall Conclusions

It was observed that the IeDDA reaction between tetrazines and strained alkenes displays superior reaction kinetics to the SPAAC reaction between cyclooctynes and azides, and for this reason has been utilised for a number of *in vivo* applications, including pretargeted imaging and therapy. The reaction between radiolabelled tetrazine **[^{68}Ga]DOTA-Tz** and a series of norbornene analogues, as described in Chapter 4, encouraged us to apply this bioorthogonal ligation to our proposed pretargeting strategy.

When functionalised with a cyclic RGD peptide, the norbornene group appeared to show none of the expected reactivity with radiolabelled tetrazine **[^{68}Ga]DOTA-Tz** in a vial or *in vitro*, suggesting further revisions of the strategy were required. Introducing a linker between RGD and the norbornene had no impact on the reactivity with the radiolabelled tetrazine. Similar results were observed by introducing a linker between the DOTA chelate and the tetrazine moiety, towards an alternative radiolabelled tetrazine **[^{68}Ga]DOTA-GA-Tz**.

Therefore, an alternative strategy was explored towards the pretargeting application. A C225 monoclonal antibody was instead modified with the more reactive TCO functional group, and approximately 17 copies of this functional handle could be introduced to each molecule of C225, increasing the probability of reaction with labelled tetrazine **[^{68}Ga]DOTA-GA-Tz**.

Pleasingly, the modified **C225-TCO** antibody showed much more promising reactivity with our labelled tetrazine, which could be translated to an *in vitro* setting. This suggests that the IeDDA reaction between TCO and our tetrazine demonstrates appropriate kinetics for application to the envisaged pretargeting strategy *in vivo*. Our radiolabelled tetrazine **[^{68}Ga]DOTA-GA-Tz** may be considered an attractive chemical reporter due to its ease of synthesis, and demonstrated stability in PBS, and consequently this strategy may enable us to demonstrate the use of short-lived isotopes, in combination with antibodies, for pretargeted PET imaging.

Chapter 6 – Final Conclusions and Future Work

6.1 Final Conclusions

The aim of this project was to evaluate the strain-promoted, copper-free azide-alkyne [3+2] cycloaddition (SPAAC) reaction, and the Inverse-electron Demand Diels-Alder (IeDDA) reaction, as a potential tools for carrying out pretargeted *in vivo* PET imaging.

This first involved the synthesis of a library of literature cyclooctyne precursors for application to the SPAAC reaction (Chapter 2), which could then be used to evaluate the reaction in the context of pretargeting. It was observed that these compounds are challenging to synthesise, with the final 'elimination' step to form the alkyne functional group often being the lowest yielding. For this reason, an alternative method towards the synthesis of symmetrical cyclooctynes was explored through use of Sonogashira couplings, but further work on this approach is still required, as initial attempts have been unsuccessful.

The kinetics of the SPAAC reaction using the synthesised cyclooctynes was examined by reacting with both 'cold' and radiolabelled (^{18}F and ^{68}Ga) azides (Chapter 3), which demonstrated that the precise structure of the chosen cyclooctyne has a significant effect on the rate of the reaction. These experiments also gave us an indication that the SPAAC reaction is more suited to organic solvents than water, and may not be achievable at very low concentrations, particularly in an environment that replicates close to physiological conditions. For this reason, the effect of reaction concentration was considered in more detail, and it was concluded that this reaction is not achievable at the low concentrations that would be found *in vivo*. This observation was supported by the initial *in vivo* experiments using antibody (Herceptin) ligated cyclooctynes and the ^{18}F-labelled azide (**[^{18}F]FEA**), which indicated that the SPAAC reaction was not occurring under these conditions.

For these reasons, the IeDDA reaction was considered as an alternative bioorthogonal reaction for pretargeting. After a minimal amount of optimisation, the tetrazine precursors required for these reactions could be synthesised in a one-pot procedure (Chapter 4). The most suitable tetrazine was tested for its reactivity with a strained alkene (norbornene) at

various concentrations, demonstrating that the rate of the IeDDA reaction is only minimally affected by the concentration of the tetrazine. A ^{68}Ga-labelled tetrazine (**[^{68}Ga]DOTA-Tz**) was reacted with a series of norbornene analogues, demonstrating superior reaction kinetics and enhanced biocompatibility when compared to the SPAAC reaction.

For this reason, it was deduced that the IeDDA reaction would be more suitable than the SPAAC reaction for application to pretargeting. It was initially imagined that RGD cyclic pentapeptides could be used as an alternative biomolecule to antibodies, to provide a proof-of-concept for the pretargeting strategy (Chapter 5). The RGD peptides were therefore ligated with norbornene functional groups, and were tested for their reactivity with the ^{68}Ga-labelled tetrazine, both in a vial and *in vitro*. However, these experiments indicated that the IeDDA reaction was not occurring as expected, which may be a result of the introduction of a bulky peptide side-chain onto the norbornene moiety.

We therefore decided to return to the antibody model, which would allow for the introduction of a greater number of alkene molecules per biomolecule, increasing the probability of the reaction with the radiolabelled tetrazine. Cetuximab ligated *trans*-cyclooctenes (TCOs), which show enhanced reaction kinetics with tetrazines as compared to norbornenes, were synthesised. The IeDDA reaction with our modified ^{68}Ga-labelled tetrazine (**[^{68}Ga]DOTA-GA-Tz**) was successfully demonstrated in a vial, and these results were supported by the validation of *in vitro* pretargeting on high EGFR expressing cells.

6.2 Summary and Future Work

Although the SPAAC reaction has not demonstrated fast enough reaction kinetics for application to pretargeting, the reaction was shown to be useful for a number of other chemical reporter applications, showing sufficient reactivity on the surface of cells. Therefore, it may be considered that further optimisation of the cyclooctyne precursors could be carried out, in order to enhance the reaction kinetics and biocompatibility of this reaction further. The synthesis of cyclooctynes may be improved, for example by use of metal-

catalysed procedures, and these could negate the need to the final, and often challenging elimination step. Further optimisation of these metal-catalysed reactions needs to be carried out, as the introduction of an alkyne into a strained ring is still difficult to achieve. For example, a Ring-Closing Metathesis (RCM) reaction may be considered as an alternative to achieve such a transformation.

The IeDDA reaction demonstrates much more favourable reaction kinetics for use as the bioorthogonal reaction for pretargeted PET imaging using short-lived isotopes such as ^{68}Ga. The use of radiolabelled tetrazine **[^{68}Ga]DOTA-GA-Tz** has been demonstrated as a suitable chemical reporter, due to its impressive reaction kinetics with the modified **C225-TCO** antibody, and good stability in PBS over a period of 2 h. This has been supported by successful validation of the reaction in a vial and *in vitro*. Future work will therefore be to validate this reaction in an *in vivo* setting, using a small animal model, with the hope that the pretargeting strategy will be equally successful in this environment. It is anticipated that sufficient accumulation of the ^{68}Ga label will be achieved within the targeted tissue, for there to be enhanced signal over background tissues. Successful validation of this system would be in accordance with work currently being carried out by other research groups.[116, 136, 140, 147, 217, 233-240]

Moreover, it could be envisaged that a library of tetrazines could be synthesised, in order to determine which compound demonstrates the most favourable reaction kinetics and stability under biological conditions. This may involve further optimisation of the synthetic procedure towards these compounds, with the existing metal-catalysed method currently being the most appropriate for the synthesis of large compound libraries. Alternative chelates for ^{68}Ga labelling, such as NOTA may also be considered, which may demonstrate different levels of stability *in vivo*.

It may additionally be possible to synthesise an ^{18}F-labelled tetrazine, for a comparative pretargeting reaction to be demonstrated; this removes the need for incorporation of chelating groups. For example, it could be imagined that a tetrazine containing an amine

moiety, such as **Tz3**, might be reacted with [^{18}F]fluorobenzaldehyde *via* reductive amination to form an ^{18}F-labelled analogue. This type of chemical reporter could be preferred over ^{68}Ga-labelled compounds due to its anticipated smaller size and enhanced cell permeability. This may well be necessary if the strategy is to be applied to intracellular targets in which the biomolecule is internalised prior to introduction of the chemical reporter.

Chapter 7 – Experimental

7.1 General Experimental Procedures, Materials and Instrumentation

All reactions were performed under anhydrous conditions and an atmosphere of nitrogen in flame-dried glassware unless otherwise stated. Yields refer to chromatographically and spectroscopically (^{1}H NMR) homogenous materials.

Solvents and reagents: All solvents were purified and dried according to standard methods prior to use. All chemicals were handled in accordance with COSHH regulations. All reagents were used as commercially supplied.

Flash chromatography (FC) was always performed on silica gel (Merck ASTM 60 F_{254} 230-400 mesh) according to the method of W. C. Still, unless otherwise stated.[243] Thin Layer Chromatography (TLC) was performed on Merck aluminium-backed plated pre-coated with silica (0.2 mm, 60 F_{254}) which were visualised either by quenching of ultraviolet fluorescence (λ = 254 and 366 nm) or by charring with 10% $KMnO_4$ in 1M H_2SO_4, unless otherwise stated. ^{1}H NMR spectra: These were recorded at 400 MHz on a Bruker AV-400 instrument. Chemical shifts (δ_H) are quoted in parts per million (ppm), referenced to the appropriate residual solvent peak. Coupling constants (J) are reported to the nearest 0.5 Hz. ^{13}C NMR spectra: These were recorded at 100 MHz on a Bruker AV-400 instrument. Chemical shifts (δ_C) are quoted in ppm, referenced to the appropriate residual solvent peak. ^{19}F NMR: These were recorded at 400 MHz on Bruker DRX-400 instrument. Chemical shifts (δ_F) are quoted in ppm, referenced to fluorobenzene at -113.5 ppm. Mass spectra: Low resolution mass spectra (m/z) and High resolution mass spectra (m/z) were recorded on either a VG platform II or VG AutoSpec spectrometers, with only molecular ions (M^+, MH^+, MNa^+, MK^+, MNH_4^+) and major peaks being reported.

Analytical reverse-phase HPLC was carried out on an Agilent 1100 series HPLC system (Agilent Technologies, Stockport, UK) equipped with a UV detector (254 nm) and a LabLogic Flow-Count radio-detector, using a Phenomenex Gemini C18 column (150 mm x 4.6 mm) at a flow rate of 1 mLmin^{-1}. Radio-HPLC was carried out on an Agilent 1100 series HPLC

system (Agilent Technologies, Stockport, UK) equipped with a γ-RAM Model 3 gamma-detector (IN/US Systems Inc., Florida, USA) and Laura 3 software (LabLogic, Sheffield, UK). One of the following gradients was used: Gradient A; (0-95% B over 15 min) Buffer A = MeCN (0.1% TFA), Buffer B = H_2O (0.1% TFA). Gradient B; (0-95% B over 15 min,) Buffer A = MeCN (10% H_2O, 0.1% TFA), Buffer B = H_2O (0.1% TFA). Gradient C; (20-80% B over 15 min) Buffer A = MeCN (0.1% TFA), Buffer B = H_2O (0.1% TFA). Semi-preparative reverse-phase HPLC was carried out on a Waters 600E system equipped with a UV detector (254 nm), using a Phenomenex Luna C18 column (100 mm x 10 mm) on either Gradient A or Gradient B, at a flow rate of 10 mLmin^{-1}. Size-exclusion HPLC was carried out on either an Agilent 1100 series HPLC system (Agilent Technologies, Stockport, UK) equipped with UV detector (215 nm) or on a Waters 600E system equipped with UV detector (215 nm) using a Phenomenex BioSep-SEC-S column (300 x 7.80 mm) on Gradient D; (100% A) Buffer A = sodium phosphate (pH 6.5) at a flow rate of 1 mLmin^{-1}. Laura 3 software was used for processing all analytical HPLC chromatograms.

[^{18}F]Fluoride was produced by a cyclotron (GE PETrace) using the $^{18}O(p,n)^{18}F$ nuclear reaction with 16.4 MeV proton irradiation of an enriched [^{18}O]H_2O target. ^{68}GaCl$_3$ was produced using an Eckert & Ziegler IGG100 ^{68}Ge/^{68}Ga-Generator using a fully-automated Modular-Lab system. ^{68}GaCl$_3$ was eluted in 2 mL of a 0.1M HCl solution, which was subsequently buffered for direct use in radiolabelling experiments.

7.2 Experimental for Chapter 2

Synthesis of cyclooct-1-yn-3-glycolic acid (OCT2)[113, 149, 150]

8,8-Dibromobicyclo[5.0.1]octane (2)[113, 149]

Potassium *tert*-butoxide (10.8 g, 145.6 mmol) was stirred in pentane (20 mL) at room temperature for 15 min. Cycloheptene **1** (8.4 mL, 72.8 mmol) was added and the mixture was cooled to -10°C. Bromoform (9.4 mL, 109.2 mmol) was added dropwise over ~20 min and the mixture turned pale brown. The reaction was allowed to warm to room temperature once the addition was complete and was stirred for 16 h, after which time H_2O (100 mL) was added, and the mixture was acidified using HCl (1M, 200 mL). The product was extracted with pentane (2 x 100 mL) and the combined organic layers were washed with H_2O (2 x 50 mL), dried over $MgSO_4$ and concentrated *in vacuo* to give crude material as an orange oil. The crude material was purified by column chromatography, eluting with 5% EtOAc in petroleum ether, to yield pure product **2** (16.7 g, 58.7 mmol, 80% yield) as a colourless oil. δ_H (400 MHz, $CDCl_3$) 1.14-1.27 (m, 3H); 1.34-1.45 (m, 2H); 1.69-1.77 (m, 2H); 1.82-1.93 (m, 3H); 2.25-2.31 (m, 2H). δ_C (100 MHz, $CDCl_3$) 28.0; 28.9; 32.2; 34.7; 40.7. *m/z* (EI$^+$) calcd. for $C_8H_{13}{}^{79}Br_2$ ([M+H]$^+$) 266.9 found: 265.9, 267.9 (1:1).
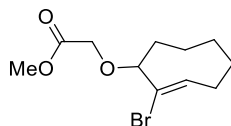
Methyl 2-bromocyclooct-1-en-3-glycolate (3)[113, 149]

Silver perchlorate (667 mg, 3.2 mmol) was added portionwise to a stirred solution of 8,8-dibromobicyclo[5.0.1]octane **2** (467 mg, 1.6 mmol) and methyl glycolate (1.09 mL, 14.4 mmol) in anhydrous toluene (1 mL). The reaction vessel was protected from light by use of

aluminium foil, and the mixture was stirred at room temperature for 1.5 h, after which time the silver salts were removed by filtration and the residue was purified straight away by column chromatography on Alumina eluting with 5-10% EtOAc/pet. ether to afford **3** as a pale yellow oil (260 mg, 0.9 mmol, 59% yield). δ_H (400 MHz, CDCl$_3$) 0.75-0.93 (m, 1H); 1.27-1.89 (m, 7H); 2.13-2.30 (m, 2H); 3.75 (s, 3H); 3.95 (d, J = 16.5 Hz, 1H); 4.10 (dd, J = 5.0 Hz, 10.0 Hz, 1H); 4.23 (d, J = 16.5 Hz, 1H); 6.35 (dd, J = 11.5 Hz, 4.0 Hz, 1H). δ_C (100 MHz, CDCl$_3$) 23.6; 27.0; 29.2; 30.3; 33.7; 51.8; 53.5; 65.6; 84.6; 126.3; 135.9; 170.7. *m/z* (EI$^+$) calcd. for C$_{11}$H$_{18}$^{79}BrO$_3$ ([M+H]$^+$) 277.0 found: 276.0, 278.0 (1:1).
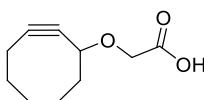
Cyclooct-1-yn-3-glycolic acid (OCT2)[113, 149]

To a solution of NaOMe in MeOH (0.5M, 13 mL) and dry DMSO (0.65 mL) was added methyl 2-bromocyclooct-1-en-3-glycolate **3** (260 mg, 0.94 mmol) and the resultant mixture was stirred at room temperature for 12 hs. The solvent was evaporated *in vacuo* to yield an orange gel-like solid. CH$_2$Cl$_2$ (10 mL) was added and the mixture was acidified to pH ~ 2 by cautious addition of 1M HCl (150 mL). The product was extracted with CH$_2$Cl$_2$ (3 x 15 mL), and the combined organic layers were washed with H$_2$O (10 mL), dried over MgSO$_4$ and concentrated *in vacuo* to obtain crude material as a yellow oil. The crude material was purified by column chromatography eluting first with 2% MeOH/CH$_2$Cl$_2$, then with 5% MeOH/CH$_2$Cl$_2$, to obtain pure **OCT2** as a pale yellow solid (14 mg, 0.08 mmol, 8% yield). δ_H (400 MHz, CDCl$_3$) 1.3-2.3 (m, 10H); 4.32-4.45 (m, 1H); 4.45 (d, J = 17.0 Hz, 1H); 4.58 (d, J = 17.0 Hz, 1H); 8.12 (s, 1H). δ_C (100 MHz, CDCl$_3$) 20.5; 26.0; 29.3; 33.7; 41.8; 65.5; 72.6; 91.2; 101.6; 173.5. *m/z* (CI$^+$) calcd. for C$_{10}$H$_{15}$O$_3$$_1$ ([M+H]$^+$) 183.2 found: 183.2.
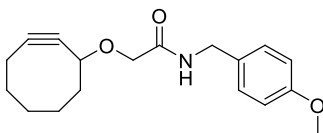
2-(Clyclooct-2-yn-1-yloxy)-*N*-(4-methoxybenzyl)acetamide (OCT4)[151]

To a stirred solution of cyclooct-1-yn-3-glycolic acid (**OCT2**) (12.5 mg, 0.07 mmol) in anhydrous DMF (1 mL) was added DIPEA (13.4 µL, 0.014 mmol) and HBTU (53 mg, 0.014 mmol). The resultant mixture was stirred at room temperature for 30 min, after which time 4-methoxy benzylamine **4** (121.0 µL, 0.084 mmol) was added and the mixture was stirred at room temperature for 16 h. TLC (1:1 EtOAC/pet. ether) indicated that the reaction had gone to completion. The reaction was stopped and the product was extracted with CH_2Cl_2 (2 x 10 mL) and washed with brine (2 x 10 mL). The combined organic layers were dried over $MgSO_4$ and the solvent was evaporated *in vacuo* to yield crude material as an orange oil. The crude material was purified by column chromatography eluting with 50-70% EtOAc/pet. ether to yield **OCT4** as a colourless oil (16 mg, 0.05 mmol, 74% yield). δ_H (400 MHz, $CDCl_3$) 1.30-2.11 (m, 10H); 3.69 (s, 3H); 3.89 (d, *J* = 15.0 Hz, 1H); 4.03 (d, *J* = 15.0 Hz, 1H); 4.33-4.43 (m, 3H); 6.84 (d, *J* = 8.5 Hz, 2H); 6.93 (bs, 1H); 7.20 (d, *J* = 8.5 Hz, 2H). δ_C (100 MHz, $CDCl_3$) 23.5; 27.0; 29.2; 31.4; 33.7; 42.3; 55.3; 68.3; 114.0; 129.0; 130.2; 135.6. *m/z* (EI^+) calcd. for $C_{18}H_{23}NO_3$ ($[M+H]^+$) 302.1756, found: 302.1760.

Synthesis of Cyclooctane-1,3-dione (5)[156]
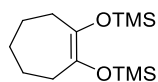
(Z)-1,2-Bis(trimethylsiloxy)cycloheptene (9)[156]

To a flame-dried reaction vessel under nitrogen gas was added anhydrous toluene (70 mL), followed by sodium (2.93 g, 128 mmol) in pieces, cut under pentane. The solution was refluxed (110°C) and stirred for 2 h to produce a sodium dispersion. The addition funnel was charged with toluene (25 mL), diethyl pimelate **8** (5.82 g, 27 mmol), and trimethylsilyl

chloride (13.5 g, 15.8 mmol) and the solution was mixed by bubbling under N_2(g). The solution was added to the refluxing reaction mixture dropwise over 2-3 h, with stirring. The reaction mixture turned deep purple upon addition, after which stirring was continued for 16 h. The mixture was then allowed to cool to room temperature, and was filtered first through glass wool, and then through 1cm of Celite® on a glass frit to remove residual sodium, washing with toluene. The solvent was evaporated *in vacuo* to give pure product **9** as a yellow oil (6.2 g, 22.6 mmol, 84% yield). $δ_H$ (400 MHz, CDCl$_3$) 0.13 (s, 18H); 1.57 (m, 6H); 2.14 (t, 4H). *m/z* (EI$^+$) calcd. for C$_{13}$H$_{29}$O$_2$Si$_2$ ([M+ H]$^+$) 273.1628, found: 273.1642.
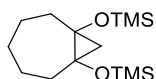
1,7-Bis(trimethylsiloxy)bicycle[5.1.0]octane (10)[156]

To a three-neck, flame-dried flask was added 1,2-bis(trimethylsiloxy)cycloheptene (4.74 g, 16.6 mmol), followed by diiodomethane (3.8 mL, 47.2 mmol) in toluene (25 mL) and the resultant mixture was cooled to -20°C under a N_2(g) atmosphere. To this was added diethylzinc in toluene (1.1M, 43.6 mL, 48.0 mmol) over a period of 30 min. The mixture was stirred for 1 h at this temperature and then at room temperature for 16 h. The mixture was quenched by pouring onto sat. aq. NH$_4$Cl and the product was extracted with toluene (3 x 50 mL). The combined organic layers were washed with H$_2$O (50 mL) and brine (50 mL), dried over MgSO$_4$, filtered and concentrated *in vacuo* to yield **2** as a yellow liquid (3.2 g,11.1 mmol, 81% yield). $δ_H$ (400 MHz, CDCl$_3$) 0.20 (s, 18H); 0.75 (d, *J* = 7.0 Hz, 1H); 0.90 (d, *J* = 7.0 Hz, 1H) 1.20-1.80 (m, 6H) 2.00-2.40 (m, 4H).
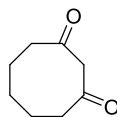
Cyclooctane-1,3-dione (5)[156]

Method 1

Anhydrous $FeCl_3$, (1.0 g, 6.2 mmol) was transferred quickly to a round-bottom flask under N_2(g). Since anhydrous $FeCl_3$ dissolves exothermically, dry DMF (1 mL) was added slowly with mechanical stirring to the ice cooled flask. A solution of **1,7-bis(trimethylsiloxy)bicyclo[5.1.0]octane 10** (420 mg, 1.5 mmol) in dry DMF (0.5 mL) was added to the mixture, and the dark brown suspension was stirred at 60°C for 16 h. After cooling, the mixture was poured into cold 10% aqueous HCl (25 mL) and the product was extracted with $CHCl_3$ (4 x 25 mL). The combined organic layers were washed with 10% HCl (2 x 20 mL) and brine (20 mL), dried over $MgSO_4$ and concentrated *in vacuo* to give crude material as a brown oil. which was Kugelrohr distilled to give product **3** as a pale yellow oil (634 mg, 4.5 mmol, 73% yield), bp 86°C (3 Torr). δ_H (400 MHz, $CDCl_3$) 1.5-1.9 (m, 6H); 2.3-2.6 (m, 4H); 3.5 (s, 2H). δ_C (100 MHz, $CDCl_3$) 24.1; 27.3; 44.0; 58.9; 206.3.

Method 2

A solution of periodic acid (1.56 g, 6.8 mmol) in absolute ethanol (12 mL) was cooled to -10°C. To this was added a solution of 1,7-bis(trimethylsiloxy)bicyclo-[5.1.0]octane (1.89 g, 6.64 mmol) **10** in ethanol (12 mL). An orange colour formed immediately. The reaction was stirred at -10°C for 30 min, by which time the colour had discharged. Following dilution with 30 mL of chloroform (30 mL), the solution was washed with H_2O (20 mL), 5% aq. Na_2SO_3 (20 mL), and brine (20 mL). The organic layers were dried over $MgSO_4$, filtered and concentrated *in vacuo* to give a yellow oil as crude, which was Kugelrohr distilled to give product **3** as a pale yellow oil (770 mg, 5.5 mmol, 81% yield), bp 86°C (3 Torr).

Synthesis of α-iodocyclooctanone (17)[174]
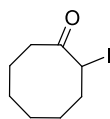
α-Iodo cyloocatnone (17)[174]

Cyclooctanone **23** (630 mg, 5.0 mmol) was added to a stirred solution of NaI (0.77 g, 5.15 mmol) in H_2O (15 mL). The flask was cooled in an ice-water bath and H_2SO_4 (1.06 mL, 20 mmol) and H_2O_2, 30% soln (3.3 mL, 30 mmol) were sequentially added. The resultant mixture was heated to 40°C for 3 h. The reaction mixture was allowed to cool, and the product was extracted with CH_2Cl_2 (3 x 25 mL). The combined organic layers were washed with H_2O (2 x 50 mL) and $Na_2S_2O_3$, 5% solution in water (2 x 50 mL), dried over $MgSO_4$, filtered and concentrated *in vacuo* to afford ketone **17** as a yellow oil (1.1 g, 4.5 mmol, 90% yield). $δ_H$ (400 MHz, $CDCl_3$) 1.04 (m, 1H); 1.29 (m, 1H); 1.51 (m, 3H), 1.69 (m, 2H), 1.87 (m, 1H), 2.29 (m, 2H), 2.46 (m, 1H), 2.94 (td, *J* = 12.0 Hz, 12.0 Hz, 3.5 Hz, 1H), 4.40 (dd, *J* = 12.5 Hz, 3.5 Hz, 1H). $δ_C$ (100 MHz, $CDCl_3$) 23.7; 25.4; 29.5; 29.7; 34.1; 35.0; 53.5; 209.8. *m/z* (EI[+]) calcd. for $C_8H_{14}OI$ ([M+H][+]) 253.0089, found: 253.0096.

Synthesis of methyl 4-(cyclooct-2-yn-1-ylmethyl)benzoate (OCT3)[113]
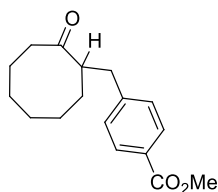
Methyl 4-[(2-oxocyclooctyl)methyl]benzoate (24)[113]

A solution of LDA, 1.8M in heptane/THF/ethylbenzene (8.54 mL, 15.4 mmol) was added drowise to a stirred solution of cyclooctanone **23** (1.76 g, 14.0 mmol) in THF (30 mL) at -78°C, and the resultant mixture was stirred at this temperature for 1 h. After this time, a solution of methyl 4-bromomethylbenzoate **18** (3.53 g, 15.4 mmol) in THF (10 mL) was

added, and the mixture was allowed to warm to rt. After 30 min, the reaction was quenched by addition of H_2O (10 Ml), and the THF was evaporated *in vacuo*. The residue was diluted with EtOAc (100 mL), washed with H_2O (3 x 100 mL) and brine (50 mL), dried over $MgSO_4$, filtered and concentrated *in vacuo* to afford the crude material as a yellow oil. The product was purified by column chromatography, eluting with 10% EtOAc/pet ether, to yield ketone **24** as a colourless oil (2.8 g, 9.9 mmol, 65% yield). R_f = 0.4 (10% EtOAc/pet ether). δ_H (400 MHz, $CDCl_3$) δ = 1.10-1.29 (m, 1H); 1.29-1.49 (m, 1H); 1.49-1.82 (m, 6H); 1.93-2.04 (m, 1H); 2.06 (ddd, *J* = 14.0 Hz, 7.5 Hz, 3.0 Hz, 1H); 2.18-2.25 (m, 1H); 2.57 (dd, *J* = 13.0 Hz, 6.0 Hz, 1H); 2.94 (m, 2H); 3.89 (s, 3H); 7.13 (d, *J* = 8.5 Hz, 2H); 7.86 (d, *J* = 8.5 Hz, 2H). δ_C (100 MHz, $CDCl_3$) 24.5; 24.6; 25.1; 27.7; 32.9; 38.1; 43.1; 51.5; 51.9; 128.0; 128.9; 129.5; 129.6; 145.5; 166.9; 218.7. *m/z* (CI^+) calcd. for $C_{17}H_{23}O_3$ ($[M+H]^+$) 275.1647, found: 275.1628.
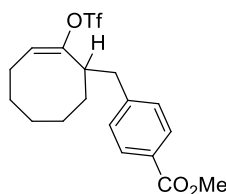
Methyl 4-{[(2*E*)-2-{[(trifluoromethyl)sulfonyl]oxy}cyclooct-2-en-1-yl]methyl}benzoate (26)[113]

To a stirred solution of methyl 4-[(2-oxocyclooctyl)methyl]benzoate **24** (500 mg, 1.8 mmol) in THF (100 mL) at -78°C was added KHMDS, 0.5M solution in toluene (3.95 mL, 2.0 mmol). After 1 h, a solution of Tf_2NPh (707 mg, 2.0 mmol) was added and the resultant mixture was allowed to warm to rt. After 30 min, the solvent was evaporated *in vacuo* to give crude material as a yellow oil. The product was purified by column chromatography, eluting with 5% EtOAc/pet ether to yield triflate **26** as a colourless oil (460 mg, 1.1 mmol, 62% yield). R_f = 0.3 (5% EtOAc/pet ether). δ_H (400 MHz, $CDCl_3$) 1.25-1.38 (m, 1H); 1.52-1.71 (m, 4H); 1.71-1.85 (m, 3H); 1.98-2.11 (m, 1H); 2.15-2.25 (m, 1H); 2.70 (dd, *J* = 14.0 Hz, 7.0 Hz, 1H); 2.95 (dd, *J* = 14.0 Hz, 8.0 Hz, 1H); 3.10 (m, 1H); 3.87 (s, 3H); 5.72 (t, *J* = 8.5 Hz, 8.5 Hz, 1H); 7.24 (d, *J* = 8.0 Hz, 2H); 7.94 (dd, *J* = 8.5 Hz, 1.5 Hz, 2H). δ_C (100 MHz, $CDCl_3$) 25.2,

25.9, 26.5, 29.8, 33.4, 37.5, 39.8, 116.8, 116.8, 119.9, 120.0, 121.3, 128.4, 128.8, 129.8, 151.1, 167.0. δ_F (376 MHz, CDCl$_3$) -74.7. *m/z* (CI$^+$) calcd. for C$_{18}$H$_{22}$O$_5$F$_3$S ([M+H]$^+$) 407.1140, found: 407.1112.
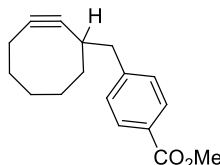
Methyl 4-(cyclooct-2-yn-1-ylmethyl)benzoate (OCT3)[113]

To a stirred solution of methyl 4-{[(2*E*)-2-{[(trifluoromethyl)sulfonyl]oxy}cyclooct-2-en-1-yl]methyl}benzoate **26** (200 mg, 0.5 mmol) in THF (3 mL) at 0°C was dropwise added LDA, , 1.8M in heptane/THF/ethyl benzene (0.32 mL, 0.5 mmol) over 1 h. The reaction was quenched by addition of H$_2$O (10 mL) and the THF was evaporated *in vacuo*. The residue was diluted with EtOAc (20 mL), and the organic layer was washed with H$_2$O (3 x 10 mL) and brine (50 mL), dried over MgSO$_4$, filtered and concentrated *in vacuo* to give crude material as a yellow oil. The product was purified by column chromatography, eluting with a gradient of 0-20% EtOAc/pet ether to yield **OCT3** as a colourless oil (15 mg, 0.05 mmol, 11% yield). R$_f$ = 0.2 (5% EtOAc/pet ether). δ_H (400 MHz, CDCl$_3$) 1.40 (m, 1H); 1.60 (m, 1H), 1.72-1.98 (m, 4H); 2.01-2.08 (m, 1H); 2.12-2.22 (m, 2H); 2.64-2.78 (m, 3H); 3.89 (s, 3H); 7.28 (m, 2H); 7.95 (m, 2H). δ_C (100 MHz, CDCl$_3$) 20.9; 28.5; 30.0; 34.8; 36.5; 40.3; 41.7; 51.9; 95.0; 96.2; 128.1; 128.9; 129.6; 145.7; 167.1. *m/z* (CI$^+$) calcd. for C$_{17}$H$_{21}$O$_2$ ([M+H]$^+$) 257.1542, found: 257.1539.

### *Synthesis of carbonic acid-2',3',2",3"-tetramethoxy-7,8-didehydro-1,2:5,6-dibenzocyclocta-1,5,7-triene-3-yl 4-nitrophenyl ester (TMDIBO1)*[178, 244]
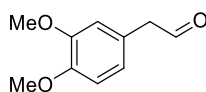
(3,4-dimethoxyphenyl)acetaldehyde (28)[178, 244]

To a stirred solution of 2-(3,4-dimethoxyphenyl)ethanol **27** (7.7 g, 42.1 mmol) in methylene chloride (50 mL) was added portionwise Dess-Martin periodinane (25 g, 58.9 mmol). The resultant mixture was stirred at room temperature for 1 h, after which time TLC in 50% EtOAc/hexane indicated that the reaction had gone to completion. The solvent was evaporated *in vacuo* to yield crude material as an orange oil. Column chromatography eluting with 30-40% EtOAc/hexane yielded (3,4-dimethoxyphenyl)acetaldehyde **28** as a pale yellow liquid (6.1 g, 33.7 mmol, 80% yield). δ_H (400 MHz, CDCl$_3$) 3.64 (d, *J* = 2.5 Hz, 2H); 3.89 (s, 6H); 6.72-6.89 (m, 3H). δ_C (100 MHz, CDCl$_3$) 50.1; 55.8; 55.9; 111.6; 112.9; 121.9; 124.1; 148.4; 149.3; 199.6. *m/z* (EI$^+$) calcd. for C$_{10}$H$_{13}$O$_3$ ([M+H]$^+$) 181.08 found: 181.1.
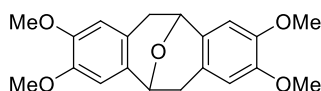
2',3',2",3"-Tetramethoxy-2,3:6,7-dibenzo-9-oxabicyclo[3.3.l]nona-2,6-diene (29)[178, 244]

To a stirred solution of (3,4-dimethoxyphenyl)acetaldehyde **28** (1.5 g, 8.7 mmol) in CH$_2$Cl$_2$ (10 mL) at -78°C was dropwise added iodo(trimethyl)silane (1.5 mL, 10.9 mmol). The solution was stirred at -78°C for 2 h, after which time it was slowly allowed to warm to room temperature. After the solution had fully warmed to room temperature, it was quenched by addition of aqueous sodium thiosulfate. The product was extracted with CH$_2$Cl$_2$ (2 x 20 mL), and the organic layer washed with H$_2$O (2 x 10 mL). The combined organic layers were dried over MgSO$_4$, filtered, and the solvent evaporated *in vacuo t*o give crude material as a brown solid. The product was recrystallised from MeOH to give **29** as an off-white powder (1.7 g, 5.0 mmol, 60% yield). δ_H (400 MHz, CDCl$_3$) 2.66 (dd, *J* = 9.5 Hz, 16.0 Hz, 2H); 3.45 (dd, *J* = 6.0 Hz, 16.0 Hz, 2H); 3.85 (d, *J* = 23.0 Hz, 12H); 5.23 (d, *J* = 6.0 Hz, 2H); 6.47 (s, 2H); 6.57 (s, 2H). δ_C (100 MHz, CDCl$_3$) 35.5; 55.7; 56.0; 108.0; 110.8; 111.5; 123.4; 129.5; 147.4; 148.0. *m/z* (EI$^+$) calcd. for C$_{20}$H$_{23}$O$_5$ ([M+H]$^+$) 343.15 found: 343.2.
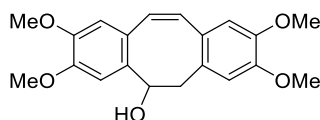
3-Hydroxy-2',3',2'',3''-tetramethoxy-1,2:5,6-dibenzocycloocta-1,5,7-triene (30)[178, 244]

To a stirred solution of ether **29** (200 mg, 0.58 mmol) in dry THF (6 mL) was added dropwise

n-butyllithium (1.4M, 0.86 mL, 1.17 mmol) at room temperature. The resultant mixture was

stirred at room temperature under nitrogen for 4 h. The reaction was stopped and H_2O (10

mL) was added with caution. The product was extracted with CH_2Cl_2 (2 x 10 mL) and the

combined organic phases were washed with brine (10 mL), dried over $MgSO_4$ and

concentrated *in vacuo* to give crude alcohol **30** as a yellow oil. The product was purified by

column chromatography eluting with 100% EtOAc to give alcohol **17** as a pale yellow solid

(114 mg, 0.3 mmol, 57% yield). δ_H (400 MHz, $CDCl_3$) 3.30 (m, 2H); 3.81-3.88 (m, 12H); 5.20

(m, 1H); 6.59-7.00 (m, 6H). δ_C (100 MHz, $CDCl_3$) 41.6; 55.9; 76.8; 111.3; 111.4; 112,4;

112.9; 125.9; 129.4; 129.8; 131.9; 146.6; 147.4. *m/z* (EI$^+$) calcd. for $C_{20}H_{23}O_5$ ([M+H]$^+$)

343.15 found: 343.2.
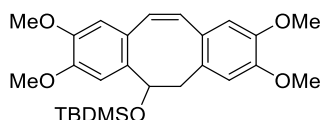
3-*tert*-Butyldimethylsilyloxy-2',3',2'',3''-tetramethoxy-1,2:5,6-dibenzocyclocta-1,5,7-

triene (31)[178]

tert-Butyldimethylsilyl chloride (440 mg, 2.9 mmol) was added to a stirred solution of 3-

hydroxy-2',3',2'',3''-tetramethoxy-1,2:5,6-dibenzocycloocta-1,5,7-triene **30** (400 mg, 1.2

mmol) in pyridine (5.6 mL, 6.9 mmol) and CH_2Cl_2 (20 mL) and the resultant mixture was

stirred at room temperature for 16 h. The mixture was diluted by addition of H_2O (20 mL) and

extracted with CH_2Cl_2 (3 x 20 mL), washed with brine and dried over $MgSO_4$. The solvent

was evaporated *in vacuo* to yield crude material as a yellow oil. The product was purified by

column chromatography eluting with 40% EtOAc/pet ether to give silyl ether **31** as a

colourless oil (1.1 g, 2.3 mmol, 80% yield). R_f = 0.5 (50% EtOAc/pet ether). δ_H (400 MHz, CDCl$_3$) -0.05 (s, 3H); 0.00 (s, 3H); 0.88 (s, 9H); 3.11 (dd, J = 15.5 Hz, 10.0 Hz, 1H); 3.40 (dd J = 15.5 Hz, 5.5 Hz, 1H); 3.80-3.88 (m, 12H); 5.39 (dd, J = 10.0 Hz, 5.5 Hz, 1H); 6.54-7.10 (m, 6H). δ_C (100 MHz, CDCl$_3$) -4.7; -4.6; 18.5; 25.9; 26.0; 46.6; 55.8; 55.9; 71.8; 109.2; 111.0; 113.4; 113.6; 126.9; 128.2; 128.8; 129.2; 132.6; 136.4; 146.7; 147.2; 147.7; 148.4. m/z (EI$^+$) calcd. for C$_{26}$H$_{36}$O$_5$SiNa ([M+Na]$^+$) 479.2 found: 479.2.
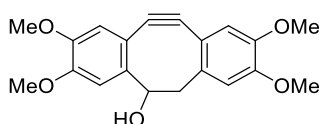
3-Hydroxy-2',3',2",3"-tetramethoxy-7,8-didehydro-1,2:5,6-dibenzocyclocta-1,5,7-triene (34)[178]

Bromine (22.6 μL, 0.44 mmol) was dropwise added to a stirred solution of 3-*tert*-Butyldimethylsilyloxy-2',3',2",3"-tetramethoxy-1,2:5,6-dibenzocyclocta-1,5,7-triene **31** (200 mg, 0.44 mmol) in CH$_2$Cl$_2$ (4 mL) and the resultant mixture was stirred at -40°C until the brown colour persisted. The mixture was concentrated *in vacuo* and the residue was dissolved in THF (4 mL). *N*-methylpiperazine (0.66 g, 6.6 mmol) was added, followed by KO^{t}Bu (198 mg, 1.8 mmol). The resulting suspension was stirred overnight, after which time it was poured over an ice/water bath, and the product was extracted with EtOAc (2 x 20 mL). The combined organic layers were concentrated *in vacuo* and the residue was dissolved in THF (4 mL). TBAF (1M in THF, 0.58 mL, 0.58 mmol) was dropwise added to the mixture at 0°C. The mixture was allowed to warm to room temperature and was stirred for an additional 30 min, after which time the reaction was quenched with NaHCO$_3$ (aq.), and the product was extracted with EtOAc (3 x 20 mL). The combined organic layers were washed with brine (2 x 20 mL), dried over MgSO$_4$, filtered and concentrated slowly *in vacuo* to afford crystallisation of the product. The crystals were filtered off to afford **34** as an off-white solid (102 mg, 0.3 mmol, 70% yield). R_f = 0.3 (50% EtOAc/pet ether). δ_H (400 MHz, CDCl$_3$) 2.64 (dd, J = 14.0 Hz, 3.5 Hz, 1H); 3.07 (dd, J = 14.0 Hz, 2.0 Hz, 1H); 3.81 (s, 6H); 3.87 (s, 6H); 4.28 (app dd,

J = 5.0 Hz, 2.0 Hz, 1H); 6.95 (s, 1H); 6.96 (s, 1H); 7.14 (s, 1H); 7.38 (s, 1H). δ_C (100 MHz, CDCl$_3$) 49.6; 55.8; 55.9; 56.2; 56.3; 74.6; 109.5; 109.5; 109.6; 110.5; 112.1; 112.3; 114.6; 115.1; 145.7; 147.4; 147.7; 148.8; 149.1; 151.1. *m/z* (EI$^+$) calcd. for $C_{20}H_{31}O_5$ ([M+H]$^+$) 341.1 found: 341.1.
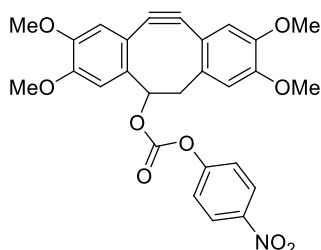
Carbonic acid-2',3',2",3"-tetramethoxy-7,8-didehydro-1,2:5,6-dibenzocyclocta-1,5,7-triene-3-yl 4-nitrophenyl ester (TMDIBO1)[178]

3-Hydroxy-2',3',2",3"-tetramethoxy-7,8-didehydro-1,2:5,6-dibenzocyclocta-1,5,7-triene (34) (50 mg, 0.15 mmol) was dissolved in CH$_2$Cl$_2$ (4.9 mL), and pyridine (0.059 mL, 0.73 mmol) and 4-nitrophenyl chloroformate (59.2 mg, 0.294 mmol) were added. The resultant mixture was stirred at room temperature for 2 h. The mixture was diluted by addition of CH$_2$Cl$_2$ (20 mL), washed with brine (2 x 10 mL) and dried over MgSO$_4$. The organic layers were filtered, and the solvent was evaporated *in vacuo* to yield crude material as an off-white solid. The product was recrystallised from EtOAc to give carbonate **TMDIBO1** as a white solid (72 mg, 0.14 mmol, 95% yield). R$_f$ = 0.25 (2.5% Et$_2$O/CH$_2$Cl$_2$). δ_H (400 MHz, CDCl$_3$) major rotamer: 2.97 (dd, *J* = 15.5 Hz, 4.0 Hz, 1H); 3.23 (dd, *J* = 15.5 Hz, 4.0 Hz, 1H); 3.89 (s, 3H); 3.90 (s, 3H); 3.91 (s, 3H); 3.95 (s, 3H); 5.51 (dd, *J* = 4.0 Hz, 2.0 Hz, 1H); 6.83 (s, 1H); 6.86 (s, 1H); 6.90 (s, 1H); 7.13 (s, 1H); 7.42 (d, *J* = 9.5 Hz, 2H); 8.28 (d, *J* = 9.5 Hz, 2H). minor rotamer: 2.90 (dd, *J* = 14.0 Hz, 2.0 Hz, 1H); 3.72 (dd, *J* = 14.0 Hz, 10.0 Hz, 1H); 3.88 (s, 3H); 3.91(s, 3H); 3.93 (s, 3H); 3.94 (s, 3H); 6.14 (dd, *J* = 10.0 Hz, 2.0 Hz, 1H); 6.84 (s, 1H); 6.87 (d, *J* = 9.0 Hz, 2H); 6.88 (s, 1H); 6.90 (s, 1H); 7.13 (s, 1H); 8.14 (d, *J* = 9.0 Hz, 1H). δ_C (100 MHz, CDCl$_3$) major+minor rotamer 39.3; 46.2; 56.1; 56.1; 56.1; 56.1; 78.5; 82.1; 107.7; 108.2; 108.7; 108.8; 109.2; 109.3; 109.5; 110.4; 112.7; 113.2; 113.9; 115.3; 115.6; 115.6; 115.6; 118.2; 121.5; 121.8; 125.1; 125.3; 139.4; 140.3; 143.0; 143.5; 145.3;

145.4; 148.1; 148.1; 148.2; 148.9; 149.2; 149.6; 151.5; 152.1; 155.3; 155.4. *m/z* (EI⁺) calc. for $C_{27}H_{24}NO_9$ ([M+H]⁺) 506.1451, found: 506.1462.

Synthesis of sym-dibenzo-1,5-cyclooctadiene-3,7-diyne (DIBOD)[182]
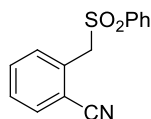
ortho-(Phenylsulfonylmethyl)benzonitrile (39)[182]

To a stirred solution of α-bromotolunitrile **38** (1 g, 5.2 mmol) in anhydrous DMF (10 mL) was added benzenesulfinic acid sodium salt dihydrate (1.01 g, 6.2 mmol). After the mixture had been stirred at 80°C for 2 h, it was cooled to room temperature. The reaction mixture was extracted with H_2O (50 mL) and EtOAc (3 x 50 mL), dried over $MgSO_4$ and the solvent was evaporated *in vacuo*. The crude residue was purified *via* recrystallisation from EtOAc/hexane to give *ortho*-(phenylsulfonylmethyl)benzonitrile **39** as colourless needles (1.1 g, 4.2 mmol, 82% yield). δ_H (400 MHz, $CDCl_3$) 4.57 (s, 2H); 7.42 (m, 4H); 7.67 (m, 5H); δ_c (100 MHz, $CDCl_3$) 60.5; 114.4; 116.6; 128.7; 129.3; 129.4; 131.6; 132.2; 132.8; 133.0; 134.3; 137.5. *m/z* (EI⁺) calcd. for $C_{14}H_{12}NO_2S$ ([M+H]⁺) 258.1 found: 258.1.
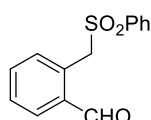
ortho-(Phenylsulfonylmethyl)benzaldehyde (40)[182]

To a stirred solution of *ortho*-(phenylsulfonylmethyl)benzonitrile **39** (1.03 g, 4.0 mmol) in CH_2Cl_2 (13 mL), was added DIBAL-H (1M in hexane, 9.3 mL, 9.3 mmol) at -78°C. After the reaction had been stirred at this temperature for 2 h, NH_4Cl (aq.) (30 mL) was poured into the mixture. The reaction mixture was extracted with 1M HCl (2 x 25 mL) and CH_2Cl_2 (2 x 25 mL), dried over $MgSO_4$ and the solvent was evaporated *in vacuo*. The crude residue was filtered and subsequently purified *via* recrystallisation from CH_2Cl_2/hexane gave *ortho*-

(phenylsulfonylmethyl)benzaldehyde **40** as colourless needles (493.5 mg, 1.9 mmol, 48% yield). δ_H (400 MHz, CDCl$_3$) 5.03 (s, 2H); 7.46 (m, 3H); 7.59 (m, 3H); 7.72 (m, 3H); 9.83 (s, 1H). δ_C (100 MHz, CDCl$_3$) 57.7; 128.7; 128.8; 129.5; 133.6; 133.8; 133.9; 134.5; 134.6; 138.2; 192.0. *m/z* (EI$^+$) calcd. for C$_{14}$H$_{13}$O$_3$S ([M+H]$^+$) 261.1, found: 261.1.
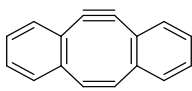
sym-Dibenzo-1,5-cyclooctadiene-3,7-diyne (DIBOD)[182]

To a stirred solution of *ortho*-(phenylsulfonylmethyl)benzaldehyde **40** (442 mg, 1.7 mmol), ClP(O)(OEt)$_2$ (0.3 mL, 2.0 mmol) in anhydrous THF (50 mL), was added LiHMDS (1M in THF, 3.4 mL, 3.4 mmol) at -78°C. After the mixture had been stirred at -78 °C for 30 min, and then at room temperature for 1.5 h, LDA, 1.8M in THF/heptane (4.7 mL, 8.5 mmol) was added dropwise at -78°C. The reaction mixture was stirred at this temperature for 2 h, and then NH$_4$Cl (aq.) (25 mL) was poured into the mixture. The product was extracted with EtOAc (2 x 25 mL) and washed with H$_2$O (2 x 25mL). The combined organic layers were dried over MgSO$_4$ and the solvent evaporated *in vacuo* to yield crude material as a brown oil. The crude material was purified by column chromatography, eluting with CH$_2$Cl$_2$ to yield **DIBOD** as a yellow solid (51.2 mg, 0.26 mmol, 15% yield). δ_H (400 MHz, CDCl$_3$) 6.71-6.77 (m, 4H); 6.90-6.95 (m, 4H). δ_C (100 MHz, CDCl$_3$) 110.1; 128.5; 129.1; 132.8. *m/z* (EI$^+$) calcd. for C$_{16}$H$_9$ ([M+H]$^+$) 201.1, found: 201.2.

Synthesis of precursors for 'Dual' Sonogashira reactions[186]
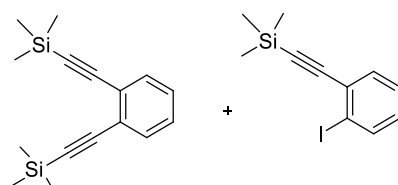
1,2-Bis((trimethylsilyl)ethynyl)benzene (44) and 1-[2-(Trimethylsilyl)ethynyl]-2-iodobenzene (45)[186]

Trimethylsilylacetylene (1.1 mL, 7.5 mmol) was added in one portion to a degassed solution of 1,2-diiodobenzene **41** (1.0 g, 3.05 mmol), $Pd(PPh_3)_4$ (0.18 g, 0.15 mmol) and CuI (0.5 g, 2.5 mmol) in Et_3N/THF (2:1, 15 mL) at room temperature. The mixture was sitrred under nitrogen at 60°C for 20 h. The reaction was cooled to room temperature, and was quenched by addition of NH_4Cl (aq) (10 mL). The product was extracted with CH_2Cl_2 (3 x 50 mL) and the combined organic layers were washed with H_2O (20 mL) and brine (20 mL) dried over $MgSO_4$ and concentrated *in vacuo* to give crude material as a brown oil. The crude material was purified by column chromatography eluting with 100% pet. ether to yield a mixture of **44** (430 mg, 52% yield) and **45** (190 mg, 21% yield) as pale yellow oils.

1,2-Bis((trimethylsilyl)ethynyl)benzene (44)[186]

δ_H (400 MHz, $CDCl_3$) 0.29 (s, 18H); 7.24-7.28 (m, 2H); 7.25-7.50 (m, 2H). δ_C (100 MHz, $CDCl_3$) 0.1; 98.5; 103.2; 125.8; 128.1; 132.3.

1-[2-(Trimethylsilyl)ethynyl]-2-iodobenzene (45)[186]

δ_H (400 MHz, $CDCl_3$) 0.28 (s, 9H); 6.97 (td, *J* = 1.5 Hz, 1H); 7.24-7.28 (m, 1H); 7.45 (dd, *J* = 1.5 Hz, 7.5 Hz, 1H); 7.81 (dd, *J* = 0.7 Hz, 8.2 Hz, 1H). δ_C (100 MHz, $CDCl_3$) 0.0; 98.8; 101.3; 106.5; 127.7; 129.2; 129.6; 132.7; 138.7.
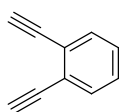
1,2-Diethynylbenzene (42)[186]

To a stirred solution of 1,2-Bis((trimethylsilyl)ethynyl)benzene **44** (310 mg, 1.5 mmol) in MeOH/THF (1:1, 100 mL) was added K_2CO_3 (800 mg, 6.0 mmol) and the resultant mixture was stirred at room temperature for 1 h. The mixture was diluted with diethyl ether (300 mL) and washed with NH_4Cl (aq) (2 x 200 mL) and H_2O (2 x 200 mL). The organic layer was dried over $MgSO_4$, filtered and concentrated *in vacuo* to afford **42** (115 mg, 0.9 mmol, 60% yield) as a yellow oil. The crude material was used for further reactions without purification.

δ_H (400 MHz, CDCl$_3$) 3.34 (s, 2H); 7.31 (dd, J = 3.5 Hz, 6.0 Hz, 2H); 7.51 (dd, J = 3.5 Hz, 5.5 Hz, 2H). δ_C (100 MHz, CDCl$_3$) 81.2; 81.8; 125.0; 128.5; 132.7. m/z (EI$^+$) calcd. for C$_{10}$H$_7$([M+H]$^+$) 128.0626, found: 128.0625.
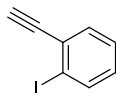
1-Ethynyl-2-iodobenzene (43)[187]

To a stirred solution of 1-[2-(trimethylsilyl)ethynyl]-2-iodobenzene **45** (370 mg, 1.2 mmol) in MeOH/CH$_2$Cl$_2$ (2:1, 6 mL) was added KOH (138 mg, 2.5 mmol) and the resultant mixture was stirred at room temperature over night. The reaction was quenched by addition of H$_2$O (10 mL) and the product was extracted with CH$_2$Cl$_2$ (3 x 10 mL) and the organic layers were washed with H$_2$O (10 mL) and brine (10 mL), filtered and concentrated *in vacuo* to afford **43** (213 mg, 72% yield) as a pale yellow oil. The crude material was used for further reactions without purification. δ_H (400 MHz, CDCl$_3$) 3.40 (s, 1H); 7.04 (m, 1H); 7.31 (td, J = 1.0 Hz, 1H); 7.51 (dd, J = 1.5 Hz, 7.5 Hz, 1H); 7.85 (dd, J = 1.0 Hz, 8.0 Hz, 1H). δ_C (100 MHz, CDCl$_3$) 81.0; 85.2; 100.5; 127.82; 128.75; 130.0; 133.5; 138.8. m/z (EI$^+$) calcd. for C$_8$H$_6$I ([M+H]$^+$) 229.9593, found: 229.9597.

7.3 Experimental for Chapter 3

Synthesis of 2-flouroethylazide (FEA)[151]
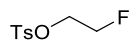
2-Fluoroethyl tosylate (56)

To a stirred solution of 2-fluoroethanol **55** (0.55 mL, 7.8 mmol) in CH_2Cl_2 (15 mL) was added tosylchloride (2.23 g, 11.7 mmol) and DIPEA (1.52 mL, 15.8 mmol) and the resultant mixture was stirred at room temperature under nitrogen for 16 h. CH_2Cl_2 (30 mL) was added and was washed with H_2O (2 x 10 mL). The solvent was evaporated *in vacuo* to yield crude 2-fluoroethyl tosylate **56** (1.83 g), which was carried through to the next step without further purification.
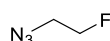
2-Fluoroethyl azide (FEA)

To a stirred solution of 2-fluoroethyl tosylate **56** (200mg, 0.92 mmol) in DMF (5 mL) was added sodium azide (178.6 mg, 2.75 mmol) and the resultant mixture was stirred at room temperature under nitrogen for 48 h, at which point TLC (1:1 EtOAc/Hex.) showed complete consumption of the starting material. The reaction mixture was then filtered to remove the white precipitate, and the filtrate was used for the next step without work-up or purification. δ_F (400 MHz, $CDCl_3$) -224.

General method for the copper-free 'click' reaction with cyclooctynes[151]

2-Fluoroethyl azide (FEA) (0.02 mmol) was added to a stirred solution of cyclooctyne (0.005 mmol) in $CDCl_3$ (0.6 mL). The resultant mixture was stirred at 40°C for 2 h. When complete, the reaction was stopped and the solvent evaporated *in vacuo*. The crude material was re-dissolved in $CDCl_3$ and the ^{19}F, ^{1}H and ^{13}C NMR spetra were taken. These crude compounds, as mixtures of regioisomers, were used as references only. The ratio of

regioisomers was determined using a combination of ^{18}F HPLC traces of the radiolabelled compounds, and by the ^{19}F NMR spectra (see appendix 2). The characterisation of these compounds is detailed below.

Characterisation of triazole products
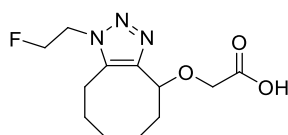
{[1-(2-Fluoroethyl)-4,5,6,7,8,9-hexahydro-1*H*-cycloocta[*d*][1,2,3]triazol-4-yl]oxyacetic acid (49) as a mixture of regioisomers in ratio 2:1.

δ_H (400 MHz, CDCl$_3$) 1.25-2.46 (m, 15H); 3.30-3.40 (m, 4.5H); 4.28 (dd, *J* = 27.0 Hz, 4.0 Hz, 3H); 4.56 (d, *J* = 47.0 Hz, 3H); 8.06 (s, 1H). δ_F (400 MHz, CDCl$_3$) -224.5 (1); -222.4 (2). *m/z* (EI$^+$) ([M+ H]$^+$) calcd. for 272.1405, found: 272.1405.
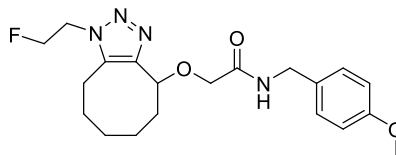
{[1-(2-Fluoroethyl)-4,5,6,7,8,9-hexahydro-1*H*-cycloocta[*d*][1,2,3]triazol-4-yl]oxy} *N*-(4-methoxybenzyl)acetamide (50)** as a mixture of regioisomers in ratio 2:1.

δ_H (400 MHz, CDCl$_3$) 1.15-2.04 (m, 13.5H); 2.80-2.64 (m, 3H); 3.31-3.53 (m, 8H); 4.13-4.31 (m, 3H); 7.13-7.19 (m, 1H); 7.53 (dd, *J* = 5.5 Hz, 3.5 Hz, 1.5H); 7.70 (dd, *J* = 5.5 Hz, 3.5 Hz); 7.78 (d, *J* = 8.0 Hz, 1H). δ_c (100 MHz, CDCl$_3$) 19.9; 23.0; 23.7; 24.2; 27.0; 29.1; 30.4; 33.3; 38.7; 48.6; 49.3 (d, J_{CF} = 25.0 Hz); 48.6; 54.3; 68.2; 81.6 (d, J_{CF} = 168.0 Hz); 125.9; 228.8; 131.0; 132.5; 165.6; 167.8. δ_F (400 MHz, CDCl$_3$) -222.5 (2); -225.5 (1). *m/z* (EI$^+$) ([M+K]$^+$) calcd. for 429.1699, found: 429.1701.
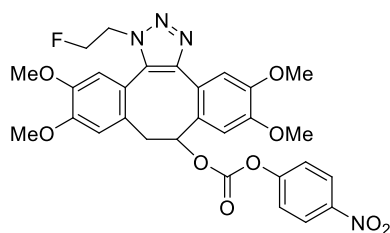
1-(2-Fluoroethyl)-carbonicacid-2',3',2",3"-tetramethoxy-7,8-didehydro-1,2:5,6-dibenzocyclocta-1,5,7-triene-[1,2 ,3]triazolyl 4-nitrophenyl ester (51) as a mixture of regioisomers in ratio 2:1.

δ_H (400 MHz, CDCl$_3$) 2.89 (app s, 1H); 2.96 (app s, 1H); 3.10 (app s, 0.5H); 3.21 (app s, 0.5H); 3.70- 4.01 (m, 18H); 4.53-4.79 (m, 6H); 5.34-5.72 (m, 1H); 6.57-6.63 (m, 1H); 6.68-6.72 (m, 1H); 6.81-6.83 (m, 1H); 6.91 (d, J = 9.0 Hz, 2H); 6.99-7.01 (m, 1H); 7.07-7.10 (m, 1H); 8.07 (d, J = 9.0 Hz, 1H); 8.14 (d, J = 9.0 Hz, 2H). δ_c (100 MHz, CDCl$_3$) 41.0; 45.6; 50.8 (d, J_{CF} = 24.0 Hz) 55.9; 55.9;, 56.0; 56.0; 81.9 (d, J_{CF} = 171.0 Hz); 107.4; 107.2; 109.3; 111.7; 113.0; 113.7; 114.7; 115.5; 115.7; 124.8; 125.9; 141.1; 142.5; 143.3; 146.5; 148.6; 149.7; 150.2; 150.7; 152.8; 154.3. δ_F (400 MHz, CDCl$_3$) -222.3 (1); -222.4 (2). m/z (EI$^+$) ([M+ 2H]$^{2+}$) calcd. for 298.0954, found: 298.1001.
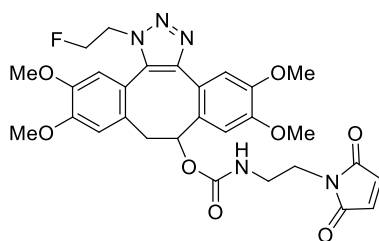
1-(2-Fluoroethyl)-carbonicacid-2',3',2",3"-tetramethoxy-7,8-didehydro-1,2:5,6-dibenzocyclocta-1,5,7-triene-[1,2,3]triazolyl *N*-(2-aminoethyl)maleimide (52) as a mixture of regioisomers in ratio 7:1.

δ_H (400 MHz, CDCl$_3$). 2.44 (s, 1H); 2.60 (s, 1H); 2.72 (s, 1H); 2.80 (s, 1H); 3.00 (s, 1H); 3.07 (s, 1H); 4.16-4.23 (m, 12H); 4.25 (dm, J = 27.0 Hz, 2H); 4.56 (dm, J = 47.0 Hz, 2H); 5.28-5.61 (m, 1H); 7.33 (s, 1H); 7.35 (s, 1H); 7.50-7.52 (m, 2H); 7.67-7.69 (m, 2H). δ_c (100 MHz,

CDCl$_3$) . 28.9; 29.7; 30.4; 36.5; 40.3; 46.1; 56.0; 67.1 (d, J_{CF} = 26.5 Hz); 68.1; 80.6 (d, J_{CF} = 174.5 Hz); 107.8; 108.7; 109.5; 112.0; 113.7; 114.1; 115.5; 128.0; 128.8; 130.8; 132.5; 145.1; 147.8; 148.5; 150.6; 151.1; 161.0; 162,6; 167.8. δ$_F$ (400 MHz, CDCl$_3$) -225.2. *m/z* (EI$^+$) ([(M-maleimide)+H]$^+$) calcd. for 430.1773, found: 430.1775.
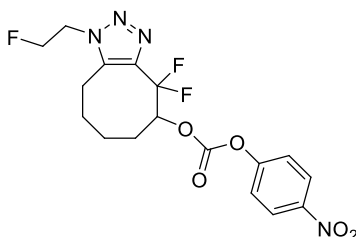
4,4-Difluoro-1-(2-fluoroethyl)-4,5,6,7,8,9-hexahydro-1*H*-cycloocta[*d*][1,2,3]triazol-5-yl 4-nitrophenyl carbonate (53) as a mixture of regioisomers in ratio 2:1.

δ$_H$ (400 MHz, CDCl$_3$) 1.18-1.37 (m, 1.5H); 1.73-1.86 (m, 1.5H); 2.30-2.39 (m, 6H); 2.43-2.47 (m, 3H); 4.57 (dm, *J* = 22.5 Hz, 3H); 4.92 (dm, *J* = 26.0 Hz, 3H); 5.35-5.38 (m, 1.5H); 7.19 (d, *J* = 8.0 Hz, 2H); 7.83 (d, *J* = 8.0 Hz, 2H). δ$_c$ (100 MHz, CDCl$_3$) 19.7; 24.1; 29.1; 29.7; 32.6; 50.6 (d, J_{CF} = 20.0 Hz); 80.4 (d, J_{CF} = 176.0 Hz); 82.0; 85.1; 111.8; 112.4; 113.1; 113.7; 115.6; 121.8; 126.0; 128.6. δ$_F$ (400 MHz, CDCl$_3$) -223.7 (2); -223.5 (1); -107.8; -107.5; -104.9; -101.3; -100.5; -93.7. *m/z* (EI$^+$) ([M+H]$^+$) calcd. for 415.1224, found: 415.1220

Radiosynthesis of [^{18}F]FEA

Radiosynthesis of [^{18}F]2-fluoroethylazide (**[^{18}F]FEA**) was carried out using the method described by Glaser *et al*.[62] Briefly, a mixture of Kryptofix 222 (5 mg, 13.3 µmol), K$_2$CO$_3$ (1 mg, 7.2 µmol, in 50 µL H$_2$O), and CH$_3$CN (1 mL) was added to [^{18}F]fluoride (74−370 MBq) in H$_2$O (1 mL). The solvent was removed by heating at 80°C under a stream of N$_2$ (g) (100 mL min^{-1}). Afterward, CH$_3$CN (0.5 mL) was added, and the distillation was continued. This procedure was repeated twice. After cooling to room temperature, a solution of 2-azidoethyl-4-toluenesulfonate (1.5 µL, 7.5 µmol) in anhydrous CH$_3$CN (0.2 mL) was added. The reaction mixture was stirred for 15 min at 80°C. After addition of CH$_3$CN (0.3 mL), **[^{18}F]FEA**

was distilled at 130°C under a flow of N_2 (g) (15 mL min^{-1}) into a trapping vial containing CH$_3$CN (0.1 mL). **[^{18}F]FEA** was collected with a radiochemical yield of 54% (decay-corrected) and 63% distillation efficiency.
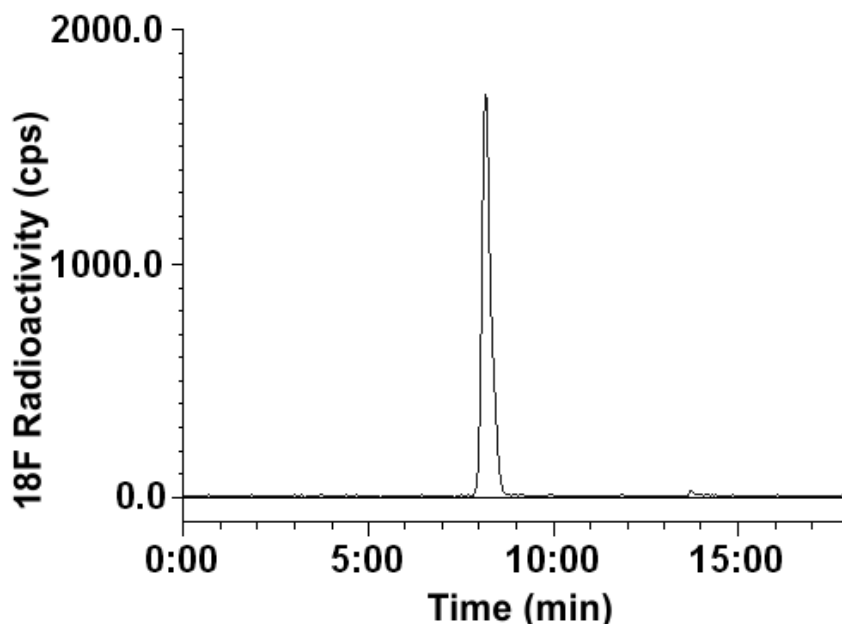
Figure SI 1. Radio-HPLC trace of **[^{18}F]FEA** using gradient A

Synthesis of maleimide-substituted cyclooctynes
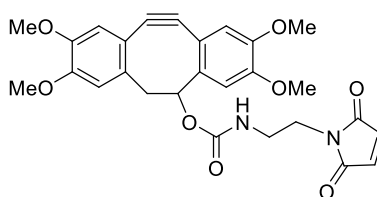
Carbamate-2',3',2",3"-tetramethoxy-7,8-didehydro-1,2:5,6-dibenzocyclocta-1,5,7-triene-3-yl *N*-(2-Aminoethyl)maleimide (TMDIBO2)

To a stirred solution of carbonic acid-2',3',2",3"-tetramethoxy-7,8-didehydro-1,2:5,6-dibenzocyclocta-1,5,7-triene-3-yl 4-nitrophenyl ester (**TMDIBO1**) (5.0 mg, 0.01 mmol) in DMF (1 mL) was added DIPEA (2.1 µL, 0.01 mmol). The resultant mixture was stirred at room temperature for 15 min, after which time *N*-(2-aminoethyl)maleimide **57** (5.1 mg, 0.02 mmol) was added and the mixture was stirred at room temperature for 16 h. The product

was extracted with EtOAc (2 x 10 mL) and washed with H_2O (2 x 10 mL). The combined organic layers were dried over $MgSO_4$ and the solvent was evaporated *in vacuo* to yield crude material as a yellow oil. The product was purified by column chromatography, eluting with 50-70% EtOAc/pet. ether to yield **TMDIBO2** as a yellow powder (5 mg, 0.01 mmol, 99% yield). δ_H (400 MHz, $CDCl_3$) 2.92 (s, 2H); 2.99 (s, 2H); 3.07-3.11 (m, 1H); 3.45-3.48 (m, 1H); 3.82-3.98 (m, 12H); 5.44 (m, 1H); 6.83-6.85 (d, *J* = 6.0 Hz, 2H); 6.92-6.94 (d, *J* = 9.0 Hz, 2H); 7.03-7.06 (d, *J* = 12.0 Hz, 2H). δ_C (100 MHz, $CDCl_3$) 30.9; 31.5; 36.5; 40.3; 46.7; 56.1; 68.2; 108.2; 108.7; 109.1; 112.5; 114.1; 115.6; 126.2; 128.8; 130.9; 134.2; 145.2; 147.8; 148.8; 150.2; 161.7; 162.4; 207.0. *m/z* (EI^+) calcd. for $C_{20}H_{21}O_5$ ($[(M-mal)+H]^+$) 341.1384, found: 341.1390.
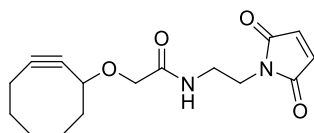
2-(Cyclooct-2-yn-1-yloxy)-*N*-(2-Aminoethyl)maleimide (OCT5)

To a stirred solution of cyclooct-1-yn-3-glycolic acid **OCT5** (25 mg, 0.14 mmol) in DMF (3 mL) was added DIPEA (50 µL, 0.30 mmol). The resultant mixture was stirred at room temperature for 15 min, after which time *N*-(2-aminoethyl)maleimide **57** (42.7 mg, 0.17 mmol) was added and the mixture was stirred at room temperature for 16 h. TLC (1:1 EtOAC/pet. ether) indicated that the reaction had gone to completion. The reaction was stopped and the product was extracted with EtOAc (2 x 25 mL) and washed with H_2O (2 x 25 mL). The combined organic layers were dried over $MgSO_4$ and the solvent was evaporated *in vacuo* to yield crude material as a yellow oil. The product was purified by column chromatography, eluting with 60-80% EtOAc/pet.ether to yield **OCT5** as a yellow solid (15 mg, 0.05 mmol, 35% yield). δ_H (400 MHz, $CDCl_3$) 1.3-2.3 (m, 10H); 3.44-2.61 (m, 2H); 3.75 (t, 2H); 3.97 (dd, *J* = 75.0 Hz, 15.0 Hz, 2H); 4.22-4.28 (m, 1H); 6.75-6.86 (m, 2H). *m/z* (EI^+) calcd. for $C_{16}H_{21}N_2O_4$ ($[(M+H]^+$) 305.14, found: 305.14.

*Cell viability assay using TMDIBO1**

A sulforhodamine B cell viability assay was carried out in order to assess the toxicity of the cyclooctyne **TMDIBO1**. On day one HCT116 colon cancer cells were seeded in a 96-well plate at a density of 2,000 cells per well in a volume of 150 µl of RPMI supplemented with 1 % penicillin/streptomycin and 10% FBS. On day two cells were treated by addition of 50 µL of **TMDIBO1** at a range of concentrations between 0 and 20 µM. After 72 h, cells were fixed by addition of 50% trichloroacetic acid and stained with a 0.4% solution of sulforhodamine B in 1% acetic acid. Finally, 10 mM tris base buffer was used to solubilise the stained protein and absorbance was measured at 540 nm.

The cell viability *versus* compound concentration curve was plotted as a percentage of non-treated control cells. The experiment was carried out on three separate occasions with n=6 replicates for each concentration.
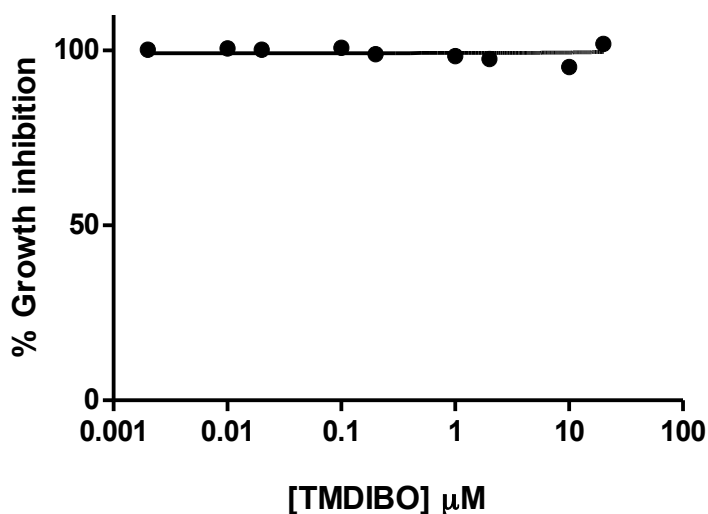
*The cell viability assay was carried out by Dr Quang-De Nguyen

Figure SI 2. Growth inhibition of HCT116 cells after 72 h incubation with an increasing concentration of TMDIBO1.

Conjugation of Herceptin to cyclooctynes

Thiol-substituted Herceptin/IgG$_1$ (61/62)

Herceptin/IgG$_1$ (21 mgmL^{-1}, 700 µL) **59/60** was stirred at room temperature with 2-imino thiolane **58** (3 µmol, 0.4 mg) for 1 h and the resultant solution was used for direct conjugation to the cyclooctyne.

OCT-Herceptin/IgG$_1$

OCT5 (0.25 mg, 0.6 µmol) was dissolved in a 1:1 DMF/DMA solution (0.25 mL) and the resultant mixture was added dropwise to the solution of **59/60**. The mixture was agitated in the dark for 1 h. 0.5 mL of the reaction mixture was loaded onto a NAP^{TM}-5 column and the ligated antibody was eluted with 0.25 M sodium acetate buffer (1.0 mL).

TMDIBO-Herceptin/IgG$_1$

TMDIBO2 (0.25 mg, 0.6 µmol) was dissolved in a 1:1 DMF/DMA solution (0.25 mL) and the resultant mixture was added dropwise to the solution of **59/60**. The mixture was agitated in the dark for 1 h. 0.5 mL of the reaction mixture was loaded onto a NAP^{TM}-5 column and the ligated antibody was eluted with 0.25 M sodium acetate buffer (1.0 mL).

Characterisation of Herceptin-conjugated cyclooctynes

In order to determine the number of cyclooctynes attached to the Herceptin antibody, the mass spectra was determined first of the antibody alone, and then with the antibody conjugated to the cyclooctyne. Mass spectral analysis of the Herceptin conjugates was carried out by the DCMR facility in Ecole Polytechnique, France. For example, the mass of OCT-Herceptin was determined as described below. The molecular masses measured for Herceptin were found to be 148 063, 148 219 and 148 379. These probably correspond to three isoforms differing in the number of hexoses (162 Da).
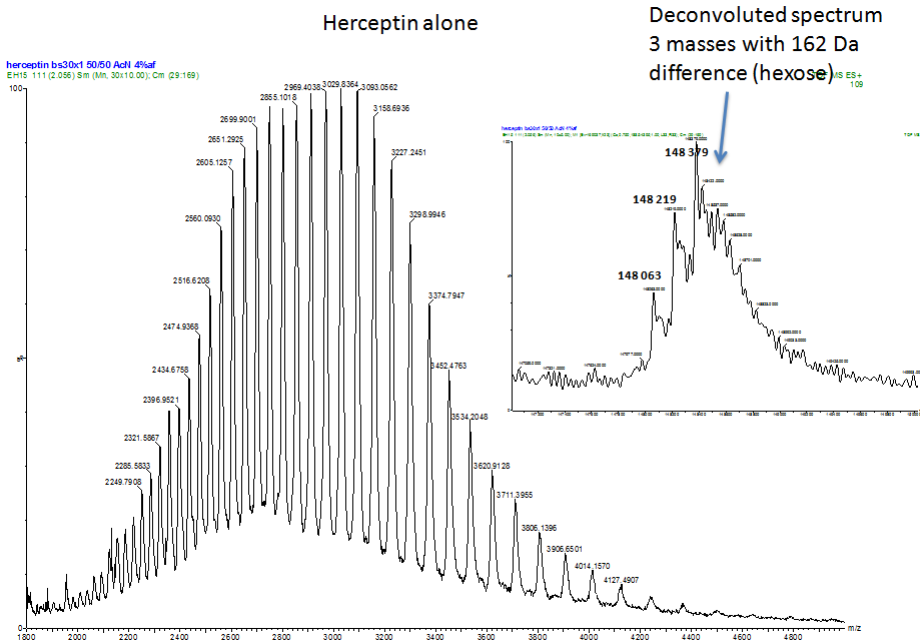
Figure SI 3. MALDI MS of unmodified Herceptin

The molecular mass measured for **OCT-Herceptin** was calculated at approximately 149 060. The difference between both can be calculated as 148 380 (to take the average mass of the pattern) - 149 060 = 680 Da. This mass corresponds probably to two molecules of **OCT5**. Then 337*2-2= 672 which is close to 680 and would indicate the presence of 2 OCT molecules (as an average). The spectrum indicates that we probably have a mixture of 1, 2 and 3 OCT, with 2 being the major isoform.
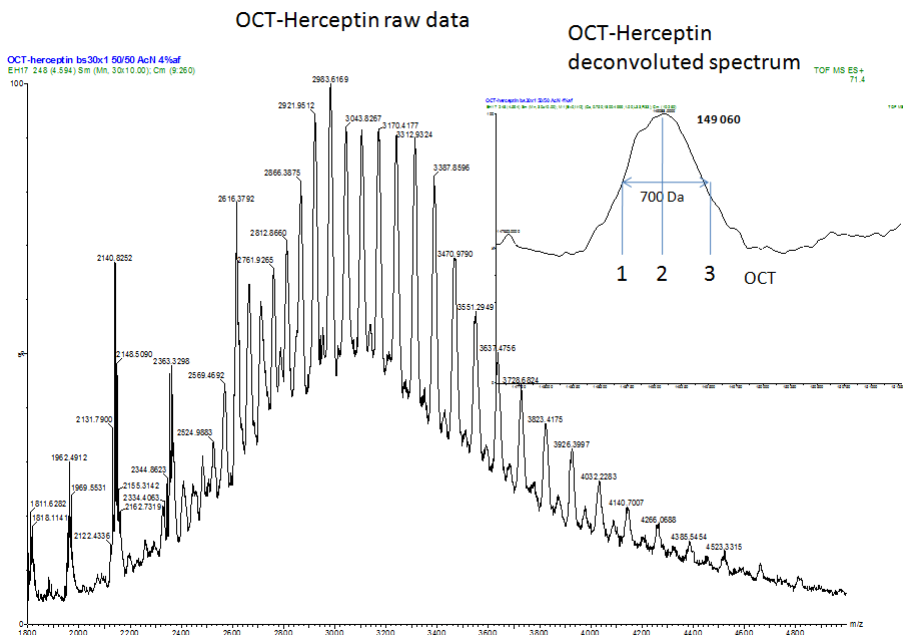
Figure SI 4. MALDI MS of OCT-Herceptin

[^{18}F]FEA small animal PET imaging and tissue biodistribution.*

BALB/c mice (n=3, Harlan, UK) were scanned on a dedicated small animal PET scanner (Siemens Multimodality Inveon, Siemens Molecular Imaging Inc., Knoxville, USA) following a bolus *i.v.* injection of ~3.7 MBq of **[^{18}F]FEA**. All animal experiments were done in accordance with the United Kingdom Home Office Guidance on the Operation of the Animal (Scientific Procedures) Act 1986 (HMSO, London, United Kingdom, 1990) and within guidelines set out by the United Kingdom National Cancer Research Institute Committee on Welfare of Animals in Cancer Research.[10] Dynamic emission scans were acquired in list-mode format over 60 min. The acquired data were then sorted into 0.5 mm sinogram bins and 19 time frames for image reconstruction, which was done by filtered back projection. Direct **[^{18}F]FEA** tissue biodistribution was assessed subsequent to the PET scan. For this, blood was taken by cardiac puncture from the animals and tissues were excised. The tissues were weighted and immediately counted for fluorine-18 radioactivity. Data were expressed as percentage injected dose per gram (%ID/ g).

Tissues	%ID/g
Plasma	3.55 ± 0.30
Blood	2.90 ± 0.23
Heart	2.43 ± 0.15
Lung	2.34 ± 0.06
Liver	3.74 ± 0.21
Gallbladder	3.47 ± 0.20
Stomach	2.22 ± 0.52
Duodenum	3.11 ± 0.22
Jejunum	2.85 ± 0.32
Caecum	3.73 ± 0.26
Colon	2.92 ± 0.33
Rectum	3.38 ± 1.01
Spleen	2.47 ± 0.08
Kidney	3.92 ± 0.18
Muscle	1.96 ± 0.09
Bone	7.11 ± 1.17
Brain	3.16 ± 0.24
Urine	46.33 ± 16.54

**Figure SI 5. [^{18}F]FEA tissue biodistribution in BALB/c mice*** *in vivo* work was carried out by Dr Quang-De Nguyen

Synthesis of 2,2',2"-(11-Azido-3,6,9-trioxaundecan-1-amino)-2-oxoethyl)-1,4,7,10-tetraazacyclododecane-1,4,7-triyl)triacetic acid (DOTA-Az)[203]

1,4,7-Tris(tert-butoxycarbonylmethyl)-1,4,7,10-tetraazacyclododecane-10-acetic acid **(71)** was synthesised in accordance with the literature procedure. [204, 205] DOTA-NHS ester **72** was purchased from Macrocyclics, Inc. (Dallas, TX).
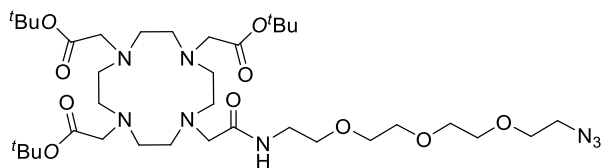
2,2′,2″-(11-Azido-3,6,9-trioxaundecan-1-amino)-2-oxoethyl)- 1,4,7-tris(tert-butoxycarbonylmethyl)-1,4,7,10-tetraazacyclododecane (72)[203]

To a stirred solution of **71** (400 mg, 0.7 mmol) in DMF (8 mL) was added HBTU (530 mg, 1.4 mmol) and DIPEA (134 µL, 1.4 mmol) and the resultant mixture was stirred at room temperature for 30 min. After this time, 11-azido-3,6,9-trioxaundecan-1-amine (200 µL, 0.85 mmol) was added and the resultant mixture was stirred at 40°C for 16 h. The mixture was allowed to cool to room temperature, and the product was extracted with CH_2Cl_2 (3 x 10 mL). The combined organic layers were washed with H_2O (2 x 10 mL) and brine (10 mL), dried over $MgSO_4$, filtered, and concentrated *in vacuo* to yield the crude material as an orange oil. The product was purified by column chromatography, eluting with 5% $MeOH/CH_2Cl_2$, to give pure product **72** as an off-white oil (421 mg, 78% yield). *m/z* (ES$^+$) calcd for: $C_{36}H_{69}N_8O_{10}$ ([(M+H]$^+$) 773.5137, found: 773.5148.
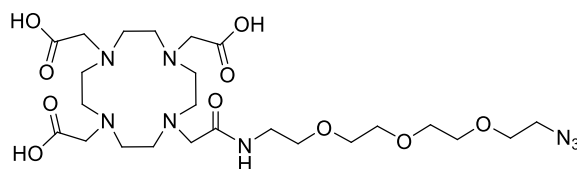
2,2′,2″-(11-Azido-3,6,9-trioxaundecan-1-amino)-2-oxoethyl)-1,4,7,10-

tetraazacyclododecane-1,4,7-triyl)triacetic acid (DOTA-Az)[203]

Method 1:

To a stirred solution of **72** (400 mg, 0.52 mmol) in CH_2Cl_2 (22.5 mL) was added TFA (30 mL) and the resultant mixture was stirred at room temperature for 2 h. The mixture was concentrated *in vacuo* and azeotroped 3 times with chloroform (3 x 25 mL). The residue was dissolved in acetone (5 mL) and the solution was added to diethyl ether (25 mL). The resulting precipitate was filtered off, and the supernatant was evaporated *in vacuo* to yield the crude material as a yellow oil. The product was purified by HPLC to yield **DOTA-Az** as a yellow oil (213 mg, 69% yield). δ_H (400 MHz, DMSO-d_6) 3.00-3.30 (m, 18H), 3.38-3.48 (m, 8H), 3.50-3.61 (m, 14H). *m/z* (ES$^+$) calcd for: $C_{24}H_{45}N_8O_{10}$ 605.3259 ([(M+H]$^+$), found: 605.3251

Method 2:

11-Azido-3,6,9-trioxaundecan-1-amine **74** (13.5 mg, 0.07 mmol) was dissolved in DMF (1 mL) and DOTA-NHS ester **73** (48.5 mg, 0.063 mmol) and triethylamine (105 µL, 0.7 mmol) were added, and the resultant mixture was stirred at room temperature for 2 h. The mixture was concentrated *in vacuo*, to give a yellow oil as crude. A portion of the crude material was purified by preparative HPLC to yield **DOTA-Az** as a yellow oil (29 mg, 69% yield)..

General procedure for Ga-labelling DOTA compounds (synthesis of 'cold' reference compounds)

To a stirred solution of DOTA-compound (1.5 µmol) in NaOAc buffer (0.2 M, pH 6) was added $Ga(NO_3)_2$ (15 µmol) and the resultant mixture was stirred at 80°C for 30 min. The mixture was cooled to room temperature, before being applied to a pre-conditioned (5 mL EtOH, followed by 5 mL H_2O) Sep-pak light C_{18} cartridge. The cartridge was washed with H_2O (5 mL), and the compound was eluted in EtOH (0.5 mL). The EtOH was evaporated *in vacuo*, and the compound re-dissolved in H_2O, before being freeze-dried to give the [69]Ga-labelled cold reference compound.
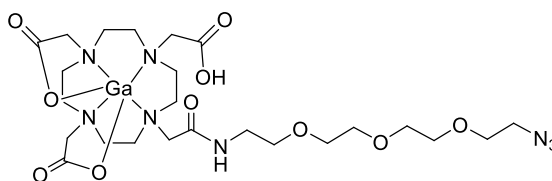
[69]Ga]2,2′,2″-(11-Azido-3,6,9-trioxaundecan-1-amino)-2-oxoethyl)-1,4,7,10-tetraazacyclododecane-1,4,7-triyl)triacetic acid ([Ga]DOTA-Az)

[Ga]**DOTA-Az** was synthesised from **DOTA-Az**, in accordance with the general procedure. *m/z* (ES) calcd for $C_{24}H_{42}N_8O_{10}{}^{69}Ga$, 671.2280 ([(M+H]^+), found 671.2297

General procedure for the SPAAC reaction between [Ga]DOTA-Az and DBCO cyclooctynes

DOTA-Az (50.0 µmol) was dissolved EtOH/DMSO (5:1, 500 mL), and cyclooctyne (55.0 µmol, 1.1 eq.) was added. The mixture was stirred at 50°C for 4 h. The mixture was purified by preparative HPLC, to form the triazole products as white solids. The triazole products were labelled with [69]Ga, as described in the general procedure.

Characterisation of triazole products
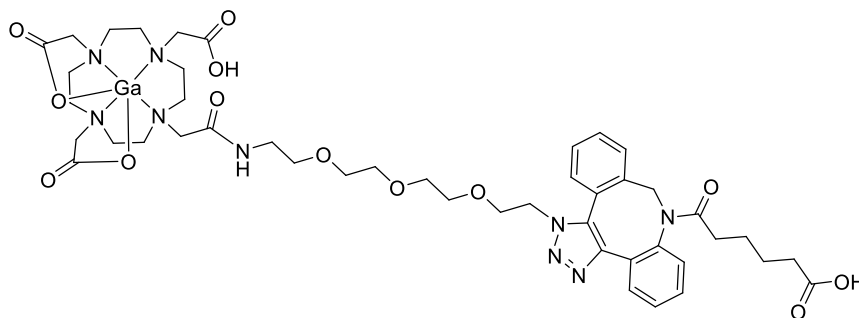
Triazole **75**: *m/z* (ES) calcd for $C_{45}H_{64}N_9O_{13}$, 938.4624 (M$^+$), found 938.4664. **[Ga]75**: *m/z* (ES) calcd for $C_{45}H_{61}N_9O_{13}$ ^{69}Ga ([M+H]$^+$), 1004.3645, found 1004.3627
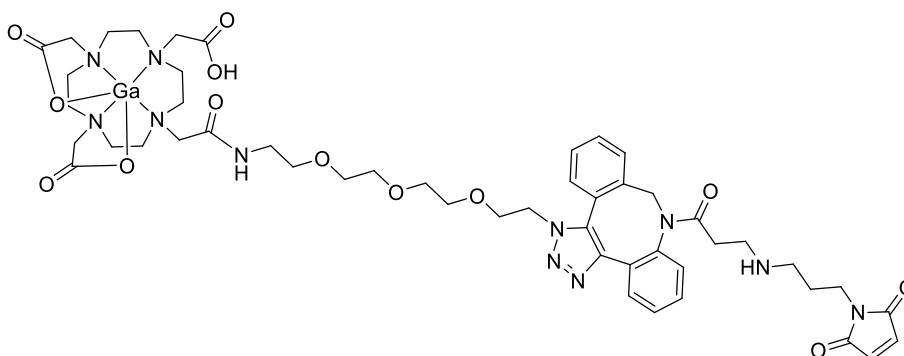
Triazole **76:** *m/z* (ES) calcd for $C_{49}H_{65}N_{11}O_{14}$, 1032.47 (M$^+$), found 1032.4581; 515.735 (M^{2+}), found 516.7386. **[Ga]76**: *m/z* (ES) calcd for $C_{49}H_{60}N_{11}O_{14}$ ^{69}Ga ([M+H]$^{2+}$) 549.8743 found 549.8743

Radiosynthesis of [^{68}Ga]DOTA-Az
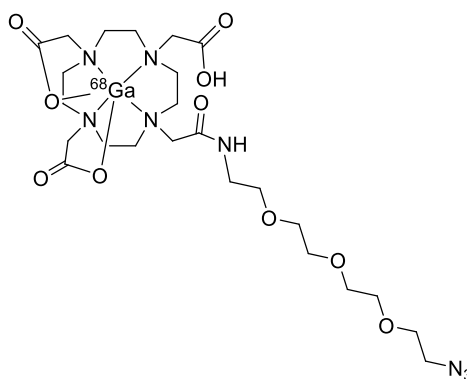
A solution of **DOTA-Az** (50 µL, 1 mgmL^{-1} in DMSO) was diluted with NaOAc buffer solution (pH 4), and the ^{68}GaCl$_3$ was eluted directly into the reaction vial (~1.5 mCi). The radiosynthesis of **[^{68}Ga]DOTA-Az** was achieved in 10 min at 90°C, in >95% radiochemical conversion, and the product was obtained in >95% radiochemical purity, and in 60% isolated RCY (n.d.c) by passing through a Sepak light C$_{18}$ cartridge, eluting in 100% EtOH. The mixture was then diluted with water or acetonitrile for application to the ^{68}Ga-labeled click reactions.
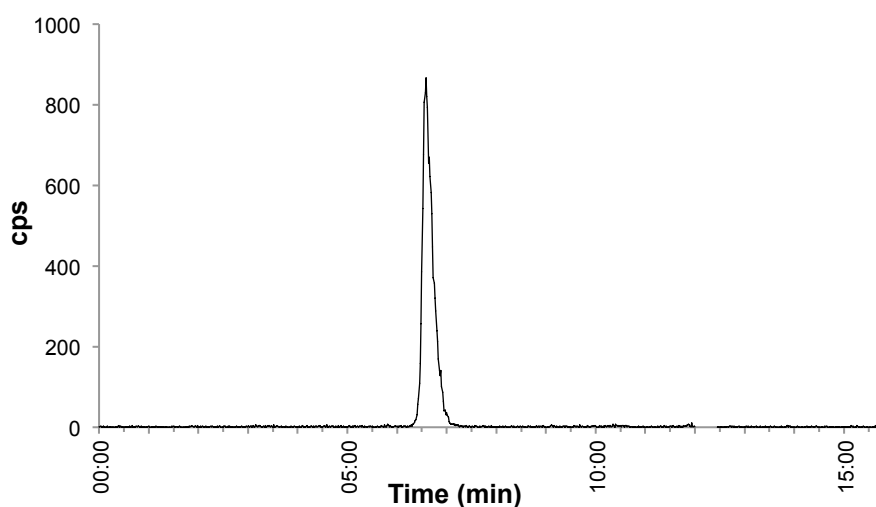
Figure SI 6. Radio-HPLC trace of **[^{68}Ga]DOTA-Az** using gradient A

General procedure for ^{68}Ga-labeled SPAAC reactions between [^{68}Ga]DOTA-Az and DIBAC cyclooctynes

To a 10 mg mL^{-1} solution of cyclooctyne (**DIBAC1**/**DIBAC2**) (50 µL) in either H$_2$O (10 % DMSO) or MeCN, was added **[^{68}Ga]DOTA-Az** (100 µL), and the mixture was heated to either 37°C or 90°C for the given time-point, without stirring. The progress of the reaction was monitored by radio-HPLC.

7.4 Experimental for Chapter 4

Synthesis of 6-(6-(Pyridin-2-yl)-1,2,4,5-tetrazine-3-yl)pyridine-3-amine (Tz1)[116]
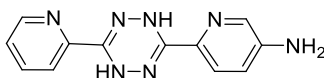
6-(6-Pyridin-2-yl-1,4-dihydro-1,2,4,5-tetrazin-3-yl)-pyridin-3-ylamine (81)[116]

A dry round-bottomed flask was charged with 5-amino-2-cyanopyridine **79** (572 mg, 4.8 mmol), 2-cyanopyridine **80** (500 mg, 4.8 mmol) and hydrazine hydrate (50-60 %, 1.2 mL, 19.2 mmol). The flask was fitted with a reflux condenser, and the mixture was stirred at 90°C for 12 h. The mixture was cooled to room temperature, and the orange precipitate formed was isolated by filtration and was washed with H_2O (3 x 10 mL). The orange solid **81** (1.03 g, 4.0 mmol, 85% yield) obtained was used for the next step without further purification. δ_H (400 MHz, DMSO-d_6) 5.88 (s, 2H) 6.98 (dd, J = 2.5 Hz, 8.5 Hz, 1H); 7.50 (m, 1H); 7.63 (d, J = 8.5 Hz, 1H); 7.92 (m, 3H); 8.61 (m, 1H); 8.65 (s, 1H); 8.70 (s, 1H). δ_C (100 MHz, DMSO-d_6) 120.8; 121.3; 122.3; 125.7; 134.5; 134.6; 137.8; 146.7; 147.1; 147.1; 147.3; 149.0. HRMS (ESI) m/z calcd for $C_{12}H_{12}N_7$ ([M+H]$^+$) 254.1154, found 254.1147.
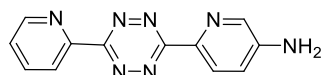
6-(6-(Pyridin-2-yl)-1,2,4,5-tetrazine-3-yl)pyridine-3-amine (Tz1)[116]

To a stirred solution of 6-(6-Pyridin-2-yl-1,4-dihydro-[1,2,4,5]tetrazin-3-yl)-pyridin-3-ylamine **81** (1.0 g, 3.95 mmol) in toluene (25 mL) was added DDQ (1.8 g, 7.9 mmol) and the resultant mixture was stirred under reflux for 16 h. The crude product was concentrated *in vacuo* onto silica deactivated with triethylamine (5% in hexane), and was purified by column chromatography eluting with 20-100% acetone in hexane. **Tz1** (eluted in 100% acetone) was isolated as a brown/purple solid (735 mg, 2.9 mmol, 75% yield). δ_H (400 MHz, DMSO-d_6) 6.38 (s, 1H); 7.13 (dd, J = 8.7, 2.8, 1H); 7.69 (ddd, J = 7.5 Hz, 4.5 Hz, 1.0 Hz, 1H); 8.12 (td, J = 8.0 Hz, 2.0 Hz, 1H); 8.24 (d, J = 3.0 Hz, 1H); 8.36 (d, J = 8.5 Hz, 1H); 8.53 (d, J = 8.0 Hz,

1H); 8.89-8.91 (m, 1H). δ_C (100 MHz, DMSO-d_6) 119.4; 124.2; 126.2; 126.7; 136.5; 137.7; 138.2; 148.5; 150.9; 163.0; 163.4. HRMS (ESI) m/z calcd for $C_{12}H_{10}N_7$ ([M+H]$^+$) 252.0098, found 252.1002.

Synthesis of 4-(6-methyl-1,2,4,5-tetrazin-3-yl)benzylamine (Tz3)[144]
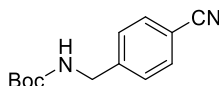
tert-Butyl [4-(Boc-aminomethyl)benzonitrile] (87)[144]

4-(Aminomethyl)benzonitrile·HCl **85** (5.0 g, 30.0 mmol) was azeotroped with toluene (3 x 20 mL) and dissolved in CH_2Cl_2 (4.0 mL). Triethylamine (11.0 mL, 75.0 mmol) and Boc$_2$O (7.4 g, 33.0 mmol) were added and the resultant mixture was stirred at room temperature for 16 h. The mixture was concentrated *in vacuo* to yield a white solid, which was recrystallised from EtOAc/pet ether, to yield *tert*-butyl (4-(aminomethyl)benzocarbamate) **87** (6.0 g, 25.8 mmol, 87% yield) as a white powder. δ_H (400 MHz, CDCl$_3$) 1.43 (s, 9H); 4.33 (d, J = 6.0 Hz, 2H); 5.10 (bs, 1H); 7.36 (d, J = 8.5 Hz, 2H); 7.58 (d, J = 8.5 Hz, 2H). δ_C (100 MHz, CDCl$_3$) 28.3; 44.1; 79.9; 111.0; 118.7; 127.7; 132.3; 144.7; 155.8. m/z (ES$^+$) calcd for: $C_{13}H_{17}N_2O$ ([M+H]$^+$) 233.1290, found: 233.1294.
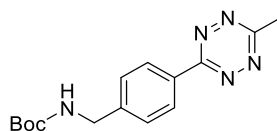
tert-Butyl 4-(6-methyl-1,2,4,5-tetrazin-3-yl)benzylcarbamate (89)[144]

A high pressure reaction tube was treated with 4-(boc-aminomethyl)benzonitrile **87** (232 mg, 1.0 mmol)*,* MeCN (525 µL, 10.0 mmol), Ni(OTf)$_2$ (178 mg, 0.5 mmol) and hydrazine hydrate (50-60% NH$_2$NH$_2$) (3.1 mL, 50.0 mmol). The tube was sealed and heated to 60°C for 24 h, after which time the mixture had turned deep purple in colour. NaNO$_2$ (1.4 g, 20.0 mmol) in H$_2$O (5 mL), was added to the mixture, followed by dropwise addition of HCl (1M), until the pH reached 3 and gases stopped evolving, at which point the mixture had turned bright red. The product was extracted with EtOAc (3 x 20 mL), and the combined organic layers were

washed with H_2O (2 x 10 mL) and brine (10 mL), dried over $MgSO_4$, filtered, and concentrated *in vacuo* to yield a bright pink oil as crude. The product was purified by column chromatography, eluting with 0-3% diethyl ether/CH_2Cl_2, to give *tert*-butyl 4-(6-methyl-1,2,4,5-tetrazin-3-yl)benzylcarbamate **89** (74 mg, 0.3 mmol, 60% yield) as a bright pink solid. R_f = 0.35 (2% diethyl ether/CH_2Cl_2). δ_H (400 MHz, $CDCl_3$) 1.47 (s, 9H); 3.08 (s, 3H); 4.42 (d, *J* = 4.5 Hz, 2H); 5.04 (bs, 1H); 7.48 (d, *J* = 7.5 Hz, 2H); 8.53 (d, *J* = 7.5 Hz, 2H). δ_C (100 MHz, $CDCl_3$) 20.5; 27.8; 43.7; 79.2; 127.5 (d, *J* = 14.0 Hz); 130.1; 143.3; 155.3; 163.3; 166.6. *m/z* (ES$^+$) calcd for: $C_{11}H_{11}N_5O_2$ ([M-^{t}Bu]$^+$) 246.0991 found: 246.0983.
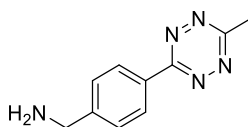
4-(6-Methyl-1,2,4,5-tetrazin-3-yl)benzylamine (Tz3)[144]

tert-Butyl 4-(6-methyl-1,2,4,5-tetrazin-3-yl)benzylcarbamate **89** (45.0 mg, 0.15 mmol) was treated with TFA/CH_2Cl_2 (1/1, *v/v*, 4 mL) for 1 h. The resultant mixture was concentrated *in vacuo* to yield 4-(6-methyl-1,2,4,5-tetrazin-3-yl)benzylamine **Tz3** as a bright pink solid (30 mg, 0.14 mmol, >95% yield). δ_H (400 MHz, DMSO-d_6) 3.01 (s, 3H); 4.18 (bs, 2H); 7.73 (d, *J* = 8.5 Hz, 2H); 8.26 (bs, 2H); 8.52 (d, *J* = 8.5 Hz, 2H). δ_C (100 MHz, DMSO-d_6) 27.8; 41.9; 127.5; (d, *J* = 14.0 Hz); 129.7; 131.9; 138.2; 162.9; 167.2. *m/z* (CI) calcd for $C_{10}H_{12}N_5$ 202.1093 (M$^+$), found 202.1096. *m/z* (CI) calcd for $C_{10}H_{12}N_5$ ([M+H]$^+$) 202.1093, found 202.1096.
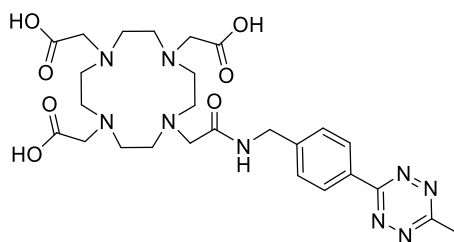
2,2′,2″-(10-(2-((4-(6-methyl-1,2,4,5-Tetrazin-3-yl)benzyl)amino)-2-oxoethyl)-1,4,7,10-tetraazacyclododecane-1,4,7-triyl)triacetic acid (DOTA-Tz)

4-(6-methyl-1,2,4,5-tetrazin-3-yl)benzylamine **Tz3** (13.5 mg, 0.07 mmol) was dissolved in DMF (1 mL) and DOTA-NHS ester **73** (48.5 mg, 0.06 mmol) and triethylamine (105 µL, 0.7 mmol) were added, and the resultant mixture was stirred at room temperature for 2 h. The mixture was concentrated *in vacuo*, to give a pink oil as crude. The crude material was purified by preparative HPLC to yield **DOTA-Tz** as a pink solid (25 mg, 0.04 mmol, 60% yield). δ_H (400 MHz, DMSO-d_6) 3.00 (s, 3H); 3.06-3.17 (m, 8H); 3.19-3.35 (m, 8H); 3.60-3.70 (m, 4H); 3.85-4.02 (m, 4H); 4.48 (d, J = 5.5 Hz, 2H); 7.59 (d, J = 8.5 Hz, 2H); 8.46 (d, J = 8.5 Hz, 2H); 9.00 (bs, 1H). m/z (ES$^+$) calcd. for $C_{26}H_{38}N_9O_7$ ([M+H]$^+$) 588.2894, found 588.2870.
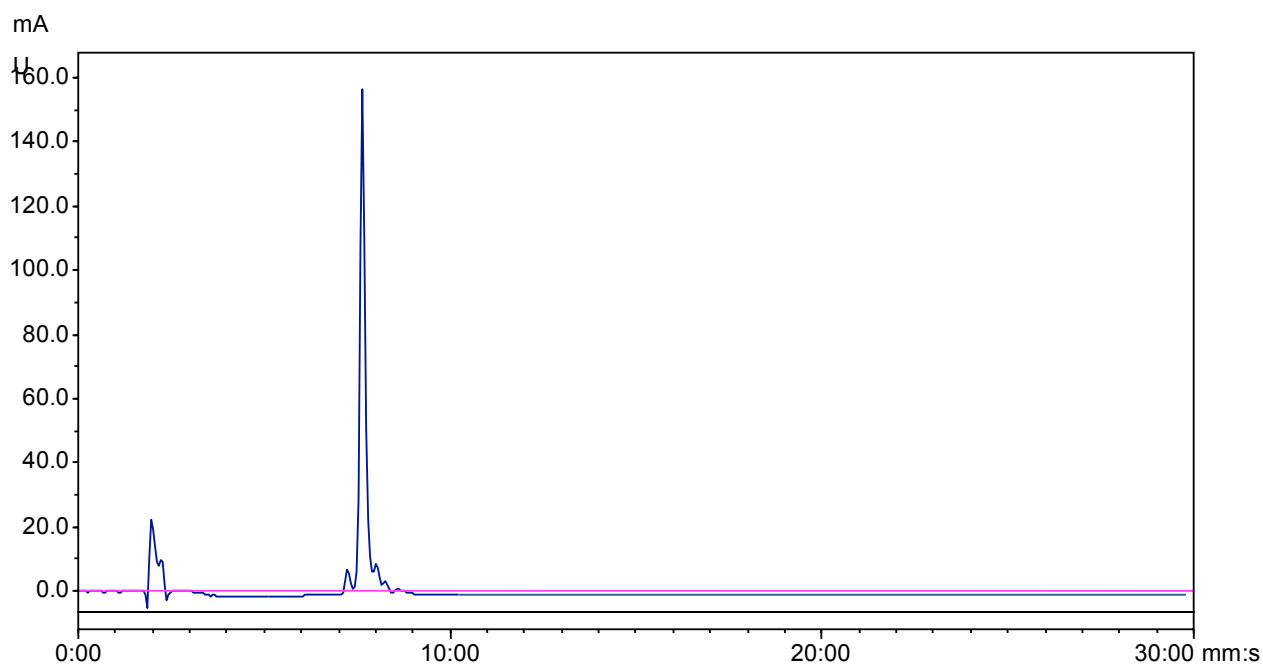
Figure SI 7. HPLC (UV) trace of **DOTA-Tz** at 254 nm using gradient B

General procedure for the synthesis of norbornene analogues

91
mixutre of *endo* and *exo*-
predominantly *endo*

104/105

100-102
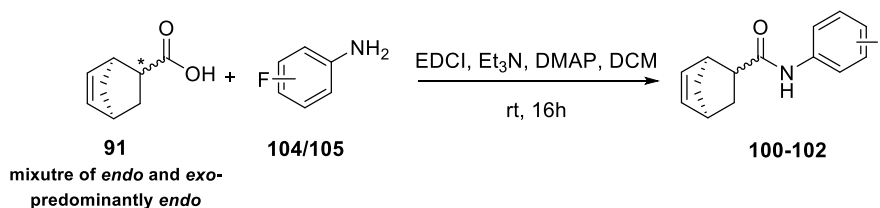
5-Norbornene-2-carboxylic acid (mixture of *endo* and *exo*, predominantly *endo*) **(91)** (130.2 mg, 1.0 mmol) was dissolved in CH_2Cl_2 (10 mL), and EDCI (230 mg, 1.2 mmol), DMAP (30.5 mg, 0.25 mmol) and triethylamine (167 µL, 1.2 mmol) were added, and the mixture was stirred at room temperature for 30 min. Fluoro-aniline (1.2 mmol) was added, and the resultant mixture was stirred at room temperature for 4 h. The mixture was partitioned between CH_2Cl_2 (20 mL) and $NaHCO_3$ (20 mL, sat. aq.), and the organic layer was washed with H_2O (2 x 20 mL) and brine (2 x 20 mL), dried over $MgSO_4$, filtered and concentrated *in vacuo*. The crude material was purified by column chromatography eluting with 100% CH_2Cl_2, and the solid was recrystallised from EtOAc/hexane to yield the product

(exo)
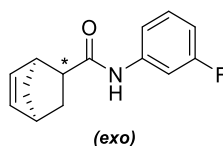
### (1*S*,4*S*)-*N*-(3-Fluorophenyl)bicyclo[2.2.1]hept-5-ene-2-carboxamide (*exo*) (100)

Using the general procedure, 3-fluoroaniline provided amide **100** as a white powder (162 mg, 0.7 mmol, 70% yield). δ_H (400 MHz, $CDCl_3$) 1.16 (m, 1H); 1.31 (m, 2H); 1.81 (ddd, J = 3.5 Hz, 9.5 Hz, 11.5 Hz, 1H); 2.83 (m, 2H); 3.05 (s, 1H); 5.85 (dd, J = 3.0 Hz, 5.5 Hz, 1H); 6.12 (dd, J = 3.0 Hz, 5.5 Hz, 1H); 6.59 (ddt, J = 0.5 Hz, 2.5 Hz, 8.5 Hz, 1H); 6.93 (dd, J = 1.0 Hz, 8.0 Hz, 1H); 7.06 (m, 1H); 7.29 (m, 1H). δ_C (101 MHz, $CDCl_3$) 29.6; 42.6; 45.6; 46.3; 50.0; 106.8; 110.2; 114.6; 129.7 (d, J_{CF} = 9.5 Hz); 131.6; 137.9; 139.3; 161.5; 172.6. δ_F (376 MHz, $CDCl_3$) -111.62 (m). *m/z* (ES) calcd for $C_{14}H_{15}NOF$ ([M+H]$^+$) 232.1138, found 232.1149.
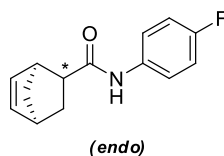
(endo)

(1S,4S)-N-(4-Fluorophenyl)bicyclo[2.2.1]hept-5-ene-2-carboxamide (*endo*) (101)

Using the general procedure, 4-fluoroaniline provided amide **101** as a white powder (111 mg, 0.5 mmol 50% yield). δ_H (400 MHz, CDCl$_3$) 1.40 (m, 2H); 1.76 (d, J = 8.5 Hz, 1H); 2.02 (td, J = 4.0 Hz, 11.5 Hz, 1H); 2.14 (dd, J = 4.5 Hz, 10.0 Hz, 1H); 3.00 (d, J = 30.5 Hz, 2H); 6.16 (ddd, J = 3.0 Hz, 5.5 Hz, 22.0 Hz, 2H); 7.00 (t, J = 8.5 Hz, 2H); 7.48 (dd, J = 5.0 Hz, 9.0 Hz, 2H). δ_C (100 MHz, CDCl$_3$) 30.3; 41.3; 45.4; 46.0; 47.0; 115.1; 115.3; 121.2 (d, J_{CF} = 8.0 Hz), 133.9; 135.5; 138.2; 157.7; 160.1; 173.6. δ_F (376 MHz, CDCl$_3$) -118.41 (m). *m/z* (ES) calcd for C$_{14}$H$_{15}$NOF ([M+H]$^+$) 232.1138, found 232.1145.

(exo)
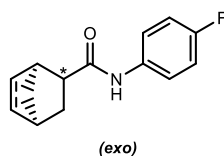
(1S,4S)-N-(4-Fluorophenyl)bicyclo[2.2.1]hept-5-ene-2-carboxamide (*exo*) (102)

Using the general procedure, 4-fluoroaniline provided amide **102** as a white powder (74 mg, 0.32 mmol, 30% yield). δ_H (400 MHz, CDCl$_3$) 1.34 (d, J = 8.0 Hz, 1H); 1.48 (m, 2H); 2.01 (m, 1H); 2.98 (m, 2H); 3.22 (s, 1H); 6.04 (dd, J = 3.0 Hz, 5.5 Hz, 1H); 6.30 (dd, J = 3.0 Hz, 5.5 Hz, 1H); 6.98 (t, J = 8.5 Hz, 2H), 7.15 (bs, 1H), 7.42 (m, 1H). δ_C (101 MHz, CDCl$_3$) 30.0; 42.9; 45.8; 46.5; 50.2; 115.4; 115.6; 121.5 (d, J_{CF} = 8.0 Hz); 132.0; 134.0; 138.1; 158.0; 160.4; 172.5. δ_F (376 MHz, CDCl$_3$) -118.52 (m). *m/z* (ES) calcd for C$_{14}$H$_{15}$NOF ([M+H]$^+$) 232.1138, found 232.1133.

General procedure for the IeDDA reaction between DOTA-Tz and alkenes
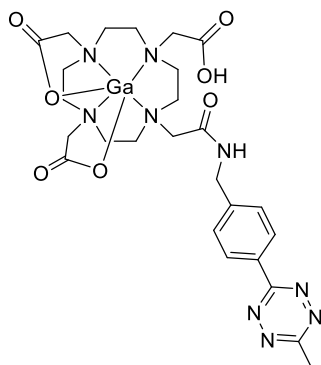
[Ga]DOTA-Tz was synthesised from DOTA-Tz as described in the general procedure for ^{69}Ga-labelling. *m/z* (ES) calcd for $C_{26}H_{35}N_9O_7{}^{69}Ga$, ([M+H]$^+$) 654.1915, found 654.1927

Synthesis of dihydropyridazine products ('cold' reference compounds)

DOTA-Tz3 (5.0 µmol) was dissolved in H_2O/10% MeOH (1 mL), and alkene (5.5 µmol, 1.1 eq.) was added. The mixture was stirred at 50°C for 2-4 h. Completion of reaction was indicated by the colour change of solution from pink to colourless. The mixture was purified by preparative HPLC, to form the dihydropyridazine products as white solids. The obtained dihydropyridazine products were labelled with Ga using the general procedure.

Characterisation of dihydropyridazine products
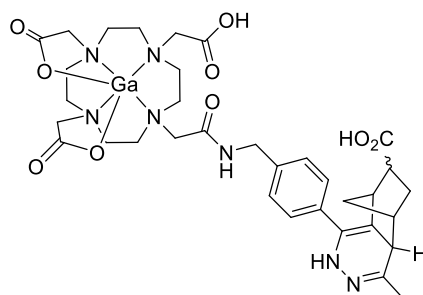
(mixture of regioisomers)

Dihydropyridazine **95:** *m/z* (ES+) calcd. for: $C_{34}H_{47}N_7O_9$, ([M+H]$^+$) 698.34, found: 698.4279;

[Ga]95: *m/z* (ES) calcd. for: $C_{34}H_{47}N_7O_9Ga$, ([M+H]$^+$) 764.2535, found: 764.2502

Figure SI 8. ES m/z for **[Ga]95**

(mixture of regioisomers)
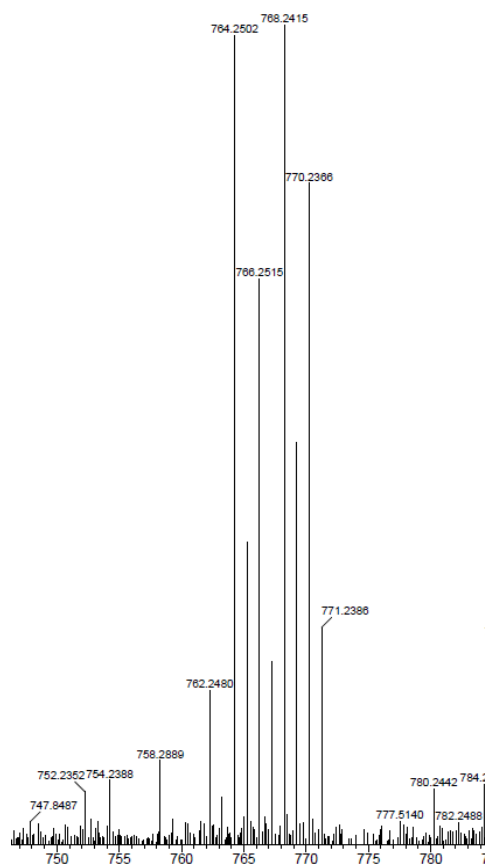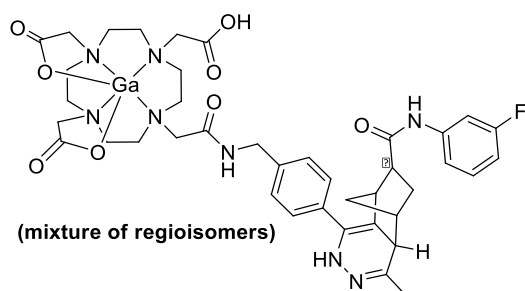
Dihydropyridazine **96**: *m/z* (ES) calcd for $C_{40}H_{52}N_8O_8F$ ([M+H]$^+$) 791.3892, found 791.3884;

[Ga]**96**: *m/z* (ES) calcd for: $C_{40}H_{49}N_8O_8FGa$ ([M+H]$^+$) 857.2913, found: 857.2924

Figure SI 9. ES m/z for **[Ga]96**

(mixture of regioisomers)
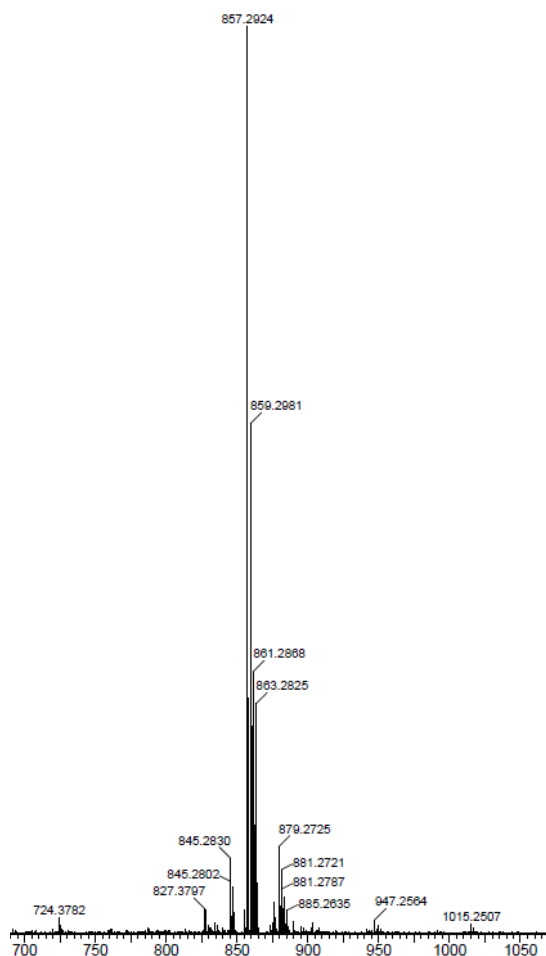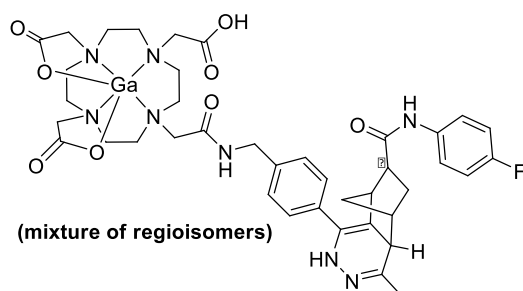
Dihydropyridazine **97**: m/z (ES) calcd for $C_{40}H_{52}N_8O_8F$ ([M+H]$^+$) 791.3892, found 791.3909;

[Ga]**97**: m/z (ES) calcd for $C_{40}H_{49}N_8O_8FGa$ ([M+H]$^+$) 857.2903, found 857.2893

Dihydropyridazine **98**: m/z (ES) calcd for $C_{40}H_{52}N_8O_8F$ ([M+H]$^+$) 791.3892, found 793.3568;

[Ga]**98**: m/z (ES) calcd for $C_{40}H_{48}N_8O_8FNaGa$ ([M+H]$^+$) 855.2508, found 855.2477.
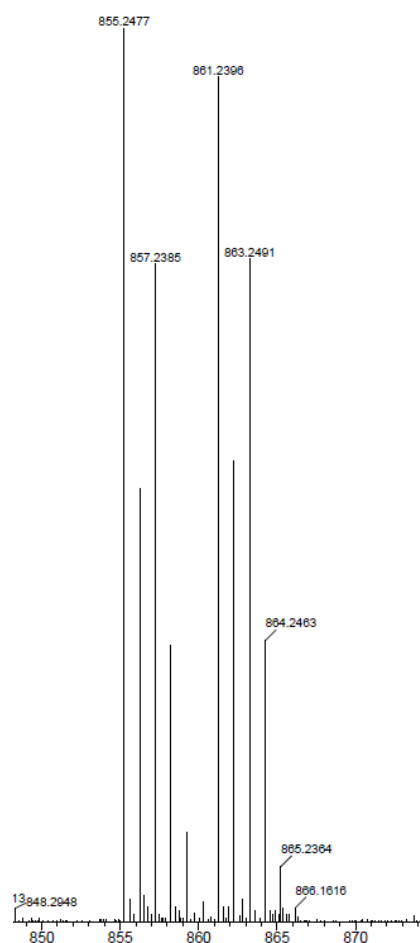
Figure SI 10. ES m/z for **[Ga]98**

Radiosynthesis of [^{68}Ga]DOTA-Tz
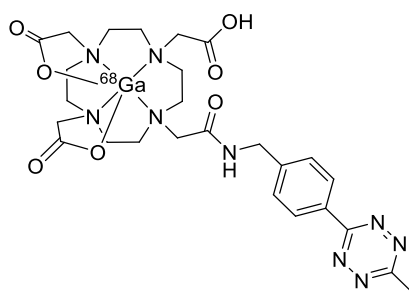
A solution of **DOTA-Tz** (25 µL, 1 mgmL^{-1} in DMSO) was diluted with NaOAc buffer solution (pH 6), and the ^{68}GaCl$_3$ was eluted directly into the reaction vial (~ 6.0 mCi). The radiosynthesis of **[^{68}Ga]DOTA-Tz** was achieved in 10 min at 90°C, in >95 % radiochemical conversion, and the product was obtained in >95% radiochemical purity, and in 60-70%

isolated RCY (n.d.c) by passing through a Sepak light C_{18} cartridge, eluting in 100% EtOH. The mixture was then diluted with water or acetonitrile for application to the ^{68}Ga-labeled IeDDA reactions.
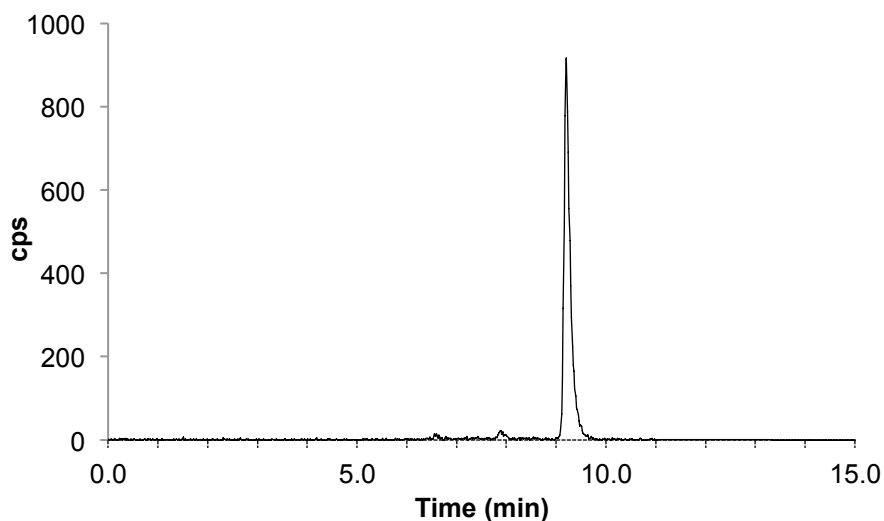
Figure SI 11. Radio-HPLC trace of **[^{68}Ga]DOTA-Tz** using gradient B

General procedure for ^{68}Ga-labeled IeDDA reactions between [^{68}Ga]DOTA-Tz and alkenes

To a 10 mgmL^{-1} solution of alkene (50 µL) in either H_2O or MeCN was added **[^{68}Ga]DOTA-Tz** (100 µL), and the mixture was heated to 37°C for the given time-point, without stirring. The progress of the reaction was monitored by radio-HPLC.

7.5 Experimental for Chapter 5

General Procedure for the Synthesis of RGD Cyclic Pentapeptides

Synthesis of RGD cyclic pentapeptides were carried out according to standard Fmoc coupling procedures[225] or from RGDfK(NH$_2$), which was purchased from FutureChem.

Characterisation of RGD Cyclic Pentapeptides
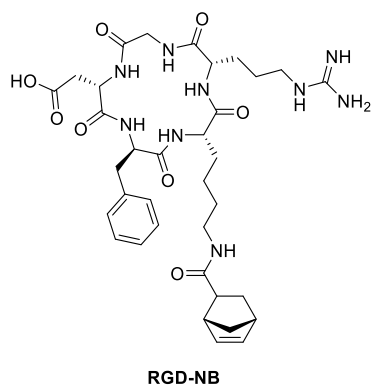
RGD-NB

C$_{35}$H$_{50}$N$_9$O$_8$
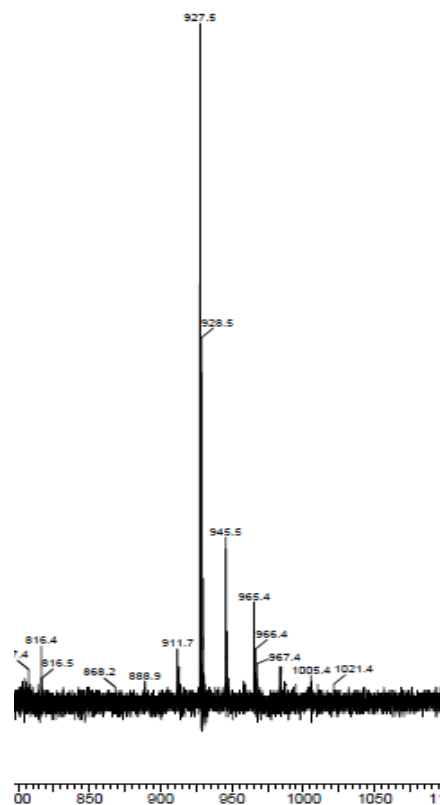
MALDI calc for: 724.37, found: 724.4
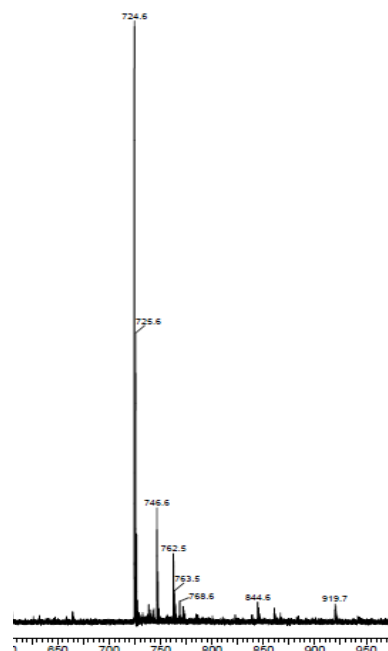
Figure SI 12. MALDI m/z for **RGD-NB**
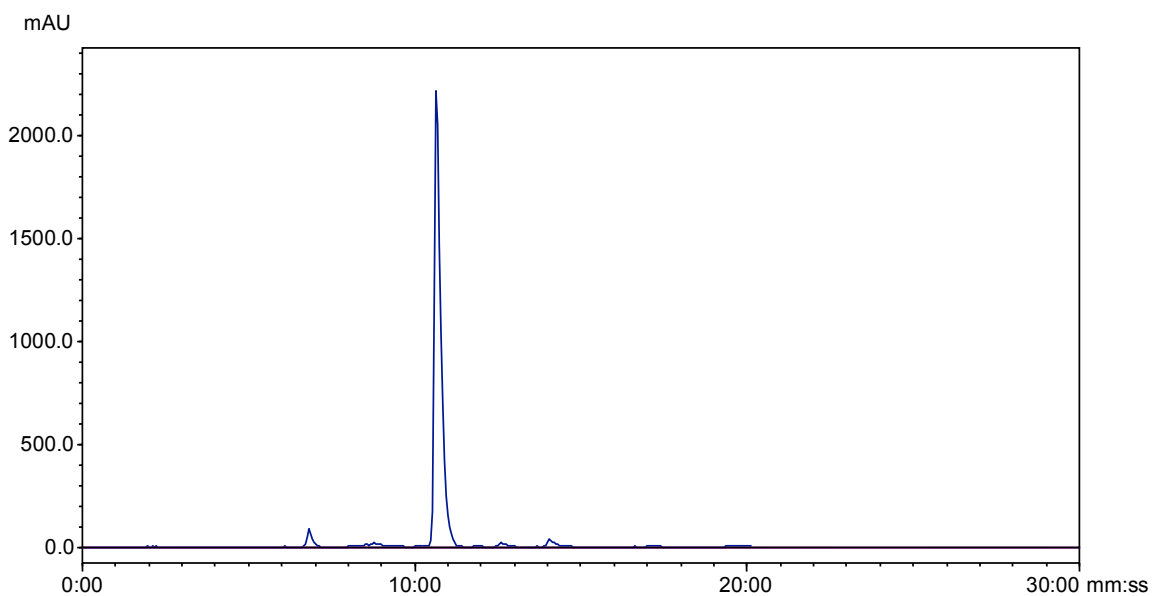
Figure SI 13. HPLC (UV) trace of **RGD-NB** at 254 nm using gradient A
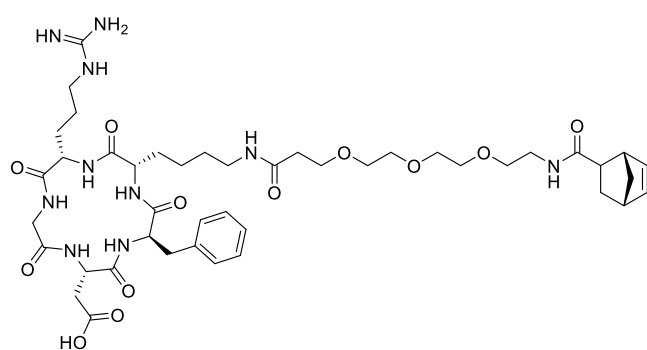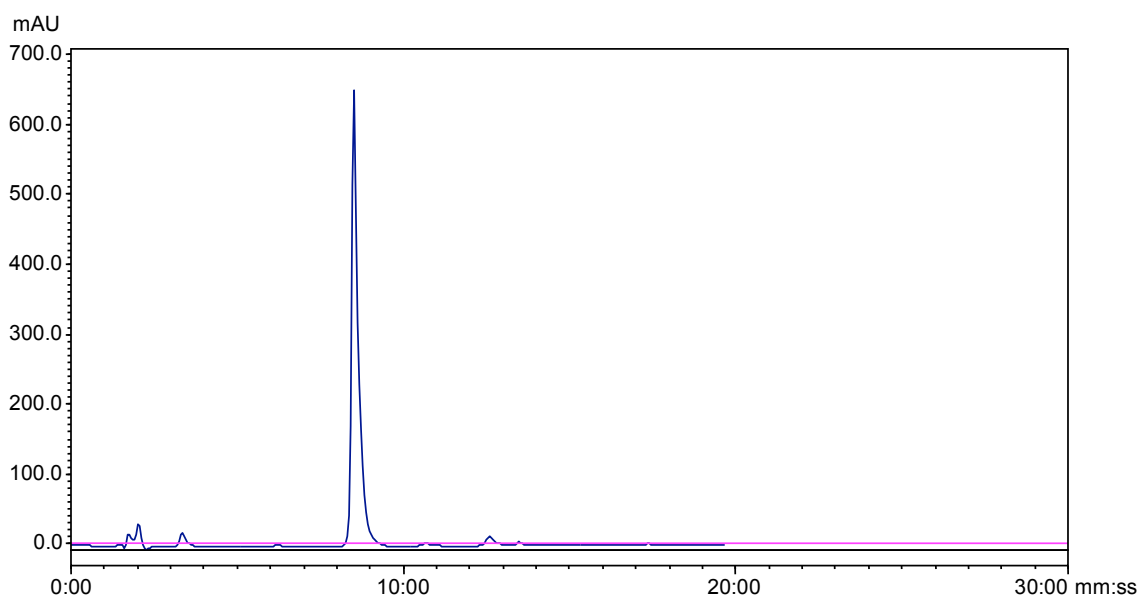
RGD-PEG3-NB

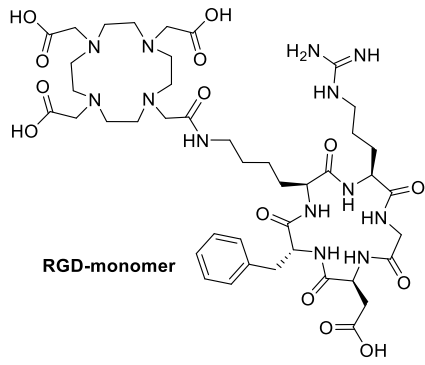$C_{44}H_{67}N_{10}O_1$

MALDI calc for: 926.49, found 927.6

Figure SI 14. MALDI m/z for **RGD-PEG3-NB**

Figure SI 15. HPLC (UV) trace of **RGD-PEG3-NB** at 254 nm using gradient A

256

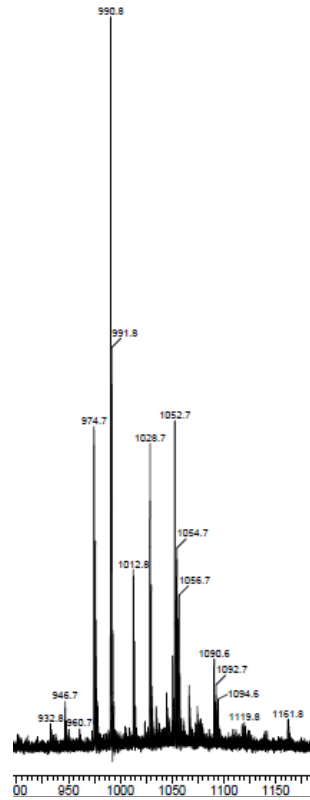$C_{43}H_{68}N_{13}O_{14}$

MALDI calc for: 990.49, found 990.8
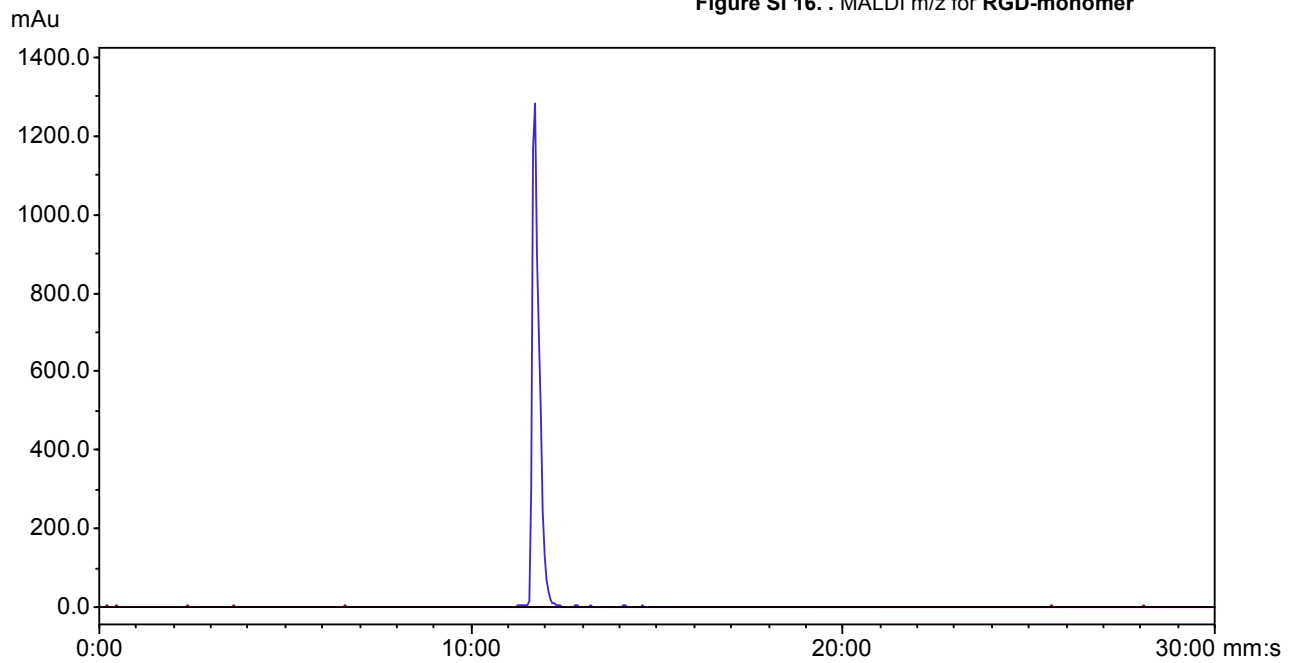

Figure SI 16. . MALDI m/z for **RGD-monomer**

Figure SI 17. HPLC (UV) trace of **RGD-monomer** at 254 nm using gradient A

257

Radiosynthesis of [^{68}Ga]RGD-monomer

A solution of **RGD-monomer** (50 µL, 1 mgmL^{-1} in DMSO) was diluted with NaOAc buffer

solution (pH 6), and the ^{68}GaCl$_3$ was eluted directly into the reaction vial (~ 1.2 mCi).   The

radiosynthesis of **[^{68}Ga]RGD-monomer** was achieved in 10 min at 100°C, in >90%

radiochemical conversion, and the product was obtained in >95% radiochemical purity, and

in 75% isolated RCY (n.d.c) by passing through a Sepak light C$_{18}$ cartridge, eluting in 100%
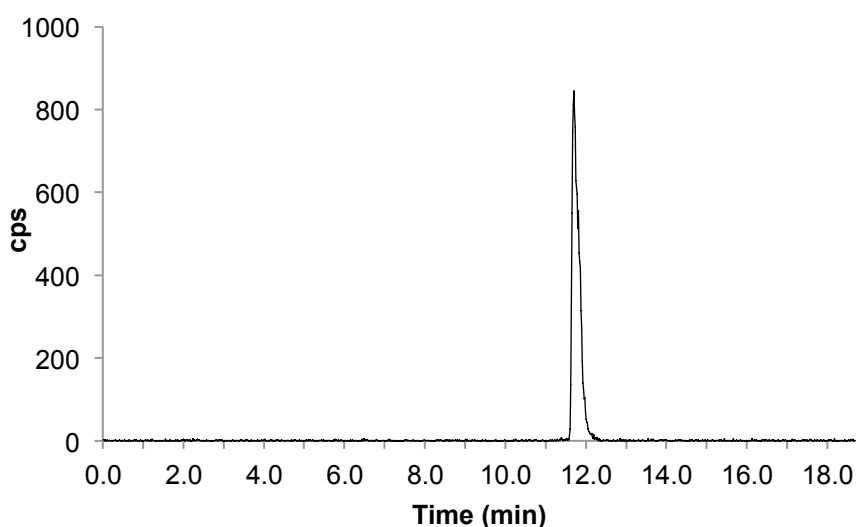
EtOH (500µL total volume).

Figure SI 18. Radio-HPLC trace of **[^{68}Ga]RGD-monomer** using gradient A

Radiosynthesis of [^{68}Ga]RGD-dimer

A solution of **RGD-dimer** (50 µL, 1 mgmL^{-1} in DMSO) was diluted with NaOAc buffer solution

(pH 6), and the ^{68}GaCl$_3$ was eluted directly into the reaction vial (~ 1.2 mCi).   The

radiosynthesis of **[^{68}Ga]RGD-dimer** was achieved in 10 min at 100°C, in >90%

radiochemical conversion, and the product was obtained in >95 % radiochemical purity, and

in 55% isolated rcy (n.d.c) by passing through a Sepak light C$_{18}$ cartridge, eluting in 100%
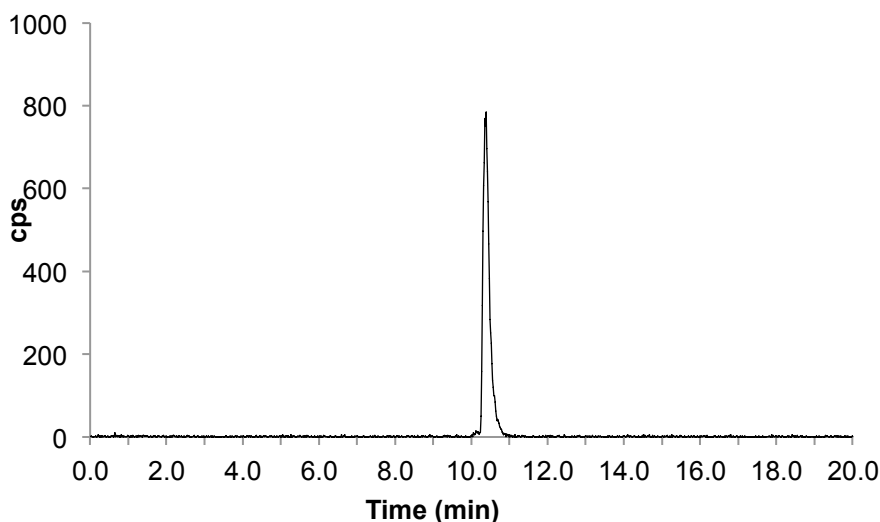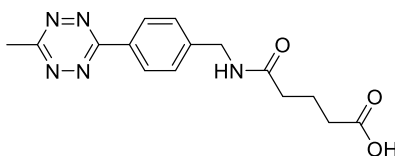
EtOH (500µL total volume).

Figure SI 19. Radio-HPLC trace of [^{68}Ga]RGD-dimer using gradient A

Synthesis of DOTA-GA-Tz
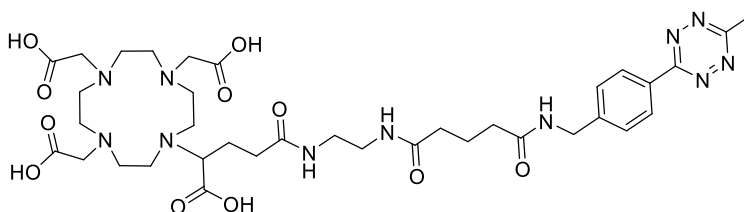

5-{[4-(6-Methyl-1,2,4,5-tetrazin-3-yl)benzyl]amino}-5-oxopentanoic acid (105)

A dry flask was treated with T**z3** (66.4 mg, 0.33 mmol), glutaric anhydride (188 mg, 1.65 mmol) and THF (10 mL), and the resultant mixture was heated to 70°C for 4 h. The mixture was cooled to 50°C, and was stirred at this temperature for a further 16 h. The solvent was evaporated *in vacuo*, to give the crude material as a pink oil. The product was purified by column chromatography eluting with a gradient of 0-5% MeOH/CH$_2$Cl$_2$ to give **105** as a red solid (100 mg, 0.32 mmol, >95% yield). R_f = 0.3 (5% MeOH/ CH$_2$Cl$_2$). δ_H (400 MHz, DMSO-d_6) 2.24 (m, 6H); 2.99 (s, 3H); 3.36 (bs, 1H); 4.38 (d, J = 6.0 Hz, 2H); 7.52 (d, J = 8.5 Hz, 2H); 8.42 (d, J = 8.5 Hz, 2H); 12.08 (bs, 1H). δ_C (100 MHz, DMSO-d_6) 21.2; 21.3; 33.2; 33.5; 34.8; 42.3; 127.9; 128.5; 130.8; 145.0; 163.6; 167.5; 172.3; 174.6; 174.6. *m/z* (ES$^+$) calcd for C$_{15}$H$_{18}$N$_5$O$_3$ 316.1410 (M$^+$), found 316.1409.
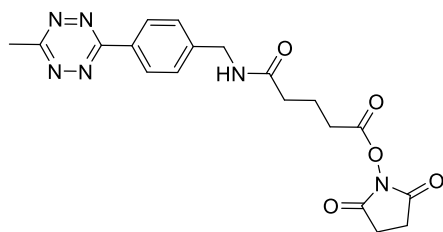
5-[(2,5-Dioxopyrrolidin-1-yl)oxy]-*N*-[4-(6-methyl-1,2,4,5-tetrazin-3-yl)benzyl]-5-

oxopentanamide (106)

To a stirred solution of **105** (63.1 mg, 0.2 mmol) in dichloroethane (2 mL), was added N-hydroxysuccinimide (92.1 mg, 0.8 mmol) and EDCI·HCl (153.4 mg, 0.8 mmol) and the resultant mixture was stirred for 16 h at rt. The mixture was diluted with CH_2Cl_2, and the organic layer was washed with HCl (1M, 2 x 40 mL), dried over $MgSO_4$, filtered and concentrated *in vacuo* to give a fushia-coloured solid (82.0 mg, 0.2 mmol, >95% yield). R_f = 0.3 (2% $MeOH/CH_2Cl_2$). The product was used for the next step without purification. *m/z* (ES$^+$) calcd for $C_{19}H_{21}N_6O_5$ 413.1573 (M$^+$), found 413.1586.

2,2',2''-(10-(1-Carboxy-4-((4-(6-methyl-1,2,4,5-tetrazin-3-yl)benzyl)amino)-4-oxobutyl)-1,4,7,10-tetraazacyclododecane-1,4,7-triyl)triacetic acid (DOTA-GA-Tz)

To a stirred solution of **106** (38.1 mg, 0.08 mmol) in DMF (5 mL), was added DOTA-GA-NH$_2$ (number) and triethylamine (290 μL), and the resultant mixture was stirred at rt for 4 h. The solvent was evaporated *in vacuo* to give a pink oil as crude. The product was purified by preparative HPLC, to yield **DOTA-GA-Tz** as a pink oil. *m/z* (ES$^+$) calcd for $C_{36}H_{54}N_{11}O_{11}$ 816.4004 (M$^+$), found 816.4001 .
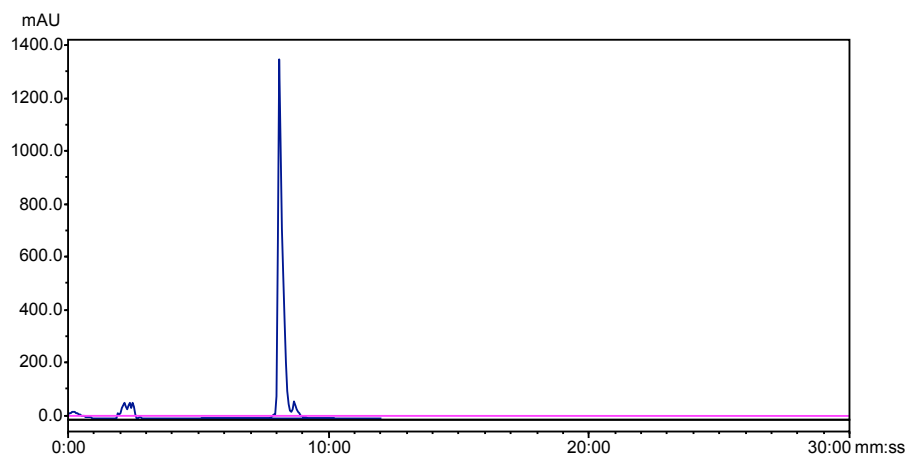
Figure SI 20. HPLC (UV) trace of **DOTA-GA-Tz** at 254 nm using gradient A

Radiosynthesis of [^{68}Ga]DOTA-GA-Tz

A solution of **DOTA-GA-Tz** (25 µL, 1 mgmL^{-1} in DMSO) was diluted with NaOAc buffer solution (pH 6), and the ^{68}GaCl$_3$ was eluted directly into the reaction vial (~ 6.0 mCi). The radiosynthesis of **[^{68}Ga]DOTA-Tz** was achieved in 10 min at 90°C, in >95% radiochemical conversion, and the product was obtained in >95% radiochemical purity, and in 60-70% isolated RCY (n.d.c) by passing through a Sepak light C$_{18}$ cartridge, eluting in 100% EtOH (500µL total volume).

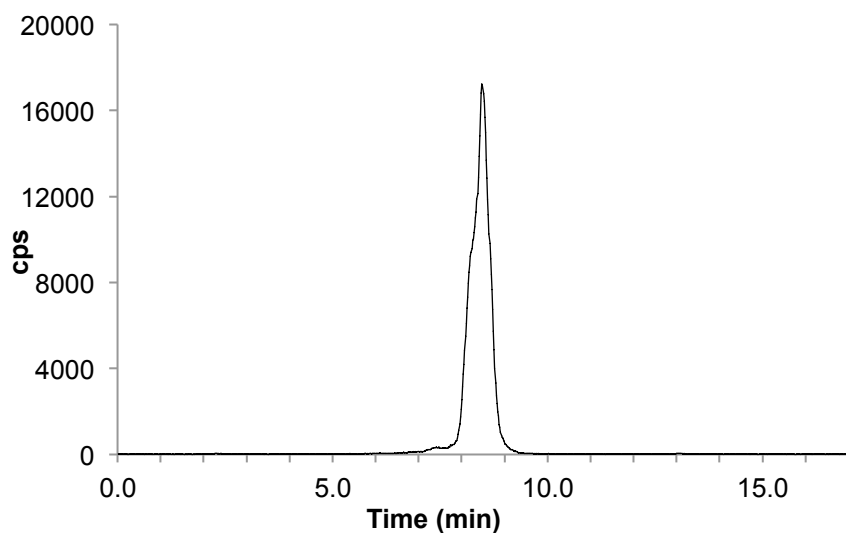**Figure SI 21.** Radio-HPLC trace of **[^{68}Ga]DOTA-Tz** using gradient A

Procedure for modification of Cetuximab (C225) with TCO

A 5 mgmL^{-1} stock solution of C225 (3 mL, 15 mg, 1.02 x 10^{-4} mmol) was concentrated down to a final concentration of 7 mgmL^{-1} (2.14 mL) by buffer exchange into NaHCO$_3$ (pH 8.5) *via* centrifugal filtration using Amicon Ultra® Centrifual filters (0.5 mL) with a 30K MW cut-off. TCO-PEG4-NHS (purchased from Jena bioscience) **108** (257 µL, 1.02 x 10^{-2} mmol, 40 mM solution in DMF) was added to the C225 solution, and the mixture was sonicated for 60 sec, followed by incubation at 4°C for 16 h. The modified antibody was purified from unconjugated TCO by centrifugal filtration using Amicon Ultra® Centrifual filters (30K MW cut-off), for a total spin-time of 40 min. Complete removal of unmodified TCO from the antibody mixture was confirmed by SEC HPLC. C225-TCO was re-dissolved in PBS (pH 7.4) to a final concentration of 5 mgmL^{-1}. MALDI MS confirmed an average of ~17 additions of TCO-PEG4 per C225 molecule (see appendix 2). MALDI MS of all Cetuximab antibody conjugates was carried out by the EPSRC National Mass Spectrometry Facility, at the College of Medicine in Swansea.

Radiolabelling C225-TCO with [^{68}Ga]DOTA-GA-Tz

[^{68}Ga]DOTA-GA-Tz (~50 µCi) was added to a solution of **C225-TCO** (50 µL, diluted to 1 mgmL^{-1} in PBS). Progress of the reaction was monitored by radio-HPLC (see appendix 1 for example HPLC traces).

Chapter 8 – References

8.1 Publications and Presentations Associated with this Work

Publications

1. ***Copper-free click - a promising tool for pre-targeted PET imaging***

   <u>**Helen L. Evans**</u>, Rozanna L. Slade, Laurence Carroll, Graham Smith, Quang-De Nguyen, Lisa Iddon, Nazila Kamaly, Henning Stöckmann, Finian J. Leeper, Eric O. Aboagye and Alan C. Spivey.

   *Chem.Commun., **2012**, 48**, 991-993.*** **DOI:** 10.1039/C1CC16220A

2. ***Bioorthogonal Chemistry for Pre-targeted Therapy and Imaging – Progress and Prospects***

   Laurence Carroll, <u>**Helen L. Evans,**</u> Eric O. Aboagye and Alan C. Spivey.

   Org. Biomol. Chem., **2013**, 11, **5772-5781**. **DOI**: 10.1039/c3ob40897c

3. ***Bioorthogonal chemistry for ^{68}Ga radiolabelling of DOTA-containing compounds***

   <u>**Helen L. Evans**</u>, Laurence Carroll, Eric O. Aboagye and Alan C. Spivey

   *J. Labell. Compd. Radiopharm., **2013**, early view article.* **DOI:** 10.1002/jlcr.3153

Presentations

The 20th International Symposium on Radiopharmaceutical Sciences (2013), Jeju, South Korea: *Poster entitled "Bioorthogonal chemistry as a pre-targeting tool for Positron Emission Tomography (PET) imaging."*

The Department of Surgery & Cancer Research Student Skills Afternoon (2013): *Poster entitled "Copper-free 'click' chemistry as a promising tool for PET imaging."*

The 3rd Annual Cancer Research UK & EPSRC Cancer Imaging Conference (2012): *Oral presentation entitled "Copper-free 'click' chemistry as a potential tool for PET imaging."*

CRUK PhD Symposium (2012): *Oral presentation entitled "Copper-free 'click' chemistry - a promising tool for pre-targeted PET imaging"*

CRUK King's College London & Imperial College London Chemistry Symposium (2011): *Oral presentation entitled "Copper-free 'click' chemistry - a promising tool for pre-targeted PET imaging"*

8.2 Bibliography

1. Nguyen, Q.-D.; Aboagye, E. O., Imaging the life and death of tumors in living subjects: Preclinical PET imaging of proliferation and apoptosis. *Integr. Biol.* **2010,** *2*, 483-495.

2. Hanahan, D.; Weinberg, R. A., The Hallmarks of Cancer. *Cell* **2000,** *100*, 57-70.

3. Hanahan, D.; Weinberg, Robert A., Hallmarks of Cancer: The Next Generation. *Cell* **2011,** *144*, 646-674.

4. Clarke, P. R.; Allan, L. A., Cell-cycle control in the face of damage – a matter of life or death. *Trends Cell Biol.* **2009,** *19*, 89-98.

5. Kummar, S.; Gutierrez, M.; Doroshow, J. H.; Murgo, A. J., Drug development in oncology: classical cytotoxics and molecularly targeted agents. *Br. J. Clin. Pharmacol.* **2006,** *62*, 15-26.

6. Alford, R.; Ogawa, M.; Choyke, P. L.; Kobayashi, H., Molecular probes for the in vivo imaging of cancer. *Mol. BioSyst.* **2009,** *5*, 1279-1291.

7. Biomarkers and surrogate endpoints: preferred definitions and conceptual framework. *Clin. Pharmacol. Ther.* **2001,** *69*, 89-95.

8. Alymani, N. A.; Smith, M. D.; Williams, D. J.; Petty, R. D., Predictive biomarkers for personalised anti-cancer drug use: Discovery to clinical implementation. *Eur. J. Cancer* **2010,** *46*, 869-879.

9. Multimodality Molecular Imaging Disciplines. http://mips.stanford.edu/grants/ccne/graphics/mmi_disciplines.gif

10. Workman, P.; Aboagye, E. O.; Balkwill, F.; Balmain, A.; Bruder, G.; Chaplin, D. J.; Double, J. A.; Everitt, J.; Farningham, D. A.; Glennie, M. J.; Kelland, L. R.; Robinson, V.; Stratford, I. J.; Tozer, G. M.; Watson, S.; Wedge, S. R.; Eccles, S. A., Guidelines for the welfare and use of animals in cancer research. *Br. J. Cancer* **2010,** *102*, 1555-77.

11. Glunde, K.; Pathak, A. P.; Bhujwalla, Z. M., Molecular–functional imaging of cancer: to image and imagine. *Trends Mol. Med.* **2007,** *13*, 287-297.

12. Workman, P.; Aboagye, E. O.; Chung, Y.-L.; Griffiths, J. R.; Hart, R.; Leach, M. O.; Maxwell, R. J.; McSheehy, P. M. J.; Price, P. M.; Zweit, J.; For the Cancer Research, U. K. P. P. T. A. C., Minimally Invasive Pharmacokinetic and Pharmacodynamic Technologies in Hypothesis-Testing Clinical Trials of Innovative Therapies. *J. Natl. Cancer Inst.* **2006,** *98*, 580-598.

13. Fenster, A.; Downey, D. B.; Cardinal, H. N., Three-dimensional ultrasound imaging. *Phys. Med. Biol.* **2001,** *46*, R67.

14. Workman, P.; Balmain, A.; Hickman, J. A.; McNally, N. J.; Rohas, A. M.; Mitchison, N. A.; Pierrepoint, C. G.; Raymond, R.; Rowlatt, C.; Stephens, T. C.; et al., UKCCCR guidelines for the welfare of animals in experimental neoplasia. *Lab. Anim.* **1988,** *22*, 195-201.

15. Srinivas, M.; Heerschap, A.; Ahrens, E. T.; Figdor, C. G.; Vries, I. J. M. d., 19F MRI for quantitative in vivo cell tracking. *Trends Biotechnol.* **2010,** *28*, 363-370.

16. Schenck, J. F., Safety of Strong, Static Magnetic Fields. *J. Magn. Reson. Imaging* **2000,** *12*, 2-19.

17. Geraldes, C. F.; Laurent, S., Classification and basic properties of contrast agents for magnetic resonance imaging. *Contrast Media Mol. Imaging* **2009,** *4*, 1-23.

18.   Chen, H.; Rogalski, M. M.; Anker, J. N., Advances in functional X-ray imaging techniques and contrast agents. *Phys. Chem. Chem. Phys.* **2012,** *14*, 13469-13486.

19.   Smith-Bindman, R.; Lipson, J.; Marcus, R.; et al., RAdiation dose associated with common computed tomography examinations and the associated lifetime attributable risk of cancer. *Arch. Intern. Med.* **2009,** *169*, 2078-2086.

20.   Körner, M.; Christ, E.; Wild, D.; Reubi, J. C., Glucagon-like peptide-1 receptor overexpression in cancer and its impact on clinical applications. *Front. Endocrinol. (Lausanne)* **2012,** *3*.

21.   Christ, E.; Wild, D.; Forrer, F.; Brandle, M.; Sahli, R.; Clerici, T.; Gloor, B.; Martius, F.; Maecke, H.; Reubi, J. C., Glucagon-like peptide-1 receptor imaging for localization of insulinomas. *J. Clin. Endocrinol. Metab.* **2009,** *94*, 4398-405.

22.   van Swieten, P. F.; Leeuwenburgh, M. A.; Kessler, B. M.; Overkleeft, H. S., Bioorthogonal organic chemistry in living cells: novel strategies for labeling biomolecules. *Org. Biomol. Chem.* **2005,** *3*, 20-27.

23.   Cai, L.; Lu, S.; Pike, V. W., Chemistry with [^{18}F]Fluoride Ion (Eur. J. Org. Chem. 2008). *Eur. J. Org. Chem.* **2008**, 2843-2843.

24.   Phelps, M. E.; Hoffman, E. J.; Mullani, N. A.; Ter-Pogossian, M. M., Application of Annihilation Coincidence Detection to Transaxial Reconstruction Tomography. *J. Nucl. Med.* **1975,** *16*, 210-224.

25.   Sharma, R.; Aboagye, E., Development of radiotracers for oncology – the interface with pharmacology. *Br. J. Pharmacol.* **2011,** *163*, 1565-1585.

26.   Miller, P. W.; Long, N. J.; Vilar, R.; Gee, A. D., Synthesis of 11C, 18F, 15O, and 13N Radiolabels for Positron Emission Tomography. *Angew. Chem. Int. Ed.* **2008,** *47*, 8998-9033.

27.   Stahl, A.; Wieder, H.; Piert, M.; Wester, H.-J.; Senekowitsch-Schmidtke, R.; Schwaiger, M., Positron emission tomography as a tool for translational research in oncology. *Mol. Imaging Biol. 6*, 214-224.

28.   Burns, H. D.; Hamill, T. G.; Eng, W.-s.; Francis, B.; Fioravanti, C.; Gibson, R. E., Positron emission tomography neuroreceptor imaging as a tool in drug discovery, research and development. *Curr. Opin. Chem. Biol.* **1999,** *3*, 388-394.

29.   Wängler, C.; Schirrmacher, R.; Bartenstein, P.; Wängler, B. r., Click-Chemistry Reactions in Radiopharmaceutical Chemistry: Fast & Easy Introduction of Radiolabels into Biomolecules for *in vivo* Imaging. *Curr. Med. Chem.* **2010,** *17*, 1092-1116.

30.   Papathanassiou, D.; Bruna-Muraille, C.; Liehn, J.-C.; Nguyen, T. D.; Curé, H., Positron Emission Tomography in oncology: Present and future of PET and PET/CT. *Crit. Rev. Oncol. Hematol.* **2009,** *72*, 239-254.

31.   Harpen, M. D., Positronium: review of symmetry, conserved quantities and decay for the radiological physicist. *Med. Phys.* **2004,** *31*, 57-61.

32.   Zanzonico, P., Positron emission tomography: a review of basic principles, scanner design and performance, and current systems. *Semin. Nucl. Med.* **2004,** *34*, 87-111.

33.   Volkow, N. D.; Brodie, J.; Bendriem, B., Positron Emission Tomography: Basic Principles and Applications in Psychiatric Researcha. *Ann. N.Y. Acad. Sci.* **1991,** *620*, 128-144.

34.   Levin, C., Primer on molecular imaging technology. *Eur. J. Nucl. Med. Mol. Imaging* **2005,** *32*, S325-S345.

35. Schlyer, D. J., *Production of Radionuclides in Accelerators*. John Wiley & Sons, New York, Ltd2005; p 1-70.

36. Schöder, H.; Erdi, Y.; Larson, S.; Yeung, H. D., PET/CT: a new imaging technology in nuclear medicine. *Eur. J. Nucl. Med. Mol. Imaging* **2003,** *30*, 1419-1437.

37. Wagner, H. N., Jr., Clinical PET: Its Time Has Come. *J. Nucl. Med.* **1991,** *32*, 561-564.

38. Nordberg, A., PET imaging of amyloid in Alzheimer's disease. *Lancet Neurol.* **2004,** *3*, 519-527.

39. PET CT scan. http://www.clermontradiology.com/images/pet/pet-ct_06.jpg (accessed Oct 2013)

40. Judenhofer, M. S.; Cherry, S. R., Applications for preclinical PET/MRI. *Semin. Nucl. Med.* **2013,** *43*, 19-29.

41. Gillings, N., Radiotracers for positron emission tomography imaging. *Magn. Reson. Mater. Phys., Biol. Med.* **2013,** *26*, 149-158.

42. Smith, G.; Carroll, L.; Aboagye, E., New Frontiers in the Design and Synthesis of Imaging Probes for PET Oncology: Current Challenges and Future Directions. *Mol. Imaging Biol.* **2012,** *14*, 653-666.

43. Haubner, R.; Kuhnast, B.; Mang, C.; Weber, W. A.; Kessler, H.; Wester, H.-J.; Schwaiger, M., [18F]Galacto-RGD: Synthesis, Radiolabeling, Metabolic Stability, and Radiation Dose Estimates. *Bioconjugate Chem.* **2003,** *15*, 61-69.

44. Grant, F. D.; Fahey, F. H.; Packard, A. B.; Davis, R. T.; Alavi, A.; Treves, S. T., Skeletal PET with ^{18}F-Fluoride: Applying New Technology to an Old Tracer. *J. Nucl. Med.* **2008,** *49*, 68-78.

45. O'Hagan, D., Understanding organofluorine chemistry. An introduction to the C-F bond. *Chem. Soc. Rev.* **2008,** *37*, 308-19.

46. O'Hagan, D., Understanding organofluorine chemistry. An introduction to the C-F bond. *Chem. Soc. Rev.* **2008,** *37*, 308-319.

47. Alauddin, M. M., Positron emission tomography (PET) imaging with (18)F-based radiotracers. *Am. J. Nucl. Med. Mol. Imaging* **2012,** *2*, 55-76.

48. Guillaume, M.; Luxen, A.; Nebeling, B.; Argentini, M.; Clark, J. C.; Pike, V. W., Recommendations for fluorine-18 production. *Int. J. Rad. Appl. Instrum. A* **1991,** *42*, 749-762.

49. Watson, D. A.; Su, M.; Teverovskiy, G.; Zhang, Y.; García-Fortanet, J.; Kinzel, T.; Buchwald, S. L., Formation of ArF from LPdAr(F): Catalytic Conversion of Aryl Triflates to Aryl Fluorides. *Science* **2009,** *325*, 1661-1664.

50. Chun, J.-H.; Pike, V. W., Single-step syntheses of no-carrier-added functionalized [18F]fluoroarenes as labeling synthons from diaryliodonium salts. *Org. Biomol. Chem.* **2013,** *11*, 6300-6306.

51. Lasne, M.-C.; Perrio, C.; Rouden, J.; Barré, L.; Roeda, D.; Dolle, F.; Crouzel, C., Chemistry of B^{+};Emitting Compounds Based on Fluorine-18. In *Contrast Agents II*, Krause, W., Ed. Springer Berlin / Heidelberg2002; Vol. 222, pp 201-258.

52. Laughlin, S. T.; Bertozzi, C. R., Metabolic labeling of glycans with azido sugars and subsequent glycan-profiling and visualization via Staudinger ligation. *Nat. Protoc.* **2007,** *2*, 2930-44.

53. Hausner, S. H.; Marik, J.; Gagnon, M. K. J.; Sutcliffe, J. L., *In Vivo* Positron Emission Tomography (PET) Imaging with an αvβ6 Specific Peptide Radiolabeled using [18]F-"Click"

Chemistry: Evaluation and Comparison with the Corresponding 4-[18F]Fluorobenzoyl- and 2-[^{18}F]Fluoropropionyl-Peptides. *J. Med. Chem.* **2008,** *51*, 5901-5904.

54. Glaser, M.; Robins, E. G., 'Click labelling' in PET radiochemistry. *J. Labelled Compd. Radiopharm.* **2009,** *52*, 407-414.

55. Codelli, J. A.; Baskin, J. M.; Agard, N. J.; Bertozzi, C. R., Second-Generation Difluorinated Cyclooctynes for Copper-Free Click Chemistry. *J. Am. Chem. Soc.* **2008,** *130*, 11486-11493.

56. Huisgen, R., Kinetics and reaction mechanisms: selected examples from the experience of forty years. In *Ninth International Conference on Physical Organic Chemistry* Pure and Applied Chemistry: Regensburg, Federal Republic of Germany, **1989**; Vol. 61, pp 613-628.

57. Baskin, J. M.; Bertozzi, C. R., Copper-Free Click Chemistry:Bioorthogonal Reagents for Tagging Azides. *Aldichim. ACTA* **2010,** *43*, 15-23.

58. Baskin, J. M.; Prescher, J. A.; Laughlin, S. T.; Agard, N. J.; Chang, P. V.; Miller, I. A.; Anderson, L.; Codelli, J. A.; Bertozzi, C. R., Copper-Free Click Chemistry for Dynamic *in vivo* Imaging. *Proc. Natl. Acad. Sci. USA* **2007,** *104*, 16793-16797.

59. Michael B, D., Reactions of L-ascorbic acid with transition metal complexes. *Polyhedron* **1992,** *11*, 285-321.

60. Kolb, H. C.; Sharpless, K. B., The growing impact of click chemistry on drug discovery. *Drug Discovery Today* **2003,** *8*, 1128-1137.

61. Iddon, L.; Leyton, J.; Indrevoll, B.; Glaser, M.; Robins, E. G.; George, A. J. T.; Cuthbertson, A.; Luthra, S. K.; Aboagye, E. O., Synthesis and *in vitro* evaluation of [^{18}F]fluoroethyl triazole labelled [Tyr3]octreotate analogues using click chemistry. *Bioorg. Med. Chem. Lett.* **2011,** *21*, 3122-3127.

62. Glaser, M.; Årstad, E., "Click Labeling" with 2-[^{18}F]Fluoroethylazide for Positron Emission Tomography. *Bioconjugate Chem.* **2007,** *18*, 989-993.

63. Li, Z. B.; Wu, Z.; Chen, K.; Chin, F. T.; Chen, X., Click chemistry for (18)F-labeling of RGD peptides and microPET imaging of tumor integrin alphavbeta3 expression. *Bioconjugate Chem.* **2007,** *18*, 1987-94.

64. Wuest, F.; Kohler, L.; Berndt, M.; Pietzsch, J., Systematic comparison of two novel, thiol-reactive prosthetic groups for 18F labeling of peptides and proteins with the acylation agent succinimidyl-4-[^{18}F]fluorobenzoate ([18F]SFB). *Amino Acids* **2009,** *36*, 283-95.

65. Ido, T.; Wan, C. N.; Casella, V.; Fowler, J. S.; Wolf, A. P.; Reivich, M.; Kuhl, D. E., Labeled 2-deoxy-D-glucose analogs. ^{18}F-labeled 2-deoxy-2-fluoro-D-glucose, 2-deoxy-2-fluoro-D-mannose and 14C-2-deoxy-2-fluoro-D-glucose. *J. Labelled Compd. Radiopharm.* **1978,** *14*, 175-183.

66. Warburg, O., On the Origin of Cancer Cells. *Science* **1956,** *123*, 309-314.

67. Couturier, O.; Luxen, A.; Chatal, J.-F.; Vuillez, J.-P.; Rigo, P.; Hustinx, R., Fluorinated tracers for imaging cancer with positron emission tomography. *Eur. J. Nucl. Med. Mol. Imaging* **2004,** *31*, 1182-1206.

68. Hamacher, K.; Coenen, H. H.; Stocklin, G., Efficient Stereospecific Synthesis of No-Carrier-Added 2-[^{18}F]-Fluoro-2-Deoxy-D-Glucose Using Aminopolyether Supported Nucleophilic Substitution. *J. Nucl. Med.* **1986,** *27*, 235-238.

69.   Langen, K.-J.; Hamacher, K.; Weckesser, M.; Floeth, F.; Stoffels, G.; Bauer, D.; Coenen, H. H.; Pauleit, D., O-(2-[18F]fluoroethyl)-l-tyrosine: uptake mechanisms and clinical applications. *Nucl. Med. Biol.* **2006,** *33*, 287-294.

70.   Bauman, G.; Belhocine, T.; Kovacs, M.; Ward, A.; Beheshti, M.; Rachinsky, I., 18F-fluorocholine for prostate cancer imaging: a systematic review of the literature. *Prostate Cancer Prostatic Dis.* **2012,** *15*, 45-55.

71.   Soloviev, D.; Lewis, D.; Honess, D.; Aboagye, E., [18F]FLT: An imaging biomarker of tumour proliferation for assessment of tumour response to treatment. *Eur. J. Cancer* **2012,** *48*, 416-424.

72.   Koh, W.-J.; Bergman, K. S.; Rasey, J. S.; Peterson, L. M.; Evans, M. L.; Graham, M. M.; Grierson, J. R.; Lindsley, K. L.; Lewellen, T. K.; Krohn, K. A.; Griffin, T. W., Evaluation of oxygenation status during fractionated radiotherapy in human nonsmall cell lung cancers using [F-18]fluoromisonidazole positron emission tomography. *Int. J. Radiat. Oncol. Biol. Phys.* **1995,** *33*, 391-398.

73.   Wadas, T. J.; Wong, E. H.; Weisman, G. R.; Anderson, C. J., Coordinating Radiometals of Copper, Gallium, Indium, Yttrium, and Zirconium for PET and SPECT Imaging of Disease. *Chem. Rev.* **2010,** *110*, 2858-2902.

74.   Eckert & Ziegler Strahlen- und Medizintechnik AG: Modular-Lab Standard. http://www.ezag.com/home/products/radiopharma/radiosynthesis-technology/modular-lab-standard.html (accessed Oct 2013)

75.   Bandoli, G.; Dolmella, A.; Tisato, F.; Porchia, M.; Refosco, F., Mononuclear six-coordinated Ga(III) complexes: A comprehensive survey. *Coord. Chem. Rev.* **2009,** *253*, 56-77.

76.   Green, M. A.; Welch, M. J., Gallium radiopharmaceutical chemistry. *Int. J. Rad. Appl. Instrum. B.* **1989,** *16*, 435-48.

77.   Moerlein, S. M.; Welch, M. J., The chemistry of gallium and indium as related to radiopharmaceutical production. *Int. J. Nucl. Med. Biol.* **1981,** *8*, 277-87.

78.   Zeglis, B. M.; Lewis, J. S., A practical guide to the construction of radiometallated bioconjugates for positron emission tomography. *Dalton trans.* **2011,** *40*, 6168-95.

79.   Fani, M.; André, J. P.; Maecke, H. R., 68Ga-PET: a powerful generator-based alternative to cyclotron-based PET radiopharmaceuticals. *Contrast Media Mol. Imaging* **2008,** *3*, 53-63.

80.   Vosjan, M. J.; Perk, L. R.; Roovers, R. C.; Visser, G. W.; Stigter-van Walsum, M.; van Bergen En Henegouwen, P. M.; van Dongen, G. A., Facile labelling of an anti-epidermal growth factor receptor Nanobody with 68Ga via a novel bifunctional desferal chelate for immuno-PET. *Eur. J. Nucl. Med. Mol. Imaging* **2011,** *38*, 753-63.

81.   Kruper, W. J.; Rudolf, P. R.; Langhoff, C. A., Unexpected selectivity in the alkylation of polyazamacrocycles. *J. Org. Chem.* **1993,** *58*, 3869-3876.

82.   Lewis, M. R.; Raubitschek, A.; Shively, J. E., A Facile, Water-Soluble Method for Modification of Proteins with DOTA. Use of Elevated Temperature and Optimized pH To Achieve High Specific Activity and High Chelate Stability in Radiolabeled Immunoconjugates. *Bioconjugate Chem.* **1994,** *5*, 565-576.

83.   Chappell, L. L.; Rogers, B. E.; Khazaeli, M. B.; Mayo, M. S.; Buchsbaum, D. J.; Brechbiel, M. W., Improved synthesis of the bifunctional chelating agent 1,4,7,10-tetraaza-N-(1-carboxy-3-(4-nitrophenyl)propyl)-N′,N″,N‴-tris(acetic acid)cyclododecane (PA-DOTA). *Biorg. Med. Chem.* **1999,** *7*, 2313-2320.

84. Viola-Villegas, N.; Doyle, R. P., The coordination chemistry of 1,4,7,10-tetraazacyclododecane-N,N′,N″,N‴-tetraacetic acid (H4DOTA): Structural overview and analyses on structure–stability relationships. *Coord. Chem. Rev.* **2009,** *253*, 1906-1925.

85. Breeman, W. A.; Verbruggen, A. M., The 68Ge/ 68Ga generator has high potential, but when can we use 68Ga-labelled tracers in clinical routine? *Eur. J. Nucl. Med. Mol. Imaging* **2007,** *34*, 978-81.

86. Viola, N. A.; Rarig Jr, R. S.; Ouellette, W.; Doyle, R. P., Synthesis, structure and thermal analysis of the gallium complex of 1,4,7,10-tetraazacyclo-dodecane-N,N′,N″,N‴-tetraacetic acid (DOTA). *Polyhedron* **2006,** *25*, 3457-3462.

87. Heppeler, A.; Froidevaux, S.; Mäcke, H. R.; Jermann, E.; Béhé, M.; Powell, P.; Hennig, M., Radiometal-Labelled Macrocyclic Chelator-Derivatised Somatostatin Analogue with Superb Tumour-Targeting Properties and Potential for Receptor-Mediated Internal Radiotherapy. *Chem. Eur. J.* **1999,** *5*, 1974-1981.

88. Clarke, E. T.; Martell, A. E., Stabilities of the Fe(III), Ga(III) and In(III) chelates of N,N′,N″-triazacyclononanetriacetic acid. *Inorg. Chim. Acta* **1991,** *181*, 273-280.

89. Clarke, E. T.; Martell, A. E., Stabilities of trivalent metal ion complexes of the tetraacetate derivatives of 12-, 13- and 14-membered tetraazamacrocycles. *Inorg. Chim. Acta* **1991,** *190*, 37-46.

90. Ma, R.; Welch, M. J.; Reibenspies, J.; Martell, A. E., Stability of metal ion complexes of 1,4,7-tris(2-mercaptoethyl)-1,4,7-triazacylclonane (TACN-TM) and molecular structure of In(C12H24N3S3). *Inorg. Chim. Acta* **1995,** *236*, 75-82.

91. Craig, A. S.; Parker, D.; Adams, H.; Bailey, N. A., Stability, 71Ga NMR, and crystal structure of a neutral gallium(III) complex of 1,4,7-triazacyclononanetriacetate: a potential radiopharmaceutical? *J. Chem. Soc., Chem. Commun.* **1989,** *0*, 1793-1794.

92. Broan, C. J.; Cox, J. P. L.; Craig, A. S.; Kataky, R.; Parker, D.; Harrison, A.; Randall, A. M.; Ferguson, G., Structure and solution stability of indium and gallium complexes of 1,4,7-triazacyclononanetriacetate and of yttrium complexes of 1,4,7,10-tetraazacyclododecanetetraacetate and related ligands: kinetically stable complexes for use in imaging and radioimmunotherapy. X-Ray molecular structure of the indium and gallium complexes of 1,4,7-triazacyclononane-1,4,7-triacetic acid. *J. Chem. Soc. Perk. Trans. 2* **1991,** *0*, 87-99.

93. Prata, M. I. M.; Santos, A. C.; Geraldes, C. F. G. C.; de Lima, J. J. P., Structural and in vivo studies of metal chelates of Ga(III) relevant to biomedical imaging. *J. Inorg. Biochem.* **2000,** *79*, 359-363.

94. Prata, M. I. M.; Santos, A. C.; Geraldes, C. F. G. C.; Lima, J. J. P. d., Characterisation of 67Ga3+ complexes of triaza macrocyclic ligands: biodistribution and clearance studies. *Nucl. Med. Biol.* **1999,** *26*, 707-710.

95. Notni, J.; Pohle, K.; Wester, H.-J., Comparative gallium-68 labeling of TRAP-, NOTA-, and DOTA-peptides: practical consequences for the future of gallium-68-PET. *EJNMMI Research* **2012,** *2*, 28.

96. Gabriel, M.; Decristoforo, C.; Kendler, D.; Dobrozemsky, G.; Heute, D.; Uprimny, C.; Kovacs, P.; Von Guggenberg, E.; Bale, R.; Virgolini, I. J., 68Ga-DOTA-Tyr3-Octreotide PET in Neuroendocrine Tumors: Comparison with Somatostatin Receptor Scintigraphy and CT. *J. Nucl. Med.* **2007,** *48*, 508-518.

97. Graham, M. M.; Menda, Y., Radiopeptide imaging and therapy in the United States. *J. Nucl. Med.* **2011,** *52 Suppl 2*, 56S-63S.

98. Sharkey, R. M.; Goldenberg, D. M., Cancer radioimmunotherapy. *Immunotherapy* **2011,** *3*, 349-370.

99. Reardan, D. T.; Meares, C. F.; Goodwin, D. A.; McTigue, M.; David, G. S.; Stone, M. R.; Leung, J. P.; Bartholomew, R. M.; Frincke, J. M., Antibodies against metal chelates. *Nature* **1985,** *316*, 265-8.

100. Knox, S. J.; Goris, M. L.; Tempero, M.; Weiden, P. L.; Gentner, L.; Breitz, H.; Adams, G. P.; Axworthy, D.; Gaffigan, S.; Bryan, K.; Fisher, D. R.; Colcher, D.; Horak, I. D.; Weiner, L. M., Phase II Trial of Yttrium-90-DOTA-Biotin Pretargeted by NR-LU-10 Antibody/Streptavidin in Patients with Metastatic Colon Cancer. *Clin. Cancer Res.* **2000,** *6*, 406-414.

101. Sharkey, R. M.; Rossi, E. A.; McBride, W. J.; Chang, C. H.; Goldenberg, D. M., Recombinant bispecific monoclonal antibodies prepared by the dock-and-lock strategy for pretargeted radioimmunotherapy. *Semin. Nucl. Med.* **2010,** *40*, 190-203.

102. Frampas, E.; Rousseau, C.; Bodet-Milin, C.; Barbet, J.; Chatal, J.-F.; Kraeber-Bodéré, F., Improvement of radioimmunotherapy using pretargeting. *Front. Oncol.* **2013,** *3*.

103. Paganelli, G.; Orecchia, R.; Jereczek-Fossa, B.; Grana, C.; Cremonesi, M.; De Braud, F.; Tradati, N.; Chinol, M., Combined treatment of advanced oropharyngeal cancer with external radiotherapy and three-step radioimmunotherapy. *Eur. J. Nucl. Med.* **1998,** *25*, 1336-1339.

104. Grana, C.; Chinol, M.; Robertson, C.; Mazzetta, C.; Bartolomei, M.; De Cicco, C.; Fiorenza, M.; Gatti, M.; Caliceti, P.; Paganelli, G., Pretargeted adjuvant radioimmunotherapy with Yttrium-90-biotin in malignant glioma patients: A pilot study. *Br. J. Cancer* **2002,** *86*, 207-212.

105. Kolb, H. C.; Finn, M. G.; Sharpless, K. B., Click Chemistry: Diverse Chemical Function from a Few Good Reactions. *Angew. Chem. Int. Ed.* **2001,** *40*, 2004-2021.

106. Jewett, J. C.; Bertozzi, C. R., Cu-free click cycloaddition reactions in chemical biology. *Chem. Soc. Rev.* **2010,** *39*, 1272-1279.

107. Saxon, E.; Armstrong, J. I.; Bertozzi, C. R., A "Traceless" Staudinger Ligation for the Chemoselective Synthesis of Amide Bonds. *Org. Lett.* **2000,** *2*, 2141-2143.

108. Saxon, E.; Bertozzi, C. R., Cell Surface Engineering by a Modified Staudinger Reaction. *Science* **2000,** *287*, 2007-2010.

109. Debets, M. F.; van Hest, J. C. M.; Rutjes, F. P. J. T., Bioorthogonal labelling of biomolecules: new functional handles and ligation methods. *Org. Biomol. Chem.* **2013,** *11*, 6439-6455.

110. Schlick, T. L.; Ding, Z.; Kovacs, E. W.; Francis, M. B., Dual-surface modification of the tobacco mosaic virus. *J. Am. Chem. Soc.* **2005,** *127*, 3718-23.

111. Zhang, Z.; Smith, B. A.; Wang, L.; Brock, A.; Cho, C.; Schultz, P. G., A new strategy for the site-specific modification of proteins in vivo. *Biochemistry* **2003,** *42*, 6735-46.

112. Debets, M. F.; van der Doelen, C. W. J.; Rutjes, F. P. J. T.; van Delft, F. L., Azide: A Unique Dipole for Metal-Free Bioorthogonal Ligations. *ChemBioChem* **2010,** *11*, 1168-1184.

113. Agard, N. J.; Baskin, J. M.; Prescher, J. A.; Lo, A.; Bertozzi, C. R., A Comparative Study of Bioorthogonal Reactions with Azides. *ACS Chem. Biol.* **2006,** *1*, 644-648.

114. Sletten, E. M.; Bertozzi, C. R., From Mechanism to Mouse: A Tale of Two Bioorthogonal Reactions. *Acc. Chem. Res.* **2011,** *44*, 666-676.

115. Devaraj, N. K.; Weissleder, R.; Hilderbrand, S. A., Tetrazine-Based Cycloadditions: Application to Pretargeted Live Cell Imaging. *Bioconjugate Chem.* **2008,** *19*, 2297-2299.

116. Blackman, M. L.; Royzen, M.; Fox, J. M., Tetrazine Ligation: Fast Bioconjugation Based on Inverse-Electron-Demand Diels−Alder Reactivity. *J. Am. Chem. Soc.* **2008,** *130*, 13518-13519.

117. Kiick, K. L.; Saxon, E.; Tirrell, D. A.; Bertozzi, C. R., Incorporation of azides into recombinant proteins for chemoselective modification by the Staudinger ligation. *Proc. Natl. Acad. Sci. USA* **2002,** *99*, 19-24.

118. Staudinger, H.; Meyer, J., Über neue organische Phosphorverbindungen III. Phosphinmethylenderivate und Phosphinimine. *Helv. Chim. Acta* **1919,** *2*, 635-646.

119. Prescher, J. A.; Dube, D. H.; Bertozzi, C. R., Chemical remodelling of cell surfaces in living animals. *Nature* **2004,** *430*, 873-877.

120. Lin, F. L.; Hoyt, H. M.; van Halbeek, H.; Bergman, R. G.; Bertozzi, C. R., Mechanistic Investigation of the Staudinger Ligation. *J. Am. Chem. Soc.* **2005,** *127*, 2686-2695.

121. Brewer, G. J.; Yuzbasiyangurkan, V., Wilson Disease. *Medicine* **1992,** *71*, 139-164.

122. Pizarro, F.; Olivares, M.; Uauy, R.; Contreras, P.; Rebelo, A.; Gidi, V., Acute gastrointestinal effects of graded levels of copper in drinking water. *Environ. Health Perspect.* **1999,** *107*, 117-121.

123. Araya, M.; McGoldrick, M. C.; Klevay, L. M.; Strain, J. J.; Robson, P.; Nielsen, F.; Olivares, M.; Pizarro, F.; Johnson, L.; Poirier, K. A., Determination of an Acute No-Observed-Adverse-Effect Level (NOAEL) for Copper in Water. *Regul. Toxicol. Pharm.* **2001,** *34*, 137-145.

124. Brewer, G. J., Wilson disease and canine copper toxicosis. *Am. J. Clin. Nutr.* **1998,** *67*, 1087S-1090S.

125. Becer, C. R.; Hoogenboom, R.; Schubert, U. S., Click Chemistry beyond Metal-Catalyzed Cycloaddition. *Angew. Chem. Int. Ed.* **2009,** *48*, 4900-4908.

126. Agard, N. J.; Prescher, J. A.; Bertozzi, C. R., A Strain-Promoted [3 + 2] Azide−Alkyne Cycloaddition for Covalent Modification of Biomolecules in Living Systems. *J. Am. Chem. Soc.* **2004,** *126*, 15046-15047.

127. Ning, X.; Guo, J.; Wolfert, M. A.; Boons, G.-J., Visualizing Metabolically Labeled Glycoconjugates of Living Cells by Copper-Free and Fast Huisgen Cycloadditions. *Angew. Chem. Int. Ed.* **2008,** *47*, 2253-2255.

128. Carroll, L.; Evans, H. L.; Aboagye, E. O.; Spivey, A. C., Bioorthogonal chemistry for pre-targeted molecular imaging - progress and prospects. *Org. Biomol. Chem.* **2013,** *11*, 5772-5781.

129. Debets, M. F.; van Berkel, S. S.; Schoffelen, S.; Rutjes, F. P. J. T.; van Hest, J. C. M.; van Delft, F. L., Aza-dibenzocyclooctynes for fast and efficient enzyme PEGylation via copper-free [3+2] cycloaddition. *Chem. Commun.* **2010,** *46*, 97-99.

130. Meier, H.; Hanold, N.; Molz, T.; Bissinger, H. J.; Kolshorn, H.; Zountsas, J., Strained cycloalkenynes. *Tetrahedron* **1986,** *42*, 1711-1719.

131. Dommerholt, J.; Schmidt, S.; Temming, R.; Hendriks, L. J.; Rutjes, F. P.; van Hest, J. C.; Lefeber, D. J.; Friedl, P.; van Delft, F. L., Readily accessible bicyclononynes for bioorthogonal labeling and three-dimensional imaging of living cells. *Angew. Chem. Int. Ed.* **2010,** *49*, 9422-5.

132. Dehnert, K. W.; Baskin, J. M.; Laughlin, S. T.; Beahm, B. J.; Naidu, N. N.; Amacher, S. L.; Bertozzi, C. R., Imaging the Sialome during Zebrafish Development with Copper-Free Click Chemistry. *ChemBioChem* **2012,** *13*, 353-357.

133. Laughlin, S. T.; Baskin, J. M.; Amacher, S. L.; Bertozzi, C. R., In vivo imaging of membrane-associated glycans in developing zebrafish. *Science* **2008,** *320*, 664-667.

134. Baskin, J. M.; Dehnert, K. W.; Laughlin, S. T.; Amacher, S. L.; Bertozzi, C. R., Visualizing enveloping layer glycans during zebrafish early embryogenesis. *Proc. Natl. Acad. Sci. USA* **2010,** *107*, 10360-10365.

135. Ji, P.; Atherton, J. H.; Page, M. I., Copper catalysed azide-alkyne cycloaddition (CuAAC) in liquid ammonia. *Org. Biomol. Chem.* **2012,** *10*, 7965-7969.

136. Carboni, R. A.; Lindsey, R. V., Reactions of Tetrazines with Unsaturated Compounds. A New Synthesis of Pyridazines. *J. Am. Chem. Soc.* **1959,** *81*, 4342-4346.

137. Bach, R. D., Ring Strain Energy in the Cyclooctyl System. The Effect of Strain Energy on [3 + 2] Cycloaddition Reactions with Azides. *J. Am. Chem. Soc.* **2009,** *131*, 5233-5243.

138. Rossin, R.; Renart Verkerk, P.; van den Bosch, S. M.; Vulders, R. C. M.; Verel, I.; Lub, J.; Robillard, M. S., In Vivo Chemistry for Pretargeted Tumor Imaging in Live Mice. *Angew. Chem. Int. Ed.* **2010,** *49*, 3375-3378.

139. Šečkutė, J.; Devaraj, N. K., Expanding room for tetrazine ligations in the in vivo chemistry toolbox. *Curr. Opin. Chem. Biol.* **2013**, 17, 761-767.

140. Devaraj, N. K.; Upadhyay, R.; Haun, J. B.; Hilderbrand, S. A.; Weissleder, R., Fast and Sensitive Pretargeted Labeling of Cancer Cells through a Tetrazine/trans-Cyclooctene Cycloaddition. *Angew. Chem. Int. Ed.* **2009,** *48*, 7013-7016.

141. Devaraj, N. K.; Weissleder, R., Biomedical Applications of Tetrazine Cycloadditions. *Acc. Chem. Res.* **2011,** *44*, 816-827.

142. Zeglis, B. M.; Mohindra, P.; Weissmann, G. I.; Divilov, V.; Hilderbrand, S. A.; Weissleder, R.; Lewis, J. S., Modular Strategy for the Construction of Radiometalated Antibodies for Positron Emission Tomography Based on Inverse Electron Demand Diels–Alder Click Chemistry. *Bioconjugate Chem.* **2011,** *22*, 2048-2059.

143. Zeglis, B. M.; Sevak, K. K.; Reiner, T.; Mohindra, P.; Carlin, S. D.; Zanzonico, P.; Weissleder, R.; Lewis, J. S., A Pretargeted PET Imaging Strategy Based on Bioorthogonal Diels–Alder Click Chemistry. *J. Nucl. Med.* **2013,** *54*, 1389-1396.

144. Yang, J.; Karver, M. R.; Li, W.; Sahu, S.; Devaraj, N. K., Metal-Catalyzed One-Pot Synthesis of Tetrazines Directly from Aliphatic Nitriles and Hydrazine. *Angew. Chem. Int. Ed.* **2012,** *51*, 5222-5225.

145. Karver, M. R.; Weissleder, R.; Hilderbrand, S. A., Synthesis and Evaluation of a Series of 1,2,4,5-Tetrazines for Bioorthogonal Conjugation. *Bioconjugate Chem.* **2011,** *22*, 2263-2270.

146. Rossin, R.; van den Bosch, S. M.; Ten Hoeve, W.; Carvelli, M.; Versteegen, R. M.; Lub, J.; Robillard, M. S., Highly Reactive trans-Cyclooctene Tags with Improved Stability for Diels-Alder Chemistry in Living Systems. *Bioconjugate Chem.* **2013**.

147. Li, Z.; Cai, H.; Hassink, M.; Blackman, M. L.; Brown, R. C. D.; Conti, P. S.; Fox, J. M., Tetrazine-trans-cyclooctene ligation for the rapid construction of 18F labeled probes. *Chem. Commun.* **2010,** *46*, 8043-8045.

148. Baskin, J. M.; Prescher, J. A.; Laughlin, S. T.; Agard, N. J.; Chang, P. V.; Miller, I. A.; Lo, A.; Codelli, J. A.; Bertozzi, C. R., Copper-free click chemistry for dynamic in vivo imaging. *Proc. Natl. Acad. Sci. USA* **2007,** *104*, 16793-16797.

149. Bernardin, A.; Cazet, A. l.; Guyon, L.; Delannoy, P.; Vinet, F. o.; Bonnaffé, D.; Texier, I., Copper-Free Click Chemistry for Highly Luminescent Quantum Dot Conjugates: Application to in Vivo Metabolic Imaging. *Bioconjugate Chem.* **2010,** *21*, 583-588.

150. Reese, C. B.; Shaw, A., Preparation of cyclo-octyn-3-ol, cyclononyn-3-ol, and derivatives. *Chem. Commun.* **1970**, 1172-1173.

151. Evans, H. L.; Slade, R. L.; Carroll, L.; Smith, G.; Nguyen, Q.-D.; Iddon, L.; Kamaly, N.; Stockmann, H.; Leeper, F. J.; Aboagye, E. O.; Spivey, A. C., Copper-free click-a promising tool for pre-targeted PET imaging. *Chem. Commun.* **2012,** *48*, 991-993.

152. Allen, F. H.; Kennard, O.; Watson, D. G.; Brammer, L.; Orpen, A. G.; Taylor, R., Tables of bond lengths determined by X-ray and neutron diffraction. Part 1. Bond lengths in organic compounds. *J. Chem. Soc. Perk. Trans. 2* **1987**, S1-S19.

153. Schoenebeck, F.; Ess, D. H.; Jones, G. O.; Houk, K. N., Reactivity and Regioselectivity in 1,3-Dipolar Cycloadditions of Azides to Strained Alkynes and Alkenes: A Computational Study. *J. Am. Chem. Soc.* **2009,** *131*, 8121-8133.

154. Laughlin, S. T.; Bertozzi, C. R., Imaging the glycome. *Proc. Natl. Acad. Sci. USA* **2009,** *106*, 12-17.

155. Chang, P. V.; Prescher, J. A.; Sletten, E. M.; Baskin, J. M.; Miller, I. A.; Agard, N. J.; Lo, A.; Bertozzi, C. R., Copper-free click chemistry in living animals. *Proc. Natl. Acad. Sci. USA* **2010,** *107*, 1821-1826.

156. Pirrung, M. C.; Webster, N. J. G., Mechanism of intramolecular photocycloadditions of cyclooctenones. *J. Org. Chem.* **1987,** *52*, 3603-3613.

157. Banks, R. E.; Lawrence, N. J.; Popplewell, A. L., Efficient electrophilic fluorination of ß -dicarbonyl compounds with the selectfluor reagent F-TEDA-BF4{1-chloromethyl-4-fluoro-1,4-diazoniabicyclo[2.2.2]octane bis(tetrafluoroborate)}. *Chem. Commun.* **1994**, 343-344.

158. Beatty, K. E.; Fisk, J. D.; Smart, B. P.; Lu, Y. Y.; Szychowski, J.; Hangauer, M. J.; Baskin, J. M.; Bertozzi, C. R.; Tirrell, D. A., Live-Cell Imaging of Cellular Proteins by a Strain-Promoted Azide-Alkyne Cycloaddition. *ChemBioChem* **2010,** *11*, 2092-2095.

159. Lutz, J.-F., Copper-Free Azide–Alkyne Cycloadditions: New Insights and Perspectives. *Angew. Chem. Int. Ed.* **2008,** *47*, 2182-2184.

160. Ito, Y.; Fujii, S.; Saegusa, T., Reaction of 1-silyloxybicyclo[n.1.0]alkanes with iron(III) chlorides. A facile synthesis of 2-cycloalkenones via ring enlargement of cyclic ketones. *J. Org. Chem.* **1976,** *41*, 2073-2074.

161. Shimizu, M.; Hiyama, T., Modern Synthetic Methods for Fluorine-Substituted Target Molecules. *Angew. Chem. Int. Ed.* **2005,** *44*, 214-231.

162. Eisenberger, P.; Gischig, S.; Togni, A., Novel 10-I-3 Hypervalent Iodine-Based Compounds for Electrophilic Trifluoromethylation. *Chem. Eur. J.* **2006,** *12*, 2579-2586.

163. Ruppert, I.; Schlich, K.; Volbach, W., Die ersten CF3-substituierten organyl(chlor)silane. *Tetrahedron Lett.* **1984,** *25*, 2195-2198.

164. Umemoto, T.; Ishihara, S., Power-variable electrophilic trifluoromethylating agents. S-, Se-, and Te-(trifluoromethyl)dibenzothio-, -seleno-, and -tellurophenium salt system. *J. Am. Chem. Soc.* **1993,** *115*, 2156-2164.

165. Wang, X.; Ye, Y.; Zhang, S.; Feng, J.; Xu, Y.; Zhang, Y.; Wang, J., Copper-Catalyzed C(sp3)–C(sp3) Bond Formation Using a Hypervalent Iodine Reagent: An Efficient Allylic Trifluoromethylation. *J. Am. Chem. Soc.* **2011,** *133*, 16410-16413.

166. Matoušek, V.; Togni, A.; Bizet, V.; Cahard, D., Synthesis of α-CF3-Substituted Carbonyl Compounds with Relative and Absolute Stereocontrol Using Electrophilic CF3-Transfer Reagents. *Org. Lett.* **2011,** *13*, 5762-5765.

167. Shibata, N.; Matsnev, A.; Cahard, D., Shelf-stable electrophilic trifluoromethylating reagents: A brief historical perspective. *Beilstein J. Org. Chem.* **2010,** *6*. No. 65.

168. Kieltsch, I.; Eisenberger, P.; Togni, A., Mild electrophilic trifluoromethylation of carbon- and sulfur-centered nucleophiles by a hypervalent iodine(III)-CF3 reagent. *Angew. Chem. Int. Ed.* **2007,** *46*, 754-7.

169. Grieco, L. M.; Halliday, G. A.; Junk, C. P.; Lustig, S. R.; Marshall, W. J.; Petrov, V. A., Reactions of 1,1,2,2-tetrafluoroethyl-N,N-dimethylamine with linear and cyclic 1,3-diketones. *J. Fluorine Chem.* **2011,** *132*, 1198-1206.

170. Pauling, L., The nature of the chemical bond. IV. The energy of single bonds and the relative electronegativity of atoms. *J. Am. Chem. Soc.* **1932,** *54*, 3570-3582.

171. Terent'ev, A. O.; Borisov, A. M.; Platonov, M. M.; Starikova, Z. A.; Chernyshev, V. V.; Nikishin, G. I., Reaction of Enol Ethers with the I2-H2O2 System: Synthesis of 2-Iodo-1-methoxy Hydroperoxides and Their Deperoxidation and Demethoxylation to 2-Iodo Ketones. *Synthesis* **2009,** *2009*, 4159-4166.

172. Sreedhar, B.; Surendra Reddy, P.; Madhavi, M., Rapid and Catalyst-Free α-Halogenation of Ketones using N-Halosuccinamides in DMSO. *Synth. Commun.* **2007,** *37*, 4149-4156.

173. Moorthy, J. N.; Senapati, K.; Singhal, N., An expedient protocol for conversion of olefins to α-bromo/iodoketones using IBX and NBS/NIS. *Tetrahedron Lett.* **2009,** *50*, 2493-2496.

174. Barluenga, J.; Marco-Arias, M.; Gonzalez-Bobes, F.; Ballesteros, A.; Gonzalez, J. M., New reactions in water: metal-free conversion of alcohols and ketones into [small alpha]-iodoketones. *Chem. Commun.* **2004**, 2616-2617.

175. Sletten, E. M.; Nakamura, H.; Jewett, J. C.; Bertozzi, C. R., Difluorobenzocyclooctyne: Synthesis, Reactivity, and Stabilization by β-Cyclodextrin. *J. Am. Chem. Soc.* **2010,** *132*, 11799-11805.

176. Jewett, J. C.; Sletten, E. M.; Bertozzi, C. R., Rapid Cu-Free Click Chemistry with Readily Synthesized Biarylazacyclooctynones. *J. Am. Chem. Soc.* **2010,** *132*, 3688-3690.

177. Jung, M. E.; Mossman, A. B.; Lyster, M. A., Direct synthesis of dibenzocyclooctadienes via double ortho Friedel-Crafts alkylation by the use of aldehyde-trimethylsilyl iodide adducts. *J. Org. Chem.* **1978,** *43*, 3698-3701.

178. Stockmann, H.; Neves, A. A.; Stairs, S.; Ireland-Zecchini, H.; Brindle, K. M.; Leeper, F. J., Development and evaluation of new cyclooctynes for cell surface glycan imaging in cancer cells. *Chem. Sci.* **2011,** *2*, 932-936.

179. Seitz, G.; Pohl, L.; Pohlke, R., 5,6-Didehydro-11,12-dihydrodibenzo[a,e]-cyclooctene. *Angew. Chem. Int. Ed.* **1969,** *8*, 447-448.

180. Neves, A. A.; Stockmann, H.; Wainman, Y. A.; Kuo, J. C.; Fawcett, S.; Leeper, F. J.; Brindle, K. M., Imaging cell surface glycosylation in vivo using "double click" chemistry. *Bioconjugate Chem.* **2013,** *24*, 934-41.

181. Kii, I.; Shiraishi, A.; Hiramatsu, T.; Matsushita, T.; Uekusa, H.; Yoshida, S.; Yamamoto, M.; Kudo, A.; Hagiwara, M.; Hosoya, T., Strain-promoted double-click reaction for chemical modification of azido-biomolecules. *Org. Biomol. Chem.* **2010**, *8*, 4051-4055.

182. Orita, A.; Hasegawa, D.; Nakano, T.; Otera, J., Double Elimination Protocol for Synthesis of 5,6,11,12-Tetradehydrodibenzo[a,e]cyclooctene. *Chem. Eur. J.* **2002**, *8*, 2000-2004.

183. Arkhypchuk, A. I.; Svyaschenko, Y. V.; Orthaber, A.; Ott, S., Mechanism of the phospha-Wittig-Horner reaction. *Angew. Chem. Int. Ed.* **2013**, *52*, 6484-7.

184. Doucet, H.; Hierso, J.-C., Palladium-Based Catalytic Systems for the Synthesis of Conjugated Enynes by Sonogashira Reactions and Related Alkynylations. *Angew. Chem. Int. Ed.* **2007**, *46*, 834-871.

185. Chinchilla, R.; Nájera, C., The Sonogashira Reaction: A Booming Methodology in Synthetic Organic Chemistry. *Chem. Rev.* **2007**, *107*, 874-922.

186. LaBeaume, P.; Wager, K.; Falcone, D.; Li, J.; Torchilin, V.; Castro, C.; Holewa, C.; Kallmerten, A. E.; Jones, G. B., Synthesis, functionalization and photo-Bergman chemistry of enediyne bioconjugates. *Biorg. Med. Chem.* **2009**, *17*, 6292-6300.

187. Holmes, B. T.; Pennington, W. T.; Hanks, T. W., Efficient Synthesis of a Complete Donor/Acceptor bis(Aryl)diyne Family. *Synth. Commun.* **2003**, *33*, 2447-2461.

188. Offermann, D. A.; McKendrick, J. E.; Sejberg, J. J. P.; Mo, B.; Holdom, M. D.; Helm, B. A.; Leatherbarrow, R. J.; Beavil, A. J.; Sutton, B. J.; Spivey, A. C., Synthesis and Incorporation into Cyclic Peptides of Tolan Amino Acids and Their Hydrogenated Congeners: Construction of an Array of A–B-loop Mimetics of the Cε3 Domain of Human IgE. *J. Org. Chem.* **2012**, *77*, 3197-3214.

189. Li, N.; Lim, R. K.; Edwardraja, S.; Lin, Q., Copper-free Sonogashira cross-coupling for functionalization of alkyne-encoded proteins in aqueous medium and in bacterial cells. *J. Am. Chem. Soc.* **2011**, *133*, 15316-9.

190. Li, P.; Wang, L.; Wang, M.; You, F., Gold(I) Iodide Catalyzed Sonogashira Reactions. *Eur. J. Org. Chem.* **2008**, *2008*, 5946-5951.

191. Neves, A. A.; Stöckmann, H.; Harmston, R. R.; Pryor, H. J.; Alam, I. S.; Ireland-Zecchini, H.; Lewis, D. Y.; Lyons, S. K.; Leeper, F. J.; Brindle, K. M., Imaging sialylated tumor cell glycans in vivo. *FASEB J* **2011**.

192. Sirion, U.; Kim, H. J.; Lee, J. H.; Seo, J. W.; Lee, B. S.; Lee, S. J.; Oh, S. J.; Chi, D. Y., An efficient F-18 labeling method for PET study: Huisgen 1,3-dipolar cycloaddition of bioactive substances and F-18-labeled compounds. *Tetrahedron Lett.* **2007**, *48*, 3953-3957.

193. Van de Waterbeemd, H.; Smith, D. A.; Beaumont, K.; Walker, D. K., Property-Based Design: Optimization of Drug Absorption and Pharmacokinetics. *J. Med. Chem.* **2001**, *44*, 1313-1333.

194. Some advantages of calculating octanol—water partition coefficients. *J. Pharm. Sci.* **1987**, *76*, 166-168.

195. Xu, Y.; Choi, S.-R.; Kung, M.-P.; Kung, H. F., Synthesis of radioiodinated 1-deoxy-nojirimycin derivatives: novel glucose analogs. *Nucl. Med. Biol.* **1999**, *26*, 833-839.

196. Lewis, F.; Jackson, P.; Lane, S.; Coast, G.; Hanby, A. M., Testing for HER2 in breast cancer. *Histopathology* **2004**, *45*, 207-217.

197. Hudis, C. A., Trastuzumab — Mechanism of Action and Use in Clinical Practice. *N. Engl. J. Med.* **2007**, *357*, 39-51.

198. Lub-de Hooge, M. N.; Kosterink, J. G. W.; Perik, P. J.; Nijnuis, H.; Tran, L.; Bart, J.; Suurmeijer, A. J. H.; de Jong, S.; Jager, P. L.; de Vries, E. G. E., Preclinical characterisation of 111In-DTPA-trastuzumab. *Br. J. Pharmacol.* **2004,** *143*, 99-106.

199. Xu, H.; Baidoo, K. E.; Wong, K. J.; Brechbiel, M. W., A novel bifunctional maleimido CHX-A″ chelator for conjugation to thiol-containing biomolecules. *Bioorg. Med. Chem. Lett.* **2008,** *18*, 2679-2683.

200. Traut, R. R.; Bollen, A.; Sun, T. T.; Hershey, J. W.; Sundberg, J.; Pierce, L. R., Methyl 4-mercaptobutyrimidate as a cleavable cross-linking reagent and its application to the Escherichia coli 30S ribosome. *Biochemistry* **1973,** *12*, 3266-73.

201. Jue, R.; Lambert, J. M.; Pierce, L. R.; Traut, R. R., Addition of sulfhydryl groups to Escherichia coli ribosomes by protein modification with 2-iminothiolane (methyl 4-mercaptobutyrimidate). *Biochemistry* **1978,** *17*, 5399-406.

202. Sletten, E. M.; Bertozzi, C. R., A Hydrophilic Azacyclooctyne for Cu-Free Click Chemistry. *Org. Lett.* **2008,** *10*, 3097-3099.

203. Martinez, G. V.; Navath, S.; Sewda, K.; Rao, V.; Foroutan, P.; Alleti, R.; Moberg, V. E.; Ahad, A. M.; Coppola, D.; Lloyd, M. C.; Gillies, R. J.; Morse, D. L.; Mash, E. A., Demonstration of a sucrose-derived contrast agent for magnetic resonance imaging of the GI tract. *Bioorg. Med. Chem. Lett.* **2013,** *23*, 2061-2064.

204. Mizukami, S.; Takikawa, R.; Sugihara, F.; Hori, Y.; Tochio, H.; Wälchli, M.; Shirakawa, M.; Kikuchi, K., Paramagnetic Relaxation-Based 19F MRI Probe To Detect Protease Activity. *J. Am. Chem. Soc.* **2007,** *130*, 794-795.

205. Pazos, E.; Torrecilla, D.; Vázquez López, M.; Castedo, L.; Mascareñas, J. L.; Vidal, A.; Vázquez, M. E., Cyclin A Probes by Means of Intermolecular Sensitization of Terbium-Chelating Peptides. *J. Am. Chem. Soc.* **2008,** *130*, 9652-9653.

206. Rossin, R.; Muro, S.; Welch, M. J.; Muzykantov, V. R.; Schuster, D. P., In Vivo Imaging of 64Cu-Labeled Polymer Nanoparticles Targeted to the Lung Endothelium. *J. Nucl. Med.* **2008,** *49*, 103-111.

207. Cioslowski, J.; Sauer, J.; Hetzenegger, J.; Karcher, T.; Hierstetter, T., Ab initio quantum-mechanical and experimental mechanistic studies of Diels-Alder reactions between unsubstituted and phenyl-substituted acetylenes and 1,2,4,5-tetrazines. *J. Am. Chem. Soc.* **1993,** *115*, 1353-1359.

208. Boger, D. L., Diels-Alder reactions of heterocyclic aza dienes. Scope and applications. *Chem. Rev.* **1986,** *86*, 781-793.

209. Clavier, G.; Audebert, P., s-Tetrazines as Building Blocks for New Functional Molecules and Molecular Materials. *Chem. Rev.* **2010,** *110*, 3299-3314.

210. Pipkorn, R.; Waldeck, W.; Didinger, B.; Koch, M.; Mueller, G.; Wiessler, M.; Braun, K., Inverse-electron-demand Diels-Alder reaction as a highly efficient chemoselective ligation procedure: Synthesis and function of a BioShuttle for temozolomide transport into prostate cancer cells. *J. Pept. Sci.* **2009,** *15*, 235-241.

211. Schoch, J.; Wiessler, M.; Jäschke, A., Post-Synthetic Modification of DNA by Inverse-Electron-Demand Diels−Alder Reaction. *J. Am. Chem. Soc.* **2010,** *132*, 8846-8847.

212. Robillard, M. S. E., Rossin, Raffaella, Lub, Johan, Renart Verkerk, Pascal, Burdinski, Dirk, pretargeting kit, method and agents used therin. US patent application 20120039803, **2012**.

213. Hsieh, C.-C.; Lee, C.-J.; Horng, Y.-C., Effects of the Counteranion on the Pyrazole−Nitrile Coupling Reaction Mediated by Nickel(II) Ions. *Organometallics.* **2009,** *28*, 4923-4928.

214. Kukushkin, V. Y.; Pombeiro, A. J. L., Additions to Metal-Activated Organonitriles†. *Chem. Rev.* **2002,** *102*, 1771-1802.

215. Han, H.-S.; Devaraj, N. K.; Lee, J.; Hilderbrand, S. A.; Weissleder, R.; Bawendi, M. G., Development of a Bioorthogonal and Highly Efficient Conjugation Method for Quantum Dots Using Tetrazine−Norbornene Cycloaddition. *J. Am. Chem. Soc.* **2010,** *132*, 7838-7839.

216. Stockmann, H.; Neves, A. A.; Stairs, S.; Brindle, K. M.; Leeper, F. J., Exploring isonitrile-based click chemistry for ligation with biomolecules. *Org. Biomol. Chem.* **2011,** *9*, 7303-7305.

217. Royzen, M.; Yap, G. P. A.; Fox, J. M., A Photochemical Synthesis of Functionalized trans-Cyclooctenes Driven by Metal Complexation. *J. Am. Chem. Soc.* **2008,** *130*, 3760-3761.

218. Dijkgraaf, I.; Kruijtzer, J. A. W.; Frielink, C.; Soede, A. C.; Hilbers, H. W.; Oyen, W. J. G.; Corstens, F. H. M.; Liskamp, R. M. J.; Boerman, O. C., Synthesis and biological evaluation of potent αvβ3-integrin receptor antagonists. *Nucl. Med. Biol.* **2006,** *33*, 953-961.

219. Dijkgraaf, I.; Rijnders, A. Y.; Soede, A.; Dechesne, A. C.; van Esse, G. W.; Brouwer, A. J.; Corstens, F. H. M.; Boerman, O. C.; Rijkers, D. T. S.; Liskamp, R. M. J., Synthesis of DOTA-conjugated multivalent cyclic-RGD peptide dendrimers via 1,3-dipolar cycloaddition and their biological evaluation: implications for tumor targeting and tumor imaging purposes. *Org. Biomol. Chem.* **2007,** *5*, 935-944.

220. Dijkgraaf, I.; Yim, C.-B.; Franssen, G.; Schuit, R.; Luurtsema, G.; Liu, S.; Oyen, W. G.; Boerman, O., PET imaging of αvβ3 integrin expression in tumours with 68Ga-labelled mono-, di- and tetrameric RGD peptides. *Eur. J. Nucl. Med. Mol. Imaging* **2011,** *38*, 128-137.

221. Knetsch, P. A.; Petrik, M.; Rangger, C.; Seidel, G.; Pietzsch, H.-J.; Virgolini, I.; Decristoforo, C.; Haubner, R., [68Ga]NS3-RGD and [68Ga] Oxo-DO3A-RGD for imaging αvβ3 integrin expression: synthesis, evaluation, and comparison. *Nucl. Med. Biol.* **2013,** *40*, 65-72.

222. Knetsch, P. A.; Petrik, M.; Griessinger, C. M.; Rangger, C.; Fani, M.; Kesenheimer, C.; Von Guggenberg, E.; Pichler, B. J.; Virgolini, I.; Decristoforo, C.; Haubner, R., NODAGA-RGD for imaging α vβ 3 integrin expression. *Eur. J. Nucl. Med. Mol. Imaging* **2011,** *38*, 1303-1312.

223. Ruoslahti, E.; Pierschbacher, M. D., New perspectives in cell adhesion: RGD and integrins. *Science* **1987,** *238*, 491-7.

224. Decristoforo, C.; Hernandez Gonzalez, I.; Carlsen, J.; Rupprich, M.; Huisman, M.; Virgolini, I.; Wester, H.-J.; Haubner, R., 68Ga- and 111In-labelled DOTA-RGD peptides for imaging of αvβ3 integrin expression. *Eur. J. Nucl. Med. Mol. Imaging* **2008,** *35*, 1507-1515.

225. Haubner, R.; Gratias, R.; Diefenbach, B.; Goodman, S. L.; Jonczyk, A.; Kessler, H., Structural and Functional Aspects of RGD-Containing Cyclic Pentapeptides as Highly Potent and Selective Integrin αVβ3 Antagonists. *J. Am. Chem. Soc.* **1996,** *118*, 7461-7472.

226. Dijkgraaf, I.; Kruijtzer, J. W.; Liu, S.; Soede, A.; Oyen, W. G.; Corstens, F. M.; Liskamp, R. J.; Boerman, O., Improved targeting of the αvβ3 integrin by multimerisation of RGD peptides. *Eur. J. Nucl. Med. Mol. Imaging* **2007,** *34*, 267-273.

227. Selvaraj, R.; Liu, S.; Hassink, M.; Huang, C.-w.; Yap, L.-p.; Park, R.; Fox, J. M.; Li, Z.; Conti, P. S., Tetrazine-trans-cyclooctene ligation for the rapid construction of integrin αvβ3 targeted PET tracer based on a cyclic RGD peptide. *Bioorg. Med. Chem. Lett.* **2011,** *21*, 5011-5014.

228. Rossin, R.; Läppchen, T.; van den Bosch, S. M.; Laforest, R.; Robillard, M. S., Diels–Alder Reaction for Tumor Pretargeting: In Vivo Chemistry Can Boost Tumor Radiation Dose Compared with Directly Labeled Antibody. *J. Nucl. Med.* **2013**, 54, No. 11.

229. Devaraj, N. K.; Thurber, G. M.; Keliher, E. J.; Marinelli, B.; Weissleder, R., Reactive polymer enables efficient in vivo bioorthogonal chemistry. *Proc. Natl. Acad. Sci. USA* **2012,** *109*, 4762-4767.

230. Vincenzi, B.; Schiavon, G.; Silletta, M.; Santini, D.; Tonini, G., The biological properties of cetuximab. *Crit. Rev. Oncol. Hematol.* **2008,** *68*, 93-106.

231. Ciardiello, F.; Tortora, G., EGFR Antagonists in Cancer Treatment. *N. Engl. J. Med.* **2008,** *358*, 1160-1174.

232. Sharma, S. V.; Bell, D. W.; Settleman, J.; Haber, D. A., Epidermal growth factor receptor mutations in lung cancer. *Nat. Rev. Cancer* **2007,** *7*, 169-181.

233. Thalhammer, F.; Wallfahrer, U.; Sauer, J., Reaktivität einfacher offenkettiger und cyclischer dienophile bei Diels-Alder-reaktionen mit inversem elektronenbedarf. *Tetrahedron Lett.* **1990,** *31*, 6851-6854.

234. Herth, M. M.; Andersen, V. L.; Lehel, S.; Madsen, J.; Knudsen, G. M.; Kristensen, J. L., Development of a 11C-labeled tetrazine for rapid tetrazine-trans-cyclooctene ligation. *Chem. Commun.* **2013,** *49*, 3805-3807.

235. Yang, K. S.; Budin, G.; Tassa, C.; Kister, O.; Weissleder, R., Bioorthogonal Approach to Identify Unsuspected Drug Targets in Live Cells. *Angew. Chem. Int. Ed.* **2013,** *52*, 10593-10597.

236. Neves, A. A.; Stöckmann, H.; Wainman, Y. A.; Kuo, J. C. H.; Fawcett, S.; Leeper, F. J.; Brindle, K. M., Imaging Cell Surface Glycosylation in Vivo Using "Double Click" Chemistry. *Bioconjugate Chem.* **2013,** *24*, 934-941.

237. Wu, Z.; Liu, S.; Hassink, M.; Nair, I.; Park, R.; Li, L.; Todorov, I.; Fox, J. M.; Li, Z.; Shively, J. E.; Conti, P. S.; Kandeel, F., Development and Evaluation of 18F-TTCO-Cys40-Exendin-4: A PET Probe for Imaging Transplanted Islets. *J. Nucl. Med.* **2013,** *54*, 244-251.

238. Liang, Y.; Mackey, J. L.; Lopez, S. A.; Liu, F.; Houk, K. N., Control and Design of Mutual Orthogonality in Bioorthogonal Cycloadditions. *J. Am. Chem. Soc.* **2012,** *134*, 17904-17907.

239. Seitchik, J. L.; Peeler, J. C.; Taylor, M. T.; Blackman, M. L.; Rhoads, T. W.; Cooley, R. B.; Refakis, C.; Fox, J. M.; Mehl, R. A., Genetically Encoded Tetrazine Amino Acid Directs Rapid Site-Specific in Vivo Bioorthogonal Ligation with trans-Cyclooctenes. *J. Am. Chem. Soc.* **2012,** *134*, 2898-2901.

240. Taylor, M. T.; Blackman, M. L.; Dmitrenko, O.; Fox, J. M., Design and Synthesis of Highly Reactive Dienophiles for the Tetrazine–trans-Cyclooctene Ligation. *J. Am. Chem. Soc.* **2011,** *133*, 9646-9649.

241. Rossin, R.; van den Bosch, S. M.; ten Hoeve, W.; Carvelli, M.; Versteegen, R. M.; Lub, J.; Robillard, M. S., Highly Reactive trans-Cyclooctene Tags with Improved Stability for Diels–Alder Chemistry in Living Systems. *Bioconjugate Chem.* **2013,** *24*, 1210-1217.

242. Lang, K.; Davis, L.; Wallace, S.; Mahesh, M.; Cox, D. J.; Blackman, M. L.; Fox, J. M.; Chin, J. W., Genetic Encoding of Bicyclononynes and trans-Cyclooctenes for Site-Specific Protein Labeling in Vitro and in Live Mammalian Cells via Rapid Fluorogenic Diels–Alder Reactions. *J. Am. Chem. Soc.* **2012,** *134*, 10317-10320.

243. Still, W. C.; Kahn, M.; Mitra, A., Rapid chromatographic technique for preparative separations with moderate resolution. *J. Org. Chem.* **1978,** *43*, 2923-2925.

244. Jung, M. E.; Miller, S. J., Total synthesis of isopavine and intermediates for the preparation of substituted amitriptyline analogs: facile routes to substituted dibenzocyclooctatrienes and dibenzocycloheptatrienes. *J. Am. Chem. Soc.* **1981,** *103*, 1984-1992.

Appendices

Appendix 1 – Example Radio-HPLC Traces

HPLC traces of SPAAC reactions between [^{18}F]FEA and cyclooctynes

Cyclooctyne: OCT2
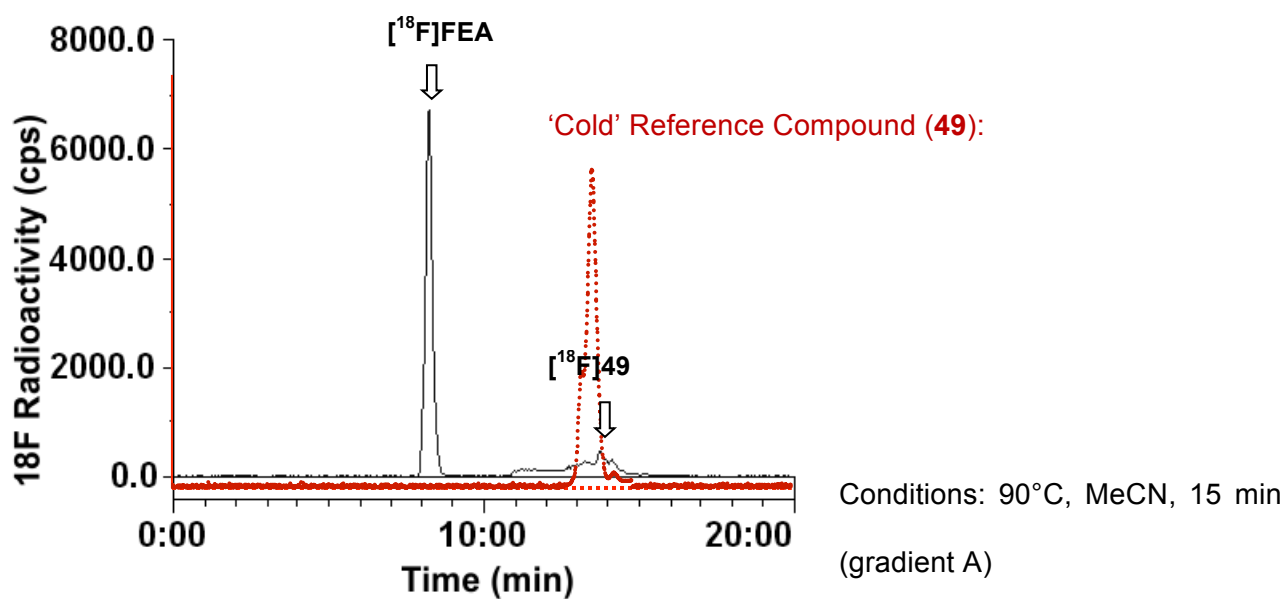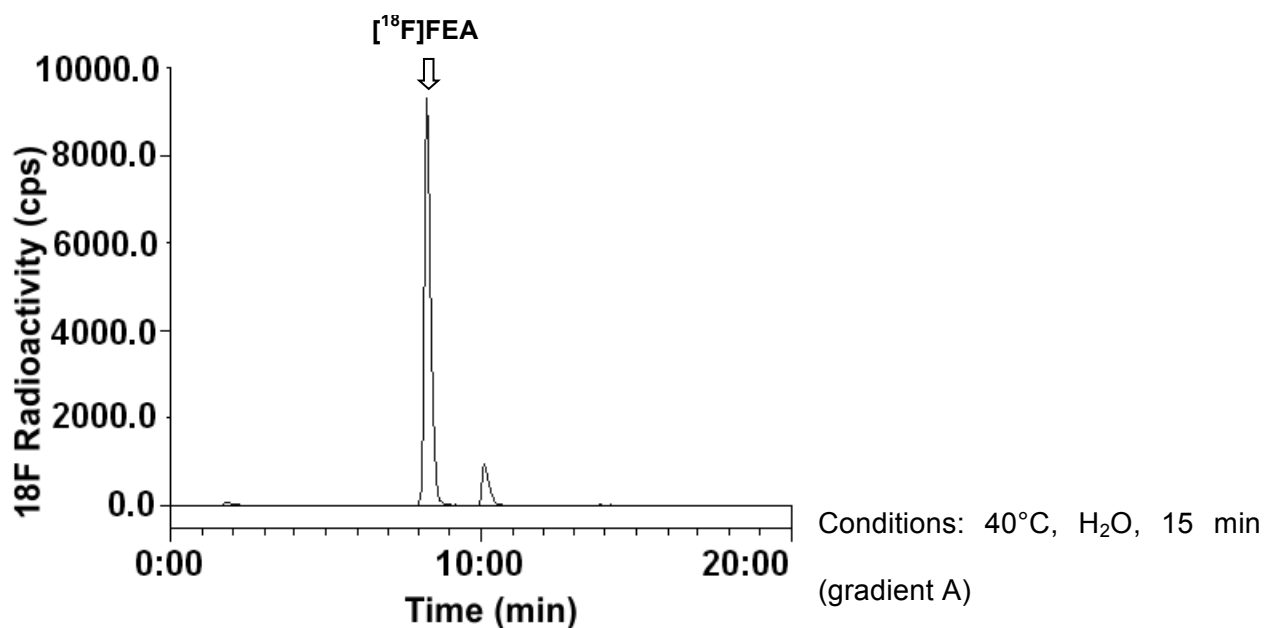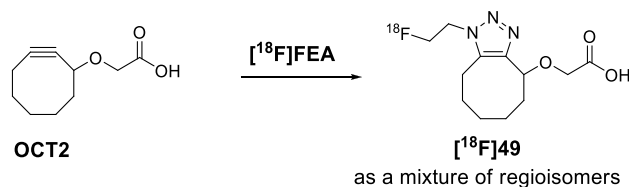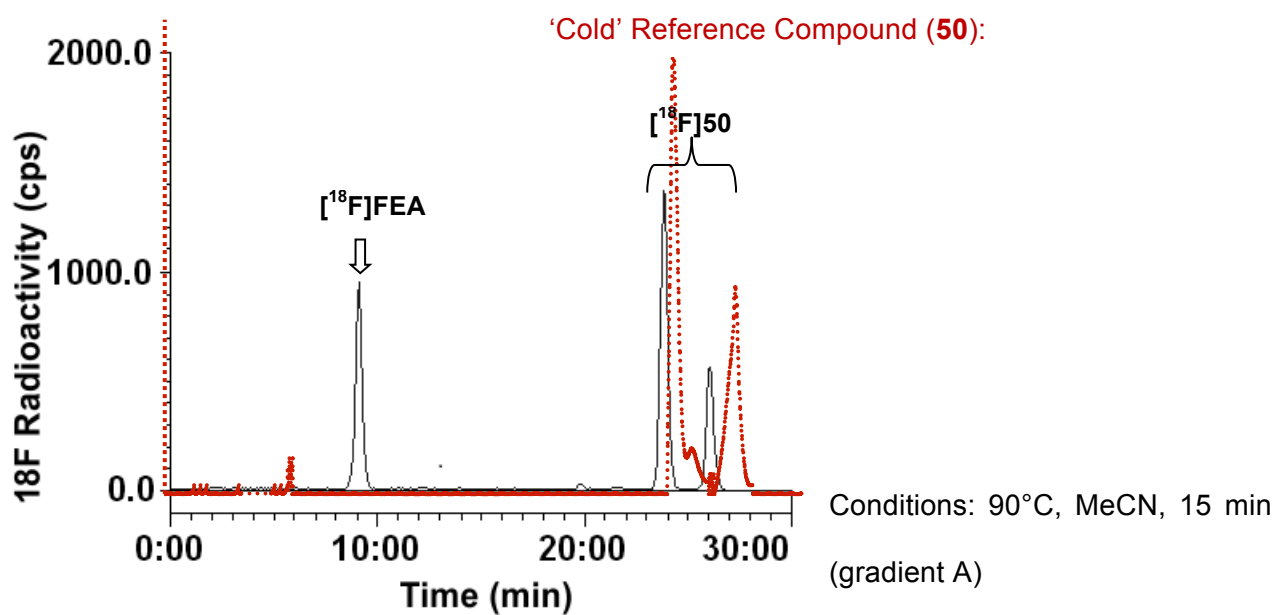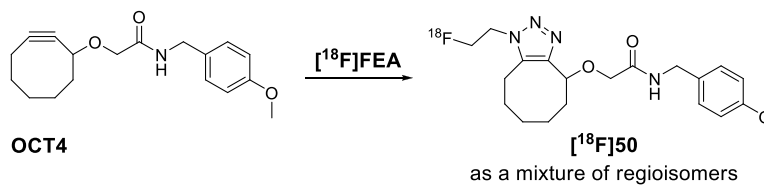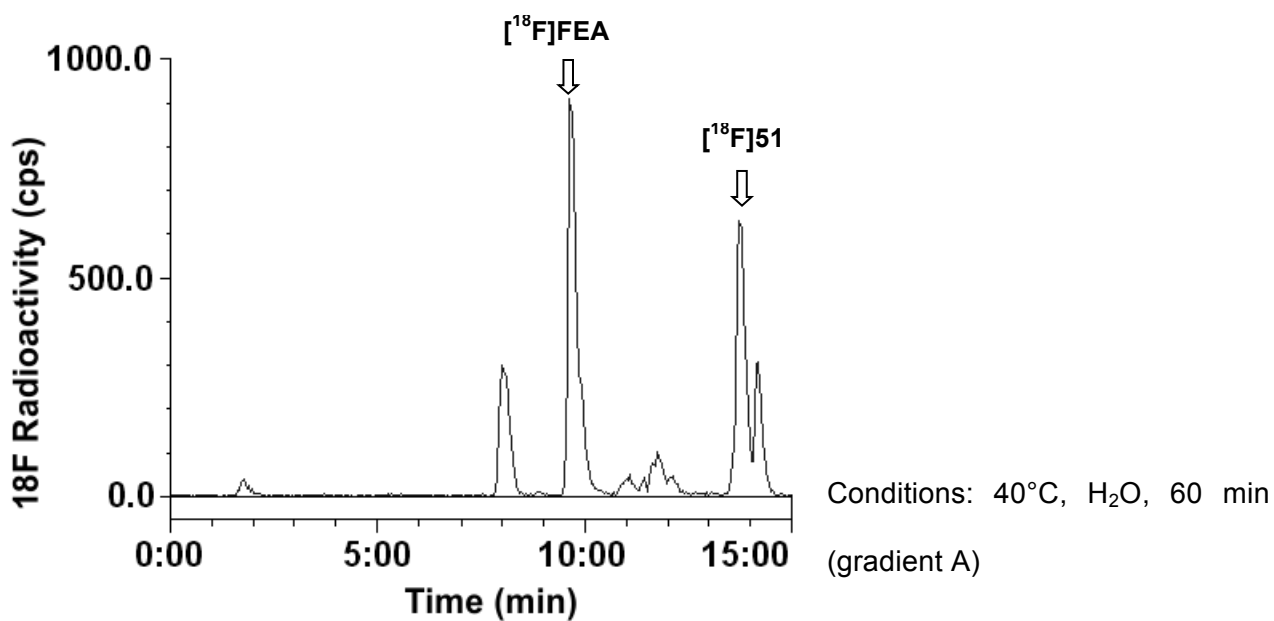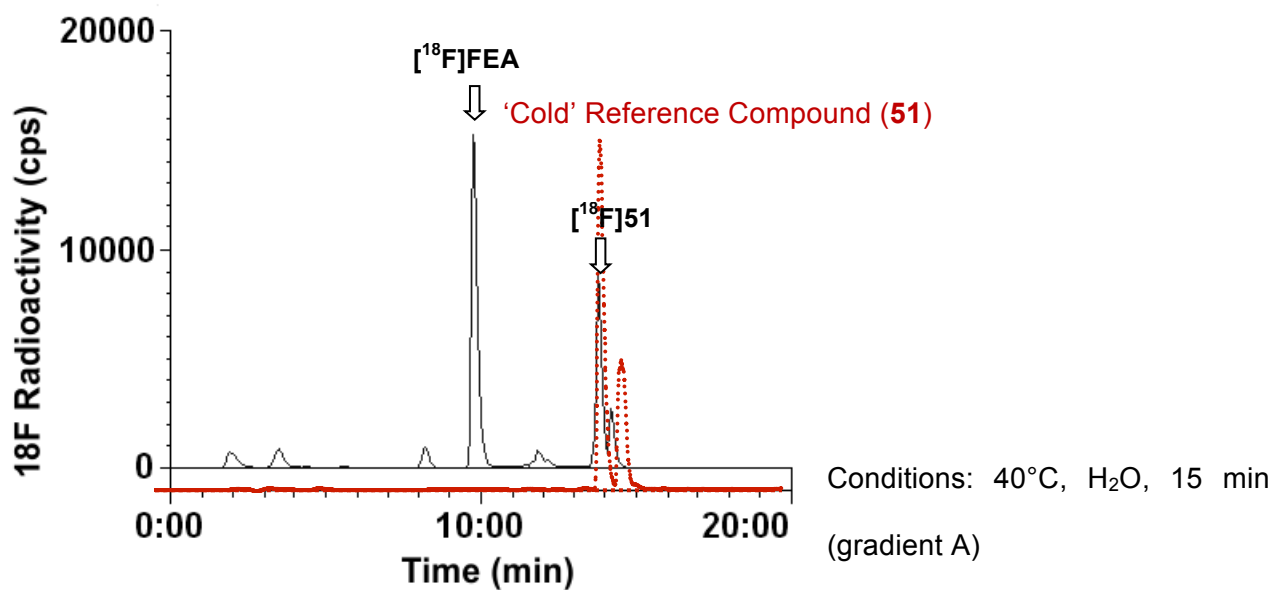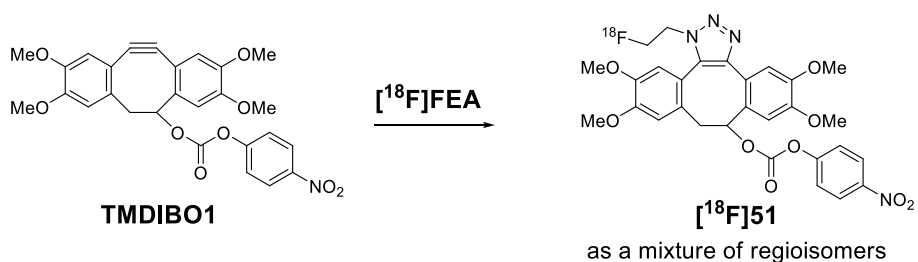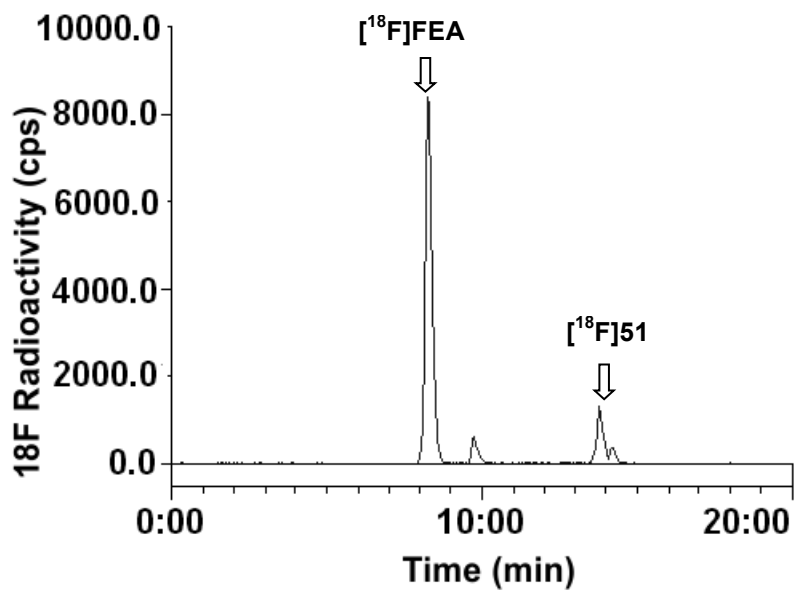
OCT2   [^{18}F]FEA   **[^{18}F]49**

as a mixture of regioisomers

Conditions: 40°C, H$_2$O, 15 min

(gradient A)

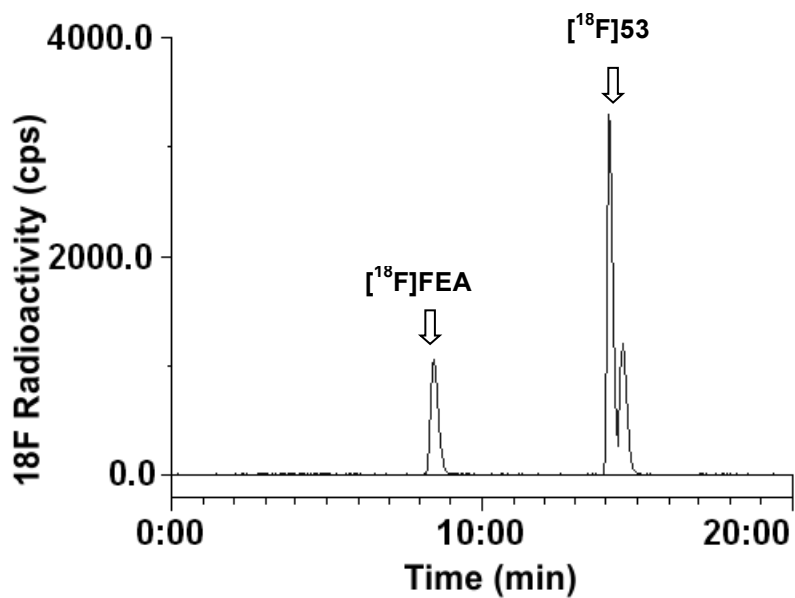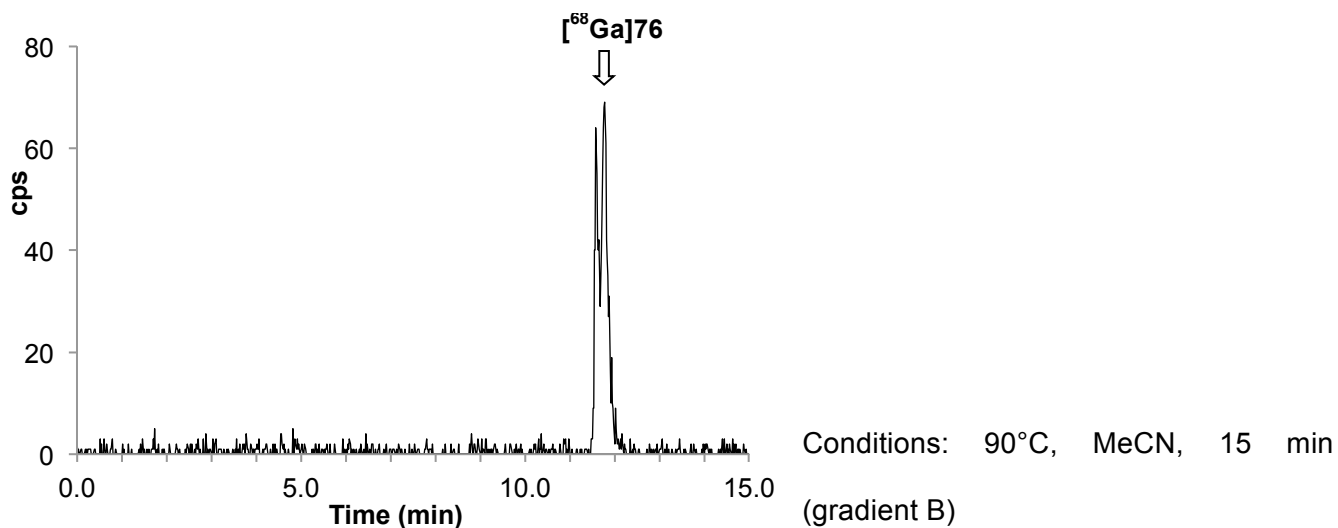Conditions: 90°C, MeCN, 15 min

(gradient A)

281

Cyclooctyne: OCT4

OCT4 →[[18F]FEA]→ **[18F]50** as a mixture of regioisomers

'Cold' Reference Compound (**50**):

Conditions: 90°C, MeCN, 15 min

(gradient A)

Cyclooctyne: TMDIBO1

[18F]FEA

TMDIBO1

[18F]51

as a mixture of regioisomers

Conditions: 40°C, H_2O, 15 min

(gradient A)

Conditions: 40°C, H_2O, 60 min

(gradient A)

Conditions: 40°C, MeCN, 15 min

(gradient A)

Conditions: 90°C, MeCN, 15 min

(gradient A)

Cyclooctyne: TMDIBO2

TMDIBO2 → [18F]51
as a mixture of regioisomers

[18F]FEA
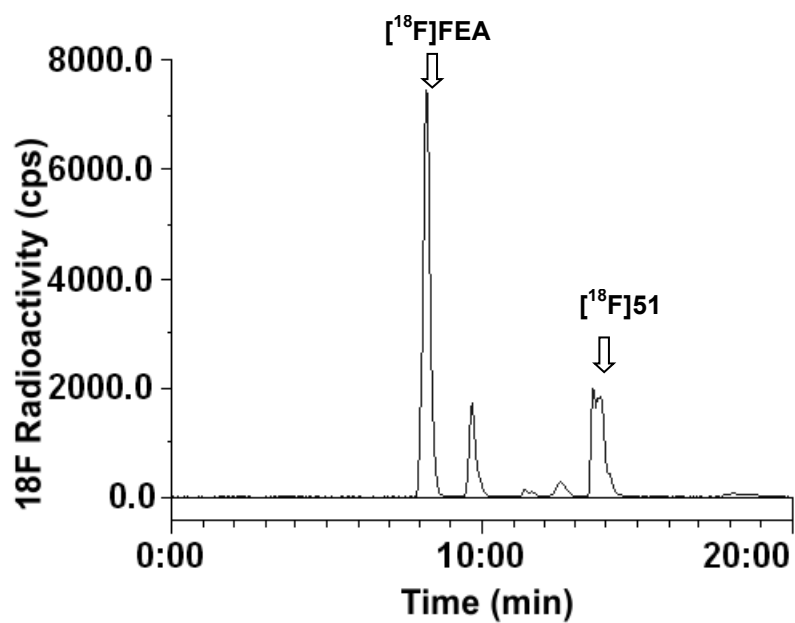
Conditions: 40°C, MeCN, 15 min

(gradient A)

Conditions: 90°C, MeCN, 15 min
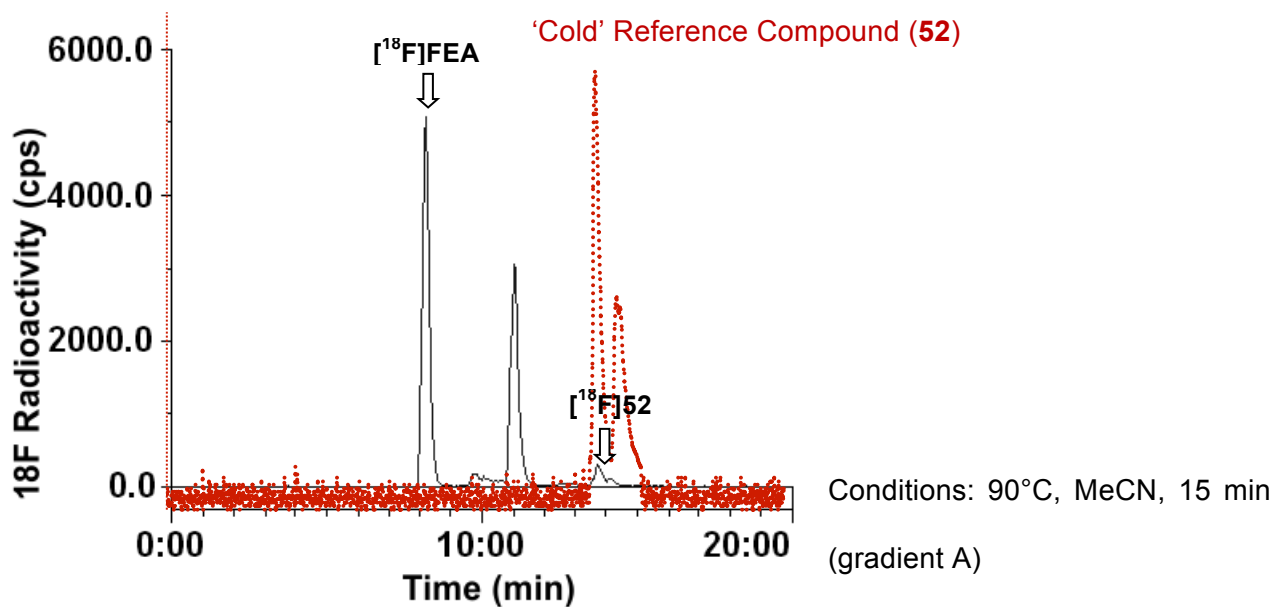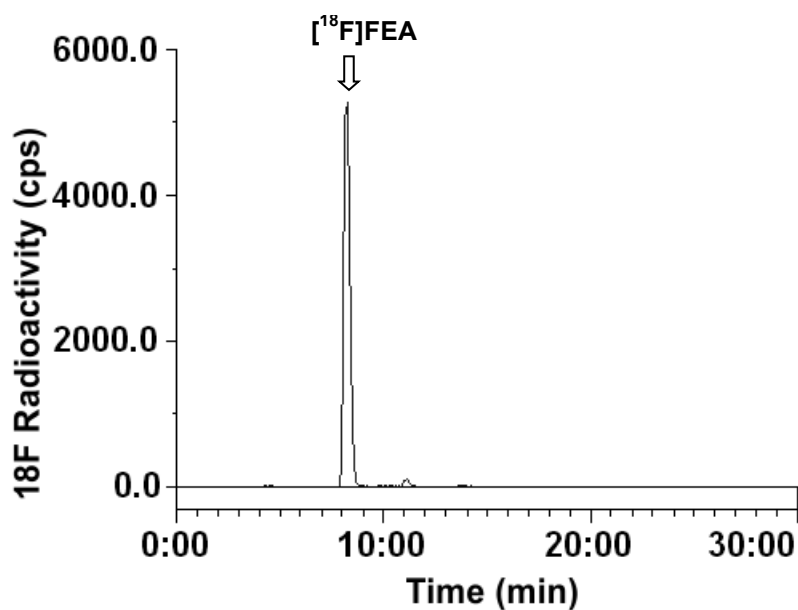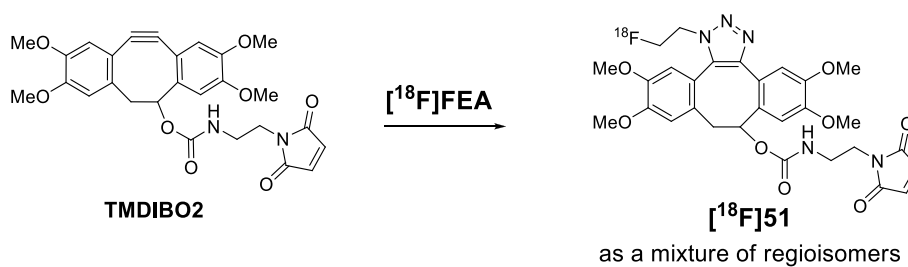
(gradient A)

Cyclooctyne: DIFO3

Conditions: 40°C, H$_2$O, 15 min

(gradient A)

Conditions: 40°C, H$_2$O, 60 min

(gradient A)

Conditions: 90°C, H_2O, 60 min (gradient A)
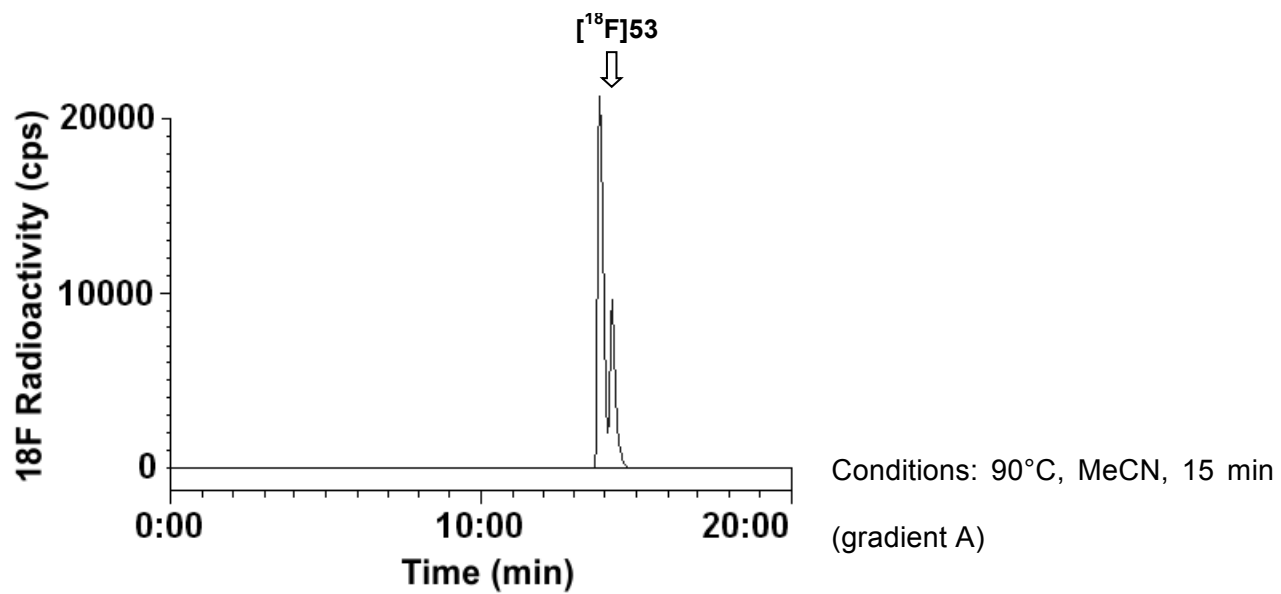
Conditions: 40°C, MeCN, 15 min (gradient A)

Conditions: 90°C, MeCN, 15 min

(gradient A)

Example HPLC traces of the reaction between [^{68}Ga]DOTA-Az and DIBAC2

[^{68}Ga]DOTA-Az   →(DIBAC2)→   [^{68}Ga]76 (mixture of regioisomers)

Conditions: 50°C, MeCN, 15 min (gradient B)

Conditions: 90°C, MeCN, 15 min (gradient B)
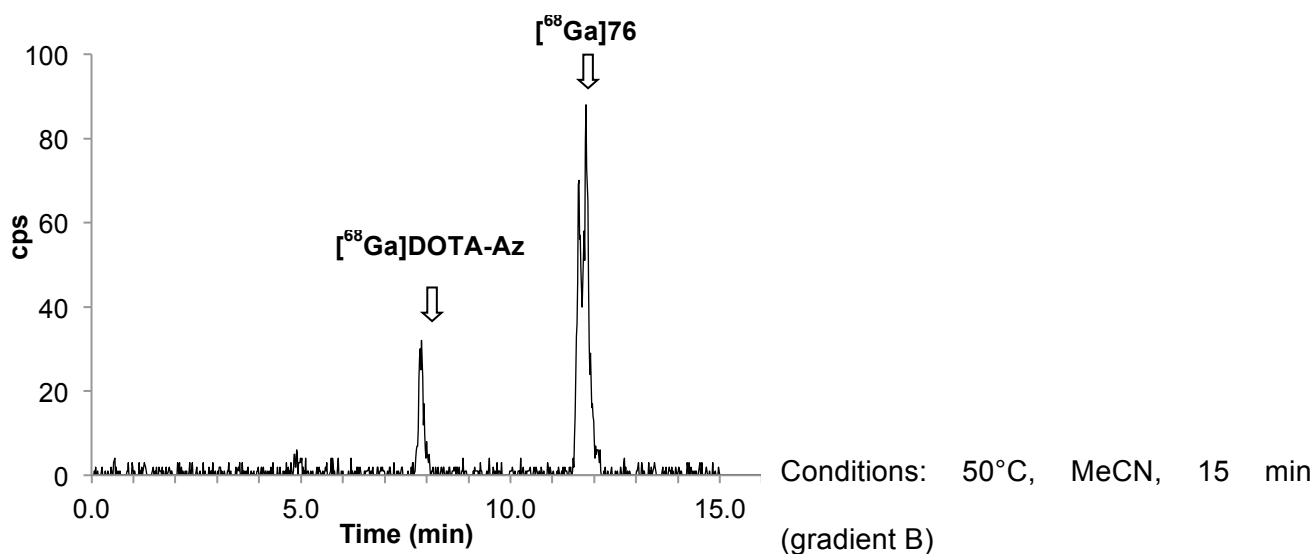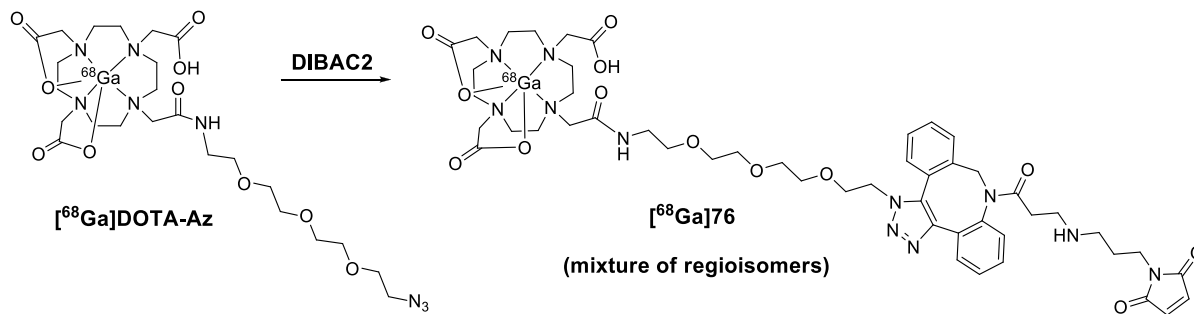
Example HPLC traces of ^{68}Ga-labeled IeDDA reactions

Alkene: ethyl vinyl ether (93)
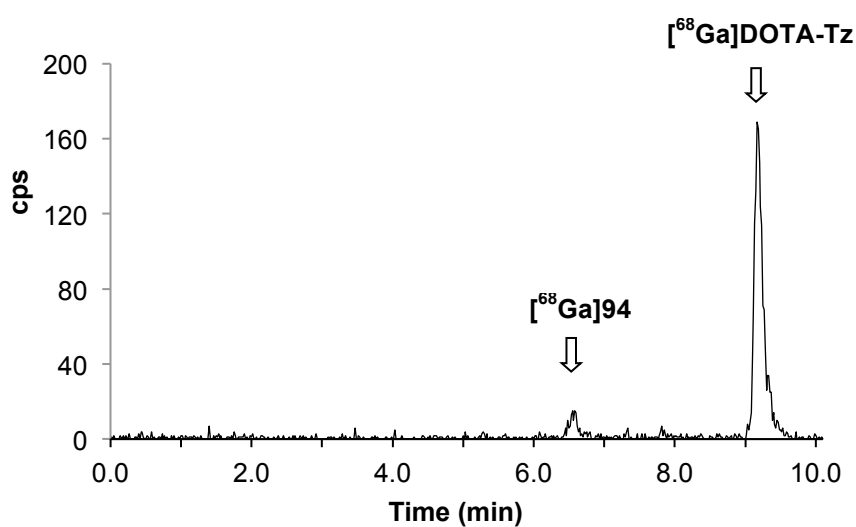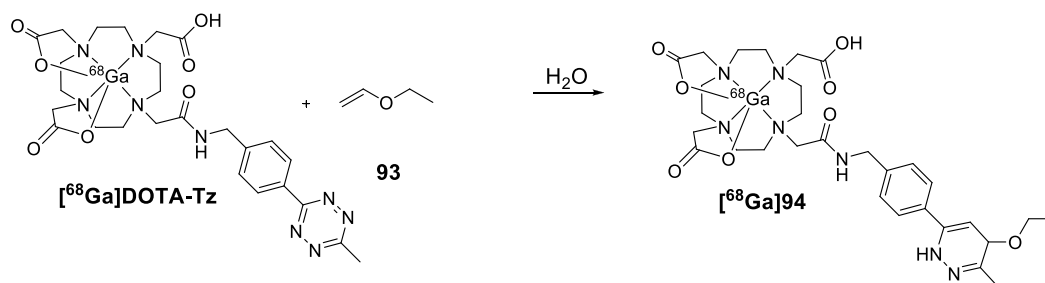
Conditions: 40°C, H$_2$O, 10 min (gradient B)
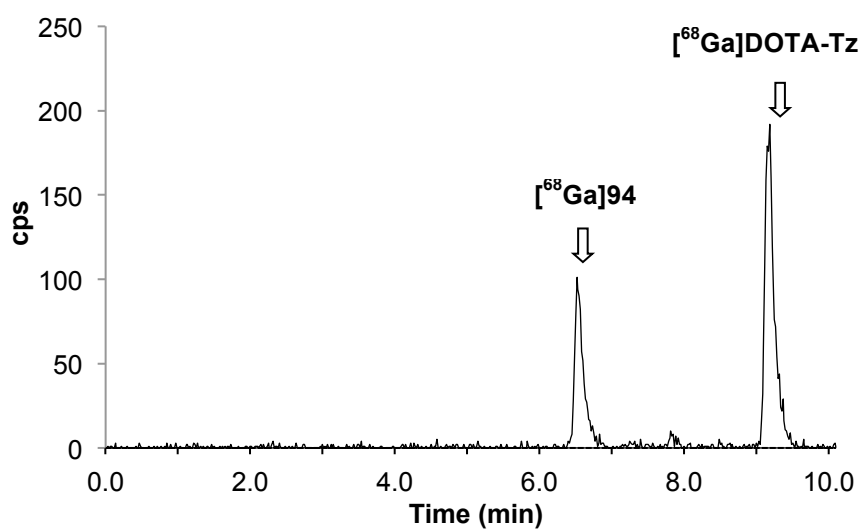
Conditions: 90°C, H$_2$O, 10 min (gradient B)

Alkene: 5-Norbornene-2-carboxylic acid (91)

Conditions: 40°C, H₂O, 10 min (gradient B)

Conditions: 40°C, H₂O, 20 min (gradient B)
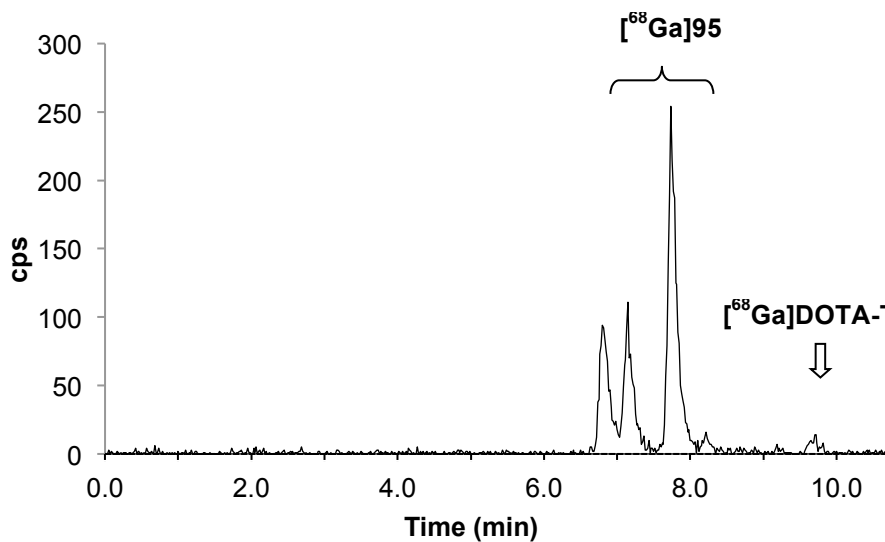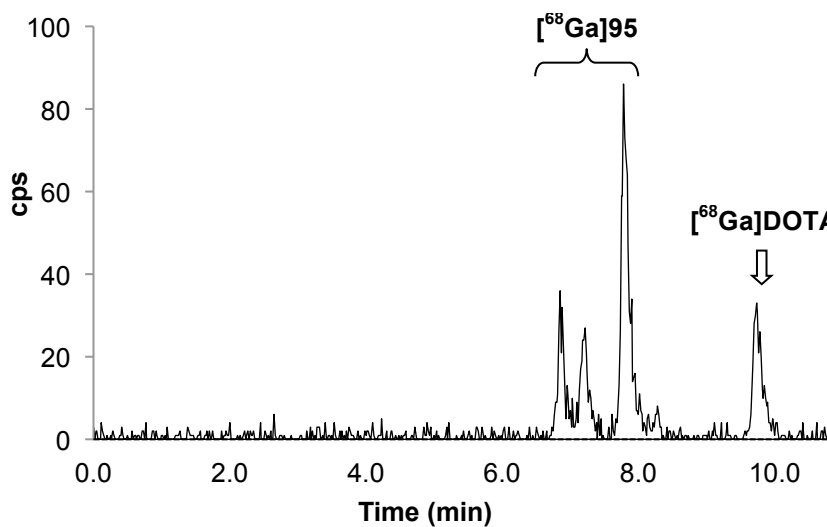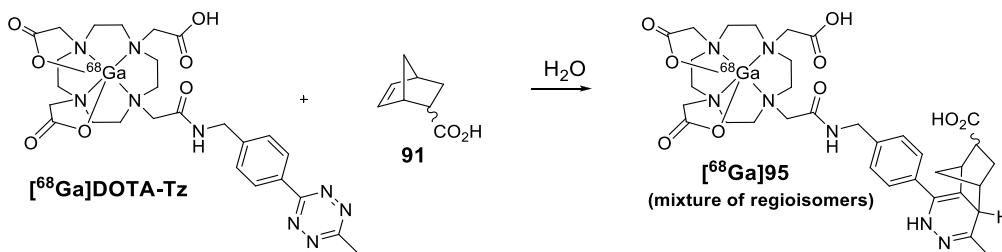
Alkene: (1*S*,4*S*)-*N*-(3-Fluorophenyl)bicyclo[2.2.1]hept-5-ene-2-carboxamide (*exo*) (100)
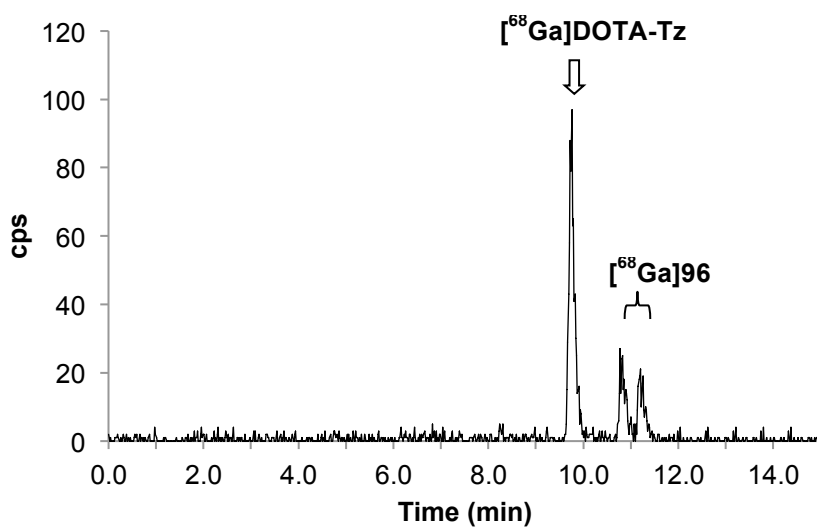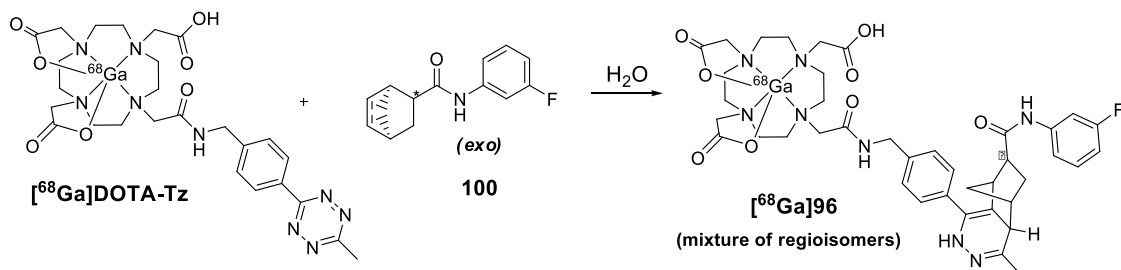
Conditions: 40°C, H$_2$O, 10 min (gradient B)
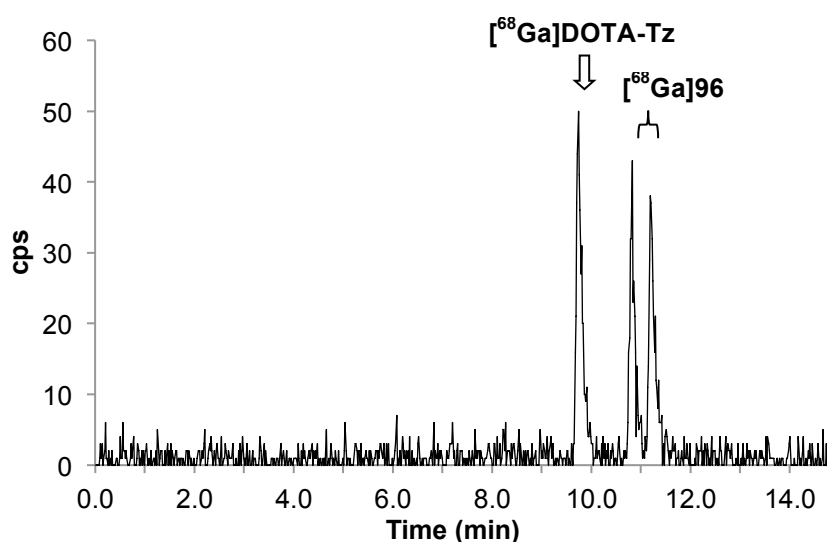
Conditions: 40°C, H$_2$O, 20 min (gradient B)

Alkene: *(1S,4S)-N*-(4-Fluorophenyl)bicyclo[2.2.1]hept-5-ene-2-carboxamide (*endo*)

(101)

Conditions: 40°C, H_2O, 10 min
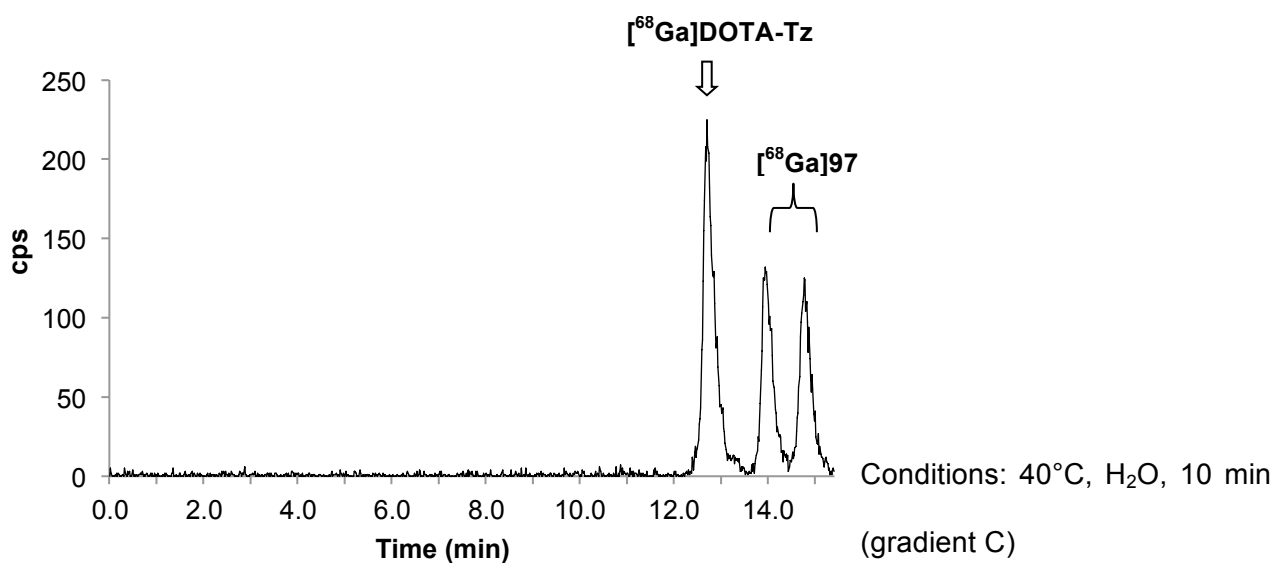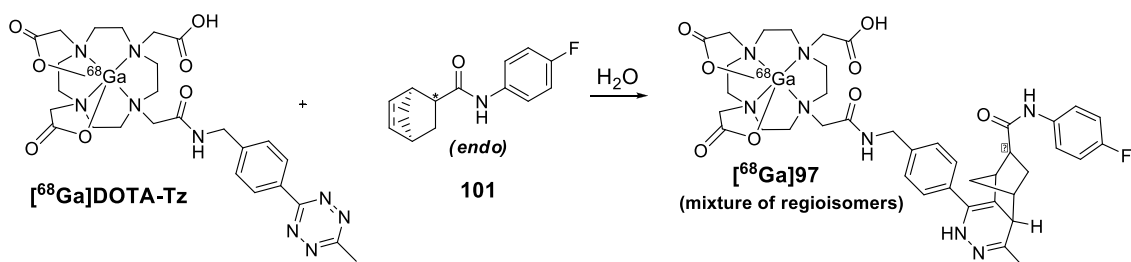
(gradient C)

Alkene: *(1S,4S)-N*-(4-Fluorophenyl)bicyclo[2.2.1]hept-5-ene-2-carboxamide (*exo*) (102)
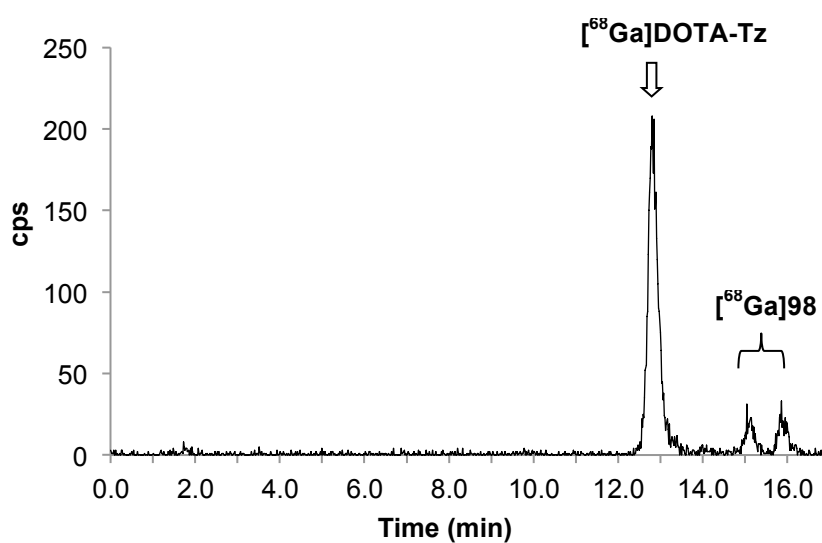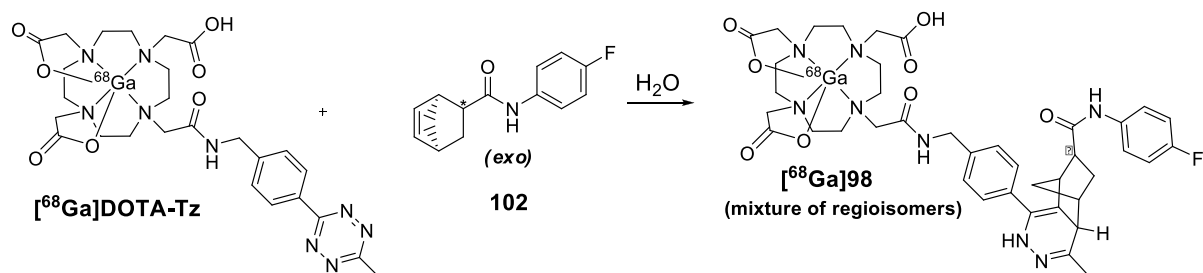
Conditions: 40°C, H_2O, 10 min

(gradient C)

Example HPLC traces of ⁶⁸Ga-labelled antibody (C225) reactions
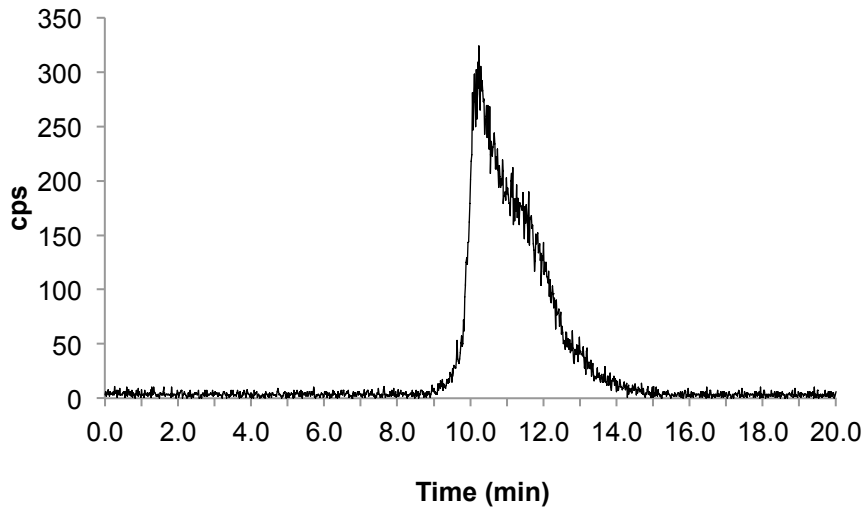
[⁶⁸Ga]DOTA-GA-Tz only,
(gradient D)
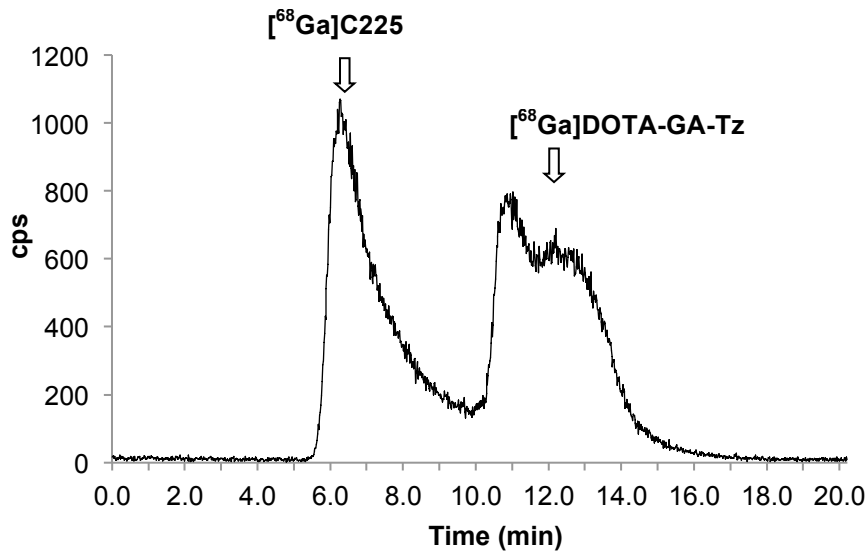
Conditions:

Batch 1, 37°C, PBS, immediate injection (gradient D)
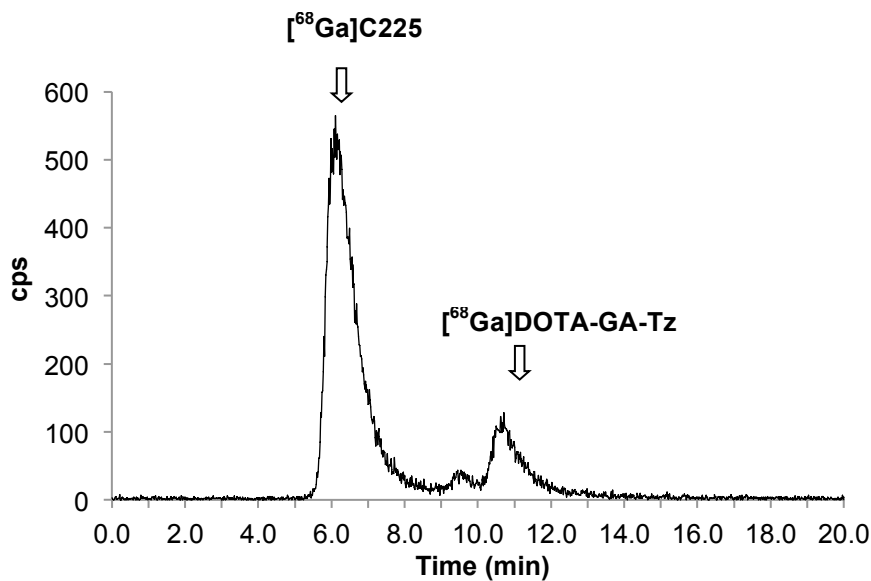
Conditions:

Batch 1, 37°C, PBS, 20 min (gradient D)

Appendix 2 – MALDI MS of C225 antibodies

MALDI m/z for C225 unmodified antibody

EPSRC National Mass Spectrometry Facility, Swansea

<<IMPSPI001-VM-MAP-C225_0001>> Voyager Spec #1=>NF0.7=>SM41=>MC[BP = 153120.5, 132]

Printed: 13:49, October 22, 2013
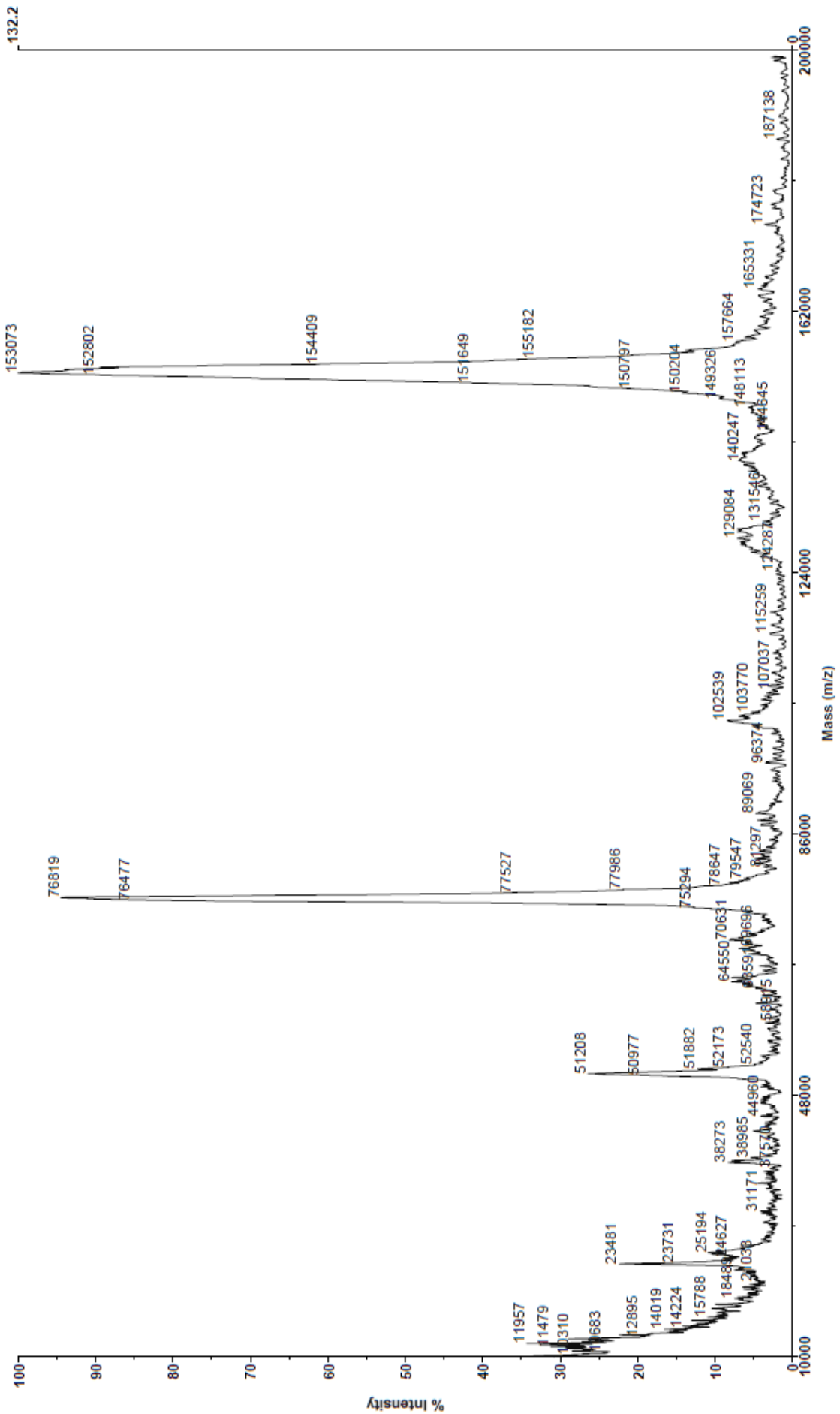
Acquired: 13:04:00, October 22, 2013
Evans C225 MW=150k?? H2O PosLin [1:24] (SA;1:1H2O:MeCN)
D:\2013\Oct13\IMPSPI001-VM-MAP-C225_0001.dat

MALDI m/z for C225-TCO modified antibody (Batch 2)

EPSRC National Mass Spectrometry Facility, Swansea

<<IMPSPI002-VM-MAP_0001>> Voyager Spec #1=>NF0.7=>SM41=>MC[BP = 9745.7, 461]

Acquired: 13:25:00, October 22, 2013
Evans   C225-TCO-2   MW=150k??   H2O   PosLin   [1:24]   (SA:1:1H2O:MeCN)
D:\2013\Oct13\IMPSPI002-VM-MAP_0001.dat

Printed: 13:55, October 22, 2013
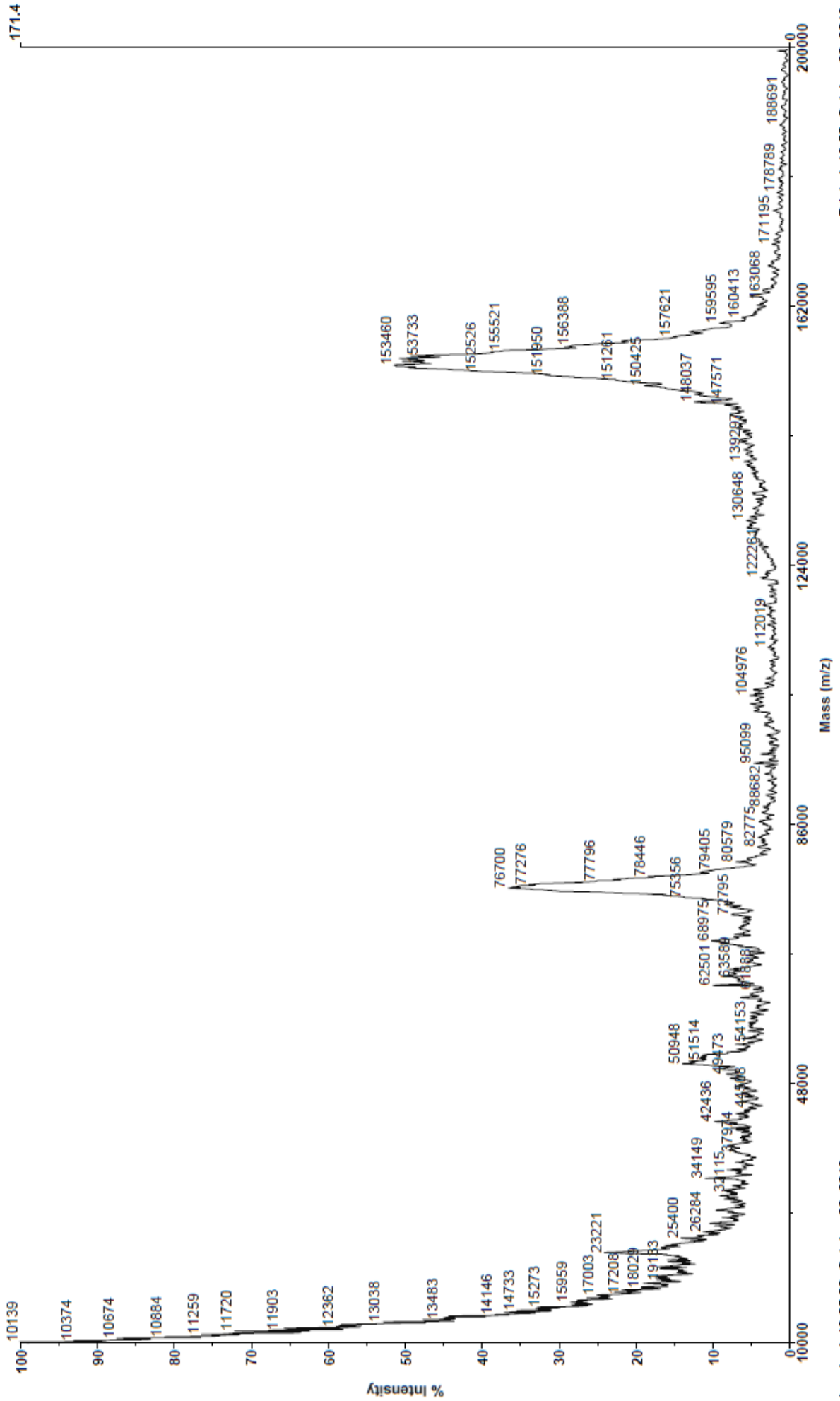
MALDI m/z for C225-TCO modified antibody (Batch 3)

Mass Spectrometry Facility, Swansea

<<IMPSPI003-VM-MAP_0001>> Voyager Spec #1=>NF0.7=>SM41=>MC[BP = 9789.8, 223]

Appendix 3 – Key NMR spectra

^{19}F NMR spectrum for Fluoroethyl azide (FEA)

19F NMR spectrum for Triazole 49 (mixture of regioisomers in ratio 2:1)
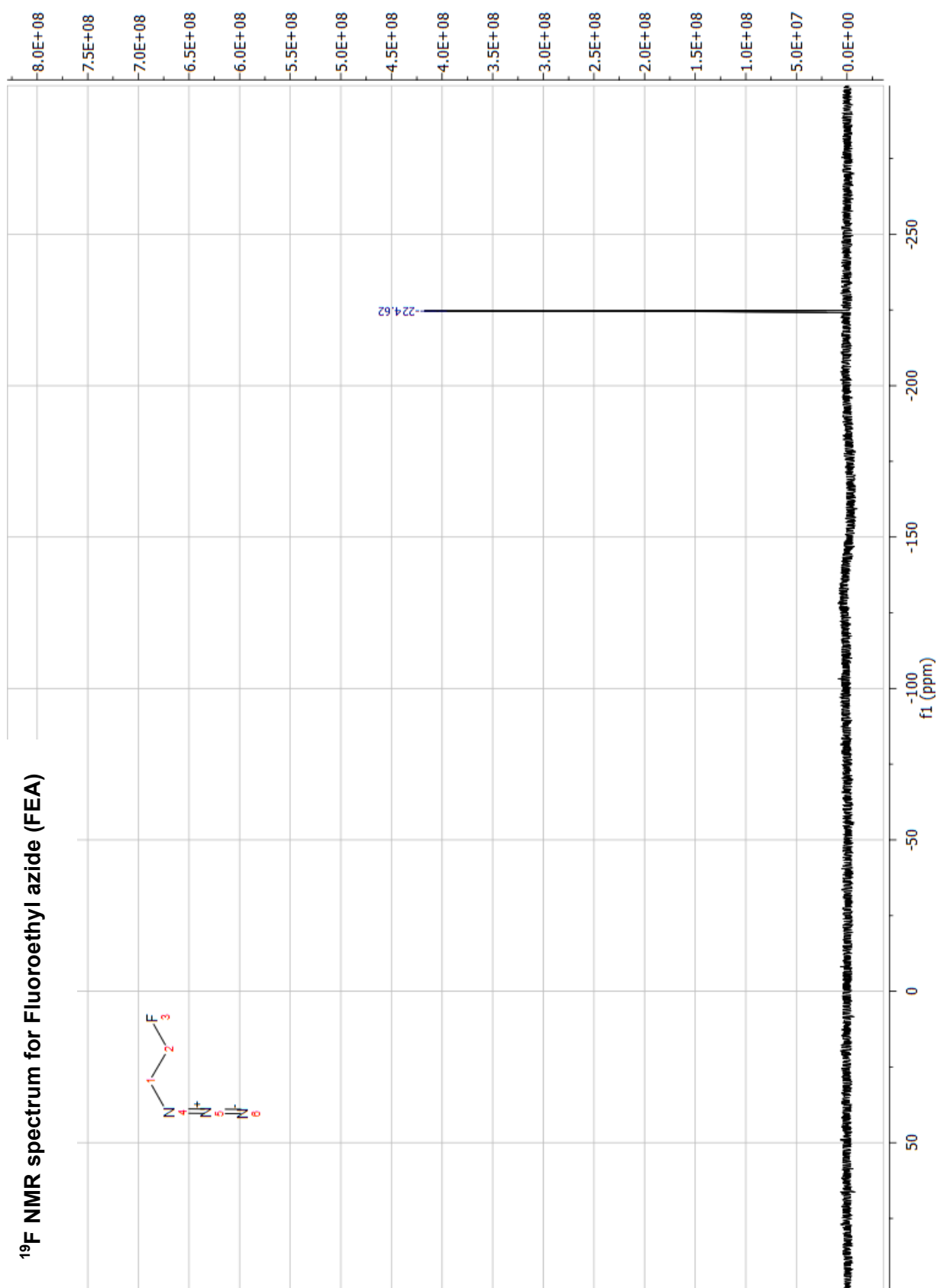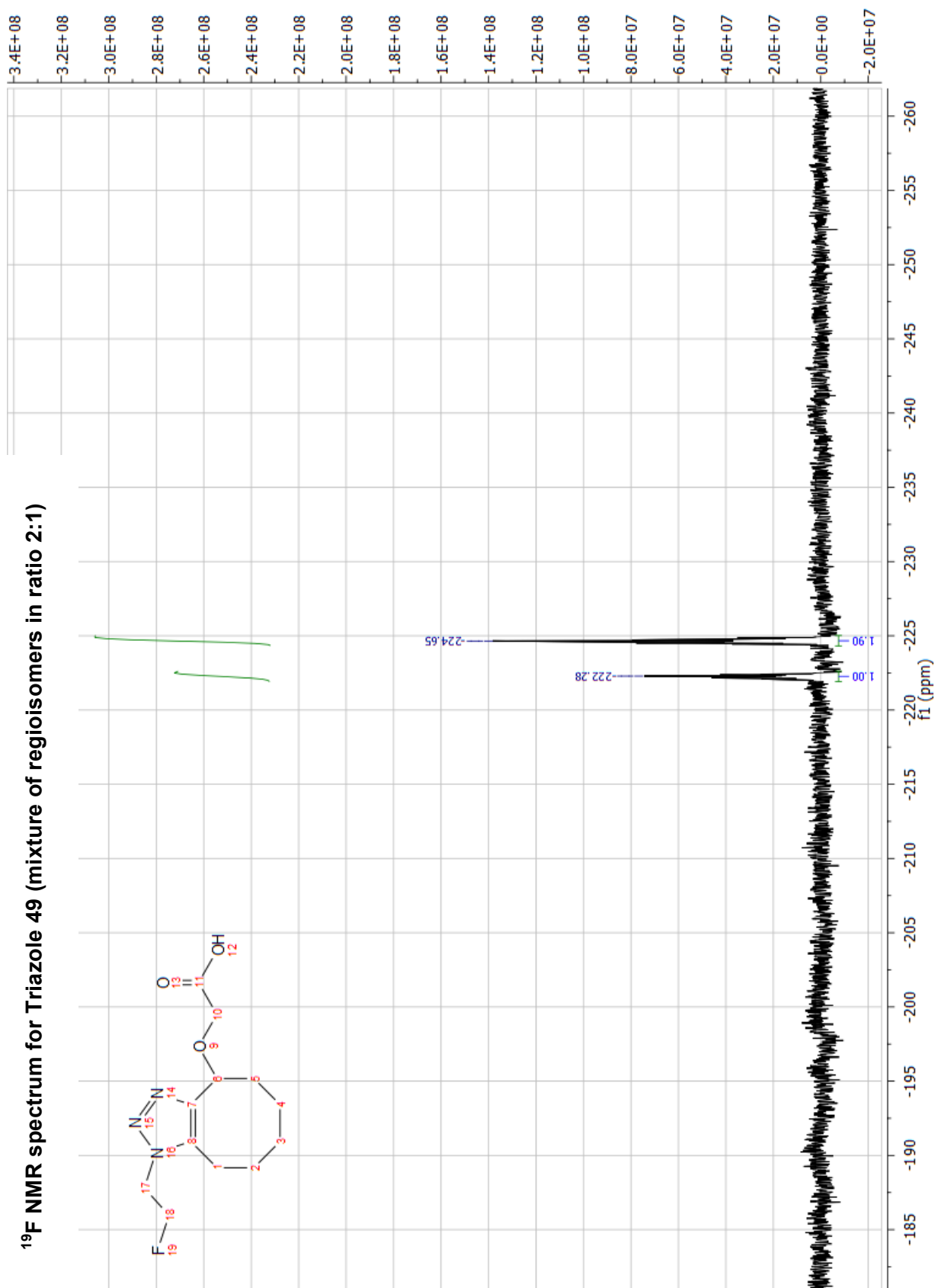
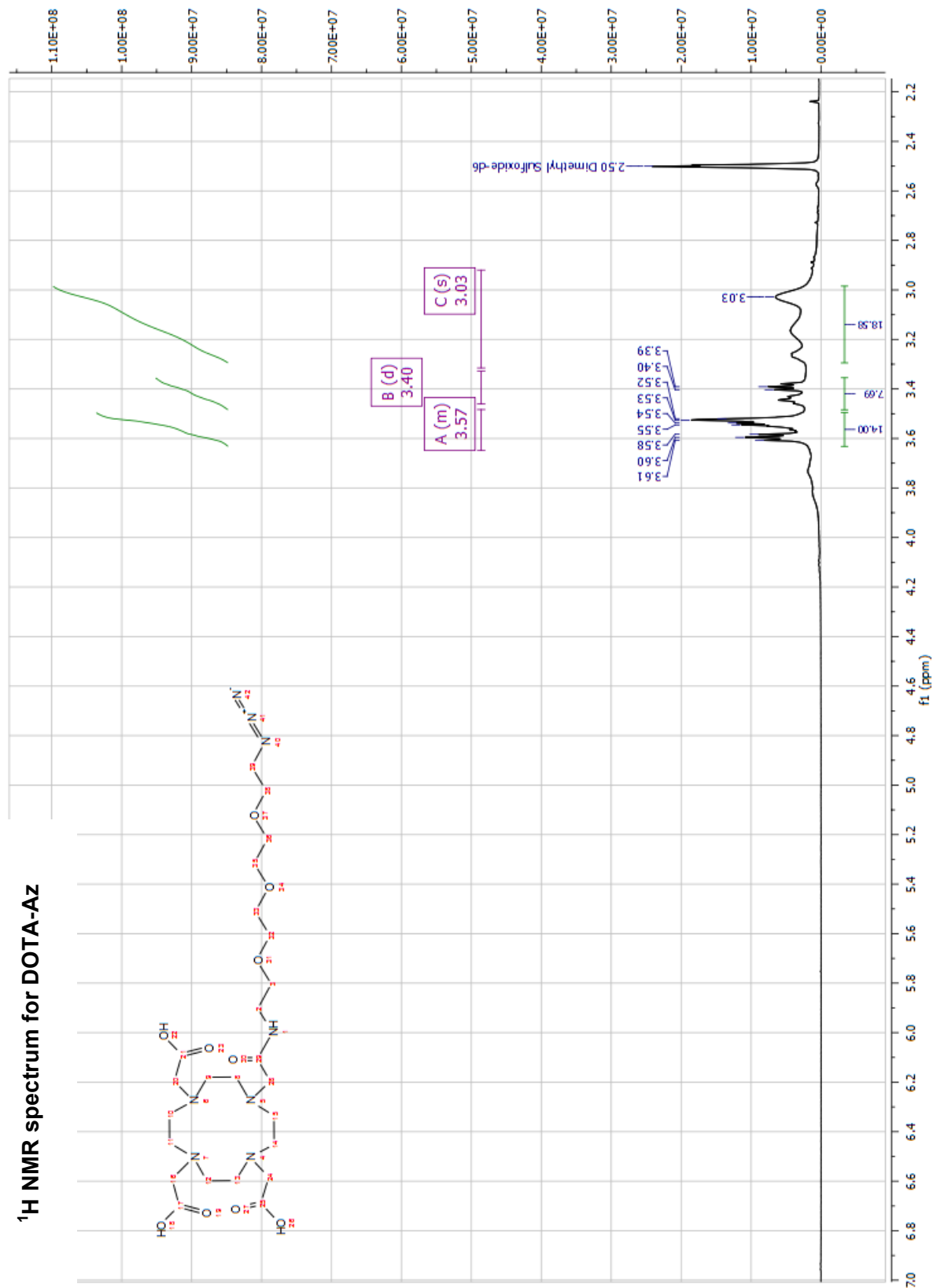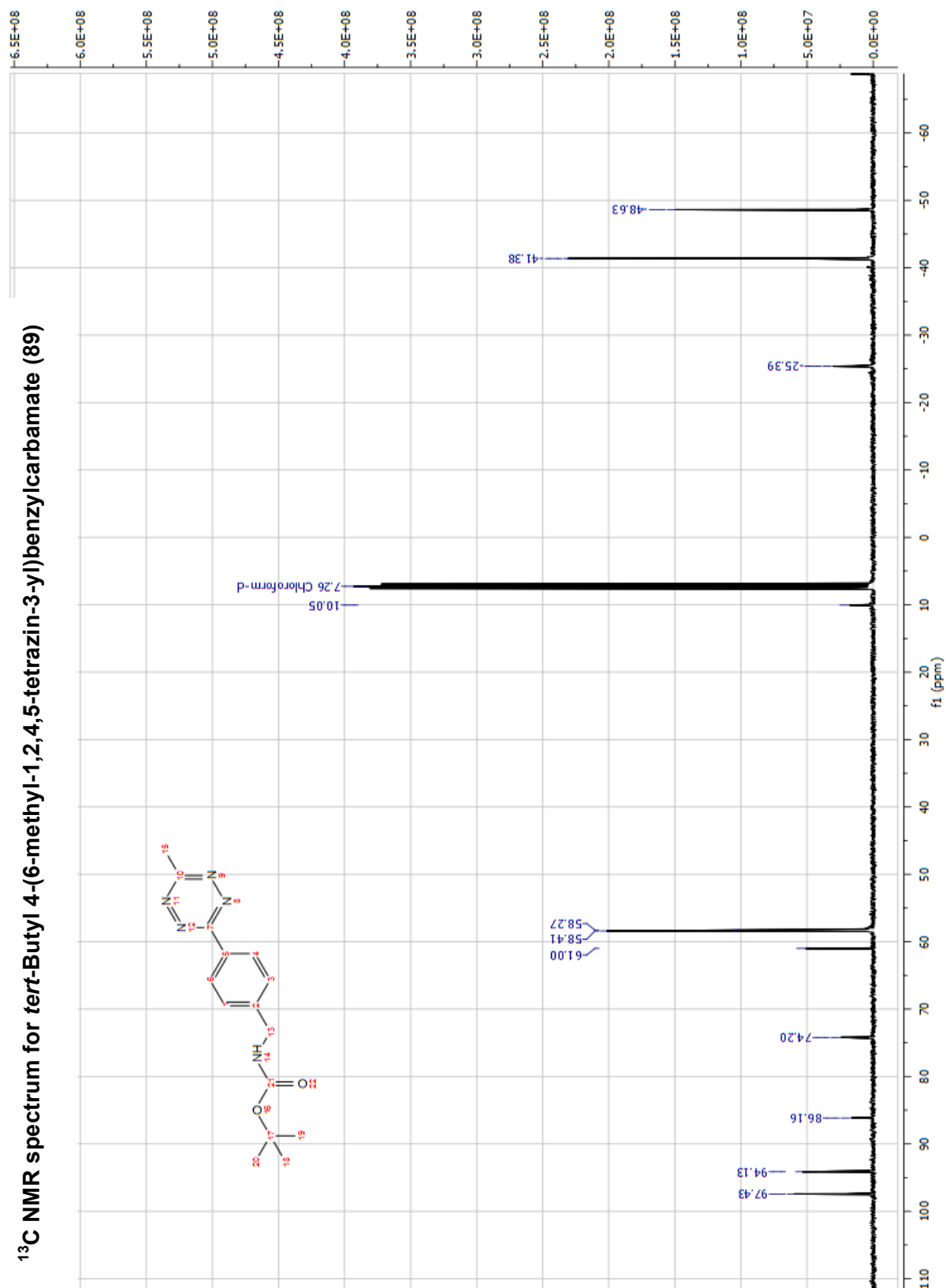**¹⁹F NMR spectrum for Triazole 50 (mixture of regioisomers in ratio 2:1)**
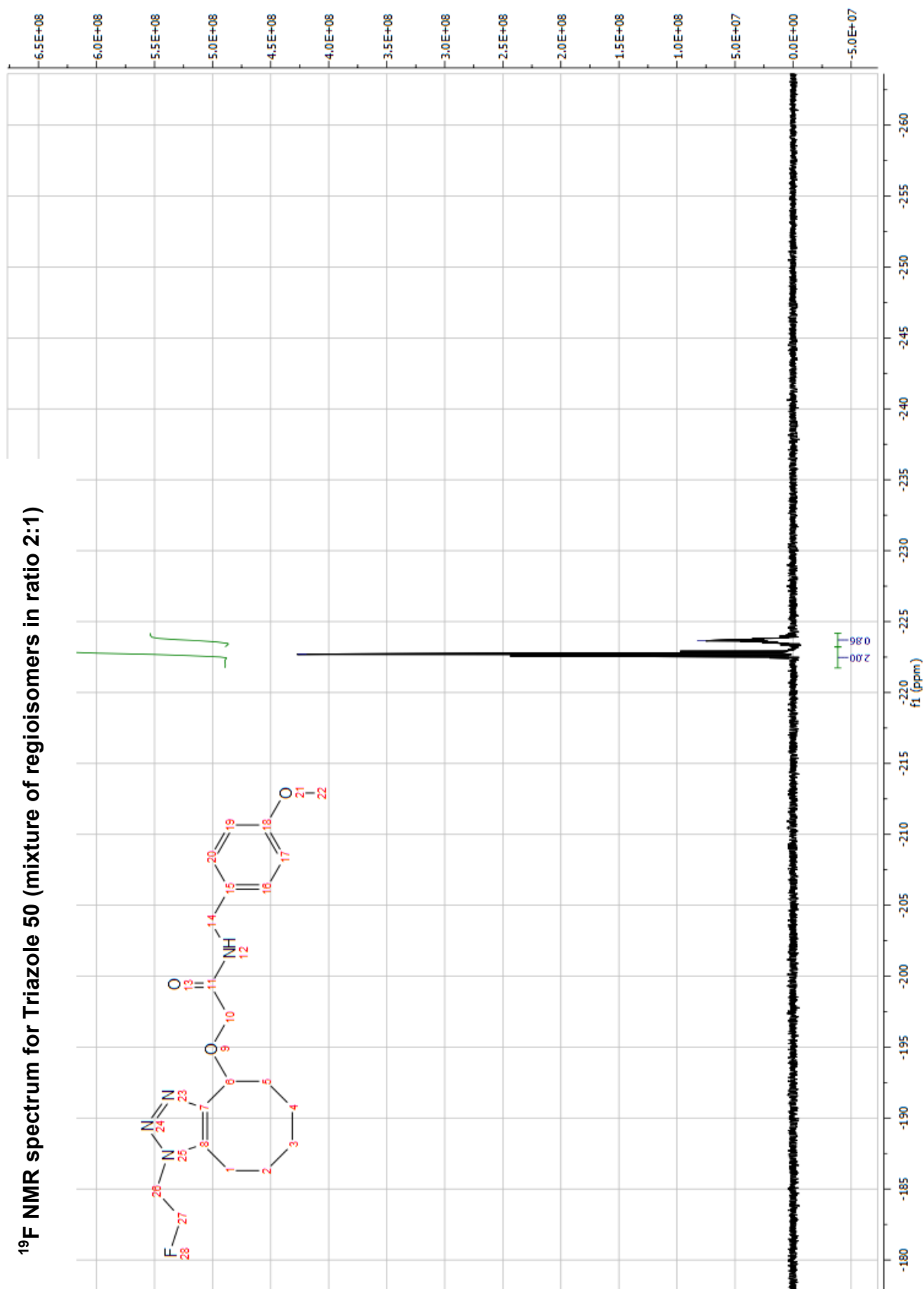
¹⁹F NMR spectrum for Triazole 51 (mixture of regioisomers in ratio 2:1)
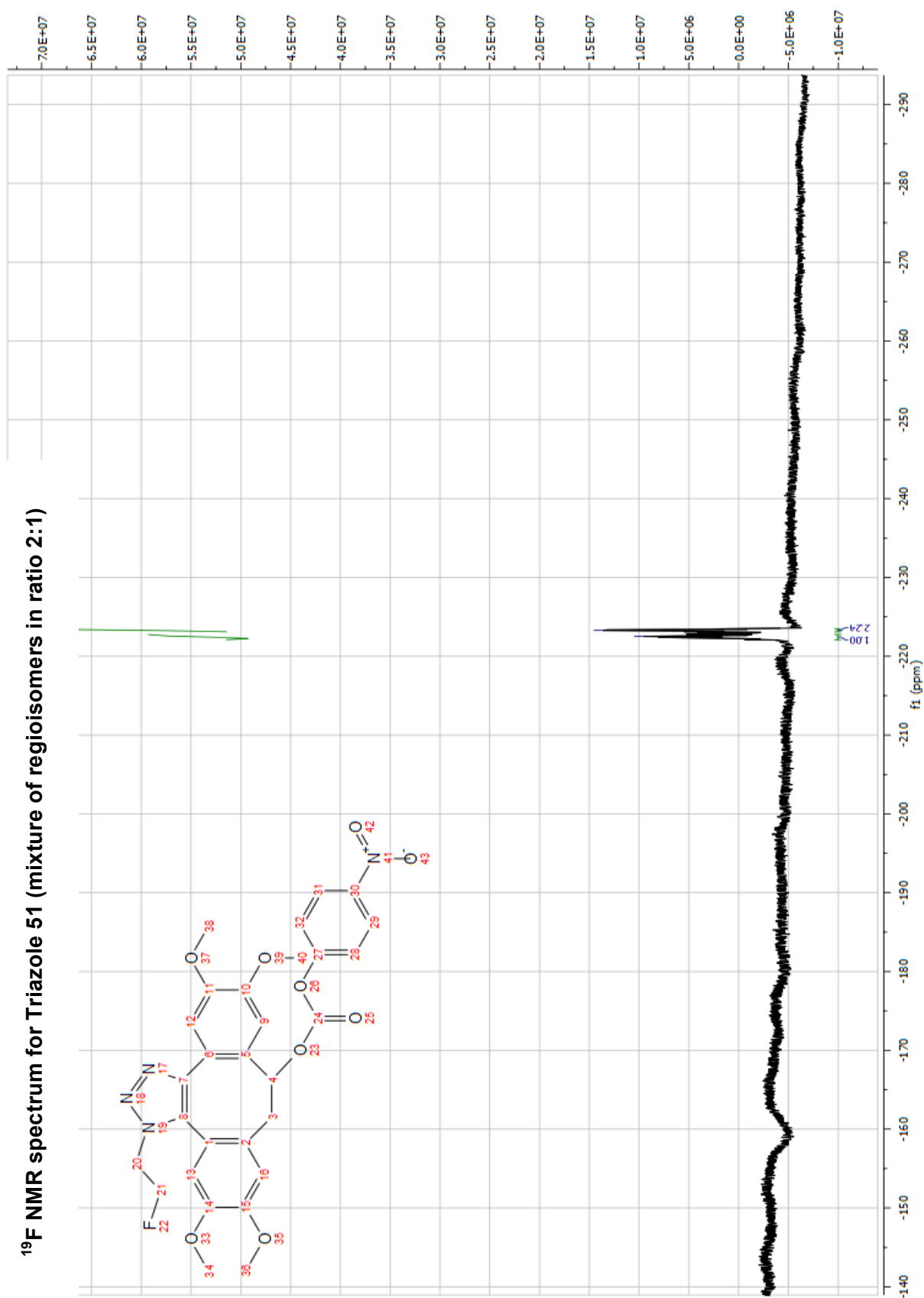
^{19}F NMR spectrum for Triazole 52 (mixture of regioisomers in ratio 7:1)

-225.10
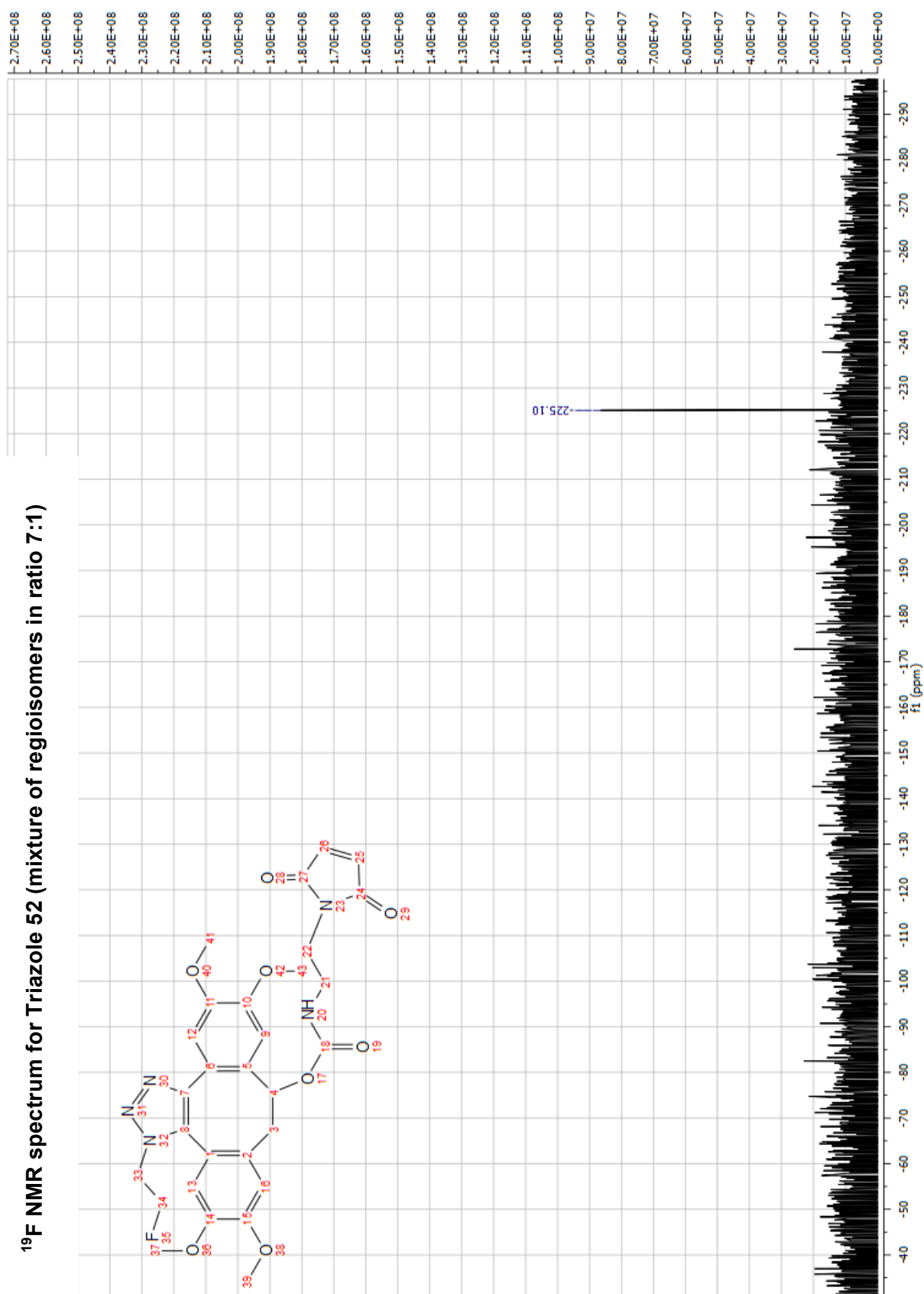
¹⁹F NMR spectrum for Triazole 53 (mixture of regioisomers in ratio 2:1)
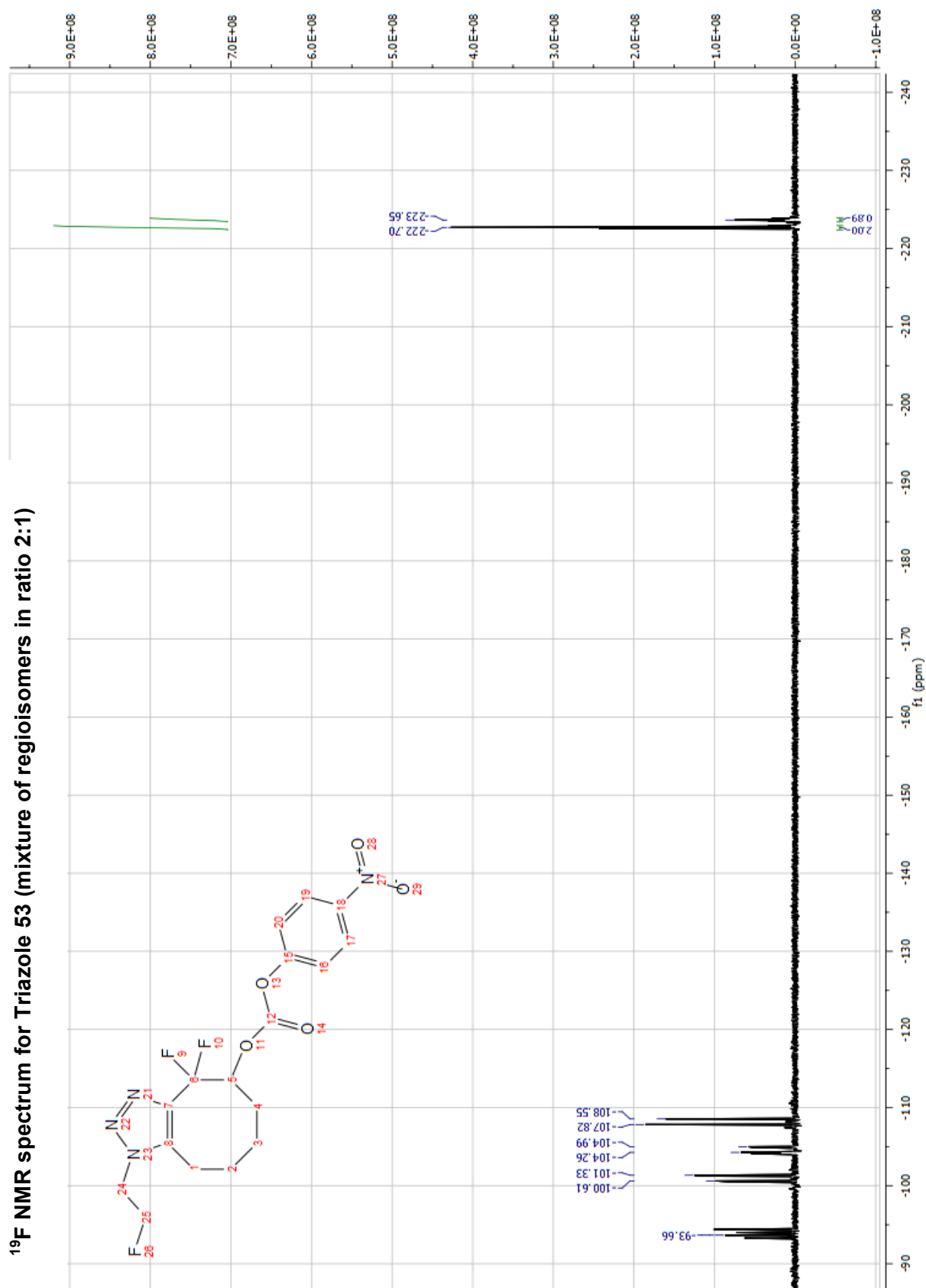
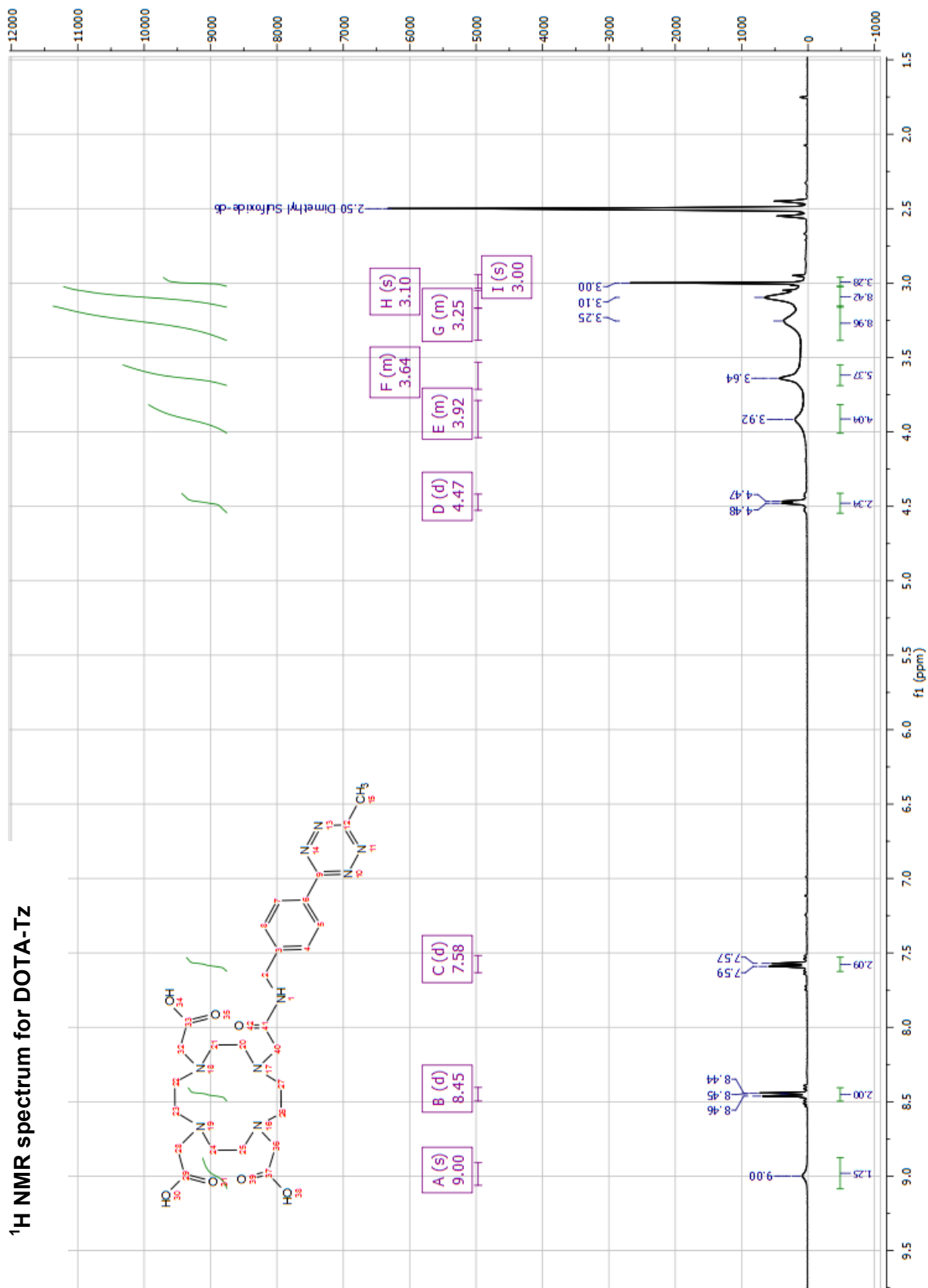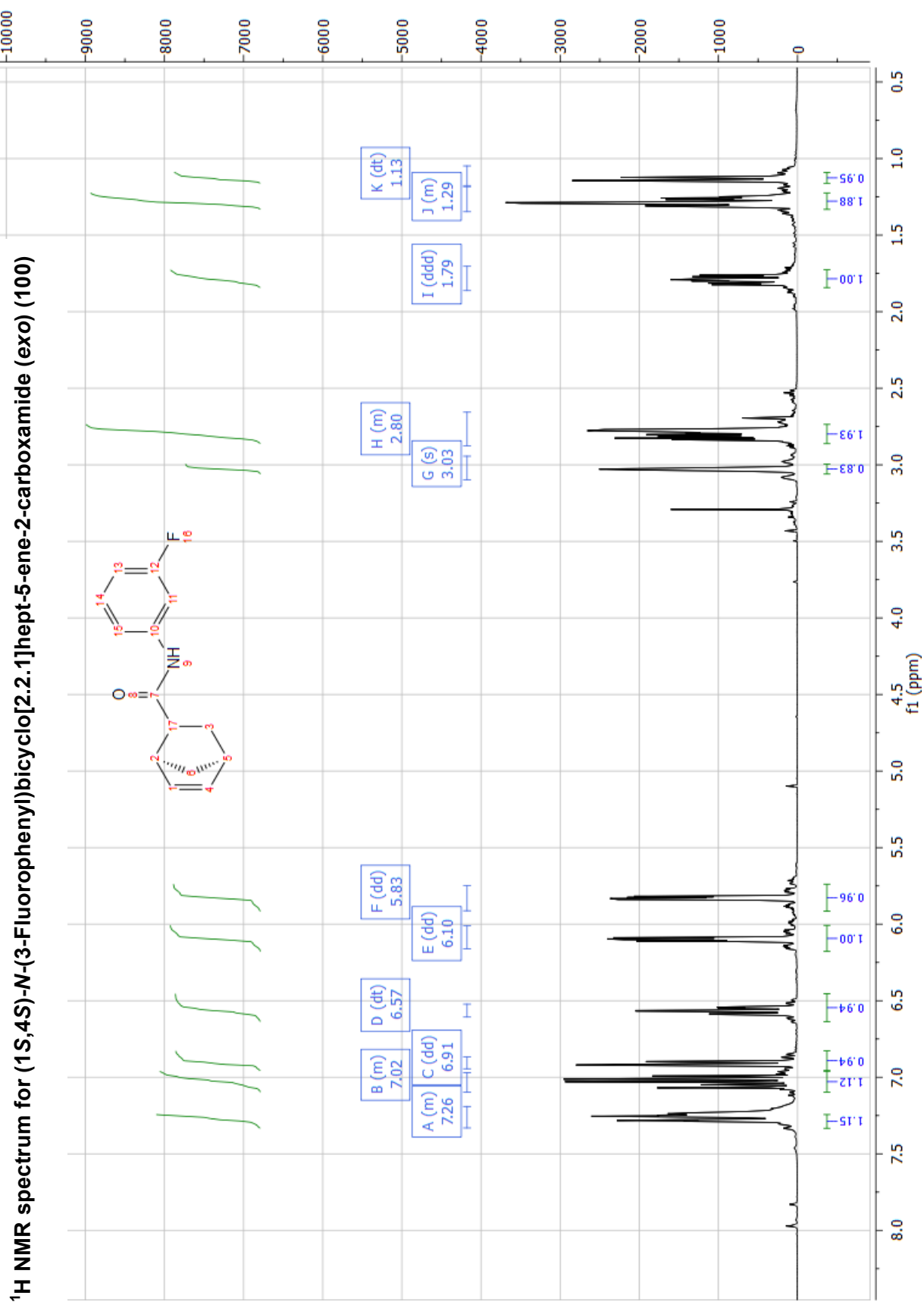**¹H NMR spectrum for DOTA-Az**

¹H NMR spectrum for *tert*-Butyl 4-(6-methyl-1,2,4,5-tetrazin-3-yl)benzylcarbamate (89)
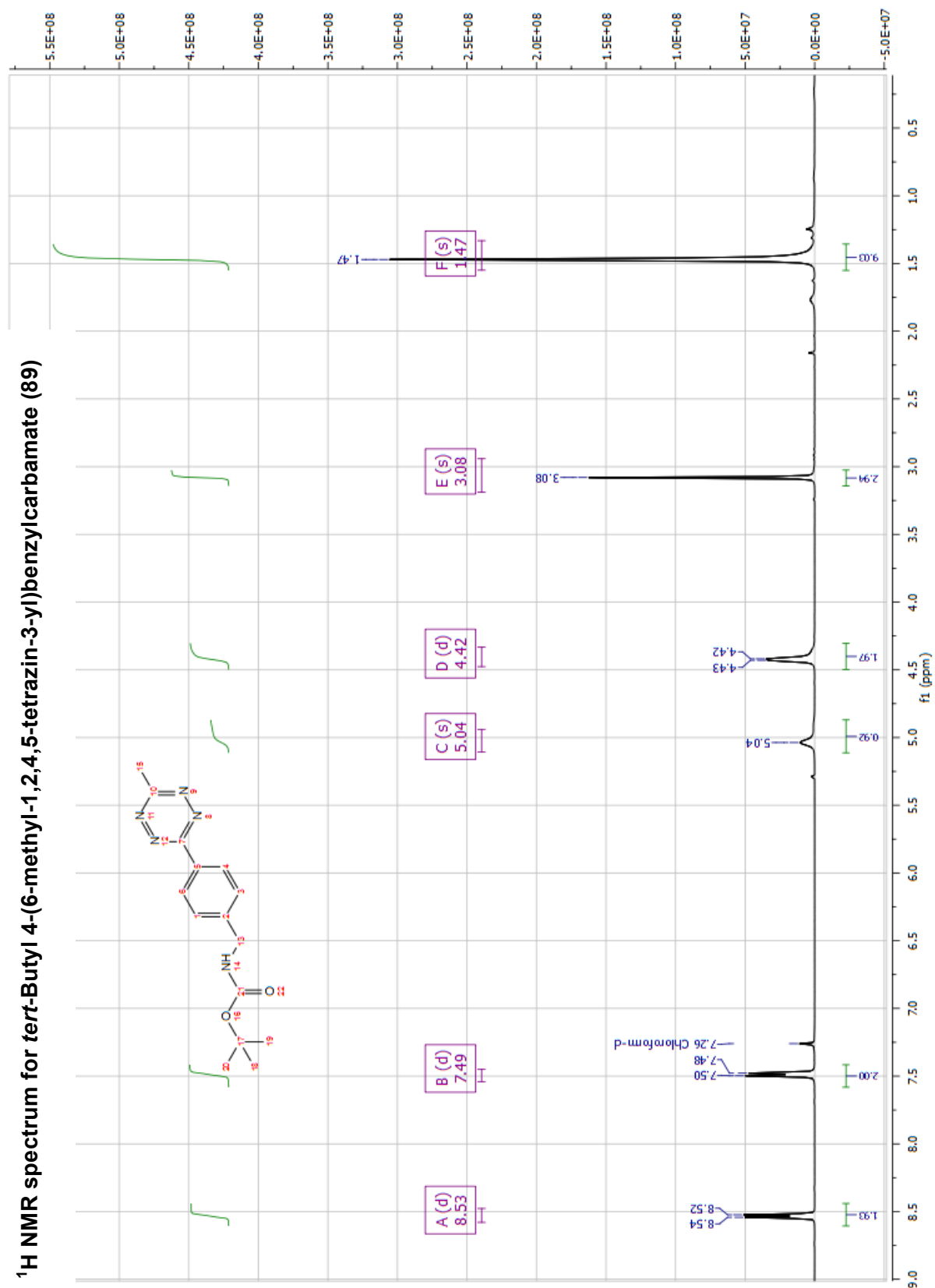
¹³C NMR spectrum for *tert*-Butyl 4-(6-methyl-1,2,4,5-tetrazin-3-yl)benzylcarbamate (89)
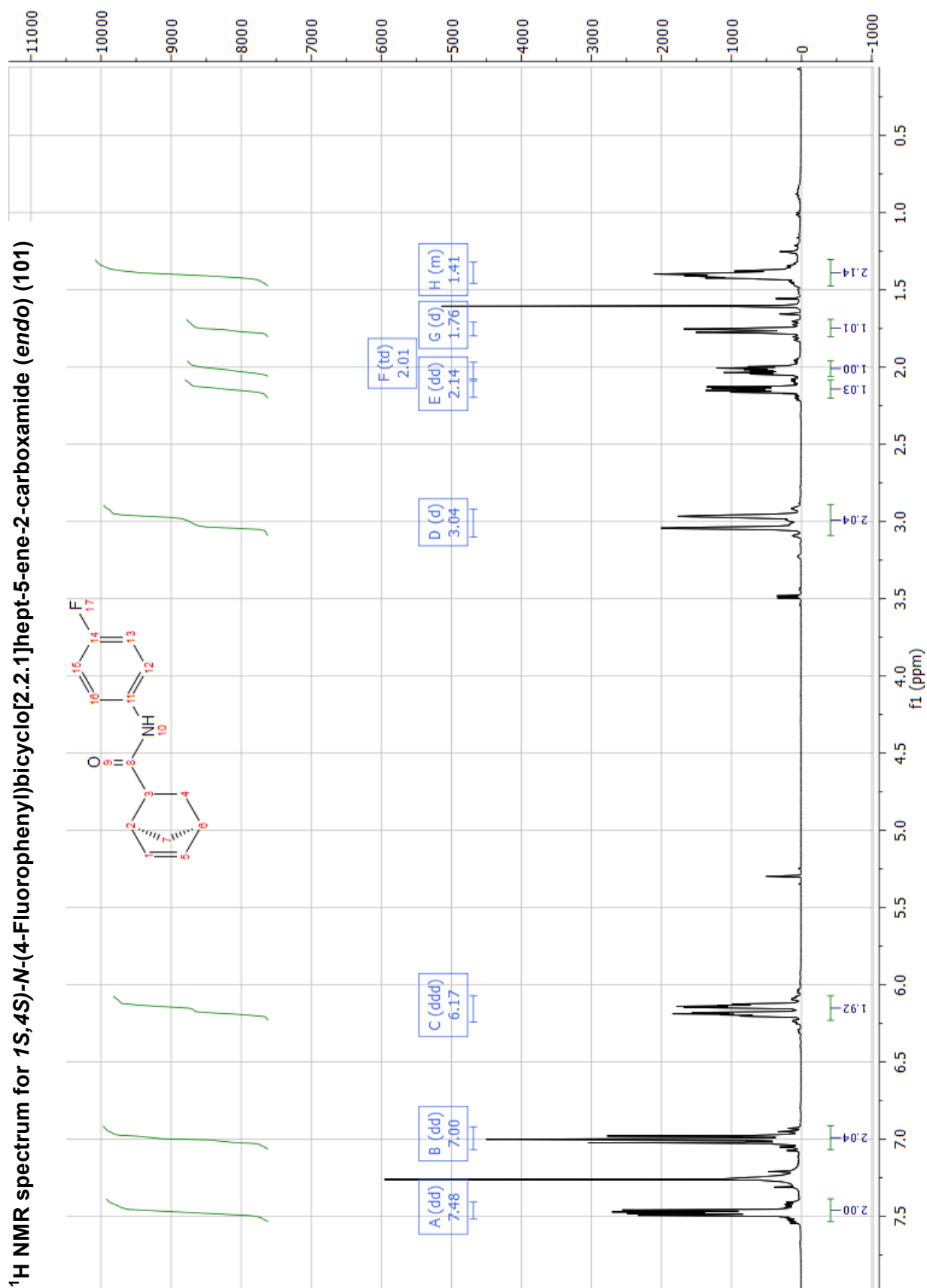
¹H NMR spectrum for DOTA-Tz

¹H NMR spectrum for (1*S*,4*S*)-*N*-(3-Fluorophenyl)bicyclo[2.2.1]hept-5-ene-2-carboxamide (*exo*) (100)

¹⁹F NMR spectrum for (1S,4S)-N-(3-Fluorophenyl)bicyclo[2.2.1]hept-5-ene-2-carboxamide (exo) (100)
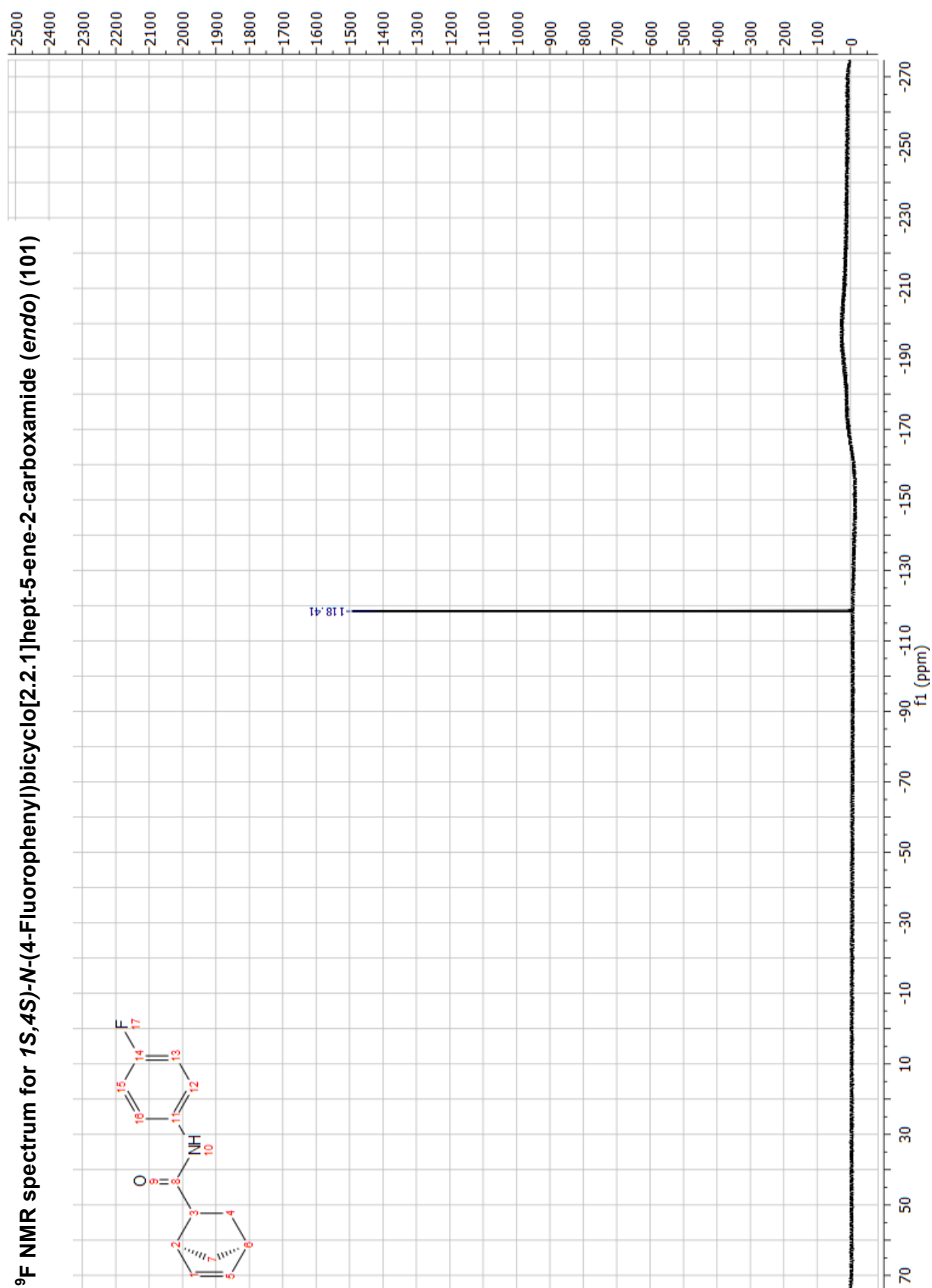

-111.64
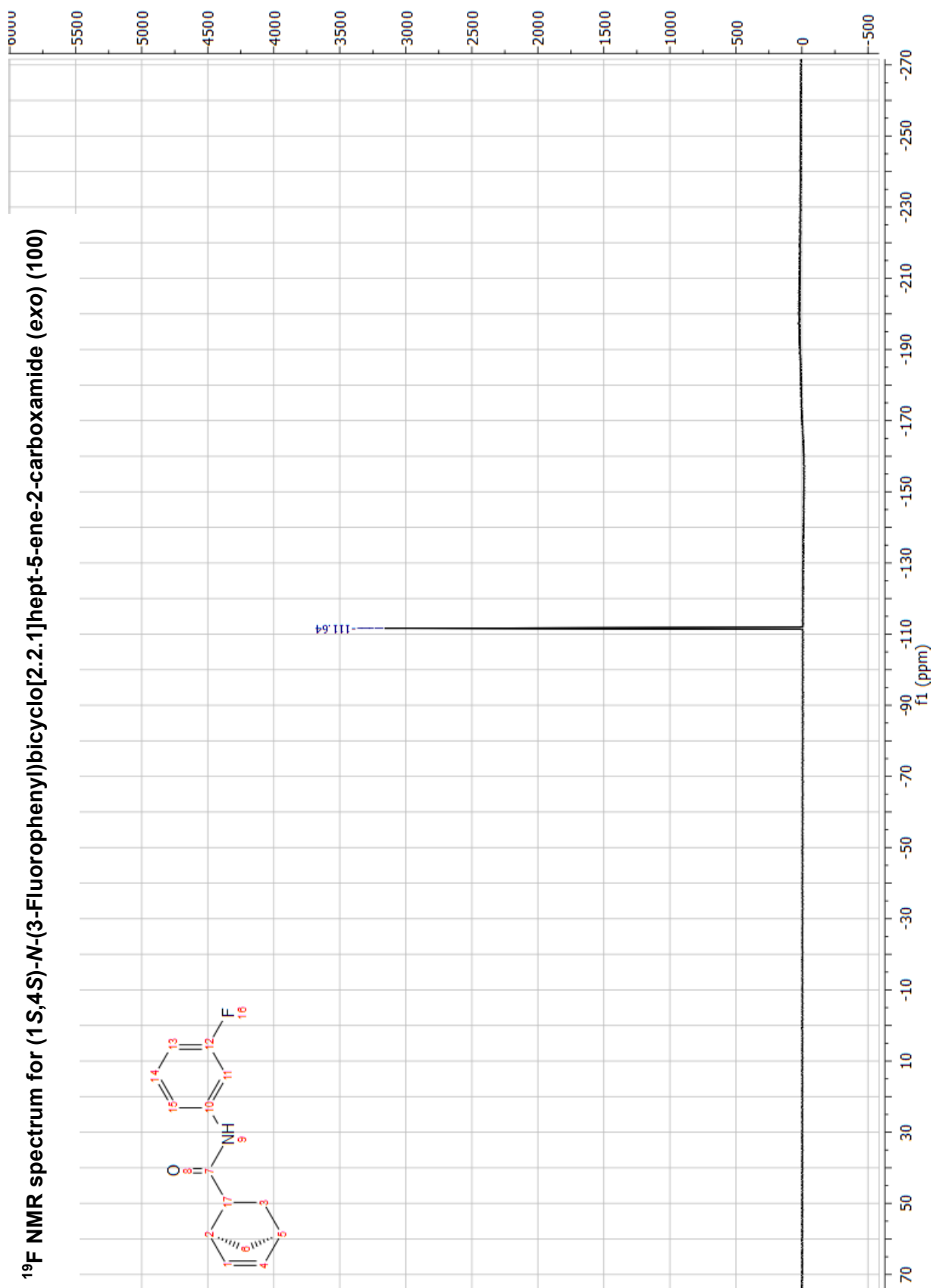
¹H NMR spectrum for *1S,4S*)-*N*-(4-Fluorophenyl)bicyclo[2.2.1]hept-5-ene-2-carboxamide (*endo*) (101)

¹⁹F NMR spectrum for *1S,4S*-*N*-(4-Fluorophenyl)bicyclo[2.2.1]hept-5-ene-2-carboxamide (*endo*) (101)
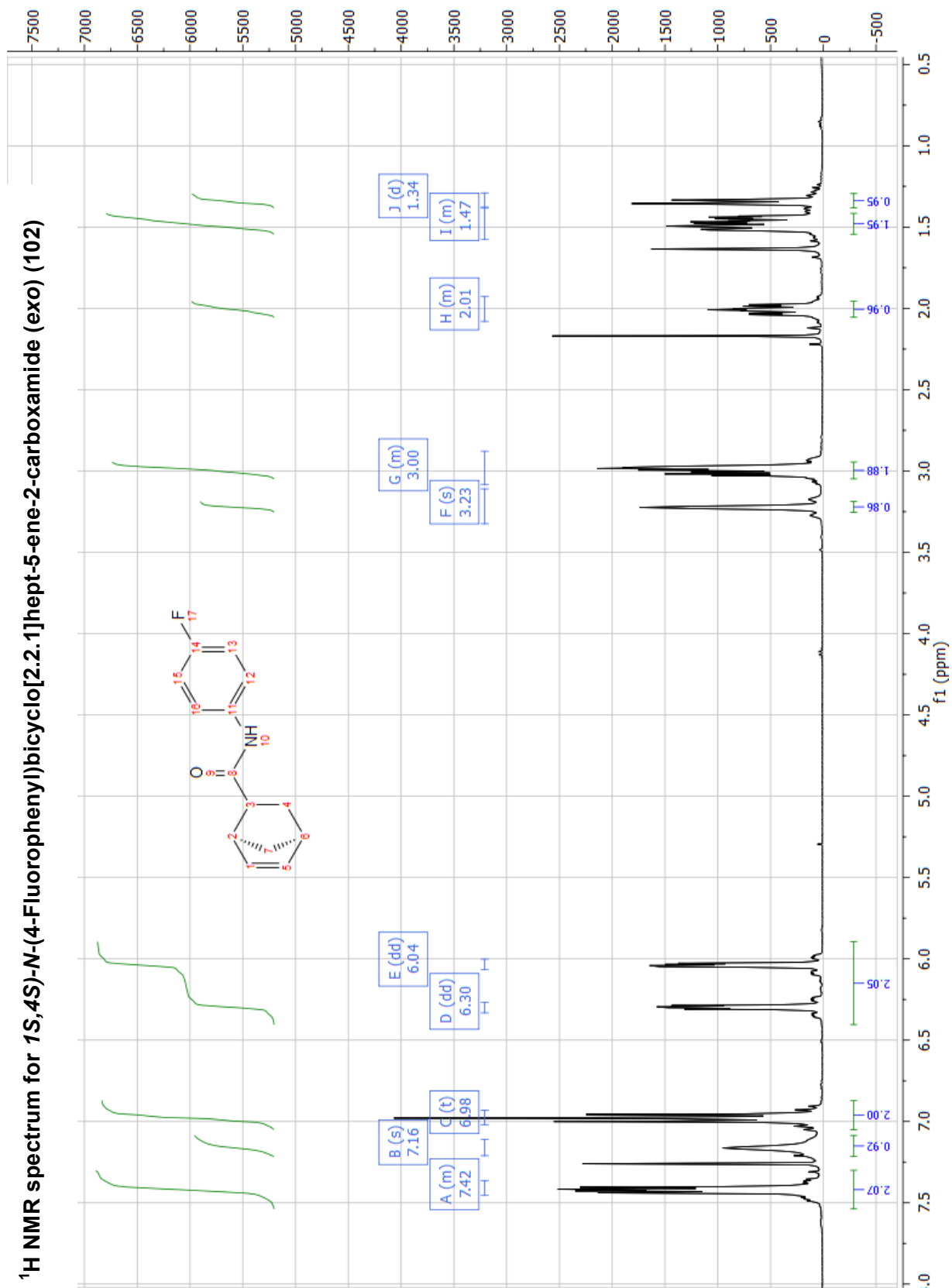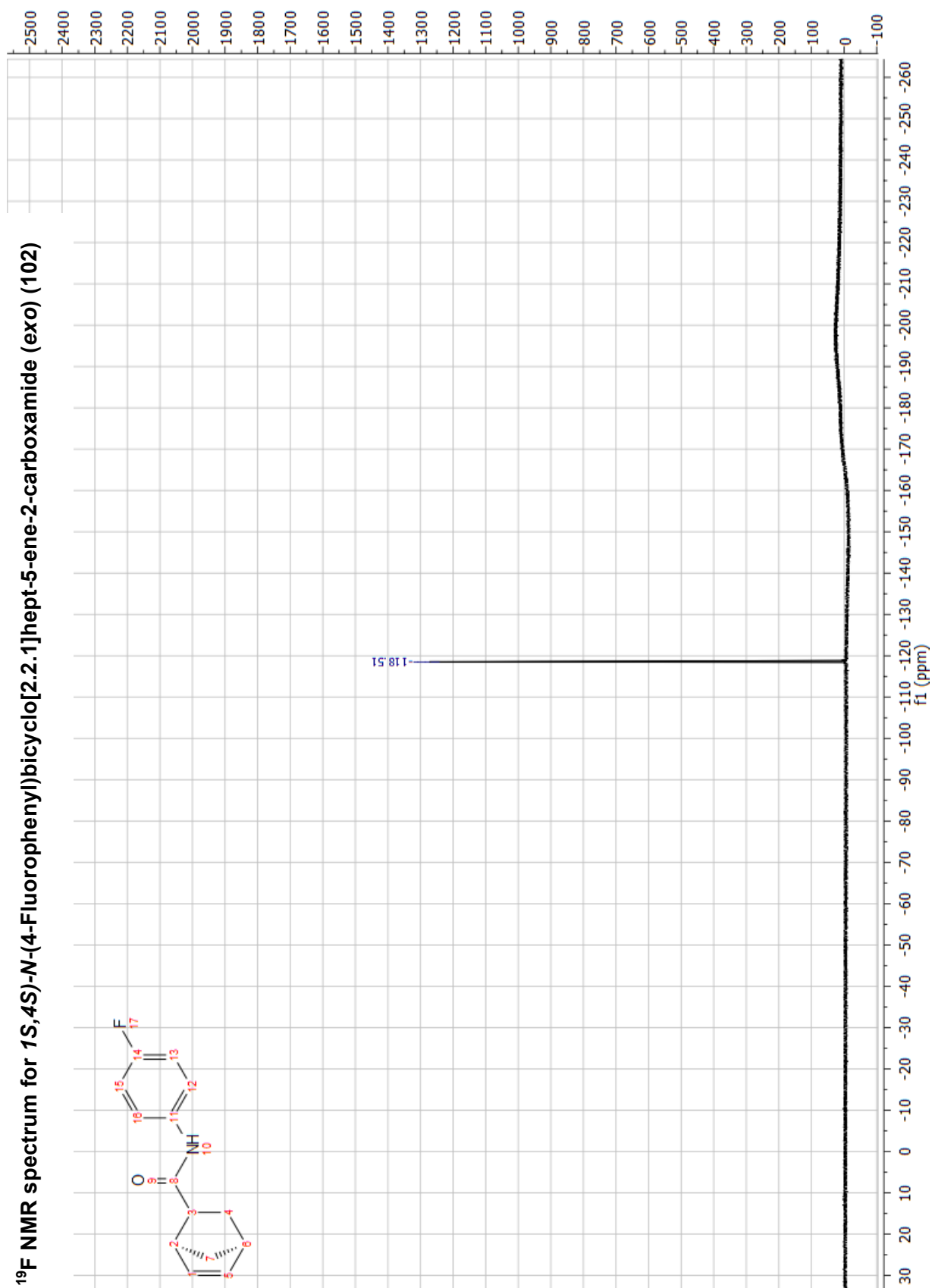

-118.41

f1 (ppm)

¹H NMR spectrum for *1S,4S*-*N*-(4-Fluorophenyl)bicyclo[2.2.1]hept-5-ene-2-carboxamide (*exo*) (102)

¹⁹F NMR spectrum for *1S,4S*-*N*-(4-Fluorophenyl)bicyclo[2.2.1]hept-5-ene-2-carboxamide (exo) (102)
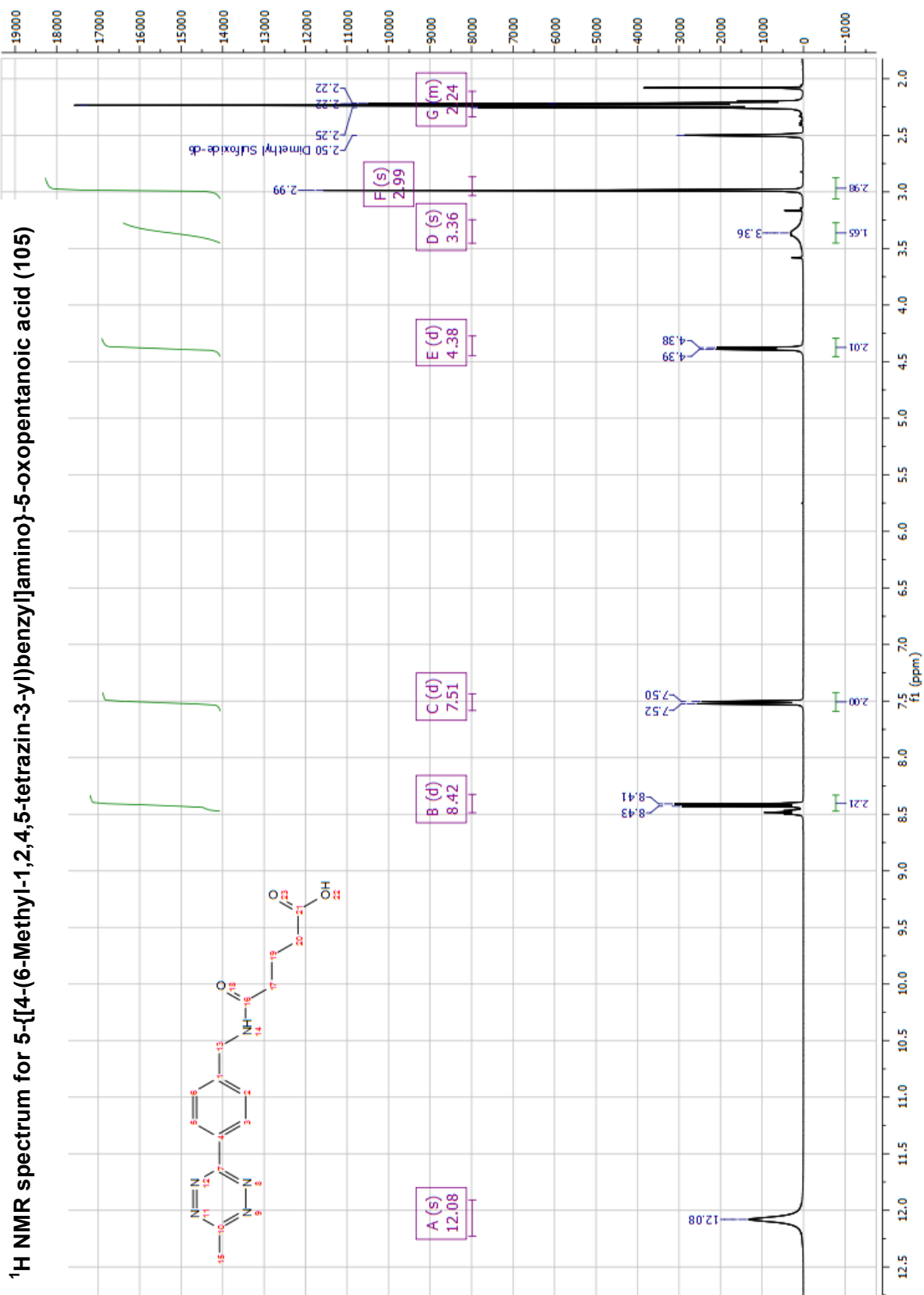
-118.51

f1 (ppm)

¹H NMR spectrum for 5-{[4-(6-Methyl-1,2,4,5-tetrazin-3-yl)benzyl]amino}-5-oxopentanoic acid (105)

^{13}C NMR spectrum for 5-{[4-(6-Methyl-1,2,4,5-tetrazin-3-yl)benzyl]amino}-5-oxopentanoic acid (105)
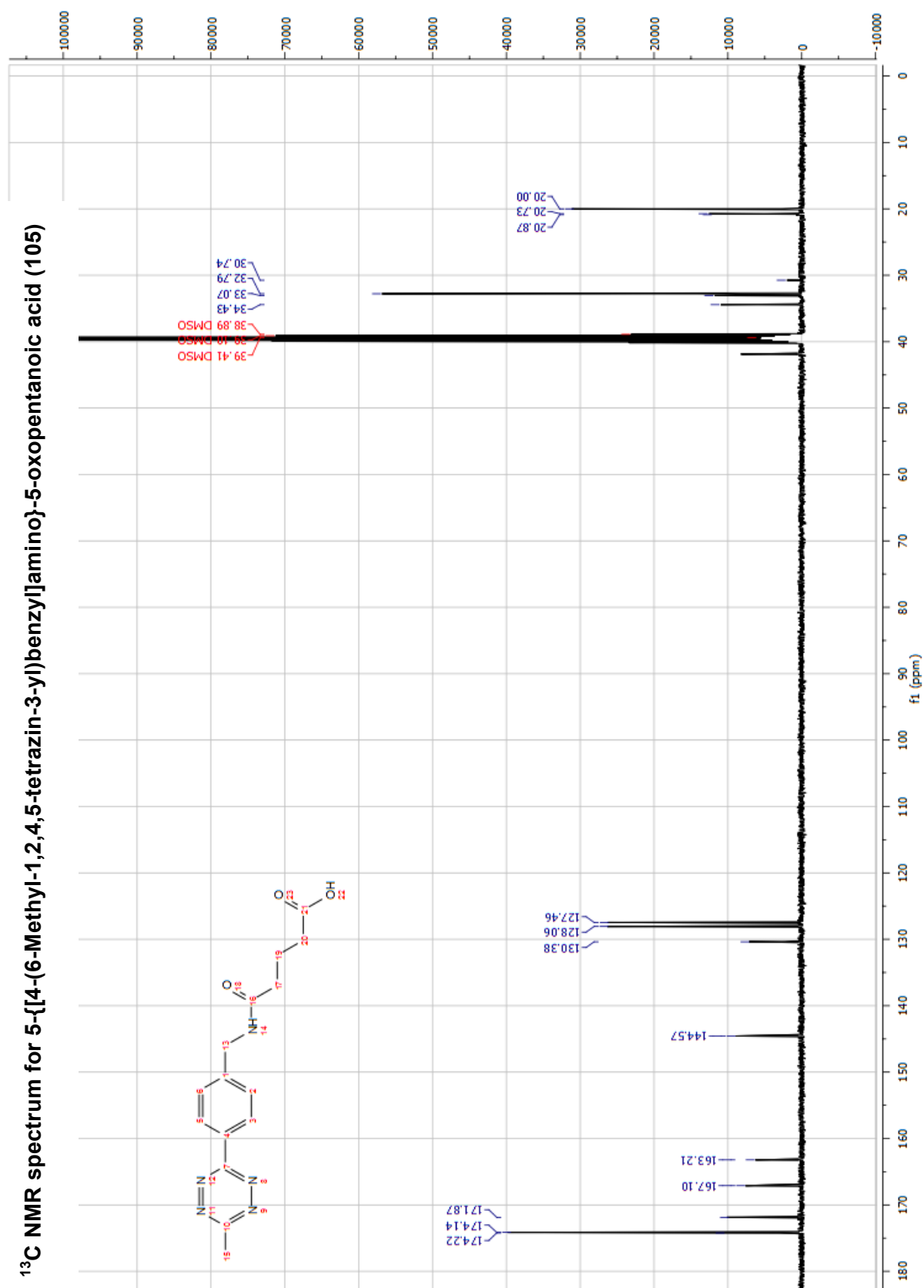
Appendix 4- Data for the Kinetics Studies
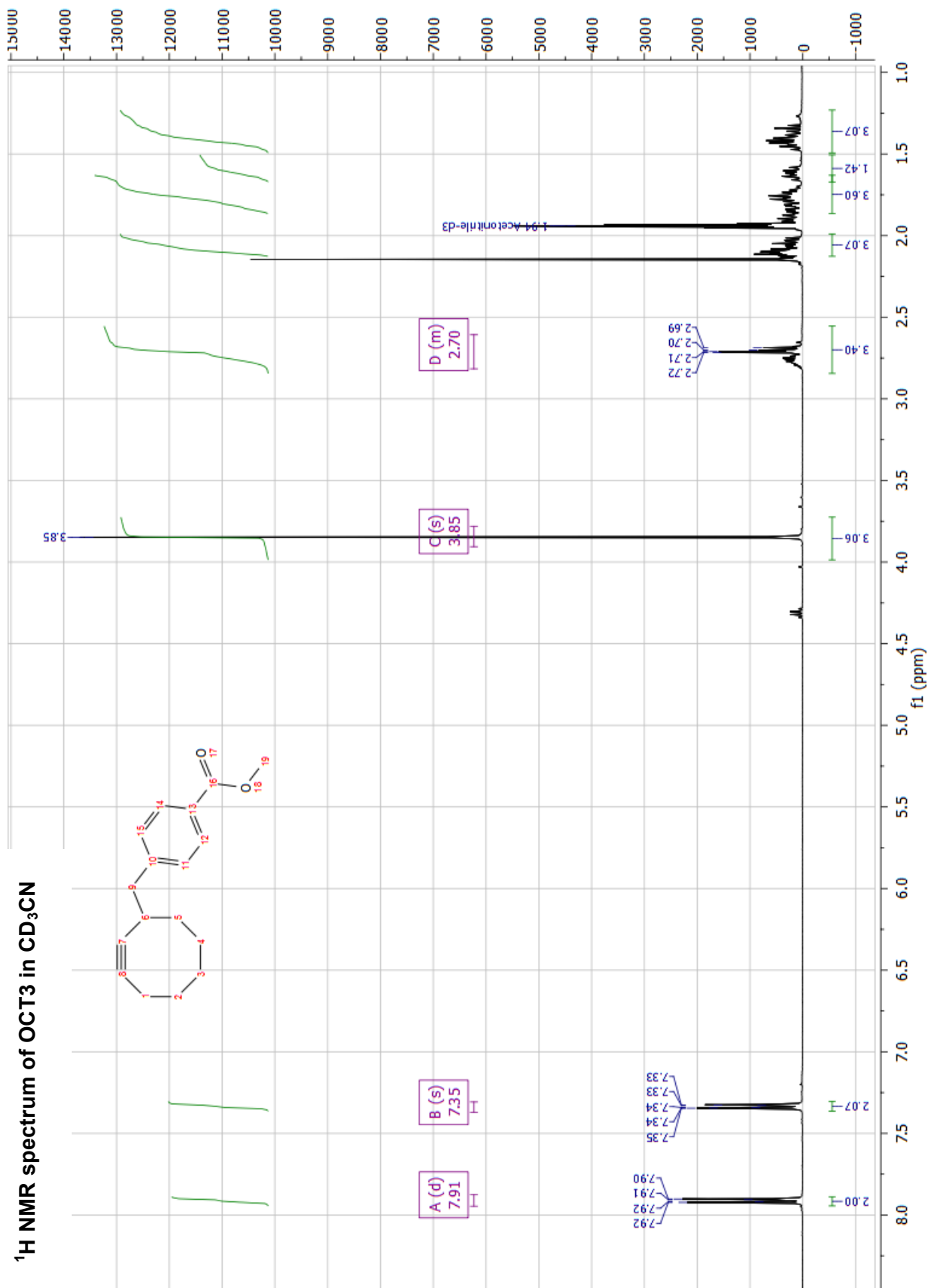
^{1}H NMR spectrum of OCT3 in CD$_3$CN

Mass spectrum of OCT3 (CI⁺)

Example ^{1}H NMR spectrum of the reaction mixture between OCT3 and benzyl azide 63 after 1h in CD$_3$CN

Example ^{1}H NMR spectrum of the reaction mixture between OCT3 and benzyl azide 63 after 16 h in CD$_3$CN
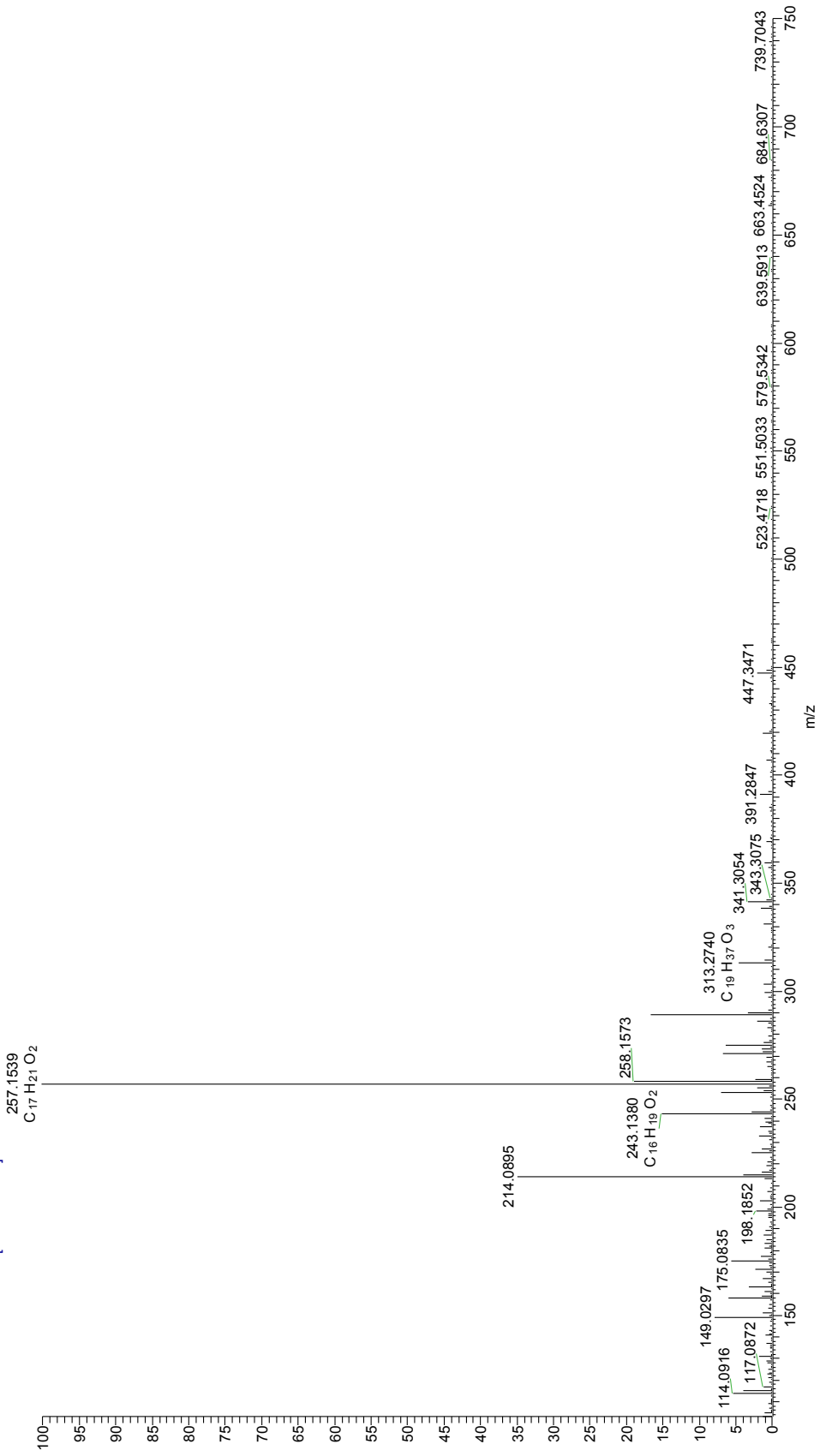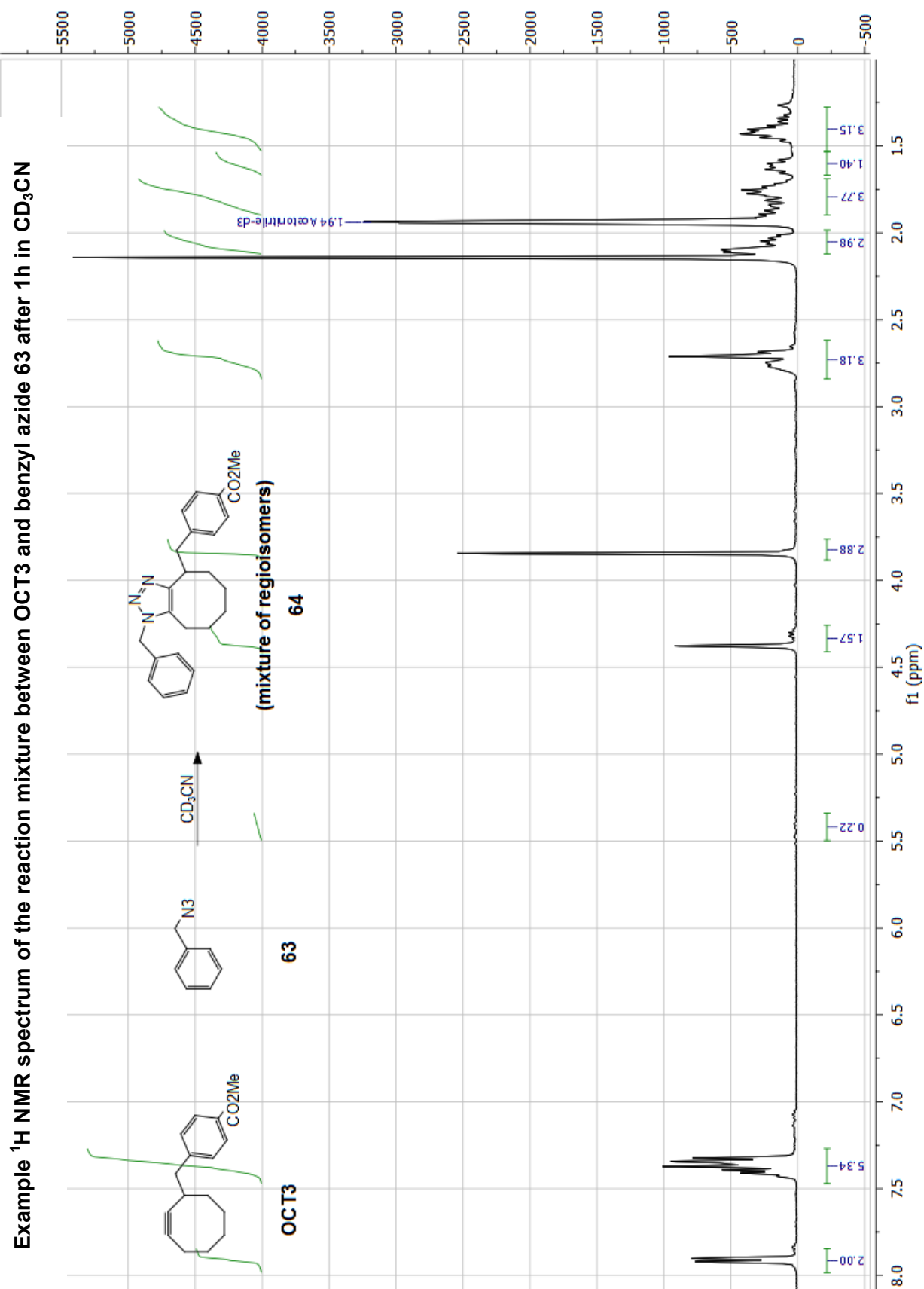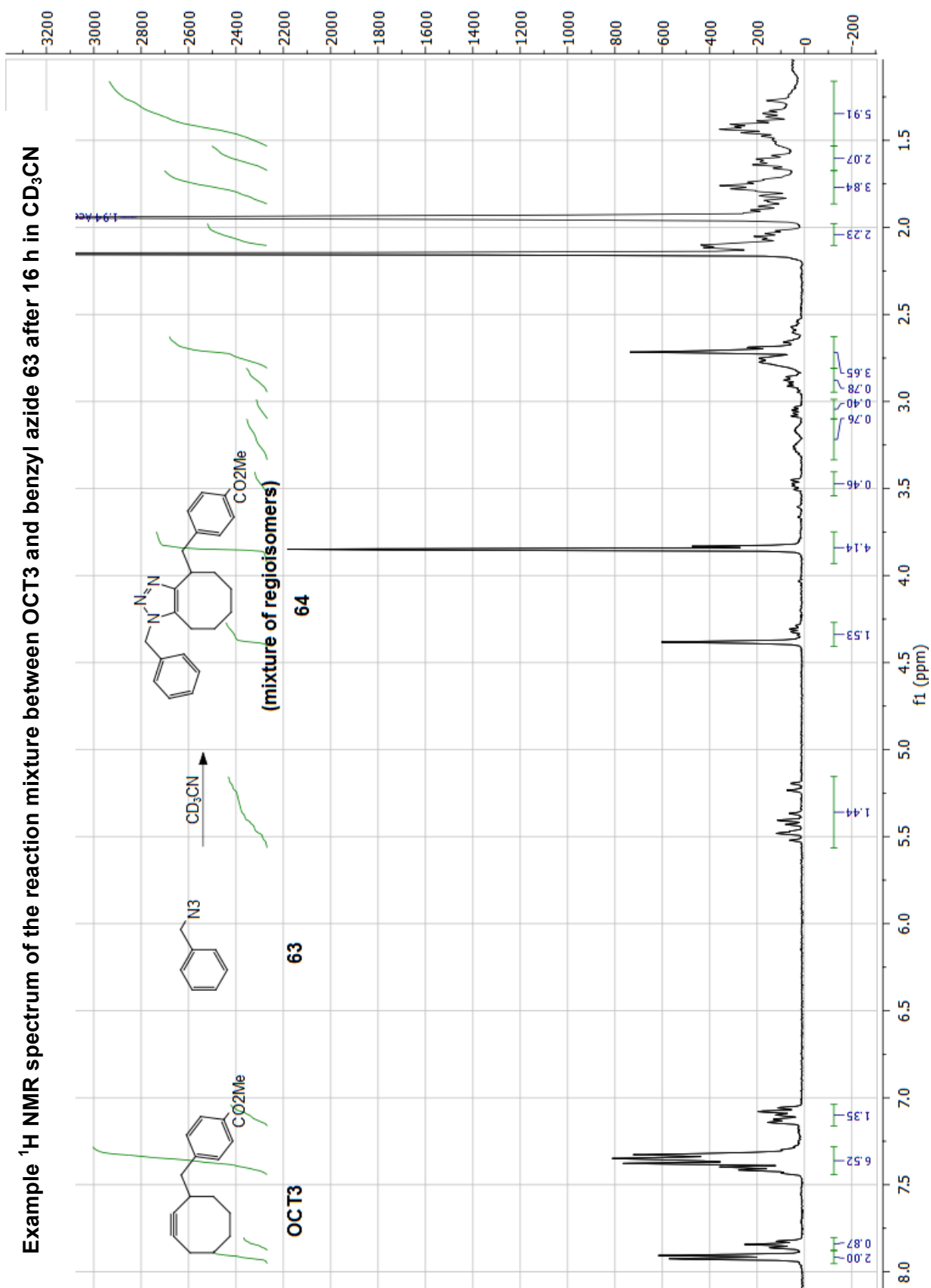
LCMS of the reaction mixture between OCT3 and benzyl azide 63 (triazole 64)

1: TOF MS ES+ :412+390 Smooth (SG, 2x2)

5.9e+004

(34)
68%
389.0 (34%)
4.00

Time

0.50 1.00 1.50 2.00 2.50 3.00 3.50 4.00 4.50

100
80
60
40
20
0

%
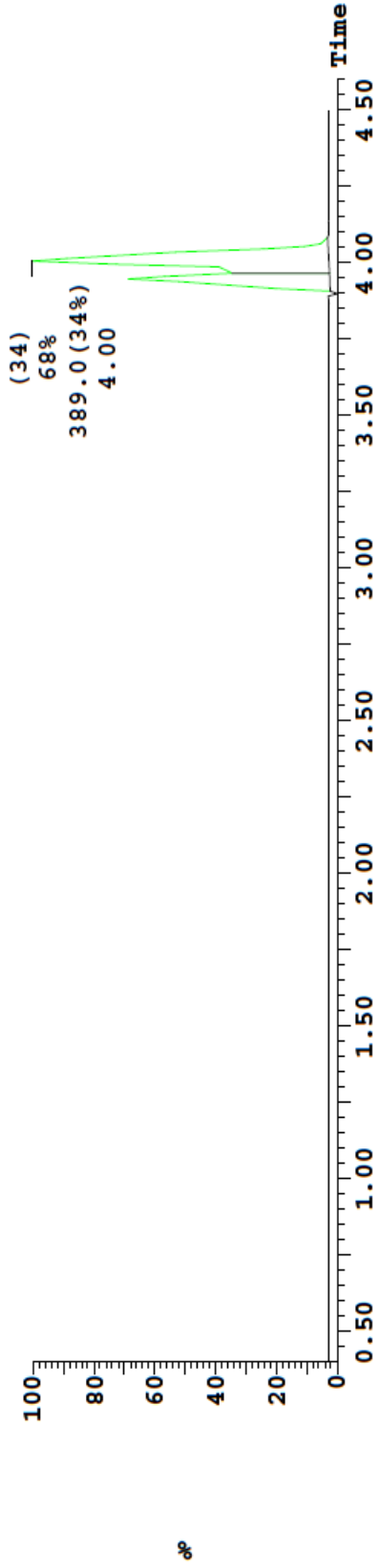
Peak ID Compound Time Mass Found
   33   3.95   390.00

33: (Time: 3.95) Combine (322:330-(309:312+340:343))

1:TOF MS ES+
2.0e+005

79.1 120.1 158.9 284.3 319.0 369.4 390.2 391.2 431.3 468.2 469.2 514.3 570.4

100.0 200.0 300.0 400.0 500.0 600.0   m/z

100
0
%
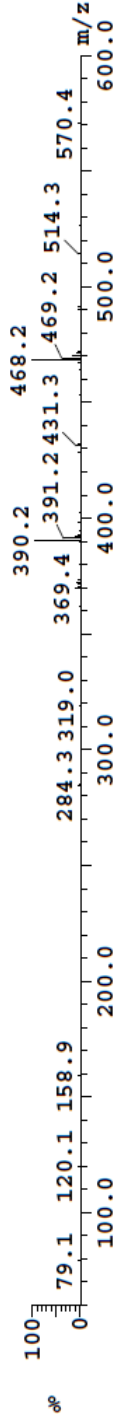
Peak ID Compound Time Mass Found
   34   4.00   412.00,390.00

34: (Time: 4.00) Combine (327:335-(314:317+345:348))
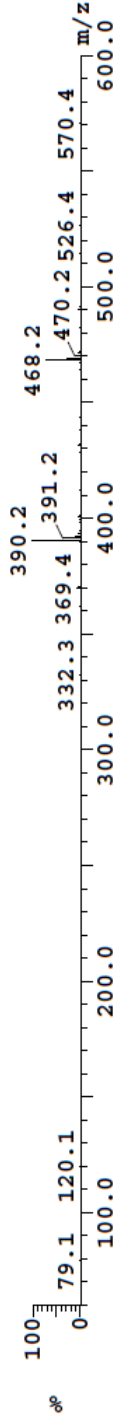
1:TOF MS ES+
2.7e+005

79.1 120.1 332.3 369.4 390.2 391.2 468.2 470.2 526.4 570.4

100.0 200.0 300.0 400.0 500.0 600.0   m/z

100
0
%

HRMS (ES$^+$) of triazole 64

Elemental Composition Report

Single Mass Analysis
Tolerance = 50.0 PPM / DBE: min = -1.5, max = 50.0
Element prediction: Off
Number of isotope peaks used for i-FIT = 3

Monoisotopic Mass, Even Electron Ions
118 formula(e) evaluated with 1 results within limits (all results (up to 1000) for each mass)
Elements Used:
C: 24-24   H: 0-1000   N: 0-10   O: 0-10

H.EVANS HE394
ms06449a 328 (3.964)

1: TOF MS ES+
1.65e+004
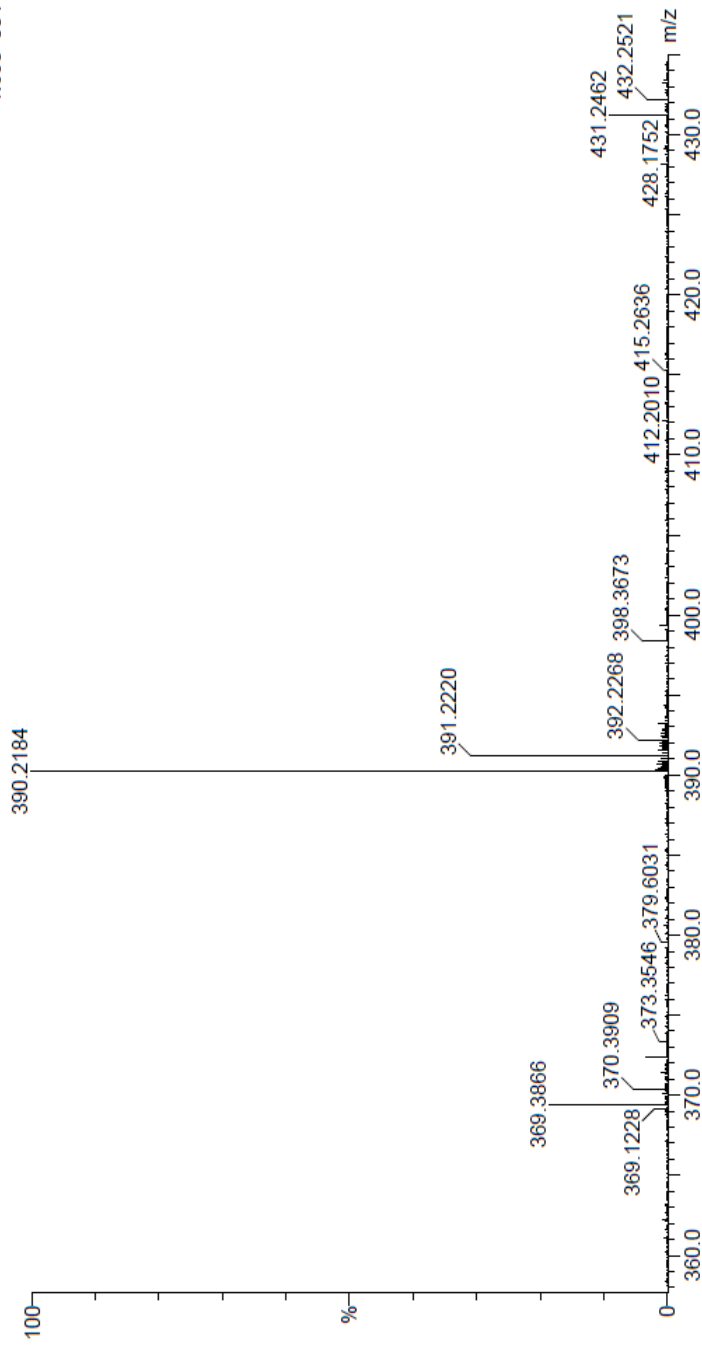
Minimum:				-1.5			
Maximum:			5.0	50.0	50.0		
Mass	Calc. Mass	mDa	PPM	DBE	i-FIT	i-FIT (Norm)	Formula
390.2184	390.2182	0.2	0.5	12.5	283.6	0.0	C24 H28 N3 O2

Raw Data for the Rate Calculation

n = 1

| Times (sec)	Ratio (63 : 64)	Conversion (%)	% [benzyl zide]	[benzyl azide] (M)	1/[benzyl azide]
900	2 : 0.05	2.4	97.6	0.0099	101.0
1800	2 : 0.12	5.7	94.3	0.0096	104.5
3600	2 : 0.20	9.0	91.0	0.0092	108.3
7200	2 : 0.31	13.4	86.6	0.0088	113.8
10800	2 : 0.43	17.7	82.3	0.0083	119.7
14400	2 : 0.54	21.3	78.7	0.0080	125.2
18000	2 : 0.68	25.4	74.6	0.0076	132.1
21600	2 : 0.79	28.3	71.7	0.0073	137.5
25200	2 : 0.95	32.2	67.8	0.0069	145.4
28800	2 : 1.06	34.6	65.4	0.0066	150.7
57600	2 : 2.29	53.4	46.6	0.0047	211.5

n = 2

Times (sec)	Ratio (63 : 64)	Conversion (%)	% [benzyl zide]	[benzyl azide] (M)	1/[benzyl azide]
900	2 : 0.07	3.4	96.6	0.0098	102.0
1800	2 : 0.13	6.1	93.9	0.0095	105.0
3600	2 : 0.15	7.0	93.0	0.0094	105.9
7200	2 : 0.27	11.9	88.1	0.0089	111.9
10800	2 : 0.34	14.5	85.5	0.0087	115.3
14400	2 : 0.43	17.7	82.3	0.0084	119.7
18000	2 : 0.52	20.6	79.4	0.0081	124.1
21600	2 : 0.64	24.2	75.8	0.0078	130.0
25200	2 : 0.72	26.5	73.5	0.0075	134.1
28800	2 : 0.80	28.6	71.4	0.0072	138.0
57600	2 : 1.53	43.3	56.7	0.0057	173.8
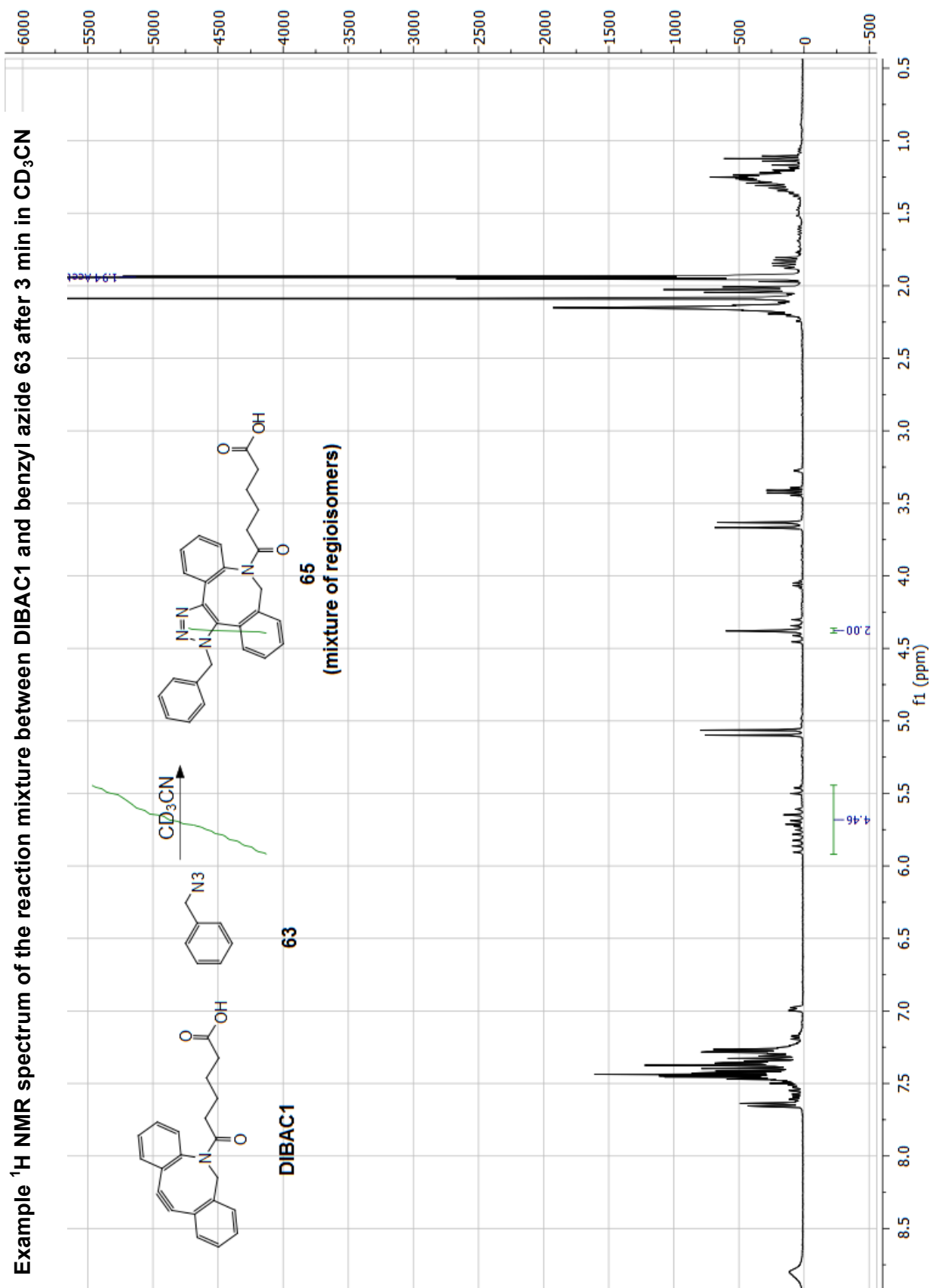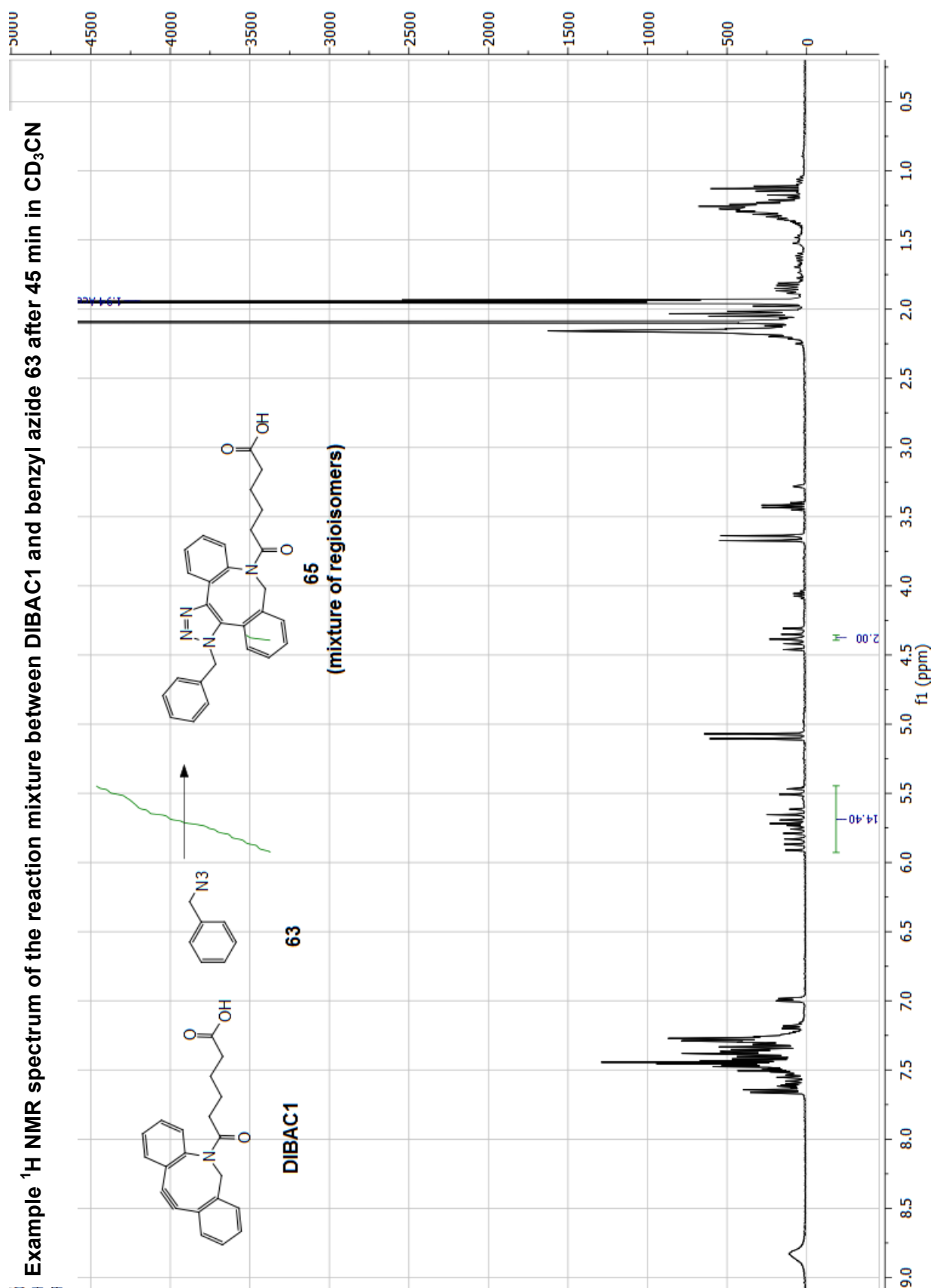
Example ^{1}H NMR spectrum of the reaction mixture between DIBAC1 and benzyl azide 63 after 3 min in CD$_3$CN

Example ¹H NMR spectrum of the reaction mixture between DIBAC1 and benzyl azide 63 after 45 min in CD₃CN

65
(mixture of regioisomers)

63

DIBAC1

LCMS of the reaction mixture between DIBAC1 and benzyl azide 63 (triazole 65)

1: TOF MS ES+ :489+467 Smooth (SG, 2x2)   4.6e+004
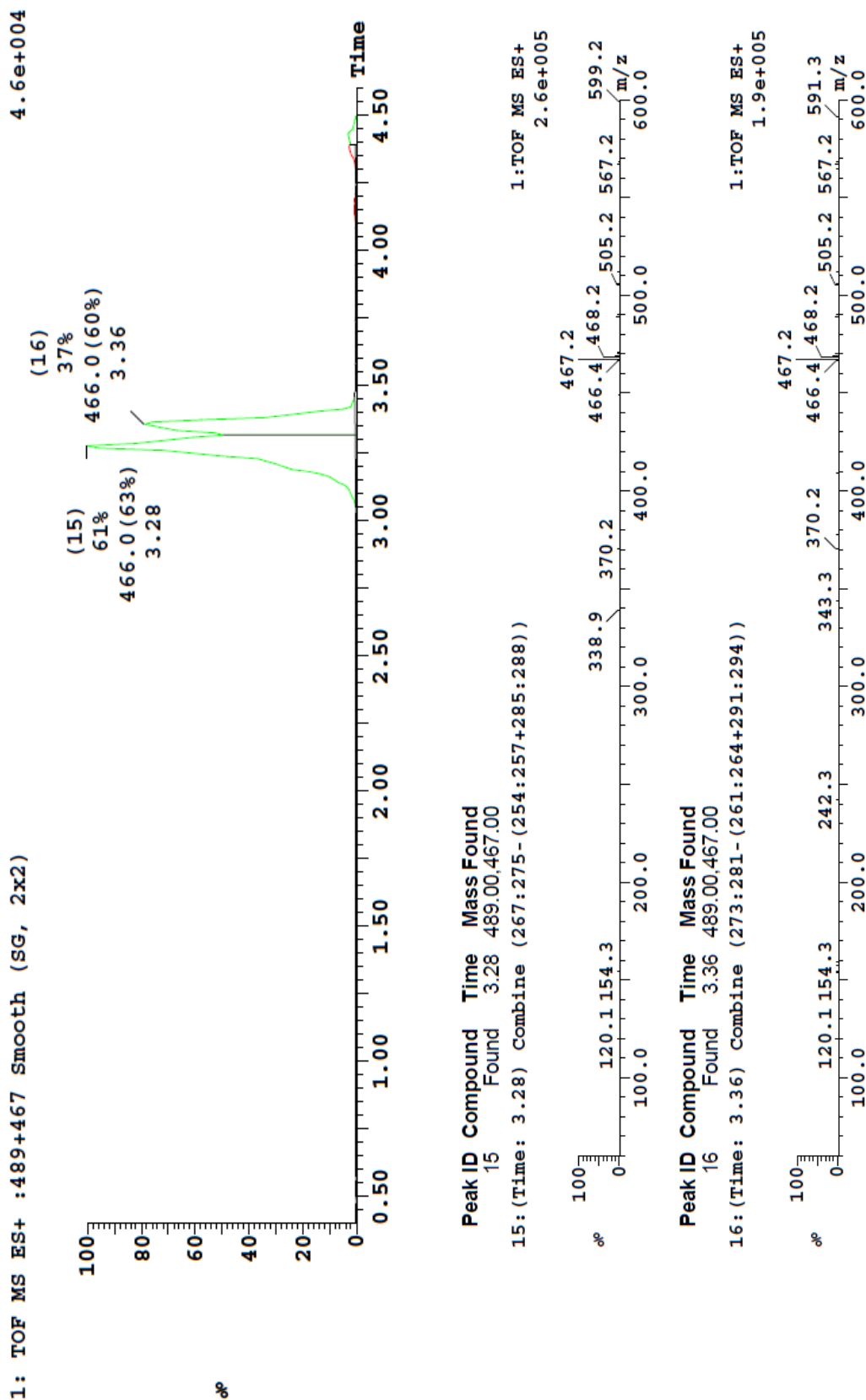
HRMS (ES⁺) of triazole 65

Elemental Composition Report

Single Mass Analysis
Tolerance = 50.0 PPM / DBE: min = -1.5, max = 50.0
Element prediction: Off
Number of isotope peaks used for i-FIT = 3

Monoisotopic Mass, Even Electron Ions
119 formula(e) evaluated with 1 results within limits (all results (up to 1000) for each mass)
Elements Used:
C: 28-28   H: 0-1000   N: 0-10   O: 0-10

H.EVANS HE398
ms06450 273 (3.308)

1: TOF MS ES+
2.45e+004
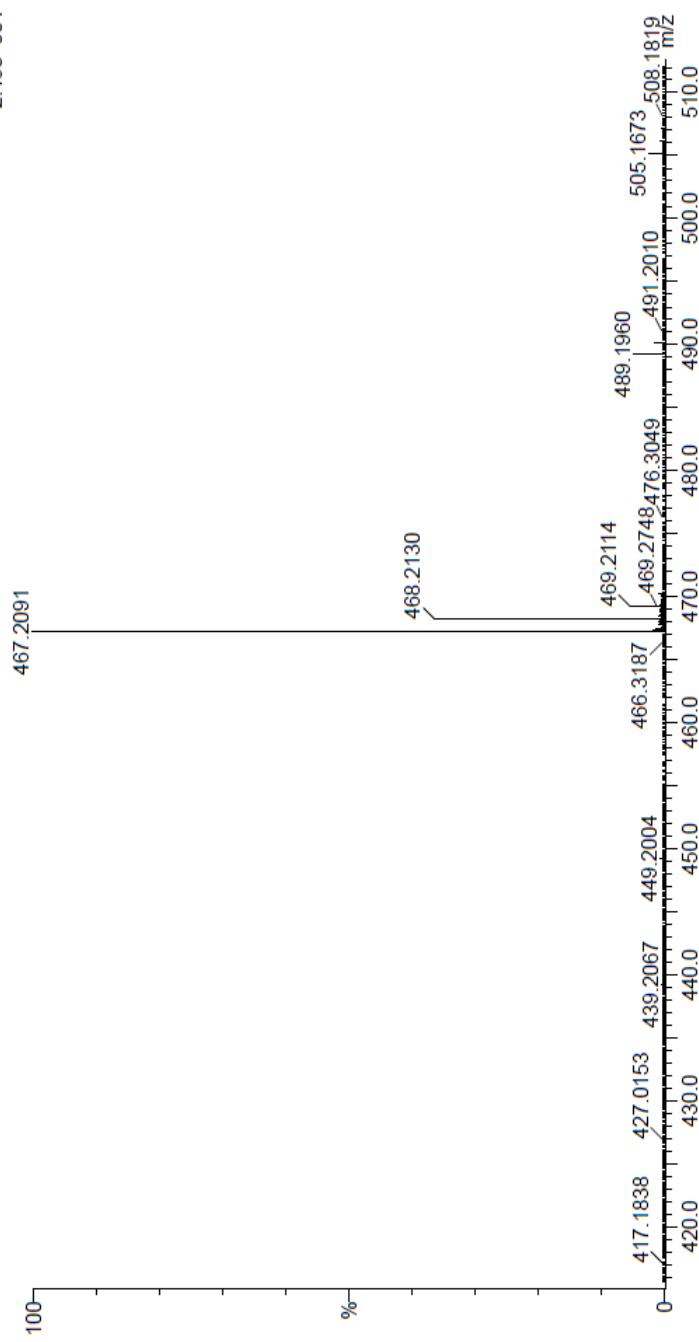
Minimum:					-1.5	
Maximum:			5.0	50.0	50.0	
Mass	Calc. Mass	mDa	PPM	DBE	i-FIT	i-FIT (Norm)	Formula
467.2091	467.2083	0.8	1.7	17.5	288.9	0.0	C28 H27 N4 O3

Raw Data for the Rate Calculation

Average Data based on 3 experiments:

Times (sec)	Ratio (63 : 65)	Conversion (%)	% [benzyl azide]	[benzyl azide] (M)	1/[benzyl azide]
180	2 : 4.46	69.0	31.0	0.0031	318.3
360	2 : 5.47	73.2	26.8	0.0027	368.1
600	2 : 6.59	76.7	23.3	0.0024	423.3
780	2 : 7.38	78.7	21.3	0.0022	462.2
960	2 : 7.73	79.4	20.6	0.0021	479.5
1200	2 : 8.57	81.1	18.9	0.0019	520.9
1380	2 : 9.42	82.5	17.5	0.0018	562.7
1560	2 : 9.82	83.1	16.9	0.0017	582.5
1740	2 : 10.47	84.0	16.0	0.0016	614.5
1980	2 : 10.92	84.5	15.5	0.0016	636.7
2160	2 : 11.41	85.1	14.9	0.0015	660.8
2340	2 : 12.19	85.9	14.1	0.0014	699.2
2580	2 : 13.16	86.8	13.2	0.0013	747.0
2760	2 : 13.58	87.2	12.8	0.0013	767.7
2940	2 : 14.40	87.8	12.2	0.0012	808.1

Evaluating the Concentration Dependence upon Rate of Reaction

Raw Data for the Reaction between DIBAC2 and Azide 66 (at 15 min)

Initial [DIBAC2] (M)	1/[DIBAC2]	Conversion (%)				Average Conversion (%)	SDEV
		n = 1	*n* = 2	*n* = 3	*n* = 4		
2.418555155	0.41347	31.49	34.31	33.15	41.36	35.1	4.34
1.209277578	0.82694	18.43	22.88	20.14	27.88	22.3	4.13
0.604638789	1.65388	22.29	10.97	14.85	32.22	12.9	9.36
0.302319394	3.30776	11.12	4.19	14.04	16.44	11.4	5.30

Raw Data for the Reaction between Tz3 and Norbornene 91 (at 0, 5, 10, 30 and 60 min)

Average data based on 3 experiments:

Initial [Tz3] (M)	Average Conversion (%)				
	0 min	5 min	10 min	30 min	60 min
0.002484596	0	82.61	92.50	95.45	98.89
0.00024846	0	80.62	89.06	98.53	98.76
2.4846E-05	0	71.71	90.20	92.92	95.20
2.4846E-06	0	49.66	80.34	89.31	96.31